Biomimetic Identification of Phase-Selective Peptide-Additives

Dissertation

zur Erlangung des Grades

“Doktor der Naturwissenschaften”

im Promotionsfach Chemie

am Fachbereich Chemie, Pharmazie und Geowissenschaften der

Johannes Gutenberg-Universität Mainz

Jochen Renkel

geboren in Bad Kreuznach

Mainz, 2019

Dekan: [redacted]

1. Berichterstatter: [redacted]

2. Berichterstatter: [redacted]

Tag der mündlichen Prüfung: 20.01.2020

Declaration

The presented dissertation was prepared between March 2010 and August 2019 under the direction of Prof. Dr. [redacted] at the Institute for Inorganic Chemistry and Analytical Chemistry of the Johannes Gutenberg University Mainz.

I hereby declare that I wrote the presented dissertation independently and without outside help. All used references and resources are completely indicated.

Erklärung

Die vorliegende Dissertation wurde in der Zeit von März 2010 bis August 2019 unter der Leitung von Univ.-Prof. Dr. [redacted] am Institut für Anorganische Chemie und Analytische Chemie der Johannes Gutenberg-Universität Mainz angefertigt.

Hiermit erkläre ich, dass ich die vorliegende Dissertation selbstständig und ohne fremde Hilfe verfasst zu haben. Alle verwendeten Quellen und Hilfsmittel sind vollständig angegeben.

Mainz, August 2019

Jochen Renkel

In Dankbarkeit meiner Familie gewidmet.

Abstract

Biomineralisation is a widespread phenomenon, which enables organisms to form highly ordered materials. During the associated processes, certain properties, such as the crystal morphology and -size or the deposited polymorph of a compound, are tightly controlled. Although the mechanisms that govern the polymorph-selective precipitations are intensively investigated, the respective experiments are often hampered by the difficulties in isolating the involved biomolecules from organisms or biominerals. To circumvent the dependence on biologic samples and related problems, this thesis has applied the Phage Display technique to identify peptides capable of biomimetically controlling the formation of the different calcium carbonate polymorphs during crystallisations.

In the first experimental part, phage display was employed for affinity selections on the calcite polymorph of calcium carbonate. The respective screening experiments allowed the identification of several, potentially calcite-affine peptide sequences unreported in the literature. Subsequently, the focus was placed on the preparation of these peptides by automated *Solid Phase Peptide Synthesis* successfully yielding these peptides or their corresponding derivatives.

The second part covered the investigation of the prepared peptides for their influence on the phase selection. Different methods for the crystallisation of calcium carbonate were adopted, modified and employed in the presence of the prepared peptides. Especially the peptide with the sequence (GQNSTTNYHTLVR) strongly shifted the phase composition towards the vaterite polymorph in a concentration-dependent manner. The crystallisation experiments further allowed to postulate a hypothesis that explained the vaterite-selective influence of the peptide by its function as a crystal growth inhibitor of the thermodynamically stable calcium carbonate-phase calcite. Additionally, several, literature-known peptides were prepared and examined in a further set of crystallisation experiments as a comparison to the peptides identified by phage display. These experiments allowed to identify similarities and differences between the individual peptides and they gave general insights into the behaviour of the respective peptide-additives.

The third part dealt with investigating the proposed effect of the vaterite-selective peptide as a crystal growth inhibitor. The intention was to demonstrate and determine the adsorptions of this peptide towards the individual polymorphs of calcium carbonate. To this purpose, a dye-labelled derivative of the vaterite-selective peptide was prepared to assess the adsorptions qualitatively and quantitatively. The tendency of the dye-labelled peptide to form hydrogels prevented the further development of the adsorption test.

In summary, calcite-affine peptides were successfully identified and the effect of these peptides on the phase composition of calcium carbonate was demonstrated through different experimental stages. The newly identified peptides complement known additive structures and facilitate future experiments to gain a deeper insight into the crystallisation- and polymorph control of calcium carbonate.

Kurzzusammenfassung

Biomineralisation ist ein weit verbreitetes Phänomen, das Organismen zur Bildung hoch geordneter Materialien befähigt. Während der dazugehörigen Prozesse werden bestimmte Eigenschaften, z. B. die Kristallmorphologie und -größe oder der abgeschiedene Polymorph einer Verbindung, streng kontrolliert. Obwohl die Mechanismen, die die polymorph-selektiven Niederschläge steuern, intensiv untersucht werden, werden die jeweiligen Experimente oft durch die Schwierigkeiten bei der Isolierung der beteiligten Biomoleküle aus Organismen oder Biomineralien gehemmt. Um die Abhängigkeit von biologischen Proben und damit verbundenen Problemen zu umgehen, wendete vorliegende Arbeit die „Phage Display"-Technik an, um Peptiden zu identifizieren, die in der Lage sind, die Bildung der verschiedenen Polymorphe des Calciumcarbonats während der Kristallisation biomimetisch zu kontrollieren.

Im ersten experimentellen Teil wurde das „Phage-Display" für Affinitätsselektionen am Calcit-Polymorph des Calciumcarbonates verwendet. Die entsprechenden Screening-Experimente erlaubten die Identifizierung mehrerer, in der Literatur nicht erfasster und potenziell Calcit-affiner Peptidsequenzen. Anschließend wurde der Schwerpunkt auf die Herstellung dieser Peptide durch automatisierte *Festphasen-Peptidsynthese* gelegt, wodurch diese Peptide oder ihre entsprechenden Derivate erfolgreich erhalten wurden.

Der zweite Teil umfasste die Untersuchung der hergestellten Peptide auf ihren Einfluss auf die Phasenselektion. Verschiedene Methoden zur Kristallisation von Calciumcarbonat wurden übernommen, modifiziert und in Gegenwart der präparierten Peptide angewandt. Insbesondere das Peptid mit der Sequenz (GQNSTTNYHTLVR) verschob die Phasenzusammensetzung stark und konzentrationsabhängig zum Polymorphen Vaterit. Außerdem ermöglichten die Kristallisationsexperimente es, eine Hypothese zu postulieren, die den Vaterit-selektiven Einfluss des Peptides durch seine Wirkung als Kristallwachstumsinhibitor der thermodynamisch stabilen Calciumcarbonat-Phase Calcit erklärte. Darüber hinaus wurden mehrere, in der Literatur bekannte Peptide hergestellt und in einer weiteren Reihe von Kristallisationsexperimenten als Vergleich zu den durch „Phage-Display" identifizierten Peptiden untersucht. Diese

Experimente ermöglichten es, Ähnlichkeiten und Unterschiede zwischen den einzelnen Peptiden zu identifizieren und ergaben allgemeine Einblicke in das Verhalten der jeweiligen Peptid-Additive.

Der dritte Teil beschäftigte sich mit der Untersuchung der vorgeschlagenen Wirkungsweise des Vaterit-selektiven Peptids als Kristallwachstumsinhibitor. Dabei war beabsichtigt, die Adsorptionen dieses Peptids an den einzelnen Polymorphen des Calciumcarbonates zu demonstrieren und zu bestimmen. Zu diesem Zweck wurde ein farbstoffmarkiertes Derivat des vateritspezifischen Peptids hergestellt, um die Adsorptionen qualitativ und quantitativ zu bewerten. Die Tendenz des farbstoffmarkierten Peptids zur Bildung von Hydrogelen verhinderte die Weiterentwicklung des Adsorptionstests.

In Summe wurden mehrere, Calcit-affine Peptide erfolgreich identifiziert und die Wirkung dieser Peptide auf die Phasenzusammensetzung von Calciumcarbonat konnte über verschiedene experimentelle Phasen nachgewiesen werden. Diese neu identifizierten Peptide ergänzen bereits bekannte Additivstrukturen und ermöglichen zukünftige Experimente, um einen tieferen Einblick in die Kristallisations- und Polymorphkontrolle von Calciumcarbonat zu gewinnen.

List of Abbreviations

A	adenine
abs.	*absolute*
ACC	Amorphous calcium carbonate
Ac_2O	Acetic anhydride
BCM	*Biologically Controlled Mineralisation*
BLAST	*Basic Local Alignment Search Tool*
BLASTp	*Protein-Protein Basic Local Alignment Search Tool*
BIM	*Biologically Induced Mineralisation*
Boc	tert-butoxycarbonyle protective-group
C	cytosine
Cbz	carboxybenzyl protective-group
CLSM	*Confocal Laser Scanning Microscope/-y*
COSY	*Correlation spectroscopy*
d	doublet
DCC	*N,N`*-Diclyclohexylcarbodiimide
dd	doublet of doublet
ddd	doublet of doublet of doublet
D*i*PEA	*N,N*-di*iso*propylethylamine
DMF	*N,N*-dimethylformamide
DMSO	Dimethyl sulfoxide
DMSO-d_6	Deuterated dimethyl sulfoxide
DNA	Deoxyribonucleic Acid
EDTA	Ethylenediaminetetraacetic Acid
eq.	Equivalent
ESI-MS	Electrospray ionization mass spectrometry
EtOH	Ethanol
Fmoc	9-(9*H*-Fluorenyl)-methoxycarbonyle
G	guanine
h	hour
HATU	*O*-(7-Azabenzotriazol-1-yl)-*N*,*N*,*N*′,*N*′-tetramethyluronium hexafluorophosphate
HBTU	*O*-(7-Benzotriazol-1-yl)-*N*,*N*,*N*′,*N*′-tetramethyluronium hexafluorphosphate
HCA	Carbonated hydroxyapatite
HOAt	1-Hydroxy-7-azabenzotriazole
HOBt	1-Hydroxy-7-benzotriazole
HMBC	*Heteronuclear multiple-bond correlation spectroscopy*
HPLC	*High-performance liquid chromatography*

HRESI-MS	*High resolution electrospray mass spectrometry*
HSQC	*Heteronuclear single-quantum correlation spectroscopy*
IPTG	Isopropyl-*β-D*--thiogalactopyranoside
LB	Lysogeny-/Luria-Broth
m	multiplet
MeCN	Acetonitrile
MeOH	Methanol
MHC	Monohydrocalcite
min	Minute
MSA	*Multiple Sequence Alignment*
m-RNA	Messenger-Ribonucleic Acid
NaAc	Sodium Acetate
*N*MM	*N*-methylmorpholine
*N*MP	*N*-methyl-2-pyrrolidone
NMR	*Nuclear magnetic resonance*
p.a.	*pro analysis*
Pbf	2,2,4,6,7-Pentamethyldihydrobenzofuran-5-sulfonyl
PEG	Polyethylene Glycol
pfu	Plaque Forming Unit
pq	pseudo quartet
ps	pseudo singlet
psext	pseudo sextet
pt	pseudo triplet
PXRD	*X-Ray Powder Diffraction*
q	quartet
R_f	Retention factor
RNA	Ribonucleic Acid
RP-HPLC	*Reversed phase High-Performance Liquid Chromatography*
rpm	Round Per Minute
s	singlet
SEM	*Scanning Electron Microscope/y*
ssDNA	single-stranded Deoxyribonucleic Acid
t	triplet
T	thymine
TBS	TRIS-buffered saline
TBS-T	TRIS-buffered saline + Tween®20
*t*Bu	*tert*-butyl
TE	TRIS/EDTA-buffer
TEM	*Transmission Electron Microscope/y*

Tet	Tetracycline
TFA	Trifluoroacetic acid
THF	Tetrahydrofuran
TIS	Triisopropylsilane
TLC	*Thin layer chromatography*
TOCSY	*Total correlation spectroscopy*
t_r	*retention time*
TRIS	tris-(hydroxymethyl) amino methane
Trt	Trityle
UV	Ultraviolet
vis	visible
X-gal	5-Bromo-4-chloro-3-indolyl-*β-D*-galactopyranoside

Abbreviations of Amino Acids

Three-Letter Code	One-Letter Code	Full Name
Ala	A	Alanine
Arg	R	Arginine
Asn	N	Asparagine
Asp	D	Aspartic acid
Cys	C	Cysteine
Gln	Q	Glutamine
Glp		Pyroglutamic acid
Glu	E	Glutamic acid
Gly	G	Glycine
His	H	Histidine
Ile	I	Isoleucine
Leu	L	Leucine
Lys	K	Lysine
Met	M	Methionine
Phe	F	Phenylalanine
Pro	P	Proline
Ser	S	Serine
Thr	T	Threonine
Trp	W	Tryptophan
Tyr	Y	Tyrosine
Val	V	Valine

Table of Content

I.

Theoretical Section

& Motivation

1.
Biomineralisation

During the course of evolution, biological organisms have developed and mastered several intriguing abilities, such as the photosynthesis, the enzymatic catalysis in general or the formation of minerals in mineralised tissues. For all processes, which form these biogenic minerals, the term *biomineralisation* has been coined. [1, 2] The biominerals precipitated during these processes, include at least 60 different mineral phases. [1, 3, 4] The most prominent examples are the calcium carbonate polymorphs aragonite and calcite, the calcium phosphate hydroxyapatite ($Ca_{10}(OH)_2(PO_4)_6$) and its carbonated derivative dahlite, amorphous silica ($SiO_2 \cdot nH_2O$) and iron oxides such as magnetite (Fe_3O_4). Furthermore, biominerals include other carbonate and phosphate minerals, metal oxides as well as sulphates, sulphides and “organic minerals” such as citrates and oxalates. [3]

Biomineralisation processes can be divided into two distinct cases, the *Biologically Induced Mineralisation* (*BIM*) [1, 5] and the *Biologically Controlled Mineralisation* (*BCM*) [1, 6]. The term *Biologically Induced Mineralisation* describes the formation of minerals by sheer presence of organisms. For instance, the mineralisation can be a consequence of metabolic activity or the presentation of charged surface structures. Biominerals formed in this manner are nearly indistinguishable from their geological analogue and are a product of both, the respective organism and its chemical surroundings.[1] Such biominerals can be beneficial for the organism, though this is not a necessity. Calcareous stromatolites [7] or manganese nodules [8, 9] are good examples for *Biologically Induced Mineralisation*.

The counterpart of *Biologically Induced Mineralisation* is the *Biologically Controlled Mineralisation*. Here, many biominerals can be found that are commonly associated with the term *Biomineralisation*, e.g. the bones and teeth in vertebrates or the magnetite nanoparticles in some magnetotactic bacteria. [1, 10, 11, 12, 13, 14] In *BCM*, the formation of minerals and mineralised tissues depends solely on the organism(s) and not on the surrounding environment. Organisms with the ability to control mineralisation processes possess specialised mechanisms to achieve this

control. Moreover, the precipitated minerals possess an intended functionality, which is beneficial to the organism. This is reflected in the properties that strongly differentiates these biominerals from their mineralogical analogues.[1] The control exerted by organisms starts at the nanoscale, as can be observed with the magnetite nanoparticles found in the magnetosomes of magnetotactic bacteria (Fig. 1a). [10, 11, 12, 13]

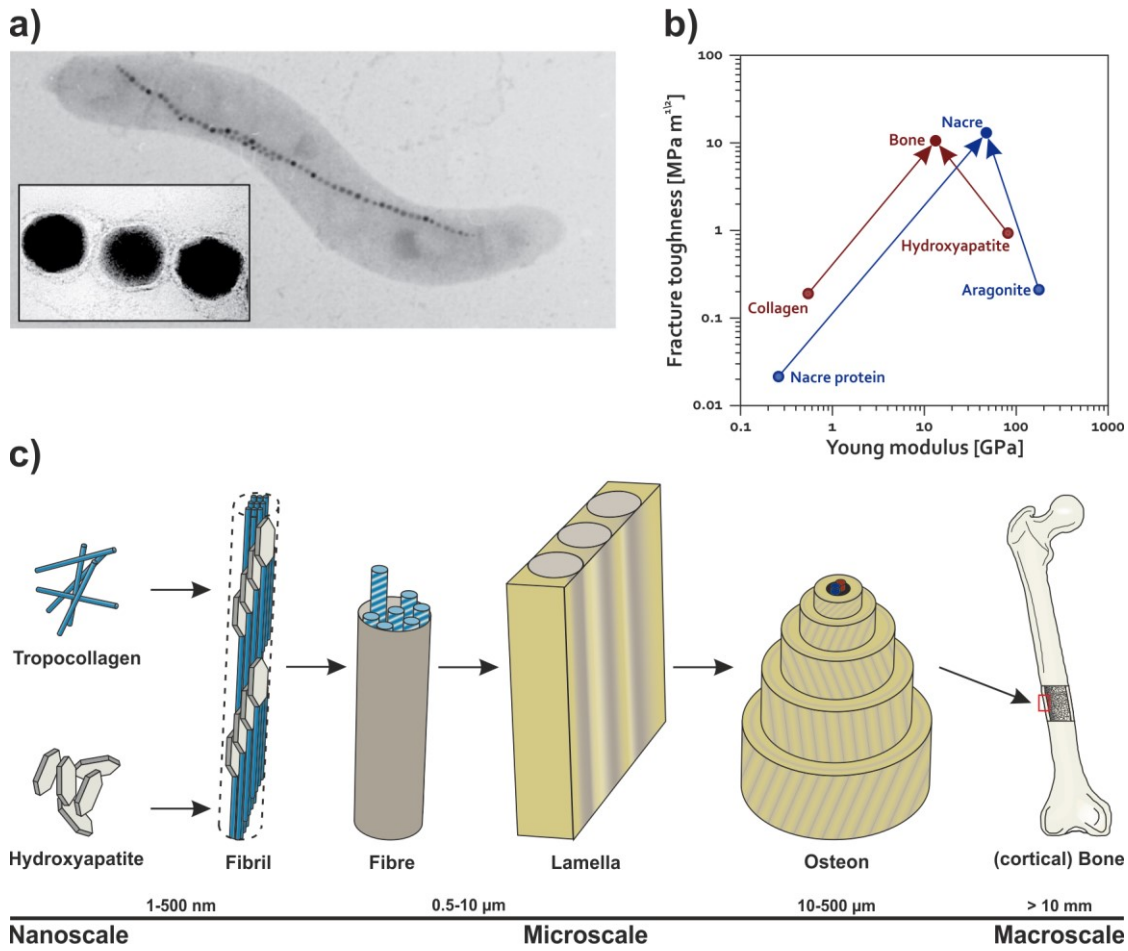

Figure 1a) Electron microscopic image of the magnetotactic bacterium *Magnetospirillum gryphiswaldense* with linearly arranged magnetite nanoparticles. Insert: Magnification of the magnetite nanoparticles. No scale-bar available. Adapted from *C. Jogler et al*. (**2009**), [15] Copyright © 2009, *Annual Reviews*. **b)** Plot of the fracture toughness as a function of the Young`s modulus. Depicted are the increased fracture toughnesses of the biocomposites Bone and Nacre, in comparison to the corresponding constituents (i.e. collagen and hydroxyapatite as well as nacre protein and aragonite). [16] **c)** Simplified scheme of the hierarchical composite structure of secondary, cortical bone. At the nanoscale the fundamental components collagen and hydroxyapatite form mineralised fibrils, which in turn are ordered into fibres. The fibres are arranged into lamellae that are cylindrically arrayed around blood vessels forming osteons, the functional subunits of cortical bone. [17, 18, 19]

Since the size of the magnetite nanoparticles is below the size of a *Weiss*-domain, they represent single domain magnets. This enables the bacteria to orient alongside the gradient of Earth`s magnetic field in sediments and water, which in turn assists the bacteria to navigate toward zones of altitude with optimal growth

conditions. * [1, 13, 14] Another intriguing example for *BCM* are the bones in vertebrates (subphylum *Craniata*). At a closer examination, bones are not simple mineral blocks, but instead are hierarchically ordered composite structures, composed of an organic matrix (~25%) and a mineral phase (~65%). ** [20, 21] This organic matrix consists of about 85-90% of collagen I, organised into fibrils. [1, 21] These fibrils are interspersed by a calcium phosphate mineral, a carbonated, non-stoichiometric hydroxyapatite termed dahlite, which can contain further foreign ions (Mg^{2+}, Na^{+}, F^{-},…). [20] This biogenic hydroxyapatite is crystallised in form of plate-like nanoparticles [22, 23] (30-50·15-30·2-10 nm [24] up to 200·30·10 nm [25]) ***. Inside the fibril, these nano-plates are aligned alongside the collagen-fibrils with their c-axes roughly parallel. The mineral-containing fibrils represent the fundamental composite-subunit, which in turn forms bone over several hierarchical levels (Fig. 1c). [1, 22, 26] Hence, bone is a nanoscopical composite that is organised up to the centimetre or metre scale, depending on species and bone type. The hierarchical structure in turn leads to improved mechanical properties, for example the fracture toughness. In cortical bone the fracture toughness (6-12 $MPam^{1/2}$) is by roughly one order of magnitude higher than the fracture toughness of the pure hydroxyapatite (~1 $MPam^{1/2}$) (Fig. 1b). [27]

In this manner, the magnetosomes of magnetotactical bacteria and the bones of vertebrates exemplify the range of control and influence; which *BCM*-enabled organisms can exert. These levels of control and influence encompass the spatial, the structural/morphological and the chemical range. [6] To achieve this level of control, an organism have to set up a corresponding mother liquor with a supersaturation towards the constituents of the respective mineral. The delineation of a crystallisation space is the first step. Such crystallisation volumes can be delineated by (cell-) membranes (i.e. in between groups of tightly bound cells or in vesicels), by insoluble polymers that form organic frameworks (i.e. proteins, polysaccharides) or by combinations of both. [1] The next step is controlling the concentration of the mineral constituent(s) inside the delineated crystallisation

*: Optimal growth conditions are depending on the specific species. Nevertheless, most magnetotatical bacteria can be found in the height of the Anoxic-Oxic-Interface and below. [13]

**: The remaining 10% are water. [20]

***: The dimensions depend on the method of determination, the bone type and the species. [25]

space, for example by active, ion-selective pumps or passive channels and similar cellular machineries.[1] Both, the space delineation and the controlled constituent concentration(s), are fundamental for the determination of the supersaturation and hence for the subsequent nucleation and crystal growth events. Moreover, both strongly predefine the aforementioned spatial and chemical range. Meanwhile, the structural/morphological range is mainly controlled by so-called additives.[1] During crystallisation, these additives are able to influence the two fundamental processes of crystallisation, i.e. nucleation and crystal growth.[1] Such additives are not defined by a common chemical nature, but by the general influence on the crystallisation of a solid. This group encompasses ions, small molecules and macromolecules.[1, 28, 29] Especially proteins and post-translationally modified proteins present a major group of additives in virtually all biomineralising organisms. In their role as additives, these proteins are thought to interact with the surfaces of growing crystallites and nascent nuclei. By this interaction, these protein additives can modify the stability of certain facets on developing crystallites or nascent nuclei. This can lead to altered growth velocities of the corresponding facets, which subsequently influences the developing crystallite morphology. Meanwhile, an interaction with nascent nuclei can lead to the stabilisation of supersaturated solutions and/or to the preference of nuclei that belong to a specific phase. Additives can also be bound to solid surfaces, such as cell membranes or organic matrices. In this way, they can form nucleation sites which allow the crystallisation to take place *via* heterogeneous nucleation.[1, 30, 31, 32]

A unique exception among these (protein) additives are the silicateins, especially the silicatein-α.[33, 34, 35] This protein can be found in marine sponges (phylum *Porifera*), more precisely in the classes *Demospongiae* and *Hexactinellida*.[36] The protein is located in close association with the siliceous spiculi, which these animals form (Fig. 2b). The formation of such spiculi was studied, among others, using the demosponge *Suberites domuncula* (Fig. 2a). Here, the formation starts intracellularly with the formation of an axial filament that consists of silicatein-α as the major constituent as well as silicatein-β and presumably silintaphin-1.[37, 38, 39] These axial filaments in turn become covered in amorphous silica ($SiO_2 \bullet nH_2O$). Subsequently, silicatein-α is deposited on the outside of the spicula in a later,

extracellular stage. Since these become covered again by more amorphous silica, the spiculi grow appositionally in alternating lamellae of silica and silicatein-α. * [35]

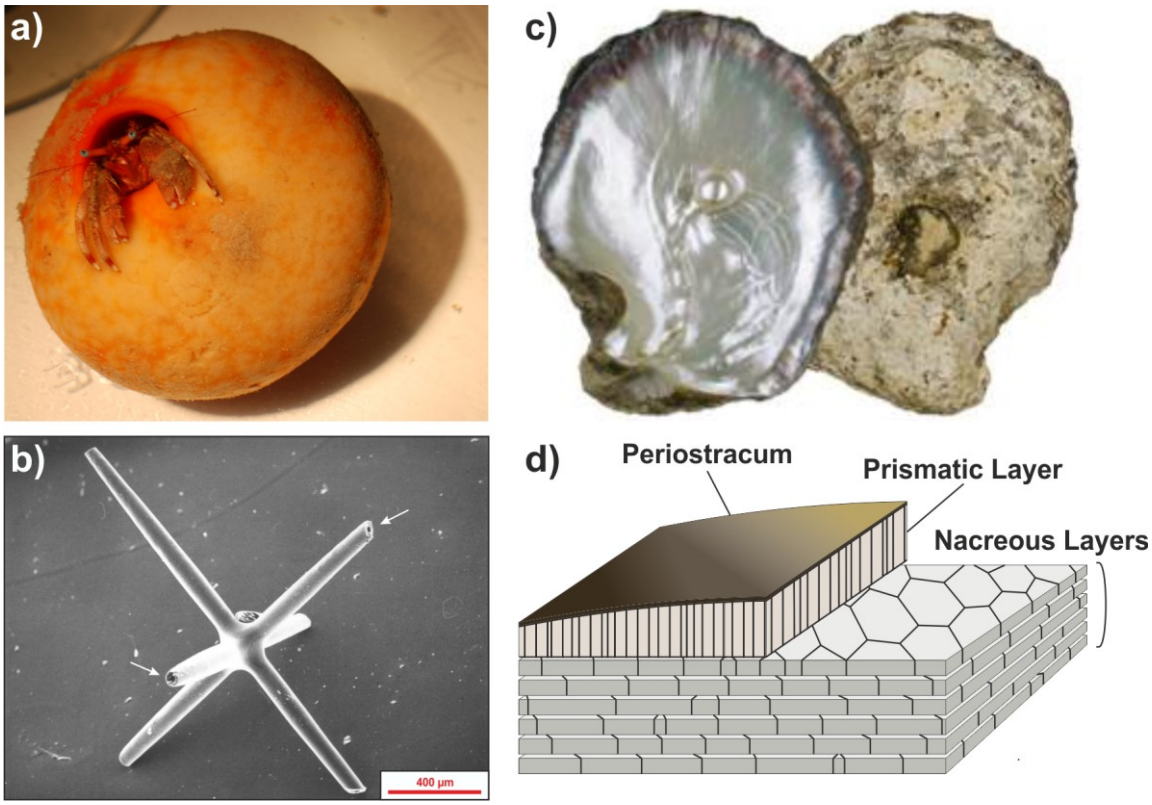

Figure 2a) Image of the demosponge *Suberites domuncula* symbiotically inhabited by a hermit crab (Reproduction of "*The sponge Suberites domuncula with Pagurus sp.*" under terms of CC BY-SA 3.0. Copyright © 2011, *Harald Berger*. https://de.wikipedia.org/wiki/Datei:Suberites_domuncula20110720.jpg, 20.02.2018). **b)** Electron-miscroscopical image of a sponge spicule, here a tetraxonal megasclere. The axial canals are visible, in which the silicatein α-containing axial filaments are located (marked by white arrows). (Adapted from "*Sponge spicule*" under terms of CC BY 3.0. Original scale bar has been removed and replaced. Copyright © 2013, *Hannes Grobe*. https://de.wikipedia.org/wiki/Datei:Sponge-spicule_gh.jpg, 20.02.2018. **c)** Image of shell and a pearl of the bivalve *Pinctada margaritifera.* The inner, nacreous layer and the exterior of the shell are depicted. (Adapted from "*Pinctada margaritifera – Two views of the same specimen*" under terms of CC By-SA 4.0. Black background has been removed. Copyright © 2013, *Didier Descouens* (*MHNT*, *Toulouse*, France), https://en.wikipedia.org/File:Pinctada_margaritifera_MHNT.CON.2002.893.jpg, 20.02.2018). **d)** Simplified, schematic cross section of a nacreous bivalve shell, depicting an outer, organic layer (periostracum), a prismatic layer and an inner, nacreous layer. Apart from the organic *β*-chitin (not shown), the nacreous layer consist of aragonite. The prismatic layer can consist of aragonite or calcite. Depending on the species, genus, family,… etc., the building plan can strongly deviate from this scheme. [1, 40, 41, 42]

Hence, silicatein-α templates the deposition during the formation of the spiculi [39], which in turn implies that it is an additive. Yet, the ability to direct the deposition of amorphous silica is already known from the silafins in diatoms. [43] The property that makes silicatein-α stand out from similar proteins is its additional ability to catalyse the polycondensation reaction of silicic acid ($Si(OH)_4$). [34, 35, 44] Otherwise, the polycondensation would be relatively slow at ambient temperature and

*: The lamellae are not visible in demosponges, as they fuse together in a process termed biosintering. Here, only a compact rod can be observed. [326, 327]

physiological pH.[45] The ability to catalyse the formation of biominerals thereby complements the well known action of peptides as additives.

Another intriguing phenomenon among the known biominerals is polymorph control. This is especially obvious in the nacreous shells of some gastropods and bivalves (Fig. 2c).[1, 46, 47, 48] Such nacreous shells are made up of alternating layers of aragonite (95 wt%) and organic, interlamellar matrix sheets (5 wt%), which itself consist of *β*-chitin sandwiched by silk fibroin-like proteins.[1, 42, 46] Similar to bone, this architecture yields superior mechanical properties in comparison to the single constituents (Fig. 1b).[16] However, the blueprint of a mollusc`s shell and consequently the presence of such nacreous layers depends on the specific species. Hence, shells can consists of several different layers, including a nacreous layer. Common examples for nacreous shells are the bivalve genus *Pinctada*[49], the gastropod *Haliotis rufescens* as well as some other members of the genus *Haliotis*[50, 51]. In these animals, the nacreous layers are terminated towards the outer side of the shell by a prismatic layer of calcite crystallites (Fig. 2d). This is intriguing, as this means a thermodynamically stable and a thermodynamically labile polymorph coexist in direct adjacency, separated only by very narrow sheets of organic compounds. This intriguing level of polymorph control is thought to be exhibited by acidic proteins with a high aspartate-content, colloquially termed Asp-rich proteins.[*] These were found in close association to the mineral phase and *in vitro* experiments showed their polymorph-selective capabilities.[30, 52, 53, 54, 55] The proteins are thought to be coated onto the sheets of *β*-chitin as well as to be present in the gel of the silk fibroin-like proteins between the *β*-chitin sheets.[1, 47, 56] In this manner, they are thought to act as both, nucleation sites in a heterogeneous nucleation path and as modifiers of crystal growth.[30, 53, 54] Though the influences of some of these proteinaceous additives have been understood, the interplay between these proteins, the proteins and the organic matrix as well as the proteins and the mineral phase still remains poorly understood.[57]

*: Meanwhile many more proteins have been isolated in association to such mineral phases. However, these possess a more varied amino acid composition.[46]

The properties of such biominerals are in many different aspects superior to their mineralogical and synthetical counterparts, which in turn have inspired many materials scientists to adopt the already gained knowledge for new biomimetic experimental approaches. Since the polymorph of a crystalline compound strongly determines the physical properties in biominerals and synthetic materials, polymorph control has been and is still in the focus of such biomimetic approaches. In this experimental context, calcium carbonate has often been applied as a model system, not only because it is a widespread biomineral but also because it is known to form several polymorphs [58]. For this purpose, different methods [59, 60, 61, 62, 63, 64] for the precipitation of calcium carbonate have been developed, which in turn have been utilised to test additive candidates as both, soluble growth modifiers and/or insoluble nucleators. [65, 66, 67, 68, 69] Here, the influence of a large number of different small molecules (e.g. amino acids, amphiphilic molecules [70, 71]) and polymers on the polymorph composition of calcium carbonate have been investigated. [69] Especially the above mentioned acidic Asp-rich proteins and their effect on the polymorph composition have been an inspiration to materials scientists. In efforts to mimic their effect, a number of small organic acids, [72] acidic poly- and oligopeptides, [73] polycarboxylates, [74, 75] (poly)phosphates [76] and other anionic molecules have been successfully tested, which implies a structure-activity relationship between these anionic additives and calcium carbonate. Still, the choice of these additives is, apart from the charge, a crude approximation. The phage display technique could represent a more selective approach to identify additives. This method has been used in the affinity-selection of peptides on a variety of targets, for example on nanoparticles. In the Tremel group, this experimental concept has been successfully transferred to the vaterite polymorph of calcium carbonate. The peptides identified in this study strongly influenced the polymorph composition in crystallisations of calcium carbonate. [77, 78] However, the polymorphs calcite and aragonite were not tested.

2.

Crystallisation Processes and the Influence of Additives

The following publications have been used as basis for this chapter: *Mullin* [28], *Sangwal* [29], *Loges* [79] and *Dietzsch* [80]. They will not be cited during the following chapter.

Crystallisation from solution implies the formation of a crystalline phase from homogeneous solutions, which lead to the development of corresponding, heterogeneous two-phase-systems with a defined interface. Such a process can only occur spontaneously, if the free enthalpy of the two-phase-system is lower than the free enthalpy of the initial solution phase

$$G_{(2-phase)} < G_{(1-phase)}. \quad (1)$$

As soon as this requirement is met, the solution becomes thermodynamically unstable with respect to the crystallisation of a solid phase. As a direct consequence, the solution is supersaturated with respect to the solute and a crystallisation can take place. For an alternative description, the law of mass action can be applied. This and the following equations will be exemplified for an ionic, binary compound. It can be written as

$$\mathrm{A}_{(solv.)}{}^{+} + \mathrm{B}_{(solv.)}{}^{-} \leftrightharpoons \mathrm{AB}\downarrow \quad (2)$$

and

$$K_{SP} = \frac{a_{A^+} \cdot a_{B^-}}{a_{AB}} \cong a_{A^+} \cdot a_{B^-}. \quad (3)$$

In this manner, a solubility product K_{SP} can be defined. As soon as the activity product * $a_{A^+} \cdot a_{B^-}$ exceeds this solubility product, the system becomes supersaturated towards the solutes, leading to the onset of a crystallisation. This expression can be further simplified by the introduction of the supersaturation

*: In diluted solutions, the concentrations can be used instead of the activity.

(4) $$S = \frac{a}{a_e}.$$

Here, a_e is the equilibrium activity of the solute, which can be substituted with the solubility product

(5) $$S = \frac{a_{A^+} \cdot a_{B^-}}{K_{SP}}.$$

The supersaturation has the advantage that its values are smaller and easier to interpret in comparison to the solubility product. In addition, it is an expression for the thermodynamical stability of a solution. In case the expression exceeds the value of one, the solution becomes thermodynamically labile and crystallisation can take place. Though this condition is met, crystallisation often does not occur, rendering the respective solutions metastable. For the description of this behaviour, a kinetic perspective is needed.

From the kinetic point of view, a crystallisation can be divided into two steps. The first step is the nucleation, which describes how a metastable, supersaturated solution starts to develop into a stable, two-phase system *via* the formation of crystalline nuclei. Separated from this nucleation step, a newly generated, stable nucleus will subsequently develop into a crystal by the addition of the solute. This second step is simply termed crystal growth. Though both processes are connected, they will be covered separately to simplify the discussion. Furthermore, the influence of additives during a crystallisation is reported to be a kinetical one as well. [28, 29] As this influence originates during nucleation and crystal growth, it will be discussed in the respective section.

Classical Nucleation Theory

As stated above, solutions become labile when the supersaturation S of a solute exceeds the value one. Hence, a crystallisation can take place, which means that a solid phase has to form from a homogeneous solution. This inevitably leads to the formation of an interface between the two phases and a corresponding increase in surface free enthalpy ΔG_S. On the other hand, the generation of the solid phase leads to a gain in the volume free enthalpy ΔG_V. Both considerations are the starting assumptions for the classical nucleation theory, in which the

increase of ΔG_S can be understood as an energy barrier for the formation of a stable nucleus. Hence, the overall change of free enthalpy can be expressed as

$$\Delta G = \Delta G_S + \Delta G_V. \quad (6)$$

Assuming a spherical nucleus, the term can be rewritten as

$$\Delta G = 4\pi r^2 \cdot \gamma + \frac{4\pi r^3}{3} \cdot \Delta G_v, \quad (7)$$

in which ΔG_v is the change in free energy per mol and γ is the respective interfacial energy. In this equation (7), it becomes apparent that as the radius r grows, it reaches a critical radius r_{crit} at which the volume term compensates the surface term (Fig. 3a). By setting the first derivative $\frac{d\Delta G}{dr}$ of equation (7) equal to zero, r_{crit} can be written as

$$r_{crit} = -\frac{2\gamma}{\Delta G_v}. \quad (8)$$

This term can be used to substitute r in equation (7) in order to express the activation energy ΔG^*

$$\Delta G^* = \frac{16\pi\gamma^3}{3\Delta G_v{}^2} = \frac{4}{3}\pi\gamma \cdot r_{crit}{}^2. \quad (9)$$

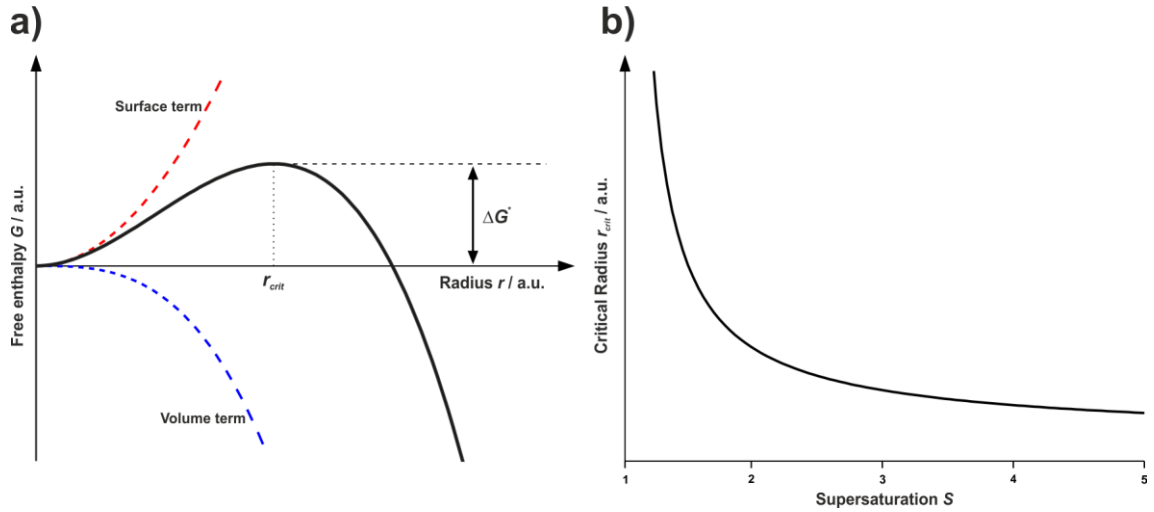

Figure 3a) Plot of the free enthalpy in dependence of the radius of a spherical nucleus. The individual contributions of the surface term and the volume term are shown. The critical radius r_{crit} is the radius, at which the volume term compensates the surface term, while ΔG^* represents the activation energy that has to be invested for the formation of a stable nucleus. **b)** Plot of the critical radius r_{crit} against the supersaturation S.

Meanwhile, the radius r is connected to the supersaturation S *via* the Gibbs-Thomson relation

$$\ln S = \frac{2\gamma V_m}{RTr}. \quad (10)$$

Here, V_m describes the molecular volume, R is the ideal gas constant and T is the thermodynamical temperature. As of this, the critical radius r_{crit} can be expressed as

$$r_{crit} = \frac{2\gamma V_m}{RT \ln S_{crit}} \quad (11)$$

and the activation energy ΔG^* as

$$\Delta G^* = \frac{16\pi}{3} \frac{\gamma^3 {V_m}^2}{(RT \ln S_{crit})^2}. \quad (12)$$

These equations show that the critical radius r_{crit} and the activation energy ΔG^* both decrease with increasing temperature T and increasing supersaturation S (Fig. 3b)*. The stable nucleus of the corresponding radius r_{crit} thereby incorporates many formula units of the solute. The formation of such a stable nucleus by the simultaneous collision of a corresponding amount of solute is extremely improbable. Instead, it can be expressed as the sequential addition of solute to a growing subcritical nucleus/cluster:

$$A + A \rightleftharpoons A_2$$
$$A_2 + A \rightleftharpoons A_3$$
$$\vdots$$
$$A_{n-1} + A \rightleftharpoons A_n \quad \text{(critical nucleus)}$$

Unfortunately, experimentally acquired data often strongly diverge from theoretical calculations that are derived from the classical nucleation theory. These differences between experiment and theory have been attributed to the assumption of a spherical nucleus and to the assumption that the interfacial energy γ of the nucleus is identical to the interfacial energy γ of the corresponding bulk material. Another aspect, the presence of impurities and respectively additives, is neglected in this theoretical approach. Additves are reported to influence the solubility of the solute and/or the interfacial energy between the nucleus and the solvent during a nucleation. [29] Still, from a mechanistic point of view, the classical nucleation theory

*: However, in reality this is more complicated, as the surface tension γ and the solubility product K_{SP} in the supersaturation S depend on the temperature as well.

and the corresponding separation of the free enthalpy into a volume and a surface dependent term yield a straightforward image of a nucleation process.

Another neglected effect in the classical nucleation theory is the interference of additional interfaces during crystallisation. Such interfaces are present in every crystallisation, e.g. the walls of a crystallisation vessel, the solution-air interface, etc. Adding a further interface to equation (6), the volume term should remain relatively unchanged, yet the surface term should be strongly altered. Here, the new interface gives rise to two additional interfacial energies, one between the nucleus and the interface and one between the solution and the interface (Fig. 4). Similar to the prior approach (equation (7)), a spherical nucleus is assumed and the additonal interface is approximated as a flat surface, though this nucleus is assumed to be cut in half by the additional interface (Fig. 4). In direct analogy to the equations (6) and (7), this can be expressed as

$$\Delta G = \underbrace{\frac{1}{2}\left(4\pi\gamma_{SN}r^2\right) + \pi\gamma_{IN}r^2 - \pi\gamma_{IS}r^2}_{\Delta G_S} + \underbrace{\frac{1}{2}\left(\frac{4\pi r^3}{3}\cdot\Delta G_v\right)}_{\Delta G_V}. \qquad (13)$$

$$\Delta G = \Delta G_S + \Delta G_V \qquad (6)$$

Here, the indices on the respective interfacial energies γ designate the corresponding interfaces (solution phase S, nucleus N and the new interface I) (Fig. 4)).

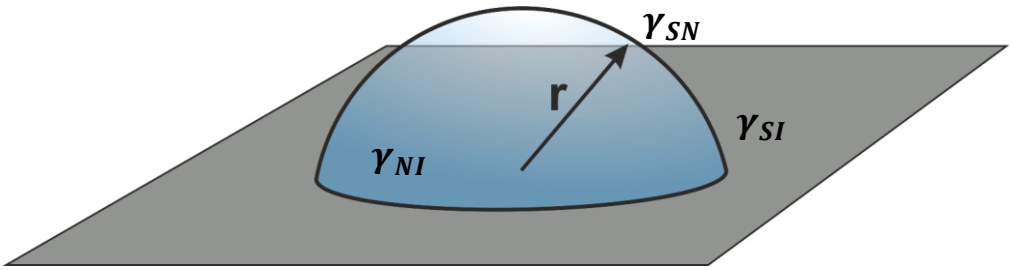

Figure 4) Schematic depiction of the heterogeneous nucleation on a flat surface. Here, γ refers to the corresponding interfacial energies between the solution phase S, the nucleus N and the interface I, while r is the radius of the forming nucleus.

In analogy to equation (8), a critical radius r_{crit} can be expressed by setting the first derivative $\frac{d\Delta G}{dr}$ of equation (13) equal zero

$$r_{crit} = -\frac{2\gamma'}{\Delta G_v} = \frac{2V_M\gamma'}{RT\ln S_{crit}}, \qquad (14)$$

in which the modified interfacial energy γ' is defined as

$$\gamma' = \gamma_{SN} \left(1 - \frac{(\gamma_{SI} - \gamma_{IN})}{2\gamma_{SN}} \right). \quad (15)$$

From this equation, it becomes apparent that the term in parentheses is less than one, if the interfacial energy γ_{IN} is smaller than the interfacial energy γ_{SI}. If this condition is fulfilled, the modified interfacial energy γ' becomes smaller than the interfacial energy γ_{SN}, which in turn implies that the critical radius r_{crit} of a nucleus on the additional interface is smaller than the critical radius r_{crit} during a homogeneous nucleation. As direct consequence of these conditions, a heterogeneous nucleation event is favoured and the critical supersaturation S_{crit}' is lower than the critical supersaturation S_{crit} of during homogeneous nucleation.

Concluding these considerations, the interfacial energies between a crystalline nucleus and a surface can be utilised to shift the nucleation from a homogeneous towards a heterogeneous mechanism and vice versa. During the crystallisation of an ionic crystal for instance, the heterogeneous nucleation on the surface of a glass vessel can be lowered by modifying the glass surface with a hydrophobic compound, as this modification should increase the interfacial energy γ_{IN}. In contrast, a decrease in interfacial energy γ_{IN} can be achieved by utilising surfaces, which possess a high crystal lattice match to the forming crystalline compound or which present an opposing surface charge. The modification of surfaces has been extensively applied to influence crystallisations towards the heterogeneous nucleation path, for instance during the crystallisation of calcium carbonate in the presence of self-assembled monolayers on gold [66, 67, 81, 82, 83] or beneath *Langmuir-Blodgett* films [84, 85, 86, 87]. For the latter two, the results strongly depend on the compounds, which are used to modify the corresponding surface, and hence the corresponding interfacial energy. These compounds can be regarded as surface-additives. In similar manner, organisms already apply such surface-additives to exert a strong control over the formation of biominerals at the nucleation step of a crystallisation process. [1, 29]

There are further models for the description of nucleation events, for example the spinodal decomposition, which are well described in the literature. [28, 29, 80] Meanwhile, after a nucleation event has occurred, a newly formed, stable nucleus is able to grow into a macroscopic crystallite. During this crystal growth, the morphology and the size of a crystallite are determined.

Crystal Growth

Crystal growth describes the microscopic processes, which occur after a first nucleation event has taken place and which result in the addition of the supersaturated solute to the surface of a stable nucleus. These processes will cause the nucleus to grow into a macroscopic crystallite. Furthermore, an overall crystallisation is exclusively governed by crystal growth, granted that the supersaturation S is above one, but below the critical supersaturation.

In the same manner as the nucleation, crystal growth is determined by the reduction of the free interfacial enthalpy. For single crystals, this free interfacial enthalpy ΔG_i can be expressed for each crystal morphology i as the sum of the interfacial energy γ_j of the individual crystal facets multiplied by the surface area of the corresponding facet A_j

$$\Delta G_i = \sum_j A_j \gamma_j . \tag{16}$$

Considering this equation, thermodynamic control should lead to the formation of the morphology, which displays the lowest interfacial free energy and which should be delimited by crystal facets with the lowest possible interfacial energy. In combination with the surface to volume relation, equation (16) implies that the formation of large crystallites is favoured over the formation of many small crystallites, assuming that the volume of the crystalline phase remains constant. This can either cause the formation of larger aggregates from smaller crystallites or the preferred growth of large crystallites, while the small crystallites dissolve simultaneously (*Ostwald* ripening).

Still, thermodynamically stable morphologies often do not form during crystallisation. This can be caused by a high supersaturation or the presence of additives, as in these cases kinetic control applies instead of thermodynamic control. Here, metastable crystal morphologies will form that are delimited by the slowest growing crystal facets (Fig. 5). Hence, influencing the growth kinetics of specific crystal facets can be achieved by altering the crystallisation conditions. In turn, this can be utilised to alter a crystal`s morphology. Nevertheless, for a further understanding of crystal growth processes a microscopic perspective is needed.

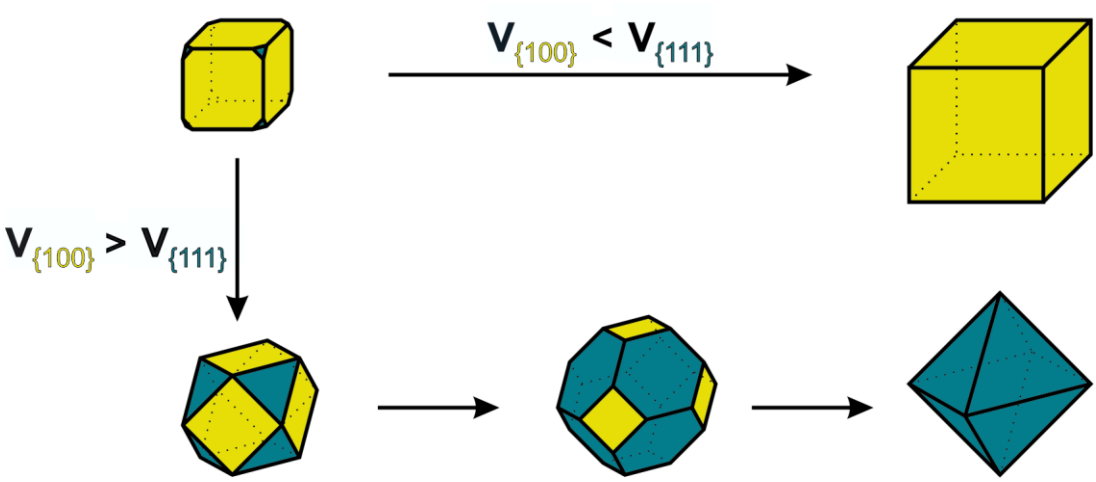

Figure 5) Depiction of the crystal growth of a crystal with a cubic elemental cell and the resulting crystal morphologies. The crystal in the upper left displays two types of different facets that either correspond to the {100} - or to the {111} crystallographic planes. In the case that the {100} planes are slower growing than the {111} planes, a cubic crystal will develop. Vice versa, if the {111} planes grow slower than the {100} planes, an octahedral crystal will form. If the growth rate of both plane types are relatively similar, both facets can develop at the same time, as in the depicted cuboctahedron (lower left).

An example for this microscopic perspective is given in Fig. 6. Here, crystal growth can be interpreted as the extraction of growth units (i.e. ions, molecules or atoms) from solution onto the surface of a growing crystal, followed by the adsorption on a flat surface terrace. This extraction/adsorption step is only the first step towards the incorporation of a growth unit into the crystal lattice. During the second step, the incorporation into the crystal lattice, the binding energy and the change in surface energy are important. The binding energy correlates with the number of attractive interactions during this incorporation, which in turn correlates with the number of nearest neighbours that a growth unit can attach to. Consequently, a growth unit prefers the incorporation at a position with a high number of nearest neighbours. At the same time, the combined surface energy of growth unit and crystal surface is reduced as the number of nearest neighbours is maximised. However, a crystal surface is not a flat plane, but instead displays a certain roughness, caused by the step edges of individual surface terraces growing upon another. Their presence gives rise to different adsorption and incorporation positions, the step edges themselves, kinks along the step edges and the flat surface terraces. Of these, each possesses an individual number of nearest neighbours, i.e. two, three and one, respectively (Fig. 6).

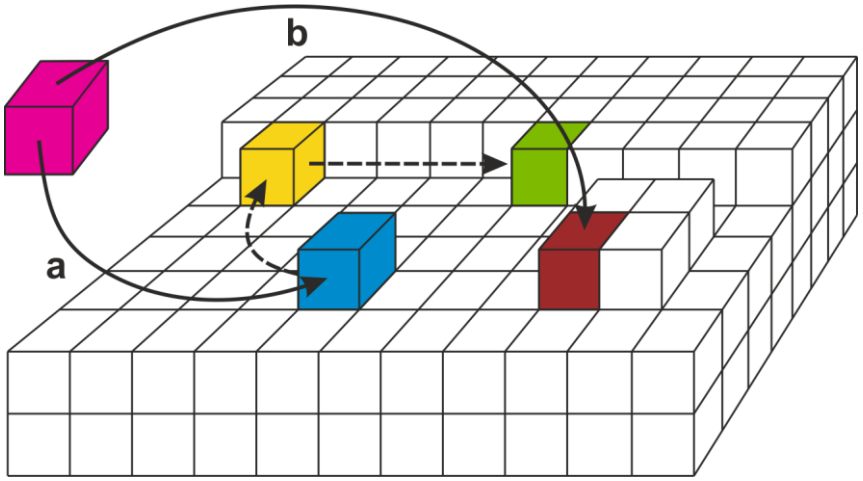

Figure 6) Depiction of crystal growth along a surface terrace. **a)** At low supersaturations, a solute **growth unit** becomes adsorbed to a **surface terrace**. The binding energy correlates with the number of nearest neighbours. A growth unit is likely to migrate over the surface terrace (1 neighbour) till it reaches a position at a **step edge** (2 neighbours). From there, it can migrate along the step ledge towards a **kink** (3 neighbours). At this positions, the growth unit can get incorporate into the crystal lattice the fastest, as here the binding energy is maximised and the surface energy is simultaneously minimised. **b)** At higher supersaturations, **growth units** can form **islands** on a flat terrace *via* heterogeneous nucleation, which can in turn act as the start of new growths steps.

Accordingly, the kink positions are the preferred site for the incorporation of a growth unit, while the relevance of the step ledges is only minor. Therefore, a growth unit, after a first adsorption onto a surface terrace, will preferably migrate towards a kink, where it can get incorporated into the crystal lattice the fastest.

However, the number of step edges and consequently of kinks is limited. During a crystallisation growth units are added to a step edge, which in turn causes the step edge to advance and to close the gap onto the underlying one. In this manner, an array of steps can become finished, simultaneously yielding a new surface terrace. At the same time, the number of kinks and step edges becomes depleted during a crystallisation, which would lead to a drastic decrease of the crystal growth rate, as only the disfavored incorporation on surface terraces would remain possible. This does not occur at high supersaturations, as at these conditions the growth units can form new “islands” that in turn function as the starting points of new step edges (Fig. 6). This process, also termed 2D nucleation, can be considered analogous to the heterogenous nucleation. For this island formation an equivalent expression to equation (14) is accessible, from which a critical radius and a corresponding critical supersaturation can be derived. Thus, crystal growth would be possible at high supersaturations, but at supersaturations below this critical supersaturation of a 2D nucleation, crystal growth should decrease as the kinks and step ledges become depleted. However, this is not the case, as screw dislocations, a specific type of

crystal defect, are omnipresent. Such screw dislocations can act as continuous sources of step edges and kinks, leading to spiral growth on the surface terrace (Fig. 7).

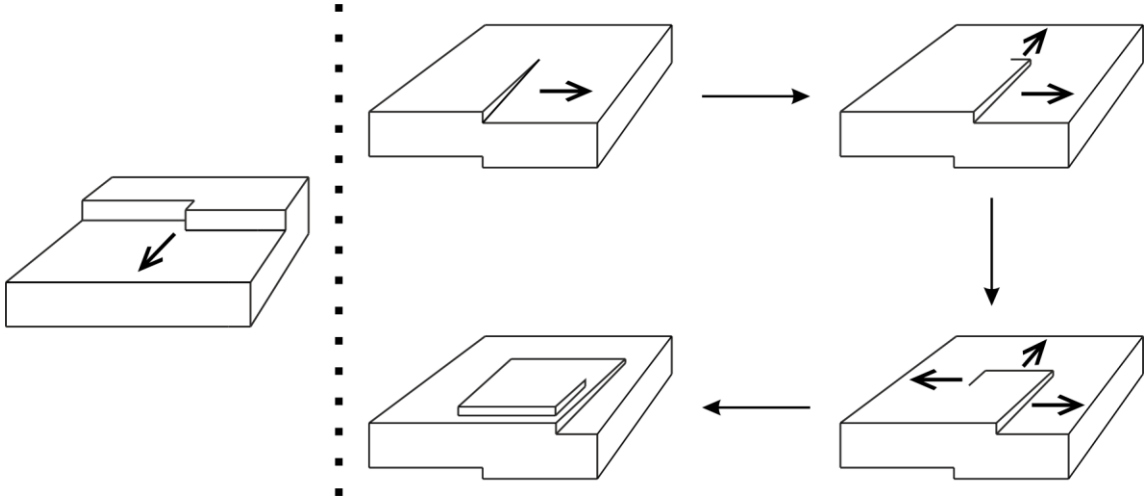

Figure 7) Depiction of the lateral growth by the advancement of a step edge (**left**) and the spiral growth induced by a screw dislocation (**right**). In the latter case, the screw dislocation acts as a continuous source of step edges. Arrows indicate the direction in which the step edges advance.

In summary, crystal growth can take place at low and high supersaturations. In both cases, this primarily happens by the addition of growth units to the kink positions on a crystal surface. Meanwhile, the source of new step edges and kinks differs. At all supersaturations, screw dislocations, a specific type of crystal defect, are present that act as continues source of steps. However, at high supersaturations, new steps are mostly generated *via* the island formation on surface terraces (2D nucleation).

Up to this point, the microscopic perspective of crystal growth has been discussed in the absence of additives. As stated above, the influence of additives results in the kinetic control of the crystal growth. Consequently, additives change the activation energy that has to be exceeded during the addition of a growth unit to a crystal. Such an influence requires a prior adsorption of an additive onto a crystal surface. Based on this, several mechanisms have been proposed. [88] For inhibitory additives, two models have been described that explain their respective influences by a prior distinction between surface mobilities. An immobile growth inhibitor will strongly adsorb to a surface terrace. This, in turn, can cause a decrease in the growth rate of a step edge, as the step edge advances between two close absorbed inhibitor units. Moreover, the step edges become curved (Fig. 8). If the surface density of the immobile inhibitor on a surface terrace is of an order that the distance

between individual additive units is below the critical radius of the 2D-nucleation, the advance of the step edges becomes pinned.[89, 90] Thus, an immobile inhibitor can halt the crystal growth by this pinning-mechanism entirely and crystal growth can only proceed further at higher supersaturation (Fig. 8).

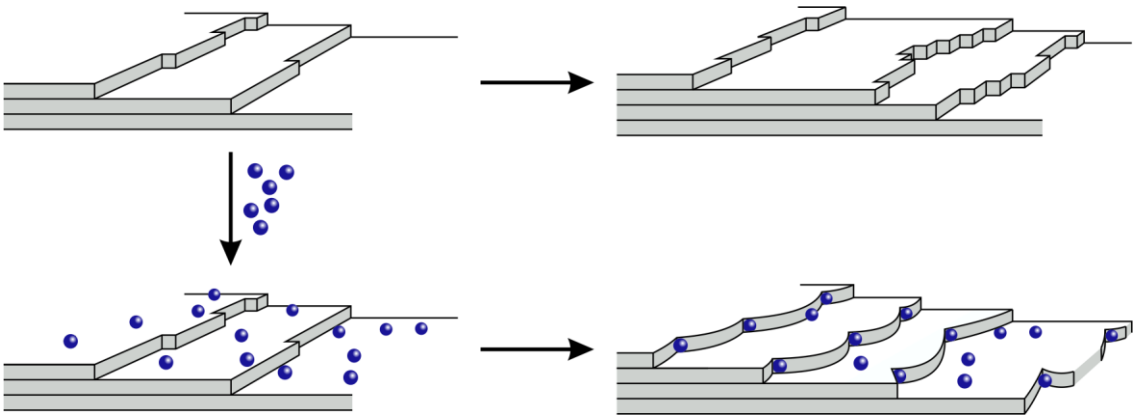

Figure 8) Comparison of crystal growth in absence and presence of an **immobilised, inhibiting additive**. In the absence of said additive the crystal growth proceeds normally (**Upper row**). In contrast, the addition of the **additive** slows the crystal growth and forces the step ledges to become curved, as they advance between two adsorbed additive units (**lower row**). If the distance between two additives is smaller than the critical radius of a 2D nucleus, crystal growth is halted completely. Inspired by *Sangwal*[29].

On the other hand, if an inhibitor remains mobile on the surface after its adsorption, it can compete with the incorporation of growth units. A competition between additive and growth units is especially effective, if the inhibitor prefers the kink positions over the step ledges. Nevertheless, a mobile inhibitor can only retard the advance of a step edge, a complete halt is not possible.[91, 90] Meanwhile, the adsorption of an additive on a surface terrace has been reported to promote crystal growth as well. This growth promoting influence has been explained by the additive lowering the interfacial energy.[88, 90] This would apply to the situation of an adsorbed, growth promoting additive that acts as the start of a new step ledge.

To conclude the microscopic considerations on additives, the discussed growth inhibiting and promoting influences of additives are translated to the macroscopic view. Here, crystals can be delimited by several crystal facets that are based on the corresponding crystallographic planes. A crystallisation of such a crystal in the presence of an inhibitory additive that indiscriminately adsorbs on all the different crystal facets would yield a slower overall crystal growth without changing the crystal morphology. Meanwhile, the situation would change drastically, if the same inhibitor adsorbs preferentially on one of the crystal facets. In this case, the growth of this facet would be slower than the growth of the remaining facets, which in turn

would result in the formation of metastable crystal morphologies (Fig. 5). It is possible to transfer this concept to the polymorph-selective additives that have been described in the prior chapter as well. Polymorphs possess individual crystal structures and thus their crystal facets are intrinsically different. Hence, the presence of a face-selective, growth-inhibiting additive could cause a polymorph-selection during the crystallisation, in case the crystallising compound can form different polymorphs. In case this additive face-selectively adsorbs to a facet of the thermodynamically stable polymorph, a thermodynamically metastable polymorph would crystallise preferentially, as the growth of the thermodynamically stable polymorph would be retarded.

In the beginning of these considerations on crystal growth, it was decided to examine crystal growth in the absence of homogeneous nucleation events. Nevertheless, crystal growth can only occur after a first nucleation event has taken place. Still, a first nucleation event does not neccesarily decrease the present supersaturation below the critical supersaturation that is required for a homogeneous nucleation. Subsequently, nucleation and crystal growth can occur simultaneously, while the supersaturation remains above the critical supersaturation. A good description of this situation can be given by a *LaMer*-curve [92] (Fig. 9), in which the supersaturation is plotted against the reaction time. Here, stage II respresents the period, in which nucleation and crystal growth take place at the same time. In the following interval of this stage, nucleation and crystal growth cause a drop in supersaturation. As the supersaturation decreases below the critical value, only crystal growth persists until the solution is in equilibrium (stage III). Nucleation and crystal growth are connected processes that represent the basis for crystallisations. Furthermore, the possible influence of additives that can emerge during crystal growth and nucleation have been shown in the respective sections as well. Additionally, the possibility of a polymorph selection by an additive has been exemplified for an inhibiting additive. Meanwhile, additives are not restricted to just one mechanism but can display more of the above described mechanisms. For example an Asp-rich protein, isolated from the nacreous shells of the bivalve *Mytilus californianus*, has been reported to act as both, a surface-additive and as soluble growth inhibitor during the crystallisation of calcium carbonate.

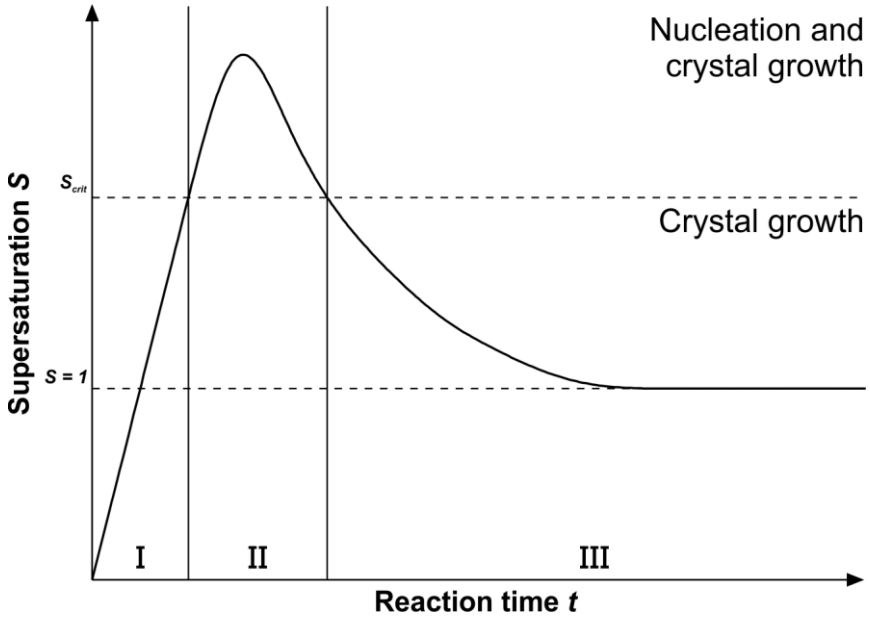

Figure 9) Plot of the supersaturation S against the reaction time t during a crystallisation in accordance to *LaMer et al.* [92]. Here, three different phases are distinguishable. In the **I** phase, the supersaturation* is below critical supersaturation S_{crit} and increases over time. In the **II** phase, the supersaturation has exceeded the critical supersaturation S_{crit} and nuclei can form, which subsequently grow. The supersaturation increases further unitl the rate of nucleation and crystal growth are equal to the increase and decreases afterwards. A crystallisation reaches the **III** phase, when the supersaturation drops below the critical supersaturation S_{crit}. Here, only crystal growth can take place until the supersaturation becomes constant at the equilibrium value ($S = 1$).

The former resulted in the nucleation of calcite crystallites, while the latter inhibited the formation of calcite. Its influence during the crystallisation of calcium carbonate indicates that this protein is presumed to be involved in the polymorph-selective formation of the nacreous shell, however no exact mechanism was reported. [30] Additionally, calcium carbonate is a very common biomineral and many organisms are known to discriminate between its polymorphs. These facts make the precipitation of calcium carbonate an interesting system for the investigation of polymorph selection.

*: In the original publication [92], the concentration was ploted against the reaction, which was here substituted against the supersaturation.

3.
Calcium Carbonate

Roughly 7% of *earth`s* crust consist of calcium carbonates ($CaCO_3$), which form widespread rocks such as limestone, chalk or marble. Such deposits play a large economical role, as calcium carbonate is a base resource. [*] [93] A large proportion of these geological deposits have been generated *via* biomineralising processes, which especially applies to deposits in marine sediments. [94] Among the known biominerals, calcium carbonate is of special importance, as it is assumed to make up a major fraction of the overall generated biominerals. [95] In this respect, calcium carbonate has been commonly utilised in the form of skeletal hard parts, but also as otoliths/statholiths in vertebrates or optical lenses [96, 97].

From a chemical point of view, calcium carbonate is the sparingly soluble salt of calcium and carbonate ions. The carbonate ion is derived from carbonic acid (H_2CO_3) by two-fold deprotonation at the respective pK_A values of 3.8 and 10.3. [**] The first dissociation step occurs at a relatively low pK_A value, making carbonic acid a comparably strong acid. However, the underlying equilibrium between carbon dioxide (CO_2) and carbonic acid favours the carbon dioxide ($pK = 2.6$, [**] equations (17)). Hence, the apparent pK_{A1}^{app} is 6.4 , which results in carbonic acid being an acid of intermediate strength. Meanwhile, the pK_{A2} of 10.3 suggests that hydrogencarbonate is a very weak acid. [**]

$$\left.\begin{aligned} &CO_2 + H_2O \leftrightharpoons H_2CO_3, && pK = 2.6^{**} \\ &H_2CO_3 + H_2O \leftrightharpoons HCO_3^- + H_3O^+, && pK_{A1} = 3.8^{**} \\ &CO_2 + 2\,H_2O \leftrightharpoons HCO_3^- + H_3O, && pK_{A1}^{app} = 6.4^{**} \\ &HCO_3^- + H_2O \leftrightharpoons CO_3^{2-} + H_3O^+, && pK_{A2} = 10.3^{**} \end{aligned}\right\} \quad (17)$$

*: Such mineralogical deposits have been mined and used for building materials and the production of cement and mortar since millenia. At present, about 1000 Mt are mined per year. The resulting calcium carbonate is mainly used in the construction industry and in the chemical industry. In the latter it is applied as precursor in the production of soda (Na_2CO_3), fertiliser and as filler material (e.g. in paper, rubber, plastics or paints). [93]

: pK- and pK_A-values adopted from Riedel (2004**) [328].

In return, the carbonate anion is a relatively strong base. Consequently, the solubility of calcium carbonate directly depends on the pH value, as the carbonate anion is easily protonated. Thus, calcium carbonate is stable at neutral and alkaline pH values, while it will dissolve at low pH values under the evolution of carbon dioxide.

As already described, calcium carbonate is crucial for different industrial branches, earth sciences and it is a major biomineral. Therefore, calcium carbonate is intensively investigated. Furthermore, calcium carbonate is able to form five polymorphs and one amorphous phase from supersaturated solutions (Fig. 10a). * These polymorphs encompass ikaite ($CaCO_3 \cdot 6H_2O$) and monohydrocalcite ($CaCO_3 \cdot H_2O$, MHC), both containing different amounts of water of crystallisation as well as the anhydrous polymorphs vaterite, aragonite and calcite. In combination with the amorphous calcium carbonate (ACC), these polymorphs make calcium carbonate an interesting model system for the investigation of crystallisations, especially in the context of polymorph control.

During the crystallisation of calcium carbonate, calcite should form upon standard conditions since it is the thermodynamically stable polymorph (i.e. the polymorph with the lowest possible solubility product K_{SP}). However, calcite is not necessarily the only precipitated polymorph during crystallisations of calcium carbonate and is frequently accompanied by polymorphs of lesser stability. In rare cases, calcite is not observed at all. Such observations can be explained *via Ostwald`s* empirical *"rule of stages"* (Fig. 10b) [98, 99]. For a general, thermodynamic system, this rule states that a system does not necessarily turn into the energetically favourable state *via* a direct path, but can take place *via* an indirect route while crossing one or more metastable states. This is caused by the activation energies $\Delta G^*_{indir.}$ along the indirect path being lower than the activation energy $\Delta G^*_{dir.}$ of the direct path. In turn, this means that a thermodynamic system follows such an indirect route, because it is faster. This applies to the calcium carbonate system as well. Therefore, calcite can precipitate from a supersaturated solution *via* the initial crystallisation of one or more metastable phases, for instance ACC and/or vaterite (Fig. 10b).

*: This excludes at least two anhydrous, high-pressure modifications of calcium carbonate. [100, 101, 139, 329]

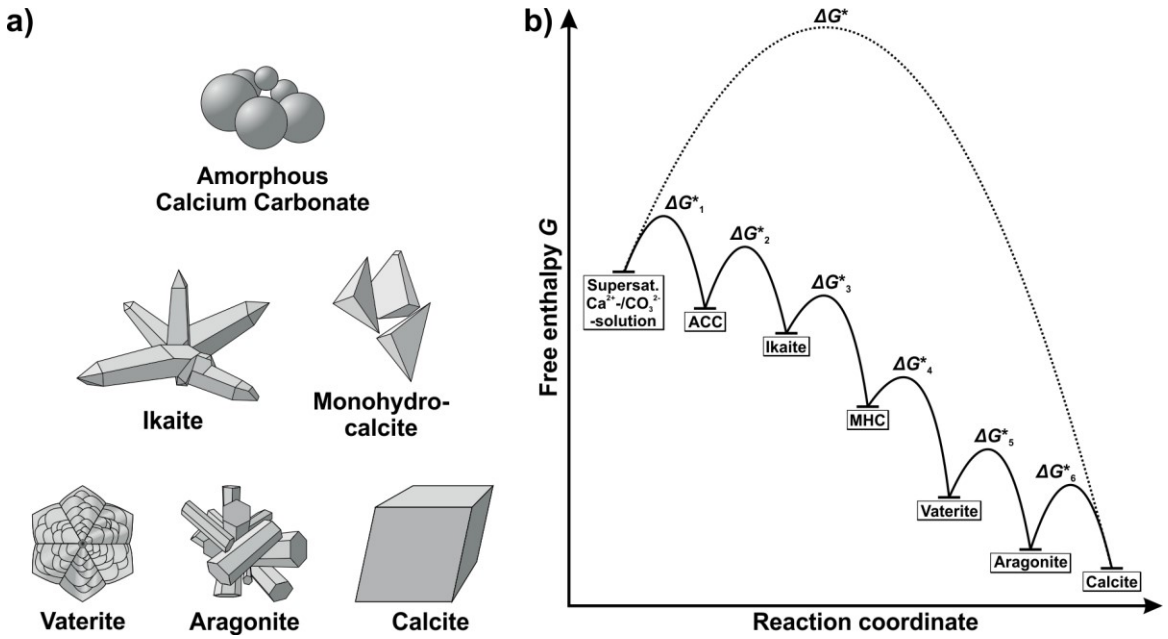

Figure 10a) The different calcium carbonate polymorphs, represented by examples of some of their corresponding morphologies (Inspired by *Cartwright et al.* (**2012**) [58]). Only polymorphs that are known to crystallise from solution, are shown; two anhydrous, high-temperature polymorphs [100, 101] are not depicted. **Upper row:** The amorphous calcium carbonate (ACC). It almost exclusively forms spherical particles, which scale up to the micrometre range (synthetic). [58, 102, 103] **Middle row:** The polymorphs ikaite ($CaCO_3 \cdot 6H_2O$, monoclinic) [104, 105, 106] and monohydrocalcite ($CaCO_3 \cdot H_2O$, trigonal) (MHC) [107, 108], both contain different amounts of crystallisation water (both mineralogical). **Lower row:** The anhydrous polymorphs vaterite (monoclinic) [109], aragonite (orthorhombic) and calcite (rhombohedral). (vaterite: polycrystalline, pseudo hexagonal example (synthetic) [110, 111]; aragonite: pseudo hexagonal, repeatedly twinned morphology (mineralogical) [112]; calcite: cleavage rhombohedron (mineralogical and synthetic). **b)** Exemplary depiction of "*Ostwald`s rule of stages*" [98, 99] on the calcium carbonate system by plotting the free enthalpy G of the individual polymorphs against the reaction coordinate. During a crystallisation of calcium carbonate at standard conditions, the stable polymorph, i.e. calcite, will form. According to "*Ostwald`s rule of stages*", the crystallisation of calcite will not directly occur in a single step (dashed line), but *via* the successive formation of metastable polymorphs(solid lines), as the corresponding activation energies ΔG^*_{1-6} being lower each than ΔG^* of the direct formation, which in turn causes the crystallisation along the route of the metastable polymorphs to be faster.*

However, *Ostwald`s* empirical *"rule of stages"* represents only a rule of thumb, as the activation energies of both, the indirect route $\Delta G^*_{indir.}$ and the direct path $\Delta G^*_{dir.}$ strongly depend on the specific conditions. Thus, depending upon the conditions certain metastable states will be crossed on the path towards the stable state, while others will be skipped. This means for the calcium carbonate system that the crystallisation of calcite can take place *via* the successive precipitation of metastable polymorphs, during which certain metastable phases will crystallise, while others will not. In extreme cases, the precipitation of calcite can take place directly.

*: Figure **10b)** The differences in free enthalpy G of the individual polymorphs are based on the corresponding solubility products K_{SP}. The heights of the activation energies ΔG^* and the free energy G of the supersaturated solution are chosen arbitrarily.

In the following, the polymorphs of calcium carbonate, known to crystallise from solution, will be introduced in order of increasing stability (decreasing solubility product K_{SP} at standard conditions).

Amorphous calcium carbonate (ACC, $CaCO_3 \cdot n\ H_2O$, n = 0-1) is the thermodynamically most labile phase ($K_{SP} = 4.0 \cdot 10^{-7}\ \frac{mol^2}{L^2}$), [113] and contains up to one unit water of crystallisation. It is prone to phase transformation into more stable polymorphs and it is mainly observed during early stages of crystallisation. In organisms, ACC has been observed to act as a transient precursor phase during the formation of more stable polymorphs, as in the formation of spicules in sea urchins. [114, 115] Additionally, ACC has been found to serve as a temporary storage deposit (e.g. in the exocuticles of crustaceans [116, 117, 118]). In contrast, ACC is generally irrelevant in geological and mineralogical contexts.

The main characteristic of the two polymorphs ikaite ($CaCO_3 \cdot 6\ H_2O$; *mS*44, 15; $K_{SP} = 2.6 \cdot 10^{-7}\ \frac{mol^2}{L^2}$) [106, 119] and monohydrocalcite ($CaCO_3 \cdot H_2O$; *hP*24, 152; $K_{SP} = 6.6 \cdot 10^{-8}\ \frac{mol^2}{L^2}$) [120, 121] is the different amount of water in the corresponding crystal structures. Both are thermodynamically labile and tend to transform quickly into the more stable phases. Ikaite occurs at marine locations that are characterised by temperatures close to the freezing point, e.g. Greenland or Antarctica [105, 122, 123]. Monohydrocalcite is reported to occur at hypersaline lakes or in close vicinity to ikaite as direct decomposition product. [124, 125] Ikaite is not yet known as a biomineral, though a possible connection to organisms *via Biologically Induced Mineralisation* has been suggested. [126, 127] In contrast, monohydrocalcite has been observed in at least four phyla [1], e.g. in the tapeworm *Mesocestoides corti* [128] or in ginuea pig`s bladder [129]. Still, both are uncommon minerals in geology and biology.

Among the three anhydrous polymorphs of calcium carbonate, vaterite is the thermodynamically most labile polymorph ($K_{SP} = 1.2 \cdot 10^{-8}\ \frac{mol^2}{L^2}$) [130] and it will readily transform into aragonite or calcite in the presence of water. As a direct consequence, vaterite is a geologically rare mineral, reported from only a few locations worldwide. [131, 132] In contrast, the importance of vaterite in organisms is significantly higher and it has been observed in a variety of organisms (e.g. fish

otoliths,[133, 134] spicules in *Ascidiacea*[135] or bivalve pearls/shells[42, 136, 137]). Still, vaterite only accompanies the more stable polymorphs aragonite or calcite as a minor fraction in a multitude of these observations. No apparent functions have been attributed to such vaterite deposits, though it has been suggested that vaterite could serve as a transient precursor towards the more stable polymorphs, similar to amorphous calcium carbonate. Additionally, some vaterite occurrences have been explained as the product of failed biomineralising processes, in which the phase transformation towards more stable polymorphs was hindered.[42, 136]

In general, macroscopic single crystallites of vaterite are unknown. Instead, vaterite forms polycrystalline aggregates, which consist of nano-sized crystallites and display spherical or (pseudo)-hexagonal morphologies. Due to the nano-sized polycrystallinity, the crystal structure has been controversially discussed for about 100 years and this discourse is still ongoing. A possible structure model by *Mugnaioli et. al.* (**2012**)[109] describes a monoclinic crystal structure,which contains two distinct calcium ions in 8-fold coordination by two different types of carbonate ions (Fig. 11). In the crystal structure, both types of calcium ions form a pseudo-hexagonal sublattice, while the carbonate ions are arranged parallel to the z-axis (≠ c), forming sheets. These sheets are twisted 180 ° against each other and shifted in a manner that the carbonate ions occupy a staggered orientation. There are further possibilities to achieve the necessary, staggered orientation of the carbonate ions, for instance other orientations of the carbonate sheets (i.e. 60 ° turns) or different sequences, in which the starting orientation is repeated.[138] The resulting, distinct superstructures would be only of little energetic difference, which implies that vaterite could be a mix of different polytypes instead of a single polymorph.[138] In addition, the superstructures of the carbonate sheets are prone to stacking defects, which have been observed already.[109, 138] Both, the stacking defects and the possibly polytypic nature of vaterite, would explain the polycrystallinity of vaterite at the nano scale as well as the long-lasting argument about its crystal structure. In addition to the proposed crystal structure by *Mugnaioli et. al.* (**2012**)[109], further structures have been proposed, which base on molecular

modelling.* However, the crystal structure published by *Mugnaioli et. al.* (**2012**)[109] is still the only proposed structure model fully relying on experimental data.

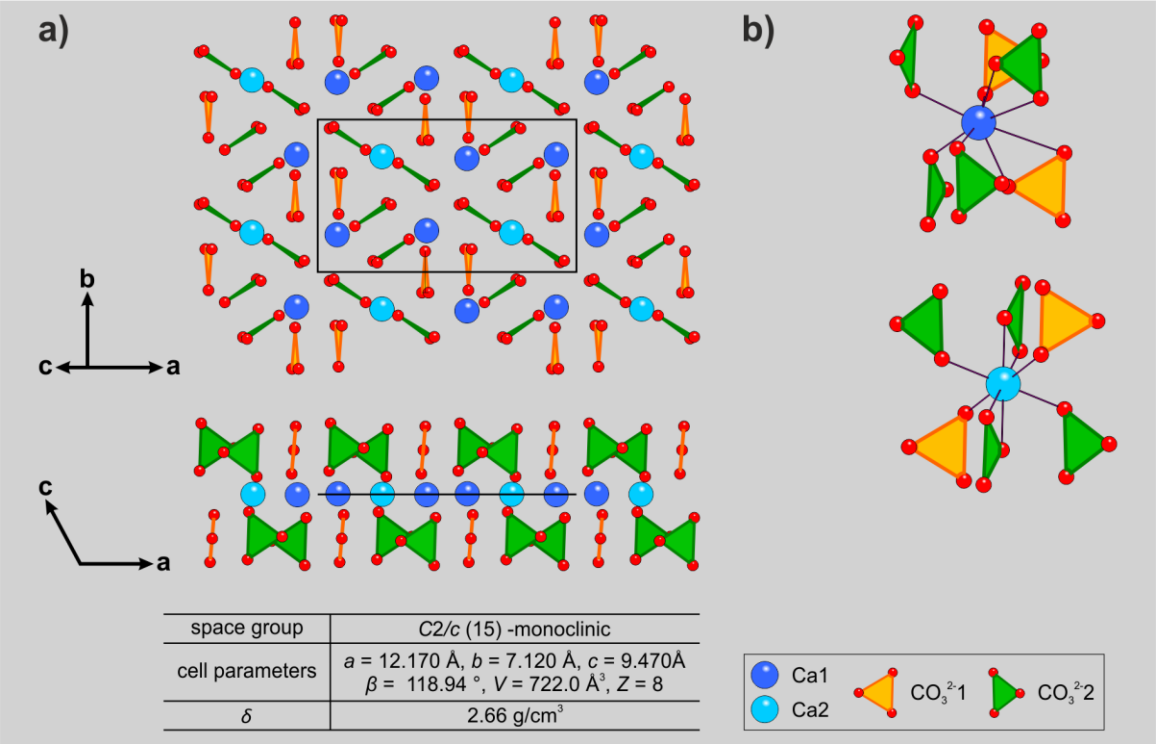

Figure 11) Crystal structure model of vaterite, according to *Mugnaioli et. al.* (**2012**).[109] **a)** View along [103] displays the hexagonally distorted arrangement of the Ca^{2+} ions (upper row), while the view along [010] illustrates the layer type structure (lower row). Black lines indicate the cell edges. **b)** Coordination of the two distinct Ca^{2+} ions (**blue**: Ca (1); **light blue**: Ca (2)) by the oxygen atoms of the two differing carbonate groups (**yellow-orange**: CO_3^{2-} (1), **green**: CO_3^{2-} (2), carbon atoms not shown). Cell parameters according to *Mugnaioli et. al.* (**2012**).[109]

In contrast, the second anhydrous polymorph, aragonite ($pK_{SP} = 5 \cdot 10^{-9} \frac{mol^2}{L^2}$)[130], is considerably less labile in comparison to the already discussed polymorphs. Aragonite crystallises in an orthorhombic structure, in which the calcium ions are coordinated nine-fold by six carbonate ions (Fig 11). This crystal structure of aragonite results in a higher density and a higher hardness than in the other polymorphs. Furthermore, it is the thermodynamically stable modification at elevated pressure.[139] In contrast to the previously discussed polymorphs, aragonite is a geologically widespread mineral forming whole rock formations.[112]

*: For further proposed structures see for example: *Demichelis et. al.* (**2012**)[330], *Demichelis et. al.* (**2013**)[331], and *Wang et. al.* (**2014**)[332]. An additional overview on the proposed crystal structures of vaterite is given in a review by *Christy* (**2017**)[138].

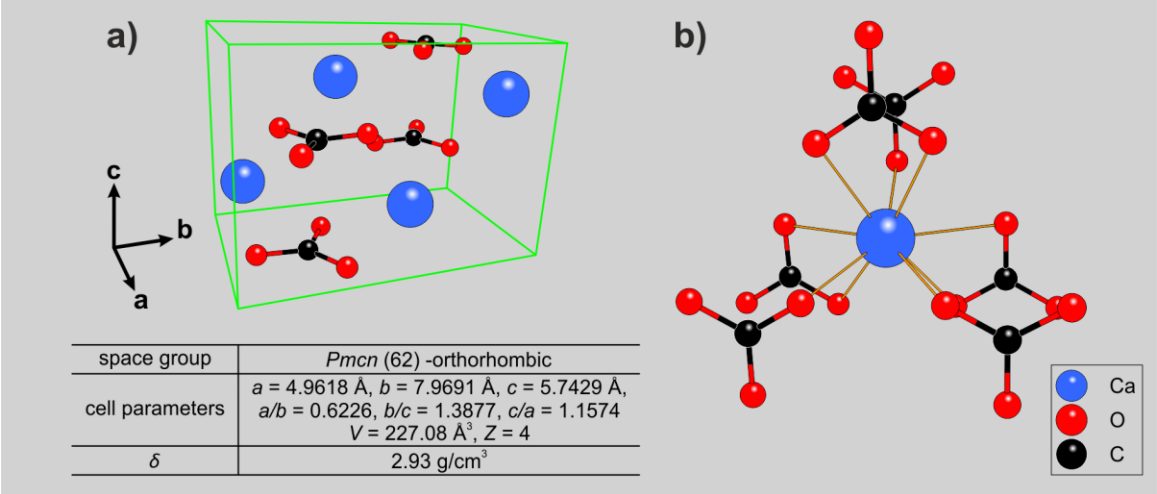

space group	*Pmcn* (62) -orthorhombic
cell parameters	*a* = 4.9618 Å, *b* = 7.9691 Å, *c* = 5.7429 Å, *a/b* = 0.6226, *b/c* = 1.3877, *c/a* = 1.1574 *V* = 227.08 Å^3, *Z* = 4
δ	2.93 g/cm^3

Figure 12) Crystal structure of aragonite. **a)** Unit cell of aragonite. **b)** Depiction of the 9-fold coordination of the calcium ions. Crystallographic data in accordance to *Caspi et. al.* (**2005**) [140].

This is also reflected in its occurrence as a biomineral, as aragonite has been observed in at least 16 *phyla.* [1] Good examples for aragonite as a biomineral are the skeletons of reef-forming stony corals (S*cleractinia*, phylum: *Cnidaria*) that consist almost entirely of aragonite [141] or the shells of different molluscs. [*] In the latter case, the nacre-containing shells of certain bivalves and gastropods are especially well known (Fig. 2c, d).

With the lowest solubility of all calcium carbonate modifications ($K_{SP} = 3 \cdot 10^{-9} \frac{mol^2}{L^2}$) [130] the anhydrous polymorph calcite is the thermodynamically stable polymorph at standard conditions. Calcite crystallises rhombohedrally and both, the calcium and carbonate ions, are 6-fold coordinated (Fig. 13). Apart from the stable, {10.4}-faceted cleavage rhombohedron (Fig. 13c), calcite shows a considerable variety of morphologies in dependence on the crystallisation conditions. As the thermodynamically stable polymorph of calcium carbonate, calcite is almost ubiquitous in *earth`s* crust and it by far surpasses the total amount of the remaining geologically occurring calcium carbonate modifications. Thus, calcite can be observed as the main constituent in several rock formations such as the above mentioned lime stone, chalk and marble, which form whole mountain ranges. [142]

*: The two examples in stony corals and mulluscs by far surpass the total amount of the remaining aragonite occurences as a biomineral. However, other examples of aragonite, such as in otoliths of certain fish species [333, 334] or in the hulls of some *Foraminifera* [1, 335] are known.

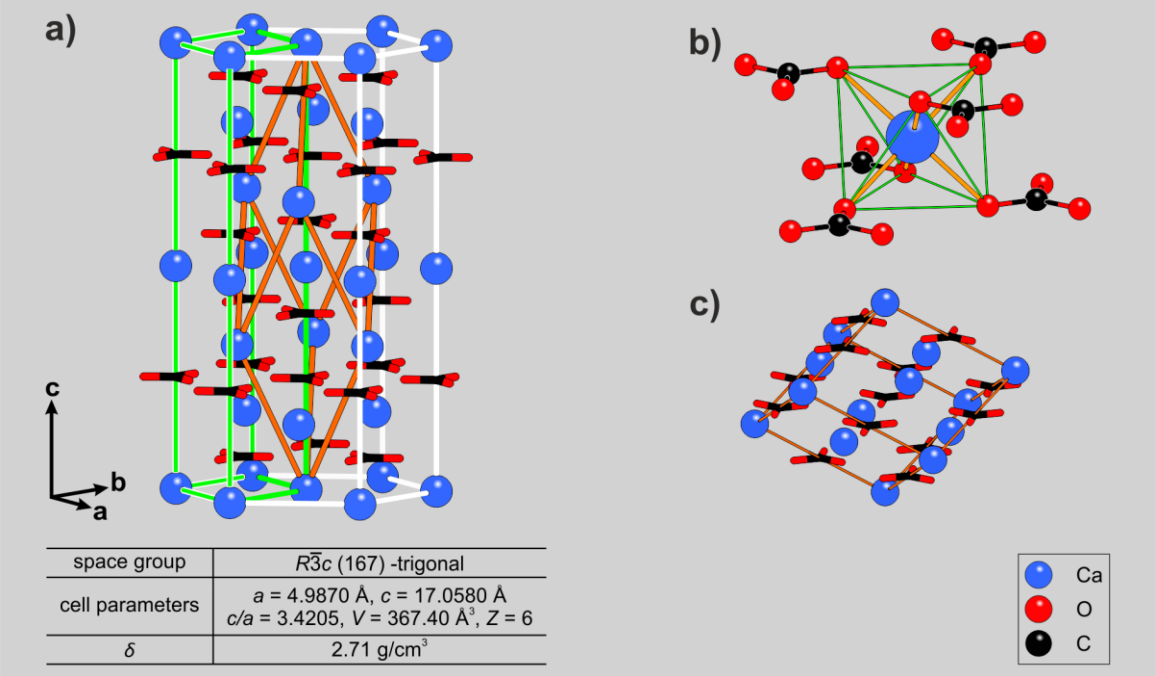

Figure 13) Crystal structure of the rhombohedral calcite. **a)** Different unit cells of the calcite and the relation between them (rhombohedral unit cell (orange), hexagonal unit cell (white) and cubic unit cell (green)). **b)** Section of the unit cell, depicting the 6-fold coordination of a calcium ion by carbonate units (orange) and the resulting coordination-octahedron (green). **c)** The octahedral coordination of the calcium ions is additionally reflected in the structure of the cleavage rhombohedron. This {10.4}-faceted cleavage rhombohedron can be considered analogous to the sodium chloride crystal structure. Inspired by *Morse et. al.* (**2007**)[94], crystallographic data in accordance to *Caspi et. al.* (**2005**)[140].

Furthermore, calcite is a very common biomineral that has been observed in different mineralised tissues of various organisms (e.g. in the egg shells of avians,[143, 144] in the spicules of sea urchins[1, 115, 145] and calcareous sponges (*Calcarea*),[146] in the tests of *Foraminifera*[1, 147] or in the coccoliths of *Coccolithophores*[1, 148]).

Calcium carbonate is a very common mineral in geology and biology. Moreover, it is a economically highly relevant base resource. Furthermore, calcium carbonate precipitates in a variety of polymorphs, which in turn makes calcium carbonate an ideal model system for the investigation of polymorph control. Such investigations have been strongly influenced by studies of biomineralisation processes, as these studies reported different polymorph-selective biomolecules. Meanwhile, another biomimetic approach to identify polymorph-selective peptides, phage display has been succesfully reported.[77] Therefore, phage display represents a promising approach that could benefit the investigation and identification of polymorph-selective additives for the calcium carbonate system.

4.
Phage Display

The experimental approach of phage display is derived from the peptide display concept originating in the combinatorial chemistry. [149] The underlying principle in all the different approaches of peptide display experiments is the screening of large, random peptide libraries for a binding affinity towards an immobilised target structure. However, from a chemical point of view two problems arise. The initial problem is the synthesis of the library itself, more specifically the synthesis of an individual peptide in a relatively large amount and the need to repeat this for an extremely large variety of different peptides. The second problem is the isolation and identification of the successfully bound peptides in excess of less affine peptides, which would require tedious separation steps and sensitive detection methods. Consequently, the concept of peptide display would not meet a combinatorial chemist`s expectations to a high-throughput screening method. In organisms however, the phenotype, in this context the sequence of a peptide or a protein, is fundamentally connected to its genotype. [150] This connection has been exploited in turn for the peptide display concept by developing libraries that present peptides on genetically engineered organisms. Phage display is one of the resulting techniques. * In phage libraries, individual groups of the phage population each display a unique (surface)-peptide. After such a phage-library is established, the required synthetic effort is drastically reduced, as the phage library can be easily replicated by infecting the corresponding host bacteria. Additionally, the latter is exploited to “amplify” the “phage-signal” during and after an affinity screening, which in turn facilitates detection and identification of the individual peptide sequences. In this manner, peptide display, in the form of phage display, has developed into a versatile method for the identification of peptide structures, which possess affinity towards specific target structures. Moreover, phage display

*: There are more approaches to realise peptide display experiments, each possessing its own advantages and drawbacks. Some are cellular based such as Bacterial [315, 316] or Yeast Display [310, 311] while others are acellular, such as Ribosome Display [314] or RNA Display [312, 313]. Among these approaches however, phage display was the first to be proposed [317] and developed. Till 1991, the proposed idea had already advanced into first randomised peptide libraries. [318, 319, 320, 336]

has been utilised to benefit the improvement of already existing peptide structures, such as enzyme inhibitors. [151]

In principle, all affinity screenings based on phage display share the same general procedure (Fig. 14a), colloqiually termed biopanning. [152] A further requirement is an immobilised target structure. This immobilised target is incubated with the phage library. Afterwards, the incubated target is washed with a buffer, often containing a detergent to remove unbound weakly affine phages. Now only phages of higher affinity remain attached to the target structure, which become detached during a subsequent elution step with a corresponding buffer. Elution buffers can for instance contain a known, specific ligand. Other buffer systems disrupt the non-covalent interactions between phage and target by exploiting denaturing conditions, for example low pH-values or high concentrations of chaotropic agents. [153] Following this, the eluted phages are “amplified” by infecting the corresponding host bacteria. This step generates a new, much smaller library with phages of differing affinity for the target, thereby finishing a first cycle of a biopanning. Using this preselected library for a second incubation of the target starts a new selection cycle of the biopanning. Generally, a complete biopanning consists of three to five individual selection cycles (Fig. 14a), though the last cycle of every biopanning deviates from the above-mentioned general cycle. In this last cycle, the eluted phages are not subsequently “amplified”, but separated on agar plates *via* a dilution series. During further processing of the separated phage, the phage genomes are sequenced and consequently the peptide sequence is identified. Essentially, one selection round should suffice for a biopanning. Nevertheless, two opposing factors, the stringency and the phage yield during the selection cycle, make iterative cycles important. Here, stringency is a value for the discrimination of higher affine phages over those of lower affinity. For example, a phage of very high affinity is difficult to detach from the target structure, while those phages of lesser affinity are easier detached. Hence, a highly affine phage might be missed in the excess of low-affinity phages during a single selection cycle. To prevent such situations, the yield of a selection cycle should be maximised during the first cycles, while during the later cycles of a biopanning an increase of stringency should be favoured. [153]

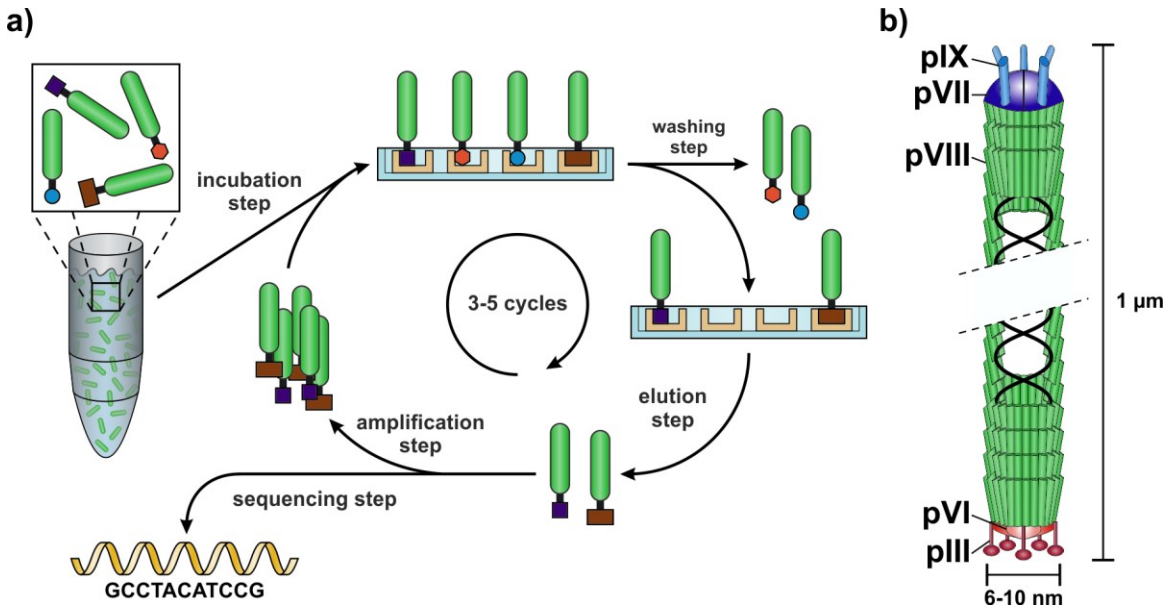

Figure 14a) General procedure for an affinity screening (biopanning) with a phage library. A biopanning is organised into three to five iterative cycles. Each cycle starts with the incubation of the target and the subsequent removal of unbound and/or lowly affine phages during the washing step. Afterwards the phages of higher affinity are detached by an elution buffer and finally amplified in the corresponding host bacteria, which finishes a cycle. The last cycle deviates from this scheme, as the eluted phages are not amplified but separated and sequenced to identify the corresponding peptide sequences. **b)** Structure of the filamentous M13-phage. The phage hull is formed by one major capsid (**pVIII**) and four minor capsids (**pVII**, **pIX**, **pVI**, **pIII**). 2700 copies of p**VIII** make up the long side of the phage and cover the single-stranded DNA, while the minor capsids form both ends of the phage. [151, 154] Inspired by *Kehoe et al.* (**2005**) [151].

For phage display libraries, it is generally possible to utilise every phage, the λ-phage [155, 156] or the T7-phage [157, 158] for instance. Even virus-particles [159] have already been utilised. However, the filamentous M13-phage is probably the most common phage used for phage display. [151, 153, 160, 161] Additionally, phage display libraries that base on the M13-phage, are commercially available. * The M13-phage is best described as a very thin rod with a diameter of 6-10 nm and a length of about 1 µm. ** [151, 154, 162] A good comparison would be a “four-foot long pencil” [151] (Fig. 14b). Its relatively small genome is organised in a circular, single stranded DNA (ssDNA) encompassing 6407 bases and encodes 11 proteins, [151, 163] of which five make up the hull of the phage particle. The major capsid **pVIII** constitutes the sides of the rod-like phage particle, thereby covering the DNA with its more than 2700 copies. Meanwhile, the four minor capsids are located at the ends of the rod-like phage in pairs of two. Here, five copies of each the capsids **pVII** and **pIX** form one end and five copies of each the capsids **pVI** and **pIII** constitute the other end

*: For example *New England Biolabs*, *Merck Millipore* or *Creative Biolabs* provide different libraries for a broad range of applications, ranging from relatively simple peptide sequences (length, amino acid composition, disulphide bridges) up to antibody libraries.

**: Diameter and length of the phage are referring to the wild-type M13-phage. Both can vary in genetically modified types.

(Fig 14b).[154] Meanwhile, all five capsids of the M13-phage have been utilised to display random peptides. Such random peptides and even larger proteins have been mainly integrated into the phage in the form of *N*-terminal fusion proteins.[151] Nevertheless, modifications at the **pVIII** and at the **pIII** capsids prevail[154], while those at the **pVI**[164], **pVII**[165] or **pIX**[166] capsids are rarely reported. Especially peptide modifications at the **pIII** capsids are interesting, as the small number of pIII`s copies allows the screening for peptides with high affinities.[151] However, it is not possible to introduce every possible modification into the phage capsids, as the capsids need to fulfil their intended roles during the life cycle of the M13-phage.

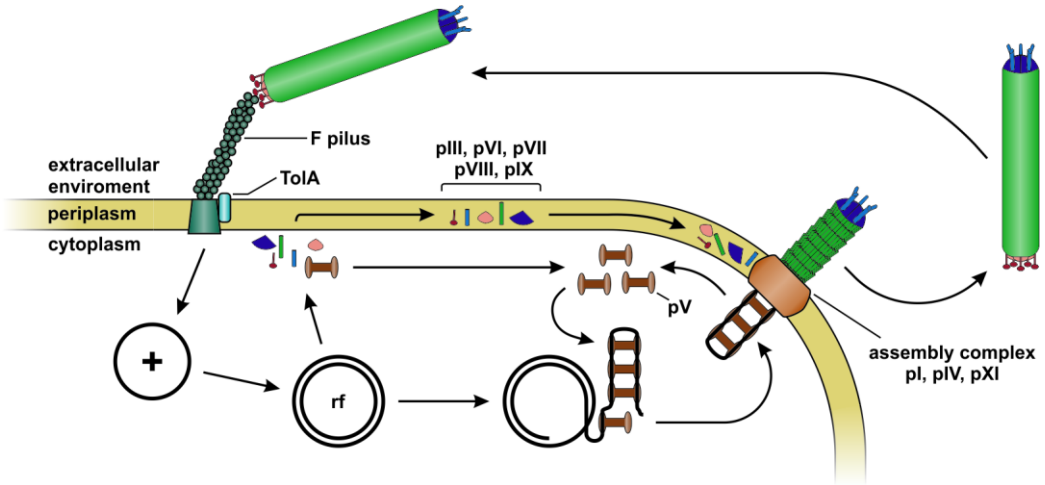

Figure 15) Schematic depiction of the life cycle of the M13-phage. The infection of E.coli by an M13-phage is induced by the interaction of a **pIII** capsid an *F pilus* on the bacterial cell membrane. The phage genome is released into the host subsequently to the additional interaction of **pIII** and *TolA*. Here, the (+)-strand ssDNA (sense-strand) is converted into the double-stranded, replicative form (rf). The proteins encoded in the phage`s genome are synthesised and the double stranded genome is replicated as well. The capsid proteins (**pIII**, **pVI**, **pVII**, **pVIII**, **pIX**) are inserted into the periplasm and accumulate at the transmembranary assembly complex, formed by **pI**, **pIV** and **pXI**. Meanwhile, the (+)-strand in the replicative form of the genome is incised and subsequently bound by the **pV** protein of the phage. This complex is bound by the capsids **pVII** and **pIX** at the assembly complex and the phage assembly is initiated. During the assembly, the **pV** proteins are striped from the (+)-strand, which becomes simultaneously covered with the **pVIII** capsids. The assembly is finished by the addition of the capsids **pIII** and **pVI** at the other end and the progeny phage is extruded from the host.[151, 154]

In comparison to most other bacteriophages, the life cycle of the M13-phage is unusual.[167] Commonly, bacteriophage transfer their genome into a host bacteria, after which new phage particles are synthesised in the host until the host bacteria becomes lysed and the new phage particles are released.[168] Bacteriophages such as the T4-phage possess such a lytic life cycle.[169] In other bacteriophages, the lytic life phase can follow upon a lysogenic phase. During this lysogenic phase, the phage genome becomes integrated into the host`s genome, where it remains dormant until certain stimuli activate it, upon which the lytic cycle is initiated.[168] The lysogenic cycle can be observed for instance in the λ-bacteriophage.[169, 170]

However, the M13-phage possesses neither a lytic nor a lysogenic life cycle. Instead, it induces a chronic infection, during which the progeny phages are extruded from the bacterial host without lysing it (Fig. 15). * Thus, the host survives, though cell growth and cell division take place at a slower rate. [151, 171] For the M13-phage, this life cycle starts with the infection of a host bacterium, i.e. *E. coli*. The infection is initiated by binding an *F pilus* on an *E. coli via* a **pIII** capsid. Afterwards, the phage is drawn towards the bacterial cell membrane, where the **pIII** capsid binds an additional membrane protein, *TolA*, and the phage subsequently introduces its genome into the bacterium. ** [154, 172] Subsequently, the introduced (+)-ssDNA (the sense strand, Fig.15) is converted by the host into the double stranded, replicative form (rf). This replicative form is copied and the encoded proteins are synthesised. The capsid proteins (**pIII**, **pVI**, **pVII**, **pVIII**, **pIX**) are inserted into the periplasm of the bacterial cell membrane and accumulate at the transmembranary assembly complex that is formed by proteins **pI**, **pIV** and **pXI**. Meanwhile, the (+)-strand of the replicative form is incised and covered with the protein **pV**. This complex is bound by the **pVII** and **pIX** capsids at the assembly complex, which starts the assembly process. Here, the ssDNA of the progeny phages becomes covered by the **pVIII** capsid, while it is striped from the **pV** proteins. The assembly is finished with the addition of the **pIII**/**pVI** capsids and the new phage extrudes from the bacterium. ** [154, 163] In this manner, a complete life cycle of the M13-phage is finished and the progeny phage can infect a new host cell.

This life cycle represents an important constraint for phage libraries, as every modification that disturbs the specific function of a capsid during the life cycle of the phage, causes a diminished survivability of the phage. For example modifications that disturb the interaction between the pIII capsid and the F-pilus and/or *TolA*, will lower the infectivity of a corresponding phage. In extreme cases, no infection will occur at all. Phages with such modifications at the **pIII** capsid are unfit in comparison to the remaining population of the library and will be

*: The chronic life cycle of the M13-phage is advantageous to the phage display procedure, as it results only in a small amount of bacterial cell debris during amplification steps in host bacteria. This in turn simplifies the phage`s purification that completes every amplification step.

**: Both processes, the phage assembly inside the bacterial membrane and the introduction of the phage genome into the host bacteria, still remain poorly understood. [321]

underrepresented in the library at least. Thus, a major limitation for modifications is the size of the inserted peptide or protein sequence. [154, 173] However, the **pIII** capsid is less prone to this size effect, though the effect still remains erratic. [151] There are other points in the life cycle that influence the displayed modifications. The assembly of the phage particle and the preceding transport of the capsid proteins into the periplasm are two of these points. Especially the transport of the capsid proteins into the periplasm is a biological “bottleneck”, as the transport of highly charge peptide sequences into to the periplasm is slower in comparison to peptide sequences without net-charge. Therefore, the relative amount of charged amino acids in the displayed sequences of a phage library is lowered in comparison to a theoretical library. [154, 174] Hence, the life cycle of the M13-phage is an important factor for the generation of phage libraries, as it creates a censorship on both, the length of the displayed peptide and the amino acid composition of the peptide. *

Numerous publications report the successful application of phage display techniques. These encompass different topics such as protein-protein interactions, [175, 176] substrate specificity of enzymes/receptors and their corresponding inhibitors, [177, 178, 179] as well as antibodies [180] and epitopes/mimitopes [181, 182]. However, phage display is not limited to applications in molecular biology, pharmacy or medicine. It has been utilised in the development of sensors/detectors [183, 184] and electrochemical devices [184] or for investigations of inorganic [185, 186] and organic [187, 188] materials. Among the investigation of inorganic materials, an especially strong focus has been placed on interaction between peptides and nanoparticles. Among these are semiconductors (GaAs [185], ZnS, [189]…), metal oxides (ZnO, [190, 191] zeolite, [192]…) or noble metals (Au, [193, 194] Ag, [195, 196]…). ** In general, the synthesis of nanoparticles strongly depends on very defined and controlled crystallisation conditions. Since biomineralisation depends on the same principles, phage display provides an alternative for the biomimetic investigation of biominerals. Following this idea, hydroxyapatite, [197, 198, 199] calcium carbonate, silica [200] and other biominerals have already been screened with different peptide display libraries. In the case of calcium carbonate, several

*: Nevertheless, it is possible to broaden the applicability of phage display by utilising more sophisticated approaches like phagemid experiments. [180, 322, 323]

**: The field is already illustrated by a number of review articles. [186, 239, 240, 324, 337]

investigations [77, 201, 202, 203, 204, 205, 206, 207] have been published. However, only four deal with the influence of library screened peptides on the polymorph selection during crystallisations. [77, 202, 205, 206] *

In summary, phage display techniques are a well-known screening method to identify peptides that possess an affinity to a great variety of different target structures. In this respect, phage libraries based on the M13-phage are especially often applied. Still, their application needs some considerations, as the selection mechanism is not solely based on the affinity against the target structure, but additionally depends upon the phage`s life cycle. In more recent time, the scope of the method has been widened to the field of material science. Still, reports on the investigation of biominerals by phage display are relatively scarce. This applies to the biomineral calcium carbonate and its polymorphs as well. Meanwhile, in a preceding experimental work, phage display has been successfully applied to screen for polymorph-selective peptides on the vaterite polymorph. [77] This biomimetic approach could be applied to additional polymorphs of calcium carbonate to broaden the control on the polymorph composition of a crystallisation.

*: Additionally, one publication used selected phages to study the polymorph selection [203] instead of peptides, while another studie used cell surface display instead of phage display [207].

5.
Motivation and Research Objectives

The oldest evidences of biological life on earth are based on microfossils, which date back to at least 3.5 billion years.[208, 209, 210] Nevertheless, the development of the first organisms is assumed to have taken place earlier.[211, 212] Since this period in earth`s history, evolution has generated a nearly inconcievable number of organisms of increasing complexity. As direct requirement, an enormous variety of functions have been brought to perfection during the advance of evolution to allow the diversity of modern biological life. Among them are fascinating processes that inspire researchers of various fields, for example photosynthesis,[213, 214 215] enzymatic catalysis in general[216, 217, 218] or molecular self-assembly[219]. In this context, biomineralisation represents another complex field of research.[1, 5, 6] Biomineralisation and biomineralising processes fascinate researchers of different disciplines, e.g. physicians and biologists as well as chemists and material scientists. The latter two place special emphases on the hierarchical build-up of biominerals and the resulting unique properties and complex forms as well as the processes by which organisms control the formation of such biominerals.[2, 95, 220] For instance, one focus is placed on the mechanical characteristics of biominerals, as some biominerals show a mechanical toughness that is far superior to their geological counterparts.[16, 221] Another biologically controlled property is the mineral polymorph.[1] In this regard, calcium carbonate is a strongly investigated biomineral, as its three anhydrous polymorphs, i.e. vaterite, aragonite and calcite, can all be found in organisms. Some striking examples for the control over the growth of calcium carbonate arise from the mollusca phylum.[1, 46, 47, 48] Many animals in this phylum produce calcium carbonate based biominerals, mostly in form of shells. Especially interesting examples are the pearl oysters of the genus *pinctada* (*bivalvia*)[49] and the abalone of the genus *haliotis* (*gastropoda*)[50, 51], which build different types of aragonitic nacre. However, these examples are not limited to the biomineralisation of aragonite, but are able to mineralise calcite in close proximity to aragonitic nacre. This polymorph selectivity during calcium carbonate mineralisation in these animals is highly interesting for materials scientist, as the

properties of a given material are directly related to its crystalline structure. This polymorph selective control during biomineralising processes is mediated by organic molecules, termed additives. Hence, numerous investigations on such additives have been reported, among which proteins are a major fraction. [1, 2, 3, 95, 222] To achieve this, a variety of methods have been applied, including the extraction of mineralised tissues and molecular-biological methods. Unfortunately, these methods suffer from a series of drawbacks. For instance, it is troublesome to identify additives, which specifically interact with a mineral polymorph, in an excess of extracted biomolecules. Some of these problems could be circumvented by applying combinatorial methods that select binding motifs. The utilisation of peptide libraries represents such an experimental approach [149], which has been realised in the form of phage display on calcium carbonate and its polymorphs. However the overall amount of such reports is still low, and those that focus on the polymorph selectivity during the crystallisation of calcium carbonate are especially rare. In a preceeding experimental work, phage display has been successfully applied to screen peptides on the vaterite polymorph. This yielded a peptide that strongly preferred vaterite over the remaining polymorphs during crystallisations. [77, 78] Nevertheless, this study focused solely on vaterite and did not screen for peptides with a polymorph-selectivity/-affinity for aragonite or calcite. Hence, we aim to complement the results of the study on the vaterite-selective peptide by identifying and testing peptides that prefer calcite during crystallisations of calcium carbonate. For this, phage display experiments are to be carried out on calcitic surfaces as a first step to identify peptides with an affinity for same. In contrast to vaterite, large, calcitic single crystals, terminated by {104}-facets, are available. According to literature, facet-selective peptides have already been identified *via* phage display. [185, 223] Hence, an additional phage display screening for peptides with an affinity to {104}-facets of calcite is to be carried out as well. In the following, the identified peptides are to be made accessible *via Solid-Phase Peptide Synthesis* (*SPPS*) and further investigated for their influence on the polymorph-composition during the crystallisation of calcium carbonate. Furthermore, the methods that were applied in the preceeding study, especially the crystallisation methods, are to be improved and advanced.

II.

Results & Discussion

6.
Phage Display on Calcite`s {10.4}-Facets

Motivation

As already explained, there are only few examples for polymorph-selective peptides identified by phage display on calcium carbonate. [77, 202, 205, 206] However, many publications report screening experiments by phage display on a large variety of inorganic materials. These investigations were not exclusively interested in the influence of the selected peptides on the polymorph selection or the crystal morphology, but also focused on peptides with additional properties, for example an affinity for specific crystal-facets. Such experiments have already been carried out on various materials, e.g. gallium arsenide- [185] or platinum-nanoparticles [223]. Successful preliminary phage display experiments on vaterite-nanoparticles in the Tremel group [77, 78] motivated to a complementary set of experiments on the calcite polymorph of calcium carbonate. Additionally, it was decided to include the idea of screening for facet-selective peptides into the planned phage display investigation of calcite. For this experimental approach, the prominent and easily accessible {10.4}-facet of calcite was chosen as screening target.

General Setup of the Phage Display on Calcite`s {10.4}-facets

For the full experimental procedure as well as the utilised materials, buffers and solutions, see Chapter 14. For the raw sequencing data and the Multiple Sequence Alignments (MSA) see Appendix IIa.

In agreement to the overview on phage display (compare Chapter 4), the following affinity selection (biopanning) of phage displayed peptides was organised in iterative cycles. The corresponding procedures were carried out in accordance to the supplier`s manual [152] and the preceding work [77].

In the preceding phage display study, vaterite nanoparticles were used as targets in affinity screenings with a corresponding phage library. [77] However, this new study aimed on identifying peptides with an affinity towards the {10.4}-facets of

calcite. Hence, large single crystals of calcite delimited by a defined {10.4}-facet were acquired (Fig. 16).*

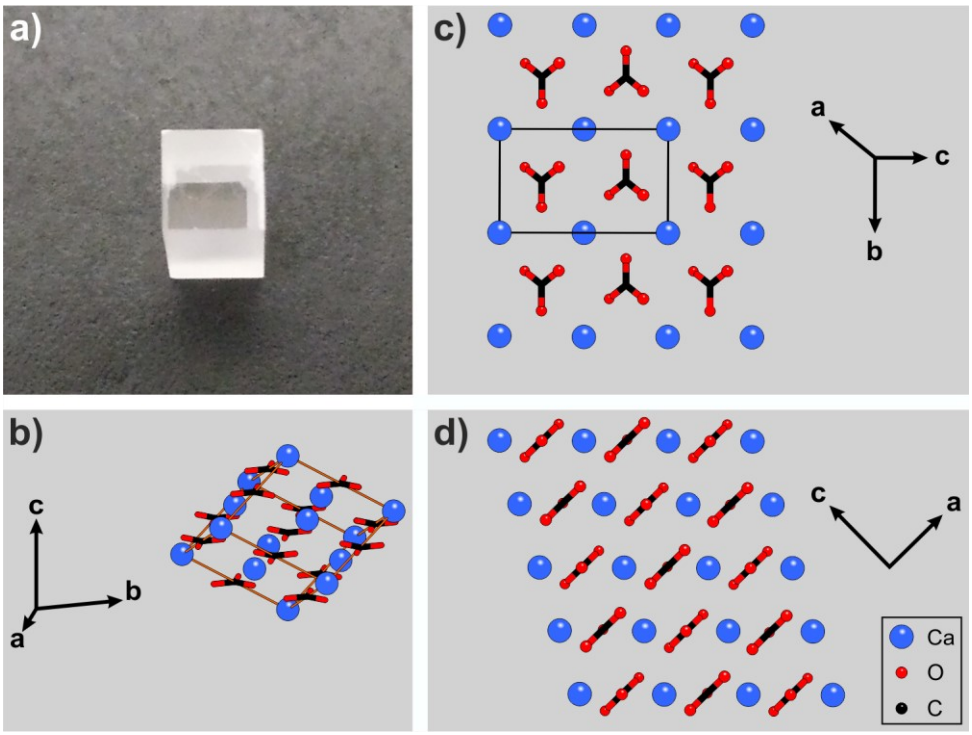

Figure 16a) View on a {10.4}-facet of a calcite single crystal used in the experiments. **b)** The {10.4}-faceted cleavage-rhombohedron of calcite. **c)** View onto a {10.4}-face of calcite. The black rectangle marks the surface unit cell. **d)** View along [01.0]. (**c** and **d** are inspired by *Rahe et. al.* (**2012**)[224] and *Marutschke et. al.* (**2014**)[225].

Prior to each cycle of the biopanning, a calcite crystal was cleaved parallel to this {10.4}-facet, creating a fresh {10.4}-facet. This new facet was subsequently washed with TBS-T·0.1 (TRIS-buffered saline + 0.1% Tween®20) and TBS (TRIS-buffered saline). In the following, these new surfaces were utilised as screening targets during the individual cycles of the biopanning.

In past experiments,[77] a library of random heptapeptides (*Ph.D.-7™*, *New England Biolab Inc.*, *Ipswich*, US-MA) had been applied. Since it was aimed to complement these experiments, the same phage library was chosen for the experiments on the {10.4}-facets of calcite. Additionally, a second phage library displaying random dodecapeptides was chosen (*Ph.D.-12™*, *New England Biolab Inc.*, *Ipswich*, US-MA). Both libraries are based on a genetically engineered variant of the M13-phage, the M13KE vector, which has been further modified with the random peptides of the respective size in form of *N*-terminal fusion proteins at the **pIII**

*: The calcite crystals with a 3·3 mm {10.4}facet were kindly provided by the [redacted], but originally supllied by *Korth Kristalle GmbH* (*Kiel*, Germany).

capsid. Furthermore, a linker/spacer consisting of three glycine moieties was additionally inserted between the random peptide and the pIII-moiety to reduce a possibly hindering influence on the function of **pIII** (Fig. 17). [152, 154]

Ph.D.-7™/Ph.D.12™

5`	TCT	CAC	TCT	$(NNK)_{(7/12)}$	GGT	GGA	GGT	TCG	***3`***
N	Ser	His	Ser	$Xxx_{(7/12)}$	Gly	Gly	Gly	Ser	***C***

K = G or T

Figure 17) Sequence of the *N*-terminal fusionprotein of both phage libraries (Ph.D.-7™/12™). Both, the genetic sequence and the peptide sequence of **the random peptide** and **the glycine-linker** are depicted. [152, 226] For the full genetic sequence of the phage, see Appendix I.

The diversity of both libraries is in the range of 10^9 different peptide sequences. [152] This is sufficient to represent the possible heptapeptides in the phage library, as this number is roughly of the same order as the number of possible random heptapeptides ($20^7 = 1.28 \times 10^9$). This is not the case for the dodecapeptide library, as the displayed peptides represent merely a fraction of the possible structures ($20^{12} = 4.096 \times 10^{15}$).

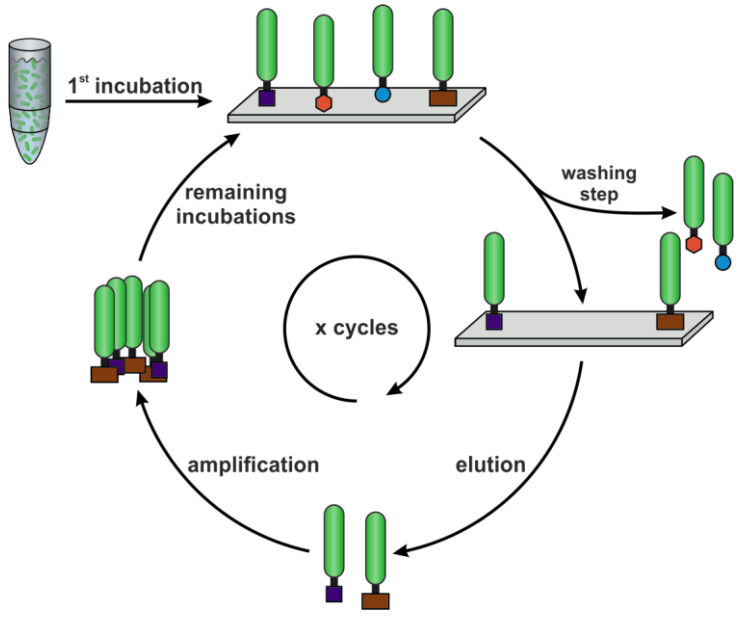

Figure 18) General scheme for the affinity selection (biopanning) on {10.4}-facets of calcite. The biopanning is organised in individual cycles, which all begin with the incubation of the target with a phage library. After a wash step, phages of higher affinity remain at the target and are subsequently eluted. The elution is followed by an amplification step, during which the phages are amplified by infecting a dispersion of host bacteria (*E. coli*). During the first cycle, the original library is applied. In contrast, in the remaining cycles the amplified libraries that were obtained during the preceding cycle are used.

Both libraries were used in individual experiments to incubate the {10.4}-facets in the first cycle of the biopanning. In the succeeding cycles, the incubations were carried out with the amplified phage dispersions that were obtained during the

preceding cycle. After incubation, the low affine or unspecifically binding phages were removed by washing with TBS-T·0.1 and TBS, while the affine phages were subsequently eluted several times with a solution of 0.1 M EDTA (sodium ethylenediaminetetraacetate). The resulting phage eluate was subsequently amplified by infecting a dilution of a *E. coli ER2738* culture, that was grown overnight. This specific strain of *E. coli* carries the F plasmid (F factor) [227, 228]. This F plasmid is of significant importance, as it encodes the sequences required for the F pili. Since F pili are in turn required for the initiation of an M13 infection (Fig. 15), this strain of *E. coli* guarantees an efficient infection. Afterwards, the bacteria were removed, the amplified phages were isolated by precipitation and subsequently redispersed. In this manner, a cycle was finished and the newly generated phage dispersions were ready to start a new cycle of the biopanning (Fig. 18).

After specific cycles, overviews of the peptide sequences were sampled. During such cycles, aliquots of the respective phage eluates were used to prepare serial dilutions prior to the normal amplification step. The resulting diluted phage suspensions were used seperately for the infection of *E. coli ER2738*. Subsequently, the suspensions of infected bacteria were spread on agar-plates, containing IPTG (Isopropyl *β-D*-1-thiogalacto-pyranoside) and X-Gal 1 (5-bromo-4-chloro-3-indolyl-*β-D*-galactopyranoside), and incubated. Both compounds are necessary for the so-called blue-white screening. [229] This screening exploits the indole galactoside X-gal as colourless precursor of a corresponding indigo dye. In the presence of *β*-galactosidase, the galactoside is cleaved yielding a indole (5-bromo-4-chloro-3-hydroxyindole), which in turn dimerises upon oxidising conditions, yielding the bluish/purple indigo-derivative (5,5'-dibromo-4,4'-dichloro-indigo) (Fig. 19a). However, the *E. coli* strain *ER2738* is not able to synthesise a functional *β*-galactosidase, as a subunit of the enzyme is defect due to a mutation (Δ(lacZ)M15). [152, 230] Therefore, the growing colonies of *ER2738* should appear transparent/colourless. In contrast, bacteria, infected by the M13KE-phage and its genetically modified progeny, are able to form a functional *β*-galactosidase *via* α-complementation, as the phage genome encodes a functional variant of the defect subunit (lacZα). [152, 226] Moreover, IPTG increases the protein biosynthesis of both subunits of the *β*-galactosidase, by deactivating the repressor of the lac operon. [229] Therefore, the colonies of infected bacteria on agar-plates which

containing X-gal and IPTG should turn blue *via* the formation of the indigo dye. [231, 232] Insufficiently or overly diluted phage suspensions yielded entirely blue or transparent plates, respectively, while sufficiently diluted phage suspensions yielded plates with well-defined blue colonies. Only blue phage colonies that grew on plates with ten to hundred well-defined colonies were chosen for sampling, as these were assumed to be derived from a single infected bacteria and respectively from a single phage.

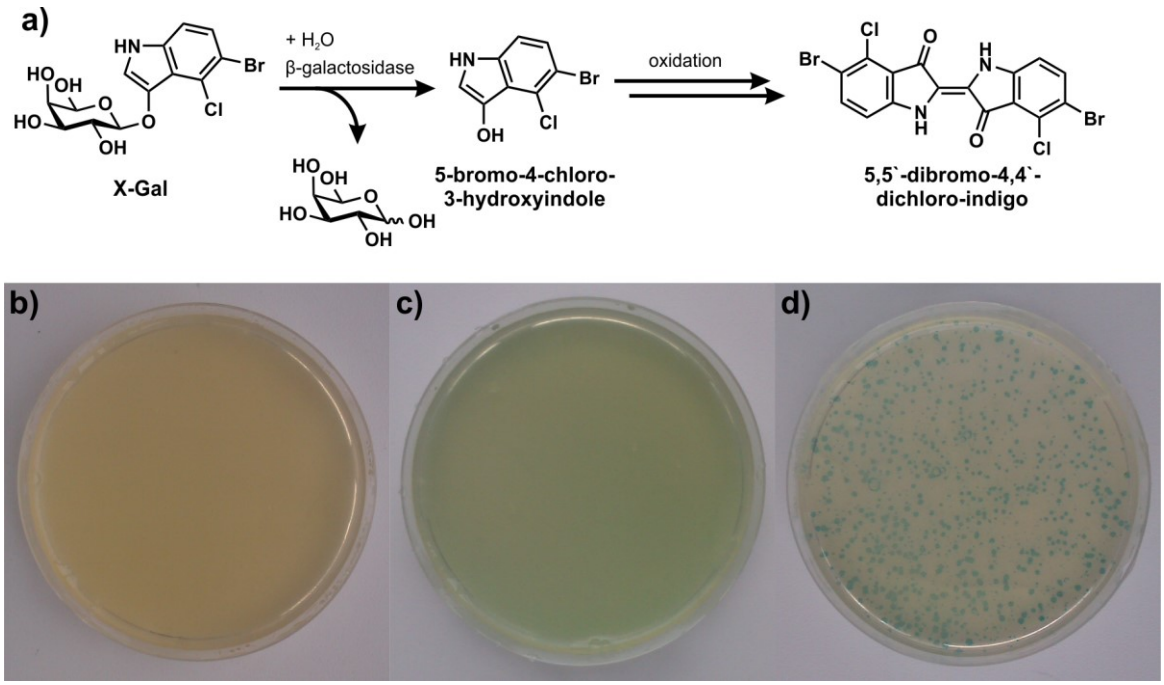

Figure 19a) Formation of the indigo dye (5,5'-dibromo-4,4'-dichloro-indigo). X-gal (5-bromo-4-chloro-3-indolyl-*β-D*-galactopyranoside) is hydrolysed under the influence of the *β*-galactosidase, yielding the indole compound (5-bromo-4-chloro-3-hydroxyindole), which in turn dimerises under oxidising conditions into the indigo dye. **b)** Dense, transparent lawn of uninfected *E. coli ER2738*, grown on an X-gal/IPTG plate. Only the yellowish background of the agar-plate is visible. **c)** *E. coli ER2738*, infected with the phage, grown on an X-gal/IPTG plate, visible as a continuous, blue bacterial lawn (appearing greenish because of the yellow background of the agar-plate). No separate colonies are observable. **d)** Diluted *E. coli ER2738*, infected with a diluted phage suspension, grown on an X-gal/IPTG plate. Here, distinct blue colonies are visible, which are surrounded by a transparent bacterial lawn.

These phage samples were separately amplified in small scale and subsequent isolation yielded phage suspensions derived from a single phage. Afterwards, the DNA of these single phage was extracted with TE-saturated phenol. [229, 233] The samples were checked by gel-electrophoresis and, if successful, an aliquot was prepared for sequencing by the addition of the 96-gIII primer (Appendix I). The actual sequencing was carried out at *StarSEQ® GmbH* (*Mainz*, Germany), using the modified Sanger-method with fluorescently marked didesoxy-nucleotides. [234, 235, 236] The resulting genomic data were processed *via* the Serial cloner software (V2.6.1, Serial Basics®) [237] yielding the peptide sequence. *Multiple*

Sequence Alingments (*MSA*) were carried out applying the *MEGA7* software (V. 7.0.21). [238]

Results and discussion

During the experiments on calcite`s {10.4}-facets both libraries, the heptapeptide and the dodecapeptide library, were applied. The procedures based on the manufacturer manual [152] and the preceding experiences in the Tremel group [77]. Both advised a biopanning comprising three to five individual cycles. Hence, the phage eluates were sampled for sequences during the third cycle. This was carried out first for the experiment with the dodecapeptide library and resulted in seven sequences with only low similarity as well as three coinciding sequences (Fig. 20). However, these coinciding sequences lacked the random peptide and the glycine linker. Since the phages were sampled from blue colonies on the IPTG/X-gal plates, a wild-type phage was ruled out as the source of this sequence. Instead, the sequence to attribute the original sequence of the M13KE-phage, on which the phage library is based (Fig. 20, cp. Appendix I).

N-	Ser	His	Ser	Ala	Glu	Thr	Val	Glu	***-C***
5`	TCT	CAC	TCG	CGG	GAA	ACT	GTT	GAA	***3`***
3`	AGA	GTG	AGC	GCC	CTT	TGA	CAA	CTT	***5`***

Figure 20) Depiction of coinciding peptide sequence identified during the experiments on {10.4}-facets of calcite. The sequence was identified as belonging to the M13KE-phage, on which the applied phage libraries are based. In the lower row, the sequenced data are shown, representing the (-)-strand (3`→ 5`). In the middle row, the corresponding (*)-strand is depicted (5`→3`) and in the upper row, the translated peptide sequence.

Hence, it was decided to carry out two additional cycles of affinity selection with the both libraries and to skip the sequence sampling during the third cycle in the experiment, which applied the heptapeptide library. The sampling during the fifth cycle yielded only sequences with low similarity for both libraries. During the biopanning with the dodecapeptide library, the sequence of the M13KE-phage was again repeatedly isolated (five in twenty samples). Since these results were not convincing, a sixth cycle was carried out with the dodecapeptide library. Since only sequences of low similarity were identified and the sequence of the M13KE-phage was more frequently identified (nine in twenty samples), the decision was made to stop further experiments with both libraries. The main reason for the decision was the increasing appearance of the M13KE-phage`s sequence. Since both libraries are directly derived from this phage by genetic modification, this phage should be

present in both libraries, though as a minor fraction of the overall population. However, this phage should possess a higher fertility in comparison to all phages, which carry the additional, *N*-terminal random peptide sequence. Thus, the increasing appearance of this sequence during the biopanning implied a selection, which was not driven by the affinity towards target, but by the fertility of the phage.

Still, we analysed the obtained peptide sequences to identify at least partially coinciding peptide sequences by *Multiple Sequence Alignments* (*MSA*). This was done separately for each library and each cycle. The alignment of the dodecapeptides that were identified during the third cycle showed the highest consensus with the sequence Ser - non-polar amino acid - Xxx_2 - (N/Q) - (K/R) (Fig. 21a). However, this possible motif was not observed in the alignments derived from the successive cycles. Meanwhile, the alignment of the heptapeptides found in the fifth cycle yielded only a single proline moiety as common motif.

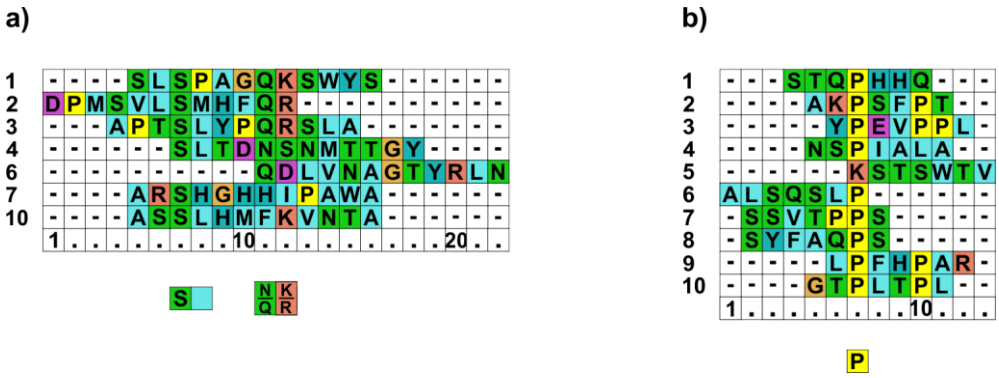

Figure 21) *Multiple Sequence Alignments* (*MSA*) **a)** *MSA* of the dodecapeptide sequences, identified during the 3rd cycle. Here, a possible consensus was observed, consisting of serine, a non-polar amino acid, asparagine/glutamine and lysine/arginine. Sequences encoding for the M13KE-phage were not included in the *MSA*. **b)** *MSA* of the sampled heptapeptide sequences during the 5th cycle. Here, the only conserved consensus was a single proline moiety. Used colour-code: G: **brown**, P: **yellow**, A, F, I, L, M, V, W: **light-blue**, Y, H: **blue**, S, T, Q, N: **green**, E, D: **pink**, R, K: **light-red**.

Additional alignments were carried out for all dodecapeptides as well as for all sequences. Nevertheless, the results of these alignments remained inconclusive and neither a repeated occurrence of single sequences nor a consensus sequence were observed.

The amino acid composition of specific cycles appeared slightly biased during the alignments. In particular, the proline content in all heptapeptides found during the fifth cycle seemed increased. Therefore, the amino acid composition was calculated for each cycle of biopanning and compared with the corresponding, expected probabilities of each amino acid. The expected probability of finding a

specific amino acid does not depend on the amount of different amino acids but on the total amount of all codons and the number of codons encoding a specific amino acid. The phage display libraries use a reduced codon set of 32 different codons instead of 64 codons for the randomised peptide sequence (cp. Appendix III). Additionally, the *ER2738* strain of *E. coli* translates the remaining stop-codon TAG as L-glutamine and hence all 32 codons are encoding. [152] Therefore, an amino acid is coded either by one, two or three codons, which results in the expected occurrence probabilities of 3.13%, 6.25% and 9.38%. Assuming a Poisson-distribution, the corresponding expectancy ranges for the amino acids were calculated to test the existence of the above-described bias in amino acid composition (Fig. 22, compare Appendix III). In this manner, a reduced level of arginine and the complete lack of any cysteine could be observed during every cycle of the biopanning, independent of the applied library. However, both observations are in accordance with the literature and are caused by the life cycles of the phage and its host. [167] Meanwhile, an increased fraction of polar amino acids (Ser, Thr, Asn) above the expectancy range was found in the third and fifth cycle in the biopanning with the dodecapeptide library (Fig. 22a, b). Meanwhile, the fraction of polar amino acids decreased in the sixth cycle (Fig 22c). Though an increased level of asparagine in phage libraries has been reported, [167] the overall increase in polar amino acids indicates the possibility that a weak target-based selection process had presumably taken place. Furthermore, the decrease of the polar amino acid in the sixth cycle coincides with the increased detection of the M13KE-phage. Thus, a weak, target-based selection mechanism was suspected, which had been outweighed by the selection for fertility during the sixth cycle. Simultaneously, the proline content was found to be strongly raised above the expectancy range in the sampled heptapeptides (Fig. 22d), which additionally suggested a successful, target-based selection. However, without the identification of a stable consensus sequence or the repeated detection of individual peptide sequences, it is difficult to distinguish between a target-based and a fertility-based selection mechanism for both biopannings and the respective, individual cycles. More sophisticated bioinformatics methods might give deeper insight. The observation of the M13KE-phage however, clearly indicates that the selection on {10.4}-facets of calcite was fertility-based.

Nevertheless, the considerations led to the conclusion that the biopannings on calcitic {10.4}-facets were unsuccessful. In consequence, the question arose, why the selection on a {10.4}-face of calcite was presumably weak, while the experimental conditions were comparable to the preceding works on vaterite nanoparticles [77].

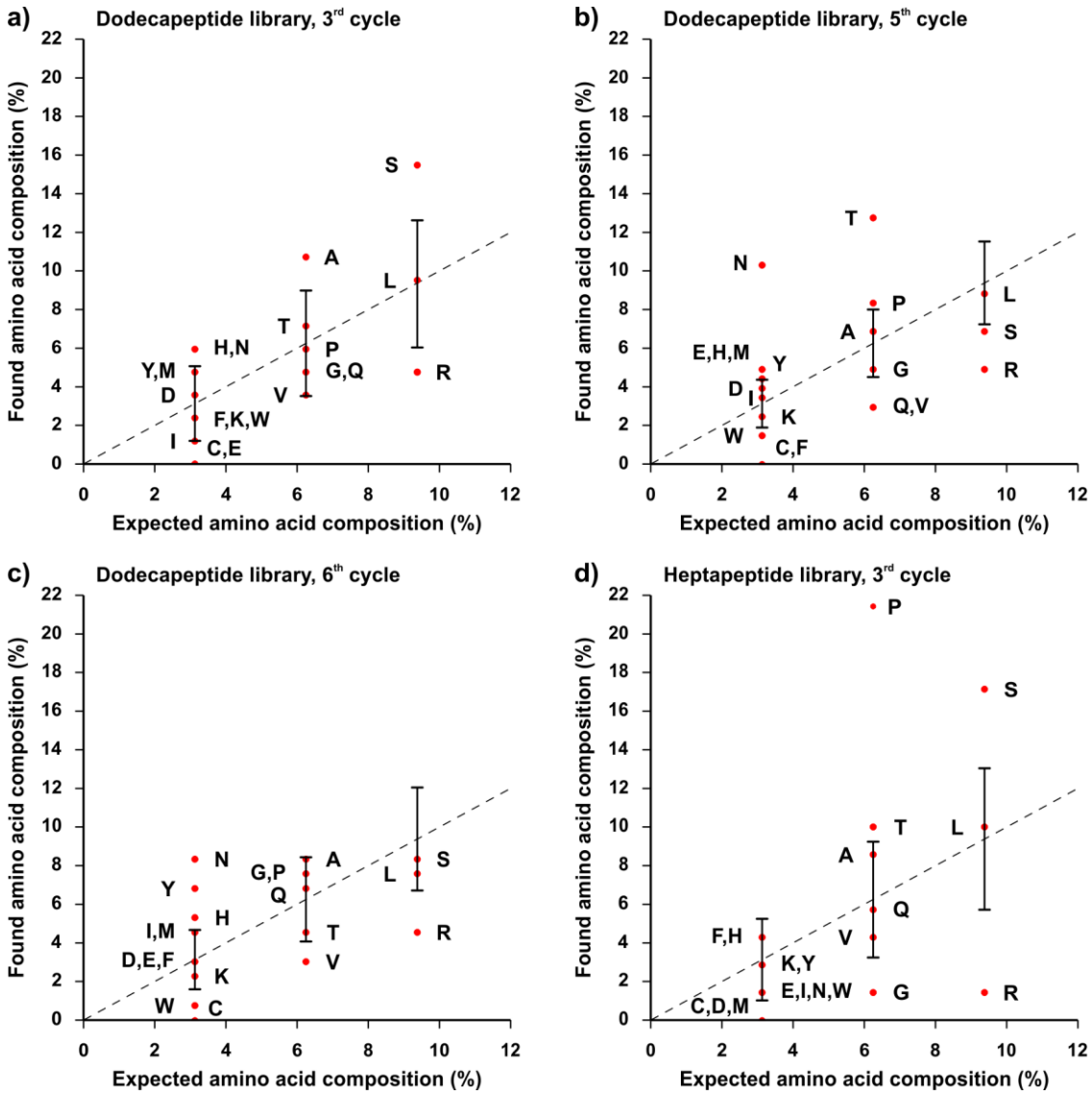

Figure 22) Plot of the observed amino acid composition (%) of all observed peptides during a specific cycle against the expected amino acid composition (%). The one-letter-code was used for all amino acids. The dashed line indicates the expected probability of observing a single amino acid. The standard-deviations are used to indicate an expectancy range for the corresponding expectancy, visualised by the black bars. The latter was calculated based on the corresponding sample sizes, while assuming a Poisson-distribution (cp. Appendix III). **a)** Dodecapeptide library, 3rd cycle. **b)** Dodecapeptide library, 5th cycle. **c)** Dodecapeptide library, 6th cycle. **d)** Heptapeptide library, 5th cycle.

Since phage display had already been proven successful during screenings on a large variety of materials, [239, 240] even in facet-selective manner, [185, 223] it appears improbable that the change of the polymorph caused the loss of selection. Meanwhile, changing the surface dimensions from a nanoscopic surface to a

macroscopic surface might result in the observed weak selection. As already explained, the basis of a phage display approach is the selection of random peptides by their corresponding interaction with a target structure. For a successful selection, all other interactions between the phage and the target need to be weaker than the aforementioned interaction. Still, further interactions besides those at the random peptide on the **pIII** capsid are possible between a target structure and the highly anisotropic M13-phage,[151] for example at the capsids **pVIII** and at the capsid pairs **pIX**/**pVII** and **pIII**/**pVI**. Though the M13-phage is small, its length of about 1 µm make it still considerably larger than a nanoparticle (Fig. 14b). Considering the possible interactions mentioned above with such a nanoparticle, it seems likely to assume that these interactions are of comparable strength and rather small (Fig. 23). In this scenario, the interaction of a random peptide with the nanoparticle can be the strongest interaction and hence it can be subsequently utilised for an affinity selection. On the other hand, considering the aforementioned interactions with a macroscopic surface larger than the phage (>> 1µm), the interaction of the **pVIII** with this surface is presumably the strongest. In this scenario, such an interaction could level off the interaction between the random peptide and the surface and would consequently disrupt the selection mechanism of the biopanning (Fig. 23).

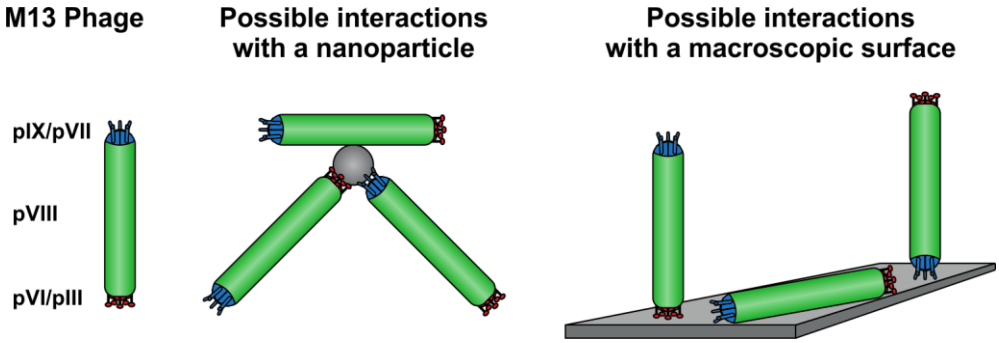

Figure 23) Schematic depiction of the M13-phage and its possible interactions *via* the capsid pVIII and the capsid pairs **pIX**/**pVII** and **pVI**/**pIII** with differently sized surfaces. As extreme cases for surfaces, a spherical nanoparticle and a macroscopic surface are depicted.

Hence, a potential explanation for the failed biopanning on calcite`s {10.4-facets} is the change from a nanoscopic target to a macroscopic one. Though this speculative hypothesis cannot be proven easily, it led to the decision to return to a nanoparticle-based affinity screening, which had already proven successful in the preceding work[77], whereas the idea of a facet-selective biopanning was abandoned.

Summary

The effort to identify peptide sequences of different length with polymorph-selective and facet-selective properties by affinity screenings on macroscopic, {10.4}-faceted calcite single crystals, was unsuccessful. Only one sequence was repeatedly identified during the third cycle of biopanning with the dodecapeptide library. The sequence belonged to the M13KE-phage, the genetic precursor of the phage library and was interpreted as a sign of a fertility-based selection. Furthermore, *Multiple Sequence Alignments* showed a small consensus for the dodecapeptides of the third cycle. This consensus did not reappear during subsequent cycles, while no consensus was observed in case of the heptapeptides. Additionally, the amino acid composition of the identified peptides showed a bias for specific amino acids, especially an increase of polar amino acids and of proline. Both, the results of the alignments and the amino acid composition, were interpreted as signs of a weak target-based selection. However, the appearance of the M13KE-phage inticated that the selection was mainly driven by the propagation of the phage and not by the affinity selection on the target.

Though only a hypothesis, the size of the target might have been the influencing factor for the unsuccessful affinity selection. Hence, it was decided to return to experimental conditions comparable to the preceding work [77] by utilising calcite nanoparticles as a screening target and to abandon the idea of a facet selective biopanning.

7.
Phage Display on Calcite Nanoparticles

Motivation

As described in the previous chapter, the first experimental approach of a phage display affinity screening on calcite had failed. The aim of this previous study was the identification of peptides by a phage display technique, which possess a selectivity towards {10.4}-facets of calcite crystallites. However, the resulting peptide sequences showed no coinciding sequences except of the sequence of the M13KE-phage, the genetic progenitor of the phage libraries. Still, hints on a consensus motif as well as a biased amino acid composition were observed, which indicated the possibility of a weak selection on the target. Though only a hypothetical explanation, the reason for these failed screening experiments might have been the comparably large size of the target surface. In contrast, a preceding work presented a successful approach to screen for polymorph-selective peptides on vaterite nanoparticles.[77] Taking the hints on the weak, target-based selection, the hypothetical target(-surface) size dependency and the successful, preceding work on vaterite nanoparticles[77] into account, an affinity screening on calcite nanoparticles appears promising. Hence, the idea to screen for peptides that possess affinity towards calcite {10.4}-facets was abandoned. Instead, a system for the selection of peptides that possess an affinity towards the surfaces of calcite should be developed on calcite nanoparticles, as to complement the results of the vaterite-selective peptides in the preceding work.

General Setup of the Phage Display on Calcite nanoparticles

For the full experimental procedure as well as the used materials and solutions, see Chapter 14. For the raw sequencing data and the *Multiple Sequence Alignments* (*MSA*), see Appendix IIb.

During the affinity selections on calcite nanoparticles, the identical phage libraries, i.e. the heptapeptide library (*Ph.D.-7*™) and the dodecapeptide library

(*Ph.D.-12*™), were used. The individual cycles of the biopanning were carried out according to the manual and the literature. [77, 152]

For the screening target, a sample of commercial calcite nanoparticles with an average diameter of 50 nm to 100 nm* (*Socal 31*) was obtained from *Solvay* (*Solvay Chemicals International*, *Brussels*, Belgium). The polymorph was confirmed by *X-ray Powder Diffraction*. Meanwhile, *TEM*-images suggested a broader distributed nanoparticle diameter (50-250 nm) (Fig. 24).

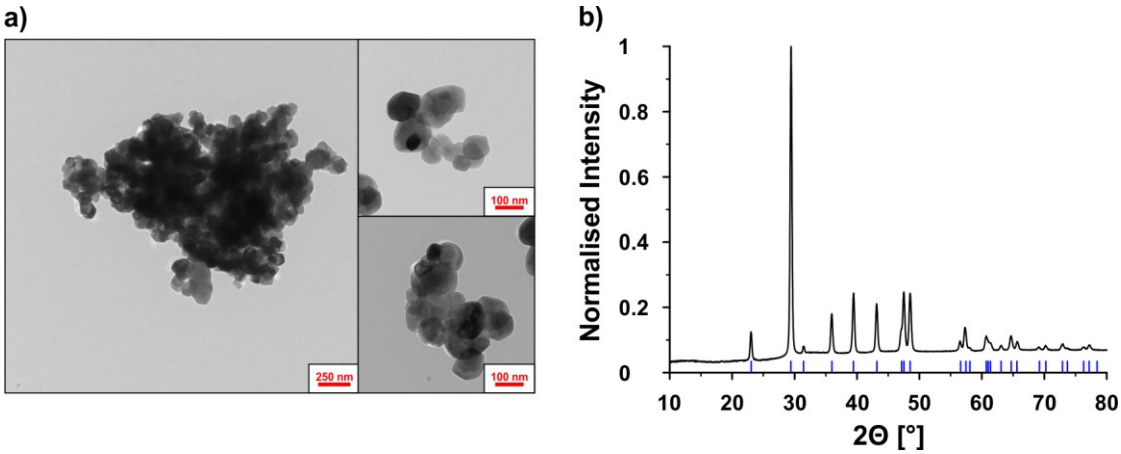

Figure 24a) *TEM*-images of the *Socal® 31* calcite nanoparticles showing a diameter ranging between 50 and 250 nm. Images provided by Dr. T. Schüler. **b)** X-ray powder diffractogram (XRPD) of the same nanoparticles, confirming calcite as the crystalline phase. Blue dashes indicate the reflex positions of the calcite reference. [140]

Since nanoparticles were used in the following biopanning experiments, additional centrifugation steps were required for precipitating the nanoparticles at the end of virtually all working steps (i.e. incubation-step, washings-steps, elution-steps,…). In preparation for an actual incubation step, the nanoparticles were dispersed at high concentration in TBS-T 0.1 in an ultrasonic bath. The suspensions were subsequently diluted and precipitated by centrifugation. After discarding the supernatant, the nanoparticles were redispersed in TBS and were ready for a subsequent incubation by a phage library.

During the conduction of the experiments, two different protocols were established. Both protocols only diverged from each other during the first cycle of the biopanning (Fig. 25). Protocol A included an additional elution step with 1 M $CaCl_2$ in TBS and an additional wash step with TBS-buffer at pH of 10, while the final elutions applied either a 0.1 M sodium acetate solution or a 0.1 M disodium

*: According to supplier information.

ethylenediaminetetraacetate solution. Afterwards, the eluates were amplified in *E. coli* and separately applied in the following iterative cycles. During these susbsequent cycles, only one eluent was applied (Fig. 25). Furthermore, the wash step with TBS (pH = 10) was not carried out during these cycles.

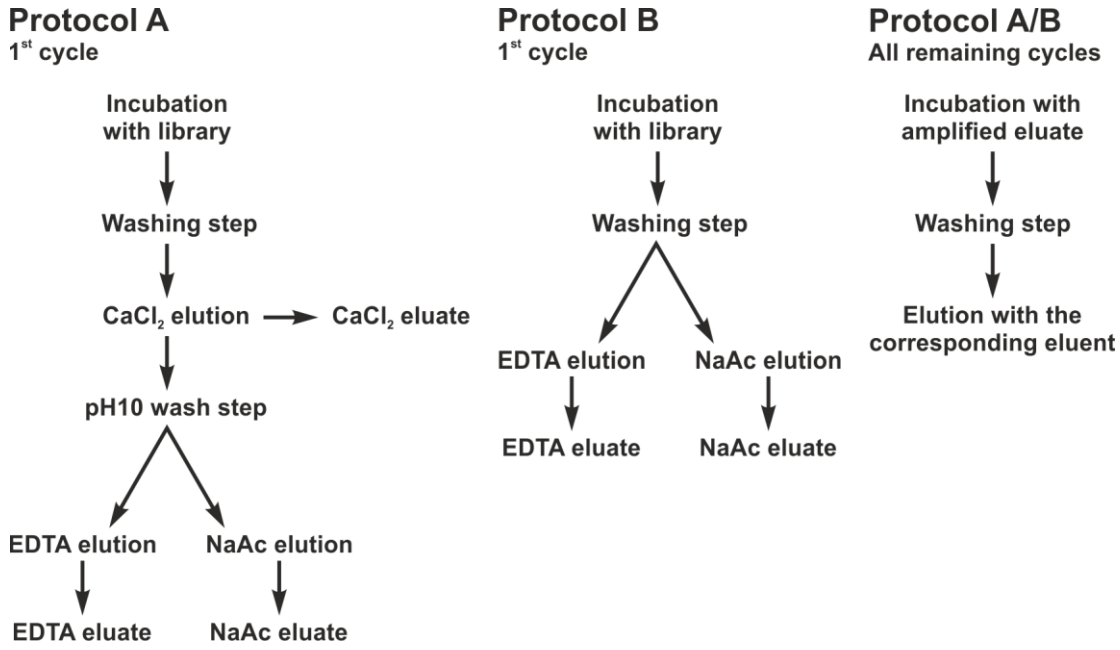

Figure 25) Schematic depiction of experimental protocols A and B.

Protocol A applied both, the random dodecapeptide library and the random heptapeptide library. In the biopanning utilising the dodecapeptide library, the peptide sequences were sampled after the third cycle, while in the biopanning with the heptapeptide library sequences were sampled from the first to the fifth cycle.

During the experiments, which applied this protocol, the additional wash and elution steps turned out unnecessary. Hence, these were abandoned in the shorter protocol B. In this protocol, the phages were eluted with either a 0.1 M sodium actetate solution or a 0.1 M disodium ethylenediaminetetraacetate solution. Nevertheless, protocols A and B were identical during the subsequent cycles. Protocol B was only applied with the random heptapeptide library. Sequences were sampled after the third round of biopanning. Apart from the differences described above, the procedures of the remaining working steps, e.g. the phage amplification or the sampling of sequences *via* the blue/white selection, were identical to the procedures described in the preceding chapter. However, it was necessary to samples sequences from amplified eluates or wash steps at certain points of the experiments. The corresponding procedures were identical to the general

sequence sampling, but the risk of identifying peptides, which were selected in a fertility-based manner, consequently increased.

Results and Discussion

Protocol A – Dodecapeptide Library

In the first experiment, protocol A was applied onto the calcite nanoparticles utilising the random dodecapeptide library. After the cycles of biopanning, only the two different sequences (**1**) and (**2**) were repeatedly indentified in all eluents (Tab. 1).*

Table 1) Dodecapeptide sequences identified during the biopanning on calcite nanoparticles. Peptides (**1**) and (**2**) were exclusively identified in all eluates of the third cycle, with peptide (**2**) representing the major proportion of the samples. (Number of overall samples: $CaCl_2$: 10, EDTA: 20; NaAc: 20). Peptide (**3**) was independently identified in the already amplified $CaCl_2$-eluate of the second cycle.

Peptide	$CaCl_2$	EDTA	NaAc	Sequence
1	4	6	7	***N*** Leu Gly Lys Thr Thr Ser Ala Gln Asn Leu Val Pro ***C***
2	6	13	13	***N*** Gln Asn Ser Thr Leu Asn Tyr Tyr Thr Leu Leu Arg ***C***
3	—	—	—	***N*** Gln Asn Ser Thr Thr Asn Tyr His Thr Leu Val Arg ***C***

In general, identifying individual sequences several times often indicates a successful selection, but identifying only two sequences in almost fifty samples was relatively uncommon. Furthermore, it was not possible to identify an underlying consensus motif by only two sequences. To ensure that these results were not caused by a fertility-based selection, further sequences were sampled in the already amplified eluates and wash suspensions of both preceding cycles.

The sequences (**1**) and (**2**) were not observed in the amplified eluates and amplified wash suspension of the first cycle. Instead, the sequence of the M13KE-phage was found, though in a smaller scale when compared to the preceding experiments on calcite`s {10.4}-facets. Apart from these observations, only unique sequences were identified. These results showed that the selection did not occur during the first cycle and that a fertility-based selection could not be excluded. In the samples of the second cycle`s eluates the peptides (**1**) and (**2**) were almost exclusively observed. The sole exception was peptide (**3**), a sequence with high similarity to peptide (**2**), differing only in three amino acids (Tab. 1). Comparing the

*: All three eluents together yielded fifty independent samples. Of the fifty samples, fourty-nine were successfully sequenced, exclusively yielding the sequences of peptides **1** and **2**.

nucleotide sequence of both peptides, apparently four nucleotides were diverging. A possible source for the differences in four nucleotides could have been an error during the sequencing procedure itself. However, these were only observed occasionally and hence the observation of four differing nucleotides in a short nucleotide sequence was not deemed an coincidence. Furthermore, the similarity between both peptides is even bigger when taking the functional groups of the differing amino acids into account. This was especially apparent in case of the exchanges of the aliphatic, sterically demanding leucine against valine (position 11) and the aromatic tyrosine against histidine (position 8) in peptide (**3**) (Tab. 1). The exchange of leucine against threonine (position 5) in peptide (**3**) is not as obvious as the former two, as it is an exchange from an aliphatic to a polar amino acid. Still, both are sterically demanding.

Only three different peptides were identified during the second cycles while the peptides that had been identified in the first cycle, possessed only unique sequences. Hence, it was concluded, that the selection had taken place during the second cycle. This conclusion was additionally supported by the absence of the M13KE-phage`s sequence during the second cycle, as this additionally implied a possible target-related selection. Furthermore, as the peptides (**2**) and (**3**) were highly similar, it was concluded that the selection of both sequences was target-based. Additional similarities between peptides (**1**) and (**3**) were observable (Tab. 1), which lead to the assumption, that the selection peptide (**1**) was target-based as well. During the preceding experimental approach on {10.4}-facets of calcite, high amounts of polar amino acids had been observed during the biopanning on {10.4}-facets of calcite, which were interpreted as a sign of a weak target-based selection. This interpretation is supported by the high portion of polar amino acids in the three dodecapeptides ((**1**): 50%, (**2**): 75%, (**3**): 83%). In reverse, this supports the conclusion, that the selection of these three peptides was target-based as well. Nevertheless, a relatively large quantity of publications report identical peptide sequences that were identified on entirely unrelated screening targets. Some of these repeatedly identified peptides are presumed to interact with parts of the selection system (e.g. polystyrene), while other peptide sequences are supposed to be related to the propagation in *E. coli*. [241] In a database for published, target-unrelated peptides, *SAROTUP* [242, 243], all three peptides were tested, but no

matching sequences were found. Two additional databases comprising published peptide sequences from various affinity selections, the *Biopanning Data Bank* [242, 243, 244] and *PepBank* [245, 246], were searched for the structural similarities. These database searches turned out negative as well.

A final comparison with the literature was conducted by the *Protein-Protein Basic Local Alignment Search Tool* (*BLASTp*) [247, 248] of the *National Centre for Biotechnology Information* (*NCBI*, *Bethesda*, US-MD). Here, the sequences were compared and aligned with a multi-species database consisting of known protein sequences and translated gene sequences. However, no putatively conserved domains were found. The highest scoring-values did not exceed the value of 40. This was further supported by the E-values, which did not decrease below 9. Hence, no similar sequences were observed in the known protein/DNA-sequences. This was expected, as the random peptide libraries per definition display sequences that are unrelated to the evolutionary development of proteins. On the other hand, these results, in combination with the negative results in the above-described databases, suggested that the peptides (**1**), (**2**) and (**3**) were unique, unreported sequences.

In summary, this first biopanning study on calcite nanoparticles by the dodecapeptide library repeatedly yielded the peptide sequences (**1**) and (**2**), while the nature of the chosen eluents had no influence. Furthermore, sequence (**3**) was identified, which possessed a high similarity to sequence (**2**) and to a lesser extent to sequence (**1**). The similarity of the sequences, the repeated identification and the searches in different databases suggest that these peptides had been selected in a target-based manner. Hence, this first biopanning on calcite nanoparticles was considered successful.

Protocol A – Heptapeptide Library

The experiences during the prior application of protocol A with the dodecapeptide library lead to the decisions to sample peptide sequences during every cycle of the biopanning and to refrain from the elution-series by the 1 M $CaCl_2$-solution. However, the corresponding elution step during the first cycle should be maintained as a wash step.

While applying this modified protocol A, no coinciding sequences were identified during the first three cycles. Hence, two additional rounds of biopanning were conducted and sequences were sampled after the fifth cycle. Here, one sequence (*N*-LPLTPLP-*C*) was repeatedly identified during the elution with 1 M NaAc. All sequences identified during this trial were compared in *Multiple Sequence Alignments*, but no consensus motifs were observed. Furthermore, the repeatedly identified peptide sequence was compared with the literature and the above mentioned databases. In all these resources, the sequence had already been described. While the literature [241] states that this peptide had been reported more than ten-times, the *Biopanning Data Bank* (*BDB*) [242, 243,244] lists 25 different reports that include the structure. Furthermore, the *SAROTUP* database [242, 243] suggested that the sequence is target-unrelated.

In summary, the biopanning on calcite nanoparticles only yielded one heptapeptide sequence (*N*-LPLTPLP-*C*) after five instead of three planned cycles. However, after consulting the literature and several databases, this heptapeptide was assumed to be a target-unrelated sequence. Hence, this biopanning study on calcite nanoparticles was considered unsuccessful and it was decided to repeat the affinity selection experiment with a simplified biopanning procedure.

Protocol B – heptapeptide library

In the prior biopanning, the affinity selection on calcite nanoparticles with the heptapeptide library following protocol A failed. However, it was decided to repeat the affinity selection with a simpler protocol, as the aim of identifying peptides with an affinity towards calcite remained. For this simpler protocol B, the wash step utilising TBS-buffer at pH 10 and the elution by 1 M $CaCl_2$ were entirely discarded, while only the separate elution steps by 0.1M NaAc and 0.1M EDTA were retained. Furthermore, the sequences were to be sampled after the third cycle of the biopanning.

During the sampling, peptide sequence (**4**) was identified almost exclusively (Tab. 2). Furthermore, it`s identification was independent of the eluent. The sole exception was the singular identification of peptide (**5**) (Tab. 2). The selection of these two peptides clearly indicated that a selection had been achieved, thus further cycles of biopanning were not necessary. However, it was not possible to

determine the cycle, during which the selection took place. Hence, sequences were sampled in the already amplified eluates and wash suspensions of the previous cycles. In the wash suspensions of the third round and in the eluates of the second round, only the sequences of the peptides (**4**) and (**5**) were observable. Again, this observation was independent of the eluent. Meanwhile, the amplified wash suspensions of the second cycle were each composed of unknown, unique sequences. Therefore, it was concluded that the selection of the peptides (**4**) and (**5**) took place during the second cycle of the affinity selection. This conclusion resulted in the additional decision to stop further sampling of sequences.

Table 2) Heptapeptide sequences identified during the biopanning on calcite nanoparticles. Peptide (**4**) was identified almost exclusively in all eluates of the third cycle (overall samples: EDTA: 20; NaAc: 20). Peptide (**5**) was identified only once during the elution with 0.1 M NaAc.

Peptide	EDTA	NaAc	Sequence
4	20	19	***N*** Trp Thr Asn Asp Pro Asp Leu ***C***
5	0	1	***N*** Val Ile Pro His Val Leu Ser ***C***

Sequence (**4**) mainly consisted of polar amino acids, notably aspartic acid and its derivative asparagine, while sequence (**5**) was mostly composed of amino acids with hydrophobic, sterically demanding side chains, i.e. valine, leucine and isoleucine (Tab. 2). Thus, both sequences displayed no similarities. Additional *Multiple Sequences Alignments* of both sequences with all sequences found during this experiment displayed no consensus. Still, it was not possible to discern between a target-based or fertility-based selection. Therefore, both sequences were compared in the same databases (i.e. *SAROTUP* [242, 243], *Biopanning Data Bank* [242, 243, 244], and *PepBank* [245, 246]), as had been done during the prior experiments. The comparisons with sequence (**4**) yielded no matches. In contrast, the *Biopanning Data Bank* [242, 243, 244] yielded one publication [249] for the minor peptide (**5**), which reported the identification of this sequence during an affinity selection study on subtypes of glycine-receptors. Additionally, both peptides had already been identified during a phage display study on calcium oxalate monohydrate nanoparticles. [250] In similarity to the present experiment, peptide (**4**) was identified as the major peptide and peptide (**5**) only as a minor peptide. Additionally, this study went further on and tested peptide (**4**) for an additive-like influence during the crystallisation of calcium oxalate. This test was unsuccessful and peptide (**4**) possessed no observable influence on on the crystal polymorph

and morphology of calcium oxalate. The identification of peptide (**5**) on the two extremely diverging screening targets led to the assumption that it had been selected by a target-unrelated mechanism. Meanwhile, the similarity between the screening targets calcium oxalate and calcium carbonate implied that peptide (**4**) had been selected by a target-based mechanism. However, because of its reported inactivity during the crystallisation of calcium oxalte, peptide (**4**) was assumed to be likewise inactive during crystallisations of calcium carbonate. Hence, further experimental trials would have been necessary to select heptapeptides on the calcite nanoparticles. However, the observed difficulties during the affinity selections dissuaded from further experiments. Instead, it was decided to concentrate on the successfully selected dodecapeptides.

Summary

The main objective of this biopanning approach was the identification and subsequent testing of peptides for a calcite-selective influence on the polymorph composition during the crystallisation of calcium carbonate. In the previous chapter, a first experimental trial is described, which had a narrower scope on screening for peptides that possess an affinity for the {10.4}-facets of calcite. As these experiments failed, the scope was widened again, by screening on calcite nanoparticles for peptides with a general affinity for calcite surfaces. In the context of this broadened focus, several affinity selections were carried out on calcite nanoparticles. In a first experiment, which followed protocol A with the dodecapeptide library, the peptide sequences (**1**), (**2**) and (**3**) were successfully identified (Tab. 1).

Table 3) Summary of all peptide sequences identified during the affinity selections on calcite nanoparticles.

Peptide	Sequence
1	***N*** Leu Gly Lys Thr Thr Ser Ala Gln Asn Leu Val Pro ***C***
2	***N*** Gln Asn Ser Thr Leu Asn Tyr Tyr Thr Leu Leu Arg ***C***
3	***N*** Gln Asn Ser Thr Thr Asn Tyr His Thr Leu Val Arg ***C***
4	***N*** Trp Thr Asn Asp Pro Asp Leu ***C***
5	***N*** Val Ile Pro His Val Leu Ser ***C***

The exceptionally high similarity between the most frequently observed peptide (**2**) and peptide (**3**) suggested a target-based selection. This assumption was

supported by both peptides being unreported in the literature. In addition, as peptide (**3**) possessed some similarity to peptide (**1**) and it could be deemed a structural link between the sequences (**1**) and (**2**). Furthermore, peptide (**1**) was not reported in the literature and thus, the selection of peptide (**1**) was likewise deemed target-based. In contrast to this successful application of protocol A, a first study with the heptapeptide library with a shortened protocol was not successful. Here, only one sequence (*N*-LPLTPLP-*C*) was identified repeatedly, which has already been reported several times in the literature for a diverse set of screening targets. Hence, it was concluded, that this peptide was selected in a target-unrelated manner. Together with the lack of further peptides with coinciding sequences or consensus motifs, this study was assumed unsuccessful and it was decided to repeat the affinity selection by the heptapeptide library with a further simplified protocol. This consideration yielded protocol B, which was used for a further biopanning with the heptapeptide library. This biopanning almost exclusively yielded peptide sequence (**4**) and an extremely minor fraction of peptide (**5**), which both shared no similarities (Tab. 3). However, both peptides had been already reported in the literature. The minor peptide (**5**) had been reported on diverging targets [249, 250] and hence it was assumed that its selection was target-unrelated. Meanwhile, only one literature report [250] described peptide (**4**). In this report, calcium oxalate monohydrate had been utilised as the target of the affinity selection. Since this target shared some similarity to calcite, it was assumed that the selection of peptide (**4**) was target-based. This detail lead to the conclusion, that the biopanning on calcite nanoparticles by the heptapeptide library was successful. However, the very same report detailed that peptide (**4**) displayed no influence during crystallisation experiments of calcium oxalate. This observation dissuaded from synthesising peptide (**4**) for up-coming crystallisation experiments. Furthermore, the difficulty of selecting peptides in a target-related manner dissuaded from carrying out further biopanning experiments. Instead, it was decided to concentrate on the syntheses of the successfully identified dodecapeptide (**1**), (**2**) and (**3**) with the aim of making these peptide structures accessible for future crystallisation experiments.

8.
Solid Phase Peptide Syntheses

Motivation

Reports of peptides and proteins, which influence the crystal polymorph and/or morphology, are common in the field of biominerals and biomineralisation. [1, 2, 46] Yet, the isolation and identification of such compounds from biological sources is laborious and complicated. [30] In contrast, peptides could also be identified in biomimetic approaches, e.g. *via* affinity selections by phage display. After a successful identification by phage display, such peptides are synthetically accessible *via Solid Phase Peptide Synthesis* (*SPPS*). This overall approach has been carried out in a previous work on vaterite nanoparticles and yielded peptides, which influenced the polymorph composition during the crystallisation of calcium carbonate towards vaterite. [77, 78] To complement the results on vaterite, it was decided to carry out affinity selections on the calcite polymorph of calcium carbonate to identify peptides with a calcite-selective influence. As described in the previous chapter, these phage display experiments on calcite nanoparticles successfully yielded three different dodecapeptide sequences, which were presumed to be selected in a target-based manner. To test these peptides for their ability to influence crystallisations of calcium carbonate, a synthetic access to these structures was necessary. For this synthesis, the *Solid Phase Peptide Synthesis* (*SPPS*) was chosen. More specifically, the automated Fmoc *Solid Phase Peptide Synthesis*, a modified variant of the *Merrifield* approach [251, 252], was selected. Since the chosen peptides were *C*-terminally linked to the larger **pIII** capsid moiety, the synthesis should be arranged in a manner, as to synthesise the *C*-terminal peptide-amides for a closer resemblance to the peptide in/on the phage.

General setup of the Fmoc-Solid Phase Peptide Synthesis

For the full experimental procedure, the characterisation of compounds and the used materials and solutions, see Chapter 15. For *NMR*-spectra and chromatograms, see Appendix IV.

In principle, peptide syntheses can be carried out in solution phase. Nevertheless, synthesis of longer peptides in solution becomes very tedious, as the reaction products need to be isolated after every reaction step. In contrast, solid phase synthesis, first introduced by *Merrifield* [251, 252], simplifies the peptide synthesis, as it reduces most of these isolation steps to mere wash steps. This is achieved by chemically linking the *C*-terminal amino acid`s carboxyl group to a polymer resin. As additional consequence, the protective group for the carboxylic groups at the *C*-terminus of a peptide chain becomes obsolete and thus, the requirements on protective groups are mitigated. However, the link of the *C*-terminal amino acid reverses the direction of peptide synthesis in comparison to the protein biosynthesis. By this approach, the synthesis of long peptides is possible, as exemplified by *Merrifield's* synthesis of bovine insulin. [253] Based on *Merrifield's* solid phase approach, different synthesis strategies have been developed, which primarily differ in the application of different protective groups and their respective chemistry.

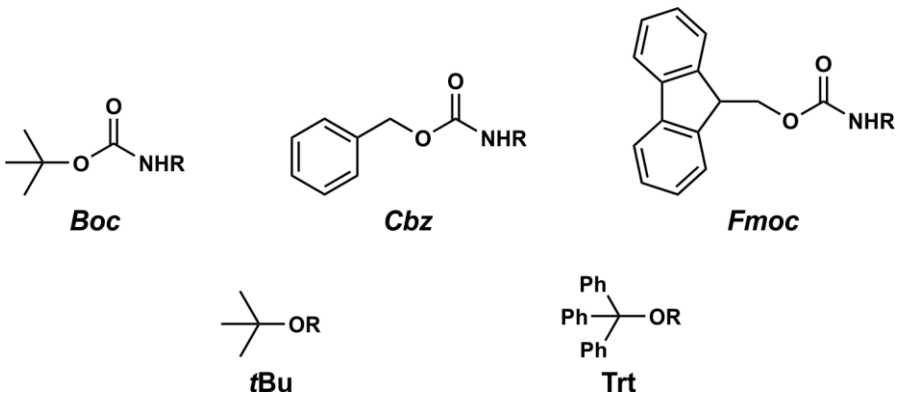

Figure 26) Different protective groups for amino acids. Upper row: Protective groups for amino functions: the acid-labile *Boc*-group, the *Cbz*-group and the base-labile Fmoc-group. Lower row: Protective groups for other functional groups. The *t*Bu-moiety can be utilised for the protection of carboxyl- and hydroxy groups. The triphenylmethyl-group (Trt) can be utilised for the protection of amides and thiols.

Of these synthesis strategies, the Fmoc *SPPS* strategy was chosen. This strategy relies on the base-labile (9*H*-fluoren-9-yl)-methoxycarbonyle (Fmoc) protective group [254, 255] as the temporary protective group of the *α*-amino functional group

instead of the more common, acid-labile *tert*.-butyloxycarbonyl (Boc) protective group [256, 257] (Fig. 26). Furthermore, this strategy allows the utilisation of acid-labile protective groups (e.g. the Boc-, the triphenylmethyl- (Trt) or *tert*.-butyl group (*t*Bu)) as fully orthogonal protective groups for the sidechain functional groups of the amino acids. In turn, the Cbz- and benzyl groups become obsolete (Fig 26).

In general, *SPPS* is executed in consecutive cycles (Fig. 27). During each cycle, a new amide bond is generated and the growing peptide chain is elongated. This can be conducted either with single amino acids or with whole (oligo-)peptides. During the first step of every cycle, the *N*-Fmoc protected amino function needs to be deblocked to enable the subsequent generation of an amide bond (Fig. 27).

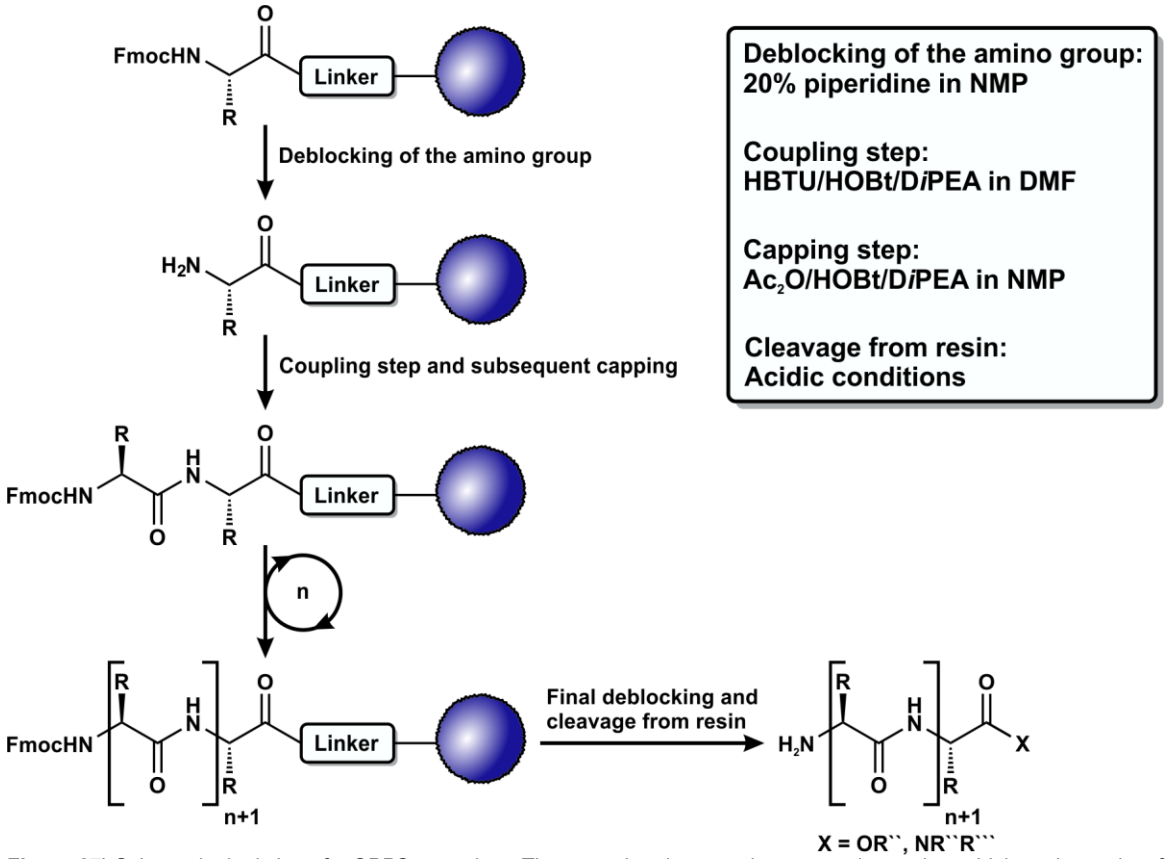

Figure 27) Schematic depiction of a *SPPS* procedure. The procedure is set up in consecutive cycles, which each consist of a deblocking step, a coupling step and a capping step. After a number of cycles, which corresponds to the length of the synthesised peptide, the *N*-Fmoc group is removed and the peptide is cleaved from the resin. In general, this cleavage step is carried out under acidic conditions. Depending on these conditions, either protected or fully deprotected peptides are available. Furthermore, depending on the linker between the *C*-terminal amino acid and the resin, different derivatives of the carboxyl group are available, e.g. amides or esters.

As already described, the Fmoc moiety is base-labile and it can be cleaved from an amino group under basic conditions. In general, this is carried out with a solution of 20% piperidine in DMF. This deblocking reaction follows an E_1cb-mechanism [258]. Furthermore, the cleaved dibenzofulvene additionally forms an adduct with an

excess of piperidine [255]. This dibenzofulvene-piperidine adduct is advantageous, because it can be photometrically measured at a wavelength of 301 nm. This can be utilised for reaction control of the ongoing peptide synthesis (Fig. 28).

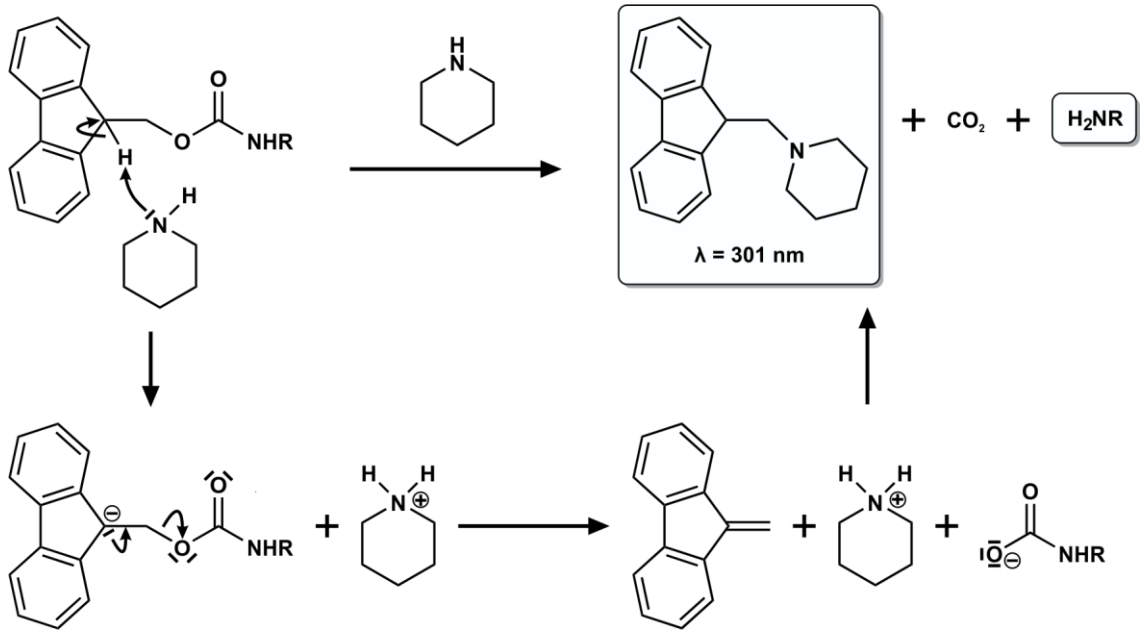

Figure 28) The deblocking reaction of a Fmoc-protective group from an amino group. In a first step, the base, in general piperidine, abstracts the proton at the carbon atom in adjacency of the aromatic systems, forming an aromatic anion. Subsequently, this aromatic anion dissociates into the dibenzofulvene and the carbamoylated amino-group. The latter further dissociates into the free amine and carbondioxide. In addition, the dibenzofulvene forms an adduct with the excess of piperidine, which can be monitored at a wavelength of 301 nm.

The main step during a cycle of *SPPS* is the actual generation of the new amide bond (Fig. 27). This is primarily carried out in two separate reactions. Initially, the free carboxyl group of the *N*-Fmoc protected amino acid which is to be introduced into the growing peptide chain, is converted into an active ester. The active ester derivative is often introduced by the reaction of the free carboxyl group with *N,N'*-dicyclohexylcarbodiimide (DCC) (Fig. 29). Usually, the reaction is carried out in the presence of catalysts such as 1-Hydroxybenzotriazole (HOBt) [259] or 1-Hydroxy-7-azabenzotriazole (HOAt) [260], yielding the intermediary formation of the respective benzotriazolyl active esters (Fig. 29). These benzotriazolyl-catalysts are advantageous, as their corresponding active esters are less prone to racemisation and form the respective amides at a higher reaction rate. However, a significant problem of the application of DCC is the formation of the corresponding *N,N´*-dicyclohexylurea, which is insoluble in many solvents used during peptide syntheses.

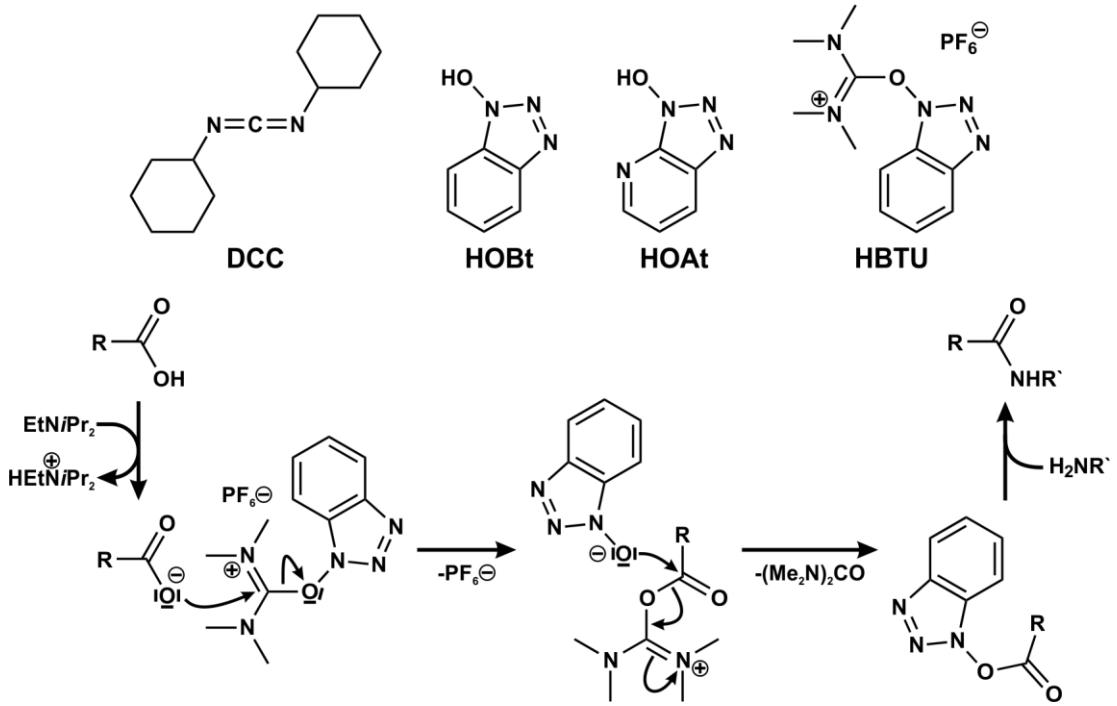

Figure 29) Upper row: Different coupling reagents applied for the formation of active esters (DCC, HBTU) and additionally applied benzotriazolyl catalysators HOAt and HOBt. **Lower row:** Mechanism for the formation of a benzotriazolyl active ester with the uronium salt coupling reagent HBTU. After a fast deprotonation of the amino acid`s carboxyl group, the carboxylate nucleophilically attacks the positivated carbon of the uronium salt, yielding the uronium salt of the amino acid. In turn, the released benzotriazolate nucleophilically attacks the carbonyl carbon of the amino acid-uronium salt in a second step. This reaction yields the corresponding benzotriazolyl active ester and the soluble tetramethylurea. In a last step, the subsequent formation of a new amide bond by the reaction of the benzotriazolyl ester with an amine can take place.

To circumvent this problem, uronium/aminium salts coupling reagents, such as *O*-(benzotriazol-1-yl)-*N,N,N′,N′*-tetramethyluronium hexafluorophosphate (HBTU) can be utilised [261, 262], as these form soluble reaction products, which can be simply washed from the resin after the coupling reaction (Fig. 29). Finally, in a second reaction, the active ester compound forms a new amide bond with the growing peptide chain`s free amino group on the resin (Fig. 29). In the automated solid phase peptide synthesis with the Fmoc protective group, uronium/aminium salts, such as HBTU 261, are standard reagents. During difficult coupling reactions, stronger reagents based on HOAt (Fig. 29) can be utilised, i.e. *O*-(7-azabenzotriazol-1-yl)-*N,N,N′,N′*-tetramethyluronium hexafluorophosphate (HATU) [260]. *

In general, the coupling reactions during the synthesis of peptides are required to be very effective, as to result in nearly quantitative yields. Still, a number of free amino functions remain after a coupling step. These free amino groups could

***:** More reactive phosphonium salts, such as benzotriazol-1-yl-oxytris(pyrrolidino)-phosphonium hexafluorophosphate (*PyBOP*) [325], are available as well.

partake in subsequent coupling reactions and thus result in additional peptides with erroneous sequences. The later isolation of the desired peptide would be impeded by these undesired peptides. To prevent the formation of such erroneous sequences, the coupling step is followed by a capping step, during which those amino functions are acetylated (Fig. 27). This is carried out by treating the resin with a solution of acetic anhydride (Ac_2O), HOBt and D*i*PEA in *N*MP. This capping step concludes a consecutive *SPPS* cycle and the next elongation cycle can be started by deblocking the next *N*-Fmoc protected amino function.

Instead of the divinylbenzene/styrene copolymer resin developed by *Merrifield* [251, 263] it was decided on applying a *Tentagel*® resin. [264] These resins consist of a similar divinylbenzene/styrene copolymer core, yet the chloromethyl linker moieties are replaced by polyethylene glycol (PEG) units (Fig. 30). [265, 266] This is advantageous, as the PEG units allow a stronger swelling of the resin in polar solvents such as DMF and *N*MP, which yields higher diffusion rates and enhanced reaction kinetics. [267]

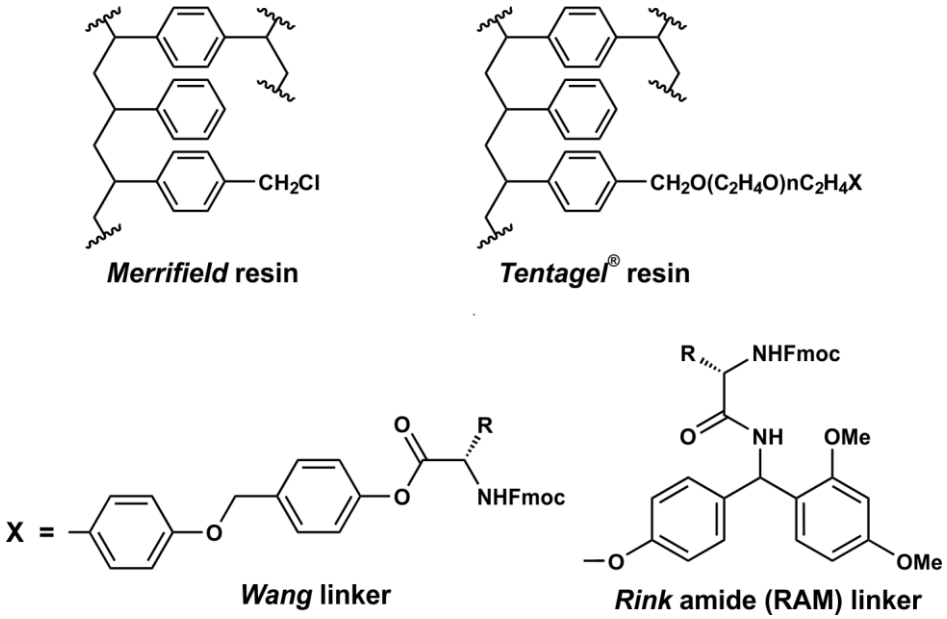

Figure 30) Structure of the styrene/divinylbenzene copolymer resin developed by *Merrifield* [251] for Solid Phase Peptide Syntheses. The chloromethyl unit is used to attach the *C*-terminal amino acid to the resin. The *Tentagel*® resins [264] still rely on a styrene/divinylbenzene core, but the chloromethyl is replaced by a polyethylene glycol (PEG) unit, which increases the swelling properties of the resin. [265, 266] Furthermore, the PEG unit carries the linker moiety (**X**). The standard linker in Fmoc *SPPS* is the *Wang* linker [268], which yields peptides with a free *C*-terminal carboxylic group after the cleavage reaction. Alternatively, the *Rink* amide (RAM) linker can be applied to yield *C*-terminal peptide amides.

The PEG units are functionalised by a linker moiety for the attachment of the *C*-terminal amino acid. This linker moiety can be chosen from a broad range to adapt to the specific target sequence. For instance, the acid labile *Wang* linker [268]

is applied in standard syntheses to generate fully deprotected *C*-terminal peptide acids. As we aimed to achieve the highest possible resemblance of the synthesised peptides to the fusion peptides in the phages, we decided on synthesising the corresponding *C*-teminal peptide amide structures. A linker for the synthesis of such a *C*-terminal peptide amide is the equally acid labile *Rink* amide linker (Fig. 30). 269 Thus, it was decided to utilise a *Rink* amide linker on a *Tentagel*® resin for syntheses of the peptide sequences (**1**), (**2**) and (**3**). For the syntheses, automated peptide synthesizer (*Perkin-Elmer ABI 433a*, *Applied Biosystems*® (*Thermo Fisher Scientific*, *Waltham*, US-MA)) was chosen, applying a standard synthesis protocol for the Fmoc *SPPS* chemistry (*FastMoc 0.1*).

Results and discussion

As shown in the preceding chapter, five different peptides sequences had been identified during affinity selection experiments by phage display with two differing peptide libraries. Three of these sequences were selected from a commercial, random dodecapeptide library (*Ph.D.-12*™), while two sequences were selected from a commercial, random heptapetide library (*Ph.D.-7*™). However, the heptapeptide (**5**) had already been reported during selections on strongly diverging target structures [249, 250] and sequence (**4**) had tuned out without influence during crystallisation in a similar study [250]. Hence, the synthetic efforts focused on the sequence (**1**), (**2**) and (**3**) (Tab. 4).

Table 4) Sequences of peptides (**1**), (**2**) and (**3**) identified during the prior affinity selection on calcite nanoparticles.

Peptide	Sequence
1	***N*** Leu Gly Lys Thr Thr Ser Ala Gln Asn Leu Val Pro ***CONH$_2$***
2	***N*** Gln Asn Ser Thr Leu Asn Tyr Tyr Thr Leu Leu Arg ***CONH$_2$***
3	***N*** Gln Asn Ser Thr Thr Asn Tyr His Thr Leu Val Arg ***CONH$_2$***

The synthesis of sequence (**1**), was carried as described above. The scale of the synthesis was set to 0.1 mmol, in accordance with the above mentioned *FastMoc 0.1* protocol, and for each coupling step, 10 equivalents (*eq.*) of the corresponding *N*-Fmoc-protected amino acids were used (Fig. 31). After preparative *HPLC*, the synthesis yielded 36% of peptide (**1**).

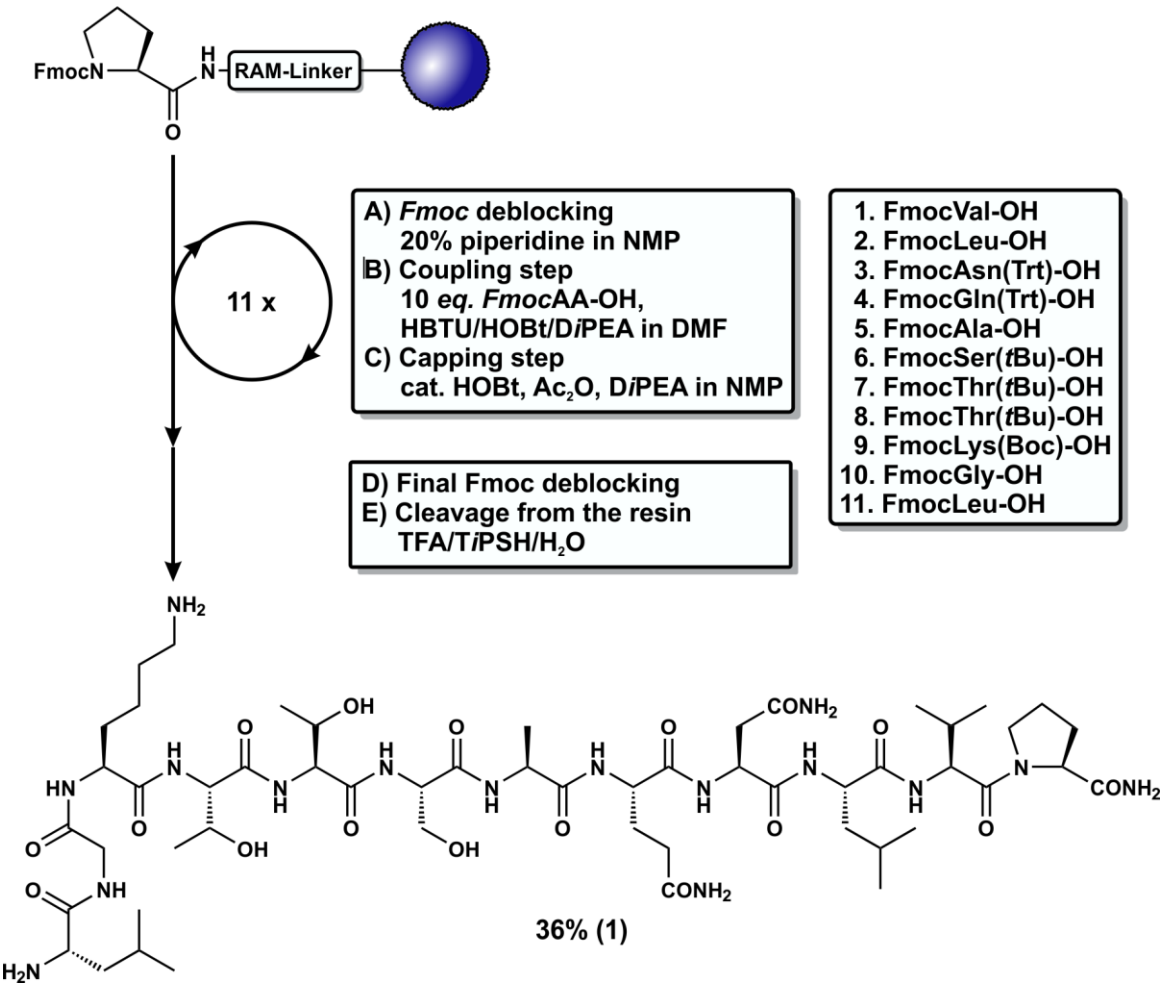

Figure 31) Schematic depiction of the synthesis of peptide (**1**). The coupling cycles were carried out in accordance to the above described procedure. Cleavage of the peptide from the resin was carried out under acidic conditions. Additionally, triisopropylsilane (TiPSH) was added as a reducing agent to prevent sidereactions of protective group`s fragments (e.g. *t*-butyl- or trityl-cations).

Meanwhile, the synthesis of sequences (**2**) and (**3**) was not straightforward. Both syntheses were carried out according to the general procedure. Prior to the product isolation by preparative *HPLC* however, *ESI*-mass spectra of each crude compound displayed two sets of mass-to-charge-ratios (*m/z*). For both peptides, the corresponding mass-to-charge-ratios of the expected quasi-molecular ions $[M+H]^+$ were observable (i.e., *m/z*: 1484.82 and *m/z*: 1432.82 for (**2**) and (**3**), respectively). These quasi-molecular ions were accompanied by additional mass-to-charge-ratios, which each were lower by 17.03 units (i.e., *m/z*: 1467.79 and *m/z*: 1415.78 for (**2**) and (**3**), respectively) (Fig. 32). The loss of 17.03 units was interpreted as a loss of ammonia and an intramolecular reaction was suspected.

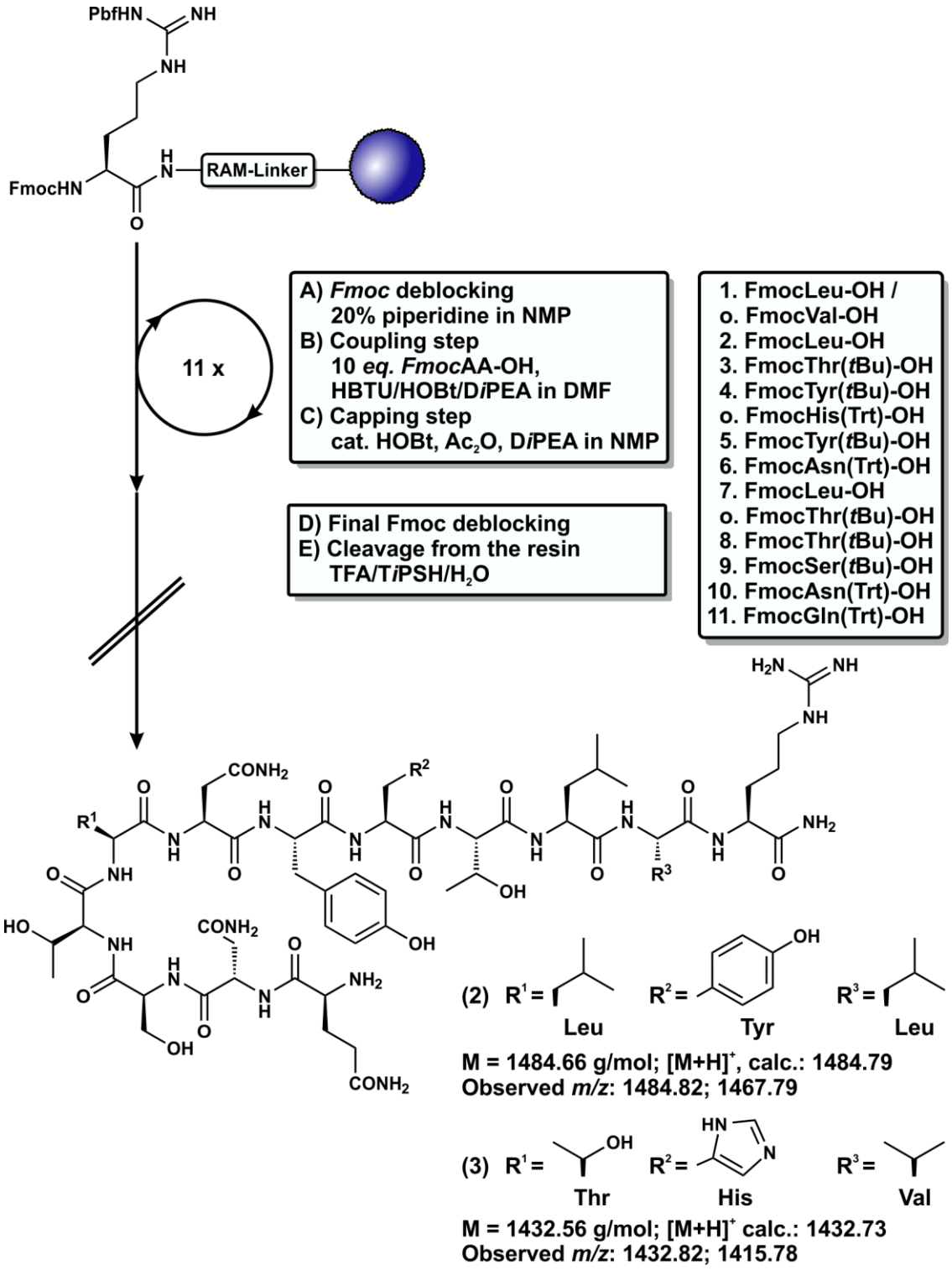

Figure 32) Scheme of the failed syntheses of the sequences (**2**) and (**3**). For both sequences the calculated mass-to-charge-ratios of quasi-molecular ions $[M+H]^+$ are shown. Both mass-to-charge ratios were observable in the corresponding *ESI*-mass spectra. However, these were accompanied by an additional set of mass-to-charge-ratios, which both were smaller by 17.03 units.

Meanwhile, in the analytic *HPLC* of the crude compound (**3**), two major peaks were observable at retention times of 14.6 min and 16.1 min, respectively (Fig. 33a). Both peaks were successfully separated by preparative *HPLC*. During subsequent analytic *HPLC* of the isolated latter peak only one major peak was observable,

while analytic *HPLC* of the first eluated peak again yielded two peaks (Fig. 33a). Additional *ESI*-mass spectra of the separated peaks displayed the lower mass-to-charge-ratio of 1415.78 for the second peak and both mass-to-charge-ratios at 1432.82 and 1415.78 for the first peak. These results suggested that the product of the supposed intramolecular reaction was the stable product. To identify this compound, different *NMR* experiments were carried out. The corresponding spectra revealed that the *N*-terminal *L*-glutamine moiety had intramolecularly cyclised into an *L*-pyroglutamic acid moiety, which resulted in the formation of peptides (**6**) and (**7**) (Fig. 33c). This was especially observable in the ^{1}H-^{13}C-*HMBC* spectrum (Fig. 33b), as the proton of the *N*-terminal *α*-amino group (strongly overlapped singlet at 7.82 ppm) showed two correlations with carbonyl groups at 177.8 ppm and at 170.7 ppm.

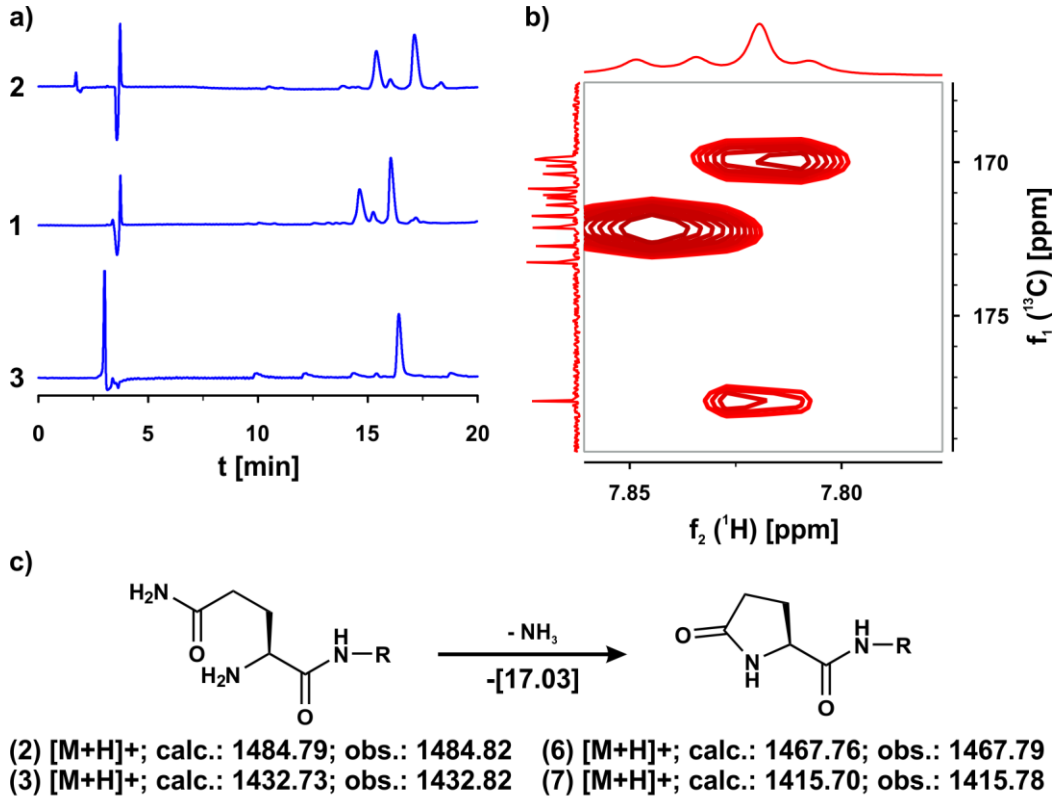

(2) [M+H]+; calc.: 1484.79; obs.: 1484.82 **(6) [M+H]+; calc.: 1467.76; obs.: 1467.79**
(3) [M+H]+; calc.: 1432.73; obs.: 1432.82 **(7) [M+H]+; calc.: 1415.70; obs.: 1415.78**

(2)/(6): R = AsnSerThrLeuAsnTyrTyrThrLeuLeuArg-CONH$_2$
(3)/(7): R = AsnSerThrThrAsnTyrHisThrLeuValArg-CONH$_2$

Figure 33) a) 1: Analytic *HPLC* chromatogram of the crude compound (**3**), showing two major peats at retention times of 14.6 min and 16.1. 2: Analytic *HPLC* chromatogram of the first peak at 14.1 min after separation by preparative *HPLC* Here, both peaks were observed, again. 3: Analytic *HPLC* chromatogram of the second peak at 16.1 min, after separation by preparative *HPLC*. Only the second major peak is observable. **b)** Section of the ^{1}H-^{13}C-*HMBC* spectrum of the isolated compound of the second peak at 16.1 min. Here, the correlation signals of two carbonyl-groups (177.8 ppm and 170.7 ppm) to the proton of an amide (7.82 ppm) indicate the *N*-terminal amino acid is *L*-pyroglutamic acid instead of *L*-glutamine, as for *L*-glutamine, the correlation to carbonyl-group at 177.8 ppm would not be observable. **c)** Intramolecular cyclisation reaction of the *N*-terminal *L*-glutamine residue into a corresponding L-pyroglutamic acid residue. Furthermore, the calculated mass-to-charge-ratios of the peptide (**2**) and (**3**) and of their corresponding *L*-pyroglutamic acid derivatives (**6**) and (**7**) are compared to the experimentally observed mass-to-charge-ratios.

Both correlations could only be explained by J^2 and J^3 couplings. This would not have been observed for glutamine, because a corresponding J^5 coupling between the proton of the amino-group to the δ-carbonyl carbon is not commonly observed in a ^1H-^{13}C-*HMBC* spectra. Furthermore, the cyclisation of *N*-terminal glutamines into pyroglutamic acid units had been reported in the literature [270]. However, this side reaction is also reported to be unavoidable. A strategy to avoid the cyclisation reaction would have been the acetylation of the *N*-terminus. Yet, this would have resulted in the loss of charge and polarity of the peptide, contradicting the aim to synthesise peptides in high similarity to the identified sequences. Instead, it was decided to elongate the peptides by an additional glycine moiety at the *N*-terminus to maintain a free amino-group (Fig. 34).

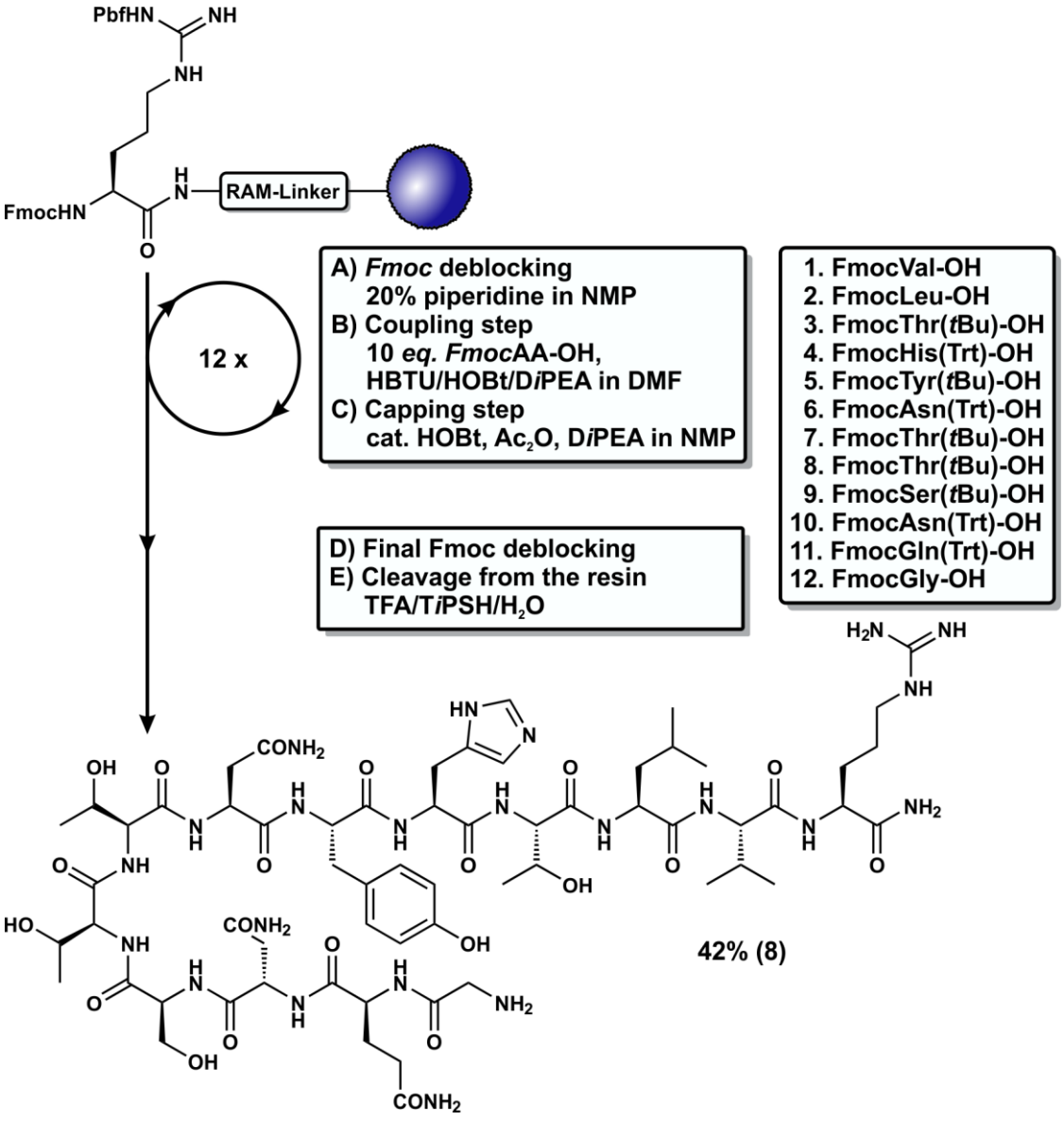

Figure 34) Schematic depiction of the synthesis of peptide (**8**). The coupling cycles were carried out according to the above described procedure, RAM corresponds to the *Rink* amide linker.

This synthesis was carried out according to the general procedure yielding 42% of sequence (**8**), the glycine derivative of sequence (**3**). Meanwhile, the corresponding glycine derivative of sequence (**2**) was not synthesised, as a simultaneous crystallisation studie showed a low solubility of the crude sequence (**2**).

Summary

The major aim of this work was the identification of peptides that possess the ability to influence the polymorph composition during the crystallisation of calcium carbonate. To identify such peptides, affinity selections by phage display on calcite nanoparticles had been carried out, which yielded three new peptide sequences, as has already been described in a previous chapter. To test the effects of these newly identified peptides, a synthetic access was required first. For the synthetic route, the automated Fmoc *Solid Phase Peptide Synthesis* was chosen, following a general procedure. In this manner, the synthesis of the peptide (**1**) was successful. However, the syntheses of peptides (**2**) and (**3**) failed, as in both cases the *N*-terminal *L*-glutamine residues cyclised into the corresponding *L*-pyroglutamic acid derivatives (**6**) and (**7**). Unfortunately, both *L*-pyroglutamic acid derivatives were the stable products of the syntheses and a separation of peptides (**2**) and (**3**) by *HPLC* was not possible. Hence, the peptide sequence of (**3**) was elongated by an *N*-terminal glycine unit leading to the successful synthesis of (**8**). This was not carried out for sequence (**2**), as simultaneous crystallisation tests showed a lower solubility for the crude compound. Nevertheless, the peptides (**1**) and (**8**) were readily available for the successive testing of their influence on the polymorph composition during the crystallisation of calcium carbonate.

Addendum

In the following experimental trials, the synthesis of different, additional peptides was necessary. The corresponding syntheses are not reported here, instead these will be properly described in the following chapters. However, these peptides were synthesised following the procedure decribed in this chapter, unless stated otherwise. For full experimental information of these peptides see Chapter 15.

9.

Development and Testing of a Crystallisation System

Motivation

As already described in the preceding chapter, the peptide sequences (**1**) and the glycine derivative (**8**) of peptide sequence (**3**) were successfully accessed *via Solid Phase Peptide Synthesis*. To investigate their respective influences on the crystal morphology and the polymorph composition during the crystallisation of calcium carbonate, a test system was required. A wide variety of methods to crystallise calcium carbonate is reported in the literature. These encompass approaches such as mixing carbonate and calcium solutions [271], the homogeneous decomposition of carbonate precursors in the presence of calcium ions [64, 272, 273] or crystallisations in (hydro-)gels [274]. Among this variety, the so-called ammonia diffusion method (ADM) [59] has been extensively applied in several (bio-)mineralisation studies [275, 276]. Furthermore, this method has been applied in several mineralisation studies in the Tremel group. [77, 78, 79, 277, 278, 279, 280] Hence, this method should be applied for the crystallisation trials with the dodecapeptides, which had been identified by the prior phage display study on calcite nanoparticles. However, before its application in the presence of the peptide additives, the method should be tested and modified, if necessary. A modification that should be implemented into the method from the beginning, was a general shift of the uninfluenced phase composition towards aragonite. This shift towards aragonite was intended, as experiences during an earlier phage display- and crystallisation study [77, 78] had shown the difficulty of distinguishing small shifts in the phase composition between vaterite and calcite. In this respect, an aragonite fraction in the polymorph composition was considered to simplify the differentiation between calcite and vaterite.

General Setup of the Crystallisation Experiments

For the full experimental procedure as well as the used materials and procedures, see Chapter 16. For the experimental data and images, see Appendix V.

As already mentioned, the ammonia diffusion method had been chosen for the crystallisation trials. For the crystallisation, an experimental procedure should be utilised, which had been reported in a publication describing the phage display study on vaterite.[77, 78] During this procedure based on the ammonia diffusion method[59] calcium solutions are exposed to an ammonia and carbon dioxide containing atmosphere. Under these conditions, ammonia and carbon dioxide diffuse into the calcium solution, where they eventually dissolve. Meanwhile, the ammonia and carbon dioxide in the atmosphere become constantly replaced by the permanent decomposition of ammonium carbonate. After dissolving in the calcium solution, the ammonia will cause an increase of the pH, while the carbon dioxide will react with water under formation of carbonic acid. In turn, the carbonic acid becomes deprotonated by the increase of the pH value, resulting in the formation of hydrogen carbonate and carbonate ions. Thus, the solution becomes increasingly saturated in respect of calcium carbonate and once the solution is supersaturated in regard of the respective polymorphs of calcium carbonate, their individual crystallisation can set on.

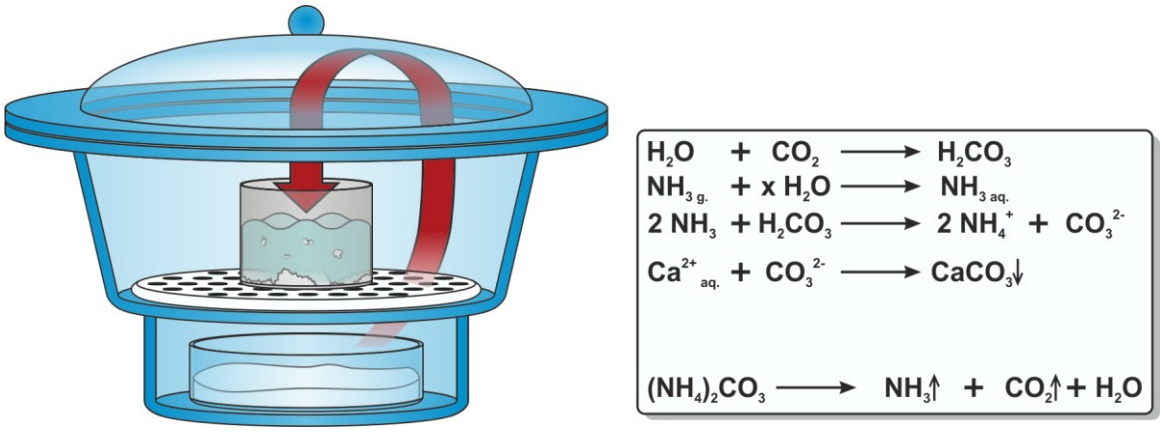

Figure 35) Schematic depiction of the precipitation of calcium carbonate utilising the ammonium carbonate diffusion method. Ammonia and carbon dioxide are constantly generated by the decomposition of ammonium carbonate at the bottom of a closed vessel (e.g. a desiccator). Ammonia and carbon dioxide diffuse into the volume of the vessel and accumulate. Furthermore, both can dissolve in a Ca^{2+} solution. Here, carbon dioxide forms carbonic acid with the excess of water. In turn, the carbonic acid is deprotonated by the dissolved ammonia resulting in the formation of carbonate ions. In this manner, the solution becomes supersaturated over time in respect of calcium carbonate and its respective polymorphs, resulting in the onset of crystallisation.

In the chosen experimental procedure, calcium chloride solutions were utilised. Except for a peptide-free control sample, the calcium chloride solutions were supplemented by the corresponding peptides at specific concentrations. These solutions were placed in a desiccator for four hours, which had already been preloaded with freshly ground ammonium carbonate (Fig. 35). To guarantee constant conditions during the crystallisation, the desiccator was additionally placed in a climate chamber.

Discussion and Results

The original reported method [77, 78] relied on additional quartz glass slides that were placed in the solutions during the crystallisation. These quartz glass slides were used to facilitate the subsequent analysis of the precipitated crystallites by *Confocal Laser Scanning Microscopy* (*CLSM*) and light microscopy. However, a pre-orientation of calcite crystals on the quartz glass slides was pointed out during discussions prior to the first experiments, which aimed at shifting the phase composition towards aragonite. In addition, this influence was suspected to depend on the pH value during the preceding cleaning procedure of the quartz glass slides. The suggested influence of the quartz glass slides hinted at the involvement of heterogeneous nucleation events. Since this influence could be presumably confused with an additive`s influence, it was intended to investigate the influence of the quartz glass slides during the crystallisations. For this investigation, quartz glass slides were treated by two different cleaning solutions prior to the crystallisation. One cleaning solution contained *Caro`s* acid (peroxymonosulfuric acid), while the other solution comprised aqueous ammonia and hydrogen peroxide. These slides were subsequently placed in the calcium chloride solutions and the crystallisations were conducted as described above. After four hours, the slides were removed from the mother liquor and examined by *CLSM* and light microscopy for differences in morphology of the precipitated crystallites. The quartz glass slide cleaned under acidic conditions was almost entirely covered by two types of rhombohedral crystallites, which differed in size and in orientation. The larger crystallites were laying upon a crystal facet, while the more numerous, smaller crystallites were standing on a corner (Fig. 36a). The rhombohedral crystal morphology indicated both types of crystallites to consist of calcite. Additionally,

the standing orientation of the smaller crystallites already implied the influence of a heterogeneous nucleation path during the crystallisation. The slide, which had been cleaned under basic conditions, was found to be covered by two types of crystallites as well. However, the crystallite density was lower and the first type of crystallites consisted of rhombohedral crystallites, while the second type consisted of large aggregates of needle-like crystallites. While the rhombohedral crystallites were assumed to consist of calcite, it was assumed that the large aggregates of needle-like crystallites were composed of aragonite, which is known to form various needle-like morphologies (Fig. 36b). No further analysis of the phase composition was carried out, as the observations clearly supported the above assumed involvement of a heterogeneous nucleation path while employing the quartz glass slides.

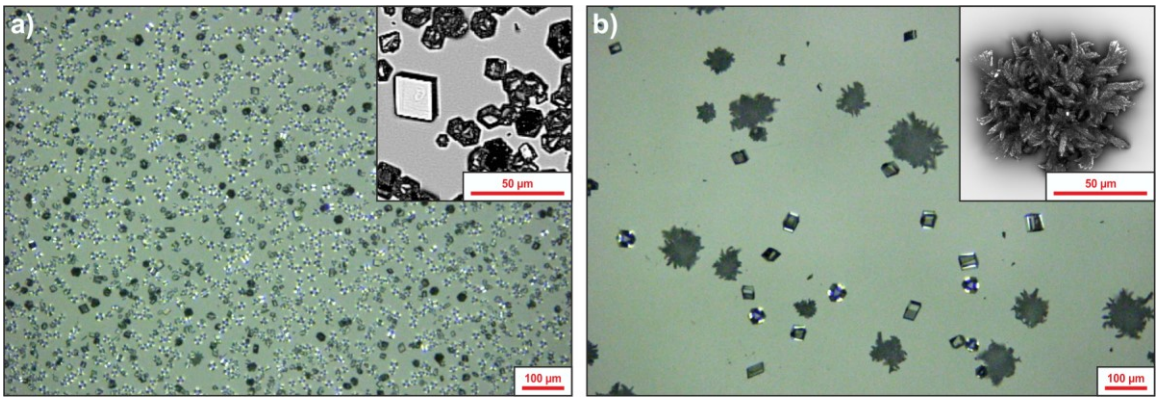

Figure 36) Microscopic images of differently treated quartz glass slides after conducting crystallisations of calcium carbonate. Both large images: Light-microscopic images. Both inlays: *CLSM*-images. **a)** Images of the quartz glass slide cleaned under acidic conditions (*Caro`s acid*). Two different types of rhombohedral crystallites were observed. The large crystallites lay on a facet, while the smaller type was orientated, as if standing on a corner. **b)** Images of the quartz glass slide cleaned under basic conditions (ammonia/hydrogen peroxide). Two different types of crystallites were observable, large, rhombohedral crystallites that lay on a facet and much larger aggregates that consisted of needle-like crystallites.

Hence, we refrained from utilising the quartz glass slides during the crystallisation from this point to prevent confusing the influence of the quartz glass slides and the peptide additives' influence. Instead, the crystallites were collected by centrifugation. Additionally, several wash steps with methanol were subsequently introduced, as to reduce the risk of recrystallisation.

In this manner, a possible source of measurement artefacts was excluded, while it was possible to concentrate on the aim of shifting the non-influenced crystallisations towards the aragonite. As already explained, the additive-influenced crystallisations in the preceding phage display study [77, 277] displayed polymorph compositions, which were dominated by calcite and especially vaterite.

Though the polymorph compositions of the additive-free control samples were different, they were similarly dominated by calcite and vaterite. Thus, the differences between some samples were difficult to observe. In contrast, aragonite was only weakly observed, if at all. Hence, the decision was made to shift the polymorph composition towards aragonite, as the presence of aragonite was assumed to simplify the observation of differences in phase composition between individual samples. A possible approach to shift the phase composition towards aragonite is the presence of magnesium ions during the crystallisation of calcium carbonate. [281, 282, 283] Based on these reports, the influence of magnesium ion was tested in the above described ADM approach. For this purpose, magnesium ions were added to the calcium chloride solution during the crystallisation at different calcium-to-magnesium ratios (i.e. 1:1, 1:2, 1:3, 1:4 and 1:5). After the crystallisations had been finished, the corresponding samples were examined *via CLSM*. Here, the magnesium-free control samples showed clear morphologies of the different calcium carbonate polymorphs, among which the rhombohedral crystallites dominated. However, all magnesium-containing samples showed morphologies, which could not be attributed to the corresponding polymorphs (compare Appendix Vb). Therefore, the samples were investigated by *X-Ray Powder Diffraction* (*XRPD*). The resulting diffractogram of the control sample confirmed the presence of all three, anhydrous polymorphs, among which calcite was the main component (Fig. 37a). In contrast, all magnesium-containing samples displayed a broad, high background with maxima at 2Θ of 25 ° and 45 ° (Fig. 37b-d), which was attributed to amorphous calcium carbonate in accordance with the literature [272]. Aside from the increasing background caused by amorphous calcium carbonate, most of the observed reflexes were attributed to calcite. However, the intensity of these reflexes decreased with decreasing calcium-to-magnesium ratio, until no sharp reflexes could be observed at calcium-to-magnesium ratio of 1:4. Additionally, a positional shift of the {10.4}-reflex was observed. While the position of this reflex in the control was close to the referenced position, it shifted towards higher degrees of 2Θ with the decreasing calcium-to-magnesium ratio (compare Appendix Vb).

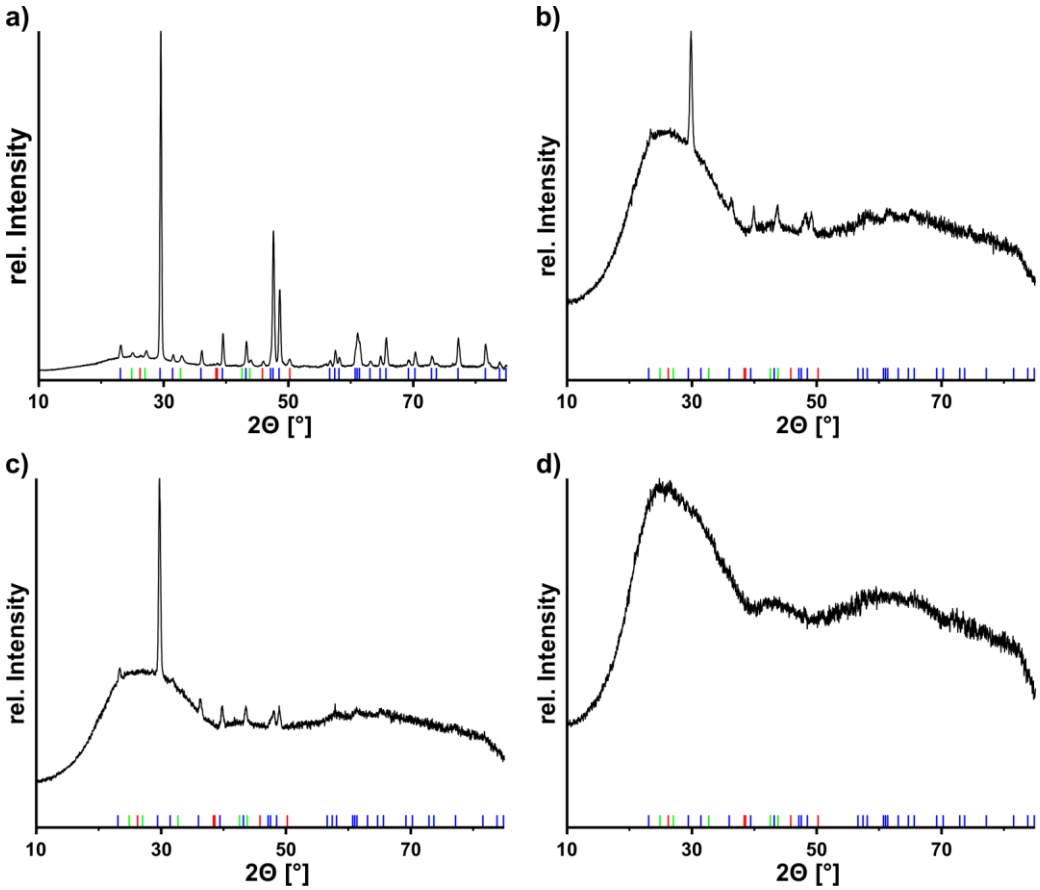

Figure 37) Normalised X-ray powder diffractograms (*XRPD*) of the magnesium-containing crystallisation series. **a)** Diffractogram of the magnesium-free control sample. **b)** Diffractogram of the sample containing a calcium-to-magnesium ratio of 1:1. **c)** Diffractogram of the sample containing a calcium-to-magnesium ratio of 1:2. **d)** Diffractogram of the sample containing a calcium-to-magnesium ratio of 1:4. Referenced reflex positions are indicated by the coloured lines. Only those are shown that where safely assigned to the control sample. Colour code and references: **Blue** lines: calcite [140]; **Red** lines: aragonite [140]; **Green** lines: vaterite [284].

This observation has been already reported in the literature and the shift was attributed to the increasing content of magnesium ions in the crystal lattice of calcite. [285] According to these observations, the presence of magnesium did not cause a shift of the phase composition towards aragonite but towards amorphous calcium carbonate. The observed precipitation of amorphous calcium carbonate in the presence of magnesium ions was supported by several other publications. [286, 287, 288] The contradictory literature reports and the observed behaviour of the crystallisation under the influence of magnesium ions can be presumably attributed to the differences in the applied methods and respective precipitation conditions.

However, the aim to shift the phase composition of the additive-free crystallisations towards aragonite still remained. Apart from the presence of magnesium ions during the crystallisation, several literature reports discuss the precipitation of

aragonite at temperatures above 40 °C.[289, 290, 291] This approach appeared especially advantageous, as it was free of any additional additive. Therefore, crystallisations were carried out at three different temperatures, i.e. at 25, 45 and 60 °C, and the resulting samples were investigated by *CLSM*. The crystallisation at 25 °C yielded mostly rhombohedral crystallites, covered in smaller, irregular crystallites. The rhombohedral crystallites were attributed to calcite (Fig. 38a). In contrast, the crystallisations at 60 °C almost exclusively resulted in needle-like crystallites, which were assigned to aragonite (Fig. 38b). Finally, the precipitate obtained at 45 °C, which consisted of a major fraction of the needle-like crystallites as well as a minor fraction of the rhombohedral morphology. In addition, unusual, feather-like crystallites were observed as a third, minor morphology, which was suspected to consist of vaterite (Fig. 38c). For further analysis of the phase composition, *X-Ray Powder Diffraction* was carried out with the precipitate obtained at 45 °C. According to the diffractogram, aragonite and calcite were present in the sample, yet clear evidence for the presence of vaterite was not found (Fig. 38d). To identify the polymorph of the feather-like crystallites, the precipitate was further investigated by *Raman*-microscopy. This allowed the clear attribution of the vaterite polymorph to this morphology. In addition, the attribution of calcite to the rhombohedral morphology and of aragonite to the needle-like morphology was confirmed (compare Appendix Vc).

In summary, the crystallisation at 25 °C yielded a phase composition, which was devoid of aragonite and dominated by calcite, while the crystallisation at 60 °C yielded almost exclusively aragonite. In contrast, the crystallisations at 45 °C successfully yielded a phase composition, which was comprised of all three, anhydrous polymorphs. Though the ideal case of an equal distribution of the three polymorphs was not achieved, the observed phase composition appeared sufficient for the general crystallisation procedure and it was decided to conduct future crystallisations at 45 °C. Additionally, a clear attribution of the three anhydrous polymorphs of calcium carbonate to specific crystallite morphologies had been achieved by *Raman* microscopy. Furthermore, this attribution was assumed to remain valid under these conditions, as long as no new, additional morphologies would be observed.

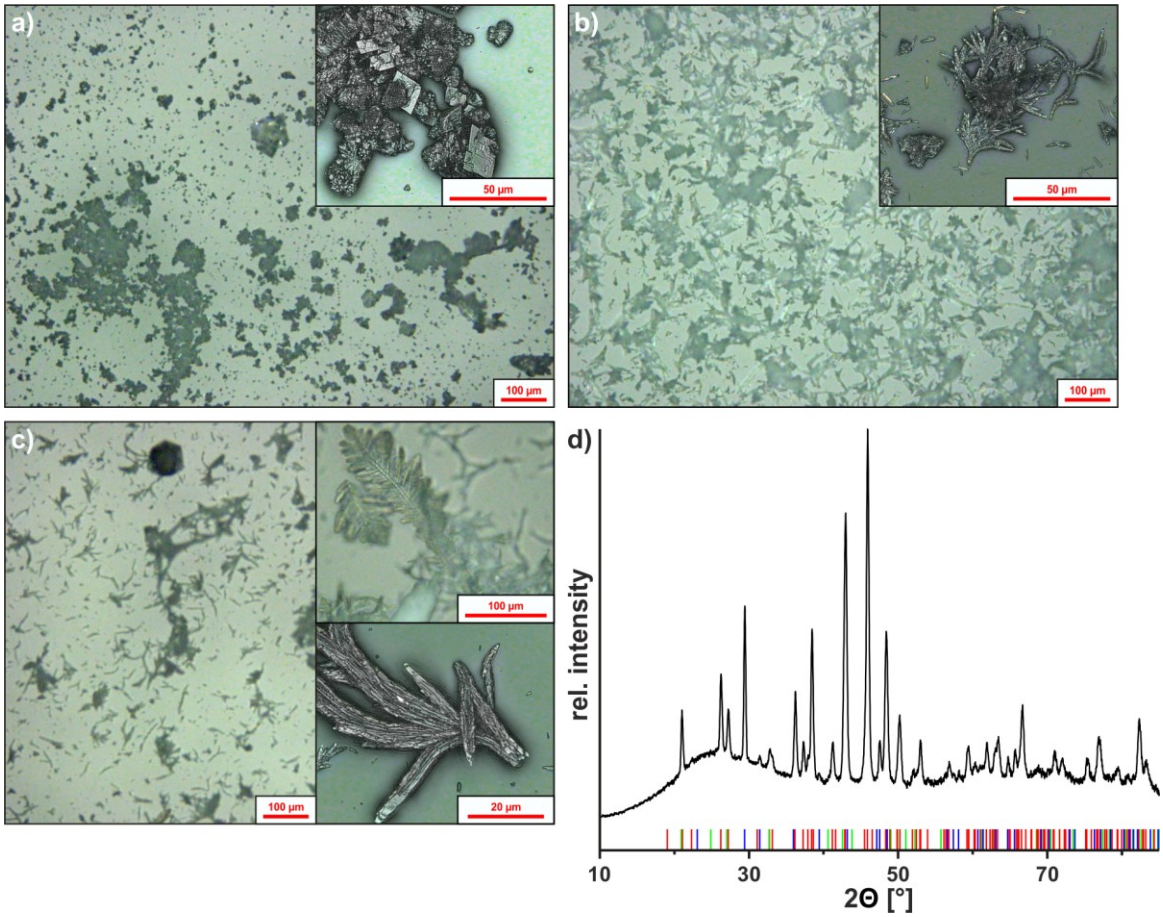

Figure 38) Results of the calcium carbonate crystallisations carried out at different temperatures. All large images: Light-microscopic images. **a)** Images of the crystallisation at 25 °C. Inlay: Overlay of light-microscopic and *CLSM*-image. **b)** Images of the crystallisation at 60 °C. Inlay: Overlay of light-microscopic and *CLSM*-image. **c)** Images of the crystallisation at 45 °C. Upper inlay: Light-microscopic image. Lower inlay: Overlay of light microscopic and *CLSM*-image. **d)** X-ray powder diffractogram (*XRPD*) of the crystallisation at 45 °C. Colour code and references: **Blue** lines: calcite [140]; **Red** lines: aragonite [140]; **Green** lines: vaterite [284].

Simultaneously, the first peptide syntheses had been carried out. Since peptides (**2**) and (**3**) had dominated the corresponding affinity selection, a special interest was placed on these very similar sequences. However, the corresponding synthesis, more precisely the purification of the crude peptides (**2**) and (**3**) proved difficult, as the *N*-terminal glutamine residues of both peptides cyclised unavoidably. Yet, the cyclisation reaction, which caused the formation of the corresponding *L*-pyroglutamic acid derivatives (**6**) and (**7**), was unidentified at this time (compare Chapter 8). Therefore, the crude peptides (**2**) and (**3**) should be employed while a preliminary crystallisation series, regardless of the impurity presence and the respective L-pyroglutamate derivatives. For this purpose, the mix of crude peptides (**2**) and (**6**) was tested at concentrations of 0.337 and 0.674 mmol/L in a first set of crystallisations. The comparison to the additive-free

control sample (Fig. 39a) displayed increasing fractions of vaterite and calcite in the presence of increasing concentrations of the crude peptide mix (Fig. 39b, c).

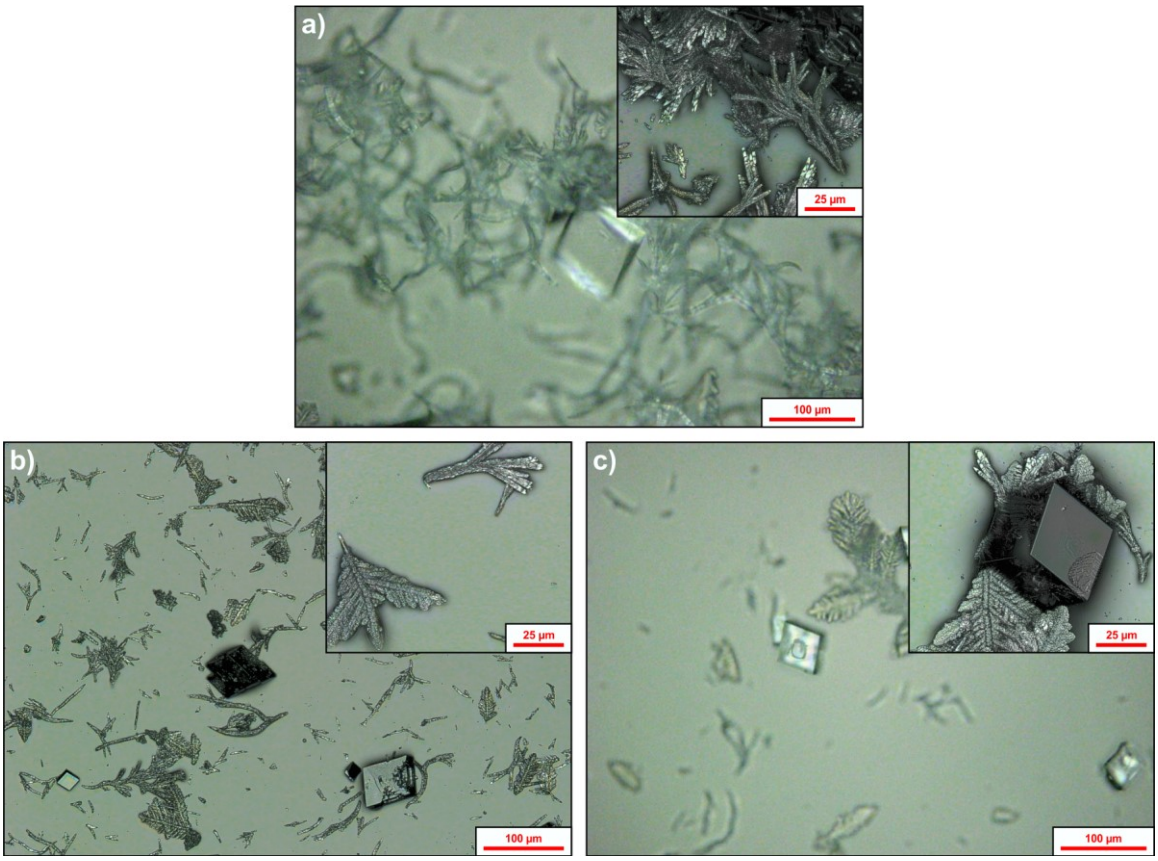

Figure 39) Images of precipitates collected after the crystallisation test applying the crude mix of peptide (**2**) and (**6**) at different concentrations. All large images: Light-microscopic-images. All inlays: Overlays of light-microscopic and *CLSM*-images. **a)** Additive-free control sample. **b)** Precipitate obtained in the presence of 0.337 mmol/L of the crude mix of peptides (**2**) and (**6**). Both images: Overlays of light-microscopic and *CLSM*-image. **c)** Precipitate obtained in the presence of 0.674 mmol/L of the crude mix of peptides (**2**) and (**6**).

Nevertheless, concentrations above 0.674 mmol/L could not be tested, because of the low solubility of the crude mix. Still, the observed shift of the phase composition towards vaterite and calcite indicated a polymorph-selective influence during the crystallisation of calcium carbonate. To improve the solubility of the mixed, crude peptides (**2**) and (**6**), a second crystallisation trial was conducted in the presence of a detergent (Tween®20). For this purpose, the crude mix was applied at concentrations of 0.05, 0.1, 0.2 and 0.5 mmol/L in the presence of 0.5% of detergent. Furthermore, a second, additive-free control sample, which contained calcium chloride and the detergent, was employed. Yet, the detergent-containing control sample already displayed a strong shift of the phase composition from aragonite towards vaterite. This shift towards vaterite persisted in the presence of the mixed, crude peptides (**2**) and (**6**) and did not display a dependence on the

applied additive concentration (not shown, for comparison see Appendix Ve). The observations suggested that the detergent`s influence superimposed the influence of the crude sequences (**2**) and (**6**). Additionally, the application of the detergent did not increase the solubility of the crude mix of sequences (**2**) and (**6**). Thus, it was desisted from applying both, the crude mix of (**2**) and (**6**) as well as any detergent, in further crystallisation experiments.

In contrast, the crude mix of sequences (**3**) and (**7**) displayed a higher solubility and it was possible to utilise this crude mix in a broader concentration range reaching from 0.05 to 5 mmol/L. Again, the corresponding control sample consisted mainly of needle-like aragonite crystallites with only minor fractions of calcite and vaterite (Fig 40a). Meanwhile, the phase composition drastically changed in the presence of the increasing additive concentrations. In the lower concentration range of the crude peptide additive(s) (i.e. in the range from 0.05 to 0.5 mmol/L) the amount of feather-like vaterite and of rhombohedral calcite crystallites increased (Fig 40b, c). At even higher concentrations (the range from 0.5 to 5 mmol/L), the calcite fraction further increased until the precipitate consisted almost entirely of rhombohedral calcite crystallites (Fig. 40c, d). Furthermore, the size of the calcite crystallites decreased with the increasing additive concentration, which again became apparent in the concentration range from 0.5 to 5 mmol/L. Here, the size of the calcite crystallites decreased from about 40 µm below 15 µm. While the size of the crystallites decreased, the total amount of individual calcite crystallites strongly increased with the increasing additive concentration (Fig. 40). Therefore, it was not only possible to show the newly established crystallisation procedure to be functional, but it was additionally possible to show a clear polymorph-selective influence of the mixed, crude peptides (**2**) and (**6**) and respectively (**3**) and (**7**). In addition, the polymorph-selective influence displayed a concentration dependency, which was much more pronounced for the more soluble, mixed crude sequences (**3**) and (**7**), while the similar crude sequences (**2**) and (**6**) were less soluble. Moreover, the observed preference of calcite in the presence of the mixed crude peptide (**3**) and (**7**) suggested that the previous affinity selection on the calcite nanoparticles had been successful. However, it was not possible to attribute the polymorph-selective influence solely to the peptides, as the nature and the influence of the present impurities was unknown.

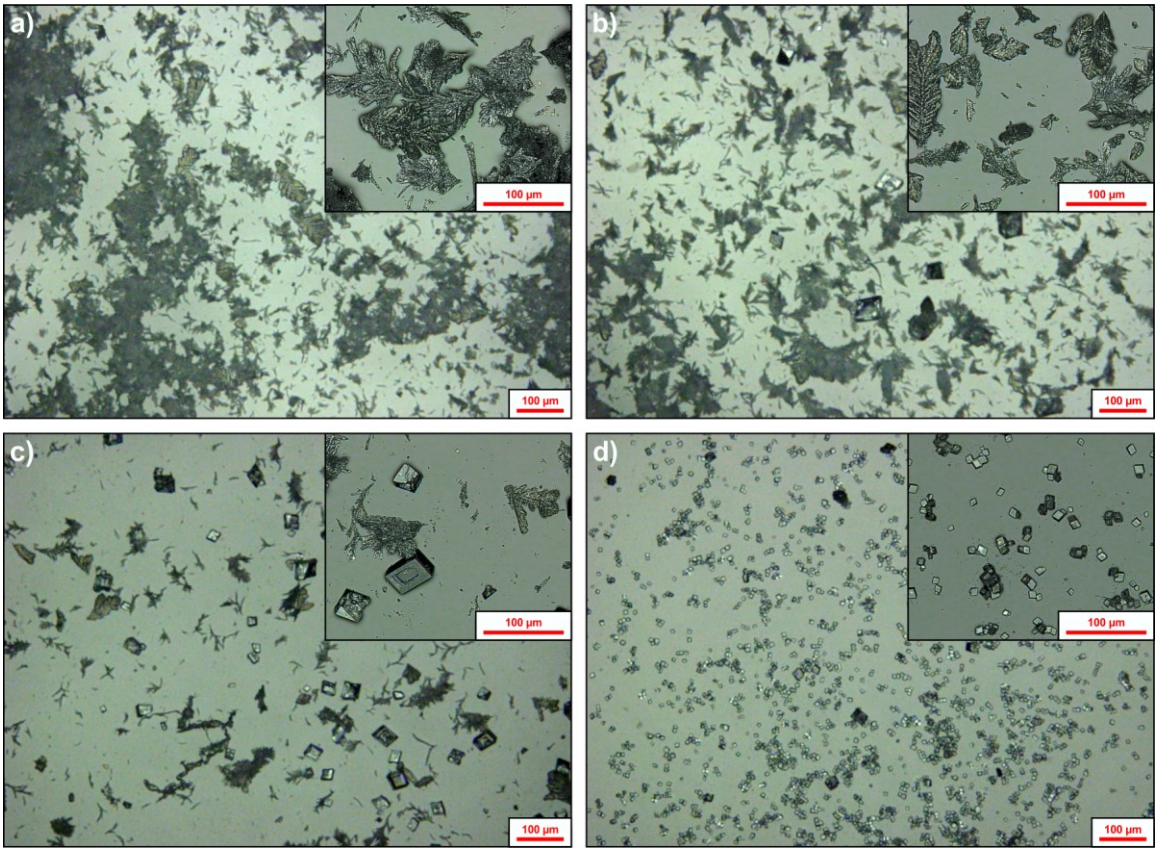

Figure 40) Images of the crystallisations in the presence of the mixed, crude peptide (**3**) and (**7**). All large images: Light-microscopic-images. All inlays: Overlays of light-microscopic and *CLSM*-images. **a)** Additive-free control sample. **b)** Precipitate obtained in the presence of 0.05 mmol/L of the crude mix of peptides (**3**) and (**7**). **c)** Precipitate obtained in the presence of 0.5 mmol/L of the crude mix of peptides (**3**) and (**7**). **d)** Precipitate obtained in the presence of 5 mmol/L of the crude mix of peptides (**3**) and (**7**).

Summary

As described above, this phase of the presented thesis aimed at establishing a crystallisation procedure for the previously identified and synthesised calcite-affine peptide sequences. For this purpose, the crystallisation procedure was chosen, which already had been applied during the previous phage display study on vaterite and based on the decomposition and diffusion of ammonium carbonate. The original crystallisation procedure resulted in the precipitation of a large calcite fraction, while a phase composition was desired that should comprise the anhydrous polymorphs of calcium carbonate in roughly equal measures. In this regard, it was decided to modify the original procedure. Yet, the quartz glass slides were excluded from the crystallisation procedure at first, as these provoked unnecessary heterogeneous nucleation events during the crystallisations. Subsequently, the influence of magnesium ions on the phase composition was investigated, as it had been reported to cause the preferred precipitation of

aragonite. However, the presence of magnesium ions yielded only amorphous calcium carbonate (ACC) instead of the wanted aragonite. An alternative approach was examined, which relied on the crystallisation at increased temperatures to induce a shift towards aragonite. Hence, the crystallisation procedure was performed at different temperatures, among which the crystallisation at 45 °C yielded a phase composition, which consisted of a major fraction of aragonite and minor fractions of vaterite and calcite. Though the three anhydrous polymorphs were not present in equal portions, it was decided to perform the future crystallisation procedure at 45 °C. In this manner, the modification of a general crystallisation procedure was successfully finished. In addition, it was possible to assign the observed crystallite morphologies to their respective polymorph by *Raman-microscopy*.

In the meantime, the peptides (**2**) and (**3**) were already available, though as crude compounds and in the presence of the corresponding *L*-pyroglutamate derivatives (**6**) and (**7**). Since the crystallisation procedure was not tested in the presence of a peptide additive, the decision was made to apply these crude mixes for preliminary crystallisation trials. During these trials, both crude mixtures displayed a clear influence on the phase composition. Here, the crude mix of peptides (**3**) and (**7**) displayed a higher solubility and subsequently a more strongly pronounced, concentration-dependent influence that almost exclusively yielded calcite at the highest concentration (5 mmol/L). Therefore, these preliminary crystallisation studies implied that the approach of identifying polymorph-selective peptides by carrying out affinity selections *via* phage display on calcite nanoparticles was successful. However, the applied peptides were non-purified raw products. Thus, the observed influence on the phase composition could have been caused by an impurity as well. Furthermore, the *L*-pyroglutamic acid derivatives (**6**) and (**7**) had been identified in the meantime (compare Chapter 8). To ensure that the influence had been caused by the original peptides, it was decided to synthesise the respective *N*-terminal glycine derivatives of sequences (**2**) and (**3**). Yet, because of the comparably lower solubility of the mixed, crude peptides (**2**) and (**6**) and the lower influence on the phase composition, the corresponding glycine derivative of sequence (**2**) was not synthesised. Instead, the following crystallisation studies should focus on examining the glycine derivative (**8**) that based on peptide (**3**).

10.
Comparative Crystallisation Studies

Motivation

During the previous experiments, a general crystallisation procedure had been established and subsequently tested with the first available peptides, the crude peptides (**2**) and (**3**). Both crude peptides displayed a calcite-selective influence, yet they contained an unknown amount of impurities and the prior identified *L*-pyroglutamic acid derivatives (**6**) and (**7**), which could have equally been the cause of this influence. Since the formation of the *L*-pyroglutamic acid derivatives was unavoidable, an *N*-terminal glycine derivative (**8**) of the more soluble peptide sequence (**3**) had been synthesised. This peptide was supposed to be examined in a new set of crystallisation experiments.

Apart from the here presented thesis, several other publications have already covered the possibility of affinity selections on different calcium carbonate polymorphs *via* phage display. [77, 78, 201, 202, 203, 204, 205, 206, 207] The peptides reported therein could potentially possess a polymorph-selective influence during the crystallisation of calcium carbonate. Therefore, these peptides appear well suited for a comparison to peptide (**8**). Hence, the decision was made to synthesise and subsequently test some of these peptides for their influence during crystallisations. Furthermore, a general aim of this thesis was the complementation of a previous study on vaterite nanoparticles. [77, 78] Thus, the therein-described vaterite-selective peptide should be synthesised and compared to peptide (**8**) as well. In the same study, an additional method had been described, which based on the recrystallisation of vaterite nanoparticles. The conditions of this recrystallisation method differed strongly from the crystallisation method described in the previous chapter. Hence, the recrystallisation method was supposed to be additionally applied for the comparisons to widen the perspective on the polymorph-selective influence of the peptides.

General Setup of the Crystallisation Experiments

For the full experimental procedure of the crystallisations as well as the used materials and procedures, see Chapter 16. For the experimental data and images, see Appendix V.

Peptide syntheses were carried out according to the previously described procedures in Chapter 8. For the corresponding materials and procedures as well as the experimental data, see Chapter 15 and Appendix IV.

An additional recrystallisation method was chosen, which had been reported along the previous phage display study on vaterite.[77, 78] This recrystallisation method relied on vaterite nanoparticles* as starting material. The nanoparticles were dispersed and shaken for 24 hours at 20 °C. During this period, the nanoparticles dissolve until the solution is saturated in respect of vaterite. Simultaneously, the solution is supersaturated in respect of aragonite and calcite, which can subsequently form. Since the nanoparticles already contained traces of the thermodynamically stable calcite (Fig. 41), the calcite fraction should increase during the 24-hour period in an additive-free experiment. Apart from a control samples, the dispersions were supplemented by the respective peptides. After 24 hours, the dispersions were precipitated by centrifugation and subsequently washed with methanol.

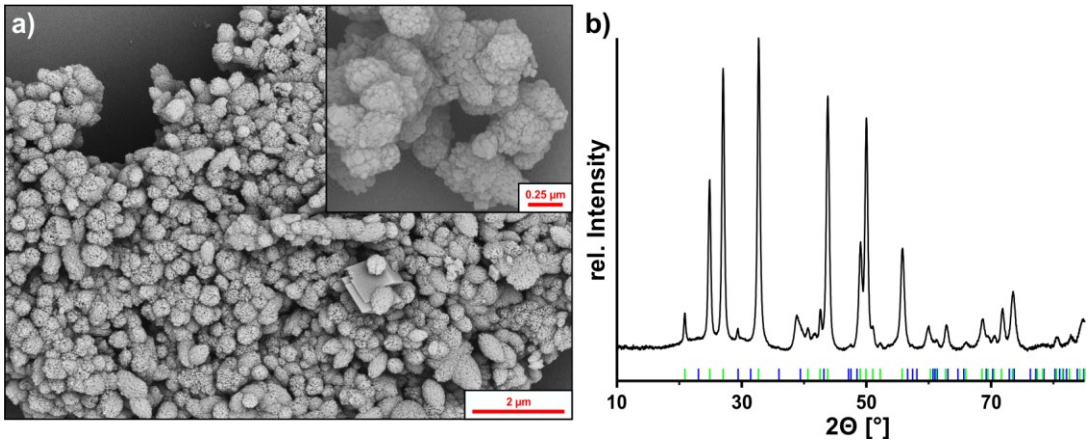

Figure 41a) *SEM*-images of the applied vaterite nanoparticles. The sample consisted of aggregated nanoparticle with a size below 50 nm. **b)** *XRPD* of the vaterite nanoparticles. Coloured lines indicate referenced reflex positions. Colour code: **Blue** lines: calcite [140]; **Green** lines: vaterite [284]. All data and images were kindly provided by *Dr. R. Schröder*.

*: The vaterite nanoparticles used during these experiment were kindly provided by [redacted]. The preparation was carried out according to *Schröder et al.* [338].

These precipitates were examined by *CLSM* and *SEM*. For full experimental procedure of the recrystallisations as well as the used materials and procedures, see Chapter 16. For the images, see Appendix VI.

Discussion and Results

In the preceding experiments, a general crystallisation procedure had been successfully established and subsequently tested in a first series of crystallisation experiments. These first crystallisation experiments displayed especially promising results in the presence of the better-soluble crude peptide (**3**), which had caused a shift of the phase composition to almost pure calcite. Still, peptide (**3**) was a crude product and hence the influence on the phase composition could have been exerted by the present impurities as well. Additionally, the crude peptide contained a considerable amount of the *N*-terminal *L*-pyroglutamic acid derivative (**7**), which further complicated conclusions. Hence, the decision was previously made to elongate peptide (**3**) by an *N*-terminal glycine moiety, which yielded peptide (**8**) (compare Tab. 5).

Table 5) Overview of relevant peptide sequences. The peptide sequences (**1**), (**2**) and (**3**) had been originally identified during the affinity selection experiments *via* phage display. However, sequences (**2**) and (**3**) unavoidably formed the corresponding L-pyroglutamic acid derivatives (**6**) and (**7**). To bypass this intramolecular cyclisation reaction, peptide (**3**), the better soluble structure, was elongated *N*-terminally by a glycine-moiety, which yielded sequence (**8**).

Peptide	Sequence
1	***N*** - Leu Gly Lys Thr Thr Ser Ala Gln Asn Leu Val Pro ***CONH$_2$***
2	***N*** - Gln Asn Ser Thr Leu Asn Tyr Tyr Thr Leu Leu Arg ***CONH$_2$***
6	***N*** - Glp Asn Ser Thr Leu Asn Tyr Tyr Thr Leu Leu Arg ***CONH$_2$***
3	***N*** - Gln Asn Ser Thr Thr Asn Tyr His Thr Leu Val Arg ***CONH$_2$***
7	***N*** - Glp Asn Ser Thr Thr Asn Tyr His Thr Leu Val Arg ***CONH$_2$***
8	***N*** Gly Gln Asn Ser Thr Thr Asn Tyr His Thr Leu Val Arg ***CONH$_2$***

Peptide (**8**) had been successfully accessed *via* Fmoc *SPPS* and the subsequent separation by semi-preparative *HPLC* yielded the pure peptide. Hence, a crystallisation trial in the presence of peptide (**8**) had become possible. In the same manner as in the previous crystallisation trial, the concentrations of peptide (**8**) ranged from 0.05 to 5 mmol/L. The resulting precipitates likewise displayed a concentration-dependent shift of the polymorph composition (Fig. 42). However, the expected shift of the phase composition from aragonite towards calcite was not observed. Instead, the crystallite morphologies shifted from the needle-like

aragonite crystallites of the control sample (Fig. 42a) towards a feather-like morphology with increasing concentration of peptide (**8**) (Fig. 42b-d). This feather-like crystallite morphology had already been attributed to vaterite *via Raman*-microscopy (compare Chapter 9 and Appendix Vc). Therefore, the increasing presence of peptide (**8**) resulted in a shift towards vaterite. At the highest concentration of peptide (**8**) (5 mmol/L), the precipitate almost exclusively consisted of feather-like vaterite crystallites (Fig. 42d).

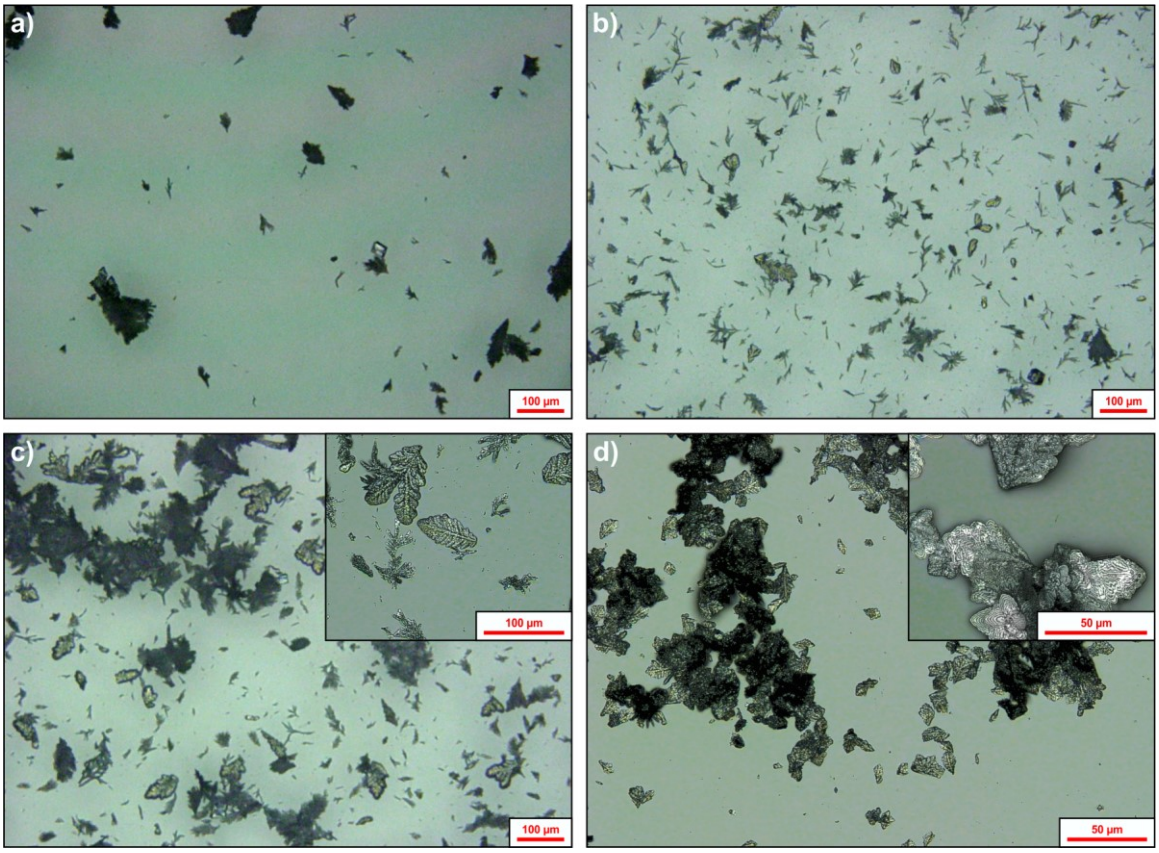

Figure 42) Images of calcium carbonate precipitates crystallised in the presence of peptide (**8**). **a)** Additive-free control sample. Light-microscopic image. **b)** Crystallites precipitated in the presence of 0.05 mmol/L of peptide (**8**). Light-microscopic image. **c)** Crystallites precipitated in the presence of 0.5 mmol/L of peptide (**8**). Large image: Light-microscopic image. Inlay: Overlay of light-microscopic and *CLSM*-images. **d)** Crystallites precipitated in the presence of 5 mmol/L of peptide (**8**). Large image and inlay: Overlays of light-microscopic and *CLSM*-images.

Therefore, it was possible to successfully demonstrate a clear polymorph-selective influence for peptide (**8**) during the crystallisation of calcium carbonate. Still, the expected shift towards calcite, previously observed in the presence of the crude mix of peptides (**3**) and (**7**), was not monitored, as peptide (**8**) exerted a polymorph-selective influence towards vaterite. In contrast to peptide (**8**), which was applied as a pure compound, peptide (**3**), more precisely the mix of peptides (**3**) and (**7**), was utilised as crude product. Hence, the change in the observed polymorph-

selective influence could have been caused by absence of one or more impurities. Alternatively, the observed shift of the phase composition in the presence of the mixed, crude peptides (**3**) and (**7**) could have been a collective effect of the peptide(s) and one or more impurities. Meanwhile, peptide (**8**) was a derivative of the originally identified peptide sequence (**3**), which had been synthesised by the introduction of an additional, *N*-terminal glycine residue. This structural change could have caused the shift in the polymorph-selective influence as well. Therefore, the decision was made to investigate the source of the observed shifts in the polymorph composition by executing an additional crystallisation series. For this investigation, a crystallisation should be conducted in the presence of the crude peptide (**8**) to test the influence of the present impurities. Additionally, the influence of the structural difference between the peptide (**3**) and (**8**) on the respective phase-selective influence should be characterised by a crystallisation. Since peptide (**3**) was not available as a pure compound (compare Chapter 8), the available, pure *L*-pyroglutamic acid derivative (**7**) should be employed as an alternative. Additionally, the crystallisations should be only carried out at the highest peptide concentration (i.e. 5 mmol/L), as to facilitate the comparison between the respective peptides.

The presence of the crude peptide (**8**) caused the formation of a precipitate, which differed entirely from the aragonite-dominated control sample (Fig. 43a) and consisted almost exclusively of rhombohedral calcite crystallites (Fig. 43b). Furthermore, it was possible to distinguish between a larger fraction of small calcite crystallites with a comparably narrow size-distribution from a smaller fraction of large calcite crystallites, which displayed a broad size-distribution. These precipitates strongly resembled the precipitates, which had been formed in the presence of the crude mix of peptides (**3**) and (**7**) (Fig. 40d). The comparison between the influence of the pure peptide (**8**) (Fig. 42d) and the crude peptide (**8**) suggested that the observed differences in the polymorph-selective influences were caused by the presence of impurities. In the presence of the pure peptide (**7**), the crystallisation had yielded a precipitate, which was composed of a minor fraction of needle-like aragonite crystallites and a major fraction of feather-like vaterite crystallites (Fig. 43c). The direct comparison to the prior, calcite-dominated crystallisation in presence of the mixed, crude peptides (**3**) and (**7**) (Fig. 40d)

displayed that the polymorph-selective influence had shifted from calcite to vaterite in the absence of impurities. Thus, both crystallisations clearly demonstrated that the calcite-selective influence had been caused by the presence of the impurities. Vice versa, the observations clearly refuted the second hypothesis, which attributed the observed shift in the polymorph-selective influence to the structural differences between pure peptide (**8**) and (**3**). The nearly identical influences of the pure peptides (**7**) and (**8**) allowed the assumption that the vaterite-selective influence is shared by the originally identified sequence (**3**), while small, *N*-terminal modifications appear to possess no effect on this vaterite-selective influence. However, without the possibility of synthesising peptide (**3**) in pure substance, this assumption cannot be proven.

Since it was possible to demonstrate that the impurities in the crude peptides were responsible for the shift of the phase composition towards calcite, the question for the nature of the responsible impurity arose. Considering the synthetic conditions of Fmoc *SPPS*, a large variety of possible impurities can form. These range from truncated or acetylated peptide sequences [292] over organic compounds, e.g. fragments of protective groups or residues of the resin, [293, 292] to salts (trifluoroacetates) [292]. Especially the salts were suspected to possess an effect on the phase composition of calcium carbonate. To investigate this suspicion, it was decided to exclude salts and other polar, water-soluble impurities from the crude peptide (**8**) and to repeat the crystallisation with this desalted peptide (**8**). Therefore, a portion of the crude peptide (**8**) was separated from salts and water-soluble impurities on a short *C18 reversed-phase* column. After the separation, the influence of this desalted peptide (**8**) was tested in a crystallisation. The subsequently obtained precipitate consisted of rhombohedral calcite crystallites as well as equal amounts of vaterite and aragonite (Fig. 43d). The presence of vaterite and aragonite indicated that the calcite-selective influence of the desalted, crude peptide (**8**) was lower in comparison to the crude peptide (**8**) and the crude, mixed peptides (**3**) and (**7**). Moreover, the still obvious formation of calcite in the absence of salts and water-soluble impurities implied that at least parts of the calcite-selective influence were exerted by one or more non-polar impurities. However, as the complexity of the impurities exceeded the available possibilities of isolating and

subsequently identifying the responsible impurity(ies), it was refrained from further investigations.

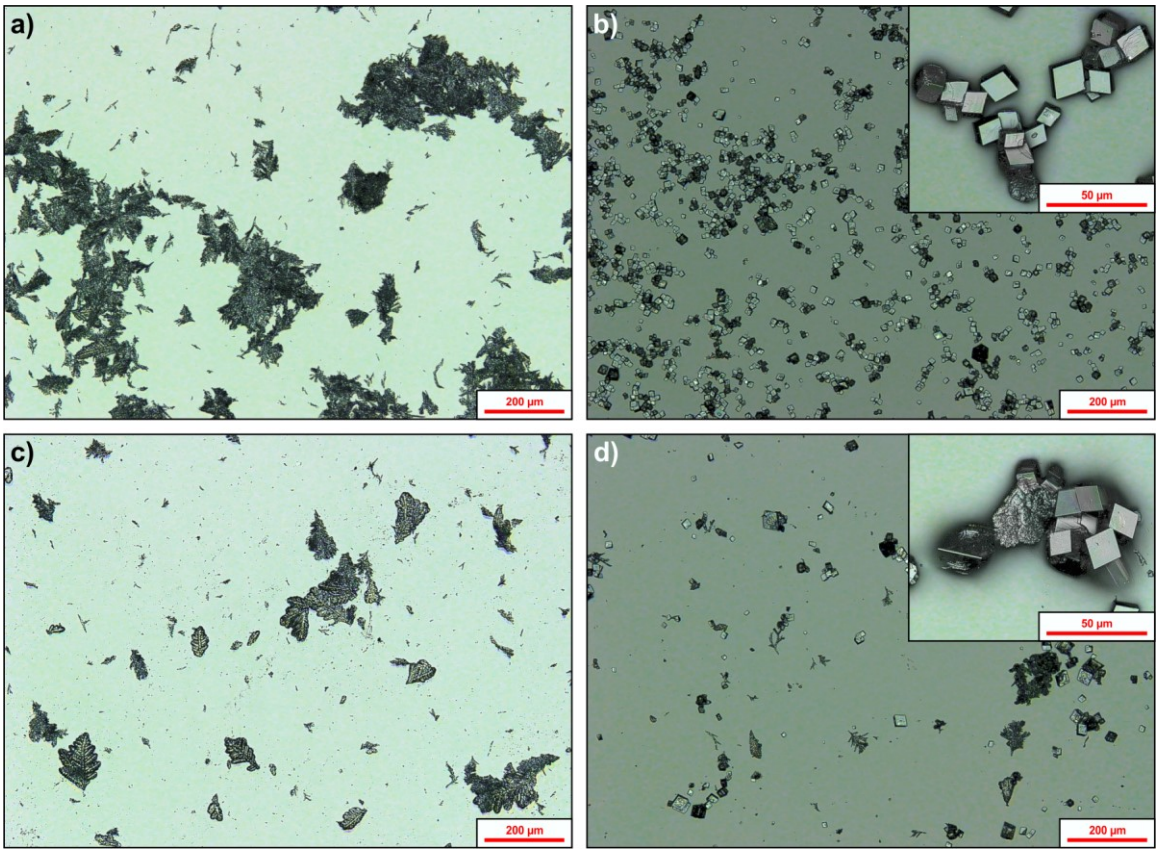

Figure 43) Images of calcium carbonate precipitates crystallised in the presence of peptides (**7**) and (**8**) in different purities. All images: Overlays of light-microscopic and *CLSM*-images. **a)** Additive-free control sample. **b)** Crystallites precipitated in the presence of 5 mmol/L of the crude peptide (**8**). **c)** Crystallites precipitated in the presence of 5 mmol/L of pure *L*-pyroglutamic acid derivative (**7**). **d)** Crystallites precipitated in the presence of 5 mmol/L of the crude, desalted peptide (**8**).

An additional aim during this stage of the thesis was the implementation of an alternative procedure to investigate the peptides and their corresponding influences on the phase composition of calcium carbonate. For this purpose, a literature-known recrystallisation method [77, 78] had been chosen, which based on the application of vaterite nanoparticles as starting material. This procedure was employed to reinvestigate the influence of the peptide (**8**) at different grades of purity. In general, the additive-free recrystallisation experiments should yield calcite. Since the vaterite nanoparticles already contained a small fraction of calcite (Fig. 41), this endpoint should be reached faster. This was confirmed, as the respective precipitate of the additive-free control sample displayed facets of larger crystallites on low magnification, which proved to be rhombohedral calcite crystallites at higher magnification (Fig. 44a). Furthermore, these calcite crystallites were covered in agglomerates of fused, roundish particles. Though the size of

these round particles was similar to the agglomerates of the vaterite nanoparticles in the starting material, they appeared as a solid mass without a nanosized substructure. In contrast, the precipitate recrystallised in the presence of the pure peptide (**8**) did not display any facets of larger crystallites on low magnification. Additionally, no rhombohedral calcite crystallites were observed at higher magnification. Instead, agglomerates of nanosized particles were monitored, which were similar to the starting material (Fig. 44b). The direct comparison with the control sample allowed the conclusion that the vaterite nanoparticles were stabilised in the presence of the pure peptide (**8**), a conclusion, which was consistent with the observations during the previous crystallisation experiment. Therefore, it was possible to confirm the vaterite-selective influence of peptide (**8**). Moreover, the crude and the desalted, crude variants were tested as well. After the corresponding recrystallisation experiments, both precipitates displayed a high degree of similarity to the precipitate in the presence of the pure peptide (**8**). Similarly, no faceted, large crystallites were observed on low magnification after the respective recrystallisations. Likewise, higher magnifications revealed that the agglomerates of the vaterite nanoparticles retained a strong similarity to the starting material (Fig. 44c, d).

In direct succession to the crystallisation trial, several mechanisms were considered to explain the confirmed vaterite-selective influence of peptide (**8**). Among the considered options, two hypotheses appeared possible. The first hypothesis assumed a prior adsorption of peptide (**8**) on the surfaces of vaterite. Subsequently, the peptide could “stabilise” the surface of vaterite by inhibiting/retarding its dissolution. The mechanism would explain the outcome of the recrystallisation experiment. Still, this mechanism appears improbable, as the surface of the employed vaterite nanoparticles should exceed the applied amount of the peptide. Additionally, the inhibition/retardation of vaterites` dissolution would vice versa imply an inhibition of vaterites` crystal growth, which would clearly contradict the preferred precipitation of vaterite during the crystallisation experiments. Thus, this mechanism appears improbable. Another possible hypothesis is the adsorption of peptide (**8**) on the facets of calcite and the subsequent inhibition of calcite`s crystal growth. This inhibition of calcite`s crystal growth would explain the retarded formation of calcite during the recrystallisation

experiment, especially as traces of calcite were already present in the starting material.

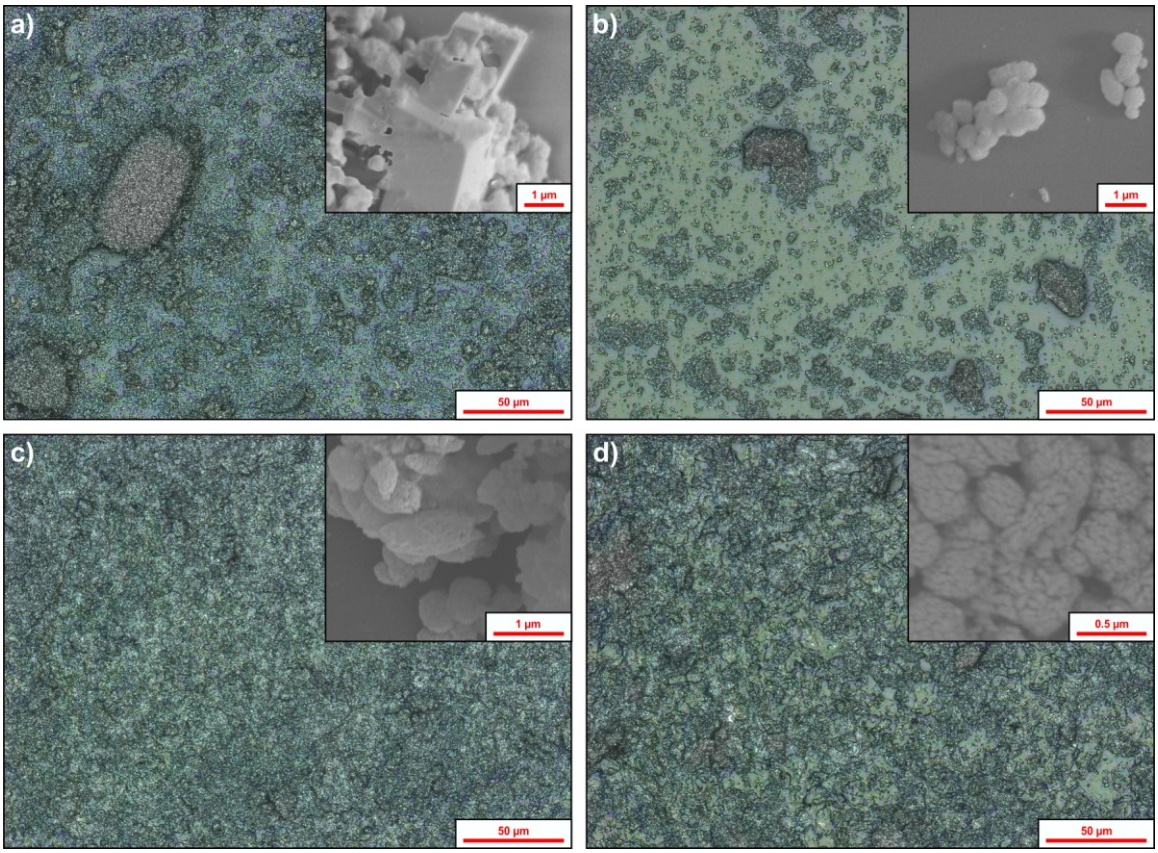

Figure 44) Images of precipitates obtained after the recrystallisation in the presence of peptide (**8**) in different purities. All large images: Overlays of light-microscopic and *CLSM*-images. All inlays: *SEM*-images. **a)** Additive-free control sample. **b)** Precipitate recrystallised in the presence of 1 mmol/L of the pure peptide (**8**). **c)** Precipitate recrystallised in the presence of 1 mmol/L of the crude peptide (**8**). **d)** Precipitate recrystallised in the presence of 1 mmol/L of the crude, desalted peptide (**8**).

Furthermore, the inhibition of calcite`s crystal growth would be consistent with the vaterite-dominated phase composition precipitated during the crystallisation experiment in the presence of peptide (**8**). This phase composition implies a growth inhibition of aragonite crystallites as well. Finally, a crystal growth inhibition of calcite would be consistent with the affinity selection on calcite, which had yielded the precursor sequence of peptide (**8**), peptide (**3**). Therefore, the hypothetical mechanism, which is based on the growth inhibition of calcite and aragonite, appears to be more probable. Nevertheless, both hypotheses neglect the nucleation stage of crystallisations. Furthermore, neither hypotheses can be proven by simple (re-)crystallisation experiments. In this regard, a different experimental approach would be required, which provides insight into the crystallisation kinetics.

The high resemblance of the precipitates obtained in the presence of the pure, the crude and the desalted peptide (**8**) indicated that the recrystallisations were solely governed by the vaterite-selective influence of peptide (**8**). This was unexpected, as the presence of the impurities had displayed a strong, calcite-selective influence during the respective crystallisation experiments. Meanwhile, the crystallisation and the recrystallisation methods differ strongly in the progression of the respective supersaturations. During the recrystallisation, the supersaturation in respect to aragonite and calcite depends solely on the dissolution of the vaterite nanoparticles and thus is limited by the solubility product of vaterite. In contrast, the supersaturation during the crystallisation procedure is principally not limited in respect of all calcium carbonate phases. Hence, a period of comparably high supersaturation in respect of each anhydrous polymorph of calcium carbonate should exist during the crystallisation procedure. While this period, nucleation events of all anhydrous polymorphs can occur simultaneously. Since the calcite-selective influence of the impurities was observed only during the crystallisation experiments, it can be assumed that the influence is only exerted at high supersaturations. This dependency on high supersaturations suggests that the impurities could facilitate the nucleation of calcite at these conditions. This assumption is supported by the occurrence of the large fraction of small calcite crystallites with a comparably even size-distribution in the presence of the impurities. This even size distribution implies a narrow period of nucleation, which could have been only cause by a different nucleation path, for instance *via* a heterogeneous nucleation. Therefore, the impurities could facilitate the nucleation *via* inducing heterogeneous nucleation events. However, a closer investigation, which could prove this hypothetical influence of the impurities, was not undertaken. Instead, it was intended to conduct the initially planned (re-)crystallisation experiments to compare the influence of peptide (**8**) with the influence of different, literature-known peptides.

For this purpose, several peptides had to be randomly chosen from several publications, which had contributed to the field of affinity selections on calcium carbonate *via* phage display.[77, 78, 201, 202, 203, 204, 206] In this regard, peptide (**9**), which had been identified by *Belcher et al.*[201], and peptide (**10**), which had been identified by *Gaskin et al.*[202] (Tab. 6), were chosen. Furthermore, the here

presented thesis aimed at complementing the previous affinity selection study on vaterite nanoparticles undertaken in the Tremel group [77, 78]. Thus, it appeared opportune to compare the here identified peptides with the previously identified ones. In this regard, the heptapeptide (**11**), which had already displayed a vaterite-selective influence [77, 78], was chosen for the comparative crystallisations. In addition, the peptide sequence (**12**), which had been identified during the first cycle of the affinity selection with the sodium acetate elution, was randomly chosen as control peptide. At last, the peptide sequence (**1**), which had already been synthetically accessed, still remained untested in (re-)crystallisation experiments. Hence, the decision was made to included peptide (**1**) in the planned comparisons with peptide (**8**).

Table 6) Sequences of literature-known peptides (**9**) [201], (**10**) [202] and (**11**) [77, 78], which were all chosen for the comparative (re-)crystallisations with peptide (**8**). Additionally, a sequence found during the first round of the affinity selection, peptide (**12**), was chosen as a control peptide.

Peptide	Sequence
9	***N*** Ala Val Gly Ser Thr Lys His Lys Trp Pro Pro Leu ***CONH$_2$***
10	***N*** His Thr Gln Asn Met Arg Met Tyr Glu Pro Trp Phe ***CONH$_2$***
11	***N*** - - - - - Ala Ser Thr Gln Pro Leu Arg ***CONH$_2$***
12	***N*** Val Ala Gln Thr Ala Val His Gly Val Met Gln Lys ***CONH$_2$***

In preparation of these comparative (re-)crystallisation experiments, the syntheses of peptides (**9**), (**10**), (**11**) and (**12**) were carried out (Fig. 45). Only the isolation of peptide (**9**) proved difficult, as it displayed two major peaks during *HPLC* at 22 °C, which could not be baseline-separated, even though the peaks eluted 4.1 min apart (Fig 45). Instead, the background level between the two peaks was near constantly increased (Fig. 45, 22 °C). This observation reminded of interconverting conformers or respectively rotamers. The assumed interconversion should display a temperature-dependent coalescence behaviour and hence the analytic *HPLC* of the crude peptide (**9**) was repeated at 8 and 40 °C. Apart from a temperature-dependent shift of the peaks, the resulting chromatograms clearly displayed a coalescence behaviour, as the two peaks were baseline-separated at 8 °C, while at 40 °C both peaks had decreased drastically and a new peak had formed in between (Fig. 45, 8 °C, 40 °C).

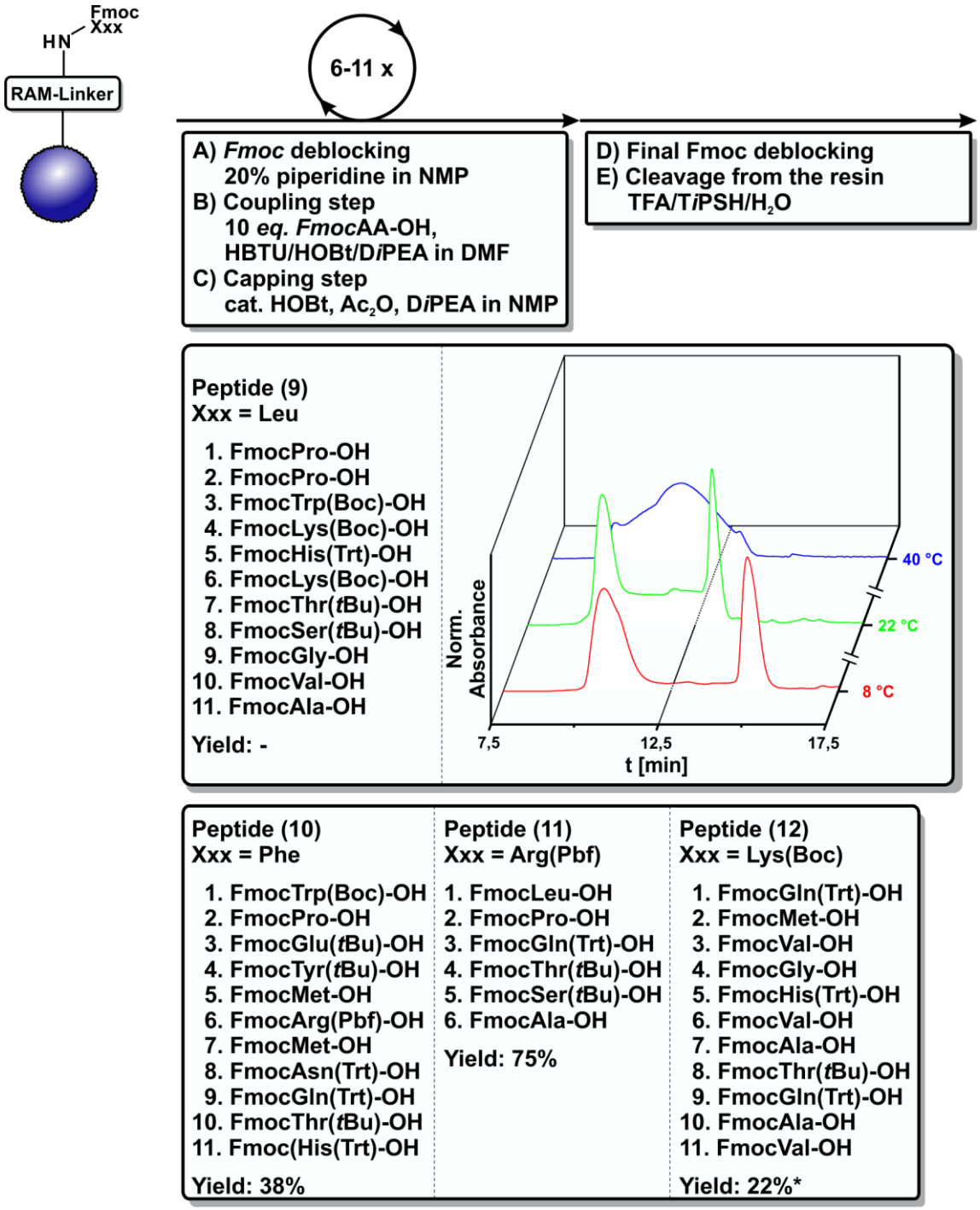

Figure 45) Schematic depiction of the synthesis of peptides (**9**), (**10**), (**11**) and (**12**). For peptide (**9**) the *HPLC* chromatograms between 7.5 and 17.5 min at 8, 20 and 40 °C. The coalescence behaviour displayed that peptide (**9**) existed in two conformers/rotamers. For the syntheses, the coupling cycles and the cleavage of the respective peptide from the resin were carried out in accordance with the standard procedures. *: Only a fraction of the crude peptide (**12**) was subjected to *HPLC*, hence the comparably low yield.

Therefore, it was concluded that peptide (**9**) equilibrated between two different forms, presumably two different rotamers. Since the broad background was suspected to hide possible impurities during the isolation of peptide (**9**), it was refrained from isolating the peptide. Instead, it was decided on reutilising the crude peptide (**9**) to further investigate the influence of the impurities.

Since all peptides required for the comparison to peptide (**8**) were available, it was possible to begin with the crystallisation experiments. The corresponding control samples were again dominated by needle-like aragonite crystallites (Fig. 46a). In the meantime, the presence of peptide (**1**) had caused the formation of a major fraction of feather-like vaterite crystallites, a very small fraction of rhombohedral calcite crystallites and traces of needle-like aragonite crystallites (Fig. 46b). The strong increase of vaterite clearly resembled the behaviour of peptide (**8**), though the presence of calcite indicated a comparably weaker, phase-selective influence of peptide (**1**). This resemblance further confirmed that the selection of peptide (**1**) and peptide (**3**), the precursor sequence of peptide (**8**), had been target-based. In contrast, the precipitate obtained in the presence of peptide (**10**), consisted almost exclusively of rhombohedral calcite crystallites, of which some formed irregular aggregates (Fig. 46c). This observation was consistent with the corresponding literature [202], which attributed a calcite-selective influence to peptide (**10**), even though the therein described experimental conditions diverged strongly from the ones applied here. Meanwhile, a large fraction of feather-like vaterite crystallites had precipitated in the presence of peptide (**11**), which was accompanied by only minor fractions of calcite and aragonite (Fig. 46d). This observation was in agreement with the literature [77, 78], though the influence of peptide (**11**) had been reported to be stronger at a lower concentration. Still, the therein described crystallisation conditions diverged strongly from the here applied method, which could have caused the difference in observation. Meanwhile, it was not possible to obtain any precipitate in the presence of peptide (**12**), as a hydrogel had formed during the experimental, which could not be redissolved. A corresponding behaviour was not displayed by the calcium-free stock solution of peptide (**12**). Therefore, the hydrogel formation could have been potentially triggered by the presence of calcium ions. Yet the change of pH during the crystallisation might have equally caused the hydrogel formation. Regardless of the cause responsible for the hydrogel formation it was refrained from further experiments in the presence of peptide (**12**). At last, a crystallisation was conducted in presence of the crude peptide (**9**) and a precipitate was obtained, which consisted mainly of feather-like vaterite crystallites as well as a minor fraction of rhombohedral calcite crystallites (Fig. 46e).

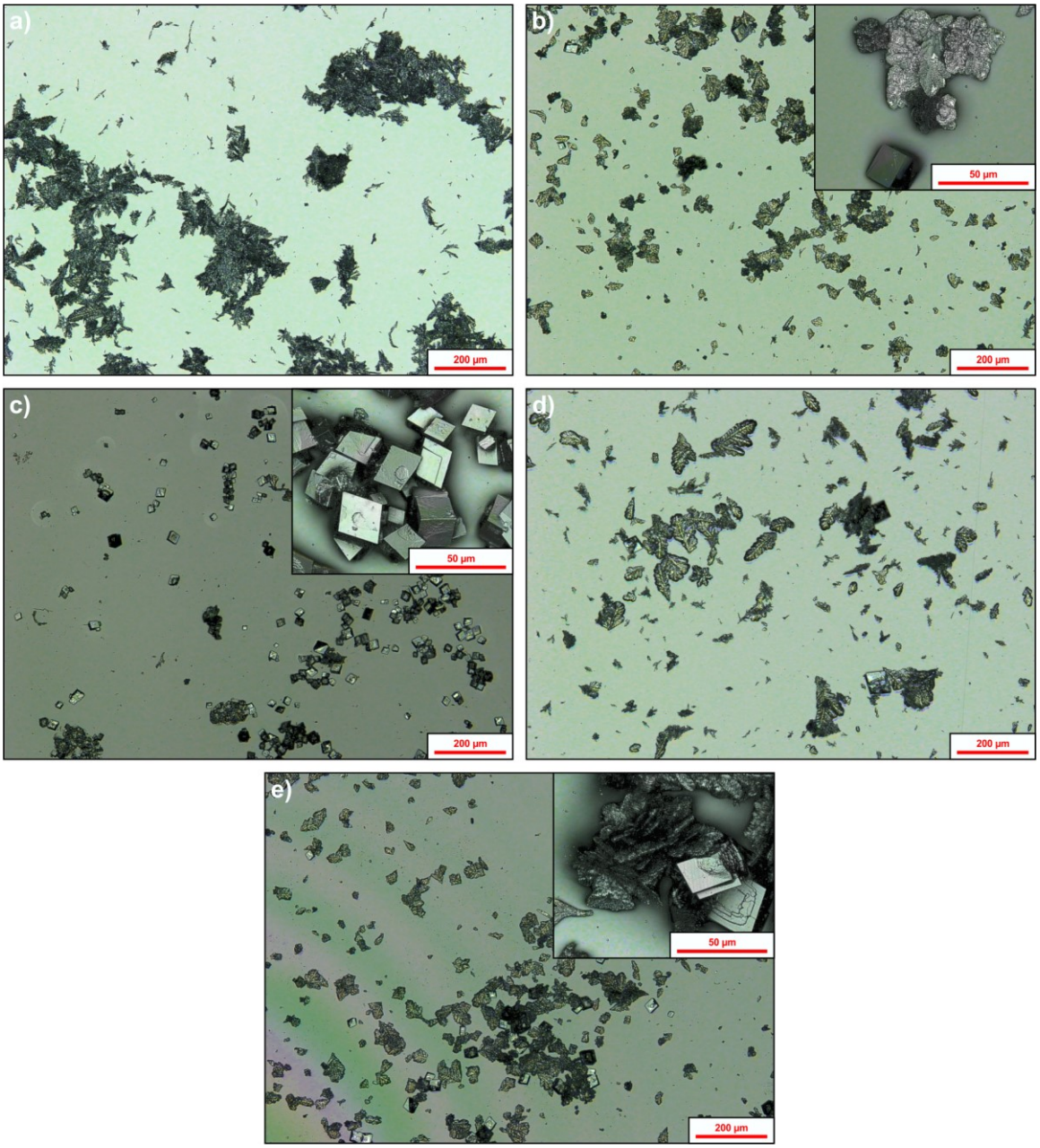

Figure 46) Precipitates crystallised in the presence of different peptides at 5 mmol/L. All images: Overlays of light-microscopic and *CLSM*-images. **a)** Additive-free control sample. **b)** Crystallisation in the presence of peptide (**1**). **c)** Crystallisation in the presence of peptide (**10**). **d)** Crystallisation in the presence of peptide (**11**). **e)** Crystallisation in the presence of the crude peptide (**9**).

Interestingly, the calcite-selective influence of the impurities, as previously observed for the crude peptide (**8**) (Fig. 43b) and the mixed, crude peptides (**3**) and (**7**) (Fig. 40d), was absent.

In direct succession to the crystallisation study, the recrystallisation experiments were carried out in the presence of the same peptides. This recrystallisation study had been carried out simultaneously with the trial described previously. Hence, the additive-free control samples were identical and displayed the same formation of

calcite crystallites covered in agglomerates of roundish, fused particles (Fig. 47a). The precipitate obtained in the presence of peptide (**1**), did not display the large amount of small, well dispersed particles at low magnification, but large aggregates of comparably well faceted crystallites. At higher magnification, these well faceted crystallites were identified as rhombohedral calcite crystallites (Fig. 47b). Hence, the presence of peptide (**1**) appeared to have accelerated the formation of calcite in comparison to the control sample. This accelerated formation of calcite conflicted with the low amount of calcite obtained after the crystallisation (Fig. 46b) and the combined observations excluded a crystal growth inhibition of calcite and vaterite. However, a facilitated nucleation of vaterite in the presence of peptide (**1**) would explain the vaterite-selective influence during the crystallisation. Still, this hypothesis could not explain the accelerated formation of calcite during the recrystallisation. Meanwhile, the precipitate obtained in presence of peptide (**10**) displayed a similar formation of well faceted, but less agglomerated crystallites, which were again identified as rhombohedral calcite crystallites at higher magnifications. Moreover, these calcite crystallites were closely connected to an irregularly shaped solid, which comprised roundish, folded lamella and flat segments (Fig. 47c). The close connection of this solid to the calcite crystallites suggested that it might be calcite, but the morphology could not be attributed to any polymorph of calcium carbonate. Regardless, the calcite-selective influence, which had been already demonstrated during the crystallisation, was retained. These observations could for instance be explained by peptide (**10**) acting as a nucleation promotor of calcite. However, this hypothetical explanation cannot be proven without further experiments. The following recrystallisation was carried out in the presence of peptide (**11**) and yielded a precipitate, which consisted of calcite (Fig. 47d). Similar to peptide (**1**), the comparison to the control sample suggested an accelerated formation of calcite in the presence of peptide (**11**), which again contradicted the observed vaterite-selective influence during the crystallisation. Additionally, the accelerated formation of calcite contradicted the literature, which had reported a retarded formation of calcite in the presence of this peptide [77, 78]. However, this inconsistency might have been caused by differences between the respective recrystallisation procedures or different purity grades of the applied peptides. The final recrystallisation was carried out in the presence of the crude peptide (**9**) and yielded a precipitate, which did not display faceted crystallites at

low magnification. Higher magnifications revealed calcite crystallites and agglomerates, of which the latter resembled the vaterite nanoparticle starting material (Fig. 47e). The observations suggested a retarded formation of calcite, which was in turn consistent with the vaterite-selective influence during the prior crystallisation. With the last recrystallisation experiment finished, it was possible to compare the influences of the individual peptides with the influence of peptide (**8**). For instance, peptide (**10**) had caused the preferred formation of calcite during the (re-)crystallisation experiments, while the presence of peptide (**8**) caused the precipitation of vaterite during the crystallisation and a retarded growth of calcite during the recrystallisation. Hence, the influences of peptides (**8**) and (**10**) possessed the least similarity. Higher similarities were observed between peptides (**1**) and (**11**) and peptide (**8**), as all three caused the preferred precipitation of vaterite during the crystallisation. However, the peptides (**1**) and (**11**) still showed the accelerated formation of calcite during the recrystallisation. Surprisingly, the influence of the crude peptide (**9**) displayed the highest similarity to the influence of peptide (**8**), as both peptides exerted a vaterite-selective influence during the crystallisation, while they both retarded the formation of calcite during the recrystallisation. This was even more surprising, as the impurities in the crude peptide (**9**) did not exert the previously observed calcite-selective influence during the crystallisation.

Since a large portion of the impurities in the crude peptides should be identical, except the presumably small amount of different peptide-based impurities, this observation appeared interesting, as it an allowed an additional hypothesis. This hypothesis assumed a collectively exerted influence of the impurities and the respective peptide(s). The formation of second, organic phase by poorly soluble impurities and the corresponding peptide could cause such a collective effect. The hypothetical influence of peptide (**8**) as an inhibitor of calcite`s crystal growth could in turn cause the heterogeneous nucleation of calcite at the interface between the solution and this new, second phase. A related behaviour had already been reported for an Asp-rich protein, which was able to inhibit the crystal growth of calcite in solution and which was able to nucleate calcite, while it was adsorbed to a surface (compare Chapter 2).[30] This hypothetical mechanism stands in agreement to the crystallisation in the presence of the desalted peptide (**8**) (Fig.

43d), which had retained the calcite-selective influence in the absence of salts and other, water-soluble impurities.

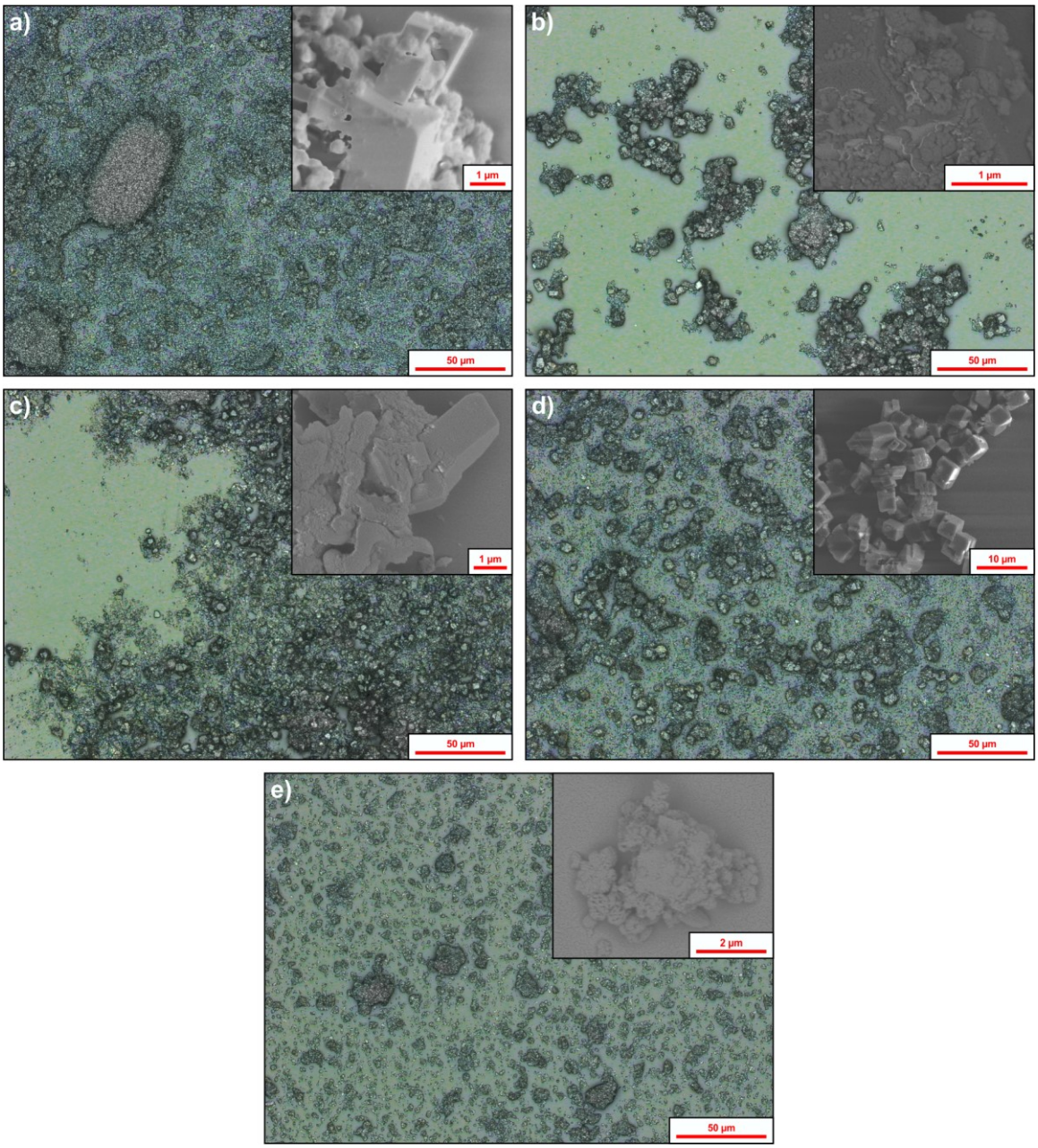

Figure 47) Images of the precipitates after the recrystallisation in the presence of different peptides. All large images: Overlays of light-microscopic and *CLSM*-images. All Inlays: *SEM*-images. **a)** Additive-free control sample. The control samples were identical with the ones of the preceding recrystallisation experiment (cp. Fig. 44a). **b)** Precipitate recrystallised in the presence of peptide (**1**). **c)** Precipitate recrystallised in the presence of peptide (**10**). **d)** Precipitate recrystallised in the presence of peptide (**11**). **e)** Precipitate recrystallised in the presence of the crude peptide (**9**).

Moreover, this new hypothesis agrees with the above presumed nucleation promotion by the impurities in the crude peptide (**8**) and the mixed, crude peptides (**3**) and (**7**). Still, the available observations during the (re-)crystallisation studies do not allow to exclude the possibility that the calcite-selective influence is exerted solely by the impurities.

Meanwhile, it had become apparent that these qualitative (re-)crystallisation experiments did not offer access to characteristic data, by which the peptides could have been compared directly. Instead, only the indirect comparisons of the phase compositions were possible. Additionally, these comparisons were further complicated by the lack of a control peptide additive, as peptide (**12**), which was intended to fill this role, formed a hydrogel during the corresponding crystallisation experiment. Thus, the comparisons of the (re-)crystallisations only allowed to point out similarities between the respective influences of the individual peptides and peptide (**8**). Nevertheless, it was possible to utilise the observed similarities and dissimilarities to deduce possible mechanisms, by which the peptide additives could exert the respective influence on the polymorph composition. Yet, it was not possible to prove a mechanism on this experimental basis. Though a quantitative determination of the phase composition would have facilitated the indirect comparisons, a direct comparison of the peptides would still not have been possible. Instead, a quantitative, kinetic test method would be required to directly compare the peptide additives and to better understand the involved mechanisms. Regardless, the qualitative (re-)crystallisation experiments and the subsequent comparisons already allowed to gain a deeper insight into the respective behaviour of the peptides, especially of peptide (**8**). Furthermore, the (re-)crystallisation experiments in general remain an appropriate approach to identify the influence of the (peptide) additives on the respective crystallisations and the resulting polymorph compositions.

Summary

During the first planned crystallisation experiments, which investigated the influence of the newly accessed, pure peptide (**8**), a concentration-dependent, strong shift of the phase composition towards vaterite was found. This vaterite-selective influence contradicted the previously observed calcite-selective influence of the crude mix of peptides (**3**) and (**7**). Therefore, an additional comparative crystallisation series was carried out, which was intended to investigate the effects of the impurities. In this regard, crystallisation experiments were performed in the presence of peptide (**8**) in different purities as well as the pure *L*-pyroglutamic acid derivative (**7**). These crystallisations clearly displayed that the previously observed

calcite-selective effect was caused by the impurities, while peptides (**7**) and (**8**) themselves possessed a vaterite-selective influence. Moreover, the latter observation allowed the assumption that the vaterite-selective influence was not perturbed by small, *N*-terminal modification and it was presumed that the precursor peptide (**3**) shared the same influence. In the meantime, the recrystallisation method had been brought forward additionally to further investigate the influence of the impurities. During these experiments, the purity of peptide (**8**) possessed no influence on the individual phase compositions. Instead, all precipitates demonstrated a preserving influence of peptide (**8**) on the vaterite nanoparticles utilised as starting material. These observations clearly confirmed the vaterite-selective influence of peptide (**8**) and allowed an assumption to explain this influence. This hypothesis suggested that peptide (**8**) presumably retards or respectively inhibits the crystal growth of calcite and aragonite, which would in turn cause the preferred crystallisation of vaterite. In addition, the observation that the impurities were active only at the comparably high supersaturation of the crystallisation experiments, allowed the assumption that the impurities could facilitate the nucleation of calcite.

After these comparative (re-)crystallisation experiments had been successfully finished, it was reverted to the initially planned comparisons of peptide (**8**) with several, already published peptides. For this purpose, the syntheses of four new peptides were carried out. Here, difficulties were encountered only during the isolation of peptide (**9**), which existed in two equilibrating conformers/rotamers according to *HPLC*. Therefore, the decision was made to utilise the crude peptide (**9**) for the further investigation on the influence of the impurities. In contrast, peptides, (**10**), (**11**) and (**12**) as well as peptide (**1**), were applicable for the planned (re-)crystallisation studies.

During the subsequent (re-)crystallisation study, peptide (**12**) was found to form a hydrogel, of which no precipitate could be obtained, and it was refrained from further experiments with this compound. Nevertheless, the experiments in the presence of the remaining peptides were carried out without meeting further complications. Still, the qualitative nature of the (re-)crystallisation experiments allowed only superficial comparisons between the individual peptides and peptide (**8**). Regardless, the comparison with the crude peptide (**9**) proved still interesting,

as it displayed the most similar influence to peptide (**8**) and the present impurities did not exert the above-described calcite-selective influence. This absence of the calcite-selective influence observed previously suggested the possibility that this calcite-selective influence was not caused solely by the impurities, but exerted collectively by the impurities and peptide (**8**) or respectively the crude mix of peptides (**3**) and (**7**). A hypothetical mechanism to explain such a collective influence was mentioned, which encompassed the formation of a second phase by the impurities and peptide (**8**) and the subsequent heterogeneous nucleation of calcite on the interface of this additional phase. However, as it was not possible to exclude that the impurities caused solely the calcite-selective influence, the hypothetical mechanism remained speculative. Furthermore, it became apparent that the comparison of the individual peptides by their respective influences on the phase composition during the (re-)crystallisations could only be utilised to show up similarities and dissimilarities, respectively. These comparisons still proved very informative, as the resulting observations were extensively utilised to consider possible mechanisms, by which some of these peptide additives could exert their corresponding influences. Additionally, (re-)crystallisation experiments remain an appropriate method to identify possible crystallisation additives. However, more precise conclusions on the influence of the peptide additives require quantitative, kinetic test methods.

11.
Development of an Adsorption Test

Motivation

During the preceding chapter, (re)crystallisation experiments had been successfully employed to demonstrate the vaterite-selective influence of peptide (**8**). Additionally, these (re)crystallisation trials had permitted the proposition of a hypothetical mechanism, which could explain this observed vaterite-selective influence. Said mechanism assumed a differentiated crystal growth inhibition of the three, anhydrous calcium carbonate polymorphs. Any crystal growth inhibitor would require a prior adsorption to a corresponding crystal or nucleus of a given material. Thus, a differentiated crystal growth inhibition would equally require a differentiated adsorption towards the respective crystallites of different materials and phases. Hence, in the context of peptide (**8**)`s observed vaterite-selective influence, the assumed differentiated growth inhibition of calcite and aragonite would need a preferred adsorption to these polymorphs. Meanwhile, the qualitative nature of the (re)crystallisation experiments did not permit to prove any of the proposed mechanisms. In this respect, a quantitative, kinetic crystallisation approach would be required to allow a deeper insight into the involved processes. However, the development of such a method appeared time-consuming and would presumably require a large up-scaling of the peptide syntheses. Nonetheless, the vaterite-selective influence of peptide (**8**) could be likewise investigated in the context of its proposed differentiated adsorption behaviour towards the anhydrous polymorphs of calcium carbonate. A similar approach had been introduced in the preceding phage display study on vaterite nanoparticles. The corresponding adsorption test on different polymorphs of calcium carbonate based on fluorescence microscopy.[77, 78] Yet, the test method relied on the immobilisation of a modified peptide onto a unique sample, a cut of a bivalve shell, which was not available anymore. Still, the concept of employing a dye-label to demonstrate different adsorption rates towards specific materials or

polymorphs of a material, appeared appealing for a possible investigation of peptide (**8**)`s vaterite-selectiveinfluence. Therefore, the synthesis of such a dye-labelled derivative of peptide (**8**) was supposed to be planned and subsequently conducted. This dye-labelled derivative was in turn intended for the subsequent development of an experimental procedure, which would allow the demonstration and the determination of this derivative`s differential adsorptions towards the anhydrous polymorphs of calcium carbonate.

General Setup

For the full experimental procedure, the characterisation of compounds and the used materials and solutions, see Chapter 15. For *NMR*-spectra and chromatograms, see Appendix IV.

For the general description and explanation of Fmoc *SPPS*, see Chapter 8.

Diverging from the standard layout applied in preceding chapters, the description of the individual organic syntheses will be given in the respective context in the discussion section. Furthermore, the here presented Fmoc *SPPS* procedure, deviated from the general procedure described in Chapter 8. The respective differences will be mentioned in the discussion section as well.

Discussion and Results

As outlined above, the planned syntheses and experiments aimed at the development of a dye-based adsorption test system. This focus had been inspired by a method developed during the course of the preceding phage display study on vaterite nanoparticles.[77, 78] The method described therein relied on the detection of a fluorescently labelled peptide, immobilised on a unique sample, by fluorescence-microscopy. In analogy to ELISA experiments, the corresponding procedure comprised two steps, an adsorption-/immobilisation step and a subsequent staining step, which exploited the interaction of streptavidin- and biotin-residues. However, the unique sample, a shell of the bivalve *Diplodon chilensis patagonicus*,[294] was no longer available. Instead, simple crystallites of the respective calcium carbonate polymorphs were intended to replace this unique sample. Furthermore, the employed derivative of peptide (**8**) should directly contain

the corresponding dye-label to simplify the experimental procedure and the decision was made to refrain from the application of fluorescent dyes. Instead, a dye with extinction maxima in the visible spectrum was intended as a label. This was thought to reduce the cost of the synthesis and to allow an easier handling during the synthesis, as fluorescent dyes are comparably expensive and sensitive. In addition, such a dye-labelled peptide was expected to be applicable for the qualitative demonstration of the different adsorptions rates towards the individual polymorphs *via* light microscopy and likewise for the quantitative, photometric determination of the adsorptions.

Regardless, before choosing a dye compound, the synthesis strategy was determined. The base for the dye-labelled compound was the sequence of peptide (**8**), which itself based on the elongation of peptide (**3**) by an additional, *N*-terminal glycine moiety. Since the *C*-termini of the peptides were linked to the **pIII**-capsids during the phage display procedures, it was assumed that *C*-terminal modifications would be less likely to alter the adsorption rates towards the polymorphs of calcium carbonate. Hence, the dye-label should be introduced at the *C*-terminus of peptide (**8**). Furthermore, the **pIII**-capsid and the *C*-terminus of the displayed peptides were not directly connected but separated by an additional glycine-spacer (compare Chapter 4). Thus, a comparable spacer-moiety should be introduced between the *C*-terminus of peptide (**8**) and the dye-label. To further simplify the synthesis, the decision was made to prepare the dye-label in a manner that would allow its direct introduction during Fmoc *SPPS*. Finally, the peptide should likewise carry a *C*-terminal amide to increase the similarity to the preceding peptides and hence a *Rink* amide linker should be employed during the synthesis. For this purpose, the corresponding, glycine-preloaded *Tentagel*® resin was arbitrarily selected (compare the concept structure (**13**), Fig. 48).

Since a general synthesis strategy had been considered, a spacer-moiety and the fundamental dye compound had to be chosen. For the spacer-moiety, it was intended to apply a well-known *N*-Fmoc protected triethylene glycol amino acid (**14**), which was compatible with the conditions during the Fmoc *SPPS* (Fig. 48). [295] In the meantime, the selection of the dye compound was more difficult, as it had to comply with additional conditions. First, the dye compound itself should possess little to no affinity for the polymorphs of calcium carbonate. Furthermore, it should

be compatible with the experimental conditions of the Fmoc *SPPS*, especially the harsh conditions during the cleavage of the peptide from the resin. Finally, the dye compound should carry a functional group that would allow the conjugation to a standard amino acid. To that end, the orange diazo dye, 2-aminoazotoluene (**15**) (Fig. 48), was selected, as its non-polar structure was expected to comply with all the above-mentioned conditions, especially with the low affinity for calcium carbonate.

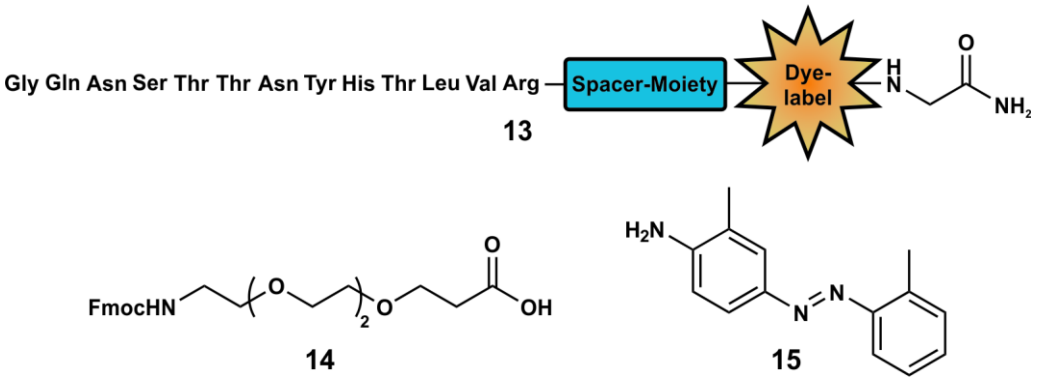

Figure 48) Depiction of the theoretical concept structure (**13**) and the chosen triethylene glycol spacer amino acid (**14**). Furthermore, the chosen, orange diazo dye compound, *2*-aminoazotoluene, (**15**) is displayed.

The free amino group of this diazo dye (**15**) should be employed in turn for the preparation of an Fmoc *SPPS* compatible dye-label. For this purpose, glutamate was chosen to connect the dye compound (**15**) *via* the *α*-carboxylic group, whereas the *γ*-carboxylic group should be utilised for the integration of the dye-label into the peptide backbone. The application of the same orthogonally protected glutamate derivative, utilised during standard Fmoc *SPPS*, was favoured, as it would simplify the synthesis route by decreasing the required protective group chemistry. Meanwhile, the aromatic amino function of the dye compound (**15**) was expected to be inert under the conditions of standard coupling reagents such as carbodiimides or uronium salts. Instead, harsher reaction conditions, i.e. more reactive active esters, would be required for the conversion of the free amine into the corresponding amide, for instance *via* an acid chloride. Yet, the formation of such an intermediary acid chloride from the *α*-carboxylic group of glutamate would greatly increase the acidity of the proton at the *α*-carbon and subsequently increase the risk of racemisation. To circumvent this problem, an additional glycine moiety was should be introduced between the *α*-carboxylic group of glutamate and the amino group of the diazo dye (**15**). Therefore, the chosen target of this synthesis

strategy was the diazo dye-labelled dipeptide (**16**), whose free carboxylic group would allow the direct application during Fmoc *SPPS* (Fig. 49).

The corresponding synthesis (Fig. 49) started with the conversion of the educt, the *N*-Fmoc protected glycine (**17**), into the respective acid chloride by thionyl chloride in dry tetrahydrofuran. [296] In direct succession, the acid chloride was converted with the diazo dye (**15**) into the amide (**18**) in the presence of *Hünig`s* base. [296] The amide (**18**) was subsequently deblocked in the presence of 20% piperidine in dichloromethane. The resulting free amine was directly reacted with the active ester of *N*-Fmoc protected *L*-glutamic acid-*γ-tert*-butyl ester, which was formed by preactivation in the presence of HOBt/HBTU and *Hünig`s* base, yielding the dipeptide compound (**19**). [297, 298] After a final deblocking step in 90% TFA [299], the diazo dye-labelled dipeptide derivative (**16**) was successfully obtained.

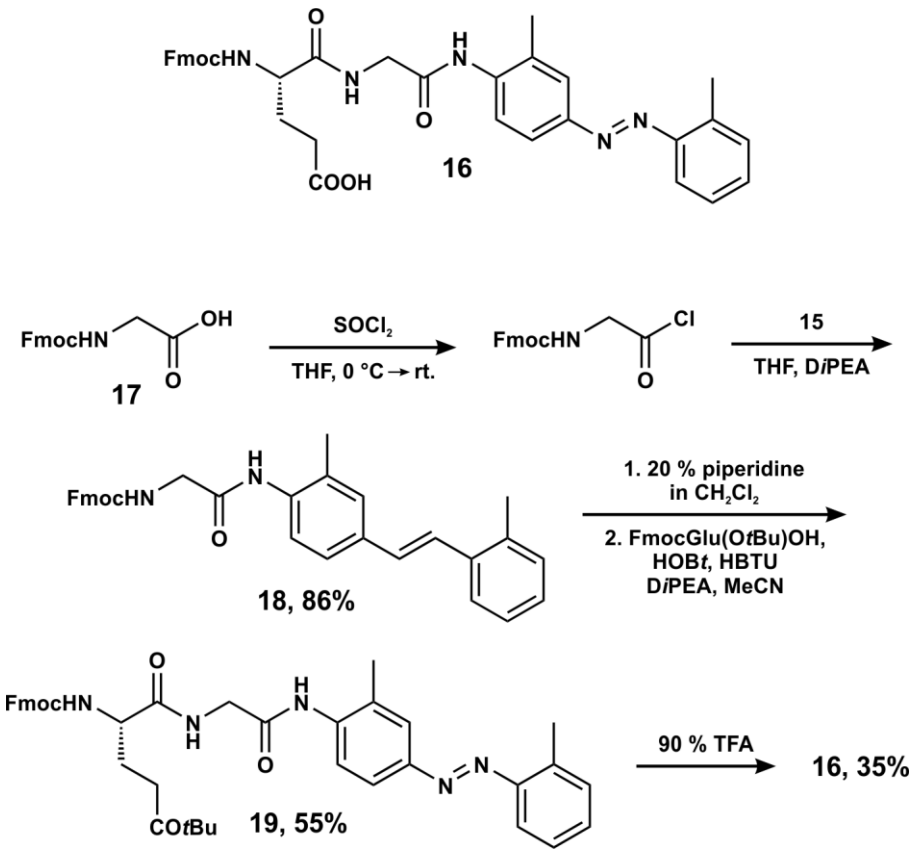

Figure 49) Depiction of the Fmoc *SPPS* compatible, dye-labelled dipeptide (**16**) as well as its corresponding synthetic route, starting with *N*-Fmoc protected glycine (**17**). After the conversion of (**17**) into the corresponding acid chloride and the subsequent reaction with the diazo dye (**15**), the dye-labelled glycine derivative (**18**) was obtained. In direct succession, the dipeptide derivative (**19**) was prepared by a deblocking step and a subsequent coupling reaction with FmocGlu(O*t*Bu)OH. After a final deblocking step, the dye-labelled building block (**16**) for the later Fmoc *SPPS* was obtained.

In the meantime, a sample of the *N*-Fmoc-protected triethylene glycol amino acid (**14**), intended for the spacer-moiety, had been obtained.* Hence, all building blocks for the solid phase synthesis of the dye-labelled derivative of peptide (**8**) were available. However, both compounds, the dye-labelled dipeptide (**16**) and the spacer amino acid (**14**), were only available in an amount, which fell short of the ten equivalents required for the coupling steps during the standard Fmoc *SPPS* procedures. In turn, the utilisation of lesser equivalents of amino acid would have risked the efficiency of the synthesis. Therefore, the first two coupling cycles, during which the dye-label (**16**) and the spacer (**14**) were to be introduced at the *C*-terminus of the peptide, required adjustment to smaller amount of equivalents. For this purpose, the decision was made to execute these first two coupling reactions manually, instead of applying the automated synthesiser. The first modification was the adoption of a stronger coupling reagent. Instead of the standard coupling reagent containing the benzotriazole HOBt[259] and its corresponding uronium salt HBTU[261], 7-azabenzotriazole HOAt[260] and its much more reactive uronium salt HATU[260] were employed for these manual coupling reactions (Fig. 29, compare Chapter 8). Moreover, the available equivalents were separated into two equal portions each and subsequently utilised in two directly consecutive coupling reactions, instead of one, as to further improve the overall coupling reaction in respect of the available equivalents (Fig. 50). Finally, the individual coupling reactions were prolonged in comparison to the standard coupling reactions. Instead of 30 min, the first reaction lasted two hours, while the second reaction lasted four hours. Meanwhile, neither the deprotecting step of the individual *N*-Fmoc protective groups nor the capping step, during which unreacted amino groups are acetylated, were modified. Apart from these first two coupling cycles, the remaining coupling cycles were conducted in accordance to the general procedure (cp. Chapter 8). After the isolation by *HPLC*, the diazo dye-labelled peptide (**20**) was successfully obtained (Fig 50). Since only a fraction of the crude peptide was separated by *HPLC*, the yield (11%) was low, yet acceptably sufficient for a first adsorption test.

***:** The *N*-Fmoc protected triethylene glycol amino acid (**14**) was kindly provided by [redacted]. The respective synthesis was carried out in accordance to *Keil et al.* [295].

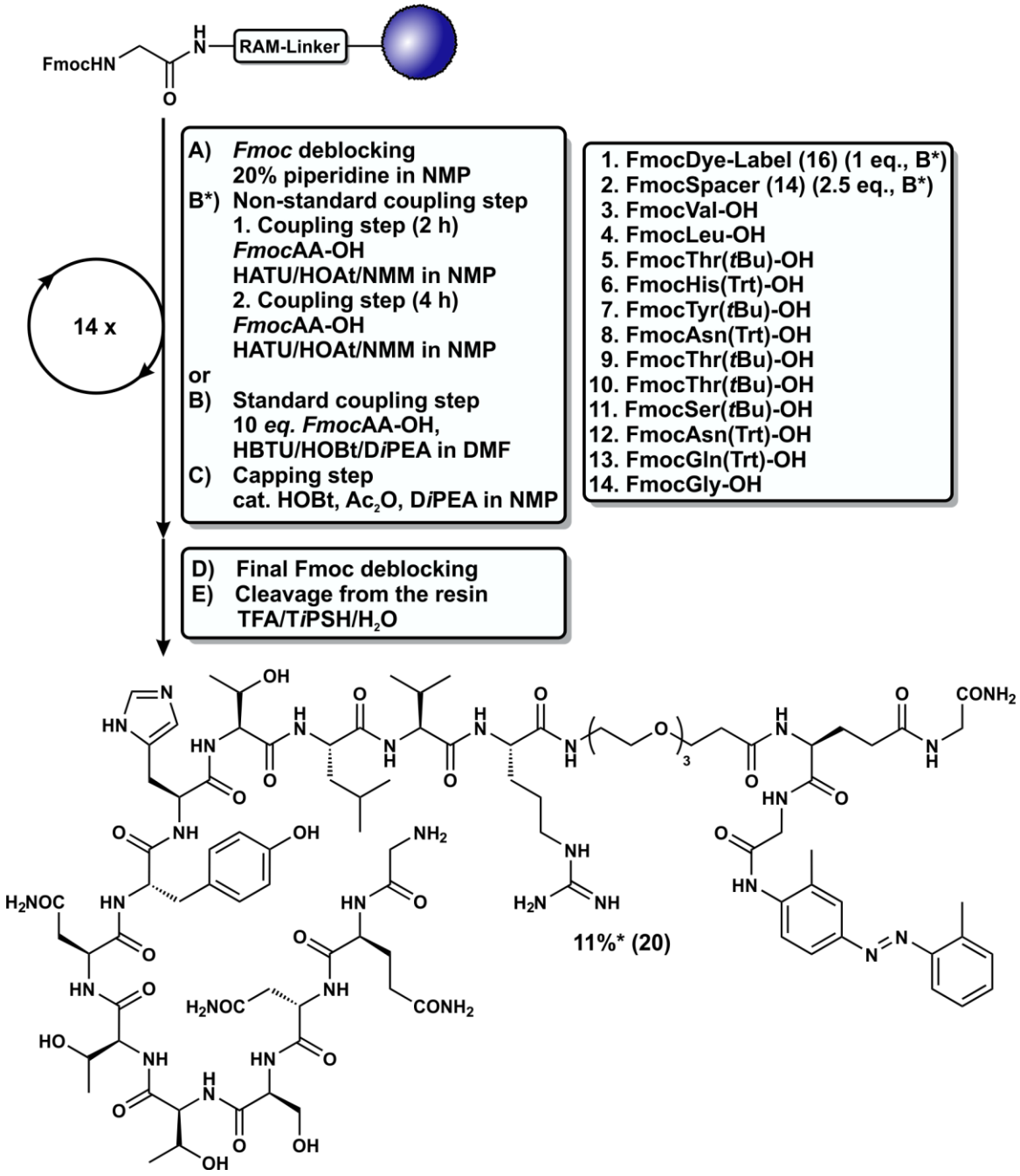

Figure 50) Synthesis scheme of the dye-labelled peptide (**20**). Two different coupling cycles were carried out. A standard procedure, relying on the coupling conditions (**B**) already described in Chapter 8 for standard amino acids, and a procedure, which relied on modified, more reactive coupling conditions (**B***) to couple the non-standard amino acids (**16**) and (**14**). These latter coupling conditions consisted of two successive coupling reaction, the first lasting 2 hours and the second 4 hours. Additionally, the more reactive coupling reagents HATU and HOAt, were employed in the presence of *N*-methyl morpholine (*N*MM). 1 *eq*. (**16**) and respectively 2.5 *eq*. (**14**) were used for the individual coupling reactions for the consecutive coupling reactions. RAM corresponds to the employed *Rink* amide linker. *****: Only a portion of the crude peptide had been isolated by *HPLC*, hence the low yield.

The last component required for the development of an adsorption test with peptide (**20**), were crystallites of each of the three anhydrous calcium carbonate polymorphs. For the later stage of this adsorption test, it was planned to photometrically determine the respective adsorption towards the respective

polymorphs individually. Hence, all three polymorphs were required to be preferably phase pure for this stage. Meanwhile, during the earlier stage, which was intended to demonstrate the differences in adsorption *via* light-microscopy, only a roughly uniform mix of the three polymorphs was required. To generate such an evenly distributed mix of these polymorphs, the decision was made to employ the already developed crystallisation method preparatively. The procedure was carried out at 25 and 45 °C, yielding a calcite-dominated and respectively an aragonite-dominated phase composition. Furthermore, both comprised a lesser vaterite fraction each. These different precipitates were mixed to generate a roughly uniformly distributed phase composition.

In direct succession, a first test was conducted, which focused at visualising and demonstrating the suspected individual adsorption rates of peptide (**20**) towards the different polymorphs *via* light-microscopy. For this purpose, the mixed calcium carbonate crystallites were dispersed at a concentration of 1 mg/mL and peptide (**20**) was added to the resulting dispersions at concentrations of 5 mg/mL (2.33 mmol/L) and 2 mg/mL (0.933 mmol/L). The resulting orange dispersions were shaken for 30 min at 25 °C. However, the precipitates could not be obtained subsequently, as the dispersions had solidified into a hydrogel each. Additional attempts at recovering the precipitates, such as wash steps with different solvents, proved unsuccessful. Therefore, a second test series was carried out, applying peptide (**20**) at lower concentrations of 1 mg/mL (0.47 mmol/L) and 0.5 mg/mL (0.23 mmol/L). Still, the slightly orange and respectively yellowish coloured dispersions both had formed a hydrogel after 30 min of agitation as well. It was not expected that even lower concentrations would allow a significant colouration of the crystallitesv observable by light-microscopy. Thus, it was refrained from further developing the simultaneous demonstration of the respective adsorption rates of peptide (**20**) towards the anhydrous polymorphs of calcium carbonate. In consequence, further tests on determining the individual adsorptions of peptide (**20**) towards the respective, anhydrous polymorphs were stopped as well.

The gel forming behaviour of the dye-labelled peptide (**20**) had been unexpected. Surprisingly, the observed gelation at the lowest concentration of 0.5 mg/mL indicated a critical gelation concentration less than 0.5‰ (w/v), a low value

compared to other gelators.* Furthermore, the stock solutions of peptide (**20**) applied for the dyeing experiments, were higher concentrated in comparison to the applied concentrations, yet they did not display the hydrogel formation. In turn, this suggested that the gelation had only taken place in the presence of calcium carbonate. Therefore, the gelation could have been initiated by calcium ions or a change of the pH. However, no further tests were conducted in this respect. Moreover, the fundamental structure of peptide (**20**), peptide (**8**), did not display the gel forming behaviour, which implies that this behaviour has been caused by the introduction of the hydrophobic diazo dye label. A hydrophobic interaction between these diazo dye-moieties of several molecules and a subsequent cross-linking of the hydrophilic peptide-moieties by calcium ions or a change in the pH value could explain the gel forming behaviour, though this remains a speculative hypothesis. Regardless, the hypothesis implied that choosing a different, more polar dye-label for the synthesis of a new derivative of peptide (**8**) could circumvent the hydrogel formation. Furthermore, the observed gel forming behaviour of the dye-labelled peptide forced the consideration of alternative test methods to investigate and determine the presumed adsorptions of a (peptide-)additive towards the anhydrous polymorphs of calcium carbonate. For instance, *NMR* experiments could represent such an alternative. Though the ^{1}H- and ^{13}C-*NMR*-spectra of peptide (**8**) would be presumably too complicated for such an application, the introduction of a fluorine-label for the detection *via* ^{19}F-*NMR* could be a viable approach. However, neither the modified strategy of choosing a more polar dye component, nor the alternative application of ^{19}F-*NMR* could be carried out for reasons of limited time. Nevertheless, both approaches could offer deeper insight into the behaviour of peptide (**8**) and other (peptide-)additives in future experiments.

Summary

In the preceding crystallisation trials, a vaterite-selective influence had been observed in the presence of peptide (**8**). A possible hypothesis, which would explain this influence, was the assumption of peptide (**8**) acting as a crystal growth

*: Critical gelation concentrations of different, known gelators: gelatine ≈ 1% (w/w) [339], alginate ≥0.35% (w/v) [340], gellan ≥ 0.15% (w/w) [341].

inhibitor of calcite and aragonite. This hypothesis in turn implied that peptide (**8**) possessed different adsorption rates towards the individual calcium carbonate polymorphs. Motivated by a fluorescence-microscopy based method, which had been introduced during a previous phage display study on vaterite nanoparticles [77, 78], the decision was made to develop a comparable method for the investigation of these presumed adsorption rates. For this purpose, the diazo-dye (**15**) was selected and successfully utilised in the synthesis of an Fmoc *SPPS* compatible dye-label (**16**). Along with the additionally obtained spacer amino acid (**14**), the dye-label (**16**) was employed in the solid phase synthesis of the dye-labelled peptide (**20**), a derivative of peptide (**8**). This newly accessed dye-labelled peptide (**20**) was intended for the demonstration of the individual adsorptions towards the respective anhydrous calcium carbonate polymorphs in a first stage. Moreover, it was planned to apply the dye-labelled peptide (**20**) for the determination of the respective adsorptions *via* photometry at a later stage. However, during the first adsorption tests the solution of peptide (**20**) solidified into a hydrogel in the presence of the calcium carbonate crystallites and thus prohibited further characterisation. Further experiments at lower concentrations of peptide (**20**) yielded similar results and simultaneously indicated a comparably low critical gelation concentration below 0.5 ‰ (w/v). Even lower concentrations of peptide (**20**) were not expected to allow the photometric determination of the individual adsorptions, let alone the simultaneous demonstration of the individual adsorptions by light-microscopy. Hence, it was refrained from further applications of peptide (**20**). Regardless, the general approach of demonstrating and subsequently determining the adsorption rates still appears viable. In this regard, it was suggested that a different, more polar dye compound could be applied to circumvent the impeding hydrogel formation. Furthermore, an additional alternative approach had been considered, which proposed the application of a fluorine-labelled derivative of peptide (**8**) in combination with ^{19}*F-NMR* experiments, to demonstrate and determine the individual adsorptions of such a peptide towards the different polymorphs of calcium carbonate. However, because of time constraints, both approaches could not be covered in the scope of this thesis.

III.

Conclusion & Outlook

12.
Conclusion

Some organisms exploit a variety of minerals for purposes such as protection, mobility or perception. The respective biomineralising processes, which control the respective crystallisations across different orders of scale and hierarchy, are mediated by biomolecules, mainly proteins, which act as crystallisation additives. This control includes the selective precipitation of specific polymorphs of a given mineral. Inspired by this polymorph control, it was aimed to investigate the possibility of influencing the polymorph composition of the model system calcium carbonate *via* peptide additives. In this respect, the identification of such peptide-additives was planned *via* phage display-based biomimetic affinity screenings on the calcite polymorph of calcium carbonate. The identified calcite-affine peptides were intended for subsequent solid-phase syntheses and crystallisations of calcium carbonate to investigate the suspected polymorph-selective influence. Additionally, a further set of affinity screenings on {10.4}-facets of calcite was planned to allow the identification of facet-selective peptides.

In respect of these aims, several series of affinity selections were conducted on {10.4}-faceted large calcite crystals and on calcite nanoparticles. During the screenings on the {10.4}-facets, no target-related peptide sequences were identified and it was consequently refrained from further experiments to identify {10.4}-facet-selective peptides. In contrast, five peptide sequences were identified during screenings on calcite nanoparticles, among which peptides (**1**), (**2**) and (**3**) were novel compounds. Since sequences (**2**) and (**3**) were especially similar, both were assumed target-related and the subsequent solid phase syntheses focused on these sequences. Yet, peptides (**2**) and (**3**) were unstable towards the formation of the respective *L*-pyroglutamic acid derivatives (**6**) and (**7**). Simultaneously, a crystallisation method was adopted from the literature, modified and subsequently tested with the already available, crude peptides (**2**) and (**3**). Here, it was possible to successfully attribute a strong, calcite-selective influence to the more soluble, crude peptide (**3**). Therefore, the stable, *N*-terminal glycine derivative (**8**) of peptide

(**3**) was successfully synthesised for further (re-)crystallisation trials. During these, peptide (**8**) displayed a vaterite-selective influence, which conflicted the calcite-selective influence of the crude peptide (**3**). A further comparative set of (re-)crystallisations allowed to assign the calcite-selective influence to the present impurities, while the strong, vaterite-selective influence could be ascribed to peptide (**8**). Therefore, it had been possible to successfully demonstrate a polymorph-selective influence for the derivative (**8**) of the priorly identified peptide (**3**).

In regard of these successful results, it was further decided on expanding the scope of this study by comparing different peptides, which had been identified in previous phage display studies, to peptide (**8**) in an additional set of (re-)crystallisations. Though these (re-)crystallisations emphasised similarities and dissimilarities between the vaterite-selective influence of peptide (**8**) and the respective influences of the literature-known peptides, a direct comparison of these peptides was not possible. In this respect, the need for a kinetic crystallisation approach became apparent. Nevertheless, the (re-)crystallisations allowed to propose a hypothetic mechanism, which could explain the vaterite-selective influence of peptide (**8**). According to this hypothesis, peptide (**8**) acts as a crystal growth inhibitor of aragonite and calcite. This proposed mechanism implied the existence of different adsorption rates of peptide (**8**) towards the individual calcium carbonate polymorphs. Hence, it was further aimed at demonstrating and determining these individual adsorptions *via* a dye-labelled derivative of peptide (**8**) in a final set of experiments. In this respect, a dye-labelled derivative (**20**) was successfully synthesised. However, the solutions of compound (**20**) solidified in the presence of calcium carbonate into a hydrogel, which prevented subsequent adsorption tests. Therefore, it was not possible to demonstrate the different adsorptions rates of peptide (**8**) or respectively its derivative (**20**) towards the polymorphs of calcium carbonate. Because of time constraints, neither further attempts to directly compare phase-selective peptides *via* a kinetic (re-)crystallisation approach nor further investigations on peptide (**8**)`s individual adsorptions towards the different polymorphs of calcium carbonate were conducted. Still, both general experimental approaches appear promising to elucidate the behaviour of phase-selective (peptide) additives in future experiments.

13.
Outlook

As described above, several peptides had been biomimetically identified on the calcite polymorph of calcium carbonate *via* phage display and subsequently investigated for a phase-selective influence in (re-)crystallisations of calcium carbonate. Especially peptide (**8**) displayed a strong, vaterite-selective influence. Therefore, subsequent experiments aimed at comparing the individual influences of the newly identified peptides *via* (re-)crystallisation experiments with influences of literature-known peptides identified during similar phage display studies. However, these (re-)crystallisation experiments only allowed indirect comparisons of resulting phase compositions, while the need for a new crystallisation method with a kinetic perspective on crystal growth became evident. Such a crystallisation method would have to distinguish between the individual crystal growth rates of the different polymorphs of calcium carbonate. These conditions could be met by seeded crystallisations, during which crystallites of one polymorph are introduced into an additive solution to induce the crystal growth of the same polymorph. Additionally, the respective additive solution is required to be supersaturated in respect of the anhydrous calcium carbonate polymorphs, though the supersaturation should be in the metastable range to reduce homogenous nucleation events. At these conditions, the crystal growth rate of the individual polymorphs would be proportional to the change of the calcium ion concentration, which could be monitored *via* a calcium selective electrode. If the surface area of the employed seed crystallites is known, the additives` influence on the crystal growth rate could be quantitatively determined, which would allow the direct comparison of additives. Still, the strong intertwining of nucleation and crystal growth might prove problematic. In this respect, the reverse reaction, the dissolution of crystals, could prove informative, as it should occur independently of a prior reaction, yet it should be similarly influenced by additives as crystal growth. Monitoring the individual dissolution rate of a polymorph could be realised in an additive solution, which is saturated in regard of this polymorph and is in direct contact to crystallites of the same polymorph with known surface area. Diluting this

solution to a small degree should cause a dissolution and a subsequent increase of the calcium ion concentration, which should be directly proportional to the dissolution rate. Nevertheless, dissolution rates and crystal growth rates are usually of different orders and not directly proportional.[28] Still, determining the dissolution rate could represent an alternative to provide useful insights into the kinetic influence of an additive and thus might allow the direct comparison of additives.*

Furthermore, it had been attempted to determine the adsorption rates of peptide (**8**) or respectively its dye-labelled derivative (**20**) towards the anhydrous polymorphs of calcium carbonate. However, the determination was unsuccessful, as the derivative (**20**) formed a hydrogel in the presence of calcium carbonate. Still, the investigation of the presumed individual adsorption rates remains a possibility to explain peptide (**8**)`s vaterite-selective influence during crystallisations. In this regard, the selection of a different, more polar dye-label to synthesise a new derivative of peptide (**8**), which avoids the hydrogel formation, could prove successful. Moreover, the application of other methods, for example *NMR*, should be considered. The employment of comparably small fluorine labels, for instance fluorinated amino acids, could represent an alternative, as such small fluorine labels could presumably exert less influence on the behaviour of the respective peptide additive. Moreover, a fluorine label should be easily monitorable *via* ^{19}*F-NMR*.

Finally, this thesis had additionally aimed at the complementation of a prior phage display study on vaterite[77, 78]. In this respect, the here presented thesis added a successful phage display study on calcite nanoparticles, during which for instance the vaterite-selective influence of peptide (**8**) was demonstrated. Therefore, future experiments could attempt to further extend the scope of the method by conducting a corresponding phage display study on the remaining anhydrous polymorph, aragonite. However, the above-described problem of directly comparing the respective additives should be addressed prior.

*: Similar experiments have been already described in the literature.[28, 342]

IV.

Experimental Section

14.
Experimental Section: Phage Display

14.1 General Information

Chemicals and Reagents

If not otherwise mentioned, all chemicals and reagents were purchased in the highest commercially available purity. Distilled water was used for the preparation of materials and solutions, if not stated differently.

Chemicals and reagents were supplied by:

Acros Organics (*Thermo Fisher Scientific*, *Geel*, Belgium) = AO
Carl Roth GmbH & Co. KG (*Karlsruhe*, Germany) = CR
Iris Biotech GmbH (*Marktredwitz*, Germany) = IB
Sigma-Aldrich Chemie GmbH (*St. Louis*, US-MO) = SA
VWR International GmbH (*Darmstadt*, Germany) = VWR

Phage Display Library Kits

The phage display libraries were purchased from *New England Biolabs Inc.* (*Ipswich*, US-MA). The libraries are based upon the M13KE-vector system of NEB [152, 226] (cp. Appendix I). The following libraries were used:

The random heptapeptide library *Ph.D.-7*™.

The random dodecapeptide library Ph.D.-12™.

Required materials (i.e. 96 gIII sequencing primer, *E. coli ER2738*) were included in the library kit. However, additional primer was supplied by *biomers GmbH* (*Ulm*, Germany) and additional batches of *E. coli ER2738* were supplied by *New England Biolabs Inc.* (*Ipswich*, US-MA). For the structure of the primer, the plasmid map of the M13KE-phage as well as the specific genetical modifications s. Appendix I.

Sequencing of the phage genomes were carried out at *StarSEQ® GmbH* (*Mainz*, Germany).

Programs for Analysis

Serial cloner v2.6.1 (*Serial Basics*®) [237] was used for the extraction of sequence information from the raw data measured at *StarSEQ® GmbH*.

Multiple Sequence Analysis (*MSA*) and *BLASTp* were performed with the *MEGA 7* software (V. 7.0.21). [238]

14.2 Preparation of materials and Solutions

The preparations of materials for phage display was carried out according to the supplier`s manual [152] and *Schüler* (**2012**) [77].

LB-medium (Lysogeny Broth, Lennox)

For 1 L: 20 g of ready-LB-medium (10 g bacto-tryptone, 5 g yeast extract, 5 g sodium chloride; CR) were dissolved in 1 L of deionised water, treated by an autoclave and stored at room temperature.

TBS-buffer

For 1 L: 6.06 g (50 mmol) TRIS (SA) and 8.77 g (150 mmol) sodium chloride (VWR) were dissolved in deionised water. pH was adjusted to 8.6 with 1 M hydrochloric acid (SA) and the volume filled up to 1 L. The solution was treated by an autoclave and stored at room temperature.

TBS-T·0.1 buffer

For 1 L: 6.06 g (50 mmol) TRIS, 8.77 g (150 mmol) sodium chloride and 1 mL Tween®20 (CR) were dissolved in deionised water. pH was adjusted to 8.6 with 1 M hydrochloric acid and the volume was filled up to 1 L. The solution was treated by an autoclave and stored at room temperature.

Tetracycline stock solution

For 1 mL: 20 mg tetracycline hydrochloride (SA) were dispersed in 1 mL ethanol (SA)/water (1:1) and stored at -20 °C.

LB/Tet-Plates

For 1 L (~25 plates): 20 g of ready-LB-medium (CR) and 15 g agar (Kobe I, CR) were dispersed in 1 L deionised water and treated by an autoclave. After cooling

to 60 °C, 1 mL of the tetracycline stock was added and the solution was poured into *Petri* dishes. After the gelling, the plates were stored at 4 °C.

IPTG/X-gal stock

1.25 g (5.25 mmol) IPTG (IB) and 1 g (2.5 mmol) X-gal (CR) were dissolved in 25 mL DMF (AO) and stored at -20 °C.

LB +IPTG/X-gal Plates

For 1 L (~25 plates): 20 g of ready LB-medium (CR) and 15 g agar were dispersed in 1 L deionised water and treated by an autoclave. After cooling to 60 °C, 1 mL of the IPTG/X-gal stock was added and the solution was poured into petri dishes. After the gelling, the plates were stored at 4 °C.

Top-Agar

For 1 L: 20 g of ready-LB-medium and 7 g agar were dispersed in 1 L deionised water. The dispersion was treated by an autoclave and the resulting gel was stored at room temperature. For use, the gel was molten in a microwave.

PEG/NaCl solution

20% (w/v) polyenthylene glycol (SA, M = 8000 g/mol) in 2.5 M sodium chloride were autoclaved. The separated layers were mixed while cooling and stored at room temperature.

TE-buffer

10x TE-buffer (CR) were diluted (1:10) in the appropriate volume of nuclease-free, sterile water (CR) and stored at room temperature.

3M NaAc

For 250 mL: 61.5 g (0.75 mol) anhydrous sodium acetate were dissolved in 250 mL deionised water, treated by an autoclave and stored at room temperature.

TAE-buffer

10x TAE-buffer (CR) were diluted (1:10) in the appropriate volume of nuclease-free, sterile water (CR) and stored at room temperature.

0.1 M EDTA solution

For 0.5 L: 14.61 g (50 mmol) ethylenediaminetetraacetic acid (EDTA, SA) were dissolved in deionised water and the pH was adjusted to 8.6 with 1 M sodium hydroxide. The volume was filled up to 0.5 L. The solution was treated by an autoclave and stored at room temperature.

0.1 M NaAc

For 0.5 L: 4.1 g (50 mmol) sodium acetate (NaAc, SA) were dissolved in deionised water and the pH was adjusted to 8.6 with 1 M hydrochloric acid. The volume was filled up to 0.5 L. The solution was treated by an autoclave and stored at room temperature.

TBS-buffer pH 10

For 1 L: 6.06 g (50 mmol) TRIS (SA) and 8.77 g (150 mmol) sodium chloride (VWR) were dissolved in deionised water and the pH was adjusted to 10 with 1 M sodium hydroxide (SA). The volume was filled up to 1 L. The solution was treated by an autoclave and stored at room temperature.

0.1 M $CaCl_2$ in TBS-buffer

For 1 L: 6.06 g (50 mmol) TRIS (SA), 8.77 g (150 mmol) sodium chloride (VWR) and 14.70 g calcium chloride dehydrate (100 mmol) were dissolved in deionised water. The pH was adjusted to 8.6 with 1 M hydrochloric acid (SA) and the volume was filled up to 1 L. The solution was treated by an autoclave and stored at room temperature.

14.3 General protocols

The procedures were carried out according to the supplier's manual [152] and *Schüler* (**2012**) [77].

Maintenance of *E. coli ER2738*

E. coli ER2738 from the supplier's glycerol stock were streaked out on a freshly prepared LB/Tet plate and incubated at 37 °C overnight. Afterwards the plate was ready to use for starting a culture. When wrapped with *Parafilm*, the plates could be stored for 2-4 weeks at 4 °C. From such plates, new *ER2738* suspension cultures were grown, by picking a bacteria colony on the plate with a pipette tip and

adding the tip to LB-medium, kept at 37 °C under constant shaking. An aliquot (1:1000 dilution) of the tetracycline stock solution was additionally added.

General amplification protocol

10 mL of LB-medium were inoculated with *ER2738* from a fresh plate and incubated overnight at 37 °C while shaking. 250 µL of the overnight-culture were added to 25 mL LB-medium (preferably in a 100 mL Erlenmeyer flask) and incubated at 37 °C for 15 min. The amplification was started by adding a phage solution (combined solutions of washing steps or the elution solutions). The suspension was incubated at 37 °C for 4.5 h while shaking. The obtained solution was cooled to 4 °C and centrifuged at 9000 rpm for 15 min. The supernatant was decanted into a new tube, 1/6 volume of PEG/NaCl was added and the phage were precipitated overnight at 4 °C. The phages were separated by centrifugation at 9000 rpm for 20 min and the supernatant was carefully discarded, the centrifugation was repeated if necessary. The phage pellet was resuspended in 1 mL TBS in a new tube and centrifuged at 14500 rpm (4 °C) for 5 min. The supernatant was transferred into a new tube, mixed with 1/6 volume of PEG/NaCl-solution and the phages were precipitated 30 min on ice. The phages were separated by centrifugation 14500 rpm at 4°C for 10 min, the supernatant was discarded and the phage pellet was suspended in 200 µL of TBS.

Phage titering

10 mL of LB-medium were inoculated with *ER2738* from a fresh plate and incubated overnight at 37 °C while shaking. The LB/IPTG/X-gal-plates were pre-warmed at 37 °C on the next day. Serial dilutions of the phage-suspensions were prepared, each with a total volume in 1 mL of LB-medium. Dilutions of 10^{-2}, 10^{-4} and 10^{-6} for unamplified phage or 10^{-2}, 10^{-4}, 10^{-6}, 10^{-8} and 10^{-10} for amplified phage solutions were prepared. Top-Agar was molten in a microwave and cooled down to 50 °C. 1 mL of the overnight-culture was diluted to 10 mL with LB-medium. 10 µL of the individual phage dilutions was added to 200 µL of the diluted *ER2738* culture and incubated at 37 °C while shaking. After 5 min, the incubated/infected bacteria were added to a 3 mL aliquot of molten Top-Agar (T < 50 °C), rapidly mixed and poured on a pre-warmed prepared LB/IPTG/X-gal-plate. The plate was tilted and rotated to spread the suspension evenly. After cooling for 5 min, the

plates were inverted on the lid and incubated overnight at 37 °C. For titering and the amplification of single phage, it is preferable to use plates with about 100 plaques or less.

Amplification of single phages

10 mL of LB-medium were inoculated with *ER2738* from a fresh plate and incubated overnight at 37 °C while shaking. 1 µL of the overnight-culture was diluted in 1 mL of LB-medium. A blue plaque from an incubated LB/IPTG/X-gal-plate (prepared according to the phage tittering protocol), was picked with a pipette tip. Only plates with less than one hundred colonies were used. Each tip was added to an individual, diluted overnight-culture. The tubes were covered with perforated *parafilm* to maintain oxygen exchange and incubated at 37 °C while shaking for 4.5 h. The tips were discarded and the bacteria were sedimented by centrifugation at 8000 rpm and 4 °C. The supernatant was transferred into a new tube. 500 µL of PEG/NaCl were added. The suspension was mixed and incubated for 15 min to precipitate the phage. The phages were precipitated by centrifugation for 10 min at 14500 rpm (4 °C). The supernatant was carefully discarded. If necessary, the centrifugation was repeated. The precipitated phages were redispersed in 100 µL TE-buffer. The dispersions were used for DNA-extractions. For storage, 10 µL of the phage dispersion were mixed with the same volume of sterile glycerol and stored at -20 °C.

DNA-extraction *

The phage dispersions in TE-buffer, as prepared during the amplification of single phage, were incubated on ice for 10 min. During this time, the dispersion were vigorously mixed three times for 10 s. 60 µL TE-saturated Phenol (CR) were added, and the suspension was mixed vigorously for 30 s and incubated on ice. After 5 min incubation on ice, it was mixed again for 30 s. The phases were separated by centrifugation for 10 min at 14500 rpm (room temperature). 80 µL of the upper phase were carefully transferred to a new tube and 5 µL 3 M NaAc and 200 µL *abs.* EtOH (SA) were added. The solution was briefly mixed and incubated for 15 min at room temperature. The DNA was precipitated by centrifugation for 10 min at 14500 rpm (4 °C) and the supernatant was discarded. The pellet was suspended

*: Modified method according to the literature [229, 233].

in 200 µL of 70% EtOH and the DNA was precipitated by centrifugation at 14500 rpm for 10 min (4 °C). The supernatant was discarded and the DNA pellet was dried. The pellet was dissolved in 25 µL nuclease-free, sterile water (CR). The DNA-extraction was tested by an agarose-gel-electrophoresis. For a 0.7% agarose-gel: 0.7% (210 mg) agarose MEEO (CR) were dispersed in 30 mL TEA-buffer and molten in a microwave. 2 µL *Roti®-GelStain* (CR) were added. After cooling below 70 °C, the solution was cast into a gel chamber. Meanwhile, 1 µL of loading buffer (blue 6x, NEB) was added to 5 µL of an individual DNA-extract. The marker was prepared by mixing 1 µL of the 1 kB DNA-ladder (NEB) with 4 µL nuclease-free, sterile water and 1 µL loading buffer (blue 6x, NEB). After complete gelling, the chamber was filled with TEA-buffer, while the samples and the marker were transferred into the corresponding gel pockets. The electrophoresis was carried out at 100 V. For the visualisation of the DNA bands, a UV lamp at 254 nm was used.

DNA sequencing

For one sample, 6 µL of a corresponding DNA-extract and 1 µL of the 96 gIII sequencing primer (1 nmol/mL) were added into a sterile, nuclease-free PCR-tube. The further addition of reagents (dNTPs, DNA-polymerase,…) and sequencing were carried out at *StarSEQ® GmbH* (*Mainz*, Germany). After receiving, the raw data were processed with the *Serial Cloner* (V2.61, *SerialBasics*) software. The sequence information was translated into to the antiparallel strand and for reasons of orientation, the recognition sites of the restriction enzymes Acc65I and EagI were searched (cp. Appendix I). All three reading frames between these recognition sites were checked for the peptide sequence Ser-His-Ser-$(Xxx)_n$-$(Gly)_3$ (n = 7/12). The sequence in between, is the sought after, randomised peptide sequence. The stop-codon TAG translates as Gln.

Multiple Sequence Analysis

Multiple Sequence Analysis (*MSA*) were carried in the *MEGA 7* software (V. 7.0.21) [238], by applying the built-in algorithms of ClustalW. [300, 301, 302, 303] During the pairwise and the multiple alignments, the gap opening penalty was set to 100 to avoid the peptide sequences being split up. As a weight matrix, the amino acid identity was used. For the amino acids, the following colour-code was used:

brown (G), **yellow** (P), **light-blue** (non-polar amino acids: I, A, L, W, V, F, M, C), **blue** (polar, aromatic amino acids: Y, H), **green** (uncharged, polar amino acids: S, T, Q, N), **pink** (acidic amino acids: E, D) and **light-red** (basic amino acids: R, K).

***Protein-Protein Basic Local Alignment Search Tool* (*BLASTp*)**

The *Protein-Protein Basic Local Alignment Search Tool* (*BLASTp*)[248] of the *National Center for Biotechnoligy Information* (*NCBI*, *United States National Library of Medicine*, *Bethesda*, US-*MD*) was accesed by the *MEGA 7* software (V. 7.0.21)[238]. The non-redundant sequences database (including the *GenBank* CDS translations as well as the databases *PDB*, *SwissProt*, *PIR* and *PRF*), was checked for matching sequences with a word size of 6. PAM30 was used as matrix, with gap cost of 9 and 1.

14.4 Protocol for Phage Display on a calcite {10.4} face

The biopanning were carried out according to the supplier's manual[152] and *Schüler* (**2012**)[77].

For one cycle of biopanning:
A calcite crystal* (3 x 3 mm, cut perpendicular to a {10.4}-facet) was cleaved with a razor blade parallel to the {10.4}-facet. The fresh surface was washed five times with 25 µL TBS-T·0.1 and twice with 25 µL TBS. 10 µL of the corresponding phage library were added onto the surface and incubated for 30 min. After the incubation was finished, the surface was carefully washed six-times with 25 µL TBS-T·0.1. Subsequently, the phage were eluted seven times with 10 µL 0.1 M EDTA and the eluates were combined. Finally, the combined eluates were amplified according to the general amplification protocol.

For the first round of phage display, the commercially available phage libraries, i.e. the random heptapeptide library (Ph.D.-7™) or the random dodecapeptide library (Ph.D.™-12), were used. In the following cycles, the amplified, corresponding eluates of the preceding cycle were used.

At the end of specific cycles of the biopanning, but prior to the general amplification, the combined eluates were sampled for DNA/peptide sequences. For the

*: Obtained from the Kühnle group. Original supplier: *Korth Kristalle GmbH* (*Kiel*, Germany).

sequencing, the phage tittering protocol was first applied, the amount of pfu on the resulting plates was counted and a plate with clearly distinguishable, blue plaques (≤ 100 pfu/plate) was chosen. Ten to twenty individual, blue colonies on such a plate were selected and sampled according to the single phage amplification protocol. It was proceeded with the DNA-extraction protocol and the DNA sequencing. The received raw data were extracted accordingly and the displayed peptide sequences were identified.

Sequences were sampled during the 3rd, 5th and 6th cycle, while screening with the random dodecapeptide library (*Ph.D.-12*™). During the biopanning with the random heptapeptide library (Ph.D.-7™), sequences were sampled in the 5th cycle.

A list of all sampled and identified peptide sequences is attached in the one-letter amino acid code. The sequences are ordered by the utilised library and the cycle, during which the sequences were identified. For the raw DNA-sequencing data and the corresponding complementary strands, see Appendix IIa.

Identified dodecapeptides during the biopanning on {10.4}-facets of calcite

During the 3rd cycle

Sample	Sequence
1	SLSPAGQKSWYS
2	DPMSVLSMHFQR
3	APTSLYPQRSLA
4	SLTDNSNMTTGY
6	QDLVNAGTYRLN
7	ARSHGHHIPAWA
10	ASSLHMFKVNTA

During the 5th cycle

Sample	Sequence
1	NSNNIVYYQRSL
2	ETTHMHIPMPPG
3	NHSPNEAYILST
5	STIPYMHTRTLK
6	MTDEGAIEPQTR
7	NALNNNWTARWP
8	NTTYGTDHDAAL
9	GGHNLWPTATTV
11	QLSSSAMVTLGD
12	KDLAYLGAGANK
13	ERIYEAESRTTL
15	GPLKHTVNTHMP
16	TSNNRDPGLSML
17	HPLTLNPQRPMN
18	YTTALNEMSHTN
19	RPYSELDSIPPR
20	QNINVEMQAVKT

During the 6th cycle

Sample	Sequence
2	HFLLPQMATPYW
9	NFTYAGTYVVHR
10	YPQIAVSYLHMN
12	YRMQELPNISEV
13	SALFDPGINKSR
15	GFSYHKQPNDMS
16	TGHLNPQHQGAQ
17	NDANTRLRIANS
18	SPLTIPSMAYGQ
19	EHASKNANISGL
20	GLAEGRYPQDMG

Identified heptapeptides during the biopanning on {10.4}-facets of calcite

During the 5th cycle

Sample	Sequence
1	STQPHHQ
2	AKPSFPT
3	YPEVPPL
4	NSPIALA
6	KSTSWTV
7	ALSQSLP
10	SSVTPPS

14.5 Protocol for Phage Display on Calcite Nanoparticles

Preparation of nanoparticles

10 mg of calcite nanoparticles (*SOCAL®31*, *Solvay Chemicals International*, *Brussels*, Belgium) were dispersed in 10 mL TBS-T·0.1 buffer in an ultrasonic bath for 10 min. An aliquot of 100 µL was transferred into a 1.5 mL *DNA LoBind Eppendorf* tube (VWR) and the nanoparticles were precipitated by centrifugation at 14500 rpm for 15 min. The supernatant was discarded and the nanoparticles were redispersed in 100 µL TBS buffer. These dispersions were ready for a round of biopanning.

Biopanning

The biopannings were carried out according to the supplier's manual [152] and *Schüler* (**2012**) [77]. However, two different protocols, i.e. A and B, were used for the biopanning on calcite nanoparticles.

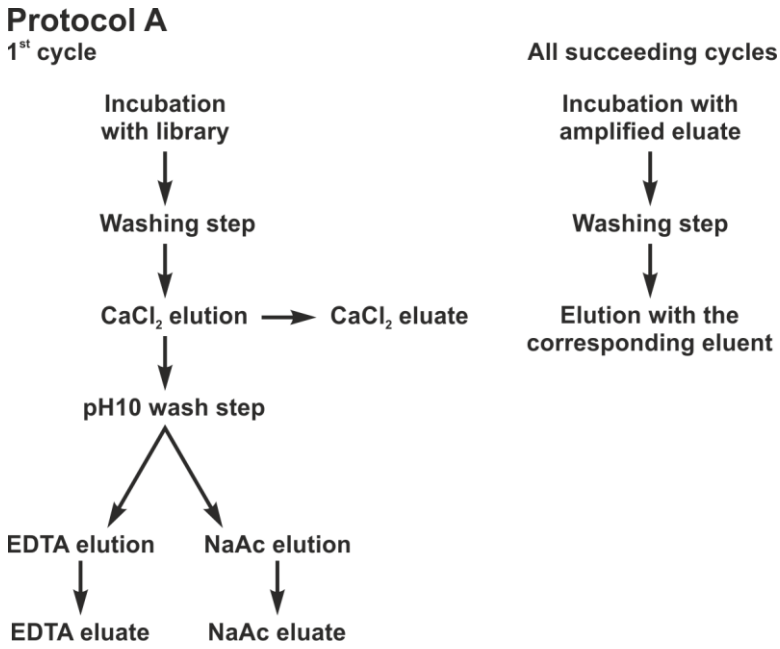

Figure 51) Schematic procedure of protocol A.

During protocol A, the procedure of the first cycle of the biopanning and the procedure of the succeeding cycles deviate strongly from each other (Fig. 51).

For the first cycle of the biopanning:

10 µL of the desired phage library were added to a prepared suspension of the calcite nanoparticles and incubated for 30 min while shaking. The nanoparticles were precipitated by centrifugation at 14500 rpm for 15 min and the supernatant was discarded. 100 µL TBS-T·0.1 buffer were added to the pellet, mixed vigorously and again precipitated by centrifugation at 14500 rpm for 15 min. The wash step was repeated six-times and the corresponding supernatants were collected and combined. The phages were eluted three times by washing the particles with 100 µL 0.1 M $CaCl_2$ in TBS and subsequent centrifugation at 14500 rpm for 15 min. The supernatants of the elution were collected and combined (C1). In the next step, the pellet was washed once with TBS pH 10. After the subsequent centrifugation at 14500 rpm for 15 min, the supernatant was discarded. In the following, the phage were eluted from the nanoparticles six-times by washing with 100 µL of either 0.1 M EDTA or 0.1 M NaAc and subsequent centrifugation at 14500 rpm for 15 min. The corresponding supernatants were collected and combined (E1, N1). The combined eluates C1, E1, N1 and the combined supernatants of the wash step were amplified in *E. coli ER2738* according to the general amplification protocol.

The resulting amplified phage eluates were ready for the second cycle of biopanning.

For the first cycle, the commercially available phage libraries, i.e. the random heptapeptide library (Ph.D.-7™, NEB) or the random dodecapeptide library (Ph.D.™-12, NEB), were used.

For the succeeding cycles of biopanning:
The amplified eluates of the preceding cycle (C, E, N) were used for separate incubations. 10 µL of the corresponding amplified eluate were added to a prepared suspension of the calcite nanoparticles and incubated for 30 min while shaking. After centrifugation at 14500 rpm for 15 min, the supernatant was discarded. The nanoparticles were washed with 100 µL TBS-T·0.1 while mixing vigorously. After centrifugation at 14500 rpm for 15 min, the supernatants were collected and combined. In the following, the phages were eluted from the nanoparticles by washing six-times with 100 µL of the corresponding buffer (i.e. 1M $CaCl_2$ in TBS for C, 0.1M NaAc for N, 0.1M EDTA for E) and subsequent centrifugation at 14500 rpm for 15 min. The supernatants were collected and combined. The combined eluates and the combined supernatants of the wash step were individually amplified in *E. coli ER2738* according to the general amplification protocol. The resulting amplified phage eluates were ready for another cycle of biopanning.

At the end of specific cycles of biopanning, but prior to the general amplification, the combined eluates were sampled for DNA/peptide sequences. For the sequencing, the phage tittering protocol was applied first. The amount of pfu on the resulting plates was determined and a plate with clearly distinguishable, blue plaques (≤ 100 pfu/plate) was selected. On this plate, ten to twenty individual, blue colonies were chosen and sampled according to the single phage amplification protocol. It was proceeded with the DNA-extraction protocol and the DNA sequencing. The received raw data were extracted accordingly and the displayed peptide sequences were identified. For the dodecapeptide library (Ph.-D.12™), sequences were sampled after the third cycle. Additionally, sequences were sampled in the already amplified eluates and the amplified suspension of the wash steps. For the heptapeptide library (Ph.-D.7™), the eluates sampled for peptide

sequences during every cycle of biopanning. Exceptions from the sampling were the eluates of the elution with 1M $CaCl_2$ in TBS and the entire fourth cycle.

A list of all sampled and identified peptide sequences is attached in the one-letter amino acid code. The sequences are ordered according to the utilised library and the corresponding cycle of the biopanning, during which the sequences were identified. For the raw DNA-sequencing data and the corresponding complementary strands, see Appendix IIb.

Identified dodecapeptides on a calcite nanoparticle (Protocol A)

Elution by 1M CaCl2 in TBS-buffer (C)

During the 3rd cycle (C3)

Sample	Sequence
1,3,8,10	LGKTTSAQNLVP
2,4-7,9	QNSTLNYYTLLR

After the 2nd cycle and amplification (C2)

Sample	Sequence
1,2,4-7,10	QNSTLNYYTLLR
3	QNSTTNYHTLVR
8,9	LGKTTSAQNLVP

Sequences in the amplified wash step of the 2nd cycle (WSC2)

Sample	Sequence
1,7	QNSTLNYYTLLR
4	DTFLWWNNELTA
5	STLSWESGWSLW
6	NDTSSKLLLDYS
8	IVDPLLNRTALP

After 1st cycle and amplification (C1)

Sample	Sequence
1	VQSNGLNGWPLH
2	LQNDATHGAGHR
3	SVNYPDFPRWMM
4	SVLTTYPITFQI
5	Sequence matches the M13KE-phage
6	GYTYSDPSSPPK
7	QGYPHYEYEPLP
8	LWKPSWTNQMPT
9	QTLYNGRDDVMA

Sequences in the amplified wash step of the 1st cycle (WSC1) *

Sample	Sequence
1,7	Sequences match the M13KE-phage
2	EHDSLGNDTIPN
3	ANRPNSDIHMSE
4	NLQSGIVNKIVV

*: The elution with 1M CaCl in TBS preceded the elution with 0.1M EDTA during the first cycle. Hence, the identified sequences in the wash step are the same.

Sequences in the amplified wash step of the 1st cycle (WSC1) *

Sample	Sequence
5	AMIKPQLHSAKF
6	NSSLTHPYNYPV
8	TPTQTRYDQSSV
9	FGLSMSTRLTKV
10	HWNSKAPIAHQL

Elution by 0.1M EDTA (E)

During the 3rd cycle (E3)

Sample	Sequence
1,2,5,7-10,12,15,17-20	QNSTLNYYTLLR
3,4,6,11,13,14	LGKTTSAQNLVP

After the 2nd cycle and amplification (E2)

Sample	Sequence
1,2,4,5,7-10	QNSTLNYYTLLR
3,6	LGKTTSAQNLVP

Sequences in the amplified wash step of the 2nd cycle (WSE2)

Sample	Sequence
1	GLGNIWPGMPIN
2,8	QNSTLNYYTLLR
3	AKMSQSSFNLAA
4	LDMDSLSPDNEN
5	VPNTTPWWKYSR
6	AQSHKHRLTEAI
7	FPPYGWVQTRAN

After 1st cycle and amplification (E1)

Sample	Sequence
1	VDRDVILGRYTV
2	SNGYESNKMNRF
3	THSIATKLKPNT
4	QSLKNTGAPILP
5,9	Sequences match the M13KE-phage
6	TTLINPIRSDWK
7	SVYQLAHVSSIP
8	SNSLRNSEWMML
10	MIPSPYKSSVQT

Sequences in the amplified wash step of the 1st cycle (WSE1) *

Sample	Sequence
1,7	Sequences match the M13KE-phage
2	EHDSLGNDTIPN
3	ANRPNSDIHMSE
4	NLQSGIVNKIVV
5	AMIKPQLHSAKF
6	NSSLTHPYNYPV
8	TPTQTRYDQSSV
9	FGLSMSTRLTKV
10	HWNSKAPIAHQL

*: The elution with 1M CaCl in TBS preceded the elution with 0.1M EDTA during the first cycle. Hence, the identified sequences in the wash step are the same.

Elution by 0.1M NaAc (N)

During the 3rd cycle (N3)

Sample	Sequence
1-3,5,9-11,13-17,19	QNSTLNYYTLLR
4,6-8,12,18,20	LGKTTSAQNLVP

After the 2nd cycle and amplification (N2)

Sample	Sequence
1-3,5,6,8,9	QNSTLNYYTLLR
4,7,10	LGKTTSAQNLVP

Sequences in the amplified wash step of the 2nd cycle (WSN2)

Sample	Sequence
2	ILPPDIYERADM
3	IYAAPPWALSVL
4	HLHANPAKKHFA
5	VNRGSHPPDSAM
6	LTDVNKTGFTLV
8	VSASFLTPYKSV
9	NLNHMYPEAPHH

After the 1st cycle and amplification (N1)

Sample	Sequence
1	VAQTAVHGVMQK
2	NKHWSTSNSTLN
3	LNLSTHRHSVNA
4	TGTLNTTSTQPR
5	KLPQTTPYNSLQ
6	DVTLRNSPLTRH
7	SVPLRHGLSWNS

Sequences in the amplified wash step of the 1st cycle (WSN1)

Sample	Sequence
1	MIGFGARNVSNH
2	Sequences matches the M13KE-phage
3	LTEPLTSRLSEQ
4	GWIPQLAGKHPL
6	LGNYPYKSILTQ
7	SMASRMTQAIQP
8	AVLTNPPQRSPN
9	TLFDRANWMGPA
10	QHFEWLKDNLKD

Identified heptapeptides on a calcite nanoparticle (Protocol A)

Elution by 0.1M EDTA (E)

During 1st cycle (E1)

Sample	Sequence
1	HQLLQPP
2	HPAVHSP
3	SPVSFRT
4	VLHPSPR
5	INGHSYA
6	IPKQVLL
7	TVVALVR
8	SISMVKK
9	HQHNNTP

During 2nd cycle (E2)

Sample	Sequence
1	GSHVNLQ
3	TLSAPWF
4	TTTQALG
5	SMSAPGR
6	NISLTRM
7	IPHSYNF
8	WTSVLSA
10	NPPDRPK

During 3rd cycle (E3)

Sample	Sequence
1	TVSVAPL
2	YAIRLPG
3	IAIPALR
4	NYVLSSQ
5	EFLWPAF
6	RLDSSVA
7	SPQLQIQ
8	MYSPGLP
9	HPYNQAG
10	SLNISNW
11	ETPPLSA
12	GYSPFNN
13	TLPQPPT
14	INPYTPG
15	STNPFTN
16	GGPWQTH
17	HYSNGTL
18	SLVNQFR
19	SSLSTDW
20	NHDAIMP

During 5th cycle (E5)

Sample	Sequence
1	GLQNSLP
2	TQNQPWF
3	TWAWRTP
4	TNAWDPQ
5	DPPSLVP
6	SLHYTTH
7	LSNANWS
8	GNTPSRA
9	LERANAH
10	TSPLRNL
11	YPGWSTR
12	TPAKPSP
13	SAISMTY
14	SSHTISF
15	VQSMHSP
16	VLPWYSP
17	SSSNSPP
18	DTYSPTP
19	TVPSKVQ
20	HLPPPHR

Elution by 0.1M NaAc (N)

During 1st cycle (N1)

Sample	Sequence
1	NLMVTMS
2	TPLEHHP
4	TVLGNTS
5	SPSTKPL
6	FSAPKTY
7	WALTRHQ
8	SHYLAPP
9	SNPTDWL
10	AIEPMTR

During 2nd cycle (N2)

Sample	Sequence
1	MEPSNTP
2	TLRLPQP
4	VGLHRYP
5	SLIISRA
6	AIGASPA
7	GLQNSLP
8	SVIAARY
9	MNSPLPA
10	ALNSTQS

During 3rd cycle (N3)

Sample	Sequence
1	TSMSHPL
2	SMPTAPY
3	QASAYYS
4	QPWPTSI
5	GRVLDRI
6	YHTHQNL
8	YVGAMVS
9	AQWAPQD
10	ANMPLQP
11	AFASVPT
12	WSWKQLV
13	VYSVGHT
14	APTLIRY
15	TAKFTPF
16	HPPTSVV
17	LPLTPLP
19	ATTSQPT
20	MIDPSLY

During 5th cycle (N5)

Sample	Sequence
1	ALENPFR
2	GSSNATT
3	LPKPAYR
4	LPPLATT
5	WHLPVTM
6	SILPYPY
7	IQSPHFF
8,17,20	LPLTPLP
9	TNPPGAQ
10	NDSVSLP
11	DSHWALN

During 5th cycle (N5)	
Sample	**Sequence**
12	GETLPPA
13	SQPLFIT
14	TQVPFLA
15	GETRAPL
16	STASYTR
18	NPAAYHT
19	TLPQTSS

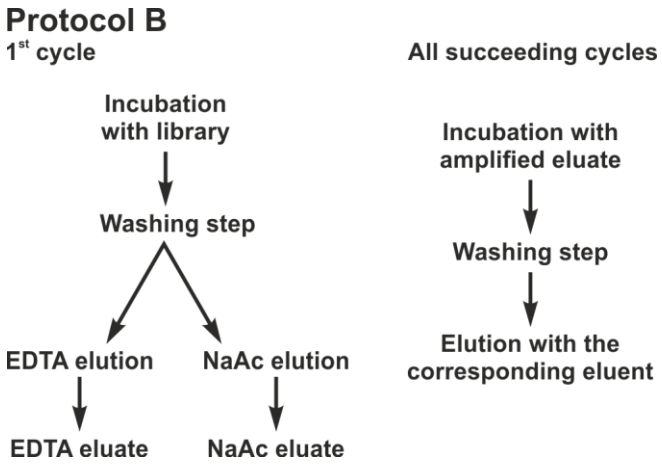

Figure 52) Schematic procedure of protocol B.

In protocol B, the procedure of the first cycle of the biopanning and the procedure of the succeeding cycles did not deviate from each other (Fig. 52).

For one cycle of biopanning:

10 µL of the desired phage library were added to a prepared suspension of the calcite nanoparticles and incubated for 30 min while shaking. After centrifugation at 14500 rpm for 15 min, the supernatant was discarded. The pellet was resuspended and washed with 100 µL TBS-T·0.1 buffer, the nanoparticles were precipitated again by centrifugation at 14500 rpm for 15 min. The supernatant was collected. The wash step was repeated six-times and the supernatants were combined. Subsequently, the phages were eluted from the nanoparticles six-times by washing with 100 µL of either 0.1M EDTA (E1) or 0.1M NaAc (N1) and centrifugation at 14500 rpm for 15 min. The supernatants were collected and combined. The respective eluates and the combined supernatants of the wash step were separately amplified in *E. coli ER2738* according to the general amplification protocol. Afterwards, the amplified eluates were ready for a new cycle of biopanning.

At the end of specific cycles of the biopanning, but prior to the general amplification, the eluates were sampled for DNA/peptide sequences. For the sequencing, the phage tittering protocol was first applied. The amount of pfu on the resulting plates was determined and a plate with clearly distinguishable, blue plaques (≤ 100 pfu/plate) was chosen. On this plate, ten to twenty individual, blue colonies were chosen and sampled according to the single phage amplification protocol. Subsequently, the DNA-extraction protocol and the DNA sequencing were carried out. The received raw data were extracted and the displayed peptide sequences were identified.

Only the heptapeptide library (*Ph.D.7*™) was used. In the following cycles, the nanoparticles were incubated with the amplified eluates of the preceding cycles. Sequences were sampled after the third cycle. Additionally, sequences were sampled in the amplified eluates of preceding cycles as well as in the corresponding amplified suspension of the wash steps.

A list of all sampled and identified peptide sequences is attached in the one-letter amino acid code. The sequences are ordered according to the corresponding cycle of the biopanning, during which the sequences were identified. For the raw DNA-sequencing data and the corresponding complementary strands, see Appendix IIb.

Identified heptapeptides on a calcite nanoparticle (Protocol B)

Elution by 0.1M EDTA (E)

During the 3rd cycle (E3)

Sample	Sequence
1-20	WTNDPDL

Sequences in the amplified wash step of the 3rd cycle (WSE3)

Sample	Sequence
1-9	WTNDPDL
10	VIPHVLS

After 2nd cycle and amplification (E2)

Sample	Sequence
1-10	WTNDPDL

Sequences in the amplified wash step of the 2nd cycle (WSE2)

Sample	Sequence
1	MLTQISP
2	TVSSTSQ
3	ANLLPYT
4	YSVNPHH
5	SNPTLAV

Sequences in the amplified wash step of the 2nd cycle (WSE2)

Sample	Sequence
6	NNGEMSQ
7	FSYQLPH
8	HDPASSK
9	MIQGALR
10	SMFHTSA

Elution by 0.1M NaAc (N)

During the 3rd cycle (N3)

Sample	Sequence
1-4,6-20	WTNDPDL
5	VIPHVLS

Sequences in the amplified wash step of the 3rd cycle (WSN3)

Sample	Sequence
1-10	WTNDPDL

After 2nd cycle and amplification (N2)

Sample	Sequence
1,2,4-6,8,9	WTNDPDL
3,7,10	VIPHVLS

Sequences in the amplified wash step of the 2nd cycle (WSN2)

Sample	Sequence
1	VVPPLKS
2	SLYHFTL
3	GPLDKPQ
4	NGAVSTR
5	TLALTHR
6	THKPLAF
7	QPTLHGK
8	SLWFNPT
9	KLSPPPE
10	ANTNMHL

15.
Experimental Section: Organic Part

15.1 General Information

Solvents and Chemicals

All chemicals and solvents were purchased in the highest commercially available purity. Amino acids were available at *Orpegen Peptide Chemicals GmbH* (*Heidelberg*, Germany). *N*MP, DMF, D*i*PEA and piperidine were purchased at *Iris Biotech GmbH* (*Marktredwitz*, Germany). HOBt, HOAt, HBTU and HATU were procured at AK Scientific, Inc. (*Union City*, US-CA). Water was purified by a *Simplicity 185* ultrapure water system (*Merck-Millipore*, *Bellerica*, US-MA) and *absolute* solvents were prepared according to literature procedures. [304]

Thin layer chromatography

TLC was carried out on *ALUGRAM® SIL G/UV* aluminium sheets pre-coated with silica gel and fluorescent indicator (*Macherey-Nagel GmbH & Co. Kg.*, *Düren*, Germany). Visualization of the chromatograms was done by UV-detection using light with the wavelength λ = 254 nm and/or by staining with ninhydrin-reagent (1.5 g ninhydrin, 15 mL glacial acetic acid, 500 mL methanol).

High-performance liquid chromatography

Analytic RP-HPLC was done using a system consisting of: a *Knauer* (*Knauer, Wissenschaftliche Geräte GmbH*, *Berlin*, Germany) S-1050 pump, a *Knauer K-1001 pump*, a *Knauer* Diode-Array-Detector *K-2800*, a *Knauer* Dynamic Mixing Chamber and a *Knauer* Degasser. As column, a *phenomenex* (*Phenomenex Inc*., *Torrance*, US-CA) *Jupiter C18* (4.6 x 250 mm, 5 µm particles, 300 Å pore size) column was used. Separations were carried out at a flowrate of 1 ml min^{-1}.

Preparative RP-HPLC was done using a system consisting of: two *Knauer Preparative Pump 1800*, a *Knauer Dynamic Mixing Chamber* and a *Knauer UV-detector S 2600*. As column, a *phenomenex Jupiter C18* (21.2 x 250 mm, 5 µm particles, 300 Å pore size) was used. Separations were carried out at a flowrate of 20 mL min^{-1}.

Acetonitrile (HPLC-grade) was commercially available, ultrapure water was produced with a *Simplicity 185* (*Merck-Millipore*, *Bellerica*, US-MA).

Mass Spectrometry

ESI-MS ans *HRESI-MS* were measured on a *Q-TOF Ultima 3* (*Waters Corporation*, *Milford*, US-MA) in methanol.

Nuclear magnetic resonance

The *NMR*-spectra were measured on the following systems:

- *Bruker* Avance III 600: 600 MHz-^{1}*H-NMR*, ^{1}*H-*^{1}*H-COSY*, *TOCSY*, 150.9 MHz-^{13}*C-NMR*, *HSQC*, *HMBC*
- *Bruker* AM-400: 400 MHz-^{1}*H-NMR*, ^{1}*H-*^{1}*H-COSY*, *TOCSY*, 100.6 MHz-^{13}*C-NMR*, *HSQC*, *HMBC*
- Bruker Avance DXR 400: 400 MHz-^{1}*H-NMR*, ^{1}*H-*^{1}*H-COSY*, 100.6 MHz-^{13}*C-NMR*, *HSQC*

Bruker (*Bellerica*, US-MA)

For the multiplicity of *NMR*-signals the following abbreviations will be used:

s	singlet
d	doublet
dd	doublet of doublet
ddd	doublet of doublet of doublet
t	triplet
q	quartet
sext	sextet
m	multiplet
ps	pseudo singlet
pt	pseudo triplet
pq	pseudo quartet
psext	pseudo sextet

15.2 Organic syntheses

N-((9*H*-Fluoren-9-yl)-methoxycarbonyle)-glycyl-(2-methyl-4-(o-tolyldiazenyl)phenyl)-amide (18) [296]

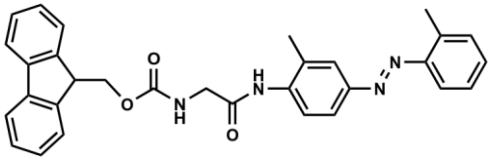

To a suspension of 2.97 g (10 mmol) *N*-((9*H*-Fluoren-9-yl)-methoxycarbonyle)-glycine in 50 mL of dry THF, 0.1 ml (95 mg, 1.3 mmol) of DMF and 1 mL (1.48 g, 11.7 mmol) thionyl chloride were added at 0 °C in a N_2-atmosphere under stirring. The ice-water bath was removed and the reaction was allowed to stir 30 min at ambient temperature. Under stirring the mixture was added to a solution of 4 g (17.9 mmol) of 4`-amino-2,3`-dimethyl-diazobenzene and 5 mL (3.7 g, 28.7 mmol) of D*i*PEA in 50 mL dry THF. After an additional hour of stirring at ambient temperature the solvent was removed under reduced pressure. The resulting crude product was recrystallized in toluene yielding 4.32 g (8.6 mmol, 86%) of the orange product.

TLC (Cyclohexane/Ethyl acetate = 3:1): r_f = 0.19

$C_{31}H_{28}N_4O_3$ (M = 504.58 g/mol) [504.2161]

ESI-MS (positive ion mode) *m/z*: 2039.78 ($[4M+Na]^+$, calc.: 2039.85), 1535.59 ($[3M+Na]^+$, calc.: 1535.64), 1047.37 ($[2M+K]^+$, calc.: 1047.40), 1031.38 ($[2M+Na]^+$, calc.: 1031.42), 1009.41 ($[2M+H]^+$, calc.: 1009.44), 543.16 ($[M+K]^+$, calc.: 543.18), 527.18 ($[M+Na]^+$, calc.: 527.21), 505.20 ($[M+H]^+$, calc.: 505.22)

HRESI-MS (positive ion mode) *m/z*: 527.2053 ($C_{31}H_{28}N_4O_3Na$ ≙ $[M+Na]^+$, calc.: 527.2059)

^{1}H-NMR (400 MHz, DMSO-d_6, *^{1}H*, *COSY*, *^{13}C-HSQC*), *δ* (ppm) = 9.46 (s, 1H, $azo^{NH4`}$), 7.90 (d, 2H, $J_{FmocH4/5,FmocH3/6}$ = 7.5 Hz, $Fmoc^{H4/5}$), 7.83 (d, 1H, $J_{azoH5`,azoH6`}$ = 8.5 Hz, $azo^{H5`}$), 7.79-7.69 (m, 4H, $Fmoc^{H1/8}$ {7.74}, $azo^{H6`}$ {7.74}, G^{NH} {7.73}), 7.55 (d, 1H, $J_{AzoH6,AzoH5}$ = 7.9 Hz, azo^{H6}), 7.45-7.38 (m, 4H, azo^{H4} {7.42}, azo^{H3} {7.42}, $Fmoc^{H3/6}$ {7.42}), 7.37-7.28 (m, 3H, $Fmoc^{H2/7}$ {7.35}, azo^{H5} {7.32}), 4.34 (d, 2H, $J_{FmocH10,FmocH9}$ = 6.8 Hz, $Fmoc^{H10}$), 4.26 (t, 1H, $J_{FmocH9,FmocH10}$ = 6.8 Hz, $Fmoc^{H9}$), 3.93 (d, 2H, $J_{Gα,GNH}$ = 6.1 Hz, $G^α$), 2.67 (s, 3H, azo^{Me2}), 2.34 (s, 3H, $azo^{Me3`}$).

^{13}C-NMR (100.6 MHz, DMSO-d_6, *^{13}C*, *^{13}C-HSQC*), *δ* (ppm) = 168.4 (G^{CO}), 156.6 ($Fmoc^{CO\text{-}urethane}$), 150.0 ($azo^{C1}$), 149.0 ($azo^{C1`}$), 143.8 ($Fmoc^{C1a/8a}$), 140.73 ($Fmoc^{C4a/5a}$), 139.1 ($azo^{C4`}$), 137.3 ($azo^{C2}$), 131.4 ($azo^{C3}$), 131.3 ($azo^{C3`}$), 131.1 ($azo^{C4}$), 127.6 ($Fmoc^{C3/6}$), 127.1 ($Fmoc^{C2/7}$), 126.6 ($azo^{C5}$), 125.2 ($Fmoc^{C1/8}$), 124.7 ($azo^{C2`}$), 124.1 ($azo^{C5`}$), 120.7 ($azo^{C6`}$), 120.1 ($Fmoc^{C4/5}$), 115.0 ($azo^{C6}$), 65.8 ($Fmoc^{C10}$), 46.7 ($Fmoc^{C9}$), 44.1 ($G^{\alpha}$), 18.0 ($azo^{Me3`}$), 17.1 ($azo^{Me2}$).

_N_-((9_H_-Fluoren-9-yl)-methoxycarbonyle)-_L_-glutamyl-(α-glycyl-_N_-(2-methyl-4-(o-tolyldiazenyl)phenyl)-amid)-γ-_t_-butyl ester (19) [296, 297, 298]

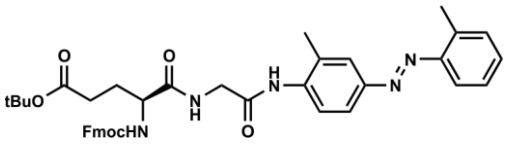

First step: cleavage of the *N*-Fmoc protective group [296]

4.32 g (8.6 mmol) of *N*-((9*H*-Fluoren-9-yl)-methoxycarbonyle)-glycyl-4`-amido-2,3`-dimethyl-diazobenzene) were dissolved in 220 mL CH_2Cl_2. The solution was treated with 44 mL (18.96 g, 222 mmol) piperidine and stirred for 20 min under nitrogen atmosphere. The solvent was removed under reduced pressure. The compound was used without further purification.

$C_{16}H_{18}N_4O$ (M = 282.34 g/mol) [282.1481]

ESI-MS (positive ion mode) *m/z*: 847.43 ($[3M+H]^+$, calc. 847.45), 587.27 ($[2M+Na]^+$, calc.: 587.29), 565.29 ($[2M+H]^+$, calc.: 565.30), 305.13 ($[M+Na]^+$, calc.: 305.14), 283.14 ($[M+H]^+$, calc.: 283.16)

HRESI-MS (positive ion mode) *m/z*: 283.1559 ($C_{16}H_{19}N_4O$ ≙ $[M+H]^+$, calc.: 283.1559)

Second step: coupling of the *N*-Fmoc-*L*-Glu(*t*Bu)-OH moiety [297, 298]

8.09 g (19 mmol) *N*-Fmoc-*L*-Glu(*t*Bu)-OH, 3.36 g (21.9 mmol) HOBt·H_2O and 8.31 g (21.9 mmol) HBTU were dissolved in 110 mL MeCN. Under stirring 3.72 mL (2.83 g, 21.9 mmol) D*i*PEA were added slowly. The crude product of step 1 was suspended in 55 mL MeCN and added to the solution. After stirring for 3 h the solvent was evaporated in vacuo and the residue was dissolved in 150 mL CH_2Cl_2. The solution was washed twice with 50 mL saturated sodium bicarbonate solution and twice with water. The organic phase was dried with Na_2SO_4 and the solvent was removed under reduced pressure. The crude product was purified by column

chromatography on silica gel (cyclohexane/ethyl acetate = 3:1 → 2:1 → 1:1) yielding 3.26 g (4.73 mmol, 55%) of product as an orange solid.

TLC (cyclohexane/ethyl acetate = 3:1): r_f = 0.11

$C_{40}H_{43}N_5O_6$ (M = 689.80 g/mol) [689.3213]

ESI-MS (positive ion mode) *m/z*: 1417.61 ($[2M+K]^+$, calc.: 1417.60), 1401.62 ($[2M+Na]^+$, calc.: 1401.63), 728.28 ($[M+K]^+$, calc.: 728.29), 712.29 ($[M+Na]^+$, calc.: 712.31), 690.33 ($[M+H]^+$, calc.: 690.33)

HRESI-MS (positive ion mode) *m/z*: 712.3127 ($C_{40}H_{43}N_5O_6Na$ ≙ $[M+Na]^+$, calc.: 712.3111)

^{1}H-NMR (400 MHz, DMSO-d_6, *^{1}H*, *COSY*, *^{13}C-HSQC*), *δ* (ppm) = 9.35 (s, 1H, $azo^{NH4`}$), 8.38 (t, 1H, J = 5.7 Hz, $G^{NH}$); 7.91-7.85 (m, 2H, $Fmoc^{H4/5}$), 7.80 (d, 1H, $J_{azoH5`,azoH6`}$ = 8.6 Hz, $azo^{H5`}$), 7.77-7.68 (m, 4H, $azo^{H6`}$ {7.72}, $azo^{H2`}$ {7.72}, $Fmoc^{H1/8}$ {7.71}), 7.68-7.61 (m, 1H, E^{NH}), 7.55 (d, 1H, $J_{azoH6,azoH5}$ = 8.1 Hz, azo^{H6}), 7.45-7.37 (m, 4H, azo^{H4} {7.42}, azo^{H3} {7.42}, $Fmoc^{H3/6}$ {7.40}), 7.36-7.28 (m, 3H, $Fmoc^{H2/7}$ {7.32}, azo^{H5} {7.32}), 4.34-4.26 (m, 2H, $Fmoc^{H10}$), 4.25-4.20 (m, 1H, $Fmoc^{H9}$), 4.13-4.06 (m, 1H, E^{α}), 4.03-3.98 (m, 2H, G^{α}), 2.67 (s, 3H, azo^{Me2}), 2.35-2.27 (m, 5H, $azo^{Me3`}$ {2.33}, E^{γ} {2.29}), 2.03-1.92 (m, 1H, $E^{\beta a}$), 1.86-1.72 (m, 1H, $E^{\beta b}$), 1.39 (s, 9H, *t*Bu^{CH3})

^{13}C-NMR (100.6 MHz, DMSO-d_6, *^{13}C*, *^{13}C-HSQC*), *δ* (ppm) = 173.5 ($E^{\delta CO}$), 171.7 (E^{CO}), 168.0 (G^{CO}), 156.1 ($Fmoc^{CO\text{-}urethane}$), 150.0 ($azo^{C1}$), 149.1 ($azo^{C1`}$), 143.8 ($Fmoc^{C1a/8a}$), 140.7 ($Fmoc^{C4a/5a}$), 139.0 ($azo^{C4`}$), 137.4 ($azo^{C2}$), 131.5 ($azo^{C3}$), 131.4 ($azo^{C3`}$), 131.1 ($azo^{C4}$), 127.7 ($Fmoc^{C3/6}$), 127.1 ($Fmoc^{C2/7}$), 126.6 ($azo^{C5}$), 125.3 ($Fmoc^{C1/8}$), 124.8 ($azo^{C2`}$), 124.1 ($azo^{C5`}$), 120.7 ($azo^{C6`}$), 120.1 ($Fmoc^{C4/5}$), 115.0 ($azo^{C6}$), 79.7 (*t*$Bu^{Cq}$), 65.8 ($Fmoc^{C10}$), 54.0 ($E^{\alpha}$), 46.7 ($Fmoc^{C9}$), 43.0 ($G^{\alpha}$), 31.3 ($E^{\gamma}$), 27.8 (*t*$Bu^{CH3}$), 27.1 ($E^{\beta}$), 17.9 ($azo^{Me3`}$), 17.1 ($azo^{Me2}$)

N-((9*H*-fluoren-9-yl)-methoxycarbonyl)-*L*-glutamyl-(α-glycyl-*N*-(2-methyl-4-(o-tolyldiazenyl)phenyl)-amide) (16) [299]

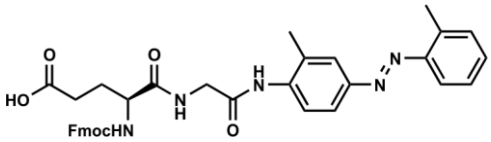

3.26 g (4.73 mmol) ω-(*tert*-butyl-ester)-*N*-((9*H*-fluoren-9-yl)-methoxycarbonyl)-*L*-glutamyl-glycyl-4`-amido-2,3`-dimethyl-diazobenzene were dissolved in 20 mL CH_2Cl_2. A solution of 2 mL water in 20 mL TFA was added under stirring at 0 °C.

The reaction was allowed to reach ambient temperature and was stirred for additional 30 min. 30 mL of toluene were added and the solvent was evaporated in vacuo. Additionally the residue was co-distilled three times with 25 mL toluene. The crude product was purified by column chromatography on silica gel (cyclohexane/ethyl acetate/acetic acid = 20:10:1 → 10:10:1) yielding 1.05 g (1.66 mmol, 35%) of the orange, solid product.

TLC (cyclohexane/ethyl acetate/acetic acid = 10:10:1): r_f = 0.31

$C_{36}H_{35}N_5O_6$ (M = 633.69 g/mol) [633.2587]

ESI-MS (positive ion mode) *m/z*: 1305.58 ($[2M+K]^+$, calc.: 1305.48), 1289.61 ($[2M+Na]^+$, calc.: 1289.51), 1267.63 ($[2M+H]^+$, calc.: 1267.53), 672.27 ($[M+K]^+$, calc.: 672.22), 656.29 ($[M+Na]^+$, calc.: 656.2485), 634.30 ($[M+H]^+$, calc.: 634.27)

HRESI-MS (positive ion mode) *m/z*: 634.2662 ($C_{36}H_{36}N_5O^6$ ≙ $[M+H]^+$, calc.: 634.2666)

^{1}H-NMR (400 MHz, DMSO-d_6, *^{1}H*, *COSY*, *^{13}C-HSQC*), *δ* (ppm) = 9.37 (s, 1H, $azo^{NH4`}$), 8.42 (t, 1H, $J_{GlyNH,Glyα}$ = 5.8 Hz, $G^{NH}$), 7.88 (d, 2H, $J_{FmocH4/5,FmocH3/6}$ = 7.5 Hz, $Fmoc^{H4/5}$), 7.81-7.67 (m, 6H, $azo^{H5`}$ {7.76}, E^{NH} {7.75}, $azo^{H2`}$ {7.74}, $Fmoc^{H1/8}$ {7.71}, $azo^{H6`}$ {7.71}), 7.54 (d, 1H, $J_{azoH6,azoH5}$ = 8.0 Hz, azo^{H6}), 7.44-7.37 (m, 4H, azo^{H3} {7.42}, azo^{H4} {7.41}, $Fmoc^{H3/6}$ {7.41}), 7.35-7.28 (m, 3H, $Fmoc^{H2/7}$ {7.31}, azo^{H5} {7.31}), 4.29-4.18 (m, 3H, $Fmoc^{H10}$ {4.26}, $Fmoc^{H9}$ {4.22}), 4.13-4.06 (m, 1H, $E^{α}$), 4.03-3.97 (m, 2H, $G^{α}$), 2.67 (s, 3H, azo^{Me2}), 2.37-2.28 (m, 5H, $azo^{Me3`}${2.34}, $E^{γ}$ {2.33}), 2.03-1.93 (m, 1H, $E^{βa}$), 1.89-1.78 (m, 1H, $E^{βb}$)

^{13}C-NMR (100.6 MHz, DMSO-d_6, *^{13}C*, *^{13}C-HSQC*), *δ* (ppm) = 174.2 ($E^{δCO}$), 172.8 (E^{CO}), 168.0 (G^{CO}), 156.2 ($Fmoc^{CO\text{-}urethane}$), 150.0 ($azo^{C1}$), 149.1 ($azo^{C1`}$), 143.9 ($Fmoc^{C1a/8a}$), 140.7 ($Fmoc^{C4a/5a}$), 139.0 ($azo^{C4`}$), 137.4 ($azo^{C2}$), 131.4 ($azo^{C3}$), 131.4 ($azo^{C3`}$), 131.1 ($azo^{C4}$), 127.7 ($Fmoc^{C3/6}$), 127.1 ($Fmoc^{C2/7}$), 126.6 ($azo^{C5}$), 125.3 ($Fmoc^{C1/8}$), 124.7 ($azo^{C2`}$), 124.1 ($azo^{C5`}$), 120.7 ($azo^{C6`}$), 120.1 ($Fmoc^{C4/5}$), 115.0 ($azo^{C6}$), 65.8 ($Fmoc^{C10}$), 54.2 ($E^{α}$), 46.7 ($Fmoc^{C9}$), 42.9 ($G^{α}$), 30.6 ($E^{γ}$), 27.7 ($E^{β}$), 17.90 ($azo^{Me3`}$), 17.2 ($azo^{Me2}$)

15.3 Solid Phase Peptide Synthesis

General Procedure for the automated *Solid-Phase-Peptide-Synthesis*

For the *Solid-Phase-Peptide-Synthesis*, a *Perkin-Elmer ABI433a* peptide synthesiser (*Applied Biosystems*®/*Thermo Fisher Scientific*, *Waltham*, US-MA), combined with an external *Series 200 UV/Vis-detector* (*Perkin-Elmer)* was applied. *Tentagel*® *S*-resins by *Rapp Polymere* (*Tübingen*, Germany), functionalized with a *Rink-Amide-Linker* (*RAM*) and preloaded with the corresponding *Fmoc*-protected amino acid, were used. The standard procedure (*FastMoc* 0.1 mmol), consisting of iterative cycles, was carried out in an 8 mL reaction vessel. The first step in one synthesis cycle was the deblocking of the *N*-*Fmoc*-protective group by treating the resin with a solution of 20% piperidine in *N*-methylpyrrolidinone (*N*MP) (three-times for 2.5 min). The resulting dibenzofulvene/piperidine adduct in *N*MP was exploited for the synthesis control by the analysis of the UV-absorption at λ = 301 nm. The following second step was the coupling step. Here, the resin is shaken vigorously for 30 min with 1 mmol (10 *eq*.) of the *Fmoc*-protected amino acid, which had been pre-activated with 1 mmol *O*-(benzotriazol-1-yl)-*N*,*N*,*N*`,*N*`-tetramethyluronium hexafluorophosphate (HBTU), 1 mmol 1-hydroxy-benzotriazole (HOBt) and 2 mmol *N*-ethyldiisopropylamine (D*i*PEA, *Hünig`s base*) in *N*,*N*-dimethylformamide (DMF). Subsequently, the last step in a cycle, the capping step, was carried out to reduce the formation of erroneous sequences. This was done by treating remaining, free amino groups with a solution of 0.5 M acetic anhydride, 0.125 M *N*-ethyldiisopropyl-amine and 0.015 M 1-hydroxybenzotriazole in *N*MP. After each step of a cycle the resin is washed thoroughly with *N*MP. After finishing the overall synthesis, the last Fmoc-protective group is removed as described above. The resin is washed with *N*MP and subsequently with dichloromethane. Finally, the resin is dried in a stream of nitrogen.

General Procedure for the desalting of a peptide

A *Sep-Pak C18 Plus Long Cartridge* (820 mg sorbent per cartridge, 55-105 µm particle size, *Waters Corporation* (*Milford*, US-MA) was activated by washing with 30 mL of MeCN and subsequently, by 30 mL of water. The cartridge was subsequently loaded with 40 mg of the peptide in 1mL of water. To ensure the adsorption the collected water was run through the cartridge twice. The cartridge was washed with 30 mL of water and the peptide was eluted with MeOH/water

(7:3). The resulting solution was evaporated under reduced pressure. The remaining solid was dissolved in 10 mL of water and lyophilisated.

_L_-Leucyl-glycyl-_L_-lysyl-_L_-threonyl-_L_-threony-_L_-seryl-_L_-alanyl-_L_-glutaminyl-_L_-asparaginyl-_L_-leucyl-_L_-valyl-_L_-prolinamide (1)
(Leu-Gly-Lys-Thr-Thr-Ser-Ala-Gln-Asn-Leu-Val-Pro-amide)

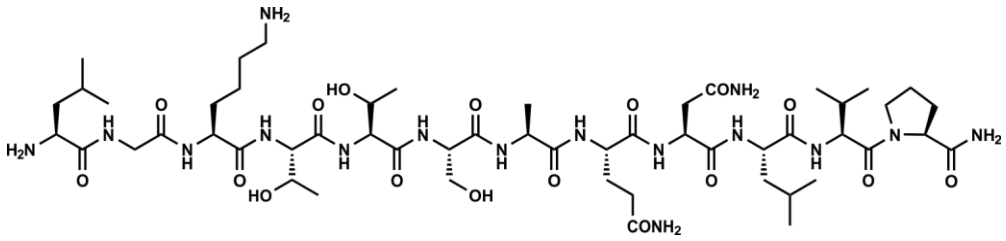

The automated *Solid-Phase-Peptide-Synthesis* was carried out as described in the general procedure, using 417 mg (0.1 mmol) of the *N-Fmoc*-Pro preloaded *RAM-Tentagel*® *S*-resin (loading capacity: 0.24 mmol/g). After the final deblocking of the *Fmoc*-protective group the resin was transferred into a *Merrifield*-reaction vessel. A mixture of 15 mL trifluoroacetic acid (TFA), 0.9 mL water and 0.9 mL triisopropylsilane (TIS) was added and the suspension was shaken for 3 h. The suspension was filtrated and the resin was washed with TFA (3·3 ml). 25 mL of toluene were added to the combined filtrates, the solution was concentrated in vacuo and codistilled with toluene (3·25 mL). The residue was washed with cold diethyl ether (Et_2O) (3·3 mL), dissolved in water and lyophilised, yielding 70 mg of crude product. The crude peptide was purified by semi-preparative HPLC (phenomenex, Jupiter C18, acetonitrile/water + 0.1% TFA, isocratic: 15:85, λ = 214 nm; t_R = 9.0 min) yielding 44 mg (0.036 mmol, 36%) of the peptide after lyophilisation.

Analytic HPLC: t_R = 13.9 min (phenomenex Jupiter C18, MeCN/H2O + 0.1% TFA, isocratic: 15:85, λ = 214 nm)

$C_{53}H_{94}N_{16}O_{17}$ (M = 1227.41 g/mol) [1226.6983]

ESI-MS (positive ion mode) *m/z*: 1249.66 ([M+Na]$^+$, calc.: 1249.69), 1227.69 ([M+H]$^+$, calc.: 1227.71), 636.34 ([M+2Na]$^+$, calc.: 636.34), 625.24 ([M+H+Na]$^+$, calc.: 625.34), 614.34 ([M+2H]$^+$, calc.: 614.36)

HRESI-MS (positive ion mode) *m/z*: 1227.7090 ($C_{53}H_{95}N_{16}O_{17}$ ≙ [M+H]$^+$, calc.: 1227.7061)

^{1}H-NMR (600 MHz, DMSO-d_6, *^{1}H*, *COSY*, *TOCSY*, *^{13}C-HSQC*, *HMBC*), *δ* (ppm) = 8.77 (t, 1H, $J_{G(2)NH,G(2)\alpha}$ = 5.7 Hz, G(2)^{NH}), 8.21-8.11 (m, 3H, K(3)^{NH} {8,17}, L(1)^{NH2} {8.16}), 8.13-8.06 (m, 2H, A(7)^{NH} {8.10}, N(9)^{NH} {8.10}), 8.06-7.99 (m, 2H, T(4)^{NH} {8.03}, Q(8)^{NH} {8.02}), 7.98 (d, 1H, $J_{S(6)NH,S(6)\alpha}$ = 7.5 Hz, S(6)^{NH}), 7.85 (d, 1H, $J_{V(11)NH,V(11)\alpha}$ = 8.4 Hz, V(11)^{NH}), 7.79 (d, 1H, $J_{L(10)NH,L(10)\alpha}$ = 8.3 Hz, L(10)^{NH}), 7.78-7.71 (m, 3H, K(3)$^{\zeta NH3+}$), 7.65 (d, *J* = 8.1 Hz, T(5)^{NH}), 7.38 (s, 1H, N(9)$^{\gamma CONH2a}$), 7.27 (s, 1H, P(12)^{CONH2a}), 7.25 (s, 1H, Q(8)$^{\delta CONH2a}$), 6.93 (s, 1H, N(9)$^{\gamma CONH2b}$), 6.85 (s, 1H, P(12)^{CONH2b}), 6.83 (s, 1H, Q(8)$^{\delta CONH2b}$), 4.50 (pq, 1H, *J* = 7.1 Hz, N(9)$^{\alpha}$), 4.44-4.37 (m, 1H, K(3)$^{\alpha}$), 4.37-4.12 (m, 8H, S(6)$^{\alpha}$ {4.35}, T(5)$^{\alpha}$ {4.31}, T(4)$^{\alpha}$ {4.28}, L(10)$^{\alpha}$ {4.27}, A(7)$^{\alpha}$ {4.25}, V(11)$^{\alpha}$ {4.24}, P(12)$^{\alpha}$ {4.20}, Q(8)$^{\alpha}$ {4.17}), 4.05-4.00 (m, 2H, T(4)$^{\beta}$ {4.02}, T(5)$^{\beta}$ {4.02}), 3.90 (dd, 1H, $J_{G(2)\alpha a,G(2)\alpha b}$ = 16.7 Hz, $J_{G(2)\alpha a,G(2)NH}$ = 5.9 Hz, G(2)$^{\alpha a}$), 3.81 (pq, 1H, *J* = 6.5 Hz, L(1)$^{\alpha}$), 3.77 (dd, 1H, $J_{G(2)\alpha b,G(2)\alpha a}$ = 16.8 Hz, $J_{G(2)\alpha b,G(2)NH}$ = 5.4 Hz, G(2)$^{\alpha b}$), 3.72- 3.67 (m, 1H, P(12)$^{\delta a}$), 3.64 (dd, 1H, *J* = 10.7 Hz, *J* = 5.7 Hz, S(6)$^{\beta a}$), 3.57 (overlapped by water signal, 1H, S(6)$^{\beta b}$), 3.53 (overlapped by water signal, 1H, P(12)$^{\delta b}$), 2.80-2.72 (m, 2H, K(3)$^{\varepsilon}$), 2.56-2.50 (overlapped by DMSO-signal, 1H, N(9)$^{\beta a}$), 2.41 (dd, 1H, *J* = 15.5, *J* = 7.6 Hz, N(9)$^{\beta b}$), 2.15-2.04 (m, 2H, Q(8)$^{\gamma}$), 2.03-1.95 (m, 2H, V(11)$^{\beta}$ {2.00}, P(12)$^{\beta a}$ {2.00}), 1.94-1.83 (m, 2H, P(12)$^{\gamma a}$ {1.90}, Q(8)$^{\beta a}$ {1.85}), 1.82-1.64 (m, 5H, P(12)$^{\gamma b}$ {1.80}, P(12)$^{\beta b}$ {1.75}, Q(8)$^{\beta b}$ {1.72}, K(3)$^{\beta a}$ {1.68}, L(1)$^{\gamma}$ {1.67}), 1.60-1.47 (m, 6H, L(10)$^{\gamma}$ {1.56}, L(1)$^{\beta a/b}$ {1.54}, K(3)$^{\delta}$ {1.52}, K(3)$^{\beta b}$ {1.51}), 1.47-1.39 (m, 2H, L(10)$^{\beta a/b}$), 1.37-1.25 (m, 2H, K(3)$^{\gamma}$), 1.22 (d, 3H, $J_{A(7)\beta,A(7)\alpha}$ = 7.0 Hz, A(7)$^{\beta}$), 1.07-1.00 (m, 6H, T(4)$^{\gamma}$ {1.03}, T(5)$^{\gamma}$ {1.03}), 0.91-0.87 (m, 9H, L(1)$^{\delta}$ {0.90}, V(11)$^{\gamma}$ {0.89}, L(1)$^{\delta`}$ {0.88}), 0.86-0.83 (m, 6H, V(11)$^{\gamma`}$ {0.85}, L(10)$^{\delta}$ {0.84}), 0.79 (d, 3H, $J_{L(10)\delta`,L(10)\gamma}$ = 6.4 Hz, L(10)$^{\delta`}$)

^{13}C-NMR (150.9 MHz, DMSO-d_6, *^{13}C*, *^{13}C-HSQC*, *HMBC*), *δ* (ppm) = 174.0 (Q(8)$^{\delta CONH2}$), 173.6 (P(12)^{CONH2}), 172.4 (A(7)^{CO}), 171.8 (L(10)^{CO}), 171.8 (K(3)^{CO}), 171.6 (N(9)$^{\gamma CONH2}$), 171.1 (Q(8)^{CO}), 170.6 (N(9)^{CO}), 170.0 (T(4)^{CO}), 170.0 (T(5)^{CO}), 169.9 (S(6)^{CO}), 169.7 (V(11)^{CO}), 169.4 (L(1)^{CO}), 168.0 (G(2)^{CO}), 66.7 (T(5)$^{\beta}$), 66.5 (T(4)$^{\beta}$), 61.6 (S(6)$^{\beta}$), 59.3 (P(12)$^{\alpha}$), 58.0 (T(4)$^{\alpha}$), 57.7 (T(5)$^{\alpha}$), 55.8 (V(11)$^{\alpha}$), 55.0 (S(6)$^{\alpha}$), 52.4 (Q(8)$^{\alpha}$), 52.3 (K(3)$^{\alpha}$), 51.1 (L(10)$^{\alpha}$), 50.9 (L(1)$^{\alpha}$), 49.8 (N(9)$^{\alpha}$), 48.6 (A(7)$^{\alpha}$), 47.1 (P(12)$^{\delta}$), 41.8 (G(2)$^{\alpha}$), 40.8 (L(10)$^{\beta}$), 40.4 (L(1)$^{\beta}$), 38.8 (K(3)$^{\varepsilon}$), 36.9 (N(9)$^{\beta}$), 31.5 (Q(8)$^{\gamma}$), 30.0 (V(11)$^{\beta}$), 29.4 (P(12)$^{\beta}$), 28.0 (Q(8)$^{\beta}$), 26.7 (K(3)$^{\delta}$), 24.6 (P(12)$^{\gamma}$), 24.1 (L(10)$^{\gamma}$), 23.6 (L(1)$^{\gamma}$), 23.3 (L(10)$^{\delta}$), 22.7 (L(1)$^{\delta}$),

22.3 (K(3)$^{\gamma}$), 22.0 (L(1)$^{\delta`}$), 21.5 (L(10)$^{\delta`}$), 19.6 (T(4)$^{\gamma}$), 19.3 (T(5)$^{\gamma}$), 19.2 (V(11)$^{\gamma}$), 18.6 (V(11)$^{\gamma`}$), 17.7 (A(7)$^{\beta}$)

_L_-Glutaminyl-_L_-asparaginyl-_L_-seryl-_L_-threonyl-_L_-leucyl-_L_-asparagyl-_L_-tyrosyl-_L_-tyrosyl-_L_-threonyl-_L_-leucyl-_L_-leucyl-_L_-arginine amide (2)
(Gln-Asn-Ser-Thr-Leu-Asn-Tyr-Tyr-Thr-Leu-Leu-Arg-amide)

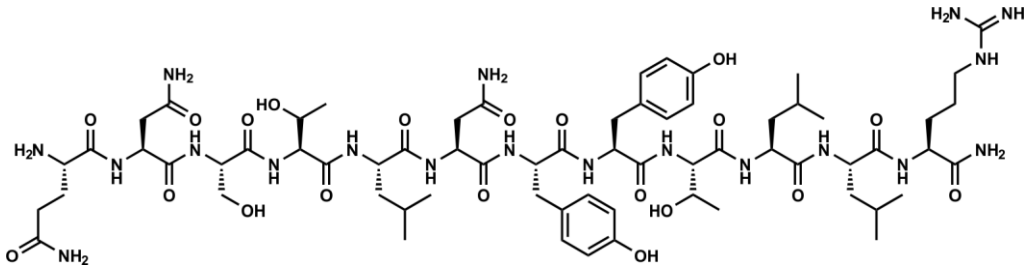

_L_-Pyroglutamyl-_L_-asparaginyl-_L_-seryl-_L_-threonyl-_L_-leucyl-_L_-asparagyl-_L_-tyrosyl-_L_-tyrosyl-_L_-threonyl-_L_-leucyl-_L_-leucyl-_L_-arginine amide (6)
(Glp-Asn-Ser-Thr-Leu-Asn-Tyr-Tyr-Thr-Leu-Leu-Arg-amide)

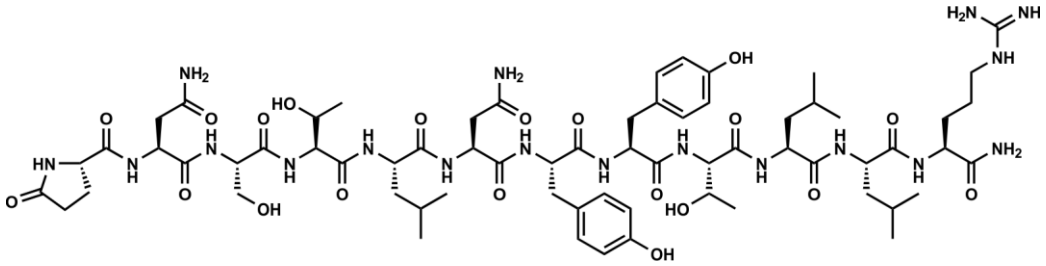

The automated *Solid-Phase-Peptide-Synthesis* was carried out as described in the general procedure, using 476 mg (0.1 mmol) of the *N-Fmoc*-Arg(Pbf) preloaded *RAM-Tentagel*® *S*-resin (loading capacity: 0.21 mmol/g). After the final deblocking of the *Fmoc*-protective group the resin was transferred into a *Merrifield*-reaction vessel. A mixture of 15 mL trifluoroacetic acid (TFA), 0.9 mL water and 0.9 mL triisopropylsilane (TIS) was added and the suspension was shaken for 3 h. The suspension was filtrated and the resin was washed with TFA (3·3 ml). 25 mL of toluene were added to the combined filtrates, afterwards the solution was concentrated in vacuo and co-evaporated with toluene (3·25 mL). The residue was washed with cold diethyl ether (Et_2O) (3·3 mL), dissolved in water and lyophilised, yielding 128 mg of crude product, containing peptide (**2**) as well as the *L*-pyroglutamic acid derivative (**6**). Both were not separated.

Product molecule (**2**): $C_{66}H_{109}N_{19}O_{20}$ (M = 1484.66 g/mol) [1483.7856]

L-Pyroglutamic acid derivate (**6**): $C_{66}H_{102}N_{18}O_{20}$ (CM ≙ 1467.62 g/mol) [1466.7518]

ESI-MS (positive ion mode) *m/z*: 1484.82 ($[M+H]^+$, calc.: 1484.79), 1467.79 ($[CM+H]^+$, calc.: 1467.76), 753.89 ($[M+Na+H]^{2+}$, calc.: 753.89), 745.37 ($[CM+Na+H]^{2+}$, calc.: 745.38), 742.90 ($[M+2H]^{2+}$, calc.: 742.90), 734.38 ($[CM+2H]^{2+}$, calc: 734.39)

_L_-Glutaminyl-_L_-asparaginyl-_L_-seryl-_L_-threonyl-_L_-threony-_L_-asparagyl-_L_-tyrosyl-_L_-histidyl-_L_-threonyl-_L_-leucyl-_L_-valyl-_L_-argininamide (3)
(Gln-Asn-Ser-Thr-Thr-Asn-Tyr-His-Thr-Leu-Val-Arg-amide)

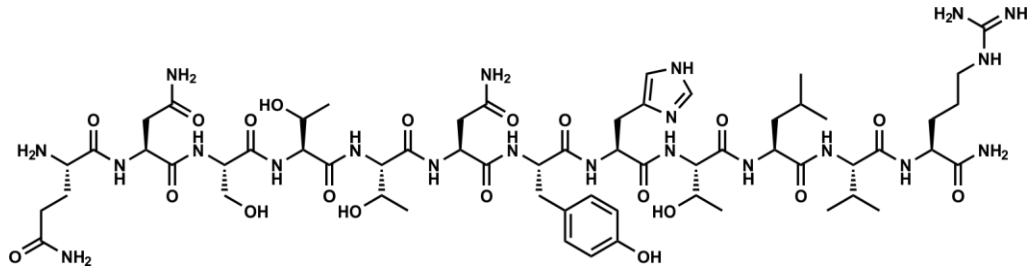

_L_-Pyroglutamyl-_L_-asparaginyl-_L_-seryl-_L_-threonyl-_L_-threony-_L_-asparagyl-_L_-tyrosyl-_L_-histidyl-_L_-threonyl-_L_-leucyl-_L_-valyl-_L_-argininamide (7)
(Glp-Asn-Ser-Thr-Thr-Asn-Tyr-His-Thr-Leu-Val-Arg-amide)

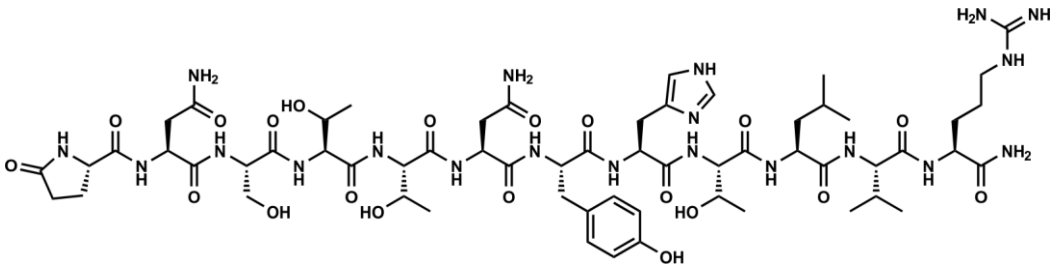

The automated *Solid-Phase-Peptide-Synthesis* was carried out as described in the general procedure, using 476 mg (0.1 mmol) of the *N-Fmoc*-Arg(Pbf) preloaded *RAM-Tentagel*® *S*-resin (loading capacity: 0.21 mmol/g). After the final deblocking of the *Fmoc*-protective group the resin was transferred into a *Merrifield*-reaction vessel. A mixture of 15 mL trifluoroacetic acid (TFA), 0.9 mL water and 0.9 mL triisopropylsilane (TIS) was added and the suspension was shaken for 3 h. The suspension was filtrated and the resin was washed with TFA (3·3 ml). 25 mL of toluene were added to the combined filtrates, afterwards the solution was concentrated in vacuo and co-evaporated with toluene (3·25 mL). The residue was washed with cold diethyl ether (Et_2O) (3·3 mL), dissolved in water and lyophilised, yielding 122 mg of a crude product, containing peptide (**3**) and its L-pyroglutamic acid derivative (**7**).

Product molecule (**3**): $C_{66}H_{109}N_{21}O_{20}$ (M = 1432.56 g/mol) [1431.7219]
L-Pyroglutamic acid derivate (**7**): $C_{60}H_{97}N_{20}O_{20}$ (CM ≙ 1415.51 g/mol) [1414.6953]
ESI-MS (positive ion mode) *m/z*: 1432.82 ($[M+H]^+$, calc.: 1432.73), 1415.78 ($[CM+H]^+$, calc.: 1415.70), 716.89 ($[M+2H]^{2+}$, calc.: 716.87), 708.34 ($[CM+2H]^{2+}$, calc: 708.36)

The L-pyroglutamic acid derivative (7) was isolated by semi-preparative *HPLC* (phenomenex, Jupiter C18, acetonitrile/water + 0.1% TFA, grad.: 13:87 (5 min const.) → 19:81, 20 min, λ = 214 nm, t_R = 15,0 min) yielding 20 mg (0.014 mmol, 14%) of the peptide after lyophilisation.
Analytic HPLC: t_R = 16,4 min (phenomenex Jupiter C18, MeCN/H2O + 0.1% TFA, grad.: 13:87 (5 min const.) → 19:81, 20 min, λ = 214 nm)
$C_{60}H_{94}N_{20}O_{20}$ (M = 1415.51 g mol^{-1}) [1414.6953 g mol^{-1}]
ESI-MS (positive ion mode) *m/z*: 1415.71 ($[M+H]^+$, calc.: 1415.70), 738.39 ($[M+Na+K]^{2+}$, calc.: 738.33), 730.36 ($[M+2Na]^{2+}$, calc.: 730.34), 719.35 ($[M+H+Na]^{2+}$, calc.: 719.35), 708.32 ($[M+2H]^{2+}$, calc.: 708.36), 485.22 ($[M+2H+K]^{3+}$, calc.: 485.22), 479.90 ($[M+2H+Na]^{3+}$, calc.: 479.90)
HRESI-MS (positive ion mode) *m/z*: 1415.7052 ($C_{60}H_{95}N_{20}O_{20}$ ≙ $[M+H]^+$, calc.: 1415.7032)
^{1}H-NMR (600 MHz, DMSO-d_6, *^{1}H*, *COSY*, *TOCSY*, *^{13}C-HSQC*, *HMBC*), δ (ppm) = 8.95 (s, 1H, $H(8)^{H2}$), 8.39 (d, 1H, $J_{H(8)NH,H(8)\alpha}$ = 8.2 Hz, $H(8)^{NH}$), 8.24 (d, 1H, $J_{N(2)NH,N(2)\alpha}$ = 7.8 Hz, $N(2)^{NH}$), 8.11-8.03 (m, 2H, $L(10)^{NH}$ {8.06}, $N(6)^{NH}$ {8.06}), 8.00 (d, 1H, $J_{Y(7)NH,Y(7)\alpha}$ = 7.4 Hz, $Y(7)^{NH}$), 7.95-7.87 (m, 3H, $S(3)^{NH}$ {7.93}, $R(12)^{NH}$ {7.93}, $T(4)^{NH}$ {7.90}), 7.86-7.79 (m, 3H, $V(11)^{NH}$ {7.84}, $Glp(1)^{NH}$ {7.82}, $T(9)^{NH}$ {7.81}), 7.70 (d, 1H, $J_{T(5)NH,T(5)\alpha}$ = 8.3 Hz, $T(5)^{NH}$), 7.66 (t, 1H, $J_{R(12)\varepsilon NH,R(12)\delta}$ = 5.8 Hz, $R(12)^{\varepsilon NH}$), 7.47 (s, 1H, $N(2)^{CONH2a}$), 7.42 (s, 1H, $N(6)^{CONH2a}$), 7.37-7.32 (m, 2H, $H(8)^{H5}$ {7.35}, $R(12)^{CONH2a}$ {7.33}), 7.09 (s, 1H, $R(12)^{CONH2b}$), 7.04-6.96 (m, 4H, $N(2)^{CONH2b}$ {7.01}, $N(6)^{CONH2b}$ {6.98}, $Y(7)^{H2/6}$ {6.98}), 6.62 (d, 2H, $J_{Y(7)3/5,Y(7)2/6}$ = 8.4 Hz, $Y(7)^{H3/5}$), 4.66 (pq, 1H, J = 7.8 Hz, $H(8)^{\alpha}$), 4.64-4.58 (m, 1H, $N(2)^{\alpha}$), 4.55 (pq, 1H, J = 7.0 Hz, $N(6)^{\alpha}$), 4.40-4.34 (m, 2H, $S(3)^{\alpha}$ {4.38}, $L(10)^{\alpha}$ {4.37}), 4.33-4.21 (m, 4H, $Y(7)^{\alpha}$ {4.32}, $T(4)^{\alpha}$ {4.28}, $T(5)^{\alpha}$ {4.26}, $T(9)^{\alpha}$ {4.24}), 4.19-4.15 (m, 2H, $R(12)^{\alpha}$ {4.18}, $V(11)^{\alpha}$ {4.15}), 4.07-4.02 (m, 2H, $T(4)^{\beta}$ {4.05}, $Glp(1)^{\alpha}$ {4.05}), 4.00-3.94 (m, 2H $T(9)^{\beta}$ {3.98}, $T(5)^{\beta}$ {3.97}), 3.64 (dd, 1H, J = 10.8 Hz, J = 5.7 Hz, $S(3)^{\beta a}$), 3.57 (dd, 1H, J = 10.9 Hz, J = 5.8 Hz, $S(3)^{\beta b}$),

3.14-3.06 (m, 3H, H(8)$^{\beta a}$ {3.12}, R(12)$^{\delta a/b}$ {3.09}), 2.99 (dd, 1H, *J* = 15.3 Hz, *J* = 8.3 Hz, H(8)$^{\beta b}$), 2.89-2.82 (m, 1H, Y(7)$^{\beta a}$), 2.66 (dd, 1H, *J* = 14.3 Hz, *J* = 9.4 Hz, Y(7)$^{\beta b}$), 2.61-2.53 (m, 2H, N(2)$^{\beta a}$ {2.57}, N(6)$^{\beta a}$ {2.55}), 2.44 (dd, 1H, *J* = 15.4 Hz, *J* = 7.8 Hz, N(2)$^{\beta b}$), 2.35 (dd, 1H, *J* = 15.6 Hz, *J* = 6.7 Hz, N(6)$^{\beta b}$), 2.29-2.21 (m, 1H, Glp(1)$^{\beta a}$), 2.14 (ddd, 1H, *J* = 16.9 Hz, *J* = 9.5 Hz, *J* = 7.6 Hz, Glp(1)$^{\gamma a}$), 2.05 (ddd, 1H, *J* = 16.5 Hz, *J* = 9.9 Hz, *J* = 5.1 Hz, Glp(1)$^{\gamma b}$), 1.96 (psext, 1H, *J* = 6.8 Hz, V(11)$^{\beta}$), 1.93-1.87 (m, 1H, Glp(1)$^{\beta b}$), 1.70-1.56 (m, 2H, R(12)$^{\beta a}$ {1.65}, L(10)$^{\gamma}$ {1.62}), 1.56-1.38 (m, 5H, R(12)$^{\beta b}$ {1.52}, L(10)$^{\beta a/b}$ {1.48}, R(12)$^{\beta a/b}$ {1.45}), 1.07-1.03 (m, 6H, T(9)$^{\gamma}$ {1.06}, T(4)$^{\gamma}$ {1.04}), 1.00 (d, 3H, $J_{T(5)\gamma,T(5)\beta}$ = 6.2 Hz, T(5)$^{\gamma}$), 0.87 (d, 3H, $J_{L(10)\delta,L(10)\gamma}$ = 6.6 Hz, L(10)$^{\delta}$), 0.85-0.80 (m, 9H, V(11)$^{\gamma}$ {0.84}, L(10)$^{\delta`}$ {0.83}, V(11)$^{\gamma`}$ {0.83})

^{13}C-NMR (150.9 MHz, DMSO-d$_6$, *^{13}C*, *^{13}C-HSQC*, *HMBC*), *δ* (ppm) = 177.8 (Glp(1)$^{\delta CONH}$), 173.3 (R(12)^{CO}), 172.7 (Glp(1)^{CO}), 172.1 (N(2)$^{\gamma CONH2}$), 172.1 (L(10)^{CO}), 171.8 (N(6)$^{\gamma CONH2}$), 171.4 (Y(7)^{CO}), 171.2 (N(6)^{CO}), 171.1 (N(2)^{CO}), 170.9 (V(11)^{CO}), 170.4 (S(3)^{CO}), 170.1 (T(4)^{CO}), 170.0 (H(8)^{CO}), 169.9 (T(9)^{CO}), 169.9 (T(5)^{CO}), 156.9 (R(12)$^{\zeta}$), 156.0 (Y(7)^{C4}), 133.9 (H(8)^{C2}), 130.2 (Y(7)$^{C2/6}$), 129.4 (H(8)^{C4}), 127.7 (Y(7)^{C1}), 117.2 (H(8)^{C5}), 115.1 (Y(7)$^{C3/5}$), 66.9 (T(9)$^{\beta}$), 66.8 (T(4)$^{\beta}$), 66.6 (T(5)$^{\beta}$), 61.8 (S(3)$^{\beta}$), 58.5 (T(4)$^{\alpha}$), 58.4 (T(9)$^{\alpha}$), 58.1 (T(5)$^{\alpha}$), 58.0 (V(11)$^{\alpha}$), 55.6 (Glp(1)$^{\alpha}$), 55.1 (S(3)$^{\alpha}$), 54.9 (Y(7)$^{\alpha}$), 52.1 (R(12)$^{\alpha}$), 51.8 (H(8)$^{\alpha}$), 51.4 (L(10)$^{\alpha}$), 49.9 (N(2)$^{\alpha}$), 49,7 (N(6)$^{\alpha}$), 40.8 (L(10)$^{\beta}$), 40.5 (R(12)$^{\delta}$), 37.3 (N(2)$^{\beta}$), 37.1 (N(6)$^{\beta}$), 36.2 (Y(7)$^{\beta}$), 30.6 (V(11)$^{\beta}$), 29.4 (R(12)$^{\beta}$), 29.3 (Glp(1)$^{\gamma}$), 27.0 (H(8)$^{\beta}$), 25.5 (Glp(1)$^{\beta}$), 25.3 (R(12)$^{\gamma}$), 24.3 (L(10)$^{\gamma}$), 23.3 (L(10)$^{\delta}$), 21.8 (L(10)$^{\delta`}$), 19.7 (T(4)$^{\gamma}$), 19.6 (T(9)$^{\gamma}$), 19.5 (T(5)$^{\gamma}$), 19.4 (V(11)$^{\gamma}$), 18.4 (V(11)$^{\gamma`}$)

Glycyl-*L*-glutaminyl-*L*-asparaginyl-*L*-seryl-*L*-threonyl-*L*-threony-*L*-asparagyl-*L*-tyrosyl-*L*-histidyl-*L*-threonyl-*L*-leucyl-*L*-valyl-*L*-arginin-amide (8)

(Gly-Gln-Asn-Ser-Thr-Thr-Asn-Tyr-His-Thr-Leu-Val-Arg-amide)

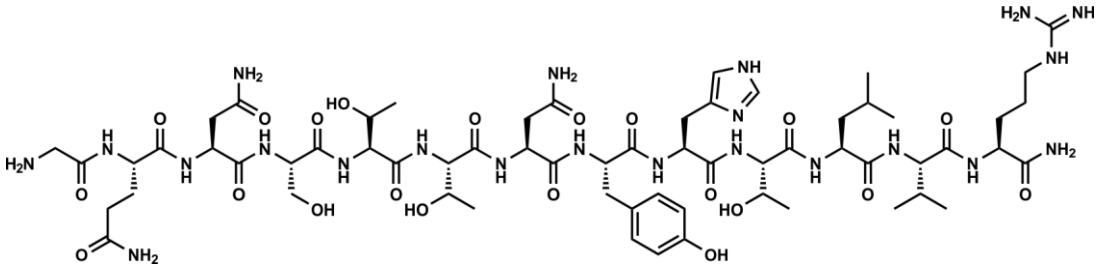

The automated *Solid-Phase-Peptide-Synthesis* was carried out as described in the general procedure, using 476 mg (0.1 mmol) of the *N-Fmoc*-Arg(Pbf) preloaded *RAM-Tentagel*® *S*-resin (loading capacity: 0.21 mmol/g). After the final deblocking of the *N-Fmoc*-protective group the resin was transferred into a *Merrifield*-reaction vessel. A mixture of 15 mL trifluoroacetic acid (TFA), 0.9 mL water and 0.9 mL triisopropylsilane (TIS) was added and the suspension was shaken for 3 h. The suspension was filtrated and the resin was washed with TFA (3·3 ml). 25 mL of toluene were added to the combined filtrates, the solution was concentrated in vacuo and codistilled with toluene (3·25 mL). The residue was washed with cold diethyl ether (Et_2O) (3·3 mL), dissolved in water and lyophilised, yielding 123 mg of crude product. The crude peptide was purified by semi-preparative *HPLC* (phenomenex, Jupiter C18, acetonitrile/water + 0.1% TFA, grad.: 13:87 (5 min const.) → 21:79, 20 min, λ = 214 nm; t_R = 8.6 min) yielding 63 mg (0.042 mmol, 42%) of the peptide after lyophilisation.

Analytic HPLC: t_R = 15.6 min (phenomenex Jupiter C18, MeCN/H2O + 0.1% TFA, grad.: 13:87 (5 min const.) → 21:79, 20 min, λ = 214 nm)

$C_{62}H_{100}N_{22}O_{21}$ (M = 1489.59 g/mol) [1488.7433]

ESI-MS (positive ion mode) *m/z*: 1489.79 ($[M+H]^+$, calc.: 1489.75), 764.38 ($[M+H+K]^{2+}$, calc.: 764.35), 756.39 ($[M+H+Na]^{2+}$, calc.: 756.37), 745.38 ($[M+2H]^{2+}$, calc.: 745.38), 509.91 ($[M+2H+K]^{3+}$, calc.: 509.90), 504.59 ($[M+2H+Na]^{3+}$, calc.: 504.58), 497.26 ($[M+3H]^{3+}$, calc.:597.26)

HRESI-MS (positive ion mode) *m/z*: 1489.7471 ($C_{62}H_{101}N_{22}O_{21}$ ≙ $[M+H]^+$, calc.: 1489.7512)

^{1}H-NMR (600 MHz, DMSO-d_6, *^{1}H*, *COSY*, *TOCSY*, *^{13}C-HSQC*, *HMBC*), *δ* (ppm) = 8.94 (s, 1H, H(9)^{H2}), 8.60 (d, 1H, $J_{Q(2)NH,Q(2)\alpha}$ = 8.0 Hz, Q(2)^{NH}), 8.43-8.35 (m, 2H, N(3)^{NH} {8.39}, H(9)^{NH} {8.39}), 8.11-7.97 (m, 6H, N(7)^{NH} {8.08}, L(11)^{NH} {8.06}, G(1)$^{NH3+}$ {8.01}, Y(8)^{NH} {8.01}), 7.96-7.88 (m, 3H, T(10)^{NH} {7.92}, R(13)^{NH} {7.92}, S(4)^{NH} {7.91}), 7.87-7.78 (m, 2H, V(12)^{NH} {7.84}, T(5)^{NH} {7.82}), 7.77-7.67 (m, 2H, R(13)$^{\varepsilon NH}$ {7.73}, T(6)^{NH} {7.71}), 7.47 (s, 1H, N(7)$^{\gamma CONH2a}$), 7.43 (s, 1H, N(3)$^{\gamma CONH2a}$), 7.36-7.30 (m, 2H, H(9)^{H5} {7.34}, R(13)^{CONH2a} {7.33}), 7.26 (s, 1H, Q(2)$^{\delta CONH2a}$), 7.08 (s, 1H, R(13)^{CONH2b}), 7.01 (s, 1H, N(7)$^{\gamma CONH2b}$), 7.00-6.93 (m, 3H, N(3)$^{\gamma CONH2b}$ {6.98}, Y(8)$^{H3/5}$ {6.98}), 6.80 (s, 1H, Q(2)$^{\gamma CONH2b}$), 6.62 (d, 2H, $J_{Y(8)3/5,Y(8)2/6}$ = 8.0 Hz, Y(8)$^{H3/5}$), 4.69-4.58 (m, 2H, H(9)$^{\alpha}$ {4.66}, N(3)$^{\alpha}$ {4.61}), 4.56 (pq, 1H, *J* = 7.0 Hz, N(7)$^{\alpha}$), 4.41-4.20 (m, 7H, S(4)$^{\alpha}$ {4.38}, Q(2)$^{\alpha}$ {4.37}, L(11)$^{\alpha}$ {4.36}, Y(8)$^{\alpha}$ {4.31}, T(10)$^{\alpha}$ {4.28}, T(6)$^{\alpha}$ {4.25}, T(5)$^{\alpha}$ {4.22}), 4.20-4.13 (m, 1H, R(13)$^{\alpha}$), 4.12 (pt, 1H, V(12)$^{\alpha}$), 4.07-4.01 (m, 1H, T(10)$^{\beta}$), 4.01-3.92 (m, 2H, T(5)$^{\beta}$ {3.98}, T(6)$^{\beta}$ {3.95}), 3.66-3.54 (m, 4H, S(4)$^{\beta a}$ {3.63}, G(1)$^{\alpha}$ {3.59}, S(4)$^{\beta b}$ {3.57}), 3.15-3.05 (m, 3H, H(9)$^{\beta a}$ {3.11}, R(13)$^{\delta}$ {3.08}), 2.99 (dd, 1h, *J* = 15.6 Hz, *J* = 8.4 Hz, H(9)$^{\beta b}$), 2.87-2.82 (m, 1H, Y(8)$^{\beta a}$), 2.65 (dd, 1H, *J* = 14.3 Hz, *J* = 9.5 Hz, Y(8)$^{\beta b}$), 2.60-2.52 (m, 2H, N(3)$^{\beta a}$ {2.58}, N(7)$^{\beta a}$ {2.54}), 2.41 (dd, 1H, *J* = 15.6 Hz, *J* = 8.0 Hz, N(3)$^{\beta b}$), 2.34 (dd, 1H, *J* = 15.5 Hz, *J* = 6.8 Hz, N(7)$^{\beta b}$), 2.14-2.01 (m, 2H, Q(2)$^{\beta a/b}$), 1.96 (psext, 1H, *J* = 6.9 Hz, V(12)$^{\beta}$), 1.91-1.84 (m, 1H, Q(2)$^{\beta a}$), 1.76-1.69 (m, 1H, Q(2)$^{\beta b}$), 1.68-1.57 (m, 2H, R(13)$^{\beta a}$ {1.64}, L(11)$^{\gamma}$ {1.60}), 1.54-1.40 (m, 5H, R(13)$^{\beta b}$ {1.51}, R(13)$^{\gamma}$ {1.47}, L(11)$^{\beta a/b}$ {1.47}), 1.07-1.02 (m, 6H, T(5)$^{\gamma}$ {1.06}, T(10)$^{\gamma}$ {1.04}), 0.99 (d, 3H, $J_{T(6)\beta/T(6)\gamma}$ = 6.2 Hz, T(6)$^{\gamma}$), 0.86 (d, 3H, $J_{L(11)\delta/L(11)\gamma}$ = 6.5 Hz, L(11)$^{\delta}$), 0.85-0.79 (m, 9H, V(12)$^{\gamma}$ {0.83}, L(11)$^{\delta`}$ {0.82}, V(12)$^{\gamma`}$ {0.81})

^{13}C-NMR (150.9 MHz, DMSO-d_6, *^{13}C*, *^{13}C-HSQC*, *HMBC*), *δ* (ppm) = 173.8 (Q(2)$^{\delta CONH2}$), 173.2 (R(13)^{CONH2}), 172.0 (L(11)^{CO}), 172.0 (N(7)$^{\gamma CONH2}$), 171.6 (N(3)$^{\gamma CONH2}$), 171.3 (Y(8)^{CO}), 171.1 (N(7)^{CO}), 171.0 (V(12)^{CO}), 170.8 (Q(2)^{CO}), 170.8 (N(3)^{CO}), 170.3 (S(4)^{CO}), 170.0 (T(6)^{CO}), 169.9 (T(5)^{CO}), 169.8 (T(19)^{CO}), 169.7 (H(9)^{CO}), 165.9 (G(1)^{CO}), 156.8 (R(13)$^{\zeta}$), 155.9 (Y(8)^{C4}), 133.8 (H(9)^{C2}), 130.0 (Y(8)$^{C2/6}$), 129.3 (H(9)^{C4}), 127.7 (Y(8)^{C1}), 117.1 (H(9)^{C5}), 115.0 (Y(8)$^{C3/5}$), 66.8 (T(6)$^{\beta}$), 66.7 (T(5)$^{\beta}$), 66.5 (T(10)$^{\beta}$), 61.7 (S(4)$^{\beta}$), 58.3 (T(10)$^{\alpha}$), 58.3 (T(5)$^{\alpha}$), 57.9 (T(6)$^{\alpha}$), 57.9 (V(12)$^{\alpha}$), 55.0 (S(8)$^{\alpha}$), 54.8 (T(8)$^{\alpha}$), 52.1 (Q(2)$^{\alpha}$), 52.0 (R(13)$^{\alpha}$), 51.7 (H(9)$^{\alpha}$), 49.7 (N(3)$^{\alpha}$), 49.6 (N(7)$^{\alpha}$), 40.6 (L(11)$^{\beta}$), 40.4 (R(13)$^{\delta}$), 40.2 (G(1)$^{\alpha}$), 37.2 (N(3)$^{\beta}$), 37.1 (N(7)$^{\beta}$), 36.1 (Y(8)$^{\beta}$), 31.3 (Q(2)$^{\gamma}$), 30.4 (V(12)$^{\beta}$),

29.2 (R(13)$^{\beta}$), 28.6 (Q(2)$^{\beta}$), 26.9 (H(9)$^{\beta}$), 25.2 (R(13)$^{\gamma}$), 24.2 (L(11)$^{\gamma}$), 23.2 (L(11)$^{\delta}$), 22.6 (L(11)$^{\delta`}$), 19.5 (T(10)$^{\gamma}$), 19.5 (T(5)$^{\gamma}$), 19.3 (T(6)$^{\gamma}$), 19.2 (V(12)$^{\gamma}$), 18.2 (V(12)$^{\gamma`}$)

_L_-Alanyl-_L_-valyl-glycyl-_L_-seryl-_L_-threonyl-_L_-lysyl-_L_-histidyl-_L_-lysyl-_L_-tryptophyl-_L_-prolyl-_L_-prolyl-_L_-leucine amide (9)
(Ala-Val-Gly-Ser-Thr-Lys-His-Lys-Trp-Pro-Pro-Leu-amide)

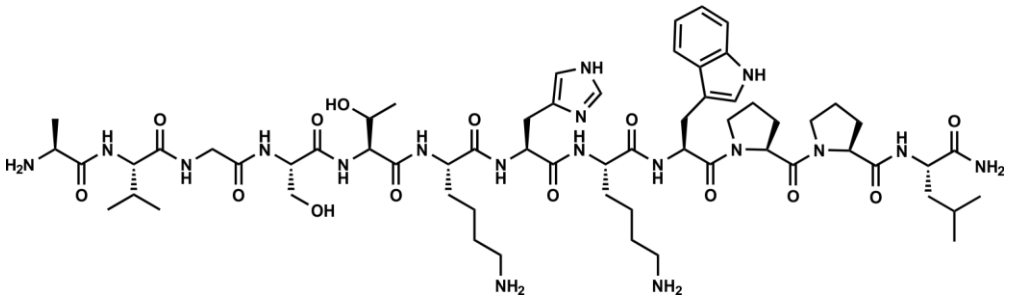

The automated *Solid-Phase-Peptide-Synthesis* was carried out as described in the general procedure, using 417 mg (0.1 mmol) of the *N-Fmoc*-Leu preloaded *RAM-Tentagel*® *S*-resin (loading capacity: 0.24 mmol/g). After the final deblocking of the *N-Fmoc*-protective group the resin was transferred into a *Merrifield*-reaction vessel. A mixture of 15 mL trifluoroacetic acid (TFA), 0.9 mL water and 0.9 mL triisopropylsilane (TIS) was added and the suspension was shaken for 3 h. The suspension was filtrated and the resin was washed with TFA (3·3 ml). 25 mL of toluene were added to the combined filtrates, afterwards the solution was concentrated in vacuo and co-evaporated with toluene (3·25 mL). The residue was washed with cold diethyl ether (Et_2O) (3·3 mL), dissolved in water and lyophilised, yielding 143 mg of crude product. 40 mg of the crude peptide were desalted yielding 24mg (0.018 mmol, 18%) of the peptide after lyophilisation.

Analytic HPLC: conformer 1: t_R = 9.6 min, conformer 2: 13.7 min (phenomenex Jupiter C18, MeCN/H2O + 0.1% TFA, grad.: 20:80 (5 min const.) → 25:75, 20 min, λ = 214 nm, T = 22 °C)

$C_{62}H_{98}N_{18}O_{14}$ (M = 1319.55 g/mol) [1318.7510]

ESI-MS (positive ion mode) *m/z*: 1341.80 ($[M+Na]^+$, calc.: 1341.74), 1319.81 ($[M+H]^+$, calc.: 1319.76), 698.37 ($[M+2K]^{2+}$, calc.: 698.34), 690.38 ($[M+K+Na]^{2+}$, calc.: 690.35), 682.41 ($[M+2Na]^{2+}$, calc.: 682.37), 679.39 ($[M+K+H]^{2+}$, calc.: 679.36), 671.40 ($[M+Na+H]^{2+}$, calc.: 671.38), 660.40 ($[M+2H]^{2+}$, calc.: 660.39), 440.61 ($[M+3H]^{3+}$, calc.: 440.59)

HRESI-MS (positive ion mode) *m/z*: 1319.7581 ($C_{62}H_{99}N_{18}O_{14}$ ≙ $[M+H]^+$, calc.: 1319.7588)

_L_-Histidyl-_L_-threonyl-_L_-glutaminyl-_L_-asparaginyl-_L_-methionyl-_L_-arginyl-_L_-methionyl-_L_-tyrosyl-_L_-glutamyl-_L_-prolyl-_L_-tryptophyl-_L_-phenylalanin-amide (10)

(His-Thr-Gln-Asn-Met-Arg-Met-Tyr-Glu-Pro-Trp-Phe-amide)

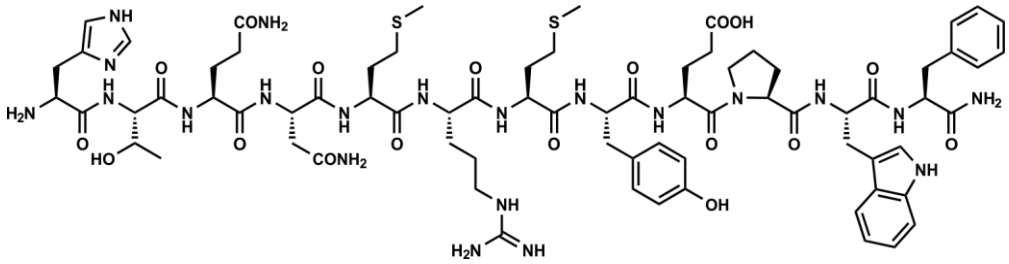

The automated *Solid-Phase-Peptide-Synthesis* was carried out as described in the general procedure, using 476 mg (0.1 mmol) of the *N-Fmoc*-Phe preloaded *RAM-Tentagel*® *S*-resin (loading capacity: 0.21 mmol/g). After the final deblocking of the *N-Fmoc*-protective group the resin was transferred into a *Merrifield*-reaction vessel. A mixture of 15 mL trifluoroacetic acid (TFA), 0.9 mL water and 0.9 mL triisopropylsilane (TIS) was added and the suspension was shaken for 3 h. The suspension was filtrated and the resin was washed with TFA (3·3 ml). 25 mL of toluene were added to the combined filtrates, afterwards the solution was concentrated in vacuo and codistilled with toluene (3·25 mL). The residue was washed with cold diethyl ether (Et_2O) (3·3 mL), dissolved in water and lyophilised, yielding 127 mg of crude product. The crude peptide was purified by semi-preparative *HPLC* (phenomenex, Jupiter C18, acetonitrile/water + 0.1% TFA, grad.: 25:75 (5 min const.) → 30:70, 20 min, λ = 214 nm; t_R = 7.13 min) yielding 63 mg (0.038 mmol, 38%) of the peptide after lyophilisation.

Analytic HPLC: t_R = 17.3 min (phenomenex Jupiter C18, MeCN/H2O + 0.1% TFA, grad.: 25:75 (5 min const.) → 30:70, 20 min, λ = 214 nm)

$C_{74}H_{103}N_{21}O_{18}S_2$ (M = 1638.87 g/mol) [1637.7231]

ESI-MS (positive ion mode) *m/z*: 1638.77 ([M+H]+, calc.: 1638.73), 841.88 ($[M+2Na]^{2+}$, calc.: 841.85), 838.87 ($[M+K+H]^{2+}$, calc.: 838.85), 830.88 ($[M+Na+H]^{2+}$, calc.: 830.86), 819.85 ($[M+2H]^{2+}$, calc.: 819.87), 554.30 ($[M+Na+2H]^{3+}$, calc.: 554.24), 546.92 ($[M+3H]^{3+}$, calc.: 546.92)

HRESI-MS (positive ion mode) *m/z*: 819.8687 ($[M+2H]^{2+}$, calc.: 819.8694)

^{1}H-NMR (600 MHz, DMSO-d$_6$, *^{1}H*, *COSY*, *TOCSY*, *^{13}C-HSQC*, *HMBC*), *δ* (ppm) = 10.81 (ps, 1H, W(11)^{H1}), 9.01 (s, 1H, H(1)^{H2}), 8.58 (d, 1H, $J_{T(2)NH,T(2)\alpha}$ = 7.0 Hz, T(2)^{NH}), 8.47-8.31 (m, 3H, Q(3)^{NH} {8.41}, H(1)^{NH2} {8.38}), 8.29 (d, 1H, $J_{N(4)NH,N(4)\alpha}$ = 7.0 Hz, N(4)^{NH}), 8.18 (d, 1H, $J_{E(9)NH,E(9)\alpha}$ = 7.8 Hz, E(9)^{NH}), 8.14 (d, 1H, $J_{R(6)NH,R(6)\alpha}$ = 7.6 Hz, R(6)^{NH}), 8.09 (d, 1H, $J_{M(7)NH,M(7)\alpha}$ = 7.6 Hz, M(7)^{NH}), 8.00 (d, 1H, $J_{W(11)NH,W(11)\alpha}$ = 7.4 Hz, W(11)^{NH}), 7.93-7.87 (m, 2H, M(5)^{NH} {7.91}, Y(8)^{NH} {7.91}), 7.80 (d, 1H, $J_{F(12)NH,F(12)\alpha}$ = 8.1Hz, F(12)^{NH}), 7.63-7.57 (m, 1H, R(6)$^{\varepsilon NH}$), 7.53-7.49 (m, 2H, W(11)^{H4} {7.51}, N(4)$^{\gamma CONH2a}$ {7.51}), 7.48 (s, 1H, H(1)^{H5}), 7.30 (d, 1H, $J_{W(11)H7,W(11)H6}$ = 8.1 Hz, W(11)^{H7}), 7.27-7.22 (m, 3H, Q(3)$^{\delta CONH2a}$ {7.25}, F(12)$^{H3/5}$ {7.24}), 7.21-7.16 (m, 4H, F(12)^{CONH2a} {7.19}, F(12)^{H4} {7.18}, F(12)$^{H3/5}$ {7.17}), 7.11 (s, 1H, F(12)^{CONH2b}), 7.07 (d, 1H, $J_{W(11)H2,W(11)H1}$ = 2.3 Hz, W(11)^{H2}), 7.04 (t, J = 7.6 Hz, W(11)^{H6}), 7.02-6.95 (m, 4H, N(4)$^{\gamma CONH2b}$ {7.01}, Y(8)$^{H2/6}$ {6.99}, W(11)^{H5} {6.96}), 6.87 (s, 1H, Q(3)$^{\delta CONH2b}$), 6.62 (d, 2H, $J_{Y(8)H3/5,Y(8)H2/6}$ = 8.0 Hz), 4.56-4.47 (m, 2H, N(4)$^{\alpha}$ {4.53}, E(9)$^{\alpha}$ {4.51}), 4.44-4.36 (m, 3H, Y(8)$^{\alpha}$ {4.42}, F(12)$^{\alpha}$ {4.39}, W(11)$^{\alpha}$ {4.38}), 4.35-4.23 (m, 6H, M(7)$^{\alpha}$ {4.32}, Q(3)$^{\alpha}$ {4.31}, M(5)$^{\alpha}$ {4.29}, H(1)$^{\alpha}$ {4.28}, P(10)$^{\alpha}$ {4.28}, T(2)$^{\alpha}$ {4.26}), 4.18 (pq, 1H, J = 7.3 Hz, R(6)$^{\alpha}$), 4.04-3.98 (m, 1H, T(2)$^{\beta}$), 3.51-3.44 (m, 1H, P(10)$^{\delta a}$), 3.43-3.37 (m, 1H, P(10)$^{\delta b}$), 2-26-3.15 (m, 2H, H(1)$^{\beta a/b}$), 3.10-2.96 (m, 4H, R(6)$^{\delta}$ {3.07}, W(11)$^{\beta a}$ {3.03}, F(12)$^{\beta a}$ {2.99}), 2.91 (dd, 1H, *J* = 15.0 Hz, *J* = 8.3 Hz, W(11)$^{\beta b}$), 2.87-2.79 (m, 2H, Y(8)$^{\beta a}$ {2.85}, F(12)$^{\beta b}$ {2.82}), 2.65 (dd, 1H, *J* = 14.0 Hz, *J* = 8.7 Hz, Y(8)$^{\beta b}$), 2.56 (dd, 1H, *J* = 15.6 Hz, *J* = 6.3 Hz, N(4)$^{\beta a}$), 2.48-2.22 (m, 7H, N(4)$^{\beta b}$ {2.43}, M(7)$^{\gamma}$ {2.42}, M(5)$^{\gamma}$ {2.36}, E(9)$^{\gamma}$ {2.28}), 2.16-2.09 (m, 2H, Q(3)$^{\gamma}$), 2.01-1.98 (m, 6H, M(5)$^{\varepsilon}$ {2.00}, M(7)$^{\varepsilon}$ {2.00}), 1.95-1.81 (m, 5H, P(10)$^{\beta a}$ {1.92}, M(7)$^{\beta a}$ {1.92}, Q(3)$^{\beta a}$ {1.91}, M(5)$^{\beta a}$ {1.88}, E(9)$^{\beta a}$ {1.85}), 1.81-1.63 (m, 8H, M(7)$^{\beta b}$ {1.78}, Q(3)$^{\beta b}$ {1.76}, M(5)$^{\beta b}$ {1.72}, P(10)$^{\gamma}$ {1.72}, P(10)$^{\beta b}$ {1.68}, E(9)$^{\beta b}$ {1.68}, R(6)$^{\beta a}$ {1.67}), 1.57-1.39 (m, 3H, R(6)$^{\beta b}$ {1.53}, R(6)$^{\gamma}$ {1.47}), 1.11 (d, 3H, $J_{T(2)\gamma,T(2)\beta}$ = 6.2 Hz, T(2)$^{\gamma}$)

^{13}C-NMR (150.9 MHz, DMSO-d$_6$, *^{13}C*, *^{13}C-HSQC*, *HMBC*), *δ* (ppm) = 174.3 (E(9)$^{\delta CO}$), 174.2 (Q(3)$^{\delta CONH2}$), 172.7 (F(12)^{CONH2}), 171.8 (N(4)$^{\gamma CONH2}$), 171.7 (P(10)^{CO}), 171.3 (M(5)^{CO}), 171.3 (M(7)^{CO}), 171.1 (R(6)^{CO}), 171.1 (W(11)^{CO}), 171.0 (Y(8)^{CO}), 170.9 (Q(3)^{CO}), 170.8 (N(4)^{CO}), 170.3 (T(2)^{CO}), 169.8 (E(9)^{CO}), 167.8 (H(1)^{CO}), 156.8 (R(6)$^{\zeta}$), 155.9 (Y(8)^{C4}), 137.9 (F(12)^{C1}), 136.1 (W(11)^{C7a}), 134.5 (H(1)^{C2}), 130.2 (Y(8)$^{C2/6}$), 129.3 (F(12)^{C4}), 128.1 (F(12)$^{C3/5}$), 127.5 (Y(8)^{C1}), 127.4 (W(11)^{C3a}), 126.7 (H(1)^{C4}), 126.3 (F(12)$^{C2/6}$), 123.5 (W(11)^{C2}),

121.0 (W(11)^{C6}), 118.4 (W(11)^{C4}), 118.4 (W(11)^{C5}), 118.3 (H(1)^{C5}), 114.9 (Y(8)$^{C3/5}$), 111.3 (W(11)^{C7}), 110.0 (W(11)^{C7}), 66.6 (T(2)$^{\beta}$), 59.6 (P(10)$^{\alpha}$), 59.0 (T(2)$^{\alpha}$), 54.0 (Y(8)$^{\alpha}$), 53.8 (W(11)$^{\alpha}$), 52.6 (R(6)$^{\alpha}$), 52.3 (Q(3)$^{\alpha}$), 52.1 (M(5)$^{\alpha}$), 51.9 (M(7)$^{\alpha}$), 51.2 (H(1)$^{\alpha}$), 49.9 (N(4)$^{\alpha}$), 49.7 (E(9)$^{\alpha}$), 46.8 (P(10)$^{\delta}$), 40.5 (R(6)$^{\delta}$), 37.4 (F(1)$^{\beta}$), 36.9 (N(4)$^{\beta}$), 36.6 (Y(8)$^{\beta}$), 32.2 (M(5)$^{\beta}$), 31.8 (M(7)$^{\beta}$), 31.4 (Q(3)$^{\gamma}$), 29.6 (E(9)$^{\gamma}$), 29.5 (M(5)$^{\gamma}$), 29.5 (M(7)$^{\gamma}$), 29.0 P(10)$^{\beta}$), 28.6 (R(6)$^{\beta}$), 28.3 (Q(3)$^{\beta}$), 27.2 (F(12)$^{\beta}$), 26.7 (H(1)$^{\beta}$), 26.6 (E(9)$^{\beta}$), 25.2 (R(6)$^{\gamma}$), 24.4 (P(10)$^{\gamma}$), 20.0 (T(2)$^{\gamma}$), 14.7 (M(5)$^{\varepsilon}$), 14.7 (M(7)$^{\varepsilon}$)

_L_-Alanyl-_L_-seryl-_L_-threonyl-_L_-glutaminyl-_L_-prolyl-_L_-leucyl-_L_-arginin-amide (11) (Ala-Ser-Thr-Gln-Pro-Leu-Arg-amide)

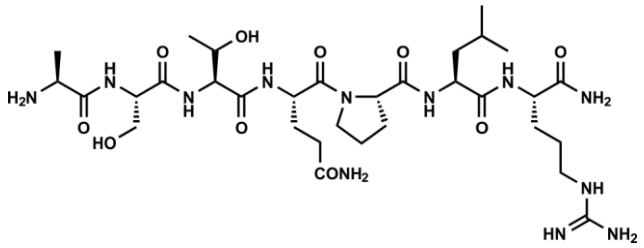

The automated *Solid-Phase-Peptide-Synthesis* was carried out as described in the general procedure, using 476 mg (0.1 mmol) of the *N-Fmoc*-Arg(Pbf)) preloaded *RAM-Tentagel*® *S*-resin (loading capacity: 0.21 mmol/g). After the final deblocking of the *N-Fmoc*-protective group the resin was transferred into a *Merrifield*-reaction vessel. A mixture of 15 mL trifluoroacetic acid (TFA), 0.9 mL water and 0.9 mL triisopropylsilane (TIS) was added and the suspension was shaken for 3 h. The suspension was filtrated and the resin was washed with TFA (3·3 ml). 25 mL of toluene were added to the combined filtrates, afterwards the solution was concentrated in vacuo and codistilled with toluene (3·25 mL). The residue was washed with cold diethyl ether (Et_2O) (3·3 mL), dissolved in water and lyophilised, yielding 75 mg of crude product. The crude peptide was purified by semi-preparative *HPLC* (phenomenex, Jupiter C18, acetonitrile/water + 0.1% TFA, grad.: 5:95 (5 min const.) → 15:85, 20 min, λ = 214 nm; t_R = 17.6 min) yielding 58 mg (0.075 mmol, 75%) of the peptide after lyophilisation.

Analytic HPLC: t_R = 16.9 min (phenomenex Jupiter C18, MeCN/H2O + 0.1% TFA, grad.: 5:95 (5 min const.) → 15:85, 20 min, λ = 214 nm)

$C_{32}H_{58}N_{12}O_{10}$ (M = 770.88 g/mol) [770.4399]

ESI-MS (positive ion mode) *m/z*: 771.45 ($[M+H]^+$, calc.: 771.45), 386.23 ($[M+2H]^{2+}$, calc.: 386.23)

HRESI-MS (positive ion mode) *m/z*: 771.4477 ($C_{32}H_{59}N_{12}O_{10}$ ≙ $[M+H]^+$; calc.: 771.4477)

^{1}H-NMR (400 MHz, DMSO-d_6, *^{1}H*, *COSY*, *TOCSY, ^{13}C-HSQC*, *HMBC*), δ (ppm) = 8.63 (d, 1H, $J_{S(2)NH,S(2)\beta}$ = 7.7 Hz, $S(2)^{NH}$) 8.16-8.05 (m, 3H, $A(1)^{NH2}$ {8.11}, $L(6)^{NH}$ {8.09}); 7.97 (d, 1H, $J_{Q(4)NH,Q(4)\alpha}$ = 7.8 Hz, $Q(4)^{NH}$); 7.80 (d, 1H, $J_{T(3)NH,T(3)\alpha}$ = 8.3 Hz, $T(3)^{NH}$); 7.74 (d, 1H, $J_{R(7)NH,R(7)\alpha}$ = 8.1 Hz, $R(7)^{NH}$); 7.70 (t, 1H, $J_{R(7)\varepsilon NH,R(7)\delta}$ = 5.7 Hz, $R(7)^{\varepsilon NH}$); 7.29 (s, 1H, $Q(4)^{\delta CONH2a}$); 7.25 (s, 1H, $R(7)^{CONH2a}$); 7.11 (s, 1H, $R(7)^{CONH2b}$); 6.88 (s, 1H, $Q(4)^{\delta CONH2b}$); 4.55-4.43 (m, 2H, $Q(4)^{\alpha}$ {4.51}, $S(2)^{\alpha}$ {4.48}); 4.34-4.27 (m, 1H, $P(5)^{\alpha}$); 4.23-4.10 (m, 3H, $T(3)^{\alpha}$ {4.20}, $L(6)^{\alpha}$ {4.18}, $R(7)^{\alpha}$ {4.15}); 4.08-4.00 (m, 1H, $T(3)^{\beta}$); 3.96-3.87 (m, 1H, $A(1)^{\alpha}$); 3.69-3.42 (m, 4H, $S(2)^{\beta a}$ {3.65}, $P(5)^{\delta}$ {3.60}, $S(2)^{\beta b}$ {3.58}); 3.08 (dd, 2H, $J_{R(7)\delta,R(7)\gamma}$ = 12.7 Hz, $J_{R(7)\delta,R(7)\varepsilon NH}$ = 6.6 Hz, $R(7)^{\delta}$); 2.12 (t, 2H, $J_{Q(4)\gamma,Q(4)\beta}$ = 7.5 Hz, $Q(4)^{\gamma}$); 2.08-1.97 (m, 1H, $P(5)^{\beta a}$); 1.93-1.76 (m, 4H, $Q(4)^{\beta a}$ {1.88}, $P(5)^{\beta b}$ {1.83}, $P(5)^{\gamma}$ {1.83}); 1.75-1.57 (m, 3H, $R(7)^{\beta a}$ {1.69}, $Q(4)^{\beta b}$ {1.67}, $L(6)^{\gamma}$ {1.60}); 1.57-1.39 (m, 5H, $R(7)^{\beta b}$ {1.50}, $L(6)^{\beta}$ {1.46}, $R(7)^{\gamma}$ {1.44}); 1.34 (d, 3H, $J_{A(1)\beta,A(1)\alpha}$ = 6.9 Hz, $A(1)^{\beta}$); 1.03 (d, 3H, $J_{T(3)\gamma,T(3)\beta}$ = 6.3 Hz, $T(3)^{\gamma}$); 0.88 (d, 3H $J_{L(6)\delta,L(6)\gamma}$ = 6.6 Hz, $L(6)^{\delta}$); 0.82 (d, 3H, $J_{L(6)\delta`,L(6)\gamma}$ = 6.5 Hz, $L(6)^{\delta`}$)

^{13}C-NMR (100.6 MHz, DMSO-d_6, *^{13}C*, *^{13}C-HSQC*, *HMBC*), δ (ppm) = 174.2 ($Q(4)^{\delta CONH2}$); 173.3 ($R(7)^{CONH2}$); 171.9 ($L(6)^{CO}$), 171.9 ($P(5)^{CO}$); 170.0 ($S(2)^{CO}$); 169.9 ($T(3)^{CO}$), 169.8 ($Q(4)^{CO}$); 169.7 ($A(1)^{CO}$); 156.8 ($R(7)^{\zeta}$); 66.4 ($T(3)^{\gamma}$); 61.6 ($S(2)^{\beta}$); 59.5 ($P(5)^{\alpha}$); 58.1 ($T(3)^{\alpha}$); 54.9 ($S(2)^{\alpha}$); 51.9 ($R(7)^{\alpha}$); 51.6 ($L(6)^{\alpha}$); 50.0 ($Q(4)^{\alpha}$); 48.1 ($A(1)^{\alpha}$); 46.9 ($P(5)^{\delta}$); 40.3 ($R(7)^{\delta}$); 40.1 (overlapped by DMSO-signal, $L(6)^{\gamma}$); 30.9 ($Q(4)^{\gamma}$); 29.2 ($P(5)^{\beta}$); 29.1 ($R(7)^{\beta}$); 27.3 ($Q(4)^{\beta}$); 25.1 ($R(7)^{\gamma}$); 24.5 ($P(5)^{\gamma}$); 24.2 ($L(6)^{\beta}$); 23.1 ($L(6)^{\delta}$); 21.5 ($L(6)^{\delta`}$); 19.9 ($T(3)^{\gamma}$); 17.3 ($A(1)^{\beta}$).

_L_-Valyl-_L_-alanyl-_L_-glutaminyl-_L_-threonyl-_L_-alanyl-_L_-valyl-_L_-histidyl-glycyl-_L_-valyl-_L_-methionyl-_L_-glutaminyl-_L_-lysinamide (12)
(Val-Ala-Gln-Thr-Ala-Val-His-Gly-Val-Met-Gln-Lys-amide)

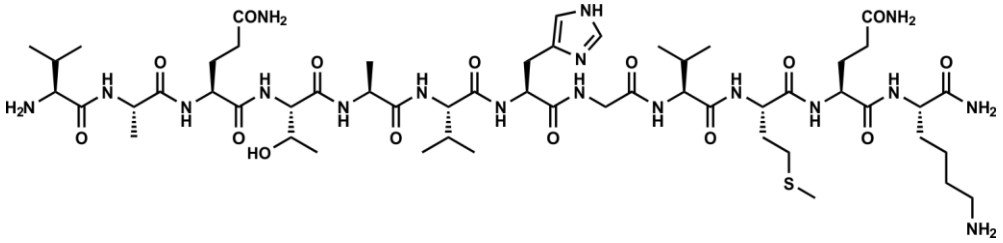

The automated *Solid-Phase-Peptide-Synthesis* was carried out as described in the general procedure, using 435 mg (0.1 mmol) of the *N-Fmoc*-Lys(*Boc*) preloaded *RAM-Tentagel*® *S*-resin (loading capacity: 0.23 mmol/g). After the final deblocking of the *N-Fmoc*-protective group the resin was transferred into a *Merrifield*-reaction vessel. A mixture of 15 mL trifluoroacetic acid (TFA), 0.9 mL water and 0.9 mL triisopropylsilane (TIS) was added and the suspension was shaken for 3 h. The suspension was filtrated and the resin was washed with TFA (3·3 ml). 25 mL of toluene were added to the combined filtrates, afterwards the solution was concentrated in vacuo and co-evaporated with toluene (3·25 mL). The residue was washed with cold diethyl ether (Et_2O) (3·3 mL), dissolved in water and lyophilised, yielding 183 mg of crude product. 75 mg of the crude peptide were purified by semi-preparative *HPLC* (phenomenex, Jupiter C18, acetonitrile/water + 0.1% TFA, grad.: 10:90 (5 min const.) → 20:80, 20 min, λ = 214 nm; t_R = 18.1 min) yielding 28 mg (0.022 mmol, 22%) of the peptide after lyophilisation.

Analytic HPLC: t_R = 18.3 min (phenomenex Jupiter C18, MeCN/H2O + 0.1% TFA, grad.: 10:90 (5 min const.) → 20:80, 20 min, λ = 214 nm)

$C_{53}H_{94}N_{16}O_{17}$ (M = 1267.50 g/mol) [1266.6867]

ESI-MS (positive ion mode) *m/z*: 1289.71 ($[M+Na]^+$, calc.: 1289.68), 1267.73 ($[M+H]^+$, calc.: 1267.69), 664.38 ($[M+K+Na]^{2+}$, calc.: 664.32), 656.35 ($[M+2Na]^{2+}$, calc.: 656.34), 653.35 ($[M+K+H]^{2+}$, calc.: 653.33), 645.36 ($[M+Na+H]^{2+}$, calc.: 645.34), 634.36 ($[M+2H]^{2+}$, calc.: 634.35), 435.90 ($[M+K+2H]^{3+}$, calc.: 435.89), 423.24 ($[M+3H]^{3+}$, calc.: 423.24)

HRESI-MS (positive ion mode) *m/z*: 634.3492 ($[M+2H]^{2+}$, calc.: 634.3512)

^{1}H-NMR (600 MHz, DMSO-d_6, *^{1}H*, *COSY*, *TOCSY*, *^{13}C-HSQC*, *HMBC*), δ (ppm) = 8.94 (s, 1H, $H(7)^{H2}$), 8.59 (d, 1H, $J_{A(2)NH,A(2)\alpha}$ = 7.0 Hz, $A(2)^{NH}$), 8.27 (d, 1H, $J_{Q(3)NH,Q(3)\alpha}$ = 7.6 Hz, $Q(3)^{NH}$), 8.24-8.17 (m, 3H, $G(8)^{NH}$ {8.22}, $H(7)^{NH}$ {8.20},

M(10)^{NH} {8.19}), 8.13-8.04 (m, 3H, V(1)^{NH2} {8.09}, V(9)^{NH} {8.07}), 8.01 (d, 1H, $J_{Q(11)NH,Q(11)\alpha}$ = 7.5 Hz, Q(11)^{NH}), 7.94 (d, 1H, $J_{A(5)NH,A(5)\alpha}$ = 7.4 Hz, A(5)^{NH}), 7.90 (d, 1H, $J_{K(12)NH,K(12)\alpha}$ = 8.0 Hz, K(12)^{NH}), 7.87 (d, 1H, $J_{V(6)NH,V(6)\alpha}$ = 8.2 Hz, V(6)^{NH}), 7.77-7.68 (m, 3H, K(12)$^{\zeta NH2}$ {7.74}, T(4)^{NH} {7.71}), 7.39-7.34 (m, 2H, K(12)^{CONH2a} {7.37}, H(7)^{H5} {7.36}), 7.27 (s, 1H, Q(3)$^{\delta CONH2a}$), 7.26 (s, 1H, Q(11)$^{\delta CONH2a}$), 7.07 (s, 1H, K(12)^{CONH2b}), 6.81 (m, 2H, Q(3)$^{\delta CONH2b}$ {6.81}, Q(11)$^{\delta CONH2b}$ {6.81}), 4.61 (pq, 1H, J = 7.1 Hz, H(7)$^{\alpha}$), 4.42-4.34 (m, 2H, A(2)$^{\alpha}$ {4.39}, A(5)$^{\alpha}$ {4.37}), 4.34-4.26 (m, 2H, M(10)$^{\alpha}$ {4.32}, Q(3)$^{\alpha}$ {4.29}), 4.24-4.17 (m, 3H, T(4)$^{\alpha}$ {4.22}, V(9)$^{\alpha}$ {4.19}, Q(11)$^{\alpha}$ {4.19}), 4.16-4.11 (m, 1H, K(12)$^{\alpha}$), 4.06 (pt, 1H, J = 7.6 Hz, V(6)$^{\alpha}$), 4.00-3.95 (m, 1H, T(4)$^{\beta}$), 3.88 (dd, 1H, $J_{G(8)\alpha a,G(8)\alpha b}$ = 16.8 Hz, $J_{G(8)\alpha a,G(8)NH}$ = 5.6 Hz, G(8)$^{\alpha a}$), 3.73 (dd, $J_{G(8)\alpha b,G(8)\alpha a}$ = 16.8 Hz, $J_{G(8)\alpha b,G(8)NH}$ = 5.5 Hz, G(8)$^{\alpha b}$), 3.59 (s, 1H, V(1)$^{\alpha}$), 3.09 (dd, 1H, $J_{H(7)\beta a,H(7)\beta b}$ = 15.5 Hz, $J_{H(7)\beta a,H(7)\alpha}$ = 5.4 Hz, H(7)$^{\beta a}$), 2.97 (dd, 1H, $J_{H(7)\beta b,H(7)\beta a}$ = 15.3 Hz, $J_{H(7)\beta b,H(7)\alpha}$ = 7.7 Hz, H(7)$^{\beta b}$), 2.78-2.72 (m, 2H, K(12)$^{\varepsilon}$), 2.48-2.38 (m, 2H, M(10)$^{\gamma}$), 2.16-2.05 (m, 4H, Q(3)$^{\gamma}$ {2.11}, Q(11)$^{\gamma}$ {2.09}), 2.06-2.00 (m, 4H, V(1)$^{\beta}$ {2.03}, M(10)$^{\varepsilon}$ {2.02}), 1.99-1.83 (m, 5H, V(9)$^{\beta}$ {1.96}, V(6)$^{\beta}$ {1.91}, M(10)$^{\beta a}$ {1.90}, Q(3)$^{\beta a}$ {1.87}, Q(11)$^{\beta a}$ {1.87}), 1.82-1.69 (m, 3H, M(10)$^{\beta b}$ {1.79}, Q(3)$^{\beta b}$ {1.73}, Q(11)$^{\beta b}$ {1.73}), 1.68-1.61 (m, 1H, K(12)$^{\beta a}$), 1.54-1.47 (m, 3H, K(12)$^{\delta}$ {1.51}, K(12)$^{\beta b}$ {1.50}), 1.33-1.22 (m, 5H, K(12)$^{\gamma}$ {1.28}, A(2)$^{\beta}$ {1.24}), 1.19 (d, 3H, $J_{A(5)\beta,A(5)\alpha}$ = 7.0 Hz, A(5)$^{\beta}$), 1.01 (d, 3H, $J_{T(4)\gamma,T(4)\beta}$ = 6.2 Hz, T(4)$^{\gamma}$), 0.95-0.90 (m, 6H, V((1)$^{\gamma}$ {0.93}, V(1)$^{\gamma`}$ {0.92}), 0.85 (d, 3H, $J_{Val(9)\gamma,Val(9)\beta}$ = 6.7 Hz, V(9)$^{\gamma}$), 0.82 (d, 3H, $J_{V(9)\gamma`,V(9)\beta}$ = 6.8 Hz, V(9)$^{\gamma`}$), 0.80-0.78 (m, 6H, V(6)$^{\gamma/\gamma`}$)

^{13}C-NMR (150.9 MHz, DMSO-d$_6$, *^{13}C*, *^{13}C-HSQC*, *HMBC*), *δ* (ppm) = 174.0 (Q(3)$^{\delta CONH2}$), 173.9 (Q(11)$^{\delta CONH2}$), 173.4 (K(12)^{CONH2}), 172.4 (A(5)^{CO}), 171.9 (A(2)^{CO}), 171.3 (Q(3)^{CO}), 171.1 (M(10)^{CO}), 171.0 (Q(11)^{CO}), 171.0 (V(6)^{CO}), 171.0 (V(9)^{CO}), 170.1 (H(7)^{CO}), 169.5 (T(4)^{CO}), 169.0 (G(8)^{CO}), 167.5 (V(1)^{CO}), 133.8 (H(7)^{C2}), 129.1 (H(7)^{C4}), 117.1 (H(7)^{C5}), 66.6 (T(4)$^{\beta}$), 58.1 (V(6)$^{\alpha}$), 57.8 (V(9)$^{\alpha}$), 57.7 (T(4)$^{\alpha}$), 57.3 (V(1)$^{\alpha}$), 52.4 (Q(11)$^{\alpha}$), 52.4 (Q(3)$^{\alpha}$), 52.1 (M(10)$^{\alpha}$), 52.0 (K(12)$^{\alpha}$), 51.4 (H(7)$^{\alpha}$), 48.2 (A(2)$^{\alpha}$), 48.1 (A(5)$^{\alpha}$), 41.9 (G(8)$^{\alpha}$), 38.7 (K(12)$^{\varepsilon}$), 31.6 (Q(3)$^{\gamma}$), 31.6 (Q(11)$^{\gamma}$), 31.5 (M(10)$^{\beta}$), 31.5 (K(12)$^{\beta}$), 30.7 (V(9)$^{\beta}$), 30.2 (V(6)$^{\beta}$), 29.9 (V(1)$^{\beta}$), 29.5 (M(10)$^{\gamma}$), 28.0 (Q(3)$^{\beta}$), 27.9 (Q(11)$^{\beta}$), 27.2 (H(7)$^{\beta}$), 26.7 (K(12)$^{\delta}$), 22.3 (K(12)$^{\gamma}$), 19.4 (T(4)$^{\gamma}$), 19.3 (V(9)$^{\gamma}$), 19.2 (V(6)$^{\gamma}$), 18.4 (V(1)$^{\gamma}$), 18.3 (V(9)$^{\gamma`}$), 18.2 (V(6)$^{\gamma`}$), 18.2 (A(2)$^{\beta}$), 18.2 (A(5)$^{\beta}$), 17.8 (V(1)$^{\gamma`}$), 14.7 (M(10)$^{\varepsilon}$)

Glycyl-*L*-glutaminyl-*L*-asparaginyl-*L*-seryl-*L*-threonyl-*L*-threonyl-*L*-asparaginyl-*L*-tyrosyl-*L*-histidyl-*L*-threonyl-*L*-leucyl-*L*-valyl-*L*-arginyl-amido-4,7,10-trioxa-dodecanylamido-*L*-Glutamyl-(α-Glycyl-*N*-(2-methyl-4-(o-tolyldiazenyl)phenyl)-amid)-γ-glycin-amide (20)

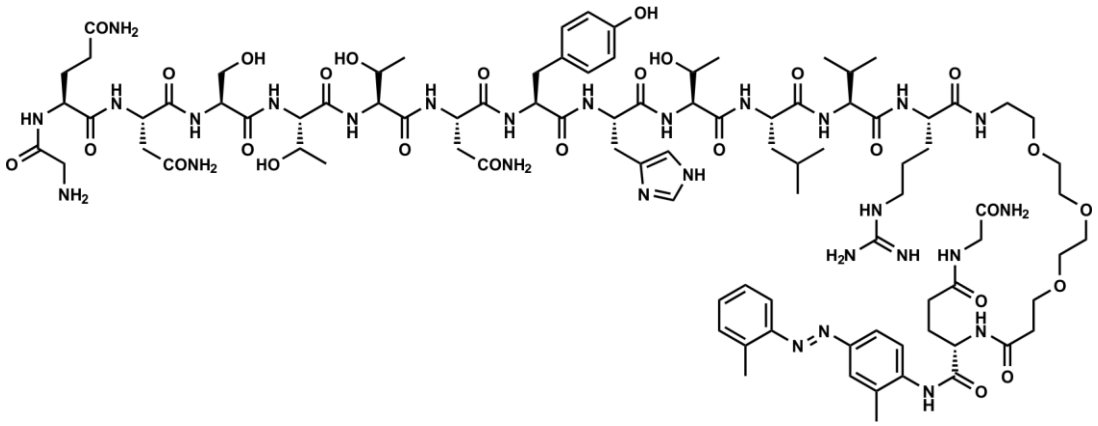

The automated *Solid-Phase-Peptide-Synthesis* was carried out as described in the general procedure, using 455 mg (0.1 mmol) of the *N-Fmoc*-Gly preloaded *RAM-Tentagel*® *S*-resin (loading capacity: 0.22 mmol/g). After the cleavage of the first Fmoc-protective group the synthesis was carried out manually. 63 mg (0.1 mmol, 1 *eq*.). of the modified amino acid (18) were mixed with 16.3 mg (0.12 mmol) HOAt, 45.6 mg (0.12 mmol) HATU in 2 mL of *N*MP. The mixture was activated with 26 µL (0.24 mmol) *N*-Methyl-morpholine (*N*MM) and mixed with the resin. The suspension was shaken vigorously for 2 h. This procedure was repeated with an additional equivalent of (18) and 4 h coupling time. Afterwards the capping step and the cleavage of the protective group were carried out. 111 mg (0.25 mmol, 2.5 *eq*.) of the spacer-amino acid were mixed with 41 mg (0.3 mmol) HOAt and 114 mg (0.3 mmol) HATU in 2 mL *N*MP. The mixture was activated with 61 µL (0.6 mmol) *N*MM and mixed with the resin. The suspension was shaken vigorously for 2 h. This procedure was repeated with an additional equivalent of spacer amino acid and a coupling time of 4 h. After the capping step the synthesis was carried out following the usual procedure. After the final deblocking of the *Fmoc*-protective group the resin was transferred into a *Merrifiled*-reaction vessel. A mixture of 15 mL trifluoroacetic acid (TFA), 0.9 mL water and 0.9 mL triisopropylsilane (TIS) was added and the suspension was shaken for 3 h. The suspension was filtrated and the resin was washed with TFA (3·3 ml). 25 mL of toluene were added to the combined filtrates, afterwards the solution was concentrated in vacuo and

codistilled with toluene (3·25 mL). The residue was washed with cold diethyl ether (Et_2O) (3·3 mL), dissolved in water and lyophilised, yielding 160 mg of crude product. 60 mg of the crude peptide were purified by semi-preparative *HPLC* (phenomenex, Jupiter C18, acetonitrile/water + 0.1% TFA, grad.: 28:72 (5 min const.) → 32:68, 20 min, λ = 214 nm; t_R = 17.0 min) yielding 23 mg (0.011 mmol, 11%) of the peptide after lyophilisation.

Analytic HPLC: t_R = 25.2 min (phenomenex Jupiter C18, MeCN/H2O + 0.1% TFA, grad.: 28:72 (5 min const.) → 32:68, 20 min, λ = 214 nm)

$C_{53}H_{94}N_{16}O_{17}$ (M = 2143.32 g/mol) [2142.0606]

ESI-MS (positive ion mode) *m/z*: 1083.23 ($[M+Na+H]^{2+}$, calc.: 1083.03), 1072.22 ($[M+2H]^{2+}$, calc.: 1072.04), 727.82 ($[M+K+2H]^{3+}$, calc.: 727.68), 722.49 ($[M+Na+2H]^{3+}$, calc.: 722.36), 715.15 ($[M+3H]^{3+}$, calc.: 715.03)

HRESI-MS (positive ion mode) *m/z*: 1072.0360 ($[M+2H]^{2+}$, calc.: 1072.0382)

^{1}H-NMR (600 MHz, DMSO-d_6, *^{1}H*, *COSY*, *TOCSY*, *^{13}C-HSQC*, *HMBC*), δ (ppm) = 9.40 (s, 1H, azo$^{4`NH}$), 8.58 (d, 1H, $J_{Q(2)NH,Q(2)\alpha}$ = 8.0 Hz, Q(2)$^{NH}$), 8.46 (t, 1H, $J_{G(16`)NH,G(16`)\alpha}$ = 5.9 Hz, G(16`)^{NH}), 8.42-8.33 (m, 2H, N(7)^{NH} {8.40}, H(9)^{NH} {8.36}), 8.20 (d, 1H, $J_{iQ(15)NH,iQ(15)\alpha}$ = 7.5 Hz, iQ(15)^{NH}), 8.10-7.89 (m, 10H, N(3)^{NH} {8.08}, L(11)^{NH} {8.06}, G(16)^{NH} {8.03}, Y(8)^{NH} {8.00}, R(13)^{NH} {7.99}, G(1)^{NH2} {7.98}, spacer^{NH} {7.98}, T(5)^{NH} {7.92} S(4)^{NH} {7.91}), 7.86-7.76 (m, 4H, V(12)^{NH} {7.84}, T(6)^{NH} {7.81}, azo$^{H5`}$ {7.78}, azo$^{H2`}$ {7.77}), 7.75-7.69 (m, 2H, azo$^{H6`}$ {7.73}, T(10)^{NH} {7.72}), 7.57-7.52 (m, 2H, R(13)$^{\varepsilon NH}$ {7.55}, azo^{H6} {7.54}), 7.47-7.39 (m, 4H, N(7)$^{\gamma CONH2a}$ {7.45}, azo^{H4} {7.42}, azo^{H3} {7.42}, N(3)$^{\gamma CONH2a}$ {7.41}), 7.37 (s, 1H, G(16)^{CONH2a}), 7.34-7.28 (m, 2H, azo^{H5} {7.31}, H(9)^{H5} {7.30}) 7.25 (s, 1H, Q(2)$^{\delta CONH2a}$), 7.07 (s, 1H, G(16)^{CONH2b}), 7.02-6.95 (m, 4H, N(7)$^{\gamma CONH2b}$ {7.00}, N(3)$^{\gamma CONH2b}$ {6.98}, Y(8)$^{H2/6}$ {6.98}), 6.81 (s, 1H, Q(2)$^{\delta CONH2b}$), 6.62 (d, 1H, $J_{Y(8)H3/5,Y(8)H2/6}$ = 8.1 Hz, Y(8)$^{H3/5}$), 4.68-4.58 (m, 2H, H(9)$^{\alpha}$ {4.64}, N(7)$^{\alpha}$ {4.62}), 4.56 (pq, 1H, J = 7.0 Hz, N(3)$^{\alpha}$), 4.41-4.18 (m, 9H, S(4)$^{\alpha}$ {4.39}, Q(2)$^{\alpha}$ {4.38}, L(11)$^{\alpha}$ {4.36}, Y(8)$^{\alpha}$ {4.31}, T(5)$^{\alpha}$ {4.28}, T(10)$^{\alpha}$ {4.25}, iQ(15)$^{\alpha}$ {4.25}, T(6)$^{\alpha}$ {4.22}, R(13)$^{\alpha}$ {4.21}), 4.13 (pt, 1H, J = 7.7 Hz, V(12)$^{\alpha}$), 4.06-3.93 (m, 5H, T(5)$^{\beta}$ {4.03}, G(16`)$^{\alpha}$ {3.99}, T(6)$^{\beta}$ {3.96}, T(10)$^{\beta}$ {3.96}), 3.67-3.54 (m, 8H, S(4)$^{\beta a}$ {3.63}, G(16)$^{\alpha}$ {3.62}, G(1)$^{\alpha}$ {3.59}, spacer^{H3} {3.58}, S(4)$^{\beta b}$ {3.57}), 3.49-3.44 (m, 10H, 5·spacer^{CH2O}), 3.36 (overlapped by the water signal, 2H, spacer^{H12}), 3.11-3.04 (m, 3H, H(9)$^{\beta a}$ {3.08}, R(13)$^{\delta}$ {3.07}), 3.01-2.93 (m, 1H, H(9)$^{\beta b}$), 2.88-2.82 (m, 1H, Y(8)$^{\beta a}$), 2.69-2.62 (m, 4H, azo^{Me2} {2.67}, Y(8)$^{\beta b}$ {2.65}), 2.60-2.52 (m, 2H,

N(7)$^{\beta a}$ {2.57}, N(3)$^{\beta a}$ {2.55}), 2.46-2.30 (m, 7H, N(7)$^{\beta b}$ {2.41}, spacer^{H2} {2.40}, N(3)$^{\beta b}$ {2.35}, azo$^{Me3`}$ {2.34}), 2.24-2.19 (m, 2H, iQ(15)$^{\gamma}$), 2.12-2.08 (m, 2H, Q(2)$^{\gamma}$), 1.97-1.83 (m, 3H, V(12)$^{\beta}$ {1.94}, iQ(15)$^{\beta a}$ {1.94}, Q(2)$^{\beta a}$ {1.87}), 1.82-1.69 (m, 2H, iQ(15)$^{\beta b}$ {1.78}, Q(2)$^{\beta b}$ {1.73}), 1.65-1.56 (m, 2H, R(13)$^{\beta a}$ {1.61}, L(11)$^{\gamma}$ {1.60}), 1.53-1.35 (m, 5H, R(13)$^{\beta b}$ {1.49}, L(11)$^{\beta}$ {1.45}, R(13)$^{\gamma}$ {1.44}), 1.06-1.02 (m, 6H, T(5)$^{\gamma}$ {1.05}, T(6)$^{\gamma}$ {1.04}), 1.00 (d, 3H, $J_{T(10)\gamma,T(10)\beta}$ = 6.2 Hz, T(10)$^{\gamma}$), 0.86 (d, 3H, $J_{L(11)\delta,L(11)\gamma}$ = 6.6 Hz, L(11)$^{\delta}$), 0.84-0.79 (m, 9H, V(12)$^{\gamma}$ {0.82}, L(11)$^{\delta`}$ {0.81}, V(12)$^{\gamma`}$ {0.80})

^{13}C-NMR (150.9 MHz, DMSO-d$_6$, *^{13}C*, *^{13}C-HSQC*, *HMBC*), *δ* (ppm) = 177.7 (Q(2)$^{\delta CONH2}$), 172.1 (L(11)^{CO}), 171.9 (Q(15)$^{\delta CO}$), 171.9 (Q(15)$^{\alpha CO}$), 171.9 (N(7)$^{\gamma CONH2}$), 171.5 (N(7)^{CO}), 171.4 (N(3)$^{\gamma CONH2}$), 171.2 (G(16)^{CONH2}), 171.2 (N(3)^{CO}), 171.0 (Y(8)^{CO}), 171.0 (R(13)^{CO}), 170.8 (V(12)^{CO}), 170.7 (T(6)^{CO}), 170.5 (spacer^{CO}), 170.5 (H(9)^{CO}), 170.3 (Q(2)^{CO}), 169.9 (T(5)^{CO}), 169.8 (T(10)^{CO}), 169.7 (S(4)^{CO}), 168.2 (G(16`)$^{CO}$), 165.8 (G(1)$^{CO}$); 156.7 (R(13)$^{\zeta}$), 155.8 (Y(8)$^{C4}$), 150.0 (azo$^{C1}$), 149.1 (azo$^{C1`}$), 139.0 (azo$^{C4`}$), 137.5 (azo$^{C2}$), 131.6 (azo$^{C3`}$), 131.5 (azo^{C3}), 131.2 (azo^{C4}), 130.0 (Y(8)$^{C2/6}$), 130.0 (H(9)^{C4}), 127.7 (Y(8)^{C1}), 126.7 (azo^{C5}), 124.7 (azo$^{C2`}$), 124.3 (azo$^{C5`}$), 120.7 (azo$^{C6`}$), 115.0 (azo^{C6}), 115.0 (H(9)^{C5}), 115.0 (Y(8)$^{C3/5}$), 69.8, 69.7, 69.7, 69.6, 69.5 (5 x spacer^{CH2O}), 69.0 (spacer^{C12}), 66.8 (T(10)$^{\beta}$), 66.8 (spacer^{C3}), 66.6 (T(6)$^{\beta}$), 66.5 (T(5)$^{\beta}$), 61.7 (S(4)$^{\beta}$), 58.3 (T(6)$^{\alpha}$), 58.3 (T(5)$^{\alpha}$), 57.9 (T(10)$^{\alpha}$), 57.8 (V(12)$^{\alpha}$), 54.9 (S(4)$^{\alpha}$), 54.8 (Y(8)$^{\alpha}$), 52.3 (iQ(15)$^{\alpha}$), 52.1 (Q(2)$^{\alpha}$), 52.0 (R(13)$^{\alpha}$), 51.2 (L(11)$^{\alpha}$), 49.7 (N(7)$^{\alpha}$), 49.6 (N(3)$^{\alpha}$), 42.8 (G(16`)$^{\alpha}$), 41.8 (G(16)$^{\alpha}$), 40.6 (L(11)$^{\beta}$), 40.4 (R(13)$^{\delta}$), 40.2 (G(1)$^{\alpha}$), 37.2 (N(7)$^{\beta}$), 37.0 (N(3)$^{\beta}$), 35.9 (Y(8)$^{\beta}$), 31.5 (iQ(15)$^{\gamma}$), 31.2 (Q(2)$^{\gamma}$), 30.5 (V(12)$^{\beta}$), 29.3 (R(13)$^{\beta}$), 28.6 (Q(2)$^{\beta}$), 27.9 (H(9)$^{\beta}$), 27.9 (iQ(15)$^{\beta}$), 25.1 (R(13)$^{\gamma}$), 24.1 (L(11)$^{\gamma}$), 23.2 (L(11)$^{\delta}$), 21.6 (L(11)$^{\delta`}$), 19.5 (T(5)$^{\gamma}$), 19.5 (T(6)$^{\gamma}$), 19.3 (T(10)$^{\gamma}$), 19.2 (V(12)$^{\gamma}$), 18.3 (V(12)$^{\gamma`}$), 18.0 (azo$^{Me3`}$), 17.2 (azo^{Me2})

16.
Experimental Section: Crystallisations

16.1 General Information

Chemicals and Reagents

All chemicals were purchased in the highest commercially available purity. 1.0 M volumetric standard solutions of calcium chloride, 0.1 M analytic standard solution of magnesium chloride, ammonium carbonate (puriss.), methanol (p.a.) and ethanol (*p.a.*) were purchased at *Sigma-Aldrich Chemie GmbH* (*St. Louis*, US-MO). Water was purified by a *Simplicity 185* ultrapure water system (*Merck-Millipore*, *Bellerica*, US-MA). Quartz glass slides *Spectrosil* were available at *Heraeus Quarzglas GmbH & Co. KG* (*Hanau*, Germany). Microscopy glass slides were purchased at *VWR International GmbH* (*Darmstadt*, Germany)).

X-Ray Powder Diffraction

X-ray diffraction patterns were recorded with a *Bruker AXS D8 Discover* diffractometer (*Bruker AXS*, *Madison*, US-WI) equipped with a *HiStar* detector using graphite monochromatized CuKα radiation. Samples were glued on top of glass using a VP/VA copolymer (vinylpyrrolidone/vinylacetate) solution in isopropanol. Individual frames were typically recorded at 2Θ = 24°, 34°, 44°, 54°, 64°, 74°, 84° (detector distance 150mm, detector range Δ(2Θ)=35°). X-ray diffraction patterns were integrated from individual frames using the *Bruker AXS GADDS* software package (*GADDS* 4.1.19, *Bruker AXS*, *Madison*, US-WI (2004)) and merged using *Bruker AXS EVA* (*EVA* 10.0, *Bruker AXS*, *Madison*, US-WI (2004)). Crystalline phases were identified the *Pearson`s Crystal Database* [305].

Crystalline compound	Pearson`s Crystal Database Entry-#
Calcite	1520914 [140]
Aragonite	1520913 [140]
Vaterite	1415671 [284]

Transmission Electron Microscopy

Transmission Electron Microscopy (*TEM*) images were recorded on a *Philips EM420* transmission electron microscope (*FEI Company*, *Hillsboro*, US-OR) at an acceleration voltage of 120 kV. The image recording was kindly carried out by Dr. T. Schüler.

Scanning Electron Microscopy

Scanning Electron Microscopy (*SEM*) images were recorded on a *FEI Nova NanoSEM 600* instrument (*FEI Company*, *Hillsboro*, US-OR), equipped with an *Everhart-Thornley* detector (ETD), a low voltage high contrast detector (vCD) and a Through Lens Detector (TLD) in high vacuum mode. The acceleration voltage was varied between 10-30 kV. The samples were attached to an aluminium stub by adhesive and conductive carbon tape. Prior to the imaging, the samples were sputtered with a 7.5nm thick gold layer on a *MED 20 Sputter Coating Unit* (*Leica Microsystems GmbH*, *Wetzlar*, Germany). The image recording was kindly carried out by Dr. A. Gehl.

Confocal Laser Scanning Microscopy

Confocal Laser Scanning Microscopy (*CLSM*) was carried out on a *Keyence VK-8710* with a *VK-8700* light- and laser-source (*Keyence*, *Osaka*, Japan). The mircroscop is provided with a set of *Nikon* objectives of 10x, 20x, 50x and 100x magnification (*Shinagawa*, *Tokyo*, Japan).

Raman Microscopy

Raman Mycroscopy was carried out on a *Horiba Jobin Yvon LabRAM HR 800 spectrometer* (*Horiba, Ltd.*, *Minami-Ku*, *Kyoto*, Japan) equipped with a Si-based charge-coupled device (CCD) detector (Peltier-cooled). The Raman spektroskop was equipped with an *Olympus BX41* optical microscope (*Olympus*, *Shinjuku*, *Tokyo*, Japan) using an automatized x – y stage. Measurements were performed, using a 50x long-distance objective (numerical aperture 0.55) and a chosen slit width of 100 µm. For excitation, a Nd:YAG laser with wavelength of 632.8 nm and a spot size of ca 2 × 2 µm was used. Spectra were recorded from 100 cm^{-1} to 1600 cm^{-1}.

Climate Chamber

For the crystallisation studies, a climate chamber *Espec* SH-241 (*Espec Corp.*, *Kita-ku*, *Osaka*, Japan) was applied.

16.2 General Procedure

General procedure for the ammonium (carbonate) diffusion crystallisation method (ADM)

For a standard crystallisation of calcium carbonate, 1 mL of a 10 mmol/L calcium chloride solution were prepared in a *LoBind-DNA-Eppendorf*™ tube. Except of the control samples, peptide additives were added in specific concentrations in dependance on the specific experiment (specific conditions of the individual experiments are listed at the end). As-prepared tubes were positioned in a dessicator together with 7 g of freshly ground ammonium carbonate, yet all tubes and the ammonium carbonate remained covered. The dessicator was placed in the climate chamber at the appropriate temperature for 30 min to equilibrate. Subsequently, the prepared solutions and the ammonium carbonate were uncovered and the precipitation was allowed to proceed at the specific conditions for 4 h. Afterwards, the samples were removed from the desiccator and centrifuged for 10 min at 14500 rpm. The supernatants were discarded and the precipitated crystallites were washed twice with 200 µL methanol. Between the wash steps, the samples were centrifuged and the supernatants were discarded as well. Finálly, the washed precipitates were dried.

Specific conditions of crystallisation experiments

<u>Influence of Quartz Glass Slides during Crystallisation:</u>

To test the influence of the quartz glass slides during crystallisation, *Spectrosil* quartz glass slides (5 x 5 mm, *Heraeus Quarzglas GmbH & Co. KG*, *Hanau*, Germany) were utilised, after cleaning by two different procedures. One set of quartz glass slides was treated in *Caro`s* acid (peroxymonosulfuric acid, H_2SO_5), prepared by carefully mixing 35% hydrogen peroxide and conc. sulfuric acid (96%) in a ratio of 1:3 at 0 °C. The slides were submerged in this solution for 10 min. The second set of quartz glass slides was treated in a solution of hydrogen

peroxide (33%) in ammonia hydroxide (32%) (1:1) at 70 °C for 10 min. After the diifferent cleaning procedures, the slides were washed several times with water and ethanol. The influence of differently treated slides was investigated, by submerging a slide in a 10 mmol/L calcium chloride solution. The actual crystallisation was carried out according to the general crystallisation procedure for 4 h at 25 °C. After 4 h, the slides were removed from the individual solutions, washed twice with water and twice with ethanol. After subsequent drying, the slides were examined by *CLSM*. For light-microscopic and *CLSM*-images, see Appendix Va.

Influence of different magnesium concentrations ion during crystallisation:

Five different calcium-to-magnesium ratios (i.e., 1:1, 1:2, 1:3, 1:4 and 1:5) were prepared by adding 10 mmol/L, 20 mmol/L, 30 mmol/L, 40 mmol/L and 50 mmol/L of magnesium chloride to 10 mmol/L of calcium chloride. Additionally, a magnesium-free 10 mmol/L solution of calcium chloride was utilised as a control sample. In accordance to the general crystallisation procedure, 1 mL aliquots of these solutions were applied for the crystallisation in a desiccator. The crystallisations carried out according to the standard protocol for 4 h at 25 °C. For light-microscopic and *CLSM*-images as well as *XRPD*-data, see Appendix Vb.

Influence of temperature on the calcium carbonate phase composition:

In accordance to the general crystallisation procedure, 1 mL aliquots of a 10 mmol/l calcium chloride solution were applied during crystallisations in a desiccator. The crystallisations were allowed to proceed for 4 h at three different temperatures, i.e., 25 °C, 45 °C and 60 °C. The individual precipitates were collected according to the general procedure. For light-microscopic and *CLSM*-images as well as *Raman*-spectra, see Appendix Vc.

Crystallisation in the presence of the mixed, crude sequences (**2**) and (**6**):

The general crystallisation procedure was carried out at 45 °C. A solution of 10 mmol/L calcium chloride was utilised as a control sample. Furthermore, the crude mix of peptides (**2**) and (**6**) was applied at concentrations of 0.5 and 1 mg/mL. in the presence of 10 mmol/L calcium chloride. The crystallisations were carried

out for 4 h as described above. For light-microscopic and *CLSM*-images, see Appendix Vd.

Crystallisations in the presence of 0.5% Tween®20 and the mixed, crude sequences (**2**) and (**6**):

The general crystallisation procedure was employed at 45 °C. Two different solutions of 10 mmol/L calcium chloride were prepared as control samples, one additionally contained 0.5% Tween®20. The mixed crude peptide (**2**) and (**6**) were utilised at concentrations of 0.5, 0.2, 0.1 and 0.05 mmol/L in the presence of 10 mmol/L $CaCl_2$-solution and 0.5% Tween®20. The procedure was carried out for 4 h as described above. For light-microscopic and *CLSM*-images, see Appendix Ve.

Crystallisation in the presence of the mixed, crude sequences (**3**) and (**7**):

The general crystallisation procedure was performed at 45 °C. A solution of 10 mmol/L calcium chloride was utilised as a control sample. Furthermore, the crude mix of peptides (**3**) and (**7**) was applied at concentrations of 5, 2, 1, 0.5, 0.2, 0.1 and 0.05 mmol/L in the presence of 10 mmol/L calcium chloride. The crystallisations were carried out for 4 h as described above. For light-microscopic and *CLSM*-images, see Appendix Vf.

Crystallisation in the presence of peptide (**8**):

The general crystallisation procedure was carried out at 45 °C. A solution of 10 mmol/L calcium chloride was utilised as a control sample. Furthermore, peptide (**8**) was applied at concentrations of 5, 2, 1, 0.5, 0.2, 0.1 and 0.05 mmol/L in the presence of 10 mmol/L calcium chloride. The crystallisations were carried out for 4 h as described above. For light-microscopic and *CLSM*-images, see Appendix Vg.

Crystallisation in the presence of the crude peptide (**8**), the desalted peptide (**8**) and the pure peptide (**7**):

The general crystallisation procedure was carried out at 45 °C. A solution of 10 mmol/L calcium chloride was utilised as control sample. Furthermore, the peptides of different purities were applied at a concentration of 5 mmol/L in the presence of 10 mmol/L calcium chloride. The crystallisations were carried out for 4 h as described above. For light-microscopic and *CLSM*-images, see Appendix Vh.

Crystallisation in the presence of the crude peptide (**9**) and the pure peptides (**10**), (**11**) and (**1**):

The general crystallisation procedure was carried out at 45 °C. A solution of 10 mmol/L calcium chloride was utilised as control sample. Furthermore, the peptides of different purities were applied at a concentration of 5 mmol/L in the presence of 10 mmol/L calcium chloride. The crystallisations were carried out for 4 h as described above. For light-microscopic and *CLSM*-images, see Appendix Vi.

General procedure for the (re)crystallisation method applying vaterite nanoparticles [77]

For a standard recrystallisation, a dispersion of vaterite-nanoparticles [*] was diluted to 1 mL volume at a concentration of 1 mg/mL. As a control, a peptide additive free sample was applied, while the remaining samples additionally contained the respective peptide additive at 1 mmol/L. The resulting dispersions were incubated on a rotary shaker at 20 °C for 24 hours. The dispersions were subsequently precipitated by centrifugation at 14500 rpm and washed three-times with methanole. The resulting precipitates were dried in vacuum and analysed by *SEM* and *CLSM*.

***:** The vaterite-nanoparticles used during these experiment were kindly provided by [redacted]. The preparation was carried out according to *Schröder et al.* [338].

Recrystallisation in the presence of the crude, the desalted and the pure peptide (**8**) as well as peptide (**10**), (**11**), (**1**) and the crude peptide (**9**):

The general crystallisation procedure was carried out, as described in the general procedure. A dispersion of 1 mg/mL vaterite nanoparticles was utilised as control sample. The respective peptides were applied at of 1 mmol/L in the presence of 1 mg/mL of vaterite nanoparticles. The crystallisations were carried out for 24 h as described above. For light-microscopic, *CLSM*- and *SEM*-images, see Appendix VIb.

Literature

(1) Lowenstam, H. A.; Weiner, S. *Biomineralisation*, Oxford University Press: New York, *1st ed.*, **1989**.

(2) Mann, S. *Biomineralization - Principles and Concepts in Bioinorganic Materials Chemistry,* Oxford Univerity Press: Oxford, *1st ed.*, **2001**.

(3) Baeuerlein, E. *Biomineralization.* Wiley-VCH: Weinheim, *1st ed.*, **2000**.

(4) Weiner, S.; Addadi, L. *Science* **2002**, *298*, 375-376.

(5) Lowenstam, H. A. *Science* **1981**, *211*, 1126-1131.

(6) Mann, S. *Struct. Bonding.* **1983**, *54*, 125-174.

(7) Dupraz, C.; Reid, R. P.; Braissant, O.; Decho, A. W.; Norman, R. S.; Visscher, P. T. *Earth-Sci. Rev.* **2009**, *96*, 141-162.

(8) Wang, X.; Schröder, H. C.; Wiens, M.; Schloßmacher, U.; Müller, W. E. G. *Micron.* **2009**, *40*, 350-358.

(9) Wang, X.; Wiens, M.; Schröder, H. C.; Schloßmacher, U.; Müller, W. E. G. "*Molecular Biomineralization: Toward an Understanding of the Biogenic Origin of Polymetallic Nodules, Seamount Crusts and Hydrothermal Vents*" in Müller, W. E. G. *Molecular Biomineralization Aquatic Organisms Forming Extraordinary Materials,* Springer-Verlag: Heidelberg, *1st ed.*, **2011**, 77-112.

(10) Blakemore, R. P. *Science* **1975**, *190*, 377-379.

(11) Faivre, D; Schüler, D. *Chem. Rev.* **2008**, *108*, 4875-4898.

(12) Baumgartner, J.; Faivre, D. "*Magnetite Biomineralization in Bacteria*" in Müller, W. E. G. *Molecular Biomineralization Aquatic Organisms Forming Extraordinary Materials,* Springer-Verlag: Heidelberg, *1st ed.*, **2011**, 3-28.

(13) Lefèvre, C. T.; Bazylinski, D. A. *Microbiol. Mol. Biol. Rev.* **2013**, *77*, 497-526.

(14) Yan, L.; Zhang, S.; Chen, P.; Liu, H.; Yin, H.; Li, H. *Microbiol. Res.* **2012**, *167*, 507-519.

(15) Jogler, C.; Schüler, D. *Annu. Rev. Microbiol.* **2009**, *63*, 501-521.

(16) Wegst, U. G. K.; Bai, H.; Saiz, E.; Tomsia, A. P.; Ritchie, R. O. *Nat. Mater.* **2015**, *14*, 23-36.

(17) Barkaoui, A.; Chamekh, A.; Merzouki, T.; Hambli, R.; Mkaddem, A. *Int. J. Numer. Meth. Biomed. Eng.* **2014**, *30*, 318-338.

(18) Ritchie, R. O.; Buehler, M. J.; Hansma, P. *Phys. Today* **2009**, *62*, 41-47.

(19) Nair, A. K.; Gautieri, A.; Chang, S.-W.; Buehler, M. J. *Nat. Commun.* **2013**, *4*, 1724.

(20) a) Dorozhkin, S. V.; Epple, M. *Angew. Chem. Int. Ed.* **2002**, *41*, 3130-3146.
b) Dorozhkin, S. V.; Epple, M. *Angew. Chem.* **2002**, *114*, 3260-3277.

(21) Beniash, E. *Wiley Interdiscip. Rev. Nanomed. Nanobiotechnol.* **2011**, *3*, 47-69.

(22) Weiner, S.; Wagner, H. D. *Annu. Rev. Mater. Sci.* **1998**, *28*, 271-298.

(23) Dorozhkin, S. V. *Materials* **2009**, *2*, 1975-2045.

(24) Weiner, S.; Price, P. A. *Calc. Tissue Int.* **1986**, *39*, 365-375.

(25) Hassenkam, T.; Fantner, G. E.; Cutroni, J. A.; Weaver, J. C.; Morse, D. E.; Hansma, P. K. *Bone.* **2004**, *35*, 4-10.

(26) Currey, J. D. *The Mechanical Adaptions Of Bone,* Princeton Univ. Press: Princeton, *1st ed.*, **1984**.

(27) Chen, Q.; Thouas, G. *Biomaterials - A Basic Introduction,* CRC Press: Boca Raton, Taylor & Francis Group, *1st ed.*, **2015**.

(28) Mullin, J. W. *Christallization,* Butterworth-Heinemann: Oxford, *4th ed.*, **2001**.

(29) Sangwal, K. *Additives And Crystallization Processes - From Fundamentals to Applications,* John Wiley & Sons Ltd.: Chichester, *1st ed.*, **2007**.

(30) Addadi, L.; Weiner, S. *Proc. Nat. Acad. Sci.* **1985**, *82*, 4110-4114.

(31) Weissbuch, I.; Popovitz-Biro, R.; Lahav, M.; Leiserowitz, L. *Acta Cryst. B* **1995**, *51*, 115-148.

(32) Song, R-Q.; Cölfen, H. *CrystEngComm.* **2011**, *13*, 1249-1276.

(33) Shimizu, K.; Cha, J.; Stucky, G. D.; Morse, D. E. *Proc. Nat. Acad. Sci.* **1998**, *95*, 6234-6238.

(34) Cha, J. N.; Shimizu, K.; Zhou, Y.; Christiansen, S. C.; Chmelka, B. F.; Stucky, G. D.; Morse, D. E. *Proc. Nat. Acad. Sci.* **1999**, *96*, 361-365.

(35) Krasko, A.; Lorenz, B.; Batel, R.; Schröder, H. C.; Müller, I. M.; Müller, W. E. G. *Eur. J. Biochem.* **2000**, *267*, 4878-4887.

(36) Müller, W. E.G.; Wang, X.; Chen, A.; Hu, S.; Gan, L.; Schröder, H. C.; Schloßmacher, U.; Wiens, M. "*The Unique Invention of the Siliceous Sponges: Their Enzymatically Made Bio-Silica Skeleton*" in Müller, W. E. G. *Molecular Biomineralization Aquatic Organisms Forming Extraordinary Materials,* Springer Verlag: Heidelberg, *1st ed.*, **2011**.

(37) Murr, M. M.; Morse, D. E. *Proc. Nat. Acad. Sci.* **2005**, *102*, 11657-11662.

(38) Müller, W. E. G.; Boreiko, A.; Schloßmacher, U.; Wang, X.; Tahir, M. N.; Tremel, W.; Brandt, D.; Kaandorp, J. A.; Schröder, H. C. *Biomaterials* **2007**, *28*, 4501-4511.

(39) Schloßmacher, U.; Wiens, M.; Schröder, H. C.; Wang, X.; Jochum, K. P.; Müller, W. E. G. *FEBS J.* **2011**, *278*, 1145-1155.

(40) Weiner, S.; Addadi, L. *J. Mater. Chem.* **1997**, *7*, 689-702.

(41) **Barthelat, F.; Tang, H.; Zavattieri, P.D.; Li, C.-M.; Espinosa, H.D.** *J. Mech. Phys. Solids.* **2007**, *55*, 306-337.

(42) Jacob, D. E.; Soldati, A. L.; Wirth, R.; Huth, J.; Wehrmeister, U.; Hofmeister, W. *Geochim. Cosmochim. Acta.* **2008**, *72*, 5401-5415.

(43) Hildebrand, M. *Chem. Rev.* **2008**, *108*, 4855-4874.

(44) Schröder, H. C.; Wiens, M.; Schloßmacher, U.; Brandt, D.; Müller, W. E. G. *Silicon* **2012**, *4*, 33-38.

(45) Müller, W. E. G.; Schröder, H. C.; Burghard, Z.; Pisignano, D.; Wang, X. *Chem. Eur. J.* **2013**, *19*, 5790-5804.

(46) Marin, F.; Luquet, G.; Marie, B.; Medakovic, D. *Curr. Top. Dev.Biol.* **2008**, *80*, 209-276.

(47) Xie, L.-P.; Zhu, F.-J.; Zhou, Y.-J.; Yang, C.; Zhang, R.-Q. "*Molecular Approaches to Understand Biomineralization of Shell Nacreous Layer*" in Müller, W. E. G. *Molecular Biomineralization Aquatic Organisms Forming Extraordinary,* Springer-Verlag: Heidelberg, *1st ed.*, **2011**, 331-352.

(48) Sun, J.; Bhushan, B. *RSC Adv.* **2012**, *2*, 7617-7632.

(49) Dauphin, Y. *J. Biol. Chem.* **2003**, *278*, 15168-15177.

(50) Dauphin, Y.; Cuif, J. P.; Mutvei, H.; Denis, A. *Bull. Geol. Inst. Univ. Uppsala* **1989**, *15*, 7-36.

(51) Heinemann, F.; Launspach, M.; Gries, K.; Fritz, M. *Biophys.Chem.* **2011**, *153*, 126-153.

(52) Weiner, S. *Amer. Zool.* **1984**, *24*, 945-951.

(53) Weiner, S.; Traub, W. *Philos. Trans. R. Soc. London Ser. B.* **1984**, *304*, 421-438.

(54) Addadi, L.; Berman, A.; Moradian-Oldak, J.; Weiner, S. *Croat. Chem. Acta.* **1990**, *63*, 539-544.

(55) Falini, G.; Albeck, S.; Weiner, S.; Addadi, L. *Science* **1996**, *271*, 67-69.

(56) Nudelman, F.; Gotliv, B. A.; Addadi, L.; Weiner, S. *J. Struct. Biol.* **2006**, *153*, 176-187.

(57) Addadi, L.; Joester, D.; Nudelman, F.; Weiner, S. *Chem. Eur. J.* **2006**, *12*, 980-987.

(58) a) Cartwright, J. H. E.; Checa, A. G.; Gale, J. D.; Gebauer, D.; Sainz-Díaz, C. I. *Angwe. Chem. Int. Ed.* **2012**, *51*, 11960-11970.
b) Cartwright, J. H. E.; Checa, A. G.; Gale, J. D.; Gebauer, D.; Sainz-Díaz, C. I. *Angew. Chem.* **2012**, *124*, 12126-12137.

(59) Ihli, J.; Bots, P.; Kulak, A.; Benning, L. G.; Meldrum, F. C. *Adv. Funct. Mater.* **2013**, *23*, 1965-1973.

(60) Tomson, M. B.; Nancollas, G. H. *Science* **1978**, *200*, 1059-1060.

(61) Beck, R.; Seiersten, M.; Andreassen, J.-P. *J. Cryst. Growth* **2013**, *380*, 187-196.

(62) Wada, N.; Okazaki, M.; Tachikawa, S. *J. Cryst. Growth* **1993**, *132*, 115-121.

(63) Loste, E.; Park, R. J.; Warren, J.; Meldrum, F. C. *Adv. Funct. Mater.* **2004**, *14*, 1211-1220.

(64) Faatz, M. *Kontrollierte Fällung von amorphem Calciumcarbonat durch homogene Carbonatfreisetzung*, *dissertation,* Johannes Gutenberg-Universität: Mainz, **2005**.

(65) Mann, S.; Heywood, B. R.; Rajam, S.; Birchall, J. D. *Nature* **1988**, *334*, 692-695.

(66) Küther, J.; Seshadri, R.; Knoll, W.; Tremel, W. *J. Mater. Chem.* **1998**, *8*, 641-650.

(67) Küther, J.; Seshadri, R.; Tremel, W. *Angew. Chem.* **1998**, *110*, 3196-3199.

(68) Lee, I.; Han, S. W.; Choi, H. J.; Kim, K. *Adv. Mater.* **2001**, *13*, 1617-1620.

(69) Sommerdijk, N. A. J. M.; de With, G. *Chem. Rev.* **2008**, *108*, 4499-4550.

(70) Suhara, T.; Esumi, K.; Meguro, K. *Bull. Chem. Soc. Jpn.* **1983**, *56*, 2932-2936.

(71) Liu, D.; Yates, M. Z. *Langmuir* **2006**, *22*, 5566-5569.

(72) Wada, N.; Yamashita, K.; Umegaki, T. *J. Colloid Interface Sci.* **1999**, *212*, 357-364.

(73) Sugawara, T.; Suwa, Y.; Ohkawa, K.; Yamamoto, H. *Macromol. Rapid. Commun.* **2003**, *24*, 847-851.

(74) Li, W.; Gao, C. *Langmuir* **2007**, *23*, 4575-4582.

(75) Meng, Q.; Chen, D.; Yue, L.; Fang, J.; Zhao, H.; Wang. L. *Macromol. Chem. Phys.* **2007**, *208*, 474-484.

(76) Abdel-Aal, N.; Sawada, K. *J. Cryst. Growth* **2003**, *256*, 188-200.

(77) Schüler, T. *Vaterite – Control of Polymorphism and Biomedical Application of Biomineral-Nanoparticles*, dissertation, Johannes Gutenberg-Universität: Mainz, **2012**.

(78) Schüler, T.; Renkel, J.; Hobe, S.; Susewind, M.; Jacob, D. E.; Hoffmann-Röder, A.; Paulsen, H.; Tremel, W. *J. Mater. Chem. B.* **2014**, *2*, 3511-3518.

(79) Loges, N. *Kontrolle der Morphologie und Polymorphie von Calciumcarbonat durch monomere und polymere, ionische Additive*, *dissertation,* Johannes Gutenberg-Universität: Mainz, **2009**.

(80) Dietzsch, M. *Precipitation of $CaCO_3$, $MgCO_3$ and $Ca(1-x)\ Mg_xCO_3$ in aqueous solution and ionic liquids*, *d*issertation, Johannes Gutenberg-Universität: Mainz, **2014**.

(81) Küther, J.; Bartz, M.; Seshadri, R.; Vaughan, G. B. M.; Tremel, W. *J. Mater. Chem.* **2001**, *11*, 503-506.

(82) Balz, M.; Therese, H. A.; Li, J.; Gutmann, J. S.; Kappl, M.; Nasdala, L.; Hofmeister, W.; Butt, H.-J.; Tremel, W. *Adv. Funct. Mater.* **2005**, *15*, 683-688.

(83) Love, J. C.; Estroff, L. A.; Kriebel, J. K.; Nuzzo, R. G.; Whitesides, G. M. *Chem. Rev.* **2005**, *105*, 1103-1169.

(84) Heywood, B. R.; Mann, S. *Chem. Mater.* **1994**, *6*, 311-318.

(85) Litvin, A. L.; Valiyaveettil, S.; Kaplan, D. I.; Mann, S. *Adv. Mater.* **1997**, *9*, 124-127.

(86) Buijnsters, P. J. J. A.; Donners, J. J. J. M.; Hill, S. J.; Heywood, B. R.; Nolte, R. J. M.; Zwanenburg, B.; Sommerdijk, N. A. J. M. *Langmuir* **2001**, *17*, 3623-3628.

(87) Popescu, D. C.; Smulders, M. M. J.; Pichon, B. P.; Chebotareva, N.; Kwak, S.-Y.; van Asselen, O. L. J.; Sijbesma, R. P.; DiMasi, E.; Sommerdijk, N. A. J. M. *J. Am. Chem. Soc.* **2007**, *129*, 14058-14067.

(88) Shtukenberg, A. G.; Lee, S. S.; Kahr, B.; Ward, M. D. *Annu. Rev. Chem. Biomol. Eng.* **2014**, *5*, 77-96.

(89) Cabrera, N.; Vermileya, D. A. *Growth and Perfection of Crystals,* John Wiley & Sons: New York, *1st ed.*, **1958**.

(90) J. J. De Yoreo, P. G. Vekilov. Principles of Crystal Nucleation and Growth. *Reviews in Mineralogy & Geochemistry -Biomineralization-.* Chantilly, VA, USA : Mineralogical Society of America, 2003.

(91) Bliznakow, G. *Fortschr. Miner.* **1958**, *36*, 149.

(92) LaMer, V. K.; Dinegar, R. H. *J. Am. Chem. Soc.* **1950**, *72*, 4847-4854.

(93) Wiberg, N. *Holleman-Wiberg - Lehrbuch der Anorganischen Chemie*, Walter de Gruyter & Co.: Berlin, *102nd ed.*, **2007**.

(94) Morse, J. W.; Arvidson, R. S.; Lüttge, A. *Chem. Rev.* **2007**, *107*, 342-381.

(95) Epple, M. *Biomaterialien und Biomineralisation*, Teubner: Wiesbaden, *1st ed.*, **2003**.

(96) Clarkson, E. N. K.; Levi-Setti, R. *Nature* **1975**, *254*, 663-667.

(97) Aizenberg, J.; Tkachenko, A.; Weiner, S.; Addadi, L.; Hendler, G. *Nature* **2001**, *412*, 819-822.

(98) Ostwald, W. *Z. Phys. Chem.* **1897**, *22*, 289-330.

(99) Threlfall, T. *Org. Proc. Res. Dev.* **2003**, *7*, 1017-1027.

(100). Mirwald, P. W. *Contrib. Mineral. Petrol.* **1976**, *59*, 33-40.

(101) Ishizawa, N. *Powder Diffr.* **2014**, *29*, 19-23.

(102) Rodriguez-Blanco, J. D.; Shaw, S.; Benning, L. G. *Nanoscale* **2011**, *3*, 265-271.

(103) Bots, P.; Benning, L. G.; Rodriguez-Blanco, J.-D.; Roncal-Herrero, T.; Shaw, S. *Cryst. Growth Des.* **2012**, *12*, 3806-3814.

(104) Johnston, J.; Merwin, H. E.; Williamson, E. D. *Am. J. Sci.* **1916**, *4*, 473-512.

(105) Pauly, H. *Arctic* **1963**, *16*, 263-264.

(106) Bischoff, J. L.; Fitzpatrick, J. A.; Rosenbauer, R. J. *J. Geol.* **1993**, *101*, 21-33.

(107) Brooks, R.; Clark, L. M.; Thurston, E. F. *Phil. Trans. Roy. Soc. London Ser. A.* **1950**, *243*, 145-167.

(108) Malone, Ph. G.; Towe, K. M. *Mar. Geol.* **1970**, *9*, 301-309.

(109) a) Mugnaioli, E.; Andrusenko, I.; Schüler, T.; Loges, N.; Dinnebier, R. E.; Panthöfer, M.; Tremel, W.; Kolb, U. *Angew. Chem. Int. Ed.* **2012**, *51*, 7041-7045.
b) Mugnaioli, E.; Andrusenko, I.; Schüler, T.; Loges, N.; Dinnebier, R. E.; Panthöfer, M.; Tremel, W.; Kolb, U. *Angew. Chem.* **2012**, *124*, 7148-7152.

(110) Hu, Q.; Zhang, J.; Teng, H.; Becker, U. *Am. Mineral.* **2012**, *97*, 1437-1445.

(111) Trushina, D. B.; Bukreeva, T. V.; Kovalchuk, M. V.; Antipina, M. N. *Mater. Sci. Eng. C.* **2014**, *45*, 644-658.

(112) mindat.org [online, 18.06.2018.] https://www.mindat.org/min-307.html.

(113) Brecevic, L.; Nielsen, A. E. *J. Cryst. Growth* **1989**, *98*, 504-510.

(114) Beniash, E.; Aizenberg, J.; Addadi, L.; Weiner, S. *Proc. Royal Soc. Lond. B.* **1997**, *264*, 461-465.

(115) Politi, Y.; Arad, T.; Klein, E.; Weiner, S.; Addadi, L. *Science* **2004**, *306*, 1161-1164.

(116) Travis, D. F. *Ann. N. Y. Acad. Sci.* **1963**, *109*, 177-245.

(117) Hild, S.; Marti, O.; Ziegler, A. *J. Struct. Biol.* **2008**, *163*, 100-108.

(118) Neues, F.; Hild, S.; Epple, M.; Ziegler, A. *J. Struct. Biol.* **2011**, *175*, 10-20.

(119) Lennie, A. R; Tang, C. C.; Thompson, S. P. *Mineral. Mag.* **2004**, *68*, 135-146.

(120) Effenberger, H. *Monatsh. Chem.* **1981**, *112*, 899-909.

(121) Kralj, D.; Brecevic, L. *Colloids Surf. A.* **1995**, *96*, 287-293.

(122) Dieckmann, G. S.; Nehrke, G.; Papadimitriou, S.; Göttlicher, J.; Steininger, R.; Kennedy, H.; Wolf-Gladrow, D.; Thomas, D. N. *Geophys. Res. Lett.* **2008**, *35*, L08501.

(123) Mindat.org [online, 02.06.2018.] https://www.mindat.org/min-2007.html.

(124) Dahl, K.; Buchardt, B. *J. Sedim. Res.* **2006**, *76*, 460-471.

(125) Mindat.org [online, 02.06.2018.] https://www.mindat.org/min-2758.html.

(126) Trampe, E.; Castenholz, R. W.; Larsen, J. E. N.; Kühl, M. *Environ. Microbiol.* **2017**, *19*, 4754-4770.

(127) Tansman, G. F.; Kindstedt, P.S.; Hughes, J. M. *Can. Mineral.* **2017**, *55*, 89-100.

(128) Senorale-Pose, M.; Chalar, C.; Dauphin, Y.; Massard, P.; Pradel, P.; Marin. M.; *Exp. Parasitol.* **2008**, *118*, 54-58.

(129) Catherine, H.; Skinner, K.; Osbaldiston, G. W.; Wilner, A. N. *Am. Mineral.* **1977**, *62*, 273-277.

(130) Plummer, L. N.; Busenberg, E. *Geochim. Cosmochim. Acta* **1982**, *46*, 1011-1040.

(131) Hazen, R. M.; Downs, R. T.; Jones, A. P.; Kah, L. *Rev. Mineral. Geochem.* **2013**, *75*, 7-46.

(132) Mindat.org [online, 02.06.2018.] https://www.mindat.org/min-4161.html.

(133) Gauldie, R. W. *Acta Zool.* **1990**, *71*, 193-199.

(134) Lenaz, D.; Miletic, M.; Pizzul, E.; Vanzo, S.; Adami, G. *Eur. J. Mineral.* **2006**, *18*, 143-148.

(135) Lowenstam, H. A. *Bull. Mar. Sci.* **1989**, *45*, 243-252.

(136) Soldati, A. L.; Jacob, D. E.; Wehrmeister, U.; Hofmeister, W. *Min. Mag.* **2008**, *72*, 579-592.

(137) Nehrke, G.; Poigner, H.; Wilhems-Dick, D.; Brey, T.; Abele, D. *Geochem. Geophys.* **2012**, *13*, Q05014.

(138) Christy, A. G. *Cryst. Growth Des.* **2017**, *17*, 3567-3578.

(139) Ono, S.; Kikegawa, T.; Ohishi, Y.; Tsuchiya, J. *Am. Mineral.* **2005**, *90*, 667-671.

(140) Caspi, E. N.; Pokroy, B.; Lee, P. L.; Quintana, J. P.; Zolotoyabko, E. *Acta Crystallogr. B.* **2005**, *61*, 129-132.

(141) Cohen, A. L.; McConnaughey, T. A. *Rev. Mineral. Geochem.* **2003**, *54*, 151-187.

(142) Mindat.org [online, 21.06.18] https://www.mindat.org/min-859.html.

(143) Heuer, A. H.; Foml, D. J.; Laraia, V. J.; Arias, J. L.; Heuer, P. *Science* **1992**, *255*, 1098-1105.

(144) Arias, J. L.; Fink, D. J.; Xiao, S.-Q.; Heuer, A. H.; Caplan, A. I. *Int. Rev. Cytol.* **1993**, *145*, 217-250.

(145) Wilt, F. H. *Zool. Sci.* **2002**, *19*, 253-261.

(146) Sethmann, I.; Wörheide, G. *Micron* **2008**, *39*, 209-228.

(147) de Nooijer, L. J.; Spero, H. J.; Erez, J.; Bijma, J.; Reichart, G. J. *Earth-Sci. Rev.* **2014**, *135*, 48-58.

(148) Brownlee, C.; Wheeler, G. L.; Taylor, A. R. *Semin. Cell Dev. Biol.* **2015**, *46*, 11-16.

(149) Ullman, C. G.; Frigotto, L.; Cooley, R. N. *Brief. Funct. Genomics.* **2011**, *10*, 125-134.

(150) Paschke, M. *Appl. Microbiol. Biotechnol.* **2006**, *70*, 2-11.

(151) Kehoe, J. W.; Kay, B. K. *Chem. Rev.* **2005**, *105*, 4056-4072.

(152) New England Biolabs GmbH (*Frankfurt am Main*, Germany). *Ph. D. TM Phage Display Libraries - Instruction Manual*.

(153) Smith, G. P.; Petrenko, V. A. *Chem. Rev.* **1997**, *97*, 391-410.

(154) Rodi, D. J.; Makowski, L. *Curr. Opin. Biotechnol.* **1999**, *10*, 87-93.

(155) Sternberg, N.; Hoess, R. H. *Proc. Nat. Acad. Sci.* **1995**, *92*, 1609-1613.

(156) Kuwabara, I.; Maruyama, H.; Mikawa, Y. G.;. Zuberi, R. I; Liu, F. T.; Maruyama, I. N. *Nat. Biotechnol.* **1997**, *15*, 74-78.

(157) Houshmand, H.; Froman, G.; Magnusson, G. *Anal. Biochem.* **1999**, *268*, 363-370.

(158) Yamamoto, M.; Kominato, Y.; Yamamoto, F. *Biochem. Biophys. Res. Commun.* **1999**, *255*, 194-199.

(159) Possee, R. D. *Curr. Opin. Biotechnol.* **1997**, *8*, 569-572.

(160) Galán, A.; Comor, L.; Horvatic, A.; Kules, J.; Guillemin, N.; Mrljak, V.; Bhide, M. *Mol. Bio. Syst.* **2016**, *12*, 2342-2358.

(161) Pande, J.; Szewczyk, M. M.; Grover, A. K. *Biotechnol. Adv.* **2010**, *28*, 849-858.

(162) Rodi, D. J.; Mandava, S.; Makowski, L. "*Filamentous Bacteriophage Structure and Biology*" in Geyer, C. R.; Sidhu, S. S. *Phage Display in Biotechnology and Drug Discovery*, CRC Press: Boca Raton, *2nd ed.*, **2015**, 1-42.

(163) Smeal, S. W.; Schmitt, M. A.; Pereira, R. R.; Prasad, A.; Fisk, J. D. *Virology.* **2017**, *500*, 259-274.

(164) Hufton, S. E.; Moerkerk, P. T.; Meulemans, E. V.; de Bruine, A.; Arends, J. W.; Hoogenboom, H. R. *J. Immunol. Methods.* **1999**, *231*, 39-51.

(165) Goa, C.; Mao, S.; Lo, C. H.; Kaufmann, G.; Wirsching, P.; Lerner, R. A.; Janda, K. D. *Proc. Nat. Acad. Sci.* **1999**, *96*, 6025-6030.

(166) Gao, C.; Mao, S.; Kaufmann, G.; Wirsching, P.; Lerner, R. A.; Janda, K. D. *Proc. Nat. Acad. Sci.* **2002**, *99*, 12612-12616.

(167) Rodi, D. J.; Soares, A. S.; Makowski, L. *J. Mol. Biol.* **2002**, *322*, 1039-1052.

(168) Weinbauer, M. G. *FEMS Microbiol. Rev.* **2004**, *28*, 127-181.

(169) Young, R. *Microbiol. Rev.* **1992**, *56*, 430-481.

(170) Gandon, S. *Trends Microbiol.* **2016**, *24*, 356-365.

(171) Wang, R.; Wang, I.-N.; Roof, W. D. *Trends Microbiol.* **2000**, *8*, 120-128.

(172) Reichmann, L.; Holliger, P. *Cell* **1997**, *90*, 351-360.

(173) Iannolo, G.; Minenkova, O.; Petruzzelli, R.; Cesareni, G. *J. Mol. Biol.* **1995**, *248*, 835-844.

(174) Fukunaga, K.; Taki, M. *J. Nuc. Acid.* **2012**, Article ID: 295719.

(175) Voss, M.; Lettau, M.; Janssen, O. *BMC Immunol.* **2009**, *10*, 53.

(176) James, K. J.; Hancock, M. A.; Gagnon, J. N.; Coulton, J. W. *Biochem.* **2009**, *48*, 9212-9220.

(177) Paradis-Bleau, C.; Lloyd, A.; Sanschagrin, F.; Maaroufi, H.; Clark, T.; Blewett, A.; Dowson, C.; Roper, D. I.; Bugg, T. D. H.; Levesque, R. C. *Biochem. J.* **2009**, *421*, 263-272.

(178) Diamond, S. L. *Curr. Opin. Mol. Biol.* **2007**, *11*, 46-51.

(179) Koolpe, M.; Burgess, R.; Dail, M.; Pasquale, E. B. *J. Biol. Chem.* **2005**, *280*, 17301-17311.

(180) Bratkovic, T. *Cell. Mol. Life Sc.* **2010**, *67*, 749-767.

(181) Böttger, V.; Böttger, A. "*Epitope mapping using phage diplay peptide libraries*" in Schutkowski, M.; Reineke, U. *Epitope Mapping Protocols - Methods in Molecular Biology*, Springer: New York, *2nd ed.*, **2009**, *524*, 181-201.

(182) Naz, R. K. *Am. J. Reprod. Immunol.* **2009**, *61*, 11-18.

(183) Cui, Y.; Kim, S. N.; Naik, R. R.; McAlpine, M. C. *Acc. Chem. Res.* **2012**, *45*, 696-704.

(184) Janczuk, M.; Niedziółka-Jönsson, J.; Szot-Karpińska, K. *J. Electoanal. Chem.* **2016**, *779*, 207-219.

(185) Whaley, S. R.; English, D. S.; Hu, E. L.; Barbara, P. F.; Belcher, A. M. *Nature* **2000**, *405*, 665-668.

(186) Sarikaya, M.; Tamerler, C.; Schwartz, D. T.; Baneyx, F. *Annu. Rev. Mater. Res.* **2004**, *34*, 373-408.

(187) Sanghvi, A. B.; Miller, K. P.-H.; Belcher, A. M.; Schmidt, C. E. *Nat. Mater.* **2005**, *4*, 496-502.

(188) Günay, K. A.; Klok, H.-A. *Bioconjugate Chem.* **2015**, *26*, 2002-2015.

(189) Mao, C.; Flynn, C. E.; Hayhurst, A.; Sweeney, R.; Qi, J.; Georgiou, G. *Proc. Nat. Acad. Sci.* **2013**, *100*, 6946-6951.

(190) Tomczak, M. M.; Gupta, M. K.; Drummy, L. F.; Rozenzhak, S. M.; Naik, R. R. *Acta Biomater.* **2009**, *5*, 876-882.

(191) a) Wei, Z.; Maeda, Y.; Matsui, H. *Angew. Chem. Int. Ed.* **2011**, *50*, 10585-10588. b) Wei, Z.; Maeda, Y.; Matsui, H. *Angew. Chem.* **2011**, *123*, 10773-10776.

(192) Nygaard, S.; Wendelbo, R.; Brown, S. *Adv. Mater.* **2002**, *14*, 1853-1856.

(193) Brown, S. *Nat. Biotechnol.* **1997**, *15*, 269-272.

(194) Brown, S.; Sarikaya, M.; Johnson, E. *J. Mol. Biol.* **2000**, *299*, 725-735.

(195) Chan, P.; Phan, T.; Kao, M. C.; Dolan, C.; Tok, J. B.-H. *Bioorg. Med. Chem. Lett.* **2006**, *16*, 5261-5264.

(196) Naik, R. R.; Stringer, S. J.; Agarwal, G.; Jones, S. E.; Stone, M. O. *Nature Mater.* **2002**, *1*, 169-172.

(197) Segvich, S.; Biswas, S.; Becker, U.; Kohn, D. H. *Cells Tissues Organs.* **2009**, *189*, 245-251.

(198) Segvich, S. J.; Smith, H. C.; Kohn, D. H. *Biomaterials* **2009**, *30*, 1287-1298.

(199) Weiger, M. C.; Park, J. J.; Roy, M. D.; Stafford, C. M.; Karim, A.; Becker, M. L. *Biomaterials* **2010**, *31*, 2955-2963.

(200) Naik, R. R.; Brott, L. L.; Clarson, S. J.; Stone, M. O. *J. Nanosci. Nanotechnol.* **2002**, *2*, 95-100.

(201) Belcher, A. M. in Bäuerlein, W. *Biomineralization*, Wiley-VCH: Weinheim, *1st ed.*, **2000**, 247.

(202) Gaskin, D. J. H.; Starck, K.; Vulfson, E. N. *Biotechnol. Lett.* **2000**, *22*, 1211-1216.

(203) Li, C.; Botsaris, G. D.; Kaplan, D. L. *Cryst. Growth Des.* **2002**, *2*, 387-393.

(204) Cunningham, S. D.; Ittel, S. D.; O'Brien, J. P.; Rouviere, P. E. *U.S. Pat. Appl. Publ.* **2009**, S. US 20090029902 A1 20090129.

(205) Gebauer, D.; Cölfen, H.; Verch, A.; Antonietti, M. *Adv. Mater.* **2009**, *21*, 435-439.

(206) Müller, W. E. G.; Wang, X.; Grebenjuk, V. A.; Korzhev, M.; Wiens, M.; Schloßmacher, U.; Schröder, H. C. *PLOS One* **2012**, *7*, Art.-#: e34617.

(207) Gresswell, C. G. *Calcium Carbonate Formation by Genetically Engineered Inorganic Binding Peptides*, master thesis, *University of Washington*: Seattle, **2012**.

(208) Cloud, P. "*Early biogeologic history: The emergence of a paradigm*" in Drake, E. T. *Earth`s Earliest Biosphere*, Princeton Univ. Press: Princeton, *1st ed.*, **1983**, 14-31.

(209) Schopf, J. W.; Kudryavtsev, A. B.; Czaja, A. D.; Tripathi, A. B. *Precambrian Res.* **2007**, *158*, 141-155.

(210) Van Kranendonk, M. J.; Phillippot, P.; Lepot, K.; Bodorkos, S.; Pirajno, F. *Precambrian Res.* **2008**, *167*, 93-124.

(211) Bell, E. A.; Boehnke, P.; Harrison, T. M.; Mao, W. L. *Proc. Nat. Acad. Sci.* **2015**, 112, 14518-14521.

(212) Mann, S. *Acc. Chem. Res.* **2012**, *45*, 2131-2141.

(213) Kudo, A.; Miseki, Y. *Chem. Soc. Rev.* **2009**, *38*, 253-278.

(214) Blankenship, R. E.; Tiede, D. M.; Barber, J.; Brudvig, G. W.; Fleming, G.; Ghirardi, M.; Gunner, M. R.; Junge, W.; Kramer, D. M.; Melis, A.; Moore, T. A.; Moser, C. C.; Nocera, D. G.; Nozik, A. J.; Ort, D. R.; Parson, W. W.; Prince, R. C.; Sayre, R. T. *Science* **2011**, *332*, S. 805-809.

(215) Dau, H.; Fujita, E.; Sun, L. *ChemSusChem* **2017**, *10*, 4228-4235.

(216) Marchetti, L.; Levine, M. *ACS Catal.* **2011**, *1*, 1090-1118.

(217) a) Wiester, M. J.; Ulmann, P. A.; Mirkin, C. A. *Angew. Chemie Int. Ed.* **2011**, *50*, 114-137.
b) Wiester, M. J.; Ulmann, P. A.; Mirkin, C. A. *Angew. Chemie* **2011**, *123*, 118-142.

(218) Ragg, R.; Korschelt, K.; Herget, K.; Natalio, F.; Tahir, M. N.; Tremel, W. in Grunwald, P. *Biocatalysis and Nanotechnology*, Pan Stanford Publishing Pte. Ltd.: Singapore, *1st ed.*, **2017**.

(219) He, Q.; Cui, Y.; Li, J. *Chem. Soc. Rev.* **2009**, *38*, 2292-2303.

(220) a) Mann, S. *Angew. Chem. Int. Ed.* **2000**, *39*, 3392-3406.
b) Mann, S. *Angew. Chem.* **2000**, *112*, 3532-3548.

(221) Wegst, U. G. K.; Ashby, M. F. *Philos. Mag.* **2004**, *84*, 2167-2186.

(222) Müller, W. E. G. *Molecular Biomineralization. - Aquatic Organisms Forming Extraordinary Materials*, Springer-Verlag: Berlin Heidelberg, *1st ed.*, **2011**.

(223) Chiu, C.-Y.; Li, Y.; Ruan, L.; Ye, X.; Murray, C. B.; Huang, Y. *Nature Chem.* **2011**, *3*, 393-399.

(224) Rahe, P.; Schütte, J.; Kühnle A.;. *J. Phys. Condens. Matter.* **2012**, *24*, 084006.

(225) Marutschke, C.; Walters, D.; Cleveland, J.; Hermes, I.; Bechstein, R.; Kühnle, A. *Nanotechnology* **2014**, *25*, 335703.

(226) Noren, K. A.; Noren, C. J. *Methods* **2001**, *23*, 169-178.

(227) Lederberg, J.; Cavalli, L. L.; Lederberg, E. M. *Genetics* **1952**, *37*, 720-730.

(228) Alvarez-Martinez, C. E.; Christie, P. J. *Microbiol. Mol. Biol. Rev.* **2009**, *73*, 775-808.

(229) Mülhardt, C. *Der Experimentator/ Molekularbiologie/Genomics.* 6th. Spektrum Akademischer Verlag: Heidelberg, *6th ed.*, **2009**.

(230) New England Biolabs. [online, 7.8.2018] https://www.neb.com/products/e4104-ecoli-k12-er2738#Product%20Information

(231) Ullmann, A.; Jacob, F.; Monod, J. *J. Mol. Biol.* **1967**, *24*, 339-343.

(232) Langley, K. E.; Villarejo, M. R.; Fowler, A. V.; Zamenhof, P.J.; Zabin, I. *Proc. Natl. Acad. Sci. U.S.A.* **1975**, *72*, 1254-1257.

(233) Greenstein, D.; Besmond, C. *Current Protocols in Molecular Biology - "Unit 1.15 Preparing and Using M13-Derived Vectors".* Brent, R.; Kingston, R. E.; Moore, D. D.; Seidman, J.G.; Smith, J. A.; Struhl, K.; Ausubel, F. M., John Wiley & Sons: Hoboken *1st ed.*, **2003**.

(234) Sanger, F.; Coulson, A. R. *J. Mol. Biol.* **1975**, *94*, 441-448.

(235) Sanger, F.; Nicklen, S.; Coulson, A. R. *Proc. Natl. Acad. Sci. U.S.A.* **1977**, *74*, 5463-5467.

(236) Smith, L.M.; Sanders, J. Z.; Kaiser, R. J.; Hughes, P.; Dodd, C.; Connel, C. R.; Heiner, C.; Kent, S. B. H.; Hood, L. E. *Nature* **1986**, *321*, 674-679.

(237) Serial Basics® [online, 8.8.2018] http://serialbasics.free.fr/Home/Home.html

(238) Kumar, S.; Stecher, G.; Tamura, K. *Mol. Biol Evol.* **2016**, *33*, 1870-1874.

(239) Sarikaya, M.; Tamerler, C.; Jen, A. K. -Y.; Schulten, K.; Baneyx, F. *Nature Mater.* **2003**, *2*, 577-585.

(240) Seker, U. O. S.; Demir, H. V. *Molecules* **2011**, *16*, 1426-1451.

(241) Vodnik, M.; Zager, U.; Strukelj, B.; Lunder, M. *Molecules* **2011**, *16*, 790-817.

(242) Huang, J.; Ru, B.; Zhu, P.; Nie, F.; Yang, J.; Wang, X.; Dai, P.; Lin, H.; Guo, F.-B.; Rao, N. *Nucleic Acids Res.* **2012**, *40*, D271-D277.

(243) Huang, J.; Ru, B.; Li, S.; Lin, H.; Guo, F. B. *J. Biomed. Biotechnol.* **2010**.

(244) He, B.; Chai, G.; Duan, Y.; Yan, Z.; Qiu, L.; Zhang, H.; Liu, Z.; He, Q.; Han, K.; Ru, B.; Guo, F.-B.; Ding, H.; Lin, H.; Wang, X.; Rao, N.; Zhou, P.; Huang, J. *Nucleic Acids Res.* **2016**, *44*, D1127-D1132.

(245) Duchrow, T.; Shtatland, T.; Guettler, D.; Pivovarov, M.; Kramer, S.; Weissleder, R. *BMC Bioinformatics* **2009**, *10*, 317.

(246) Shtatland, T.; Guettler, D.; Kossodo, M.; Pivovarov, M.; Weissleder, R. *BMC Bioinformatics* **2007**, *8*, 280.

(247) Altschul, S. F.; Gish, W.; Miller, W.; Myers, E. W.; Lipman, D. J. *J. Mol. Biol.* **1990**, *215*, 403-410.

(248) Altschul, S. F.; Madden, T. L.; Schäffer, A. A.; Zhang, J.; Zhang, Z.; Miller, W.; Lipman, D. J. *Nucleic Acids Res.* **1997**, *25*, 3389-3402.

(249) Cornelison, G. L.; Pflanz, N. C.; Tipps, M. E.; Mihic, S. J. *Eur. J. Pharmacol.* **2016**, *780*, 252-259.

(250) Hajir, M. *Calciumoxalat als potentielles Biomaterial - Kontrolle der Morphologie und Hydratphase, dissertation,* Johannes Gutenberg-Universität: Mainz, **2014**.

(251) Merrifield, R. B. *J. Am. Chem. Soc.* **1963**, *85*, 2149-2154.

(252) a) Merrifield, R. B. *Angew. Chem. Int Ed.* **1985**, *24*, 799-810.
b) Merrifield, R. B. *Angew. Chem.* **1985**, *97*, 801-812.

(253) Marglin, A.; Merrifield, R. B. *J. Am. Chem. Soc.* **1966**, *88*, 5051-5052.

(254) Carpino, L. A.; Han, G. Y. *J. Am. Chem. Soc.* **1970**, *92*, 5748-5749.

(255) Carpino, L. A.; Han, G. Y. *J. Org. Chem.* **1972**, *37*, 3404-3409.

(256) McKay, F. C.; Albertson, N. F. *J. Am. Chem. Soc.* **1957**, *79*, 4686-4690.

(257) Anderson, G. W.; McGregor, A. C. *J. Am. Chem. Soc.* **1957**, *79*, 6180-6183.

(258) Beckert, R.; Fanghänel, E.; Habicher, W. D.; Metz, P.; Pavel, D.; Schwetlick, K.; Becker, H. G. O.; Berger, W.; Domschke, G.; Faust, J.; Fischer, M.; Gentz, F.; Gewald, K.; Gluch, R.; Mayer, R.; Müller, K.; Schmidt, H.; Schollberg, K.; Seiler, E.; Zeppenfeld, G. *Organikum*, Wiley-VCH Verlag GmbH: Weinheim, *22nd ed.*, **2004**.

(259) König, W.; Geiger, R. *Chem. Ber.* **1970**, *103*, 788-798.

(260) Carpino, L. A. *J. Am. Chem. Soc.* **1993**, *115*, 4397-4398.

(261) Knorr, R.; Trzeciak, A.; Bannwarth, W.; Gillessen, D. *Tetrahedron Lett.* **1989**, *30*, 1927-1930.

(262) Albericio, F.; Carpino, L. A. in Fields, G. B. *Methods in Enzymology*, Academic Press: London, **1997**, *289*, 104-126.

(263) Frechet, J. M. J. *Tetrahedron* **1981**, *37*, 663-683.

(264) Bayer, E.; Rapp, W. *Chemistry of Peptides and Proteins*, Walter de Gruyter & Co.: Berlin, *3rd ed.*, **1986**. 3-8.

(265) Bayer, E.; Dengler, M.; Hemmasi, B. *J. Pept. Prot. Res.* **1985**, *25*, 178-186.

(266) E. Bayer, W .Rapp. *DE 3500180 A1* Germany, **1986**, Offenlegung.

(267) a) Bayer, E. *Angew. Chem. Int. Ed.* **1991**, *30*, 113-129.
b) Bayer, E. *Angew. Chem.* **1991**, *103*, 117-133.

(268) Wang, S.-S. *J. Am. Chem. Soc.* **1973**, *95*, 1328-1333.

(269) Rink, H. *Tetrahedron Lett.* **1987**, *33*, 3787-3790.

(270) Chan, W. C.; White, P. D. *Fmoc Solid Phase Peptide Synthesis*, Oxford University Press: Oxford, *1st ed.*, **2000**.

(271) Kitano, Y.; Hood, D. W. *Geochim. Cosmochim. Acta* **1965**, *29*, 29-41.

(272) Faatz, M.; Gröhn, F.; Wegener, G. *Adv. Mater.* **2004**, *16*, 996-1000.

(273) Kim, K. N.; Shin, D. Y.; Son, S. G.; Kim, Y. D. *Mater. Sci. Forum.* **2005**, *486-487*, 542-545.

(274) Moreno, A.; Rosales-Hoz, M. J. *Prog. Cryst. Growth Charact. Mater.* **2017**, *63*, 63-71.

(275) Aizenberg, J.; Albeck, S.; Weiner, S.; Addadi, L. *J. Cryst. Growth.* **1994**, *142*, 156-164.

(276) Albeck, S.; Weiner, S.; Addadi, L. *Chem. Eur. J.* **1996**, *2*, 278-284.

(277) Susewind, M. *Molekular gesteuerte Aggregation von Nano-Kompositkristallen*, dissertation, Johannes Gutenberg-Universität: Mainz, **2015**.

(278) Küther, J. *Templatinduzierte Kristallisationen anorganischer Biomineralien auf selbstorganisierten Oberflächen*, dissertation, Johannes Gutenberg-Universität: Mainz, **1998**.

(279) Balz, M. *Investigations of cooperative interactions in template induced crystallization processes and kinetic studies of nucleation and growth by small- angle neutron scattering*, dissertation, Johannes Gutenberg-Universität: Mainz, **2004**.

(280) Montingy, M. *Kristallisation von $CaCO_3$*, diploma thesis, Johannes Gutenberg-Universität: Mainz, **2015**.

(281) Folk, R. L. *J. Sediment. Res.* **1974**, *44*, 40-53.

(282) Park, W. K.; Ko, S.-J.; Lee, S. W.; Cho, K.-H.; Ahn, J.-W.; Han, C. *J. Cryst. Growth.* **2008**, *310*, 2593-2601.

(283) Choudens-Sanchez, V. D.; Gonzales, L. A. *J. Sediment. Res.* **2009**, *79*, 363-376.

(284) Sato, M.; Matsuda, S. *Z. Kristallogr.* **1969**, *129*, 405-410.

(285) Nash, M. C.; Opdyke, B. N.; Wu, Z.; Xu, H.; Trafford, J. M. *J. Sediment. Res.* **2013**, *83*, 1084-1098.

(286) Raz, S.; Weiner, S.; Addadi, L. *Adv. Mater.* **2000**, *12*, 38-42.

(287) Blue, C. R.; Guiffre, A.; Mergelsberg, S.; Han, N.; De Yoreo, J. J.; Dove, P. M. *Geochim. Cosmochim. Acta* **2017**, *196*, 179-196.

(288) Loste, E.; Wilson, R. M.; Seshadri, R.; Meldrum, F. C. *J. Cryst. Growth.* **2003**, *254*, 206-218.

(289) Wray, J. L.; Daniels, F. *J. Am. Chem. Soc.* **1957**, *79*, 2031-2034.

(290) Tai, C. Y.; Chen, F.-B. *AIChE J.* **1998**, *44*, 1790-1797.

(291) Kawano, J.; Shimobayashi, N.; Miyake, A.; Kitamura, M. *J. Phys.: Condens. Matter* **2009**, *21*, 275403.

(292) D'Hondt, M.; Bracke, N.; Taevernier, L.; Gevaert, B.; Verbeke, F.; Wynendaele, E.; De Spiegeleer, B. *J. Pharm. Biomed. Anal.* **2014**, *101*, 2-30.

(293) Rapp, W. in Jung, G. *Combinatorial peptide and nonpeptide libraries*, Verlag Chemie: Weinheim, *1st ed.*, **1996**, 425-464.

(294) Wehrmeister, U.; Jacob, D. E.; Soldati, A. L.; Loges, N.; Häger, T.; Hofmeister, W. *J. Raman Spectrosc.* **2011**, *42*, 926-935.

(295) a) Keil, S.; Claus, C.; Dippold, W.; Kunz, H. *Angwe. Chemie Int. Ed.* **2001**, *40*, 366-369. b) Keil, S.; Claus, C.; Dippold, W.; Kunz, H. *Angwe. Chemie* **2001**, *113*, 379-382.

(296) Gouin, S. G.; Benoist, E.; Gestin, J. F.; Meslin, J. C.; Deniaud, D. *Eur. J. Org. Chem.* **2004**, 878-885.

(297) Dourtoglou, V.; Ziegler, J. C.; Gross, B. *Tetrahedron Lett.* **1978**, *19*, 1269-1272.

(298) Dourtoglou, V.; Gross, B. *Synthesis* **1984**, *7*, 572-574.

(299) Herzner, H.; Kunz, H. *Carbohydrate Research* **2007**, *342*, 541-557.

(300) Higgins, D. G.; Sharp, P. M. *Gene* **1988**, *73*, 237-244.

(301) Higgins, D. G.; Sharp, P. M. *Bioinformatics (CABIOS)* **1989**, *5*, 151-153.

(302) Thompson, J. D.; Higgins, D. G.; Gibson, T. J: *Nucleic Acids Res.* **1994**, *22*, 4673-4680.

(303) Larkin, M. A.; Blackshields, G.; Brown, N. P.; Chenna, R.; McGettigan, P. A.; McWilliam, H.; Valentin, F.; Wallace, I. M.; Wilm, A.; Lopez, R.; Thompson, J. D.; Gibson, T. J.; Higgins, D. G. *Bioinformatics* **2007**, *23*, 2947-2948.

(304) Perrin, D. D.; Armarego, W. L. F. *Purification of Laboratory Chemicals*, Pergamon Press: Oxford, *3rd ed.*, **1988**.

(305) P. Villars, K. Cenzual,. *Pearson`s Crystal Data - Crystal Structure Database for Inorganic Compunds.* [CD-Rom] Materials Park, Ohio, USA : ASM International, 10 2009.

(306) New England Biolabs Inc. [online, 24.02.2017] https://www.neb.com/~/media/NebUs/Page%20Images/Tools%20and%20Resources/Interactive%20Tools/DNA%20Sequences%20and%20Maps/Text%20Documents/m13kefsa.txtm13kefsa

(307) Bischoff, W. D.; Sharma, S. K.; Mackenzie, F. T. *Am. Mineral.* **1985**, *70*, 581-589.

(308) Wehrmeister, U.; Soldati, A. L.; Jacob, D. E.; Häger, T.; Hofmeister, W. *J. Raman Spectrosc.* **2010**, *41*, 193-201.

(309) Hollet, M. J. *The Spectroscopic Analysis of Vaterite*, master thesis, Memorial University of Newfoundland: St. John, **2000**.

(310) Kondo, A.; Ueda, M. *Appl. Microb. Biotechnol.* **2004**, *64*, 28-40.

(311) Feldhaus, M. J.; Siegel, R. W.; Opresko, L. K.; Coleman, J. R.; Feldhaus, J. M.; Yeung, Y. A.; Cochran, J. R.; Heinzelman, P.; Colby, D.; Swers, J.; Graff, C.; Wiley, H. S.; Wittrup, K. D. *Nat. Biotechnol.* **2003**, *21*, 163-170.

(312) Wilson, D. S.; Keefe, A. D.; Szostak, J. W. *Proc. Nat. Acad. Sci.* **2001**, *98*, 3750-3755.

(313) Takahashi, T. T.; Austin, R. J.; Roberts, R. W. *Trends Biochem. Sci.* **2003**, *28*, 159-165.

(314) Matsuura, T.; Pluckthun, A. *FEBS Lett.* **2003**, *539*, 24-28.

(315) Georgiou, G.; Stathopoulos, C.; Daugherty, P. S.; Nayak, A. R.; Iverson, B. L.; Curtis III, R. *Nat. Biotechnol.* **1997**, *15*, 29-34.

(316) Samuelson, P.; Gunneriusson, E.; Nygren, P.-A.; Stahl, S. *J. Biotechnol.* **2002**, *96*, 129-154.

(317) Smith, G. P. *Science* **1985**, *228*, 1315-1316.

(318) Devlin, J. J.; Panganiban, L. C.; Devlin, P. E. *Science* **1990**, *249*, 404-406.

(319) Scott, J. K.; Smith, G. P. *Science* **1990**, *249*, 386-390.

(320) Smith, G. P. *Curr. Opin. Biotech.* **1991**, *2*, 668-673.

(321) Bennet, N. J.; Gagic, D.; Sutherland-Smith, A. J.; Rakonjac, J. *J. Mol. Biol.* **2011**, *411*, 972-985.

(322) Russel, M.; Lowman, H. B.; Clackson, T. "*Introduction to phage biology and phage display*" in Lowman, H.B.; Clackson, T. *Phage Display—A Practical Approach*, Oxford University Press: Oxford, *1st ed.*, **2004**, 1-26.

(323) Bradbury, A. R. M.; Sidhu, S.; Dübel, S.; McCafferty, J. *Nature biotechnol.* **2011**, *29*, 245-254.

(324) Tarmeler, C.; Khatayevich, D.; Gungormus, M.; Kacar, T.; Oren, E. E.; Hnilova, M.; Sarikaya, M. *Biopolymers Pept. Sci.* **2010**, *94*, 78-94.

(325) Coste, J.; Le-Nguyen, D.; Castro, B. *Tetrahedron Lett.* **1990**, *31*, 205-208.

(326) Müller, W. E. G.; Wang, X.; Burghard, Z.; Bill, J.; Krasko, A.; Boreiko, A.; Schloßmacher, U.; Schröder, H. C.; Wiens, M. *J. Struct. Biol.* **2009**, *168*, 548-561.

(327) Wang, X.; Wiens, M.; Schloßmacher, U.; Jochum, K. P.; Schröder, H. C.; Müller, W. E. G. *Adv. Eng. Mater.* **2012**, *14*, B4-B12.

(328) Riedel, E. *Anorganische Chemie*, Walter de Gruyter: Berlin, *6th ed.*, **2004**.

(329) Suito, K.; Namba, J.; Horikawa, T.; Taniguchi, Y.; Sakurai, N.; Kobayashi, M.; Onodera, A.; Shimomura, O.; Kikegawa, T. *Am. Mineral.* **2001**, *86*, 997-1002.

(330) Demichelis, R.; Raiteri, P.; Gale, J. D.; Dovesi, R. *CrytEngComm.* **2012**, *14*, 44-47.

(331) Demichelis, R.; Raiteri, P.; Gale, J. D.; Dovesi, R. *Cryst. Growth Des.* **2013**, *13*, 2247-2251.

(332) Wang, J.; Zhang, F.; Zhang, J.; Ewing, R. C.; Becker, U.; Cai, Z. *J. Cryst. Growth* **2014**, *407*, 78-86.

(333) Dongni, R.; Yonghua, G.; Quingling, F. *Mater. Sci. Eng. C.* **2013**, *33*, 9-14.

(334) Tohse, H.; Saruwatari, K.; Kogure, T.; Nagasawa, H.; Takagi, Y. *Cryst. Growth Des.* **2009**, *9*, 4897-4901.

(335) Marchitto, T. M.; Bryan, S. P.; Doss, W.; McCulloch, M. T.; Montagna, P. *Earth Planet. Sci. Lett.* **2018**, *481*, 20-29.

(336) Cwirla, S. E.; Peters, E. A.; Barrett, R. W.; Dower, E. J. *Proc. Nat. Acad. Sci.* **1990**, *87*, 6378-6382.

(337) Thota, V.; Perry, C. C. *Recent Pat. Nanotechnol.* **2017**, *11*, 168-180.

(338) Schröder, R.; Besch, L.; Pohlit, H.; Panthöfer, M.; Roth, W.; Frey, H.; Tremel, W.; Unger, R. E. *J. Tissue Eng. Regen. Med.* **2018**, *12*, 1754-1768.

(339) Michon, C.; Cuvelier, G.; Launay, B. *Rheol. Acta* **1993**, *32*, 94-103.

(340) Draget, K. I.; Braek, G. S.; Smidsrod, O. *Carbohydr. Polym.* **1994**, *25*, 31-38.

(341) Morris, E. R.; Nishinari, K.; Rinaudo, M. *Food Hydrocoll.* **2012**, *28*, 373-411.

(342) Kubota, N.; Fujisawa, Y.; Yokota, M.; Mullin, J.W. *J. Cryst. Growth* **1999**, *197*, 388-392.

Acknowledgements

[redacted]

[redacted]

Danksagung

[redacted]

[redacted]

Appendix

Appendix I:
Sequence Data and Plasmid Map of the M13KE-Phage

Full genome of the original M13KE-phage prior the insertion of the randomised sequence by the manufacturer [152, 306]. The region, which comprises the randomised sequence, is marked red.

>M13KE [length=7222] [version=09-MAY-2008] [topology=circular] Cloning vector M13KE, complete sequence.

AATGCTACTACTATTAGTAGAATTGATGCCACCTTTTCAGCTCGCGCCCCAAATGAAAATATAGCTAAACAG
GTTATTGACCATTTGCGAAATGTATCTAATGGTCAAACTAAATCTACTCGTTCGCAGAATTGGGAATCAACT
GTTATATGGAATGAAACTTCCAGACACCGTACTTTAGTTGCATATTTAAAACATGTTGAGCTACAGCATTAT
ATTCAGCAATTAAGCTCTAAGCCATCCGCAAAAATGACCTCTTATCAAAAGGAGCAATTAAAGGTACTCTCT
AATCCTGACCTGTTGGAGTTTGCTTCCGGTCTGGTTCGCTTTGAAGCTCGAATTAAAACGCGATATTTGAAG
TCTTTCGGGCTTCCTCTTAATCTTTTTGATGCAATCCGCTTTGCTTCTGACTATAATAGTCAGGGTAAAGAC
CTGATTTTTGATTTATGGTCATTCTCGTTTTCTGAACTGTTTAAAGCATTTGAGGGGGATTCAATGAATATT
TATGACGATTCCGCAGTATTGGACGCTATCCAGTCTAAACATTTTACTATTACCCCCTCTGGCAAAACTTCT
TTTGCAAAAGCCTCTCGCTATTTTGGTTTTTATCGTCGTCTGGTAAACGAGGGTTATGATAGTGTTGCTCTT
ACTATGCCTCGTAATTCCTTTTGGCGTTATGTATCTGCATTAGTTGAATGTGGTATTCCTAAATCTCAACTG
ATGAATCTTTCTACCTGTAATAATGTTGTTCCGTTAGTTCGTTTTATTAACGTAGATTTTTCTTCCCAACGT
CCTGACTGGTATAATGAGCCAGTTCTTAAAATCGCATAAGGTAATTCACAATGATTAAAGTTGAAATTAAAC
CATCTCAAGCCCAATTTACTACTCGTTCTGGTGTTTCTCGTCAGGGCAAGCCTTATTCACTGAATGAGCAGC
TTTGTTACGTTGATTTGGGTAATGAATATCCGGTTCTTGTCAAGATTACTCTTGATGAAGGTCAGCCAGCCT
ATGCGCCTGGTCTGTACACCGTTCATCTGTCCTCTTTCAAAGTTGGTCAGTTCGGTTCCCTTATGATTGACC
GTCTGCGCCTCGTTCCGGCTAAGTAACATGGAGCAGGTCGCGGATTTCGACACAATTTATCAGGCGATGATA
CAAATCTCCGTTGTACTTTGTTTCGCGCTTGGTATAATCGCTGGGGGTCAAAGATGAGTGTTTTAGTGTATT
CTTTTGCCTCTTTCGTTTTAGGTTGGTGCCTTCGTAGTGGCATTACGTATTTTACCCGTTTAATGGAAACTT
CCTCATGAAAAAGTCTTTAGTCCTCAAAGCCTCTGTAGCCGTTGCTACCCTCGTTCCGATGCTGTCTTTCGC
TGCTGAGGGTGACGATCCCGCAAAAGCGGCCTTTAACTCCCTGCAAGCCTCAGCGACCGAATATATCGGTTA
TGCGTGGGCGATGGTTGTTGTCATTGTCGGCGCAACTATCGGTATCAAGCTGTTTAAGAAATTCACCTCGAA
AGCAAGCTGATAAACCGATACAATTAAAGGCTCCTTTTGGAGCCTTTTTTTTGGAGATTTTCAACGTGAAAA
AATTATTATTCGCAATTCCTTTAGTGGTACCTTTCTATTCTCACTCGGCCGAAACTGTTGAAAGTTGTTTAG
CAAAATCCCATACAGAAAATTCATTTACTAACGTCTGGAAAGACGACAAAACTTTAGATCGTTACGCTAACT
ATGAGGGCTGTCTGTGGAATGCTACAGGCGTTGTAGTTTGTACTGGTGACGAAACTCAGTGTTACGGTACAT
GGGTTCCTATTGGGCTTGCTATCCCTGAAAATGAGGGTGGTGGCTCTGAGGGTGGCGGTTCTGAGGGTGGCG
GTTCTGAGGGTGGCGGTACTAAACCTCCTGAGTACGGTGATACACCTATTCCGGGCTATACTTATATCAACC
CTCTCGACGGCACTTATCCGCCTGGTACTGAGCAAAACCCCGCTAATCCTAATCCTTCTCTTGAGGAGTCTC
AGCCTCTTAATACTTTCATGTTTCAGAATAATAGGTTCCGAAATAGGCAGGGGGCATTAACTGTTTATACGG
GCACTGTTACTCAAGGCACTGACCCCGTTAAAACTTATTACCAGTACACTCCTGTATCATCAAAAGCCATGT
ATGACGCTTACTGGAACGGTAAATTCAGAGACTGCGCTTTCCATTCTGGCTTTAATGAGGATTTATTTGTTT
GTGAATATCAAGGCCAATCGTCTGACCTGCCTCAACCTCCTGTCAATGCTGGCGGCGGCTCTGGTGGTGGTT
CTGGTGGCGGCTCTGAGGGTGGTGGCTCTGAGGGTGGCGGTTCTGAGGGTGGCGGCTCTGAGGGAGGCGGTT
CCGGTGGTGGCTCTGGTTCCGGTGATTTTGATTATGAAAAGATGGCAAACGCTAATAAGGGGGCTATGACCG
AAAATGCCGATGAAAACGCGCTACAGTCTGACGCTAAAGGCAAACTTGATTCTGTCGCTACTGATTACGGTG
CTGCTATCGATGGTTTCATTGGTGACGTTTCCGGCCTTGCTAATGGTAATGGTGCTACTGGTGATTTTGCTG
GCTCTAATTCCCAAATGGCTCAAGTCGGTGACGGTGATAATTCACCTTTAATGAATAATTTCCGTCAATATT
TACCTTCCCTCCCTCAATCGGTTGAATGTCGCCCTTTTGTCTTTGGCGCTGGTAAACCATATGAATTTTCTA
TTGATTGTGACAAAATAAACTTATTCCGTGGTGTCTTTGCGTTTCTTTTATATGTTGCCACCTTTATGTATG
TATTTTCTACGTTTGCTAACATACTGCGTAATAAGGAGTCTTAATCATGCCAGTTCTTTTGGGTATTCCGTT
ATTATTGCGTTTCCTCGGTTTCCTTCTGGTAACTTTGTTCGGCTATCTGCTTACTTTTCTTAAAAAGGGCTT
CGGTAAGATAGCTATTGCTATTTCATTGTTTCTTGCTCTTATTATTGGGCTTAACTCAATTCTTGTGGGTTA
TCTCTCTGATATTAGCGCTCAATTACCCTCTGACTTTGTTCAGGGTGTTCAGTTAATTCTCCCGTCTAATGC
GCTTCCCTGTTTTTATGTTATTCTCTCTGTAAAGGCTGCTATTTTCATTTTTGACGTTAAACAAAAAATCGT
TTCTTATTTGGATTGGGATAAATAATATGGCTGTTTATTTTGTAACTGGCAAATTAGGCTCTGGAAAGACGC
TCGTTAGCGTTGGTAAGATTCAGGATAAAATTGTAGCTGGGTGCAAAATAGCAACTAATCTTGATTTAAGGC
TTCAAAACCTCCCGCAAGTCGGGAGGTTCGCTAAAACGCCTCGCGTTCTTAGAATACCGGATAAGCCTTCTA

TATCTGATTTGCTTGCTATTGGGCGCGGTAATGATTCCTACGATGAAAATAAAAACGGCTTGCTTGTTCTCG
ATGAGTGCGGTACTTGGTTTAATACCCGTTCTTGGAATGATAAGGAAAGACAGCCGATTATTGATTGGTTTC
TACATGCTCGTAAATTAGGATGGGATATTATTTTTCTTGTTCAGGACTTATCTATTGTTGATAAACAGGCGC
GTTCTGCATTAGCTGAACATGTTGTTTATTGTCGTCGTCTGGACAGAATTACTTTACCTTTTGTCGGTACTT
TATATTCTCTTATTACTGGCTCGAAAATGCCTCTGCCTAAATTACATGTTGGCGTTGTTAAATATGGCGATT
CTCAATTAAGCCCTACTGTTGAGCGTTGGCTTTATACTGGTAAGAATTTGTATAACGCATATGATACTAAAC
AGGCTTTTTCTAGTAATTATGATTCCGGTGTTTATTCTTATTTAACGCCTTATTTATCACACGGTCGGTATT
TCAAACCATTAAATTTAGGTCAGAAGATGAAATTAACTAAAATATATTTGAAAAAGTTTTCTCGCGTTCTTT
GTCTTGCGATTGGATTTGCATCAGCATTTACATATAGTTATATAACCCAACCTAAGCCGGAGGTTAAAAAGG
TAGTCTCTCAGACCTATGATTTTGATAAATTCACTATTGACTCTTCTCAGCGTCTTAATCTAAGCTATCGCT
ATGTTTTCAAGGATTCTAAGGGAAAATTAATTAATAGCGACGATTTACAGAAGCAAGGTTATTCACTCACAT
ATATTGATTTATGTACTGTTTCCATTAAAAAAGGTAATTCAAATGAAATTGTTAAATGTAATTAATTTTGTT
TTCTTGATGTTTGTTTCATCATCTTCTTTTGCTCAGGTAATTGAAATGAATAATTCGCCTCTGCGCGATTTT
GTAACTTGGTATTCAAAGCAATCAGGCGAATCCGTTATTGTTTCTCCCGATGTAAAAGGTACTGTTACTGTA
TATTCATCTGACGTTAAACCTGAAAATCTACGCAATTTCTTTATTTCTGTTTTACGTGCAAATAATTTTGAT
ATGGTAGGTTCTAACCCTTCCATTATTCAGAAGTATAATCCAAACAATCAGGATTATATTGATGAATTGCCA
TCATCTGATAATCAGGAATATGATGATAATTCCGCTCCTTCTGGTGGTTTCTTTGTTCCGCAAAATGATAAT
GTTACTCAAACTTTTAAAATTAATAACGTTCGGGCAAAGGATTTAATACGAGTTGTCGAATTGTTTGTAAAG
TCTAATACTTCTAAATCCTCAAATGTATTATCTATTGACGGCTCTAATCTATTAGTTGTTAGTGCTCCTAAA
GATATTTTAGATAACCTTCCTCAATTCCTTTCAACTGTTGATTTGCCAACTGACCAGATATTGATTGAGGGT
TTGATATTTGAGGTTCAGCAAGGTGATGCTTTAGATTTTTCATTTGCTGCTGGCTCTCAGCGTGGCACTGTT
GCAGGCGGTGTTAATACTGACCGCCTCACCTCTGTTTTATCTTCTGCTGGTGGTTCGTTCGGTATTTTTAAT
GGCGATGTTTTAGGGCTATCAGTTCGCGCATTAAAGACTAATAGCCATTCAAAAATATTGTCTGTGCCACGT
ATTCTTACGCTTTCAGGTCAGAAGGGTTCTATCTCTGTTGGCCAGAATGTTCCTTTTATTACTGGTCGTGTG
ACTGGTGAATCTGCCAATGTAAATAATCCATTTCAGACGATTGAGCGTCAAAATGTAGGTATTTCCATGAGC
GTTTTTCCTGTTGCAATGGCTGGCGGTAATATTGTTCTGGATATTACCAGCAAGGCCGATAGTTTGAGTTCT
TCTACTCAGGCAAGTGATGTTATTACTAATCAAAGAAGTATTGCTACAACGGTTAATTTGCGTGATGGACAG
ACTCTTTTACTCGGTGGCCTCACTGATTATAAAAACACTTCTCAGGATTCTGGCGTACCGTTCCTGTCTAAA
ATCCCTTTAATCGGCCTCCTGTTTAGCTCCCGCTCTGATTCTAACGAGGAAAGCACGTTATACGTGCTCGTC
AAAGCAACCATAGTACGCGCCCTGTAGCGGCGCATTAAGCGCGGCGGGTGTGGTGGTTACGCGCAGCGTGAC
CGCTACACTTGCCAGCGCCCTAGCGCCCGCTCCTTTCGCTTTCTTCCCTTCCTTTCTCGCCACGTTCGCCGG
CTTTCCCCGTCAAGCTCTAAATCGGGGGCTCCCTTTAGGGTTCCGATTTAGTGCTTTACGGCACCTCGACCC
CAAAAAACTTGATTTGGGTGATGGTTCACGTAGTGGGCCATCGCCCTGATAGACGGTTTTTCGCCCTTTGAC
GTTGGAGTCCACGTTCTTTAATAGTGGACTCTTGTTCCAAACTGGAACAACACTCAACCCTATCTCGGGCTA
TTCTTTTGATTTATAAGGGATTTTGCCGATTTCGGAACCACCATCAAACAGGATTTTCGCCTGCTGGGGCAA
ACCAGCGTGGACCGCTTGCTGCAACTCTCTCAGGGCCAGGCGGTGAAGGGCAATCAGCTGTTGCCCGTCTCA
CTGGTGAAAAGAAAAACCACCCTGGCGCCCAATACGCAAACCGCCTCTCCCCGCGCGTTGGCCGATTCATTA
ATGCAGCTGGCACGACAGGTTTCCCGACTGGAAAGCGGGCAGTGAGCGCAACGCAATTAATGTGAGTTAGCT
CACTCATTAGGCACCCCAGGCTTTACACTTTATGCTTCCGGCTCGTATGTTGTGTGGAATTGTGAGCGGATA
ACAATTTCACACAGGAAACAGCTATGACCATGATTACGCCAAGCTTGCATGCCTGCAGGTCCTCGAATTCAC
TGGCCGTCGTTTTACAACGTCGTGACTGGGAAAACCCTGGCGTTACCCAACTTAATCGCCTTGCAGCACATC
CCCCTTTCGCCAGCTGGCGTAATAGCGAAGAGGCCCGCACCGATCGCCCTTCCCAACAGTTGCGCAGCCTGA
ATGGCGAATGGCGCTTTGCCTGGTTTCCGGCACCAGAAGCGGTGCCGGAAAGCTGGCTGGAGTGCGATCTTC
CTGAGGCCGATACTGTCGTCGTCCCCTCAAACTGGCAGATGCACGGTTACGATGCGCCCATCTACACCAACG
TGACCTATCCCATTACGGTCAATCCGCCGTTTGTTCCCACGGAGAATCCGACGGGTTGTTACTCGCTCACAT
TTAATGTTGATGAAAGCTGGCTACAGGAAGGCCAGACGCGAATTATTTTTGATGGCGTTCCTATTGGTTAAA
AAATGAGCTGATTTAACAAAAATTTAATGCGAATTTTAACAAAATATTAACGTTTACAATTTAAATATTTGC
TTATACAATCTTCCTGTTTTTTGGGGCTTTTCTGATTATCAACCGGGGTACATATGATTGACATGCTAGTTTT
ACGATTACCGTTCATCGATTCTCTTGTTTGCTCCAGACTCTCAGGCAATGACCTGATAGCCTTTGTAGATCT
CTCAAAAATAGCTACCCTCTCCGGCATTAATTTATCAGCTAGAACGGTTGAATATCATATTGATGGTGATTT
GACTGTCTCCGGCCTTTCTCACCCTTTTGAATCTTTACCTACACATTACTCAGGCATTGCATTTAAAATATA
TGAGGGTTCTAAAAATTTTTATCCTTGCGTTGAAATAAAGGCTTCTCCCGCAAAAGTATTACAGGGTCATAA
TGTTTTTGGTACAACCGATTTAGCTTTATGCTCTGAGGCTTTATTGCTTAATTTTGCTAATTCTTTGCCTTG

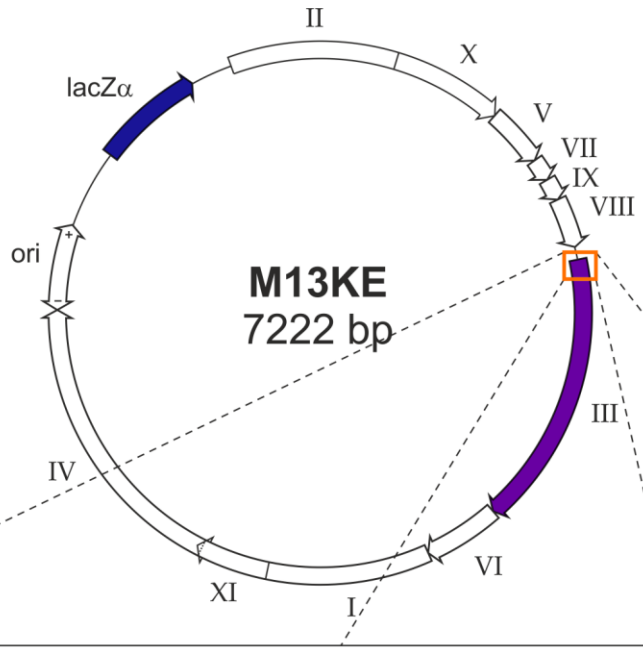

5`-...	TTA	TTC	GCA	ATT	CCT	TTA	GTG	GTA	CCT	TTC	TAT	TCT
3`-...	AAT	AAG	CGT	TAA	GGA	AAT	CAC	CAT	GGA	AAG	ATA	AGA
N-...	Leu	Phe	Ala	Ile	Pro	Leu	Val	Val	Pro	Phe	Tyr	Ser
CAC	TCT	**$(XXK)_n$**		**GGT**	**GGA**	**GGT**	TCG	GCC	GAA	ACT	GTT	GAA
GTG	AGA	**$(XXM)_n$**		**CCA**	**CCT**	**CCA**	AGC	CGG	CTT	TGA	CAA	CTT
His	Ser	**Xxx_n**		**Gly**	**Gly**	**Gly**	Ser	Ala	Glu	Thr	Val	Glu
AGT	TGT	TTA	GCA	AAA	TCC	CAT	ACA	GAA	AAT	TCA	TTT	ACT
TCA	ACA	AAT	CGT	TTT	AGG	GTA	CAC	CTT	TTA	AGT	AAA	TGA
Ser	Cys	Leu	Ala	Lys	Ser	His	Thr	Glu	Asn	Ser	Phe	Thr
AAC	GTC	TGG	AAA	GAC	GAC	AAA	ACT	TTA	GAT	CGT	TAC	GCT
TTG	CAG	ACC	TTT	CTG	CTG	TTT	TGA	AAT	CTA	**GCA**	**ATG**	**CGA**
Asn	Val	Trp	Lys	Asp	Asp	Lys	Thr	Leu	Asp	Arg	Tyr	Ala

AAC	TAT	GAG	GGC	***...-3`***
TTG	**ATA**	**CTC**	**CC**G	***...-5`***
Asn	Tyr	Glu	Gly	***...-C***

7 aa random library (Ph.D.-7): n = 7

12 aa random library (Ph.D.-7): n = 12

K = G or T; M = C or A

Figure 53) Plasmid map of the M13KE-phage [152, 226] depicting all genes and their respective positions in the genome. The gene coding for the **pIII capsid** as well as the artificially introduced sequence for a **lacZα** subunit (for blue/white screening) are highlighted. The **enlarged section** of the pIII sequence shows the sense strand (upper row), the complementary anti-sense strand (middle row) and the amino acid sequence (lower row). Here, the introduced **random sequence**, the **glycine linker** and the **96 primer sequence** (for sequencing) are highlighted. Adapted from the supplier`s manual. [152]

Appendix II:

Sequencing Data and Multiple Sequence Alignments

Full list of phage sequencing data, ordered by experimental set-up, library and round of biopanning. Only the section of the genetic sequence will be shown that contains the randomised peptid structure. First line of each set of sequencing data is the peptid sequence (marked bold), together with the adjacent sequence. Second line is the actual phage sequence ((+)-strand) and the third line is the experimentally found DNA sequence ((-)-strand).

IIa: Identified sequences during the biopanning on calcite {10.4}-facets

In addition to the sequence data, the corresponding Multiple Sequence Analyses are attached. For the amino acids, the following colour-code was used: **brown** (G), **yellow** (P), **light-blue** (non-polar amino acids: I, A, L, W, V, F, M), **blue** (polar, aromatic amino acids: Y, H), **green** (uncharged, polar amino acids: S,T, Q, N), **pink** (acidic amino acids: E, D) and **light-red** (basic amino acids: R, K).

Random dodecapeptide library

After **3rd** cycle:

Sequence 1

N **–**	Ser	His	Ser	**Ser**	**Leu**	**Ser**	**Pro**	**Ala**	**Gly**	**Gln**	**Lys**
5` **–**	TCT	CAC	TCT	TCT	CTG	TCG	CCT	GCT	GGG	TAG	AAG
3` **–**	AGA	GTG	AGA	AGA	GAC	AGC	GGA	CGA	CCC	ATC	TTC
	Ser	**Trp**	**Tyr**	**Ser**	Gly	Gly	Gly	**– *C***			
	TCG	TGG	TAT	TCT	GGT	GGA	GGT	**– *3`***			
	AGC	ACC	ATA	AGA	CCA	CCT	CCA	**– *5`***			

Sequence 2

N **–**	Ser	His	Ser	**Asp**	**Pro**	**Met**	**Ser**	**Val**	**Leu**	**Ser**	**Met**
5` **–**	TCT	CAC	TCT	GAT	CCG	ATG	AGT	GTG	CTG	AGT	ATG
3` **–**	AGA	GTG	AGA	CTA	GGC	TAC	TCA	CAC	GAC	TCA	TAC
	His	**Phe**	**Gln**	**Arg**	Gly	Gly	Gly	**– *C***			
	CAT	TTT	CAG	AGG	GGT	GGA	GGT	**– *3`***			
	GTA	AAA	GTC	TCC	CCA	CCT	CCA	**– *5`***			

Sequence 3

N **–**	Ser	His	Ser	**Ala**	**Pro**	**Thr**	**Ser**	**Leu**	**Tyr**	**Pro**	**Gln**
5` **–**	TCT	CAC	TCT	GCG	CCT	ACT	TCG	CTG	TAT	CCG	CAG
3` **–**	AGA	GTG	AGA	CGC	GGA	TGA	AGC	GAC	ATA	GGC	GTC
	Arg	**Ser**	**Leu**	**Ala**	Gly	Gly	Gly	**– *C***			
	AGG	TCG	CTT	GCT	GGT	GGA	GGT	**– *3`***			
	TCC	AGC	GAA	CGA	CCA	CCT	CCA	**– *5`***			

Sequence 4

N **–**	Ser	His	Ser	**Ser**	**Leu**	**Thr**	**Asp**	**Asn**	**Ser**	**Asn**	**Met**
5` **–**	TCT	CAC	TCT	TCT	CTG	ACT	GAT	AAT	TCG	AAT	ATG
3` **–**	AGA	GTG	AGA	AGA	GAC	TGA	CTA	TTA	AGC	TTA	TAC
	Thr	**Thr**	**Gly**	**Tyr**	Gly	Gly	Gly	**– *C***			
	ACG	ACG	GGT	TAT	GGT	GGA	GGT	**– *3`***			
	TGC	TGC	CCA	ATA	CCA	CCT	CCA	**– *5`***			

Sequences 5, 8 and 9

N **–**	Ser	His	Ser	Ala	Glu	Thr	Val	Glu	**– *C***
5` **–**	TCT	CAC	TC**G**	GCC	GAA	ACT	GTT	GAA	**– *3`***
3` **–**	AGA	GTG	AG**C**	CGG	CTT	TGA	CAA	CTT	**– *5`***

Sequences match the sequence of the M13KE-phage.

Sequence 6

N **–**	Ser	His	Ser	**Gln**	**Asp**	**Leu**	**Val**	**Asn**	**Ala**	**Gly**	**Thr**
5` **–**	TCT	CAC	TCT	CAG	GAT	TTG	GTG	AAT	GCT	GGG	ACT
3` **–**	AGA	GTG	AGA	GTC	CTA	AAC	CAC	TTA	CGA	CCC	TGA

	Tyr	**Arg**	**Leu**	**Asn**	Gly	Gly	Gly	**– *C***			
	TAT	CGT	TTG	AAT	GGT	GGA	GGT	**– *3`***			
	ATA	GCA	AAC	TTA	CCA	CCT	CCA	**– *5`***			

Sequence 7

***N* –**	Ser	His	Ser	**Ala**	**Arg**	**Ser**	**His**	**Gly**	**His**	**His**	**Ile**
***5`* –**	TCT	CAC	TCT	GCG	CGT	TCT	CAT	GGT	CAT	CAT	ATT
***3`* –**	AGA	GTG	AGA	CGC	GCA	AGA	GTA	CCA	GTA	GTA	TAA
	Pro	**Ala**	**Trp**	**Ala**	Gly	Gly	Ser	**– *C***			
	CCT	GCT	TGG	GCG	GGT	GGA	AGT	**– *3`***			
	GGA	CGA	ACC	CGC	CCA	CCT	TCA	**– *5`***			

Sequence 10

***N* –**	Ser	His	Ser	**Ala**	**Ser**	**Ser**	**Leu**	**His**	**Met**	**Phe**	**Lys**
***5`* –**	TCT	CAC	TCT	GCG	TCT	TCG	CTG	CAT	ATG	TTT	AAG
***3`* –**	AGA	GTG	AGA	CGC	AGA	AGC	GAC	GTA	TAC	AAA	TTC
	Val	**Asn**	**Thr**	**Ala**	Gly	Gly	Gly	**– *C***			
	GTT	AAT	ACT	GCT	GGT	GGA	GGT	**– *3`***			
	CAA	TTA	TGA	CGA	CCA	CCT	TCA	**– *5`***			

Multiple Sequence Analysis (Dodecapeptide library, after 3rd cycle)

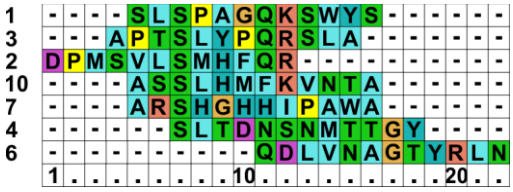

After **5th** cycle:

Sequence 1

***N* –**	Ser	His	Ser	**Asn**	**Ser**	**Asn**	**Asn**	**Ile**	**Val**	**Tyr**	**Tyr**
***5`* –**	TCT	CAC	TCT	AAT	TCT	AAT	AAT	ATT	GTG	TAT	TAT
***3`* –**	AGA	GTG	AGA	TTA	AGA	TTA	TTA	TAA	CAC	ATA	ATA
	Gln	**Arg**	**Ser**	**Leu**	Gly	Gly	Gly	**– *C***			
	CAG	CGT	TCG	CTG	GGT	GGA	GGT	**– *3`***			
	GTC	GCA	AGC	GAC	CCA	CCT	CCA	**– *5`***			

Sequence 2

***N* –**	Ser	His	Ser	**Glu**	**Thr**	**Thr**	**His**	**Met**	**His**	**Ile**	**Pro**
***5`* –**	TCT	CAC	TCT	GAG	ACG	ACG	CAT	ATG	CAT	ATT	CCT
***3`* –**	AGA	GTG	AGA	CTC	TGC	TGC	GTA	TAC	GTA	TAA	GGA
	Met	**Pro**	**Pro**	**Gly**	Gly	Gly	Gly	**– *C***			
	ATG	CCG	CCT	GGG	GGT	GGA	GGT	**– *3`***			
	TAC	GGC	GGA	CCC	CCA	CCT	CCA	**– *5`***			

Sequence 3

***N* –**	Ser	His	Ser	**Asn**	**His**	**Ser**	**Pro**	**Asn**	**Glu**	**Ala**	**Tyr**
***5`* –**	TCT	CAC	TCT	AAT	CAT	TCT	CCT	AAT	GAG	GCG	TAT
***3`* –**	AGA	GTG	AGA	TTA	GTA	AGA	GGA	TTA	CTC	CGC	ATA
	Ile	**Leu**	**Ser**	**Thr**	Gly	Gly	Gly	**– *C***			
	ATT	CTT	AGT	ACT	GGT	GGA	GGT	**– *3`***			
	TAA	GAA	TCA	TGA	CCA	CCT	CCA	**– *5`***			

Sequences 4, 10 and 14

***N* –**	Ser	His	Ser	Ala	Glu	Thr	Val	Glu	**– *C***
***5`* –**	TCT	CAC	TC**G**	GCC	GAA	ACT	GTT	GAA	**– *3`***
***3`* –**	AGA	GTG	AG**C**	CGG	CTT	TGA	CAA	CTT	**– *5`***

Sequences match the sequence of the M13KE-phage.

Sequence 5

***N* –**	Ser	His	Ser	**Ser**	**Thr**	**Ile**	**Pro**	**Tyr**	**Met**	**His**	**Thr**
***5`* –**	TCT	CAC	TCT	TCT	ACT	ATT	CCT	TAT	ATG	CAT	ACT
***3`* –**	AGA	GTG	AGA	AGA	TGA	TAA	GGA	ATA	TAC	GTA	TGA
	Arg	**Thr**	**Leu**	**Lys**	Gly	Gly	Gly	**– *C***			
	AGG	ACT	TTG	AAG	GGT	GGA	GGT	**– *3`***			
	TCC	TGA	AAC	TTC	CCA	CCT	CCA	**– *5`***			

Sequence 6

***N* –**	Ser	His	Ser	**Met**	**Thr**	**Asp**	**Glu**	**Gly**	**Ala**	**Ile**	**Glu**
***5`* –**	TCT	CAC	TCT	ATG	ACT	GAT	GAG	GGT	GCT	ATT	GAG
***3`* –**	AGA	GTG	AGA	TAC	TGA	CTA	CTC	CCA	CGA	TAA	CTC
	Pro	**Gln**	**Thr**	**Arg**	Gly	Gly	Gly	**– *C***			
	CCG	TAG	ACT	CGG	GGT	GGA	GGT	**– *3`***			
	GGC	ATC	TGA	GCC	CCA	CCT	CCA	**– *5`***			

Sequence 7

***N* –**	Ser	His	Ser	**Asn**	**Ala**	**Leu**	**Asn**	**Asn**	**Asn**	**Trp**	**Thr**
***5`* –**	TCT	CAC	TCT	AAT	GCG	CTG	AAT	AAT	AAT	TGG	ACG
***3`* –**	AGA	GTG	AGA	TTA	CGC	GAC	TTA	TTA	TTA	ACC	TGC
	Ala	**Arg**	**Trp**	**Pro**	Gly	Gly	Gly	**– *C***			
	GCG	AGG	TGG	CCT	GGT	GGA	GGT	**– *3`***			
	CGC	TCC	ACC	GGA	CCA	CCT	CCA	**– *5`***			

Sequence 8

N –	Ser	His	Ser	**Asn**	**Thr**	**Thr**	**Tyr**	**Gly**	**Thr**	**Asp**	**His**
5`–	TCT	CAC	TCT	AAT	ACG	ACG	TAT	GGT	ACT	GAT	CAT
3`–	AGA	GTG	AGA	TTA	TGC	TGC	ATA	CCA	TGA	CTA	GTA
	Asp	**Ala**	**Ala**	**Lys**	Gly	Gly	Gly	***– C***			
	GAT	GCG	GCG	AAG	GGT	GGA	GGT	***– 3`***			
	CTA	CGC	CGC	TTC	CCA	CCT	CCA	***– 5`***			

Sequence 9

N –	Ser	His	Ser	**Gly**	**Gly**	**His**	**Asn**	**Leu**	**Trp**	**Pro**	**Thr**
5`–	TCT	CAC	TCT	GGT	GGG	CAT	AAT	CTT	TGG	CCT	ACG
3`–	AGA	GTG	AGA	CCA	CCC	GTA	TTA	GAA	ACC	GGA	TGC
	Ala	**Thr**	**Thr**	**Val**	Gly	Gly	Gly	***– C***			
	GCG	ACG	ACG	GTG	GGT	GGA	GGT	***– 3`***			
	CGC	TGC	TGC	CAC	CCA	CCT	CCA	***– 5`***			

Sequence 11

N –	Ser	His	Ser	**Gln**	**Leu**	**Ser**	**Ser**	**Ser**	**Ala**	**Met**	**Val**
5`–	TCT	CAC	TCT	CAG	CTT	TCT	TCT	TCT	GCT	ATG	GTG
3`–	AGA	GTG	AGA	GTC	GAA	AGA	AGA	AGA	CGA	TAC	CAC
	Thr	**Leu**	**Gly**	**Asp**	Gly	Gly	Gly	***– C***			
	ACG	CTT	GGG	GAT	GGT	GGA	GGT	***– 3`***			
	TGC	GAA	CCC	CTA	CCA	CCT	CCA	***– 5`***			

Sequence 12

N –	Ser	His	Ser	**Lys**	**Asp**	**Leu**	**Ala**	**Tyr**	**Leu**	**Gly**	**Ala**
5`–	TCT	CAC	TCT	AAG	GAT	CTG	GCT	TAT	TTG	GGT	GCG
3`–	AGA	GTG	AGA	TTC	CTA	GAC	CGA	ATA	AAC	CCA	CGC
	Gly	**Ala**	**Asn**	**Lys**	Gly	Gly	Gly	***– C***			
	GGT	GCT	AAT	AAG	GGT	GGA	GGT	***– 3`***			
	CCA	CGA	TTA	TTC	CCA	CCT	CCA	***– 5`***			

Sequence 13

N –	Ser	His	Ser	**Glu**	**Arg**	**Ile**	**Tyr**	**Glu**	**Ala**	**Glu**	**Ser**
5`–	TCT	CAC	TCT	GAG	CGG	ATT	TAT	GAG	GCT	GAG	TCG
3`–	AGA	GTG	AGA	CTC	GCC	TAA	ATA	CTC	CGA	CTC	AGC
	Arg	**Thr**	**Thr**	**Leu**	Gly	Gly	Gly	***– C***			
	CGG	ACG	ACG	TTG	GGT	GGA	GGT	***– 3`***			
	GCC	TGC	TGC	AAC	CCA	CCT	CCA	***– 5`***			

Sequence 15

N –	Ser	His	Ser	**Gly**	**Pro**	**Leu**	**Lys**	**His**	**Thr**	**Val**	**Asn**
5`–	TCT	CAC	TCT	GGT	CCG	TTG	AAG	CAT	ACT	GTT	AAT
3`–	AGA	GTG	AGA	CCA	GGC	AAC	TTC	GTA	TGA	CAA	TTA
	Thr	**His**	**Met**	**Pro**	Gly	Gly	Gly	***– C***			
	ACG	CAT	ATG	CCG	GGT	GGA	GGT	***– 3`***			
	TGC	GTA	TAC	GGC	CCA	CCT	CCA	***– 5`***			

Sequence 16

N –	Ser	His	Ser	**Thr**	**Ser**	**Asn**	**Asn**	**Arg**	**Asp**	**Pro**	**Gly**
5`–	TCT	CAC	TCT	ACT	TCG	AAT	AAT	AGG	GAT	CCT	GGT
3`–	AGA	GTG	AGA	TGA	AGC	TTA	TTA	TCC	CTA	GGA	CCA
	Leu	**Ser**	**Met**	**Leu**	Gly	Gly	Gly	***– C***			
	TTG	TCG	ATG	CTT	GGT	GGA	GGT	***– 3`***			
	AAC	AGC	TAC	GAA	CCA	CCT	CCA	***– 5`***			

Sequence 17

N –	Ser	His	Ser	**His**	**Pro**	**Leu**	**Thr**	**Leu**	**Asn**	**Pro**	**Gln**
5`–	TCT	CAC	TCT	CAT	CCG	TTG	ACT	TTG	AAT	CCG	CAG
3`–	AGA	GTG	AGA	GTA	GGC	AAC	TGA	AAC	TTA	GGC	GTC
	Arg	**Pro**	**Met**	**Asn**	Gly	Gly	Gly	***– C***			
	AGG	CCT	ATG	AAT	GGT	GGA	GGT	***– 3`***			
	TCC	GGA	TAC	TTA	CCA	CCT	CCA	***– 5`***			

Sequence 18

N –	Ser	His	Ser	**Tyr**	**Thr**	**Thr**	**Ala**	**Leu**	**Asn**	**Glu**	**Met**
5`–	TCT	CAC	TCT	TAT	ACT	ACG	GCT	CTT	AAT	GAG	ATG
3`–	AGA	GTG	AGA	ATA	TGA	TGC	CGA	GAA	TTA	CTC	TAC
	Ser	**His**	**Thr**	**Asn**	Gly	Gly	Gly	***– C***			
	AGT	CAT	ACG	AAT	GGT	GGA	GGT	***– 3`***			
	TCA	GTA	TGC	TTA	CCA	CCT	CCA	***– 5`***			

Sequence 19

N –	Ser	His	Ser	**Arg**	**Pro**	**Tyr**	**Ser**	**Glu**	**Leu**	**Asp**	**Ser**
5`–	TCT	CAC	TCT	AGG	CCG	TAT	TCG	GAG	CTT	GAT	TCG
3`–	AGA	GTG	AGA	TCC	GGC	ATA	AGC	CTC	GAA	CTA	AGC
	Ile	**Pro**	**Pro**	**Arg**	Gly	Gly	Gly	***– C***			
	ATT	CCG	CCT	CGG	GGT	GGA	GGT	***– 3`***			
	TAA	GGC	GGA	GCC	CCA	CCT	CCA	***– 5`***			

Sequence 20

N –	Ser	His	Ser	**Gln**	**Asn**	**Ile**	**Asn**	**Val**	**Glu**	**Met**	**Gln**
5`–	TCT	CAC	TCT	TAG	AAT	ATT	AAT	GTT	GAG	ATG	CAG
3`–	AGA	GTG	AGA	ATC	TTA	TAA	TTA	CAA	CTC	TAC	GTC
	Ala	**Val**	**Lys**	**Thr**	Gly	Gly	Gly	***– C***			
	GCG	GTG	AAG	ACG	GGT	GGA	GGT	***– 3`***			
	CGC	CAC	TTC	TGC	CCA	CCT	CCA	***– 5`***			

Multiple Sequence Analysis (Dodecapeptide library, after 5th cycle)

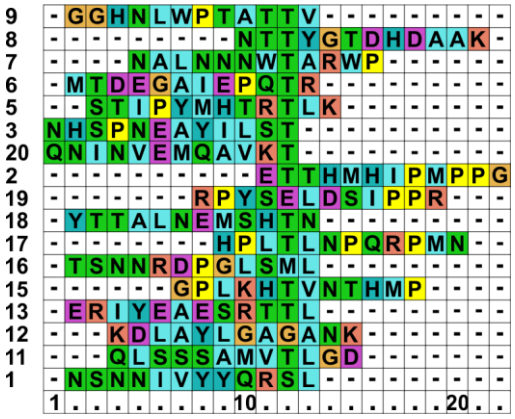

After **6th** cycle:

Sequences 1, 3-8, 11 and 14

***N* –**	Ser	His	Ser	Ala	Glu	Thr	Val	Glu	***– C***
***5`* –**	TCT	CAC	TC**G**	GCC	GAA	ACT	GTT	GAA	***– 3`***
***3`* –**	AGA	GTG	AG**C**	CGG	CTT	TGA	CAA	CTT	***– 5`***

Sequences match the sequence of the M13KE-phage.

Sequence 2

***N* –**	Ser	His	Ser	**His**	**Phe**	**Leu**	**Leu**	**Pro**	**Gln**	**Met**	**Ala**
***5`* –**	TCT	CAC	TCT	CAT	TTT	CTT	CTT	CCT	CAG	ATG	GCT
***3`* –**	AGA	GTG	AGA	GTA	AAA	GAA	GAA	GGA	GTC	TAC	CGA
	Thr	**Pro**	**Tyr**	**Trp**	Gly	Gly	Gly	***– C***			
	ACG	CCT	TAT	TGG	GGT	GGA	GGT	***– 3`***			
	TGC	GGA	ATA	ACC	CCA	CCT	CCA	***– 5`***			

Sequence 9

***N* –**	Ser	His	Ser	**Asn**	**Phe**	**Thr**	**Tyr**	**Ala**	**Gly**	**Thr**	**Tyr**
***5`* –**	TCT	CAC	TCT	AAT	TTT	ACG	TAT	GCG	GGT	ACT	TAT
***3`* –**	AGA	GTG	AGA	TTA	AAA	TGC	ATA	CGC	CCA	TGA	ATA
	Val	**Val**	**His**	**Arg**	Gly	Gly	Gly	***– C***			
	GTT	GTT	CAT	CGG	GGT	GGA	GGT	***– 3`***			
	CAA	CAA	GTA	GCC	CCA	CCT	CCA	***– 5`***			

Sequence 10

***N* –**	Ser	His	Ser	**Tyr**	**Pro**	**Gln**	**Ile**	**Ala**	**Val**	**Ser**	**Tyr**
***5`* –**	TCT	CAC	TCT	TAT	CCG	TAG	ATT	GCT	GTG	TCG	TAT
***3`* –**	AGA	GTG	AGA	ATA	GGC	ATC	TAA	CGA	CAC	AGC	ATA
	Leu	**His**	**Met**	**Asn**	Gly	Gly	Gly	***– C***			
	CTT	CAT	ATG	AAT	GGT	GGA	GGT	***– 3`***			
	GAA	GTA	TAC	TTA	CCA	CCT	CCA	***– 5`***			

Sequence 12

***N* –**	Ser	His	Ser	**Tyr**	**Arg**	**Met**	**Gln**	**Glu**	**Leu**	**Pro**	**Asn**
***5`* –**	TCT	CAC	TCT	TAT	CGT	ATG	CAG	GAG	CTG	CCG	AAT
***3`* –**	AGA	GTG	AGA	ATA	GCA	TAC	GTC	CTC	GAC	GGC	TTA
	Ile	**Ser**	**Glu**	**Val**	Gly	Gly	Gly	***– C***			
	ATT	TCT	GAG	GTG	GGT	GGA	GGT	***– 3`***			
	TAA	AGA	CTC	CAC	CCA	CCT	CCA	***– 5`***			

Sequence 13

***N* –**	Ser	His	Ser	**Ser**	**Ala**	**Leu**	**Phe**	**Asp**	**Pro**	**Gly**	**Ile**
***5`* –**	TCT	CAC	TCT	AGT	GCG	TTG	TTT	GAT	CCT	GGT	ATT
***3`* –**	AGA	GTG	AGA	TCA	CGC	AAC	AAA	CTA	GGA	CCA	TAA
	Asn	**Lys**	**Ser**	**Arg**	Gly	Gly	Gly	***– C***			
	AAT	AAG	TCG	CGT	GGT	GGA	GGT	***– 3`***			
	TTA	TTC	AGC	GCA	CCA	CCT	CCA	***– 5`***			

Sequence 15

***N* –**	Ser	His	Ser	**Gly**	**Phe**	**Ser**	**Tyr**	**His**	**Lys**	**Gln**	**Pro**
***5`* –**	TCT	CAC	TCT	GGG	TTT	AGT	TAT	CAT	AAG	CAG	CCT
***3`* –**	AGA	GTG	AGA	CCC	AAA	TCA	ATA	GTA	TTC	GTC	GGA
	Asn	**Asp**	**Met**	**Ser**	Gly	Gly	Gly	***– C***			
	AAT	GAT	ATG	TCT	GGT	GGA	GGT	***– 3`***			
	TTA	CTA	TAC	AGA	CCA	CCT	CCA	***– 5`***			

Sequence 16

***N* –**	Ser	His	Ser	**Thr**	**Gly**	**His**	**Leu**	**Asn**	**Pro**	**Gln**	**His**
***5`* –**	TCT	CAC	TCT	ACG	GGT	CAT	CTT	AAT	CCT	CAG	CAT
***3`* –**	AGA	GTG	AGA	TGC	CCA	GTA	GAA	TTA	GGA	GTC	GTA
	Gln	**Gly**	**Ala**	**Gln**	Gly	Gly	Gly	***– C***			
	CAG	GGT	GCT	CAG	GGT	GGA	GGT	***– 3`***			
	GTC	CCA	CGA	GTC	CCA	CCT	CCA	***– 5`***			

Sequence 17

***N* –**	Ser	His	Ser	**Asn**	**Asp**	**Ala**	**Asn**	**Thr**	**Arg**	**Leu**	**Arg**
***5`* –**	TCT	CAC	TCT	AAT	GAT	GCG	AAT	ACT	CGG	CTT	CGT
***3`* –**	AGA	GTG	AGA	TTA	CTA	CGC	TTA	TGA	GCC	GAA	GCA

	Ile	**Ala**	**Asn**	**Ser**	Gly	Gly	Gly	***– C***		
	ATT	GCG	AAT	TCG	GGT	GGA	GGT	***– 3`***		
	TAA	CGC	TTA	AGC	CCA	CCT	CCA	***– 5`***		

Sequence 18

N –	Ser	His	Ser	**Ser**	**Pro**	**Leu**	**Thr**	**Ile**	**Pro**	**Ser**	**Met**
5`–	TCT	CAC	TCT	AGT	CCT	CTG	ACT	ATT	CCG	AGT	ATG
3`–	AGA	GTG	AGA	TCA	GGA	GAC	TGA	TAA	GGC	TCA	TAC
	Ala	**Tyr**	**Gly**	**Gln**	Gly	Gly	Gly	***– C***			
	GCG	TAT	GGG	CAG	GGT	GGA	GGT	***– 3`***			
	CGC	ATA	CCC	GTC	CCA	CCT	CCA	***– 5`***			

Sequence 19

N –	Ser	His	Ser	**Glu**	**His**	**Ala**	**Ser**	**Lys**	**Asn**	**Ala**	**Asn**
5`–	TCT	CAC	TCT	GAG	CAT	GCT	AGT	AAG	AAT	GCG	AAT
3`–	AGA	GTG	AGA	CTC	GTA	CGA	TCA	TTC	TTA	CGC	TTA
	Ile	**Ser**	**Gly**	**Leu**	Gly	Gly	Gly	***– C***			
	ATT	TCG	GGG	CTG	GGT	GGA	GGT	***– 3`***			
	TAA	AGC	CCC	GAC	CCA	CCT	CCA	***– 5`***			

Sequence 20

N –	Ser	His	Ser	**Gly**	**Leu**	**Ala**	**Glu**	**Gly**	**Arg**	**Tyr**	**Pro**
5`–	TCT	CAC	TCT	GGG	CTG	GCT	GAG	GGG	AGG	TAT	CCT
3`–	AGA	GTG	AGA	CCC	GAC	CGA	CTC	CCC	TCC	ATA	GGA
	Gln	**Asp**	**Met**	**Gly**	Gly	Gly	Gly	***– C***			
	CAG	GAT	ATG	GGG	GGT	GGA	GGT	***– 3`***			
	GTC	CTA	TAC	CCC	CCA	CCT	CCA	***– 5`***			

Multiple Sequence Analysis (Dodecapeptide, after 6th cycle)

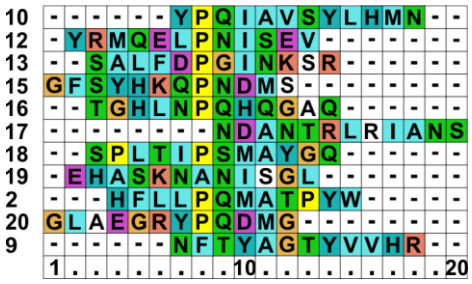

Multiple Sequence Analysis (Dodecapeptide library, all cycles)

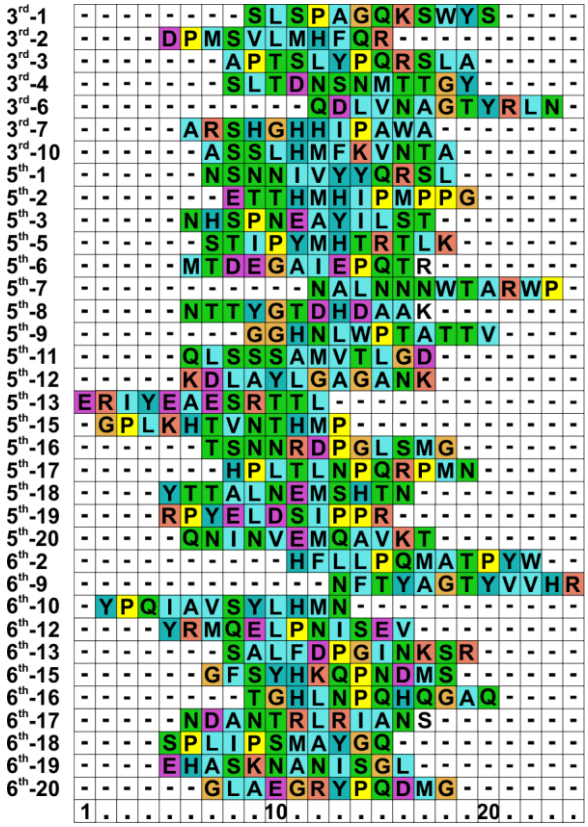

Random heptapeptide library

After 5th cycle:

Sequence 1

***N* –**	Ser	His	Ser	**Ser**	**Thr**	**Gln**	**Pro**	**His**	**His**	**Gln**
***5`* –**	TCT	CAC	TCT	TCG	ACG	CAG	CCT	CAT	CAT	CAG
***3`* –**	AGA	GTG	AGA	AGC	TGC	GTC	GGA	GTA	GTA	GTC
	Gly	Gly	**Ser**	***– C***						
	GGT	GGA	**A**GT	***– 3`***						
	CCA	CCT	**T**CA	***– 5`***						

Possible point mutation G → A, changing Gly → Ser or a failure/misinterpretation while sequencing.

Sequence 2

***N* –**	Ser	His	Ser	**Ala**	**Lys**	**Pro**	**Ser**	**Phe**	**Pro**	**Thr**
***5`* –**	TCT	CAC	TCT	GCG	AAG	CCG	AGT	TTT	CCG	ACG
***3`* –**	AGA	GTG	AGA	CGC	TTC	GGC	TCA	AAA	GGC	TGC
	Gly	Gly	Gly	***– C***						
	GGT	GGA	GGT	***– 3`***						
	CCA	CCT	CCA	***– 5`***						

Sequence 3

***N* –**	Ser	His	Ser	**Tyr**	**Pro**	**Glu**	**Val**	**Pro**	**Pro**	**Leu**
***5`* –**	TCT	CAC	TCT	TAT	CCT	GAG	GTT	CCG	CCG	CTT
***3`* –**	AGA	GTG	AGA	ATA	GGA	CTC	CAA	GGC	GGC	GAA
	Gly	Gly	Gly	***– C***						
	GGT	GGA	GGT	***– 3`***						
	CCA	CCT	CCA	***– 5`***						

Sequence 4

***N* –**	Ser	His	Ser	**Asn**	**Ser**	**Pro**	**Ile**	**Ala**	**Leu**	**Ala**
***5`* –**	TCT	CAC	TCT	AAT	AGT	CCG	ATT	GCG	CTG	GCT
***3`* –**	AGA	GTG	AGA	TTA	TCA	GGC	TAA	CGC	GAC	CGA
	Gly	Gly	Gly	***– C***						
	GGT	GGA	GGT	***– 3`***						
	CCA	CCT	CCA	***– 5`***						

Sequence 5

***N* –**	Ser	His	Ser	**Lys**	**Ser**	**Thr**	**Ser**	**Trp**	**Thr**	**Val**
***5`* –**	TCT	CAC	TCT	AAG	TCG	ACG	AGT	TGG	ACG	GTG
***3`* –**	AGA	GTG	AGA	TTC	AGC	TGC	TCA	ACC	TGC	CAC
	Gly	**Glu**	Gly	***– C***						
	GGT	G**A**A	GGT	***– 3`***						
	CCA	C**T**T	CCA	***– 5`***						

Possible point mutation G → A, changing Gly → Glu or a failure/misinterpretation while sequencing.

Sequence 6

***N* –**	Ser	His	Ser	**Ala**	**Leu**	**Ser**	**Gln**	**Ser**	**Leu**	**Pro**
***5`* –**	TCT	CAC	TCT	GCG	TTG	TCT	CAG	TCT	CTG	CCT
***3`* –**	AGA	GTG	AGA	CGC	AAC	AGA	GTC	AGA	GAC	GGA
	Gly	Gly	Gly	***– C***						
	GGT	GGA	GGT	***– 3`***						
	CCA	CCT	CCA	***– 5`***						

Sequence 7

***N* –**	Ser	His	Ser	**Ser**	**Ser**	**Val**	**Thr**	**Pro**	**Pro**	**Ser**
***5`* –**	TCT	CAC	TCT	AGT	TCG	GTT	ACT	CCT	CCT	AGT
***3`* –**	AGA	GTG	AGA	TCA	AGC	CAA	TGA	GGA	GGA	TCA
	Gly	Gly	Gly	***– C***						
	GGT	GGA	GGT	***– 3`***						
	CCA	CCT	CCA	***– 5`***						

Sequence 8

***N* –**	Ser	His	Ser	**Ser**	**Tyr**	**Phe**	**Ala**	**Gln**	**Pro**	**Ser**
***5`* –**	TCT	CAC	TCT	TCT	TAT	TTT	GCT	CAG	CCT	TCG
***3`* –**	AGA	GTG	AGA	AGA	ATA	AAA	CGA	GTC	GGA	AGC
	Gly	Gly	Gly	***– C***						
	GGT	GGA	GGT	***– 3`***						
	CCA	CCT	CCA	***– 5`***						

Sequence 9

***N* –**	Ser	His	Ser	**Leu**	**Pro**	**Phe**	**His**	**Pro**	**Ala**	**Arg**
***5`* –**	TCT	CAC	TCT	TCT	TAT	TTT	GCT	CAG	CCT	TCG
***3`* –**	AGA	GTG	AGA	AGA	ATA	AAA	CGA	GTC	GGA	AGC
	Gly	Gly	Gly	***– C***						
	GGT	GGA	GGT	***– 3`***						
	CCA	CCT	CCA	***– 5`***						

Sequence 10

***N* –**	Ser	His	Ser	**Gly**	**Thr**	**Pro**	**Leu**	**Thr**	**Pro**	**Leu**
***5`* –**	TCT	CAC	TCT	GGG	ACG	CCT	CTT	ACG	CCG	CTG
***3`* –**	AGA	GTG	AGA	CCC	TGC	GGA	GAA	TGC	GGC	GAC
	Asp	Gly	Gly	***– C***						
	G**A**T	GGA	GGT	***– 3`***						
	C**T**A	CCT	CCA	***– 5`***						

Possible point mutation G → A, changing Gly → Asp or a failure/misinterpretation while sequencing.

Multiple Sequence Analysis (Heptapeptide library, after 5th cycle)

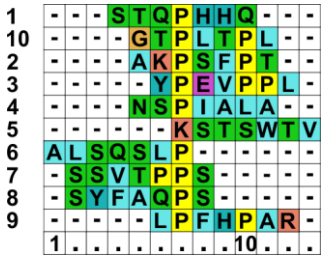

Multiple Sequence Analysis (Both libraries, all cycles)

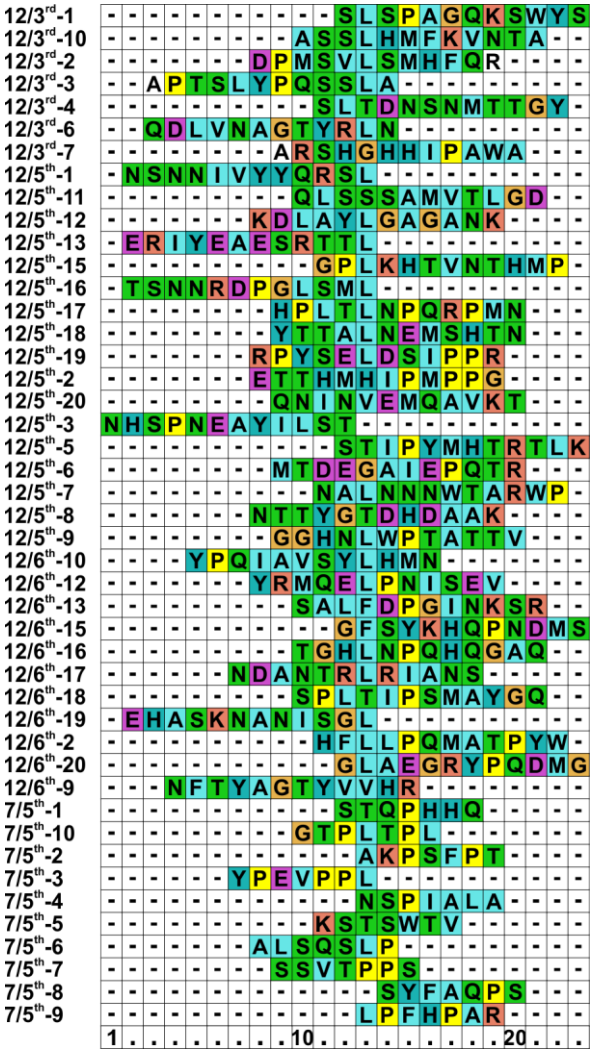

IIb: Identified sequences during the biopanning on calcite nanoparticles

In addition to the sequence data, the corresponding Multiple Sequence Analyses are attached. For the amino acids, the following colour-code was used: **brown** (G), **yellow** (P), **light-blue** (non-polar amino acids: I, A, L, W, V, F, M), **blue** (polar, aromatic amino acids: Y, H), **green** (uncharged, polar amino acids: S,T, Q, N), **pink** (acidic amino acids: E, D) and **light-red** (basic amino acids: R, K).

Sequences identified while applying protocol A

Random dodecapeptide library

Elution with 0.1M CaCl2 in TBS (**C**):

After **3rd** cycle of biopanning (**C3**):

Sequences 1,3,8,10

N –	Ser	His	Ser	**Leu**	**Gly**	**Lys**	**Thr**	**Thr**	**Ser**	**Ala**	**Gln**
5`–	TCT	CAC	TCT	CTG	GGT	AAG	ACT	ACT	TCT	GCG	CAG
3`–	AGA	GTG	AGA	GAC	CCA	TTC	TGA	TGA	AGA	CGC	GTC
	Asn	**Leu**	**Val**	**Pro**	Gly	Gly	Gly	***– C***			
	AAT	TTG	GTG	CCG	GGT	GGA	GGT	***– 3`***			
	TTA	AAC	CAC	GGC	CCA	CCT	CCA	***– 5`***			

Sequences 2,4-7,9

N –	Ser	His	Ser	**Gln**	**Asn**	**Ser**	**Thr**	**Leu**	**Asn**	**Tyr**	**Tyr**
5`–	TCT	CAC	TCT	CAG	AAT	TCT	ACT	TTG	AAT	TAT	TAT
3`–	AGA	GTG	AGA	GTC	TTA	AGA	TGA	AAC	TTA	ATA	ATA
	Thr	**Leu**	**Leu**	**Arg**	Gly	Gly	Gly	***– C***			
	ACG	CTT	CTG	CGG	GGT	GGA	GGT	***– 3`***			
	TGC	GAA	GAC	GCC	CCA	CCT	CCA	***– 5`***			

After 2nd cycle of biopanning and amplification (**C2**):

Sequences 1,2,4-7,10

N –	Ser	His	Ser	**Gln**	**Asn**	**Ser**	**Thr**	**Leu**	**Asn**	**Tyr**	**Tyr**
5`–	TCT	CAC	TCT	CAG	AAT	TCT	ACT	TTG	AAT	TAT	TAT
3`–	AGA	GTG	AGA	GTC	TTA	AGA	TGA	AAC	TTA	ATA	ATA
	Thr	**Leu**	**Leu**	**Arg**	Gly	Gly	Gly	***– C***			
	ACG	CTT	CTG	CGG	GGT	GGA	GGT	***– 3`***			
	TGC	GAA	GAC	GCC	CCA	CCT	CCA	***– 5`***			

Sequence 3

N –	Ser	His	Ser	**Gln**	**Asn**	**Ser**	**Thr**	**Thr**	**Asn**	**Tyr**	**His**
5`–	TCT	CAC	TCT	CAG	AAT	TCT	ACT	ACG	AAT	TAT	CAT
3`–	AGA	GTG	AGA	GTC	TTA	AGA	TGA	TGC	TTA	ATA	GTA
	Thr	**Leu**	**Val**	**Arg**	Gly	Gly	Gly	***– C***			
	ACG	CTT	GTG	CGG	GGT	GGA	GGT	***– 3`***			
	TGC	GAA	CAC	GCC	CCA	CCT	CCA	***– 5`***			

Sequences 8,9

N –	Ser	His	Ser	**Leu**	**Gly**	**Lys**	**Thr**	**Thr**	**Ser**	**Ala**	**Gln**
5`–	TCT	CAC	TCT	CTG	GGT	AAG	ACT	ACT	TCT	GCG	CAG
3`–	AGA	GTG	AGA	GAC	CCA	TTC	TGA	TGA	AGA	CGC	GTC
	Asn	**Leu**	**Val**	**Pro**	Gly	Gly	Gly	***– C***			
	AAT	TTG	GTG	CCG	GGT	GGA	GGT	***– 3`***			
	TTA	AAC	CAC	GGC	CCA	CCT	CCA	***– 5`***			

Sequences identified in the amplified washing step of the 2nd cycle (**WSC2**):

Sequences 1,7

N –	Ser	His	Ser	**Gln**	**Asn**	**Ser**	**Thr**	**Leu**	**Asn**	**Tyr**	**Tyr**
5`–	TCT	CAC	TCT	CAG	AAT	TCT	ACT	TTG	AAT	TAT	TAT
3`–	AGA	GTG	AGA	GTC	TTA	AGA	TGA	AAC	TTA	ATA	ATA
	Thr	**Leu**	**Leu**	**Arg**	Gly	Gly	Gly	***– C***			
	ACG	CTT	CTG	CGG	GGT	GGA	GGT	***– 3`***			
	TGC	GAA	GAC	GCC	CCA	CCT	CCA	***– 5`***			

Sequences 2,3

Deletion of a nucleotide.

Sequence 4

N –	Ser	His	Ser	**Asp**	**Thr**	**Phe**	**Leu**	**Trp**	**Trp**	**Asn**	**Asn**
5`–	TCT	CAC	TCT	GAT	ACG	TTT	CTT	TGG	TGG	AAT	AAT
3`–	AGA	GTG	AGA	CTA	TGC	AAA	GAA	ACC	ACC	TTA	TTA

	Glu	**Leu**	**Thr**	**Ala**	Gly	Gly	Gly	***– C***			
	GAG	CTT	ACG	GCT	GGT	GGA	GGT	***– 3`***			
	CTC	GAA	TGC	CGA	CCA	CCT	CCA	***– 5`***			

Sequence 5

N –	Ser	His	Ser	**Ser**	**Thr**	**Leu**	**Ser**	**Trp**	**Glu**	**Ser**	**Gly**
5`–	TCT	CAC	TCT	TCG	ACT	CTT	TCT	TGG	GAG	TCT	GGG
3`–	AGA	GTG	AGA	AGC	TGA	GAA	AGA	ACC	CTC	AGA	CCC
	Trp	**Ser**	**Leu**	**Glu**	Gly	Gly	Gly	***– C***			
	TGG	TCG	CTT	GAG	GGT	GGA	GGT	***– 3`***			
	ACC	AGC	GAA	CTC	CCA	CCT	CCA	***– 5`***			

Sequence 6

N –	Ser	His	Ser	**Asn**	**Asp**	**Thr**	**Ser**	**Ser**	**Lys**	**Leu**	**Leu**
5`–	TCT	CAC	TCT	AAT	GAT	ACT	TCG	TCG	AAG	CTG	TTG
3`–	AGA	GTG	AGA	TTA	CTA	TGA	AGC	AGC	TTC	GAC	AAC
	Leu	**Asp**	**Tyr**	**Ser**	Gly	Gly	Gly	***– C***			
	CTG	GAT	TAT	TCG	GGT	GGA	GGT	***– 3`***			
	GAC	CTA	ATA	AGC	CCA	CCT	CCA	***– 5`***			

Sequence 8

N –	Ser	His	Ser	**Ile**	**Val**	**Asp**	**Pro**	**Leu**	**Leu**	**Asn**	**Arg**
5`–	TCT	CAC	TCT	ATT	GTG	GAT	CCT	TTG	TTG	AAT	CGT
3`–	AGA	GTG	AGA	TAA	CAC	CTA	GGA	AAC	AAC	TTA	GCA
	Thr	**Ala**	**Leu**	**Pro**	Gly	Gly	Gly	***– C***			
	ACG	GCT	TTG	CCG	GGT	GGA	GGT	***– 3`***			
	TGC	CGA	AAC	GGC	CCA	CCT	CCA	***– 5`***			

After 1st cycle and amplification (**C1**)

Sequence 1

N –	Ser	His	Ser	**Val**	**Gln**	**Ser**	**Asn**	**Gly**	**Leu**	**Asn**	**Gly**
5`–	TCT	CAC	TCT	GTT	CAG	TCG	AAT	GGT	TTG	AAT	GGT
3`–	AGA	GTG	AGA	CAA	GTC	AGC	TTA	CCA	AAC	TTA	CCA
	Trp	**Pro**	**Leu**	**His**	Gly	Gly	Gly	***– C***			
	TGG	CCG	CTG	CAT	GGT	GGA	GGT	***– 3`***			
	ACC	GGC	GAC	GTA	CCA	CCT	CCA	***– 5`***			

Sequence 2

N –	Ser	His	Ser	**Leu**	**Gln**	**Asn**	**Asp**	**Ala**	**Thr**	**His**	**Gly**
5`–	TCT	CAC	TCT	TTG	CAG	AAT	GAT	GCG	ACT	CAT	GGG
3`–	AGA	GTG	AGA	AAC	GTC	TTA	CTA	CGC	TGA	GTA	CCC
	Ala	**Gly**	**His**	**Arg**	Gly	Gly	Gly	***– C***			
	GCG	GGT	CAT	CGG	GGT	GGA	GGT	***– 3`***			
	CGC	CCA	GTA	GCC	CCA	CCT	CCA	***– 5`***			

Sequence 3

N –	Ser	His	Ser	**Ser**	**Val**	**Asn**	**Tyr**	**Pro**	**Asp**	**Phe**	**Pro**
5`–	TCT	CAC	TCT	TCT	GTG	AAT	TAT	CCT	GAT	TTT	CCT
3`–	AGA	GTG	AGA	AGA	CAC	TTA	ATA	GGA	CTA	AAA	GGA
	Arg	**Trp**	**Met**	**Met**	Gly	Gly	Gly	***– C***			
	CGT	TGG	ATG	ATG	GGT	GGA	GGT	***– 3`***			
	GCA	ACC	TAC	TAC	CCA	CCT	CCA	***– 5`***			

Sequence 4

N –	Ser	His	Ser	**Ser**	**Val**	**Leu**	**Thr**	**Thr**	**Tyr**	**Pro**	**Ile**
5`–	TCT	CAC	TCT	TCT	GTT	CTG	ACG	ACG	TAT	CCG	ATT
3`–	AGA	GTG	AGA	AGA	CAA	GAC	TGC	TGC	ATA	GGC	TAA
	Thr	**Phe**	**Gln**	**Ile**	Gly	Gly	Gly	***– C***			
	ACG	TTT	CAG	ATT	GGT	GGA	GGT	***– 3`***			
	TGC	AAA	GTC	TAA	CCA	CCT	CCA	***– 5`***			

Sequence 5

N –	Ser	His	Ser	**Ala**	**Glu**	**Thr**	**Val**	**Glu**	***– C***
5`–	TCT	CAC	TC**G**	GCC	GAA	ACT	GTT	GAA	***– 3`***
3`–	AGA	GTG	AG**C**	CGG	CTT	TGA	CAA	CTT	***– 5`***

Sequence matches the sequence of the M13KE-phage.

Sequence 6

N –	Ser	His	Ser	**Gly**	**Tyr**	**Thr**	**Tyr**	**Ser**	**Asp**	**Pro**	**Ser**
5`–	TCT	CAC	TCT	GGT	TAT	ACG	TAT	AGT	GAT	CCG	AGT
3`–	AGA	GTG	AGA	CCA	ATA	TGC	ATA	TCA	CTA	GGC	TCA
	Ser	**Pro**	**Pro**	**Lys**	Gly	Gly	Gly	***– C***			
	TCT	CCT	CCT	AAG	GGT	GGA	GGT	***– 3`***			
	AGA	GGA	GGA	TTC	CCA	CCT	CCA	***– 5`***			

Sequence 7

N –	Ser	His	Ser	**Gln**	**Gly**	**Tyr**	**Pro**	**His**	**Tyr**	**Glu**	**Tyr**
5`–	TCT	CAC	TCT	CAG	GGG	TAT	CCT	CAT	TAT	GAG	TAT
3`–	AGA	GTG	AGA	GTC	CCC	ATA	GGA	GTA	ATA	CTC	ATA
	Glu	**Pro**	**Leu**	**Pro**	Gly	Gly	Gly	***– C***			
	GAG	CCT	CTG	CCG	GGT	GGA	GGT	***– 3`***			
	CTC	GGA	GAC	GGC	CCA	CCT	CCA	***– 5`***			

Sequence 8

N –	Ser	His	Ser	**Leu**	**Trp**	**Lys**	**Pro**	**Ser**	**Trp**	**Thr**	**Asn**
5`–	TCT	CAC	TCT	CTG	TGG	AAG	CCG	AGT	TGG	ACT	AAT
3`–	AGA	GTG	AGA	GAC	ACC	TTC	GGC	TCA	ACC	TGA	TTA
	Gln	**Met**	**Pro**	**Thr**	Gly	Gly	Gly	***– C***			
	TAG	ATG	CCT	ACG	GGT	GGA	GGT	***– 3`***			
	ATC	TAC	GGA	TGC	CCA	CCT	CCA	***– 5`***			

Sequence 9

***N* –**	Ser	His	Ser	**Gln**	**Thr**	**Leu**	**Tyr**	**Asn**	**Gly**	**Arg**	**Asp**
***5`* –**	TCT	CAC	TCT	CAG	ACT	CTG	TAT	AAT	GGT	CGT	GAT
***3`* –**	AGA	GTG	AGA	GTC	TGA	GAC	ATA	TTA	CCA	GCA	CTA
	Asp	**Val**	**Met**	**Ala**	Gly	Gly	Gly	***– C***			
	GAT	GTT	ATG	GCG	GGT	GGA	GGT	***– 3`***			
	CTA	CAA	TAC	CGC	CCA	CCT	CCA	***– 5`***			

Sequences identified in the amplified washing step of the 1st cycle (**WSC1**) *

Sequence 1,7

N –	Ser	His	Ser	Ala	Glu	Thr	Val	Glu	*– C*
5` –	TCT	CAC	TC**G**	GCC	GAA	ACT	GTT	GAA	*– 3`*
3` –	AGA	GTG	AG**C**	CGG	CTT	TGA	CAA	CTT	*– 5`*

Sequences match the sequence of the M13KE-phage.

Sequence 2

N –	Ser	His	Ser	**Glu**	**His**	**Asp**	**Ser**	**Leu**	**Gly**	**Asn**	**Asp**
5` –	TCT	CAC	TCT	GAG	CAT	GAT	TCG	CTG	GGT	AAT	GAT
3` –	AGA	GTG	AGA	CTC	GTA	CTA	AGC	GAC	CCA	TTA	CTA
	Thr	**Ile**	**Pro**	**Asn**	Gly	Gly	Gly	*– C*			
	ACT	ATT	CCT	AAT	GGT	GGA	GGT	*– 3`*			
	TGA	TAA	GGA	TTA	CCA	CCT	CCA	*– 5`*			

Sequence 3

N –	Ser	His	Ser	**Ala**	**Asn**	**Arg**	**Pro**	**Asn**	**Ser**	**Asp**	**Ile**
5` –	TCT	CAC	TCT	GCG	AAT	CGT	CCT	AAT	TCG	GAT	ATT
3` –	AGA	GTG	AGA	CGC	TTA	GCA	GGA	TTA	AGC	CTA	TAA
	His	**Met**	**Ser**	**Glu**	**Gly**	Gly	Gly	*– C*			
	CAT	ATG	TCT	GAG	GG**C**	GGA	GGT	*– 3`*			
	GTA	TAC	AGA	CTC	CC**G**	CCT	CCA	*– 5`*			

Possible point mutation T → C, which does not change the amino acid, or a failure/misinterpretation while sequencing.

Sequence 4

N –	Ser	His	Ser	**Asn**	**Leu**	**Gln**	**Ser**	**Gly**	**Ile**	**Val**	**Asn**
5` –	TCT	CAC	TCT	AAT	TTG	TAG	AGT	GGT	ATT	GTT	AAT
3` –	AGA	GTG	AGA	TTA	AAC	ATC	TCA	CCA	TAA	CAA	TTA
	Lys	**Ile**	**Val**	**Val**	Gly	Gly	Gly	*– C*			
	AAG	ATT	GTT	GTG	GGT	GGA	GGT	*– 3`*			
	TTC	TAA	CAA	CAC	CCA	CCT	CCA	*– 5`*			

Sequence 5

N –	Ser	His	Ser	**Ala**	**Met**	**Ile**	**Lys**	**Pro**	**Gln**	**Leu**	**His**
5` –	TCT	CAC	TCT	GCT	ATG	ATT	AAG	CCG	TAG	CTG	CAT
3` –	AGA	GTG	AGA	CGA	TAC	TAA	TTC	GGC	ATC	GAC	GTA
	Ser	**Ala**	**Lys**	**Phe**	Gly	Gly	Gly	*– C*			
	AGT	GCT	AAG	TTT	GGT	GGA	GGT	*– 3`*			
	TCA	CGA	TTC	AAA	CCA	CCT	CCA	*– 5`*			

Sequence 6

N –	Ser	His	Ser	**Asn**	**Ser**	**Ser**	**Leu**	**Thr**	**His**	**Pro**	**Tyr**
5` –	TCT	CAC	TCT	AAT	AGT	AGT	TTG	ACT	CAT	CCG	TAT
3` –	AGA	GTG	AGA	TTA	TCA	TCA	AAC	TGA	GTA	GGC	ATA
	Asn	**Tyr**	**Pro**	**Val**	Gly	Gly	Gly	*– C*			
	AAT	TAT	CCT	GTG	GGT	GGA	GGT	*– 3`*			
	TTA	ATA	GGA	CAC	CCA	CCT	CCA	*– 5`*			

Sequence 8

N –	Ser	His	Ser	**Thr**	**Pro**	**Thr**	**Gln**	**Thr**	**Arg**	**Tyr**	**Asp**
5` –	TCT	CAC	TCT	ACG	CCG	ACT	CAG	ACG	AGG	TAT	GAT
3` –	AGA	GTG	AGA	TGC	GGC	TGA	GTC	TGC	TCC	ATA	CTA
	Gln	**Ser**	**Ser**	**Val**	Gly	Gly	Gly	*– C*			
	CAG	TCG	TCT	GTT	GGT	GGA	GGT	*– 3`*			
	GTC	AGC	AGA	CAA	CCA	CCT	CCA	*– 5`*			

Sequence 9

N –	Ser	His	Ser	**Phe**	**Gly**	**Leu**	**Ser**	**Met**	**Ser**	**Thr**	**Arg**
5` –	TCT	CAC	TCT	TTT	GGT	CTT	TCT	ATG	TCG	ACG	AGG
3` –	AGA	GTG	AGA	AAA	CCA	GAA	AGA	TAC	AGC	TGC	TCC
	Leu	**Thr**	**Lys**	**Val**	Gly	Gly	Gly	*– C*			
	CTG	ACG	AAG	GTT	GGT	GGA	GGT	*– 3`*			
	GAC	TGC	TTC	CAA	CCA	CCT	CCA	*– 5`*			

Sequence 10

N –	Ser	His	Ser	**His**	**Trp**	**Asn**	**Ser**	**Lys**	**Ala**	**Pro**	**Ile**
5` –	TCT	CAC	TCT	CAT	TGG	AAT	TCG	AAG	GCT	CCT	ATT
3` –	AGA	GTG	AGA	GTA	ACC	TTA	AGC	TTC	CGA	GGA	TAA
	Ala	**His**	**Gln**	**Leu**	Gly	Gly	Gly	*– C*			
	GCG	CAT	CAG	CTT	GGT	GGA	GGT	*– 3`*			
	CGC	GTA	GTC	GAA	CCA	CCT	CCA	*– 5`*			

*: The elution with 1M CaCl in TBS preceded the elution with 0.1M EDTA during the first cycle. Hence, the identified sequences in the wash step are the same.

Multiple Sequence Analysis (protocol A, dodecapeptides, $CaCl_2$-elution, all cycles)

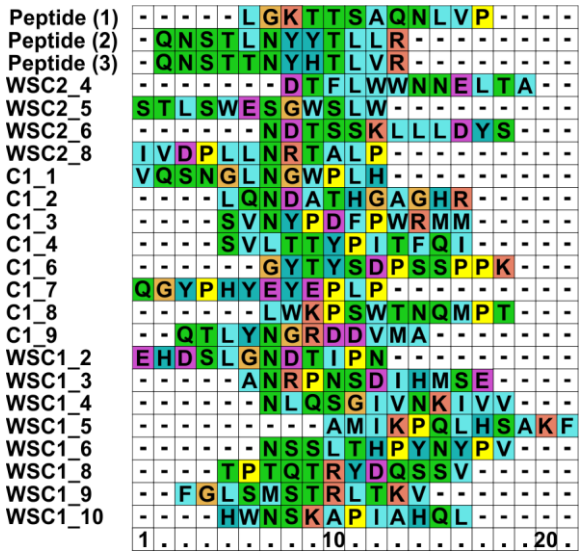

Elution method applying 0.1M EDTA (**E**)

After 3rd cycle of the biopanning (**E3**):

Sequence 1,2,5,7-10,12,15,17-20

***N* –**	Ser	His	Ser	**Gln**	**Asn**	**Ser**	**Thr**	**Leu**	**Asn**	**Tyr**	**Tyr**
***5`* –**	TCT	CAC	TCT	CAG	AAT	TCT	ACT	TTG	AAT	TAT	TAT
***3`* –**	AGA	GTG	AGA	GTC	TTA	AGA	TGA	AAC	TTA	ATA	ATA
	Thr	**Leu**	**Leu**	**Arg**	Gly	Gly	Gly	***– C***			
	ACG	CTT	CTG	CGG	GGT	GGA	GGT	***– 3`***			
	TGC	GAA	GAC	GCC	CCA	CCT	CCA	***– 5`***			

Sequence 3,4,6,11,13,14

***N* –**	Ser	His	Ser	**Leu**	**Gly**	**Lys**	**Thr**	**Thr**	**Ser**	**Ala**	**Gln**
***5`* –**	TCT	CAC	TCT	CTG	GGT	AAG	ACT	ACT	TCT	GCG	CAG
***3`* –**	AGA	GTG	AGA	GAC	CCA	TTC	TGA	TGA	AGA	CGC	GTC
	Asn	**Leu**	**Val**	**Pro**	Gly	Gly	Gly	***– C***			
	AAT	TTG	GTG	CCG	GGT	GGA	GGT	***– 3`***			
	TTA	AAC	CAC	GGC	CCA	CCT	CCA	***– 5`***			

Sequence 16

Insertion of a nucleotide.

After 2nd cycle and amplification (**E2**)

Sequence 1,2,4,5,7,8,9,10

***N* –**	Ser	His	Ser	**Gln**	**Asn**	**Ser**	**Thr**	**Leu**	**Asn**	**Tyr**	**Tyr**
***5`* –**	TCT	CAC	TCT	CAG	AAT	TCT	ACT	TTG	AAT	TAT	TAT
***3`* –**	AGA	GTG	AGA	GTC	TTA	AGA	TGA	AAC	TTA	ATA	ATA
	Thr	**Leu**	**Leu**	**Arg**	Gly	Gly	Gly	***– C***			
	ACG	CTT	CTG	CGG	GGT	GGA	GGT	***– 3`***			
	TGC	GAA	GAC	GCC	CCA	CCT	CCA	***– 5`***			

Sequence 3,6

***N* –**	Ser	His	Ser	**Leu**	**Gly**	**Lys**	**Thr**	**Thr**	**Ser**	**Ala**	**Gln**
***5`* –**	TCT	CAC	TCT	CTG	GGT	AAG	ACT	ACT	TCT	GCG	CAG
***3`* –**	AGA	GTG	AGA	GAC	CCA	TTC	TGA	TGA	AGA	CGC	GTC
	Asn	**Leu**	**Val**	**Pro**	Gly	Gly	Gly	***– C***			
	AAT	TTG	GTG	CCG	GGT	GGA	GGT	***– 3`***			
	TTA	AAC	CAC	GGC	CCA	CCT	CCA	***– 5`***			

Sequences identified in the amplified washing step of the 2nd cycle (**WSE2**)

Sequence 1

***N* –**	Ser	His	Ser	**Gly**	**Leu**	**Gly**	**Asn**	**Ile**	**Trp**	**Pro**	**Gly**
***5`* –**	TCT	CAC	TCT	GGG	CTG	GGG	AAT	ATT	TGG	CCT	GGG
***3`* –**	AGA	GTG	AGA	CCC	GAC	CCC	TTA	TAA	ACC	GGA	CCC
	Met	**Pro**	**Ile**	**Asn**	Gly	Gly	Gly	***– C***			
	ATG	CCT	ATT	AAT	GGT	GGA	GGT	***– 3`***			
	TAC	GGA	TAA	TTA	CCA	CCT	CCA	***– 5`***			

Sequences 2,8

***N* –**	Ser	His	Ser	**Gln**	**Asn**	**Ser**	**Thr**	**Leu**	**Asn**	**Tyr**	**Tyr**
***5`* –**	TCT	CAC	TCT	CAG	AAT	TCT	ACT	TTG	AAT	TAT	TAT
***3`* –**	AGA	GTG	AGA	GTC	TTA	AGA	TGA	AAC	TTA	ATA	ATA

	Thr	**Leu**	**Leu**	**Arg**	Gly	Gly	Gly	***– C***			
	ACG	CTT	CTG	CGG	GGT	GGA	GGT	***– 3`***			
	TGC	GAA	GAC	GCC	CCA	CCT	CCA	***– 5`***			

Sequence 3

N –	Ser	His	Ser	**Ala**	**Lys**	**Met**	**Ser**	**Glu**	**Ser**	**Ser**	**Phe**
5`–	TCT	CAC	TCT	GCG	AAG	ATG	TCT	GAG	AGT	TCT	TTT
3`–	AGA	GTG	AGA	CGC	TTC	TAC	AGA	CTC	TCA	AGA	AAA
	Asn	**Leu**	**Ala**	**Ala**	Gly	Gly	Gly	***– C***			
	AAT	CTT	GCT	GCG	GGT	GGA	GGT	***– 3`***			
	TTA	GAA	CGA	CGC	CCA	CCT	CCA	***– 5`***			

Sequence 4

N –	Ser	His	Ser	**Leu**	**Asp**	**Met**	**Asp**	**Ser**	**Leu**	**Ser**	**Pro**
5`–	TCT	CAC	TCT	TTG	GAT	ATG	GAT	TCG	CTT	TCT	CCG
3`–	AGA	GTG	AGA	AAC	CTA	TAC	CTA	AGC	GAA	AGA	GGC
	Asp	**Asn**	**Glu**	**Asn**	Gly	Gly	Gly	***– C***			
	GAT	AAT	GAG	AAT	GGT	GGA	GGT	***– 3`***			
	CTA	TTA	CTC	TTA	CCA	CCT	CCA	***– 5`***			

Sequence 5

N –	Ser	His	Ser	**Val**	**Pro**	**Asn**	**Thr**	**Thr**	**Pro**	**Trp**	**Trp**
5`–	TCT	CAC	TCT	GTG	CCG	AAT	ACG	ACT	CCT	TGG	TGG
3`–	AGA	GTG	AGA	CAC	GGC	TTA	TGC	TGA	GGA	ACC	ACC
	Lys	**Tyr**	**Ser**	**Arg**	Gly	Gly	Gly	***– C***			
	AAG	TAT	AGT	CGG	GGT	GGA	GGT	***– 3`***			
	TTC	ATA	TCA	GCC	CCA	CCT	CCA	***– 5`***			

Sequence 6

N –	Ser	His	Ser	**Ala**	**Gln**	**Ser**	**His**	**Lys**	**His**	**Arg**	**Leu**
5`–	TCT	CAC	TCT	GCT	CAG	TCG	CAT	AAG	CAT	AGG	CTG
3`–	AGA	GTG	AGA	CGA	GTC	AGC	GTA	TTC	GTA	TCC	GAC
	Thr	**Glu**	**Ala**	**Ile**	Gly	Gly	Gly	***– C***			
	ACG	GAG	GCT	ATT	GGT	GGA	GGT	***– 3`***			
	TGC	CTC	CGA	TAA	CCA	CCT	CCA	***– 5`***			

Sequence 7

N –	Ser	His	Ser	**Phe**	**Pro**	**Pro**	**Tyr**	**Gly**	**Trp**	**Val**	**Gln**
5`–	TCT	CAC	TCT	TTT	CCG	CCT	TAT	GGG	TGG	GTT	TAG
3`–	AGA	GTG	AGA	AAA	GGC	GGA	ATA	CCC	ACC	CAA	ATC
	Thr	**Arg**	**Ala**	**Asn**	Gly	Gly	Gly	***– C***			
	ACT	CGT	GCT	AAT	GGT	GGA	GGT	***– 3`***			
	TGA	GCA	CGA	TTA	CCA	CCT	CCA	***– 5`***			

After 1st cycle and amplification (**E1**)

Sequence 1

N –	Ser	His	Ser	**Val**	**Asp**	**Arg**	**Asp**	**Val**	**Ile**	**Leu**	**Gly**
5`–	TCT	CAC	TCT	GTG	GAT	CGT	GAT	GTG	ATT	CTG	GGT
3`–	AGA	GTG	AGA	CAC	CTA	GCA	CTA	CAC	TAA	GAC	CCA
	Arg	**Tyr**	**Thr**	**Val**	Gly	Gly	Gly	***– C***			
	CGG	TAT	ACG	GTG	GGT	GGA	GGT	***– 3`***			
	GCC	ATA	TGC	CAC	CCA	CCT	CCA	***– 5`***			

Sequence 2

N –	Ser	His	Ser	**Ser**	**Asn**	**Gly**	**Tyr**	**Glu**	**Ser**	**Asn**	**Lys**
5`–	TCT	CAC	TCT	AGT	AAT	GGG	TAT	GAG	TCT	AAT	AAG
3`–	AGA	GTG	AGA	TCA	TTA	CCC	ATA	CTC	AGA	TTA	TTC
	Met	**Asn**	**Arg**	**Phe**	Gly	Gly	Gly	***– C***			
	ATG	AAT	AGG	TTT	GGT	GGA	GGT	***– 3`***			
	TAC	TTA	TCC	AAA	CCA	CCT	CCA	***– 5`***			

Sequence 3

N –	Ser	His	Ser	**Thr**	**His**	**Ser**	**Ile**	**Ala**	**Thr**	**Lys**	**Leu**
5`–	TCT	CAC	TCT	ACT	CAT	TCG	ATT	GCG	ACT	AAG	CTT
3`–	AGA	GTG	AGA	TGA	GTA	AGC	TAA	CGC	TGA	TTC	GAA
	Lys	**Pro**	**Asn**	**Thr**	Gly	Gly	Gly	***– C***			
	AAG	CCG	AAT	ACG	GGT	GGA	GGT	***– 3`***			
	TTC	GGC	TTA	TGC	CCA	CCT	CCA	***– 5`***			

Sequence 4

N –	Ser	His	Ser	**Gln**	**Ser**	**Leu**	**Lys**	**Asn**	**Thr**	**Gly**	**Ala**
5`–	TCT	CAC	TCT	CAG	TCT	TTG	AAG	AAT	ACG	GGT	GCG
3`–	AGA	GTG	AGA	GTC	AGA	AAC	TTC	TTA	TGC	CCA	CGC
	Pro	**Ile**	**Leu**	**Pro**	Gly	Gly	Gly	***– C***			
	CCG	ATT	CTT	CCT	GGT	GGA	GGT	***– 3`***			
	GGC	TAA	GAA	GGA	CCA	CCT	CCA	***– 5`***			

Sequences 5,9

N –	Ser	His	Ser	Ala	Glu	Thr	Val	Glu	***– C***
5`–	TCT	CAC	TC**G**	GCC	GAA	ACT	GTT	GAA	***– 3`***
3`–	AGA	GTG	AG**C**	CGG	CTT	TGA	CAA	CTT	***– 5`***

Sequences match the sequence of the M13KE-phage.

Sequence 6

N –	Ser	His	Ser	**Thr**	**Thr**	**Leu**	**Ile**	**Asn**	**Pro**	**Ile**	**Arg**
5`–	TCT	CAC	TCT	ACG	ACG	CTG	ATT	AAT	CCG	ATT	CGT
3`–	AGA	GTG	AGA	TGC	TGC	GAC	TAA	TTA	GGC	TAA	GCA
	Ser	**Asp**	**Trp**	**Lys**	Gly	Gly	Gly	***– C***			
	AGT	GAT	TGG	AAG	GGT	GGA	GGT	***– 3`***			
	TCA	CTA	ACC	TTC	CCA	CCT	CCA	***– 5`***			

Sequence 7

***N* –**	Ser	His	Ser	**Ser**	**Val**	**Tyr**	**Gln**	**Leu**	**Ala**	**His**	**Val**
***5`* –**	TCT	CAC	TCT	TCT	GTT	TAT	TAG	CTG	GCT	CAT	GTG
***3`* –**	AGA	GTG	AGA	AGA	CAA	ATA	ATC	GAC	CGA	GTA	CAC
	Ser	**Ser**	**Ile**	**Pro**	Gly	Gly	Gly	***– C***			
	TCT	TCG	ATT	CCT	GGT	GGA	GGT	***– 3`***			
	AGA	AGC	TAA	GGA	CCA	CCT	CCA	***– 5`***			

Sequence 8

***N* –**	Ser	His	Ser	**Ser**	**Asn**	**Ser**	**Leu**	**Arg**	**Asn**	**Ser**	**Glu**
***5`* –**	TCT	CAC	TCT	AGT	AAT	TCG	TTG	CGT	AAT	TCG	GAG
***3`* –**	AGA	GTG	AGA	TCA	TTA	AGC	AAC	GCA	TTA	AGC	CTC
	Trp	**Met**	**Met**	**Leu**	Gly	Gly	Gly	***– C***			
	TGG	ATG	ATG	CTT	GGT	GGA	GGT	***– 3`***			
	ACC	TAC	TAC	GAA	CCA	CCT	CCA	***– 5`***			

Sequence 10

***N* –**	Ser	His	Ser	**Met**	**Ile**	**Pro**	**Ser**	**Pro**	**Tyr**	**Lys**	**Ser**
***5`* –**	TCT	CAC	TCT	ATG	ATT	CCT	TCG	CCT	TAT	AAG	AGT
***3`* –**	AGA	GTG	AGA	TAC	TAA	GGA	AGC	GGA	ATA	TTC	TCA
	Ser	**Val**	**Gln**	**Thr**	Gly	Gly	Gly	***– C***			
	TCG	GTT	CAG	ACG	GGT	GGA	GGT	***– 3`***			
	AGC	CAA	GTC	TGC	CCA	CCT	CCA	***– 5`***			

Sequences identified in the amplified washing step of the 1st cycle (**WSE1**) *

Sequences 1,7

N –	Ser	His	Ser	Ala	Glu	Thr	Val	Glu	*– C*
5` –	TCT	CAC	TC**G**	GCC	GAA	ACT	GTT	GAA	*– 3`*
3` –	AGA	GTG	AG**C**	CGG	CTT	TGA	CAA	CTT	*– 5`*

Sequences match the sequence of the M13KE-phage.

Sequence 2

N –	Ser	His	Ser	**Glu**	**His**	**Asp**	**Ser**	**Leu**	**Gly**	**Asn**	**Asp**
5` –	TCT	CAC	TCT	GAG	CAT	GAT	TCG	CTG	GGT	AAT	GAT
3` –	AGA	GTG	AGA	CTC	GTA	CTA	AGC	GAC	CCA	TTA	CTA
	Thr	**Ile**	**Pro**	**Asn**	Gly	Gly	Gly	*– C*			
	ACT	ATT	CCT	AAT	GGT	GGA	GGT	*– 3`*			
	TGA	TAA	GGA	TTA	CCA	CCT	CCA	*– 5`*			

Sequence 3

N –	Ser	His	Ser	**Ala**	**Asn**	**Arg**	**Pro**	**Asn**	**Ser**	**Asp**	**Ile**
5` –	TCT	CAC	TCT	GCG	AAT	CGT	CCT	AAT	TCG	GAT	ATT
3` –	AGA	GTG	AGA	CGC	TTA	GCA	GGA	TTA	AGC	CTA	TAA
	His	**Met**	**Ser**	**Glu**	Gly	Gly	Gly	*– C*			
	CAT	ATG	TCT	GAG	GG**C**	GGA	GGT	*– 3`*			
	GTA	TAC	AGA	CTC	CC**G**	CCT	CCA	*– 5`*			

Possible point mutation T → C, not changing the amino acid or a failure/misinterpretation while sequencing.

Sequence 4

N –	Ser	His	Ser	**Asn**	**Leu**	**Gln**	**Ser**	**Gly**	**Ile**	**Val**	**Asn**
5` –	TCT	CAC	TCT	AAT	TTG	TAG	AGT	GGT	ATT	GTT	AAT
3` –	AGA	GTG	AGA	TTA	AAC	ATC	TCA	CCA	TAA	CAA	TTA
	Lys	**Ile**	**Val**	**Val**	Gly	Gly	Gly	*– C*			
	AAG	ATT	GTT	GTG	GGT	GGA	GGT	*– 3`*			
	TTC	TAA	CAA	CAC	CCA	CCT	CCA	*– 5`*			

Sequence 5

N –	Ser	His	Ser	**Ala**	**Met**	**Ile**	**Lys**	**Pro**	**Gln**	**Leu**	**His**
5` –	TCT	CAC	TCT	GCT	ATG	ATT	AAG	CCG	TAG	CTG	CAT
3` –	AGA	GTG	AGA	CGA	TAC	TAA	TTC	GGC	ATC	GAC	GTA
	Ser	**Ala**	**Lys**	**Phe**	Gly	Gly	Gly	*– C*			
	AGT	GCT	AAG	TTT	GGT	GGA	GGT	*– 3`*			
	TCA	CGA	TTC	AAA	CCA	CCT	CCA	*– 5`*			

Sequence 6

N –	Ser	His	Ser	**Asn**	**Ser**	**Ser**	**Leu**	**Thr**	**His**	**Pro**	**Tyr**
5` –	TCT	CAC	TCT	AAT	AGT	AGT	TTG	ACT	CAT	CCG	TAT
3` –	AGA	GTG	AGA	TTA	TCA	TCA	AAC	TGA	GTA	GGC	ATA
	Asn	**Tyr**	**Pro**	**Val**	Gly	Gly	Gly	*– C*			
	AAT	TAT	CCT	GTG	GGT	GGA	GGT	*– 3`*			
	TTA	ATA	GGA	CAC	CCA	CCT	CCA	*– 5`*			

Sequence 8

N –	Ser	His	Ser	**Thr**	**Pro**	**Thr**	**Gln**	**Thr**	**Arg**	**Tyr**	**Asp**
5` –	TCT	CAC	TCT	ACG	CCG	ACT	CAG	ACG	AGG	TAT	GAT
3` –	AGA	GTG	AGA	TGC	GGC	TGA	GTC	TGC	TCC	ATA	CTA
	Gln	**Ser**	**Ser**	**Val**	Gly	Gly	Gly	*– C*			
	CAG	TCG	TCT	GTT	GGT	GGA	GGT	*– 3`*			
	GTC	AGC	AGA	CAA	CCA	CCT	CCA	*– 5`*			

Sequence 9

N –	Ser	His	Ser	**Phe**	**Gly**	**Leu**	**Ser**	**Met**	**Ser**	**Thr**	**Arg**
5` –	TCT	CAC	TCT	TTT	GGT	CTT	TCT	ATG	TCG	ACG	AGG
3` –	AGA	GTG	AGA	AAA	CCA	GAA	AGA	TAC	AGC	TGC	TCC
	Leu	**Thr**	**Lys**	**Val**	Gly	Gly	Gly	*– C*			
	CTG	ACG	AAG	GTT	GGT	GGA	GGT	*– 3`*			
	GAC	TGC	TTC	CAA	CCA	CCT	CCA	*– 5`*			

*: The elution with 1M CaCl in TBS preceded the elution with 0.1M EDTA during the first cycle. Hence, the identified sequences in the wash step are the same.

Sequence 10

N –	Ser	His	Ser	**His**	**Trp**	**Asn**	**Ser**	**Lys**	**Ala**	**Pro**	**Ile**
5` –	TCT	CAC	TCT	CAT	TGG	AAT	TCG	AAG	GCT	CCT	ATT
3` –	AGA	GTG	AGA	GTA	ACC	TTA	AGC	TTC	CGA	GGA	TAA
	Ala	**His**	**Gln**	**Leu**	Gly	Gly	Gly	*– C*			
	GCG	CAT	CAG	CTT	GGT	GGA	GGT	*– 3`*			
	CGC	GTA	GTC	GAA	CCA	CCT	CCA	*– 5`*			

Multiple Sequence Analysis (protocol A, dodecapeptides, EDTA-elution, all cycles)

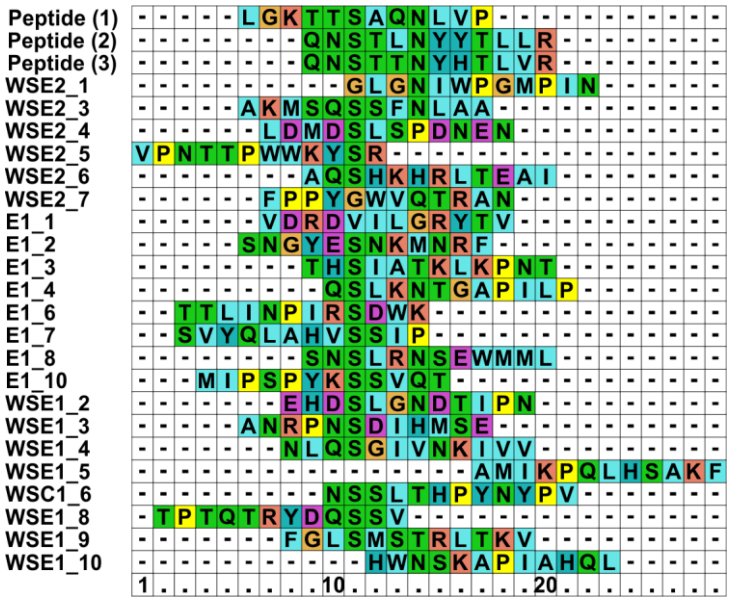

Elution method applying 0.1M NaAc (**N**)

After third cycle of biopanning (**N3**):

Sequence 1-3,5,9-11,13-17,19

N **–**	Ser	His	Ser	**Gln**	**Asn**	**Ser**	**Thr**	**Leu**	**Asn**	**Tyr**	**Tyr**
5` **–**	TCT	CAC	TCT	CAG	AAT	TCT	ACT	TTG	AAT	TAT	TAT
3` **–**	AGA	GTG	AGA	GTC	TTA	AGA	TGA	AAC	TTA	ATA	ATA
	Thr	**Leu**	**Leu**	**Arg**	Gly	Gly	Gly	***– C***			
	ACG	CTT	CTG	CGG	GGT	GGA	GGT	***– 3`***			
	TGC	GAA	GAC	GCC	CCA	CCT	CCA	***– 5`***			

Sequence 4,6-8,12,18,20

N **–**	Ser	His	Ser	**Leu**	**Gly**	**Lys**	**Thr**	**Thr**	**Ser**	**Ala**	**Gln**
5` **–**	TCT	CAC	TCT	CTG	GGT	AAG	ACT	ACT	TCT	GCG	CAG
3` **–**	AGA	GTG	AGA	GAC	CCA	TTC	TGA	TGA	AGA	CGC	GTC
	Asn	**Leu**	**Val**	**Pro**	Gly	Gly	Gly	***– C***			
	AAT	TTG	GTG	CCG	GGT	GGA	GGT	***– 3`***			
	TTA	AAC	CAC	GGC	CCA	CCT	CCA	***– 5`***			

After 2nd cycle and amplification (**N2**)

Sequences 1,2,3,5,6,8,9

N **–**	Ser	His	Ser	**Gln**	**Asn**	**Ser**	**Thr**	**Leu**	**Asn**	**Tyr**	**Tyr**
5` **–**	TCT	CAC	TCT	CAG	AAT	TCT	ACT	TTG	AAT	TAT	TAT
3` **–**	AGA	GTG	AGA	GTC	TTA	AGA	TGA	AAC	TTA	ATA	ATA
	Thr	**Leu**	**Leu**	**Arg**	Gly	Gly	Gly	***– C***			
	ACG	CTT	CTG	CGG	GGT	GGA	GGT	***– 3`***			
	TGC	GAA	GAC	GCC	CCA	CCT	CCA	***– 5`***			

Sequences 4,7,10

N **–**	Ser	His	Ser	**Leu**	**Gly**	**Lys**	**Thr**	**Thr**	**Ser**	**Ala**	**Gln**
5` **–**	TCT	CAC	TCT	CTG	GGT	AAG	ACT	ACT	TCT	GCG	CAG
3` **–**	AGA	GTG	AGA	GAC	CCA	TTC	TGA	TGA	AGA	CGC	GTC
	Asn	**Leu**	**Val**	**Pro**	Gly	Gly	Gly	***– C***			
	AAT	TTG	GTG	CCG	GGT	GGA	GGT	***– 3`***			
	TTA	AAC	CAC	GGC	CCA	CCT	CCA	***– 5`***			

Sequences identified in the amplified washing step of the 2nd cycle (**WSN2**)

Sequence 1

Insertion of a nucleotide.

Sequence 2

***N* –**	Ser	His	Ser	**Ile**	**Leu**	**Pro**	**Pro**	**Asp**	**Ile**	**Tyr**	**Glu**
***5`* –**	TCT	CAC	TCT	ATT	CTT	CCG	CCG	GAT	ATT	TAT	GAG
***3`* –**	AGA	GTG	AGA	TAA	GAA	GGC	GGC	CTA	TAA	ATA	CTC
	Arg	**Ala**	**Asp**	**Met**	Gly	Gly	Gly	***– C***			
	AGG	GCG	GAT	ATG	GGT	GGA	GGT	***– 3`***			
	TCC	CGC	CTA	TAC	CCA	CCT	CCA	***– 5`***			

Sequence 3

***N* –**	Ser	His	Ser	**Ile**	**Tyr**	**Ala**	**Ala**	**Pro**	**Pro**	**Trp**	**Ala**
***5`* –**	TCT	CAC	TCT	ATT	TAT	GCT	GCG	CCT	CCT	TGG	GCG
***3`* –**	AGA	GTG	AGA	TAA	ATA	CGA	CGC	GGA	GGA	ACC	CGC
	Leu	**Ser**	**Val**	**Leu**	Gly	Gly	Gly	***– C***			
	TTG	TCT	GTG	CTG	GGT	GGA	GGT	***– 3`***			
	AAC	AGA	CAC	GAC	CCA	CCT	CCA	***– 5`***			

Sequence 4

***N* –**	Ser	His	Ser	**His**	**Leu**	**His**	**Ala**	**Asn**	**Pro**	**Ala**	**Lys**
***5`* –**	TCT	CAC	TCT	CAT	CTT	CAT	GCG	AAT	CCT	GCG	AAG
***3`* –**	AGA	GTG	AGA	GTA	GAA	GTA	CGC	TTA	GGA	CGC	TTC
	Lys	**His**	**Phe**	**Ala**	Gly	Gly	Gly	***– C***			
	AAG	CAT	TTT	GCG	GGT	GGA	GGT	***– 3`***			
	TTC	GTA	AAA	CGC	CCA	CCT	CCA	***– 5`***			

Sequence 5

***N* –**	Ser	His	Ser	**Val**	**Asn**	**Arg**	**Gly**	**Ser**	**His**	**Pro**	**Pro**
***5`* –**	TCT	CAC	TCT	GTG	AAT	GCT	GGG	TCG	CAT	CCG	CCG
***3`* –**	AGA	GTG	AGA	CAC	TTA	CGA	CCC	AGC	GTA	GGC	GGC
	Asp	**Ser**	**Ala**	**Met**	Gly	Gly	Gly	***– C***			
	GAT	TCT	GCG	ATG	GGT	GGA	GGT	***– 3`***			
	CTA	AGA	CGC	TAC	CCA	CCT	CCA	***– 5`***			

Sequence 6

***N* –**	Ser	His	Ser	**Leu**	**Thr**	**Asp**	**Val**	**Asn**	**Lys**	**Thr**	**Gly**
***5`* –**	TCT	CAC	TCT	CTG	ACT	GAT	GTT	AAT	AAG	ACG	GGG
***3`* –**	AGA	GTG	AGA	GAC	TGA	CTA	CAA	TTA	TTC	TGC	CCC
	Phe	**Thr**	**Leu**	**Val**	Gly	Gly	Gly	***– C***			
	TTT	ACT	CTT	GTG	GGT	GGA	GGT	***– 3`***			
	AAA	TGA	GAA	CAC	CCA	CCT	CCA	***– 5`***			

Sequence 7

Insertion of a nucleotide.

Sequence 8

***N* –**	Ser	His	Ser	**Val**	**Ser**	**Ala**	**Ser**	**Phe**	**Leu**	**Thr**	**Pro**
***5`* –**	TCT	CAC	TCT	GTG	TCG	GCG	TCG	TTT	CTG	ACT	CCG
***3`* –**	AGA	GTG	AGA	CAC	AGC	CGC	AGC	AAA	GAC	TGA	GGC
	Tyr	**Lys**	**Ser**	**Val**	Gly	Gly	Gly	***– C***			
	TAT	AAG	TCT	GTG	GGT	GGA	GGT	***– 3`***			
	ATA	TTC	AGA	CAC	CCA	CCT	CCA	***– 5`***			

Sequence 9

***N* –**	Ser	His	Ser	**Asn**	**Leu**	**Asn**	**His**	**Met**	**Tyr**	**Pro**	**Glu**
***5`* –**	TCT	CAC	TCT	AAT	TTG	AAT	CAT	ATG	TAT	CCG	GAG
***3`* –**	AGA	GTG	AGA	TTA	AAC	TTA	GTA	TAC	ATA	GGC	CTC
	Ala	**Pro**	**His**	**His**	Gly	Gly	Gly	***– C***			
	GCT	CCT	CAT	CAT	GGT	GGA	GGT	***– 3`***			
	CGA	GGA	GTA	GTA	CCA	CCT	CCA	***– 5`***			

After 1st cycle and amplification (**N1**)

Sequence 1

***N* –**	Ser	His	Ser	**Val**	**Ala**	**Gln**	**Thr**	**Ala**	**Val**	**His**	**Gly**
***5`* –**	TCT	CAC	TCT	GTG	GCG	CAG	ACT	GCG	GTT	CAT	GGT
***3`* –**	AGA	GTG	AGA	CAC	CGC	GTC	TGA	CGC	CAA	GTA	CCA
	Val	**Met**	**Gln**	**Lys**	Gly	Gly	Gly	***– C***			
	GTG	ATG	CAG	AAG	GGT	GGA	GGT	***– 3`***			
	CAC	TAC	GTC	TTC	CCA	CCT	CCA	***– 5`***			

Sequence 2

***N* –**	Ser	His	Ser	**Asn**	**Lys**	**His**	**Trp**	**Ser**	**Thr**	**Ser**	**Asn**
***5`* –**	TCT	CAC	TCT	AAT	AAG	CAT	TGG	TCT	ACT	TCT	AAT
***3`* –**	AGA	GTG	AGA	TTA	TTC	GTA	ACC	AGA	TGA	AGA	TTA
	Ser	**Thr**	**Leu**	**Asn**	Gly	Gly	Gly	***– C***			
	TCT	ACG	CTG	AAT	GGT	GGA	GGT	***– 3`***			
	AGA	TGC	GAC	TTA	CCA	CCT	CCA	***– 5`***			

Sequence 3

***N* –**	Ser	His	Ser	**Leu**	**Asn**	**Leu**	**Ser**	**Thr**	**His**	**Arg**	**His**
***5`* –**	TCT	CAC	TCT	TTG	AAT	CTT	TCT	ACT	CAT	AGG	CAT
***3`* –**	AGA	GTG	AGA	AAC	TTA	GAA	AGA	TGA	GTA	TCC	GTA
	Ser	**Val**	**Asn**	**Ala**	Gly	Gly	Gly	***– C***			
	TCT	GTT	AAT	GCG	GGT	GGA	GGT	***– 3`***			
	AGA	CAA	TTA	CGC	CCA	CCT	CCA	***– 5`***			

Sequence 4

***N* –**	Ser	His	Ser	**Thr**	**Gly**	**Thr**	**Leu**	**Asn**	**Thr**	**Thr**	**Ser**
***5`* –**	TCT	CAC	TCT	ACT	GGG	ACG	CTT	AAT	ACG	ACT	TCT
***3`* –**	AGA	GTG	AGA	TGA	CCC	TGC	GAA	TTA	TGC	TGA	AGA
	Thr	**Gln**	**Pro**	**Arg**	Gly	Gly	Gly	***– C***			
	ACT	CAG	CCT	AGG	GGT	GGA	GGT	***– 3`***			
	TGA	GTC	GGA	TCC	CCA	CCT	CCA	***– 5`***			

Sequence 5

***N* –**	Ser	His	Ser	**Lys**	**Leu**	**Pro**	**Gln**	**Thr**	**Thr**	**Pro**	**Tyr**
***5`* –**	TCT	CAC	TCT	AAG	CTG	CCT	CAG	ACG	ACG	CCT	TAT
***3`* –**	AGA	GTG	AGA	TTC	GAC	GGA	GTC	TGC	TGC	GGA	ATA
	Asn	**Ser**	**Leu**	**Gln**	Gly	Gly	Gly	***– C***			
	AAT	TCG	TTG	CAG	GGT	GGA	GGT	***– 3`***			
	TTA	AGC	AAC	GTC	CCA	CCT	CCA	***– 5`***			

Sequence 6

***N* –**	Ser	His	Ser	**Asp**	**Val**	**Thr**	**Leu**	**Arg**	**Asn**	**Ser**	**Pro**
***5`* –**	TCT	CAC	TCT	GAT	GTG	ACT	CTG	CGT	AAT	AGT	CCT
***3`* –**	AGA	GTG	AGA	CTA	CAC	TGA	GAC	GCA	TTA	TCA	GGA
	Leu	**Thr**	**Arg**	**His**	Gly	Gly	Gly	***– C***			
	TTG	ACG	CGG	CAT	GGT	GGA	GGT	***– 3`***			
	AAC	TGC	GCC	GTA	CCA	CCT	CCA	***– 5`***			

Sequence 7

***N* –**	Ser	His	Ser	**Ser**	**Val**	**Pro**	**Leu**	**Arg**	**His**	**Gly**	**Leu**
***5`* –**	TCT	CAC	TCT	TCG	GTT	CCG	TTG	AGG	CAT	GGG	CTT
***3`* –**	AGA	GTG	AGA	AGC	CAA	GGC	AAC	TCC	GTA	CCC	GAA
	Ser	**Trp**	**Asn**	**Ser**	Gly	Gly	Gly	***– C***			
	AGT	TGG	AAT	TCG	GGT	GGA	GGT	***– 3`***			
	TCA	ACC	TTA	AGC	CCA	CCT	CCA	***– 5`***			

Sequences identified in the amplified washing step of the 1st cycle (**WSN1**)

Sequence 1

***N* –**	Ser	His	Ser	**Met**	**Ile**	**Gly**	**Phe**	**Gly**	**Ala**	**Arg**	**Asn**
***5`* –**	TCT	CAC	TCT	ATG	ATT	GGG	TTT	GGG	GCG	CGG	AAT
***3`* –**	AGA	GTG	AGA	TAC	TAA	CCC	AAA	CCC	CGC	GCC	TTA
	Val	**Ser**	**Asn**	**His**	Gly	Gly	Gly	***– C***			
	GTG	TCG	AAT	CAT	GGT	GGA	GGT	***– 3`***			
	CAC	AGC	TTA	GTA	CCA	CCT	CCA	***– 5`***			

Sequence 2

***N* –**	Ser	His	Ser	Ala	Glu	Thr	Val	Glu	***– C***
***5`* –**	TCT	CAC	TC**G**	GCC	GAA	ACT	GTT	GAA	***– 3`***
***3`* –**	AGA	GTG	AG**C**	CGG	CTT	TGA	CAA	CTT	***– 5`***

Sequenc matches the sequence of the M13KE-phage.

Sequence 3

***N* –**	Ser	His	Ser	**Leu**	**Thr**	**Glu**	**Pro**	**Leu**	**Thr**	**Ser**	**Arg**
***5`* –**	TCT	CAC	TCT	TTG	ACT	GAG	CCT	TTG	ACG	TCG	CGG
***3`* –**	AGA	GTG	AGA	AAC	TGA	CTC	GGA	AAC	TGC	AGC	GCC
	Leu	**Ser**	**Glu**	**Gln**	Gly	Gly	Gly	***– C***			
	CTG	TCT	GAG	CAG	GGT	GGA	GGT	***– 3`***			
	GAC	AGA	CTC	GTC	CCA	CCT	CCA	***– 5`***			

Sequence 4

***N* –**	Ser	His	Ser	**Gly**	**Trp**	**Ile**	**Pro**	**Gln**	**Leu**	**Ala**	**Gly**
***5`* –**	TCT	CAC	TCT	GGG	TGG	ATT	CCG	TAG	CTT	GCG	GGT
***3`* –**	AGA	GTG	AGA	CCC	ACC	TAA	GGC	ATC	GAA	CGC	CCA
	Lys	**His**	**Pro**	**Leu**	Gly	Gly	Gly	***– C***			
	AAG	CAT	CCG	TTG	GGT	GGA	GGT	***– 3`***			
	TTC	GTA	GGC	AAC	CCA	CCT	CCA	***– 5`***			

Sequence 5

Deletion of a nucleotide.

Sequence 6

***N* –**	Ser	His	Ser	**Leu**	**Gly**	**Asn**	**Tyr**	**Pro**	**Tyr**	**Lys**	**Ser**
***5`* –**	TCT	CAC	TCT	CTG	GGG	AAT	TAT	CCG	TAT	AAG	AGT
***3`* –**	AGA	GTG	AGA	GAC	CCC	TTA	ATA	GGC	ATA	TTC	TCA
	Ile	**Leu**	**Thr**	**Gln**	Gly	Gly	Gly	***– C***			
	ATT	TTG	ACT	TAG	GGT	GGA	GGT	***– 3`***			
	TAA	AAC	TGA	ATC	CCA	CCT	CCA	***– 5`***			

Sequence 7

***N* –**	Ser	His	Ser	**Ser**	**Met**	**Ala**	**Ser**	**Arg**	**Met**	**Thr**	**Gln**
***5`* –**	TCT	CAC	TCT	TCG	ATG	GCG	AGT	CGG	ATG	ACG	TAG
***3`* –**	AGA	GTG	AGA	AGC	TAC	CGC	TCA	GCC	TAC	TGC	ATC
	Ala	**Ile**	**Gln**	**Pro**	Gly	Gly	Gly	***– C***			
	GCT	ATT	CAG	CCT	GGT	GGA	GGT	***– 3`***			
	CGA	TAA	GTC	GGA	CCA	CCT	CCA	***– 5`***			

Sequence 8

***N* –**	Ser	His	Ser	**Ala**	**Val**	**Leu**	**Thr**	**Asn**	**Pro**	**Pro**	**Gln**
***5`* –**	TCT	CAC	TCT	GCT	GTG	CTT	ACG	AAT	CCT	CCG	TAG
***3`* –**	AGA	GTG	AGA	CGA	CAC	GAA	TGC	TTA	GGA	GGC	ATC
	Arg	**Ser**	**Pro**	**Asn**	Gly	Gly	Gly	***– C***			
	AGG	TCG	CCT	AAT	GGT	GGA	GGT	***– 3`***			
	TCC	AGC	GGA	TTA	CCA	CCT	CCA	***– 5`***			

Sequence 9

***N* –**	Ser	His	Ser	**Thr**	**Leu**	**Phe**	**Asp**	**Arg**	**Ala**	**Asn**	**Trp**
***5`* –**	TCT	CAC	TCT	ACG	CTT	TTT	GAT	CGG	GCT	AAT	TGG
***3`* –**	AGA	GTG	AGA	TGC	GAA	AAA	CTA	GCC	CGA	TTA	ACC
	Met	**Gly**	**Pro**	**Ala**	Gly	Gly	Gly	***– C***			
	ATG	GGG	CCT	GCG	GGT	GGA	GGT	***– 3`***			
	TAC	CCC	GGA	CGC	CCA	CCT	CCA	***– 5`***			

Sequence 10

***N* –**	Ser	His	Ser	**Gln**	**His**	**Phe**	**Glu**	**Trp**	**Leu**	**Lys**	**Asp**
***5`* –**	TCT	CAC	TCT	CAG	CAT	TTT	GAG	TGG	CTT	AAG	GAT
***3`* –**	AGA	GTG	AGA	GTC	GTA	AAA	CTC	ACC	GAA	TTC	CTA
	Asn	**Leu**	**Lys**	**Asp**	Gly	Gly	Gly	***– C***			
	AAT	TTG	AAG	GAT	GGT	GGA	GGT	***– 3`***			
	TTA	AAC	TTC	CTA	CCA	CCT	CCA	***– 5`***			

Multiple Sequence Analysis (protocol A, dodecapeptides, NaAc-elution, all cycles)

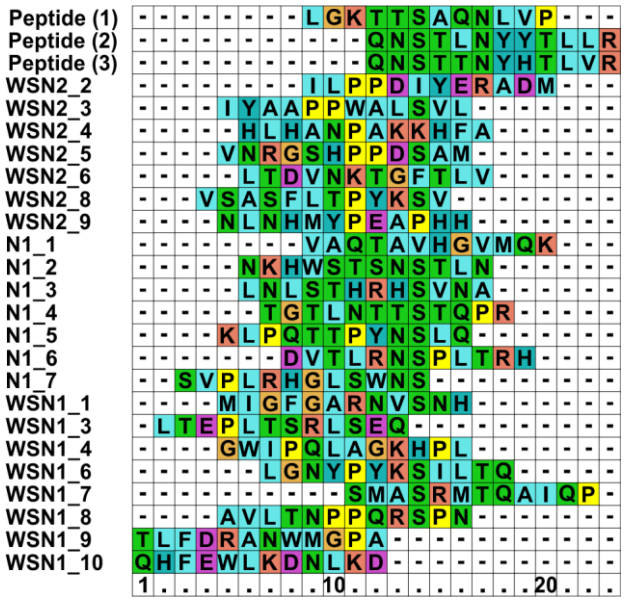

Random heptapeptide library

Elution method applying 0.1M EDTA (**E**)

After 1st cycle (**E1**)

Sequence 1

***N* –**	Ser	His	Ser	**His**	**Gln**	**Leu**	**Leu**	**Gln**	**Pro**	**Pro**
***5`* –**	TCT	CAC	TCT	CAT	CAG	CTT	CTT	CAG	CCT	CCG
***3`* –**	AGA	GTG	AGA	GTA	GTC	GAA	GAA	GTC	GGA	GGC
	Gly	Gly	Gly	***– C***						
	GGT	GGA	GGT	***– 3`***						
	CCA	CCT	CCA	***– 5`***						

Sequence 2

***N* –**	Ser	His	Ser	**His**	**Pro**	**Ala**	**Val**	**His**	**Ser**	**Pro**
***5`* –**	TCT	CAC	TCT	CAT	CCG	GCT	GTT	CAT	TCT	CCT
***3`* –**	AGA	GTG	AGA	GTA	GGC	CGA	CAA	GTA	AGA	GGA
	Gly	Gly	Gly	***– C***						
	GGT	GGA	GGT	***– 3`***						
	CCA	CCT	CCA	***– 5`***						

Sequence 3

***N* –**	Ser	His	Ser	**Ser**	**Pro**	**Val**	**Ser**	**Phe**	**Arg**	**Thr**
***5`* –**	TCT	CAC	TCT	TCG	CCT	GTG	AGT	TTT	AGG	ACT
***3`* –**	AGA	GTG	AGA	AGC	GGA	CAC	TCA	AAA	TCC	TGA
	Gly	Gly	Gly	***– C***						
	GGT	GGA	GGT	***– 3`***						
	CCA	CCT	CCA	***– 5`***						

Sequence 4

***N* –**	Ser	His	Ser	**Val**	**Leu**	**His**	**Pro**	**Ser**	**Pro**	**Arg**
***5`* –**	TCT	CAC	TCT	GTT	CTG	CAT	CCT	TCT	CCT	AGG
***3`* –**	AGA	GTG	AGA	CAA	GAC	GTA	GGA	AGA	GGA	TCC
	Gly	Gly	Gly	***– C***						
	GGT	GGA	GGT	***– 3`***						
	CCA	CCT	CCA	***– 5`***						

Sequence 5

***N* –**	Ser	His	Ser	**Ile**	**Asn**	**Gly**	**His**	**Ser**	**Tyr**	**Ala**
***5`* –**	TCT	CAC	TCT	ATT	AAT	GGT	CAT	TCG	TAT	GCT
***3`* –**	AGA	GTG	AGA	TAA	TTA	CCA	GTA	AGC	ATA	CGA
	Gly	Gly	Gly	***– C***						
	GGT	GGA	GGT	***– 3`***						
	CCA	CCT	CCA	***– 5`***						

Sequence 6

N –	Ser	His	Ser	**Ile**	**Pro**	**Lys**	**Gln**	**Val**	**Leu**	**Leu**
5`–	TCT	CAC	TCT	ATT	CCG	AAG	CAG	GTG	CTT	CTT
3`–	AGA	GTG	AGA	TAA	GGC	TTC	GTC	CAC	GAA	GAA
	Glu	Gly	Gly	***– C***						
	GAT	GGA	GGT	***– 3`***						
	CTA	CCT	CCA	***– 5`***						

Possible piont mutation G → A, changing Gly → Glu, or a failure/misinterpretation while sequencing.

Sequence 7

N –	Ser	His	Ser	**Thr**	**Val**	**Val**	**Ala**	**Leu**	**Val**	**Arg**
5`–	TCT	CAC	TCT	ACT	GTG	GTT	GCG	CTG	GTT	CGT
3`–	AGA	GTG	AGA	TGA	CAC	CAA	CGC	GAC	CAA	GCA
	Gly	Gly	Gly	***– C***						
	GGT	GGA	GGT	***– 3`***						
	CCA	CCT	CCA	***– 5`***						

Sequence 8

N –	Ser	His	Ser	**Ser**	**Ile**	**Ser**	**Met**	**Val**	**Lys**	**Lys**
5`–	TCT	CAC	TCT	TCT	ATT	TCG	ATG	GTT	AAG	AAG
3`–	AGA	GTG	AGA	AGA	TAA	AGC	TAC	CAA	TTC	TTC
	Gly	Gly	Gly	***– C***						
	GGT	GGA	GGT	***– 3`***						
	CCA	CCT	CCA	***– 5`***						

Sequence 9

N –	Ser	His	Ser	**His**	**Gln**	**His**	**Asn**	**Asn**	**Thr**	**Pro**
5`–	TCT	CAC	TCT	CAT	CAG	CAT	AAT	AAT	ACT	CCG
3`–	AGA	GTG	AGA	GTA	GTC	GTA	TTA	TTA	TGA	GGC
	Gly	Gly	Gly	***– C***						
	GGT	GGA	GGT	***– 3`***						
	CCA	CCT	CCA	***– 5`***						

Sequence 10

Deletion of nucleotides.

Multiple Sequence Analysis (protocol A, heptapeptides, EDTA-elution, 1st cycle)

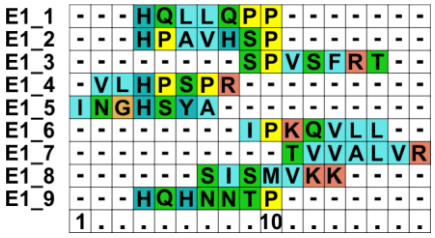

After 2nd cycle (**E2**)

Sequence 1

N –	Ser	His	Ser	**Gly**	**Ser**	**His**	**Val**	**Asn**	**Leu**	**Gln**
5`–	TCT	CAC	TCT	GGG	AGT	CAT	GTT	AAT	CTG	TAG
3`–	AGA	GTG	AGA	CCC	TCA	GTA	CAA	TTA	GAC	ATC
	Gly	Gly	Gly	***– C***						
	GGT	GGA	GGT	***– 3`***						
	CCA	CCT	CCA	***– 5`***						

Sequence 2

Insertion of a nucleotide.

Sequence 3

N –	Ser	His	Ser	**Thr**	**Leu**	**Ser**	**Ala**	**Pro**	**Trp**	**Phe**
5`–	TCT	CAC	TCT	ACT	TTG	TCT	GCT	CCG	TGG	TTT
3`–	AGA	GTG	AGA	TGA	AAC	AGA	CGA	GGC	ACC	AAA
	Gly	Gly	Gly	***– C***						
	GGT	GGA	GGT	***– 3`***						
	CCA	CCT	CCA	***– 5`***						

Sequence 4

N –	Ser	His	Ser	**Thr**	**Thr**	**Thr**	**Gln**	**Ala**	**Leu**	**Gly**
5`–	TCT	CAC	TCT	ACG	ACT	ACT	TAG	GCG	CTG	GGT
3`–	AGA	GTG	AGA	TGC	TGA	TGA	ATC	CGC	GAC	CCA
	Gly	Gly	Gly	***– C***						
	GGT	GGA	GGT	***– 3`***						
	CCA	CCT	CCA	***– 5`***						

Sequence 5

N –	Ser	His	Ser	**Ser**	**Met**	**Ser**	**Ala**	**Pro**	**Gly**	**Arg**
5`–	TCT	CAC	TCT	TCT	ATG	TCG	GCT	CCT	GGT	CGT
3`–	AGA	GTG	AGA	AGA	TAC	AGC	CGA	GGA	CCA	GCA
	Gly	Gly	Gly	***– C***						
	GGT	GGA	GGT	***– 3`***						
	CCA	CCT	CCA	***– 5`***						

Sequence 6

N –	Ser	His	Ser	**Asn**	**Ile**	**Ser**	**Leu**	**Thr**	**Arg**	**Met**
5`–	TCT	CAC	TCT	AAT	ATT	TCT	CTT	ACG	CGG	ATG
3`–	AGA	GTG	AGA	TTA	TAA	AGA	GAA	TGC	GCC	TAC

	Gly	Gly	Gly	– *C*
	GGT	GGA	GGT	– *3`*
	CCA	CCT	CCA	– *5`*

Sequence 7

N –	Ser	His	Ser	**Ile**	**Pro**	**His**	**Ser**	**Tyr**	**Asn**	**Phe**
5` –	TCT	CAC	TCT	ATT	CCT	CAT	TCG	TAT	AAT	TTT
3` –	AGA	GTG	AGA	TAA	GGA	GTA	AGC	ATA	TTA	AAA
	Gly	Gly	Gly	– *C*						
	GGT	GGA	GGT	– *3`*						
	CCA	CCT	CCA	– *5`*						

Sequence 8

N –	Ser	His	Ser	**Trp**	**Thr**	**Ser**	**Val**	**Leu**	**Ser**	**Ala**
5` –	TCT	CAC	TCT	TGG	ACG	TCT	GTT	CTG	TCG	GCT
3` –	AGA	GTG	AGA	ACC	TGC	AGA	CAA	GAC	AGC	CGA
	Gly	Gly	Gly	– *C*						
	GGT	GGA	GGT	– *3`*						
	CCA	CCT	CCA	– *5`*						

Sequence 9

Insertion of a nucleotide.

Sequence 10

N –	Ser	His	Ser	**Asn**	**Pro**	**Pro**	**Asp**	**Arg**	**Pro**	**Lys**
5` –	TCT	CAC	TCT	AAT	CCG	CCT	GAT	CGG	CCT	AAG
3` –	AGA	GTG	AGA	TTA	GGC	GGA	CTA	GCC	GGA	TTC
	Gly	Gly	Gly	– *C*						
	GGT	GGA	GGT	– *3`*						
	CCA	CCT	CCA	– *5`*						

Multiple Sequence Analysis (protocol A, heptapeptides, EDTA-elution, 2nd cycle)

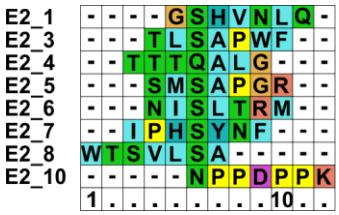

After 3rd cycle (**E3**)

Sequence 1

N –	Ser	His	Ser	**Thr**	**Val**	**Ser**	**Val**	**Ala**	**Pro**	**Leu**
5` –	TCT	CAC	TCT	ACG	GTT	TCG	GTG	GCG	CCG	CTT
3` –	AGA	GTG	AGA	TGC	CAA	AGC	CAC	CGC	GGC	GAA
	Gly	Gly	Gly	– *C*						
	GGT	GGA	GGT	– *3`*						
	CCA	CCT	CCA	– *5`*						

Sequence 2

N –	Ser	His	Ser	**Tyr**	**Ala**	**Ile**	**Arg**	**Leu**	**Pro**	**Gly**
5` –	TCT	CAC	TCT	TAT	GCG	ATT	CGT	CTG	CCT	GGG
3` –	AGA	GTG	AGA	ATA	CGC	TAA	GCA	GAC	GGA	CCC
	Gly	Gly	Gly	– *C*						
	GGT	GGA	GGT	– *3`*						
	CCA	CCT	CCA	– *5`*						

Sequence 3

N –	Ser	His	Ser	**Ile**	**Ala**	**Ile**	**Pro**	**Ala**	**Leu**	**Arg**
5` –	TCT	CAC	TCT	ATT	GCT	ATT	CCG	GCG	CTT	AGG
3` –	AGA	GTG	AGA	TAA	CGA	TAA	GGC	CGC	GAA	TCC
	Gly	Gly	Gly	– *C*						
	GGT	GGA	GGT	– *3`*						
	CCA	CCT	CCA	– *5`*						

Sequence 4

N –	Ser	His	Ser	**Asn**	**Tyr**	**Val**	**Leu**	**Ser**	**Ser**	**Gln**
5` –	TCT	CAC	TCT	AAT	TAT	GTG	TTG	TCT	TCT	CAG
3` –	AGA	GTG	AGA	TTA	ATA	CAC	AAC	AGA	AGA	GTC
	Gly	Gly	Gly	– *C*						
	GGT	GGA	GGT	– *3`*						
	CCA	CCT	CCA	– *5`*						

Sequence 5

N –	Ser	His	Ser	**Glu**	**Phe**	**Leu**	**Trp**	**Pro**	**Ala**	**Phe**
5` –	TCT	CAC	TCT	GAG	TTT	CTG	TGG	CCT	GCT	TTT
3` –	AGA	GTG	AGA	CTC	AAA	GAC	ACC	GGA	CGA	AAA
	Gly	Gly	Gly	– *C*						
	GGT	GGA	GGT	– *3`*						
	CCA	CCT	CCA	– *5`*						

Sequence 6

N –	Ser	His	Ser	**Arg**	**Leu**	**Asp**	**Ser**	**Ser**	**Val**	**Ala**
5` –	TCT	CAC	TCT	CGT	TTG	GAT	TCT	TCG	GTT	GCT
3` –	AGA	GTG	AGA	GCA	AAC	CTA	AGA	AGC	CAA	CGA

	Gly	Gly	Gly	**– *C***
	GGT	GGA	GGT	**– *3`***
	CCA	CCT	CCA	**– *5`***

Sequence 7

***N* –**	Ser	His	Ser	**Ser**	**Pro**	**Gln**	**Leu**	**Gln**	**Ile**	**Gln**
***5`* –**	TCT	CAC	TCT	TCG	CCG	CAG	CTG	TAG	ATT	CAG
***3`* –**	AGA	GTG	AGA	AGC	GGC	GTC	GAC	ATC	TAA	GTC
	Gly	Gly	Gly	**– *C***						
	GGT	GGA	GGT	**– *3`***						
	CCA	CCT	CCA	**– *5`***						

Sequence 8

***N* –**	Ser	His	Ser	**Met**	**Tyr**	**Ser**	**Pro**	**Gly**	**Leu**	**Pro**
***5`* –**	TCT	CAC	TCT	ATG	TAT	TCG	CCG	GGG	CTT	CCG
***3`* –**	AGA	GTG	AGA	TAC	ATA	AGC	GGC	CCC	GAA	GGC
	Gly	Gly	Gly	**– *C***						
	GGT	GGA	GGT	**– *3`***						
	CCA	CCT	CCA	**– *5`***						

Sequence 9

***N* –**	Ser	His	Ser	**His**	**Pro**	**Tyr**	**Asn**	**Gln**	**Ala**	**Gln**
***5`* –**	TCT	CAC	TCT	CAT	CCG	TAT	AAT	CAG	GCG	CAG
***3`* –**	AGA	GTG	AGA	GTA	GGC	ATA	TTA	GTC	CGC	GTC
	Gly	Gly	Gly	**– *C***						
	GGT	GGA	GGT	**– *3`***						
	CCA	CCT	CCA	**– *5`***						

Sequence 10

***N* –**	Ser	His	Ser	**Ser**	**Leu**	**Asn**	**Ile**	**Ser**	**Asn**	**Trp**
***5`* –**	TCT	CAC	TCT	TCG	TTG	AAT	ATT	TCT	AAT	TGG
***3`* –**	AGA	GTG	AGA	AGC	AAC	TTA	TAA	AGA	TTA	ACC
	Gly	Gly	Gly	**– *C***						
	GGT	GGA	GGT	**– *3`***						
	CCA	CCT	CCA	**– *5`***						

Sequence 11

***N* –**	Ser	His	Ser	**Glu**	**Thr**	**Pro**	**Pro**	**Leu**	**Ser**	**Ala**
***5`* –**	TCT	CAC	TCT	GAG	ACG	CCG	CCT	CTG	TCT	GCG
***3`* –**	AGA	GTG	AGA	CTC	TGC	GGC	GGA	GAC	AGA	CGC
	Gly	Gly	Gly	**– *C***						
	GGT	GGA	GGT	**– *3`***						
	CCA	CCT	CCA	**– *5`***						

Sequence 12

***N* –**	Ser	His	Ser	**Gly**	**Tyr**	**Ser**	**Pro**	**Phe**	**Asn**	**Asn**
***5`* –**	TCT	CAC	TCT	GGG	TAT	TCG	CCT	TTT	AAT	AAT
***3`* –**	AGA	GTG	AGA	CCC	ATA	AGC	GGA	AAA	TTA	TTA
	Gly	Gly	Gly	**– *C***						
	GGT	GGA	GGT	**– *3`***						
	CCA	CCT	CCA	**– *5`***						

Sequence 13

***N* –**	Ser	His	Ser	**Thr**	**Leu**	**Pro**	**Gln**	**Pro**	**Pro**	**Thr**
***5`* –**	TCT	CAC	TCT	ACT	CTG	CCG	CAG	CCT	CCG	ACG
***3`* –**	AGA	GTG	AGA	TGA	GAC	GGC	GTC	GGA	GGC	TGC
	Gly	Gly	Gly	**– *C***						
	GGT	GGA	GGT	**– *3`***						
	CCA	CCT	CCA	**– *5`***						

Sequence 14

***N* –**	Ser	His	Ser	**Ile**	**Asn**	**Pro**	**Tyr**	**Thr**	**Pro**	**Gly**
***5`* –**	TCT	CAC	TCT	ATT	AAT	CCT	TAT	ACG	CCG	GGG
***3`* –**	AGA	GTG	AGA	TAA	TTA	GGA	ATA	TGC	GGC	CCC
	Gly	Gly	Gly	**– *C***						
	GGT	GGA	GGT	**– *3`***						
	CCA	CCT	CCA	**– *5`***						

Sequence 15

***N* –**	Ser	His	Ser	**Ser**	**Thr**	**Asn**	**Pro**	**Phe**	**Thr**	**Asn**
***5`* –**	TCT	CAC	TCT	TCT	ACG	AAT	CCG	TTT	ACT	AAT
***3`* –**	AGA	GTG	AGA	AGA	TGC	TTA	GGC	AAA	TGA	TTA
	Gly	Gly	Gly	**– *C***						
	GGT	GGA	GGT	**– *3`***						
	CCA	CCT	CCA	**– *5`***						

Sequence 16

***N* –**	Ser	His	Ser	**Gly**	**Gly**	**Pro**	**Trp**	**Gln**	**Thr**	**His**
***5`* –**	TCT	CAC	TCT	GGG	GGG	CCT	TGG	CAG	ACT	CAT
***3`* –**	AGA	GTG	AGA	CCC	CCC	GGA	ACC	GTC	TGA	GTA
	Gly	Gly	Gly	**– *C***						
	GGT	GGA	GGT	**– *3`***						
	CCA	CCT	CCA	**– *5`***						

Sequence 17

***N* –**	Ser	His	Ser	**His**	**Tyr**	**Ser**	**Asn**	**Gly**	**Thr**	**Leu**
***5`* –**	TCT	CAC	TCT	CAT	TAT	TCT	AAT	GGT	ACT	CTT
***3`* –**	AGA	GTG	AGA	GTA	ATA	AGA	TTA	CCA	TGA	GAA
	Gly	Gly	Gly	**– *C***						
	GGT	GGA	GGT	**– *3`***						
	CCA	CCT	CCA	**– *5`***						

Sequence 18

***N* –**	Ser	His	Ser	**Ser**	**Leu**	**Val**	**Asn**	**Gln**	**Phe**	**Arg**
***5`* –**	TCT	CAC	TCT	TCT	CTT	GTT	AAT	CAG	TTT	CGG
***3`* –**	AGA	GTG	AGA	AGA	GAA	CAA	TTA	GTC	AAA	GCC
	Gly	Gly	Gly	***– C***						
	GGT	GGA	GGT	***– 3`***						
	CCA	CCT	CCA	***– 5`***						

Sequence 19

***N* –**	Ser	His	Ser	**Ser**	**Ser**	**Leu**	**Ser**	**Thr**	**Asp**	**Trp**
***5`* –**	TCT	CAC	TCT	TCT	TCT	CTG	TCT	ACT	GAT	TGG
***3`* –**	AGA	GTG	AGA	AGA	AGA	GAC	AGA	TGA	CTA	ACC
	Gly	Gly	Gly	***– C***						
	GGT	GGA	GGT	***– 3`***						
	CCA	CCT	CCA	***– 5`***						

Sequence 20

***N* –**	Ser	His	Ser	**Asn**	**His**	**Asp**	**Ala**	**Ile**	**Met**	**Pro**
***5`* –**	TCT	CAC	TCT	AAT	CAT	GAT	GCT	ATT	ATG	CCT
***3`* –**	AGA	GTG	AGA	TTA	GTA	CTA	CGA	TAA	TAC	GGA
	Gly	Gly	Gly	***– C***						
	GGT	GGA	GGT	***– 3`***						
	CCA	CCT	CCA	***– 5`***						

Multiple Sequence Analysis (protocol A, heptapeptides, EDTA-elution, 3rd cycle)

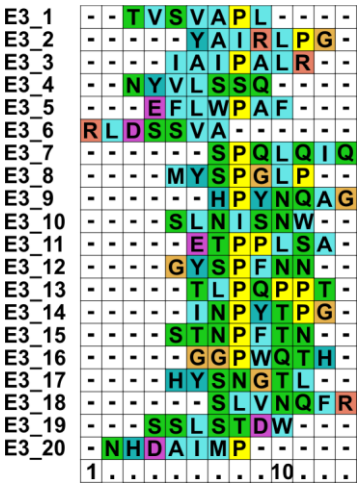

After 5th cycle (**E5**)

Sequence 1

***N* –**	Ser	His	Ser	**Gly**	**Leu**	**Gln**	**Asn**	**Ser**	**Leu**	**Pro**
***5`* –**	TCT	CAC	TCT	GGT	CTT	CAG	AAT	AGT	CTT	CCG
***3`* –**	AGA	GTG	AGA	CCA	GAA	GTC	TTA	TCA	GAA	GGC
	Gly	Gly	Gly	***– C***						
	GGT	GGA	GGT	***– 3`***						
	CCA	CCT	CCA	***– 5`***						

Sequence 2

***N* –**	Ser	His	Ser	**Thr**	**Gln**	**Asn**	**Gln**	**Pro**	**Trp**	**Phe**
***5`* –**	TCT	CAC	TCT	ACG	CAG	AAT	CAG	CCG	TGG	TTT
***3`* –**	AGA	GTG	AGA	TGC	GTC	TTA	GTC	GGC	ACC	AAA
	Gly	Gly	Gly	***– C***						
	GGT	GGA	GGT	***– 3`***						
	CCA	CCT	CCA	***– 5`***						

Sequence 3

***N* –**	Ser	His	Ser	**Thr**	**Trp**	**Ala**	**Trp**	**Arg**	**Thr**	**Pro**
***5`* –**	TCT	CAC	TCT	ACG	TGG	GCT	TGG	CGG	ACG	CCG
***3`* –**	AGA	GTG	AGA	TGC	ACC	CGA	ACC	GCC	TGC	GGC
	Gly	Gly	Gly	***– C***						
	GGT	GGA	GGT	***– 3`***						
	CCA	CCT	CCA	***– 5`***						

Sequence 4

***N* –**	Ser	His	Ser	**Thr**	**Asn**	**Ala**	**Trp**	**Asp**	**Pro**	**Gln**
***5`* –**	TCT	CAC	TCT	ACT	AAT	GCT	TGG	GAT	CCG	TAG
***3`* –**	AGA	GTG	AGA	TGA	TTA	CGA	ACC	CTA	GGC	ATC
	Gly	Gly	Gly	***– C***						
	GGT	GGA	GGT	***– 3`***						
	CCA	CCT	CCA	***– 5`***						

Sequence 5

***N* –**	Ser	His	Ser	**Asp**	**Pro**	**Pro**	**Ser**	**Leu**	**Val**	**Pro**
***5`* –**	TCT	CAC	TCT	GAT	CCG	CCG	TCG	CTG	GTG	CCT
***3`* –**	AGA	GTG	AGA	CTA	GGC	GGC	AGC	GAC	CAC	GGA
	Gly	Gly	Gly	***– C***						
	GGT	GGA	GGT	***– 3`***						
	CCA	CCT	CCA	***– 5`***						

Sequence 6

N –	Ser	His	Ser	**Ser**	**Leu**	**His**	**Tyr**	**Thr**	**Thr**	**His**
5`–	TCT	CAC	TCT	AGT	CTG	CAT	TAT	ACG	ACG	CAT
3`–	AGA	GTG	AGA	TCA	GAC	GTA	ATA	TGC	TGC	GTA
	Gly	Gly	Gly	***– C***						
	GGT	GGA	GGT	***– 3`***						
	CCA	CCT	CCA	***– 5`***						

Sequence 7

N –	Ser	His	Ser	**Leu**	**Ser**	**Asn**	**Ala**	**Asn**	**Trp**	**Ser**
5`–	TCT	CAC	TCT	CTG	TCT	AAT	GCT	AAT	TGG	TCT
3`–	AGA	GTG	AGA	GAC	AGA	TTA	CGA	TTA	ACC	AGA
	Gly	Gly	Gly	***– C***						
	GGT	GGA	GGT	***– 3`***						
	CCA	CCT	CCA	***– 5`***						

Sequence 8

N –	Ser	His	Ser	**Gly**	**Asn**	**Thr**	**Pro**	**Ser**	**Arg**	**Ala**
5`–	TCT	CAC	TCT	GGT	AAT	ACT	CCG	TCT	CGG	GCT
3`–	AGA	GTG	AGA	CCA	TTA	TGA	GGC	AGA	GCC	CGA
	Gly	Gly	Gly	***– C***						
	GGT	GGA	GGT	***– 3`***						
	CCA	CCT	CCA	***– 5`***						

Sequence 9

N –	Ser	His	Ser	**Leu**	**Glu**	**Arg**	**Ala**	**Asn**	**Ala**	**His**
5`–	TCT	CAC	TCT	CTT	GAG	CGT	GCT	AAT	GCG	CAT
3`–	AGA	GTG	AGA	GAA	CTC	GCA	CGA	TTA	CGC	GTA
	Gly	Gly	Gly	***– C***						
	GGT	GGA	GGT	***– 3`***						
	CCA	CCT	CCA	***– 5`***						

Sequence 10

N –	Ser	His	Ser	**Thr**	**Ser**	**Pro**	**Leu**	**Arg**	**Asn**	**Leu**
5`–	TCT	CAC	TCT	ACG	TCG	CCT	TTG	CGT	AAT	CTT
3`–	AGA	GTG	AGA	TGC	AGC	GGA	AAC	GCA	TTA	GAA
	Gly	Gly	Gly	***– C***						
	GGT	GGA	GGT	***– 3`***						
	CCA	CCT	CCA	***– 5`***						

Sequence 11

N –	Ser	His	Ser	**Tyr**	**Pro**	**Gly**	**Trp**	**Ser**	**Thr**	**Arg**
5`–	TCT	CAC	TCT	TAT	CCT	GGT	TGG	TCT	ACG	CGT
3`–	AGA	GTG	AGA	ATA	GGA	CCA	ACC	AGA	TGC	GCA
	Gly	Gly	Gly	***– C***						
	GGT	GGA	GGT	***– 3`***						
	CCA	CCT	CCA	***– 5`***						

Sequence 12

N –	Ser	His	Ser	**Thr**	**Pro**	**Ala**	**Lys**	**Pro**	**Ser**	**Pro**
5`–	TCT	CAC	TCT	ACG	CCG	GCT	AAG	CCG	TCG	CCT
3`–	AGA	GTG	AGA	TGC	GGC	CGA	TTC	GGC	AGC	GGA
	Gly	Gly	Gly	***– C***						
	GGT	GGA	GGT	***– 3`***						
	CCA	CCT	CCA	***– 5`***						

Sequence 13

N –	Ser	His	Ser	**Ser**	**Ala**	**Ile**	**Ser**	**Met**	**Thr**	**Tyr**
5`–	TCT	CAC	TCT	AGT	GCT	ATT	AGT	ATG	ACT	TAC
3`–	AGA	GTG	AGA	TCA	CGA	TAA	TCA	TAC	TGA	ATG
	Gly	Gly	Gly	***– C***						
	GGT	GGA	GGT	***– 3`***						
	CCA	CCT	CCA	***– 5`***						

Sequence 14

N –	Ser	His	Ser	**Ser**	**Ser**	**His**	**Thr**	**Ile**	**Ser**	**Phe**
5`–	TCT	CAC	TCT	AGT	TCG	CAT	ACG	ATT	TCT	TTT
3`–	AGA	GTG	AGA	TCA	AGC	GTA	TGC	TAA	AGA	AAA
	Gly	Gly	Gly	***– C***						
	GGT	GGA	GGT	***– 3`***						
	CCA	CCT	CCA	***– 5`***						

Sequence 15

N –	Ser	His	Ser	**Val**	**Gln**	**Ser**	**Met**	**His**	**Ser**	**Pro**
5`–	TCT	CAC	TCT	GTG	CAG	TCT	ATG	CAT	TCT	CCG
3`–	AGA	GTG	AGA	CAC	GTC	AGA	TAC	GTA	AGA	GGC
	Gly	Gly	Gly	***– C***						
	GGT	GGA	GGT	***– 3`***						
	CCA	CCT	CCA	***– 5`***						

Sequence 16

N –	Ser	His	Ser	**Val**	**Leu**	**Pro**	**Trp**	**Tyr**	**Ser**	**Pro**
5`–	TCT	CAC	TCT	GTT	CTG	CCG	TGG	TAT	TCG	CCT
3`–	AGA	GTG	AGA	CAA	GAC	GGC	ACC	ATA	AGC	GGA
	Gly	Gly	Gly	***– C***						
	GGT	GGA	GGT	***– 3`***						
	CCA	CCT	CCA	***– 5`***						

Sequence 17

N –	Ser	His	Ser	**Ser**	**Ser**	**Ser**	**Asn**	**Ser**	**Pro**	**Pro**
5`–	TCT	CAC	TCT	TCT	TCG	TCG	AAT	TCG	CCG	CCG
3`–	AGA	GTG	AGA	AGA	AGC	AGC	TTA	AGC	GGC	GGC
	Gly	Gly	Gly	***– C***						
	GGT	GGA	GGT	***– 3`***						
	CCA	CCT	CCA	***– 5`***						

Sequence 18

***N* –**	Ser	His	Ser	**Asp**	**Thr**	**Tyr**	**Ser**	**Pro**	**Thr**	**Pro**
***5`* –**	TCT	CAC	TCT	GAT	ACG	TAT	TCG	CCG	ACG	CCT
***3`* –**	AGA	GTG	AGA	CTA	TGC	ATA	AGC	GGC	TGC	GGA
	Gly	Gly	Gly	***– C***						
	GGT	GGA	GGT	***– 3`***						
	CCA	CCT	CCA	***– 5`***						

Sequence 19

***N* –**	Ser	His	Ser	**Thr**	**Val**	**Pro**	**Ser**	**Lys**	**Val**	**Gln**
***5`* –**	TCT	CAC	TCT	ACT	GTT	CCG	AGT	AAG	GTT	CAG
***3`* –**	AGA	GTG	AGA	TGA	CAA	GGC	TCA	TTC	CAA	GTC
	Gly	Gly	Gly	***– C***						
	GGT	GGA	GGT	***– 3`***						
	CCA	CCT	CCA	***– 5`***						

Sequence 20

***N* –**	Ser	His	Ser	**His**	**Leu**	**Pro**	**Pro**	**Pro**	**His**	**Arg**
***5`* –**	TCT	CAC	TCT	CAT	CTG	CCT	CCG	CCG	CAT	CGG
***3`* –**	AGA	GTG	AGA	GTA	GAC	GGA	GGC	GGC	GTA	GCC
	Gly	Gly	Gly	***– C***						
	GGT	GGA	GGT	***– 3`***						
	CCA	CCT	CCA	***– 5`***						

Multiple Sequence Analysis (protocol A, heptapeptides, EDTA-elution, 5th cycle)

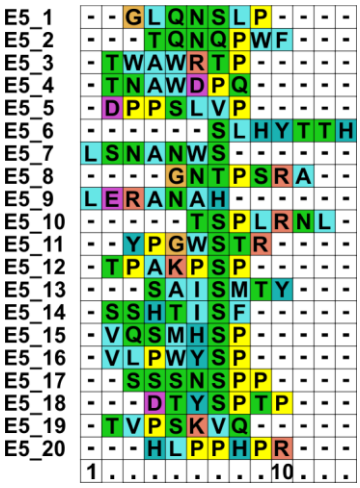

Multiple Sequence Analysis (protocol A, heptapeptides, EDTA-elution, all cycles)

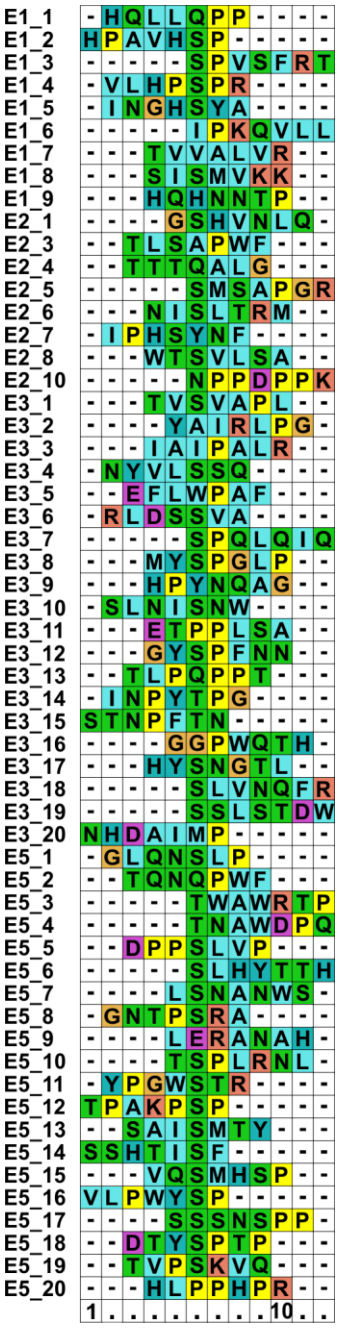

Elution method applying 0.1M NaAc (**N**)

After 1st cycle (**N1**)

Sequence 1

N **–**	Ser	His	Ser	**Asn**	**Leu**	**Met**	**Val**	**Thr**	**Met**	**Ser**
5` **–**	TCT	CAC	TCT	AAT	CTT	ATG	GTT	ACT	ATG	TCG
3` **–**	AGA	GTG	AGA	TTA	GAA	TAC	CAA	TGA	TAC	AGC
	Gly	Gly	Gly	***– C***						
	GGT	GGA	GGT	***– 3`***						
	CCA	CCT	CCA	***– 5`***						

Sequence 2

N **–**	Ser	His	Ser	**Thr**	**Pro**	**Leu**	**Glu**	**His**	**His**	**Pro**
5` **–**	TCT	CAC	TCT	ACG	CCT	TTG	GAG	CAT	CAT	CCG
3` **–**	AGA	GTG	AGA	TGC	GGA	AAC	CTC	GTA	GTA	GGC
	Gly	Gly	Gly	***– C***						
	GGT	GGA	GGT	***– 3`***						
	CCA	CCT	CCA	***– 5`***						

Sequence 3
Deletion of nucleotides.

Sequence 4

N –	Ser	His	Ser	**Thr**	**Val**	**Leu**	**Gly**	**Asn**	**Thr**	**Ser**	
5`–	TCT	CAC	TCT	ACT	GTT	TTG	GGT	AAT	ACT	TCG	
3`–	AGA	GTG	AGA	TGA	CAA	AAC	CCA	TTA	TGA	AGC	CTG
	Gly	Gly	Gly	***– C***							
	GGT	GGA	GGT	***– 3`***							
	CCA	CCT	CCA	***– 5`***							

Sequence 5

N –	Ser	His	Ser	**Ser**	**Pro**	**Ser**	**Thr**	**Lys**	**Pro**	**Leu**
5`–	TCT	CAC	TCT	TCG	CCG	TCT	ACT	AAG	CCT	TTG
3`–	AGA	GTG	AGA	AGC	GGC	AGA	TGA	TTC	GGA	AAC
	Gly	Gly	Gly	***– C***						
	GGT	GGA	GGT	***– 3`***						
	CCA	CCT	CCA	***– 5`***						

Sequence 6

N –	Ser	His	Ser	**Phe**	**Ser**	**Ala**	**Pro**	**Lys**	**Thr**	**Tyr**
5`–	TCT	CAC	TCT	TTT	TCT	GCG	CCG	AAG	ACT	TAT
3`–	AGA	GTG	AGA	AAA	AGA	CGC	GGC	TTC	TGA	ATA
	Gly	Gly	Gly	***– C***						
	GGT	GGA	GGT	***– 3`***						
	CCA	CCT	CCA	***– 5`***						

Sequence 7

N –	Ser	His	Ser	**Trp**	**Ala**	**Leu**	**Thr**	**Arg**	**His**	**Gln**
5`–	TCT	CAC	TCT	TGG	GCG	CTT	ACT	CGT	CAT	TAG
3`–	AGA	GTG	AGA	ACC	CGC	GAA	TGA	GCA	GTA	ATC
	Gly	Gly	Gly	***– C***						
	GGT	GGA	GGT	***– 3`***						
	CCA	CCT	CCA	***– 5`***						

Sequence 8

N –	Ser	His	Ser	**Ser**	**His**	**Tyr**	**Leu**	**Ala**	**Pro**	**Pro**
5`–	TCT	CAC	TCT	TCT	CAT	TAT	CTG	GCG	CCG	CCG
3`–	AGA	GTG	AGA	AGA	GTA	ATA	GAC	CGC	GGC	GGC
	Gly	Gly	Gly	***– C***						
	GGT	GGA	GGT	***– 3`***						
	CCA	CCT	CCA	***– 5`***						

Sequence 9

N –	Ser	His	Ser	**Ser**	**Asn**	**Pro**	**Thr**	**Asp**	**Trp**	**Leu**
5`–	TCT	CAC	TCT	TCT	AAT	CCT	ACT	GAT	TGG	CTG
3`–	AGA	GTG	AGA	AGA	TTA	GGA	TGA	CTA	ACC	GAC
	Gly	Gly	Gly	***– C***						
	GGT	GGA	GGT	***– 3`***						
	CCA	CCT	CCA	***– 5`***						

Sequence 10

N –	Ser	His	Ser	**Ala**	**Ile**	**Glu**	**Pro**	**Met**	**Thr**	**Arg**
5`–	TCT	CAC	TCT	GCG	ATT	GAG	CCT	ATG	ACT	AGG
3`–	AGA	GTG	AGA	CGC	TAA	CTC	GGA	TAC	TGA	TCC
	Gly	Gly	Gly	***– C***						
	GGT	GGA	GGT	***– 3`***						
	CCA	CCT	CCA	***– 5`***						

Multiple Sequence Analysis (protocol A, heptapeptides, NaAc-elution, 1st cycle)

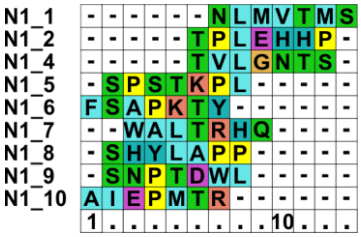

After 2nd cycle (**N2**)

Sequence 1

N –	Ser	His	Ser	**Met**	**Glu**	**Pro**	**Ser**	**Asn**	**Thr**	**Pro**
5`–	TCT	CAC	TCT	ATG	GAG	CCG	TCT	AAT	ACG	CCG
3`–	AGA	GTG	AGA	TAC	CTC	GGC	AGA	TTA	TGC	GGC
	Gly	Gly	Gly	***– C***						
	GGT	GGA	GGT	***– 3`***						
	CCA	CCT	CCA	***– 5`***						

Sequence 2

N –	Ser	His	Ser	**Thr**	**Leu**	**Arg**	**Leu**	**Pro**	**Gln**	**Pro**
5`–	TCT	CAC	TCT	ACG	TTG	CGT	CTG	CCT	CAG	CCT
3`–	AGA	GTG	AGA	TGC	AAC	GCA	GAC	GGA	GTC	GGA
	Gly	Gly	Gly	***– C***						
	GGT	GGA	GGT	***– 3`***						
	CCA	CCT	CCA	***– 5`***						

Sequence 3
Deletion of nucleotides.

Sequence 4

N –	Ser	His	Ser	**Val**	**Gly**	**Leu**	**His**	**Arg**	**Tyr**	**Pro**
5`–	TCT	CAC	TCT	GTT	GGT	CTG	CAT	CGT	TAT	CCT
3`–	AGA	GTG	AGA	CAA	CCA	GAC	GTA	GCA	ATA	GGA
	Gly	Gly	Gly	***– C***						
	GGT	GGA	GGT	***– 3`***						
	CCA	CCT	CCA	***– 5`***						

Sequence 5

N –	Ser	His	Ser	**Ser**	**Leu**	**Ile**	**Ile**	**Ser**	**Arg**	**Ala**
5`–	TCT	CAC	TCT	TCT	TTG	ATT	ATT	AGT	AGG	GCT
3`–	AGA	GTG	AGA	AGA	AAC	TAA	TAA	TCA	TCC	CGA
	Gly	Gly	Gly	***– C***						
	GGT	GGA	GGT	***– 3`***						
	CCA	CCT	CCA	***– 5`***						

Sequence 6

N –	Ser	His	Ser	**Ala**	**Ile**	**Gly**	**Ala**	**Ser**	**Pro**	**Ala**
5`–	TCT	CAC	TCT	GCT	ATT	GGT	GCG	TCT	CCG	GCG
3`–	AGA	GTG	AGA	CGA	TAA	CCA	CGC	AGA	GGC	CGC
	Gly	Gly	Gly	***– C***						
	GGT	GGA	GGT	***– 3`***						
	CCA	CCT	CCA	***– 5`***						

Sequence 7

N –	Ser	His	Ser	**Gly**	**Leu**	**Gln**	**Asn**	**Ser**	**Leu**	**Pro**
5`–	TCT	CAC	TCT	GGT	CTT	CAG	AAT	AGT	CTT	CCG
3`–	AGA	GTG	AGA	CCA	GAA	GTC	TTA	TCA	GAA	GGC
	Gly	Gly	Gly	***– C***						
	GGT	GGA	GGT	***– 3`***						
	CCA	CCT	CCA	***– 5`***						

Sequence 8

N –	Ser	His	Ser	**Ser**	**Val**	**Ile**	**Ala**	**Ala**	**Arg**	**Tyr**
5`–	TCT	CAC	TCT	TCT	GTT	ATT	GCG	GCG	CGG	TAT
3`–	AGA	GTG	AGA	AGA	CAA	TAA	CGC	CGC	GCC	ATA
	Gly	Gly	Gly	***– C***						
	GGT	GGA	GGT	***– 3`***						
	CCA	CCT	CCA	***– 5`***						

Sequence 9

N –	Ser	His	Ser	**Met**	**Asn**	**Ser**	**Pro**	**Leu**	**Pro**	**Ala**
5`–	TCT	CAC	TCT	ATG	AAT	TCT	CCG	CTG	CCT	GCT
3`–	AGA	GTG	AGA	TAC	TTA	AGA	GGC	GAC	GGA	CGA
	Gly	Gly	Gly	***– C***						
	GGT	GGA	GGT	***– 3`***						
	CCA	CCT	CCA	***– 5`***						

Sequence 10

N –	Ser	His	Ser	**Ala**	**Leu**	**Asn**	**Ser**	**Thr**	**Gln**	**Ser**
5`–	TCT	CAC	TCT	GCT	CTG	AAT	TCT	ACT	CAG	TCT
3`–	AGA	GTG	AGA	CGA	GAC	TTA	AGA	TGA	GTC	AGA
	Gly	Gly	Gly	***– C***						
	GGT	GGA	GGT	***– 3`***						
	CCA	CCT	CCA	***– 5`***						

Multiple Sequence Analysis (protocol A, heptapeptides, NaAc-elution, 2nd cycle)

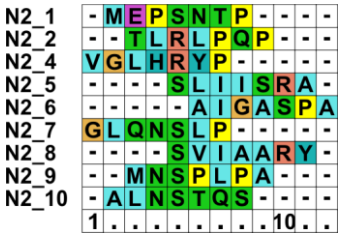

After 3rd cycle (**N3**)

Sequence 1

N –	Ser	His	Ser	**Thr**	**Ser**	**Met**	**Ser**	**His**	**Pro**	**Leu**
5`–	TCT	CAC	TCT	ACT	TCT	ATG	AGT	CAT	CCT	CTT
3`–	AGA	GTG	AGA	TGA	AGA	TAC	TCA	GTA	GGA	GAA
	Gly	Gly	Gly	***– C***						
	GGT	GGA	GGT	***– 3`***						
	CCA	CCT	CCA	***– 5`***						

Sequence 2

N –	Ser	His	Ser	**Ser**	**Met**	**Pro**	**Thr**	**Ala**	**Pro**	**Tyr**
5`–	TCT	CAC	TCT	TCG	ATG	CCT	ACT	GCT	CCG	TAT
3`–	AGA	GTG	AGA	AGC	TAC	GGA	TGA	CGA	GGC	ATA
	Gly	Gly	Gly	***– C***						
	GGT	GGA	GGT	***– 3`***						
	CCA	CCT	CCA	***– 5`***						

Sequence 3

N –	Ser	His	Ser	**Gln**	**Ala**	**Ser**	**Ala**	**Tyr**	**Tyr**	**Ser**
5`–	TCT	CAC	TCT	CAG	GCT	TCG	GCG	TAT	TAT	TCG
3`–	AGA	GTG	AGA	GTC	CGA	AGC	CGC	ATA	ATA	AGC
	Gly	Gly	Gly	***– C***						
	GGT	GGA	GGT	***– 3`***						
	CCA	CCT	CCA	***– 5`***						

Sequence 4

N –	Ser	His	Ser	**Gln**	**Pro**	**Trp**	**Pro**	**Thr**	**Ser**	**Ile**
5`–	TCT	CAC	TCT	CAG	CCT	TGG	CCG	ACG	AGT	ATT
3`–	AGA	GTG	AGA	GTC	GGA	ACC	GGC	TGC	TCA	TAA
	Gly	Gly	Gly	***– C***						
	GGT	GGA	GGT	***– 3`***						
	CCA	CCT	CCA	***– 5`***						

Sequence 5

N –	Ser	His	Ser	**Gly**	**Arg**	**Val**	**Leu**	**Asp**	**Arg**	**Ile**
5`–	TCT	CAC	TCT	GGG	AGG	GTG	TTG	GAT	AGG	ATT
3`–	AGA	GTG	AGA	CCC	TCC	CAC	AAC	CTA	TCC	TAA
	Gly	Gly	Gly	***– C***						
	GGT	GGA	GGT	***– 3`***						
	CCA	CCT	CCA	***– 5`***						

Sequence 6

N –	Ser	His	Ser	**Tyr**	**His**	**Thr**	**His**	**Gln**	**Asn**	**Leu**
5`–	TCT	CAC	TCT	TAT	CAT	ACG	CAT	CAG	AAT	TTG
3`–	AGA	GTG	AGA	ATA	GTA	TGC	GTA	GTC	TTA	AAC
	Gly	Gly	Gly	***– C***						
	GGT	GGA	GGT	***– 3`***						
	CCA	CCT	CCA	***– 5`***						

Sequence 7

Insertion of nucleotides.

Sequence 8

N –	Ser	His	Ser	**Tyr**	**Val**	**Gly**	**Ala**	**Met**	**Val**	**Ser**
5`–	TCT	CAC	TCT	TAT	GTG	GGG	GCG	ATG	GTT	TCT
3`–	AGA	GTG	AGA	ATA	CAC	CCC	CGC	TAC	CAA	AGA
	Gly	Gly	Gly	***– C***						
	GGT	GGA	GGT	***– 3`***						
	CCA	CCT	CCA	***– 5`***						

Sequence 9

N –	Ser	His	Ser	**Ala**	**Gln**	**Trp**	**Ala**	**Pro**	**Gln**	**Asp**
5`–	TCT	CAC	TCT	GCT	CAG	TGG	GCT	CCG	CAG	GAT
3`–	AGA	GTG	AGA	CGA	GTC	ACC	CGA	GGC	GTC	CTA
	Gly	Gly	Gly	***– C***						
	GGT	GGA	GGT	***– 3`***						
	CCA	CCT	CCA	***– 5`***						

Sequence 10

N –	Ser	His	Ser	**Ala**	**Asn**	**Met**	**Pro**	**Leu**	**Gln**	**Pro**
5`–	TCT	CAC	TCT	GCG	AAT	ATG	CCG	CTT	CAG	CCT
3`–	AGA	GTG	AGA	CGC	TTA	TAC	GGC	GAA	GTC	GGA
	Gly	Gly	Gly	***– C***						
	GGT	GGA	GGT	***– 3`***						
	CCA	CCT	CCA	***– 5`***						

Sequence 11

N –	Ser	His	Ser	**Ala**	**Phe**	**Ala**	**Ser**	**Val**	**Pro**	**Thr**
5`–	TCT	CAC	TCT	GCT	TTT	GCT	TCT	GTG	CCG	ACT
3`–	AGA	GTG	AGA	CGA	AAA	CGA	AGA	CAC	GGC	TGA
	Gly	Gly	Gly	***– C***						
	GGT	GGA	GGT	***– 3`***						
	CCA	CCT	CCA	***– 5`***						

Sequence 12

N –	Ser	His	Ser	**Trp**	**Ser**	**Trp**	**Lys**	**Gln**	**Leu**	**Val**
5`–	TCT	CAC	TCT	TGG	AGT	TGG	AAG	CAG	CTG	GTG
3`–	AGA	GTG	AGA	ACC	TCA	ACC	TTC	GTC	GAC	CAC
	Gly	Gly	Gly	***– C***						
	GGT	GGA	GGT	***– 3`***						
	CCA	CCT	CCA	***– 5`***						

Sequence 13

N –	Ser	His	Ser	**Val**	**Tyr**	**Ser**	**Val**	**Gly**	**His**	**Thr**
5`–	TCT	CAC	TCT	GTG	TAT	TCT	GTG	GGG	CAT	ACT
3`–	AGA	GTG	AGA	CAC	ATA	AGA	CAC	CCC	GTA	TGA
	Gly	Gly	Gly	***– C***						
	GGT	GGA	GGT	***– 3`***						
	CCA	CCT	CCA	***– 5`***						

Sequence 14

N –	Ser	His	Ser	**Ala**	**Pro**	**Thr**	**Leu**	**Ile**	**Arg**	**Tyr**
5`–	TCT	CAC	TCT	GCG	CCT	ACG	TTG	ATT	CGG	TAT
3`–	AGA	GTG	AGA	CGC	GGA	TGC	AAC	TAA	GCC	ATA
	Gly	Gly	Gly	***– C***						
	GGT	GGA	GGT	***– 3`***						
	CCA	CCT	CCA	***– 5`***						

Sequence 15

***N* –**	Ser	His	Ser	**Thr**	**Ala**	**Lys**	**Phe**	**Thr**	**Pro**	**Phe**
***5`* –**	TCT	CAC	TCT	ACT	GCT	AAG	TTT	ACG	CCT	TTT
***3`* –**	AGA	GTG	AGA	TGA	CGA	TTC	AAA	TGC	GGA	AAA
	Gly	Gly	Gly	***– C***						
	GGT	GGA	GGT	***– 3`***						
	CCA	CCT	CCA	***– 5`***						

Sequence 16

***N* –**	Ser	His	Ser	**His**	**Pro**	**Pro**	**Thr**	**Ser**	**Val**	**Val**
***5`* –**	TCT	CAC	TCT	CAT	CCT	CCT	ACG	TCT	GTG	GTT
***3`* –**	AGA	GTG	AGA	GTA	GGA	GGA	TGC	AGA	CAC	CAA
	Gly	Gly	Gly	***– C***						
	GGT	GGA	GGT	***– 3`***						
	CCA	CCT	CCA	***– 5`***						

Sequence 17

***N* –**	Ser	His	Ser	**Leu**	**Pro**	**Leu**	**Thr**	**Pro**	**Leu**	**Pro**
***5`* –**	TCT	CAC	TCT	CTG	CCG	TTG	ACT	CCG	CTT	CCG
***3`* –**	AGA	GTG	AGA	GAC	GGC	AAC	TGA	GGC	GAA	GGC
	Gly	Gly	Gly	***– C***						
	GGT	GGA	GGT	***– 3`***						
	CCA	CCT	CCA	***– 5`***						

Sequence 18

Insertion of a nucleotide.

Sequence 19

***N* –**	Ser	His	Ser	**Ala**	**Thr**	**Thr**	**Ser**	**Gln**	**Pro**	**Thr**
***5`* –**	TCT	CAC	TCT	GCG	ACT	ACT	TCT	CAG	CCT	ACT
***3`* –**	AGA	GTG	AGA	CGC	TGA	TGA	AGA	GTC	GGA	TGA
	Gly	Gly	Gly	***– C***						
	GGT	GGA	GGT	***– 3`***						
	CCA	CCT	CCA	***– 5`***						

Sequence 20

***N* –**	Ser	His	Ser	**Met**	**Ile**	**Asp**	**Pro**	**Ser**	**Leu**	**Tyr**
***5`* –**	TCT	CAC	TCT	ATG	ATT	GAT	CCG	TCG	CTG	TAT
***3`* –**	AGA	GTG	AGA	TAC	TAA	CTA	GGC	AGC	GAC	ATA
	Gly	Gly	Gly	***– C***						
	GGT	GGA	GGT	***– 3`***						
	CCA	CCT	CCA	***– 5`***						

Multiple Sequence Analysis (protocol A, heptapeptides, NaAc-elution, 3rd cycle)

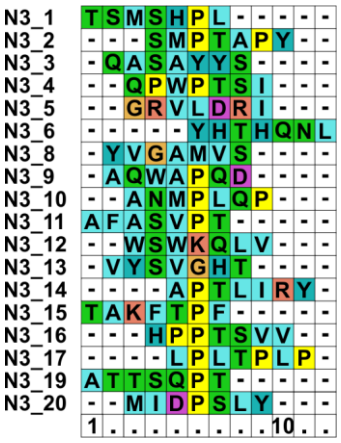

After 5th cycle (**N5**)

Sequence 1

***N* –**	Ser	His	Ser	**Ala**	**Leu**	**Glu**	**Asn**	**Pro**	**Phe**	**Arg**
***5`* –**	TCT	CAC	TCT	GCT	CTG	GAG	AAT	CCT	TTT	CGG
***3`* –**	AGA	GTG	AGA	CGA	GAC	CTC	TTA	GGA	AAA	GCC
	Gly	Gly	Gly	***– C***						
	GGT	GGA	GGT	***– 3`***						
	CCA	CCT	CCA	***– 5`***						

Sequence 2

***N* –**	Ser	His	Ser	**Gly**	**Ser**	**Ser**	**Asn**	**Ala**	**Thr**	**Thr**
***5`* –**	TCT	CAC	TCT	GGT	AGT	AGT	AAT	GCT	ACG	ACG
***3`* –**	AGA	GTG	AGA	CCA	TCA	TCA	TTA	CGA	TGC	TGC
	Gly	Gly	Gly	***– C***						
	GGT	GGA	GGT	***– 3`***						
	CCA	CCT	CCA	***– 5`***						

Sequence 3

***N* –**	Ser	His	Ser	**Leu**	**Pro**	**Lys**	**Pro**	**Ala**	**Tyr**	**Arg**
***5`* –**	TCT	CAC	TCT	CTG	CCT	AAG	CCT	GCT	TAT	CGG
***3`* –**	AGA	GTG	AGA	GAC	GGA	TTC	GGA	CGA	ATA	GCC

	Gly	Gly	Gly	***– C***
	GGT	GGA	GGT	***– 3`***
	CCA	CCT	CCA	***– 5`***

Sequence 4

N –	Ser	His	Ser	**Leu**	**Pro**	**Pro**	**Leu**	**Ala**	**Thr**	**Thr**
5`–	TCT	CAC	TCT	CTG	CCT	CCT	CTG	GCG	ACT	ACG
3`–	AGA	GTG	AGA	GAC	GGA	GGA	GAC	CGC	TGA	TGC
	Gly	Gly	Gly	***– C***						
	GGT	GGA	GGT	***– 3`***						
	CCA	CCT	CCA	***– 5`***						

Sequence 5

N –	Ser	His	**Ala**	**Trp**	**His**	**Leu**	**Pro**	**Val**	**Thr**	**Met**
5`–	TCT	CAC	**G**CT	TGG	CAT	CTT	CCT	GTT	ACG	ATG
3`–	AGA	GTG	**C**GA	ACC	GTA	GAA	GGA	CAA	TGC	TAC
	Gly	Gly	Gly	***– C***						
	GGT	GGA	GGT	***– 3`***						
	CCA	CCT	CCA	***– 5`***						

Possible point mutation T → G, changing Ser → Ala or a failure/misinterpretation while sequencing.

Sequence 6

N –	Ser	His	Ser	**Ser**	**Ile**	**Leu**	**Pro**	**Tyr**	**Pro**	**Tyr**
5`–	TCT	CAC	TCT	TCT	ATT	CTG	CCG	TAT	CCT	TAT
3`–	AGA	GTG	AGA	AGA	TAA	GAC	GGC	ATA	GGA	ATA
	Gly	Gly	Gly	***– C***						
	GGT	GGA	GGT	***– 3`***						
	CCA	CCT	CCA	***– 5`***						

Sequence 7

N –	Ser	His	Ser	**Ile**	**Gln**	**Ser**	**Pro**	**His**	**Phe**	**Phe**
5`–	TCT	CAC	TCT	ATT	CAG	TCT	CCT	CAT	TTT	TTT
3`–	AGA	GTG	AGA	TAA	GTC	AGA	GGA	GTA	AAA	AAA
	Gly	Gly	Gly	***– C***						
	GGT	GGA	GGT	***– 3`***						
	CCA	CCT	CCA	***– 5`***						

Sequences 8,17,20

N –	Ser	His	Ser	**Leu**	**Pro**	**Leu**	**Thr**	**Pro**	**Leu**	**Pro**
5`–	TCT	CAC	TCT	CTG	CCG	TTG	ACT	CCG	CTT	CCG
3`–	AGA	GTG	AGA	GAC	GGC	AAC	TGA	GGC	GAA	GGC
	Gly	Gly	Gly	***– C***						
	GGT	GGA	GGT	***– 3`***						
	CCA	CCT	CCA	***– 5`***						

Sequence 9

N –	Ser	His	Ser	**Thr**	**Asn**	**Pro**	**Pro**	**Gly**	**Ala**	**Gln**
5`–	TCT	CAC	TCT	ACT	AAT	CCG	CCG	GGT	GCG	CAG
3`–	AGA	GTG	AGA	TGA	TTA	GGC	GGC	CCA	CGC	GTC
	Gly	Gly	Gly	***– C***						
	GGT	GGA	GGT	***– 3`***						
	CCA	CCT	CCA	***– 5`***						

Sequence 10

N –	Ser	His	Ser	**Asn**	**Asp**	**Ser**	**Val**	**Ser**	**Leu**	**Pro**
5`–	TCT	CAC	TCT	AAT	GAT	AGT	GTG	TCT	TTG	CCT
3`–	AGA	GTG	AGA	TTA	CTA	TCA	CAC	AGA	AAC	GGA
	Gly	Gly	Gly	***– C***						
	GGT	GGA	GGT	***– 3`***						
	CCA	CCT	CCA	***– 5`***						

Sequence 11

N –	Ser	His	Ser	**Asp**	**Ser**	**His**	**Trp**	**Ala**	**Leu**	**Asn**
5`–	TCT	CAC	TCT	GAT	TCT	CAT	TGG	GCT	CTG	AAT
3`–	AGA	GTG	AGA	CTA	AGA	GTA	ACC	CGA	GAC	TTA
	Gly	Gly	Gly	***– C***						
	GGT	GGA	GGT	***– 3`***						
	CCA	CCT	CCA	***– 5`***						

Sequence 12

N –	Ser	His	Ser	**Gly**	**Glu**	**Thr**	**Leu**	**Pro**	**Pro**	**Ala**
5`–	TCT	CAC	TCT	GGG	GAG	ACT	CTT	CCG	CCG	GCG
3`–	AGA	GTG	AGA	CCC	CTC	TGA	GAA	GGC	GGC	CGC
	Gly	Gly	Gly	***– C***						
	GGT	GGA	GGT	***– 3`***						
	CCA	CCT	CCA	***– 5`***						

Sequence 13

N –	Ser	His	Ser	**Ser**	**Gln**	**Pro**	**Leu**	**Phe**	**Ile**	**Thr**
5`–	TCT	CAC	TCT	AGT	CAG	CCG	CTT	TTT	ATT	ACT
3`–	AGA	GTG	AGA	TCA	GTC	GGC	GAA	AAA	TAA	TGA
	Gly	Gly	Gly	***– C***						
	GGT	GGA	GGT	***– 3`***						
	CCA	CCT	CCA	***– 5`***						

Sequence 14

N –	Ser	His	Ser	**Thr**	**Gln**	**Val**	**Pro**	**Phe**	**Leu**	**Ala**
5`–	TCT	CAC	TCT	ACG	TAG	GTT	CCT	TTT	CTT	GCT
3`–	AGA	GTG	AGA	TGC	ATC	CAA	GGA	AAA	GAA	CGA
	Gly	Gly	Gly	***– C***						
	GGT	GGA	GGT	***– 3`***						
	CCA	CCT	CCA	***– 5`***						

Sequence 15

***N* –**	Ser	His	Ser	**Gly**	**Glu**	**Thr**	**Arg**	**Ala**	**Pro**	**Leu**
***5`* –**	TCT	CAC	TCT	GGG	GAG	ACT	CGT	GCG	CCG	CTT
***3`* –**	AGA	GTG	AGA	CCC	CTC	TGA	GCA	CGC	GGC	GAA
	Gly	Gly	Gly	***– C***						
	GGT	GGA	GGT	***– 3`***						
	CCA	CCT	CCA	***– 5`***						

Sequence 16

***N* –**	Ser	His	Ser	**Ser**	**Thr**	**Ala**	**Ser**	**Tyr**	**Thr**	**Arg**
***5`* –**	TCT	CAC	TCT	TCG	ACG	GCG	TCT	TAT	ACT	CGT
***3`* –**	AGA	GTG	AGA	AGC	TGC	CGC	AGA	ATA	TGA	GCA
	Gly	Gly	Gly	***– C***						
	GGT	GGA	GGT	***– 3`***						
	CCA	CCT	CCA	***– 5`***						

Sequence 18

***N* –**	Ser	His	Ser	**Asn**	**Pro**	**Ala**	**Ala**	**Tyr**	**His**	**Thr**
***5`* –**	TCT	CAC	TCT	AAT	CCT	GCT	GCG	TAT	CAT	ACG
***3`* –**	AGA	GTG	AGA	TTA	GGA	CGA	CGC	ATA	GTA	TGC
	Gly	Gly	Gly	***– C***						
	GGT	GGA	GGT	***– 3`***						
	CCA	CCT	CCA	***– 5`***						

Sequence 19

***N* –**	Ser	His	Ser	**Thr**	**Leu**	**Pro**	**Gln**	**Thr**	**Ser**	**Ser**
***5`* –**	TCT	CAC	TCT	ACG	CTT	CCT	CAG	ACT	TCT	TCT
***3`* –**	AGA	GTG	AGA	TGC	GAA	GGA	GTC	TGA	AGA	AGA
	Gly	Gly	Gly	***– C***						
	GGT	GGA	GGT	***– 3`***						
	CCA	CCT	CCA	***– 5`***						

Multiple Sequence Analysis (protocol A, heptapeptides, NaAc-elution, 5th cycle)

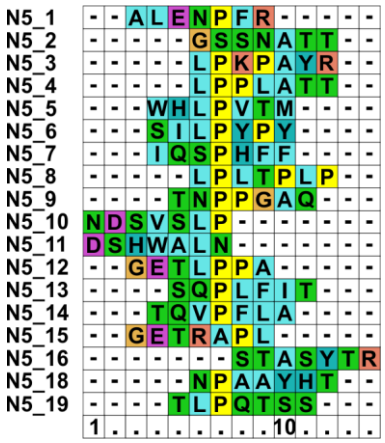

Multiple Sequence Analysis (protocol A, heptapeptides, NaAc-elution, 5th cycle)

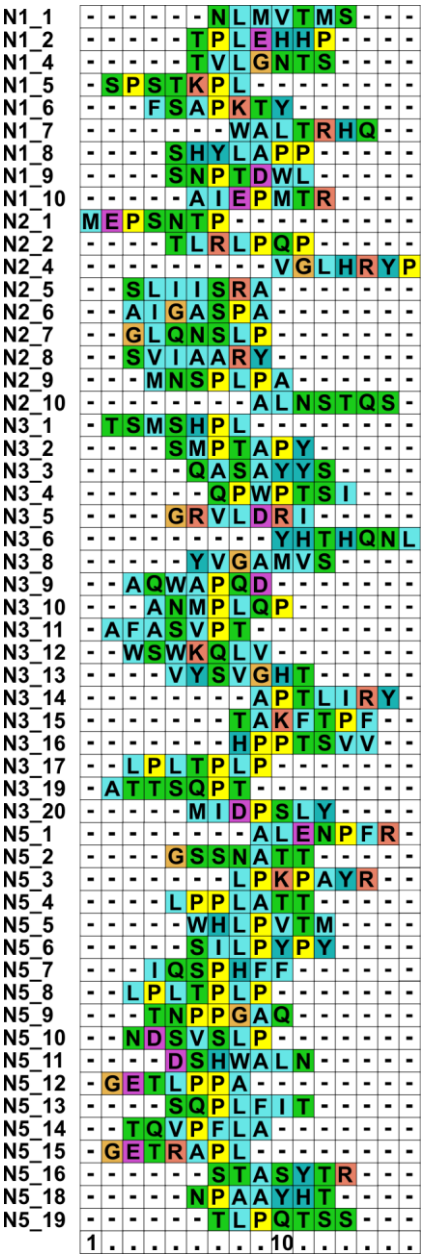

Sequences identified while following protocol B

Random heptapeptide library

Elution method applying 0.1M EDTA (**E**)

After 3rd round (**E3**)

Sequences 1-20

N –	Ser	His	Ser	**Trp**	**Thr**	**Asn**	**Asp**	**Pro**	**Asp**	**Leu**
5`–	TCT	CAC	TC**G**	TGG	ACT	AAT	GAT	CCG	GAT	TTG
3`–	AGA	GTG	AG**C**	ACC	TGA	TTA	CTA	GGC	CTA	AAC
	Gly	Gly	Gly	***– C***						
	GGT	GGA	GGT	***– 3`***						
	CCA	CCT	CCA	***– 5`***						

Point mutation T → G, but no change in amino acid sequence or a possible failure/misinterpretation while sequencing.

Sequences identified in the amplified washing step of the3rd cycle (**WSE3**)

Sequences 1-9

N –	Ser	His	Ser	**Trp**	**Thr**	**Asn**	**Asp**	**Pro**	**Asp**	**Leu**
5`–	TCT	CAC	TC**G**	TGG	ACT	AAT	GAT	CCG	GAT	TTG
3`–	AGA	GTG	AG**C**	ACC	TGA	TTA	CTA	GGC	CTA	AAC
	Gly	Gly	Gly	***– C***						
	GGT	GGA	GGT	***– 3`***						
	CCA	CCT	CCA	***– 5`***						

Point mutation T → G, but no change in amino acid sequence or a possible failure/misinterpretation while sequencing.

Sequence 10

N –	Ser	His	Ser	**Val**	**Ile**	**Pro**	**His**	**Val**	**Leu**	**Ser**
5`–	TCT	CAC	TCT	GTG	ATT	CCG	CAT	GTT	CTT	TCT
3`–	AGA	GTG	AGA	CAC	TAA	GGC	GTA	CAA	GAA	AGA
	Gly	Gly	Gly	***– C***						
	GGT	GGA	GGT	***– 3`***						
	CCA	CCT	CCA	***– 5`***						

After 2nd round of biopanning and amplification (**E2**)

Sequence1-10

N –	Ser	His	Ser	**Trp**	**Thr**	**Asn**	**Asp**	**Pro**	**Asp**	**Leu**
5`–	TCT	CAC	TC**G**	TGG	ACT	AAT	GAT	CCG	GAT	TTG
3`–	AGA	GTG	AG**C**	ACC	TGA	TTA	CTA	GGC	CTA	AAC
	Gly	Gly	Gly	***– C***						
	GGT	GGA	GGT	***– 3`***						
	CCA	CCT	CCA	***– 5`***						

Point mutation T → G, but no change in amino acid sequence or a possible failure/misinterpretation while sequencing.

Sequences identified in the amplified washing step of the 2nd cycle (**WSE2**)

Sequence 1

N –	Ser	His	Ser	**Met**	**Leu**	**Thr**	**Gln**	**Ile**	**Ser**	**Pro**
5`–	TCT	CAC	TCT	ATG	CTT	ACG	CAG	ATT	AGT	CCT
3`–	AGA	GTG	AGA	TAC	GAA	TGC	GTC	TAA	TCA	GGA
	Gly	Gly	Gly	***– C***						
	GGT	GGA	GGT	***– 3`***						
	CCA	CCT	CCA	***– 5`***						

Sequence 2

N –	Ser	His	Ser	**Thr**	**Val**	**Ser**	**Ser**	**Thr**	**Ser**	**Gln**
5`–	TCT	CAC	TCT	ACG	GTG	TCT	TCG	ACT	TCT	CAG
3`–	AGA	GTG	AGA	TGC	CAC	AGA	AGC	TGA	AGA	GTC
	Gly	Gly	Gly	***– C***						
	GGT	GGA	GGT	***– 3`***						
	CCA	CCT	CCA	***– 5`***						

Sequence 3

N –	Ser	His	Ser	**Ala**	**Asn**	**Leu**	**Leu**	**Pro**	**Tyr**	**Thr**
5`–	TCT	CAC	TCT	GCT	AAT	CTT	CTT	CCG	TAT	ACT
3`–	AGA	GTG	AGA	CGA	TTA	GAA	GAA	GGC	ATA	TGA
	Gly	Gly	Gly	***– C***						
	GGT	GGA	GGT	***– 3`***						
	CCA	CCT	CCA	***– 5`***						

Sequence 4

N –	Ser	His	Ser	**Tyr**	**Ser**	**Val**	**Asn**	**Pro**	**His**	**His**
5`–	TCT	CAC	TCT	TAT	TCG	GTT	AAT	CCT	CAT	CAT
3`–	AGA	GTG	AGA	ATA	AGC	CAA	TTA	GGA	GTA	GTA
	Gly	Gly	Gly	***– C***						
	GGT	GGA	GGT	***– 3`***						
	CCA	CCT	CCA	***– 5`***						

Sequence 5

N –	Ser	His	Ser	**Ser**	**Asn**	**Pro**	**Thr**	**Leu**	**Ala**	**Val**
5`–	TCT	CAC	TCT	AGT	AAT	CCG	ACT	CTG	GCG	GTG
3`–	AGA	GTG	AGA	TCA	TTA	GGC	TGA	GAC	CGC	CAC

	Gly	Gly	Gly	**– *C***
	GGT	GGA	GGT	**– *3`***
	CCA	CCT	CCA	**– *5`***

Sequence 6

***N* –**	Ser	**Gln**	Ser	**Asn**	**Asn**	**Gly**	**Glu**	**Met**	**Ser**	**Gln**
***5`* –**	TCT	CA**G**	TCT	AAT	AAT	GGG	GAG	ATG	TCG	CAG
***3`* –**	AGA	GT**C**	AGA	TTA	TTA	CCC	CTC	TAC	AGC	GTC
	Gly	Gly	Gly	**– *C***						
	GGT	GGA	GGT	**– *3`***						
	CCA	CCT	CCA	**– *5`***						

Possible point mutation C → G, changing His → Gln or a possible failure/misinterpretation while sequencing.

Sequence 7

***N* –**	Ser	His	Ser	**Phe**	**Ser**	**Tyr**	**Gln**	**Leu**	**Pro**	**His**
***5`* –**	TCT	CAC	TCT	TTT	TCG	TAT	CAG	CTG	CCT	CAT
***3`* –**	AGA	GTG	AGA	AAA	AGC	ATA	GTC	GAC	GGA	GTA
	Gly	Gly	Gly	**– *C***						
	GGT	GGA	GGT	**– *3`***						
	CCA	CCT	CCA	**– *5`***						

Sequence 8

***N* –**	Ser	His	Ser	**His**	**Asp**	**Pro**	**Ala**	**Ser**	**Ser**	**Lys**
***5`* –**	TCT	CAC	TCT	CAT	GAT	CCG	GCG	TCT	AGT	AAG
***3`* –**	AGA	GTG	AGA	GTA	CTA	GGC	CGC	AGA	TCA	TTC
	Gly	Gly	Gly	**– *C***						
	GGT	GGA	GGT	**– *3`***						
	CCA	CCT	CCA	**– *5`***						

Sequence 9

***N* –**	Ser	His	Ser	**Met**	**Ile**	**Gln**	**Gly**	**Ala**	**Leu**	**Arg**
***5`* –**	TCT	CAC	TCT	ATG	ATT	TAG	GGT	GCG	CTG	CGT
***3`* –**	AGA	GTG	AGA	TAC	TAA	ATC	CCA	CGC	GAC	GCA
	Gly	Gly	Gly	**– *C***						
	GGT	GGA	GGT	**– *3`***						
	CCA	CCT	CCA	**– *5`***						

Sequence 10

***N* –**	Ser	His	Ser	**Ser**	**Met**	**Phe**	**His**	**Thr**	**Ser**	**Ala**
***5`* –**	TCT	CAC	TCT	TCT	ATG	TTT	CAT	ACG	TCG	GCG
***3`* –**	AGA	GTG	AGA	AGA	TAC	AAA	GTA	TGC	AGC	CGC
	Gly	Gly	Gly	**– *C***						
	GGT	GGA	GGT	**– *3`***						
	CCA	CCT	CCA	**– *5`***						

Multiple Sequence Analysis (protocol B, heptapeptides, EDTA-elution, all sequences)

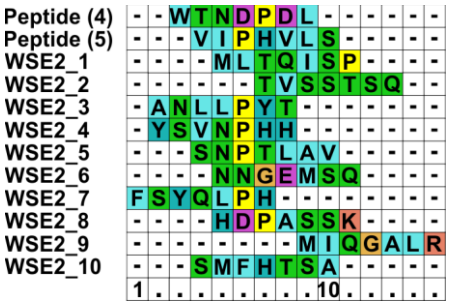

Elution method applying 0.1M NaAc (**N**)

After 3rd round (**N3**)

Sequences 1-4,6-20

***N* –**	Ser	His	Ser	**Trp**	**Thr**	**Asn**	**Asp**	**Pro**	**Asp**	**Leu**
***5`* –**	TCT	CAC	TC**G**	TGG	ACT	AAT	GAT	CCG	GAT	TTG
***3`* –**	AGA	GTG	AG**C**	ACC	TGA	TTA	CTA	GGC	CTA	AAC
	Gly	Gly	Gly	**– *C***						
	GGT	GGA	GGT	**– *3`***						
	CCA	CCT	CCA	**– *5`***						

Point mutation T → G, but no change in amino acid sequence or a possible failure/misinterpretation while sequencing.

Sequence 5

***N* –**	Ser	His	Ser	**Val**	**Ile**	**Pro**	**His**	**Val**	**Leu**	**Ser**
***5`* –**	TCT	CAC	TCT	GTG	ATT	CCG	CAT	GTT	CTT	TCT
***3`* –**	AGA	GTG	AGA	CAC	TAA	GGC	GTA	CAA	GAA	AGA
	Gly	Gly	Gly	**– *C***						
	GGT	GGA	GGT	**– *3`***						
	CCA	CCT	CCA	**– *5`***						

Sequences identified in the amplified washing step of the 3rd cycle (**WSN3**)

Sequence 1-10

N –	Ser	His	Ser	**Trp**	**Thr**	**Asn**	**Asp**	**Pro**	**Asp**	**Leu**
5`–	TCT	CAC	TC**G**	TGG	ACT	AAT	GAT	CCG	GAT	TTG
3`–	AGA	GTG	AG**C**	ACC	TGA	TTA	CTA	GGC	CTA	AAC
	Gly	Gly	Gly	***– C***						
	GGT	GGA	GGT	***– 3`***						
	CCA	CCT	CCA	***– 5`***						

Point mutation T → G, but no change in amino acid sequence or a possible failure/misinterpretation while sequencing.

After 2nd round (**N2**)

Sequences 1,2,4-6,8,9

N –	Ser	His	Ser	**Trp**	**Thr**	**Asn**	**Asp**	**Pro**	**Asp**	**Leu**
5`–	TCT	CAC	TC**G**	TGG	ACT	AAT	GAT	CCG	GAT	TTG
3`–	AGA	GTG	AG**C**	ACC	TGA	TTA	CTA	GGC	CTA	AAC
	Gly	Gly	Gly	***– C***						
	GGT	GGA	GGT	***– 3`***						
	CCA	CCT	CCA	***– 5`***						

Point mutation T → G, but no change in amino acid sequence or a possible failure/misinterpretation while sequencing.

Sequences 3,7,10

N –	Ser	His	Ser	**Val**	**Ile**	**Pro**	**His**	**Val**	**Leu**	**Ser**
5`–	TCT	CAC	TCT	GTG	ATT	CCG	CAT	GTT	CTT	TCT
3`–	AGA	GTG	AGA	CAC	TAA	GGC	GTA	CAA	GAA	AGA
	Gly	Gly	Gly	***– C***						
	GGT	GGA	GGT	***– 3`***						
	CCA	CCT	CCA	***– 5`***						

Sequences identified in the amplified washing step of the 2nd cycle (**WSN2**)

Sequence 1

N –	Ser	His	Ser	**Val**	**Val**	**Pro**	**Pro**	**Leu**	**Lys**	**Ser**
5`–	TCT	CAC	TCT	GTT	GTG	CCT	CCT	CTG	AAG	TCT
3`–	AGA	GTG	AGA	CAA	CAC	GGA	GGA	GAC	TTC	AGA
	Gly	Gly	Gly	***– C***						
	GGT	GGA	GGT	***– 3`***						
	CCA	CCT	CCA	***– 5`***						

Sequence 2

N –	Ser	His	Ser	**Ser**	**Leu**	**Tyr**	**His**	**Phe**	**Thr**	**Leu**
5`–	TCT	CAC	TCT	TCT	CTT	TAT	CAT	TTT	ACT	CTT
3`–	AGA	GTG	AGA	AGA	GAA	ATA	GTA	AAA	TGA	GAA
	Gly	Gly	Gly	***– C***						
	GGT	GGA	GGT	***– 3`***						
	CCA	CCT	CCA	***– 5`***						

Sequence 3

N –	Ser	His	Ser	**Gly**	**Pro**	**Leu**	**Asp**	**Lys**	**Pro**	**Gln**
5`–	TCT	CAC	TCT	GGT	CCG	TTG	GAT	AAG	CCT	CAG
3`–	AGA	GTG	AGA	CCA	GGC	AAC	CTA	TTC	GGA	GTC
	Gly	Gly	Gly	***– C***						
	GGT	GGA	GGT	***– 3`***						
	CCA	CCT	CCA	***– 5`***						

Sequence 4

N –	Ser	His	Ser	**Asn**	**Gly**	**Ala**	**Val**	**Ser**	**Thr**	**Arg**
5`–	TCT	CAC	TCT	AAT	GGG	GCT	GTG	AGT	ACG	CGG
3`–	AGA	GTG	AGA	TTA	CCC	CGA	CAC	TCA	TGC	GCC
	Gly	Gly	Gly	***– C***						
	GGT	GGA	GGT	***– 3`***						
	CCA	CCT	CCA	***– 5`***						

Sequence 5

N –	Ser	His	Ser	**Thr**	**Leu**	**Ala**	**Leu**	**Thr**	**His**	**Arg**
5`–	TCT	CAC	TCT	ACT	CTG	GCT	CTG	ACG	CAT	CGT
3`–	AGA	GTG	AGA	TGA	GAC	CGA	GAC	TGC	GTA	GCA
	Gly	Gly	Gly	***– C***						
	GGT	GGA	GGT	***– 3`***						
	CCA	CCT	CCA	***– 5`***						

Sequence 6

N –	Ser	His	Ser	**Thr**	**His**	**Lys**	**Pro**	**Leu**	**Ala**	**Phe**
5`–	TCT	CAC	TCT	ACT	CAT	AAG	CCT	CTT	GCT	TTT
3`–	AGA	GTG	AGA	TGA	GTA	TTC	GGA	GAA	CGA	AAA
	Gly	Gly	Gly	***– C***						
	GGT	GGA	GGT	***– 3`***						
	CCA	CCT	CCA	***– 5`***						

Sequence 7

N –	Ser	His	Ser	**Gln**	**Pro**	**Thr**	**Leu**	**His**	**Gly**	**Lys**
5`–	TCT	CAC	TCT	CAG	CCT	ACT	CTG	CAT	GGT	AAG
3`–	AGA	GTG	AGA	GTC	GGA	TGA	GAC	GTA	CCA	TTC
	Gly	Gly	Gly	***– C***						
	GGT	GGA	GGT	***– 3`***						
	CCA	CCT	CCA	***– 5`***						

Sequence 8

***N* –**	Ser	His	Ser	**Ser**	**Leu**	**Trp**	**Phe**	**Asn**	**Pro**	**Thr**
***5`* –**	TCT	CAC	TCT	TCG	CTG	TGG	TTT	AAT	CCG	ACT
***3`* –**	AGA	GTG	AGA	AGC	GAC	ACC	AAA	TTA	GGC	TGA
	Gly	Gly	Gly	***– C***						
	GGT	GGA	GGT	***– 3`***						
	CCA	CCT	CCA	***– 5`***						

Sequence 9

***N* –**	Ser	His	Ser	**Lys**	**Leu**	**Ser**	**Pro**	**Pro**	**Pro**	**Glu**
***5`* –**	TCT	CAC	TCT	AAG	CTG	TCG	CCT	CCT	CCG	GAG
***3`* –**	AGA	GTG	AGA	TTC	GAC	AGC	GGA	GGA	GGC	CTC
	Gly	Gly	Gly	***– C***						
	GGT	GGA	GGT	***– 3`***						
	CCA	CCT	CCA	***– 5`***						

Sequence 10

***N* –**	Ser	His	Ser	**Ala**	**Asn**	**Thr**	**Asn**	**Met**	**His**	**Leu**
***5`* –**	TCT	CAC	TCT	GCG	AAT	ACT	AAT	ATG	CAT	CTG
***3`* –**	AGA	GTG	AGA	CGC	TTA	TGA	TTA	TAC	GTA	GAC
	Gly	Gly	Gly	***– C***						
	GGT	GGA	GGT	***– 3`***						
	CCA	CCT	CCA	***– 5`***						

Multiple Sequence Analysis (protocol B, heptapeptides, NaAc-elution, all sequences)

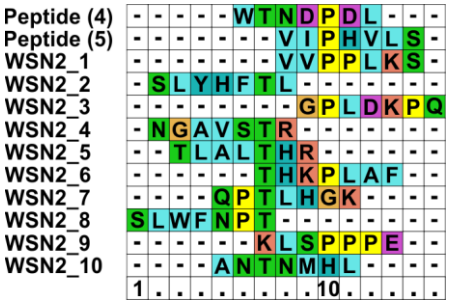

Appendix III:

Statistical Data of the Amino Acid Composition

Phage display on calcite {10.4}-facets - Amino Acid composition of the found peptides, sorted by library and cycle of biopanning

Dodecapeptide Library																					
	Amino Acid																				
Third round peptides	A	C	D	E	F	G	H	I	K	L	M	N	P	Q	R	S	T	V	W	Y	Sum
Total amino acids	9	0	3	0	2	4	5	1	2	8	4	5	5	4	4	13	6	3	2	4	84
Amino acid composition	10.7	0	3.57	0	2.38	4.76	5.95	1.19	2.38	9.52	4.76	5.95	5.95	4.76	4.76	15.4	7.14	3.57	2.38	4.76	100
Expectancy (%)	6,25	3,13	3,13	3,13	3,13	6,25	3,13	3,13	3,13	9,38	3,13	3,13	6,25	6,25	9,38	9,38	6,25	6,25	3,13	3,13	
Standard deviation (%)	±2,7	±1,9	±1,9	±1,9	±1,9	±2,7	±1,9	±1,9	±1,9	±3,3	±1,9	±1,9	±2,7	±2,7	±3,3	±3,3	±2,7	±2,7	±1,9	±1,9	

Fifth round peptides	A	C	D	E	F	G	H	I	K	L	M	N	P	Q	R	S	T	V	W	Y	Sum
Total amino acids	14	0	7	10	0	10	10	8	5	18	10	21	17	6	10	14	26	6	3	9	204
Amino acid composition	6.86	0	3.43	4.90	0	5.21	4.90	3.92	2.45	8.82	4.90	10.2	8.33	2.94	4.90	6.86	12.7	2.94	1.47	4.41	100
Expectancy (%)	6,25	3,13	3,13	3,13	3,13	6,25	3,13	3,13	3,13	9,38	3,13	3,13	6,25	6,25	9,38	9,38	6,25	6,25	3,13	3,13	
Standard deviation (%)	±1,7	±1,2	±1,2	±1,2	±1,2	±1,7	±1,2	±1,2	±1,2	±2,1	±1,2	±1,2	±1,7	±1,7	±2,1	±2,1	±1,7	±1,7	±1,2	±1,2	

Sixth round peptides	A	C	D	E	F	G	H	I	K	L	M	N	P	Q	R	S	T	V	W	Y	Sum
Total amino acids	11	0	4	4	4	10	7	6	3	10	6	11	10	9	6	11	6	4	1	9	132
Amino acid composition (%)	8.33	0	3.03	3.03	3.03	7.58	5.30	4.55	2.27	7.58	4.55	8.33	7.58	6.82	4.55	8.33	4.55	3.03	0.76	6.82	100
Expectancy (%)	6,25	3,13	3,13	3,13	3,13	6,25	3,13	3,13	3,13	9,38	3,13	3,13	6,25	6,25	9,38	9,38	6,25	6,25	3,13	3,13	
Standard deviation (%)	±2,1	±1,5	±1,5	±1,5	±1,5	±2,1	±1,5	±1,5	±1,5	±2,6	±1,5	±1,5	±2,1	±2,1	±2,6	±2,6	±2,1	±2,1	±1,5	±1,5	

Heptapeptide Library																					
	Amino acid																				
	A	C	D	E	F	G	H	I	K	L	M	N	P	Q	R	S	T	V	W	Y	Sum
Total amino acids	6	0	0	1	3	1	3	1	2	7	0	1	15	4	1	12	7	3	1	2	70
Amino acid composition (%)	8.57	0	0	1.43	4.29	1.43	4.29	1.43	2.86	10.0	0	1.43	21.4	5.71	1.43	17.1	10.0	4.29	1.43	2.86	100
Expectancy (%)	6,25	3,13	3,13	3,13	3,13	6,25	3,13	3,13	3,13	9,38	3,13	3,13	6,25	6,25	9,38	9,38	6,25	6,25	3,13	3,13	
Standard deviation (%)	±2,9	±2,1	±2,1	±2,1	±2,1	±2,9	±2,1	±2,1	±2,1	±3,6	±2,1	±2,1	±2,9	±2,9	±3,6	±3,6	±2,9	±2,9	±2,1	±2,1	

Calculation of expectancy and standard deviation, assuming a Poisson-distribution

The 20 natural amino acids are coded unevenly by the 3-base codon system, hence the probability of finding one specific amino acids is not 1/20. Instead, the probability is based on the factor n/64, as four different bases coded in three pairs equals 4^3 = 64 possible combinations. Nevertheless, in all the utilised phage libraries, the genetic code has been reduced by the manufacturer by applying only G or T as the last base in a codon. Thus the factor is reduced to n/32. Additionally, the strain *ER2738* of *E. coli* translates the stop-codon TAG into glutamine (Q). [152] Therefore, codons and the amino acid expectancy are distributed as follows:

	Amino acids																				
	A	**C**	**D**	**E**	**F**	**G**	**H**	**I**	**K**	**L**	**M**	**N**	**P**	**Q**	**R**	**S**	**T**	**V**	**W**	**Y**	**Stop**
Codons ending with A/C (not used)	GCA	TGC	GAC	GAA	TTC	GGA	CAC	ATA	AAA	CTA		AAC	CCA	CAA	AGA	AGC	ACA	GTA		TAC	TAA
	GCC					GGC		ATC		CTC			CCC		CGA	TCA	ACC	GTC			TGA
										TTA					CGC	TCC					
Codons ending on T/G	GCG	TGT	GAT	GAG	TTT	GGG	CAT	ATT	AAG	CTG	ATG	AAT	CCG	CAG	AGG	AGT	ACG	GTG	TGG	TAT	TAG
	GCT					GGT				CTT			CCT	TAG	CGG	TCG	ACT	GTT			
										TTG					CGT	TCT					
Total codons	4	2	2	2	2	4	2	3	2	6	1	2	4	2	6	6	4	4	1	2	3
Modified codon system (n)	**2**	**1**	**1**	**1**	**1**	**2**	**1**	**1**	**1**	**3**	**1**	**1**	**2**	**2**	**3**	**3**	**2**	**2**	**1**	**1**	**0**
Resulting probability (%)	**6.25**	**3.13**	**3.13**	**3.13**	**3.13**	**6.25**	**3.13**	**3.13**	**3.13**	**9.38**	**3.13**	**3.13**	**6.25**	**6.25**	**9.38**	**9.38**	**6.25**	**6.25**	**3.13**	**3.13**	**0.00**

Hence, the probability of finding a specific amino acid is either 3.13%, 6.25% or 9.68%. Since there is no standard deviation for the observed amino acid composition, the standard deviation of the expectancy value in dependence of the sample size was calculated assuming Poisson-statistics.

$$P_\lambda(k) = e^{-\lambda}\frac{\lambda^k}{k!}\ ;\ k = number\ of\ successes, \qquad \lambda = expectancy\ value$$

The expectancy value λ is given by the relative expectancy value p and the size of the sample n:

$$\lambda = n \cdot p$$

The variance $Var(x)$ in the Poisson-statistics is identical to the expectancy value and identical to the squared standard deviation σ:

$$\sigma^2 = Var(x) = \lambda\ and\ \sigma = \sqrt{np}$$

Since we are interested in relative standard deviation:

$$\sigma(\%) = \frac{\sqrt{np}}{n}$$

The following relative standard deviations were calculated:

$\boldsymbol{n}$	$\boldsymbol{p}$	$\boldsymbol{\lambda}$	$\boldsymbol{\sigma}$	$\boldsymbol{p}$ (%)	$\boldsymbol{\sigma}$ (%)
70	1/32	2.188	1.479	3.13	± 2.11
	2/32	4.375	2.092	6.25	± 2.99
	3/32	6.563	2.562	9.68	± 3.66
84	1/32	2.625	1.620	3.13	± 1.93
	2/32	5.25	2.291	6.25	± 2.73
	3/32	7.875	2.806	9.68	± 3.34
132	1/32	4.125	2.031	3.13	± 1.54
	2/32	8.25	2.872	6.25	± 2.18
	3/32	12.375	3.518	9.68	± 2.67
204	1/32	6.375	2.525	3.13	± 1.24
	2/32	12.75	3.571	6.25	± 1.75
	3/32	19.125	4.373	9.68	± 2.14

Appendix IV:

Spectroscopical and Chromatographic Data

Leu-Gly-Lys-Thr-Thr-Ser-Ala-Gln-Asn-Leu-Val-Pro-amide (1)

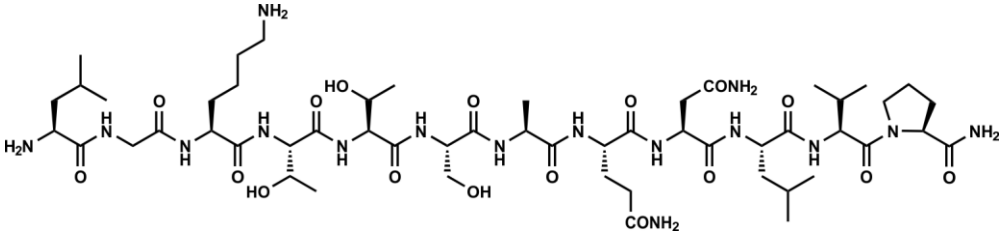

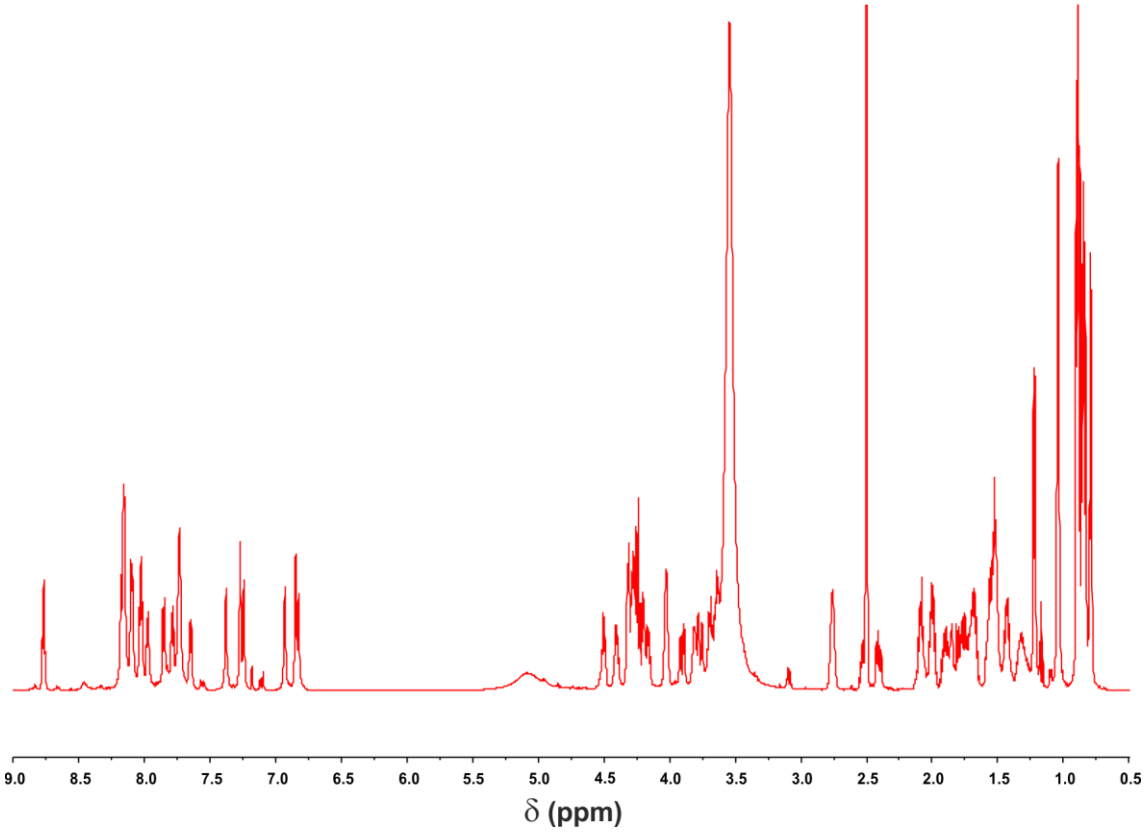

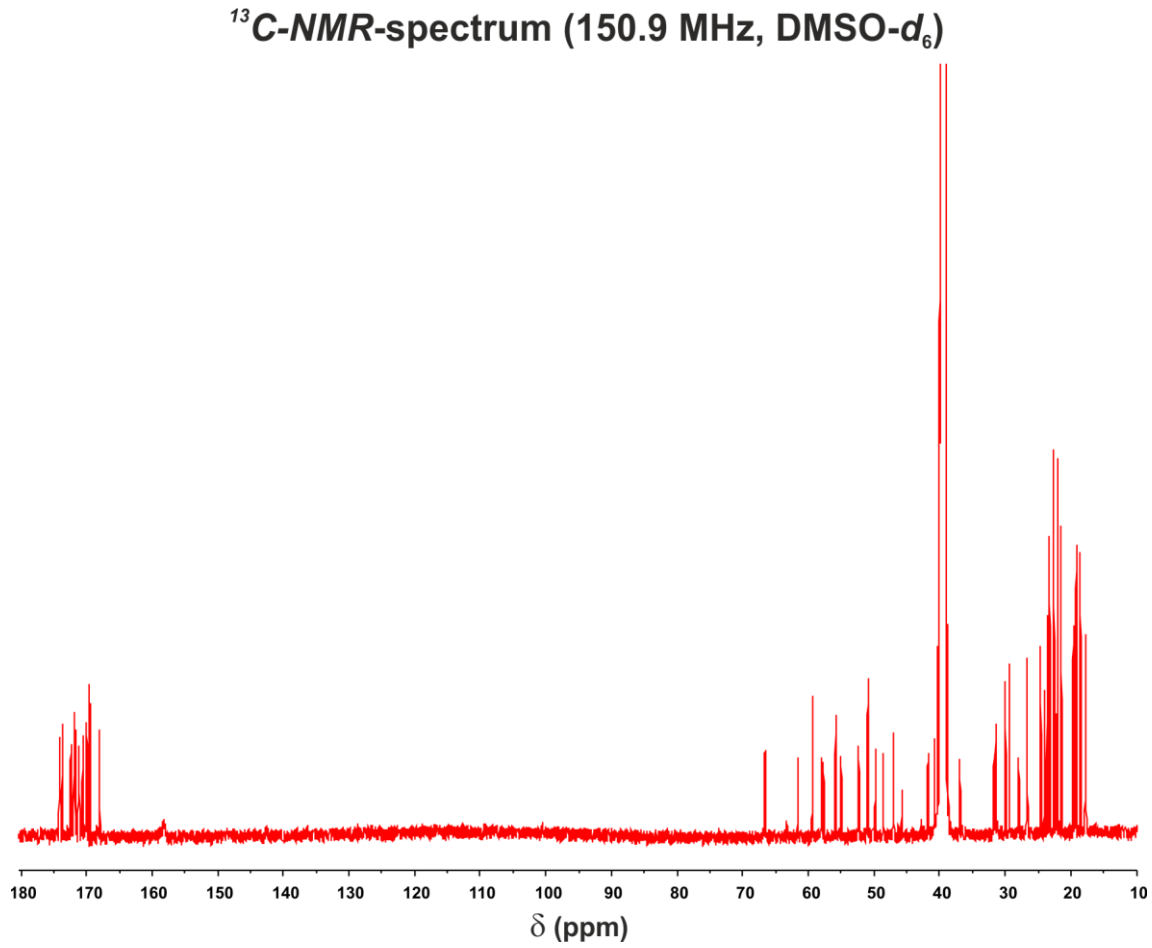
^{13}C-NMR-spectrum (150.9 MHz, DMSO-d_6)
180 170 160 150 140 130 120 110 100 90 80 70 60 50 40 30 20 10
δ (ppm)

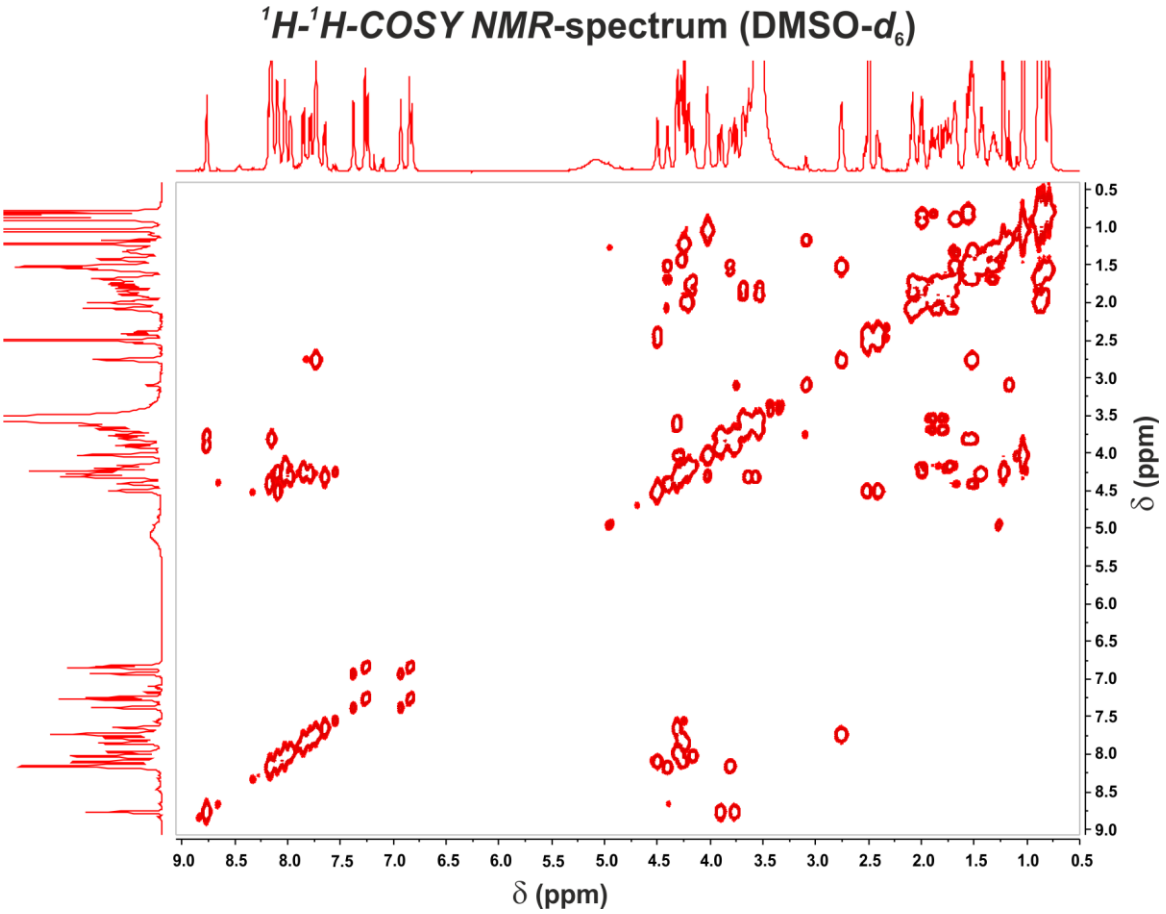
^{1}H-^{1}H-COSY NMR-spectrum (DMSO-d_6)
9.0 8.5 8.0 7.5 7.0 6.5 6.0 5.5 5.0 4.5 4.0 3.5 3.0 2.5 2.0 1.5 1.0 0.5
δ (ppm)
δ (ppm)

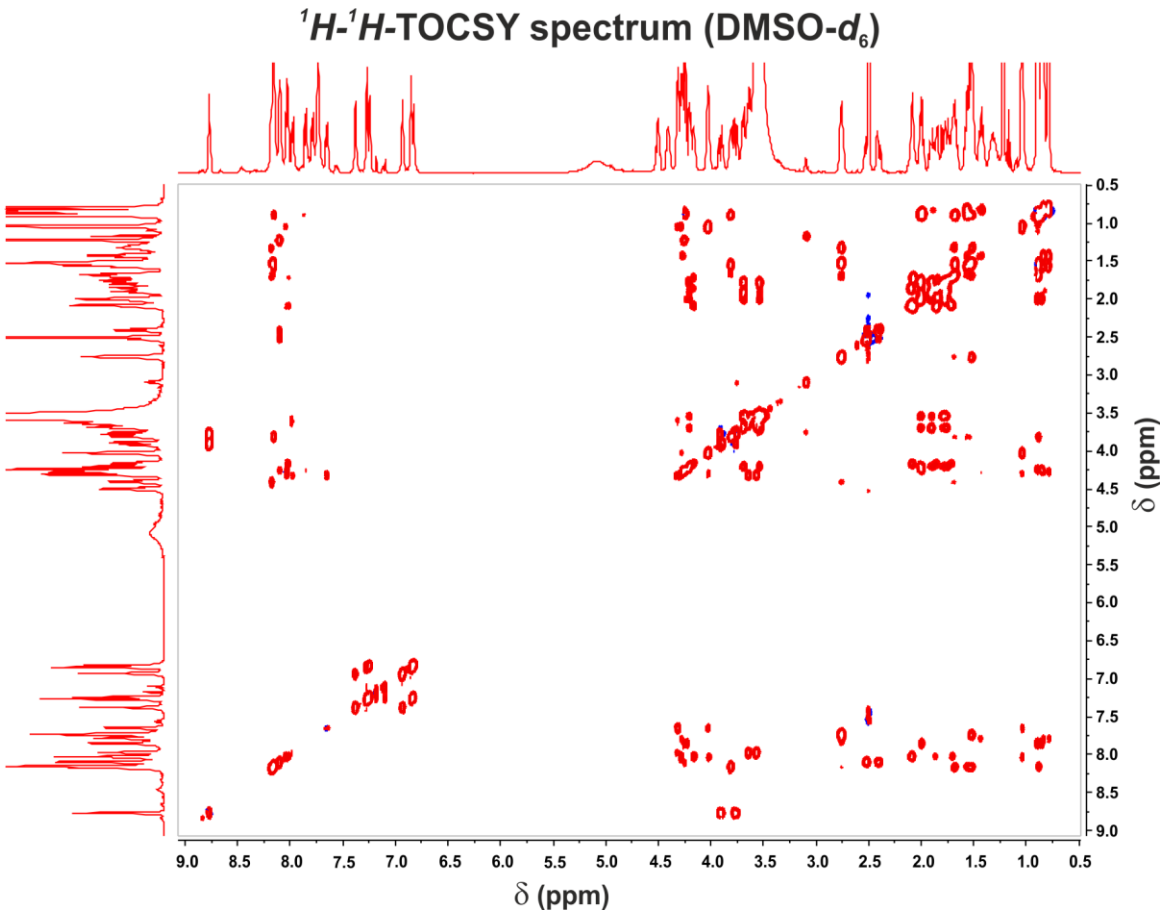
^{1}H-^{1}H-TOCSY spectrum (DMSO-d_6)
δ (ppm)
δ (ppm)

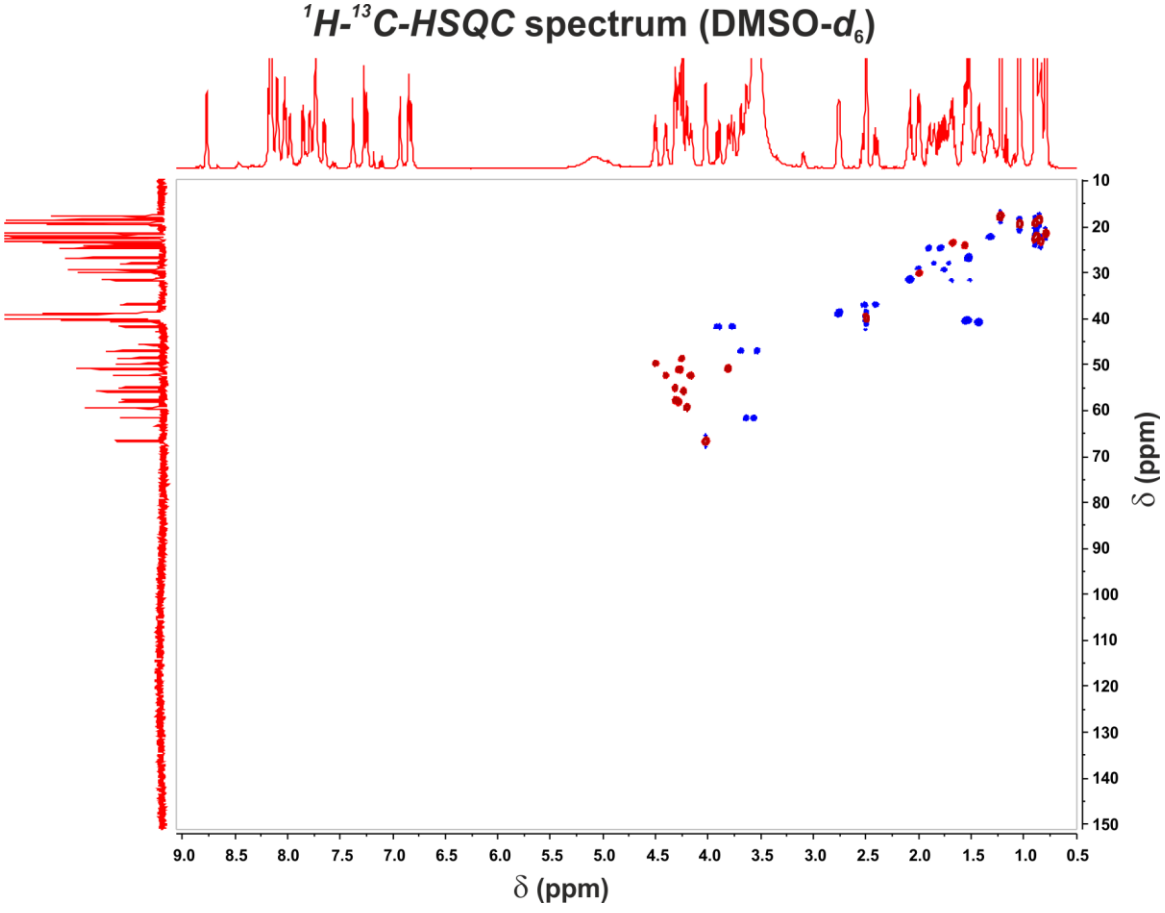
^{1}H-^{13}C-HSQC spectrum (DMSO-d_6)
δ (ppm)
δ (ppm)

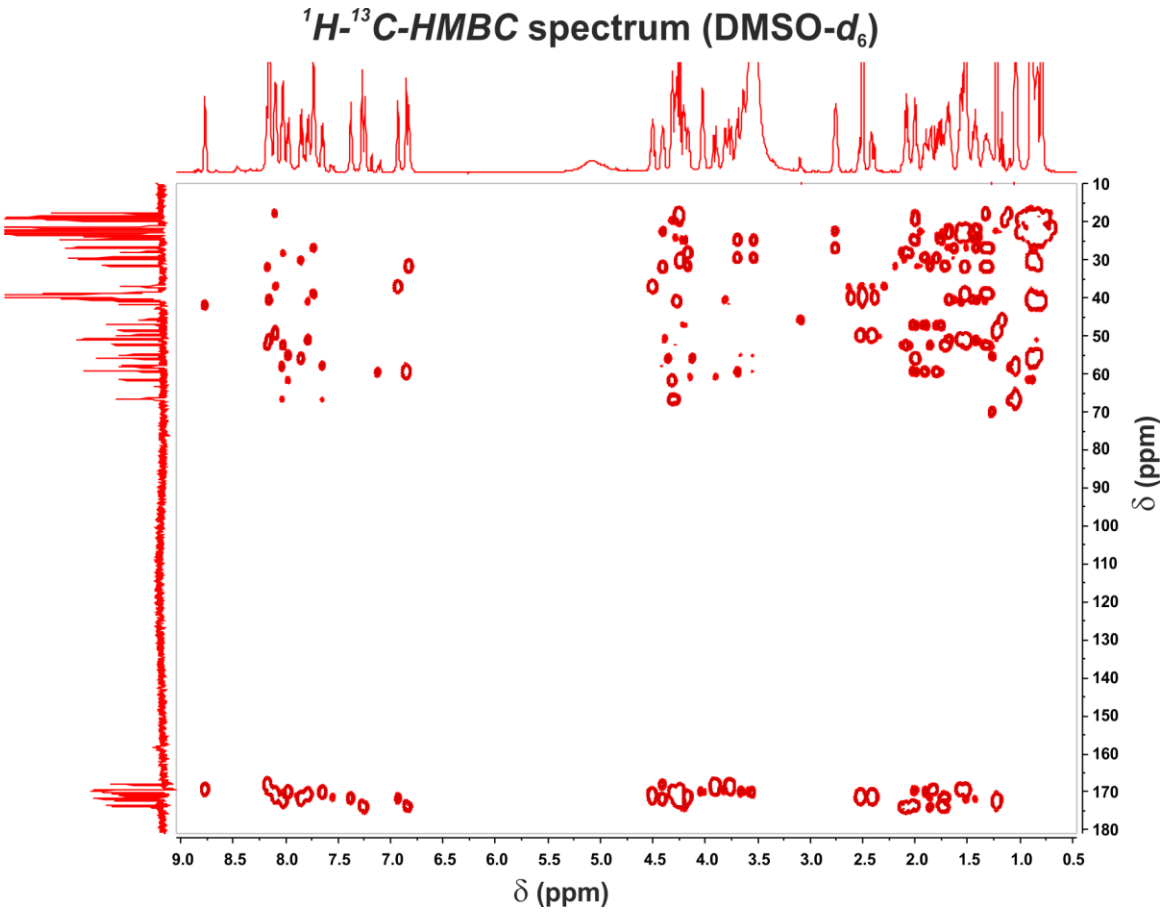
^{1}H-^{13}C-HMBC spectrum (DMSO-d_6)
δ (ppm)
δ (ppm)

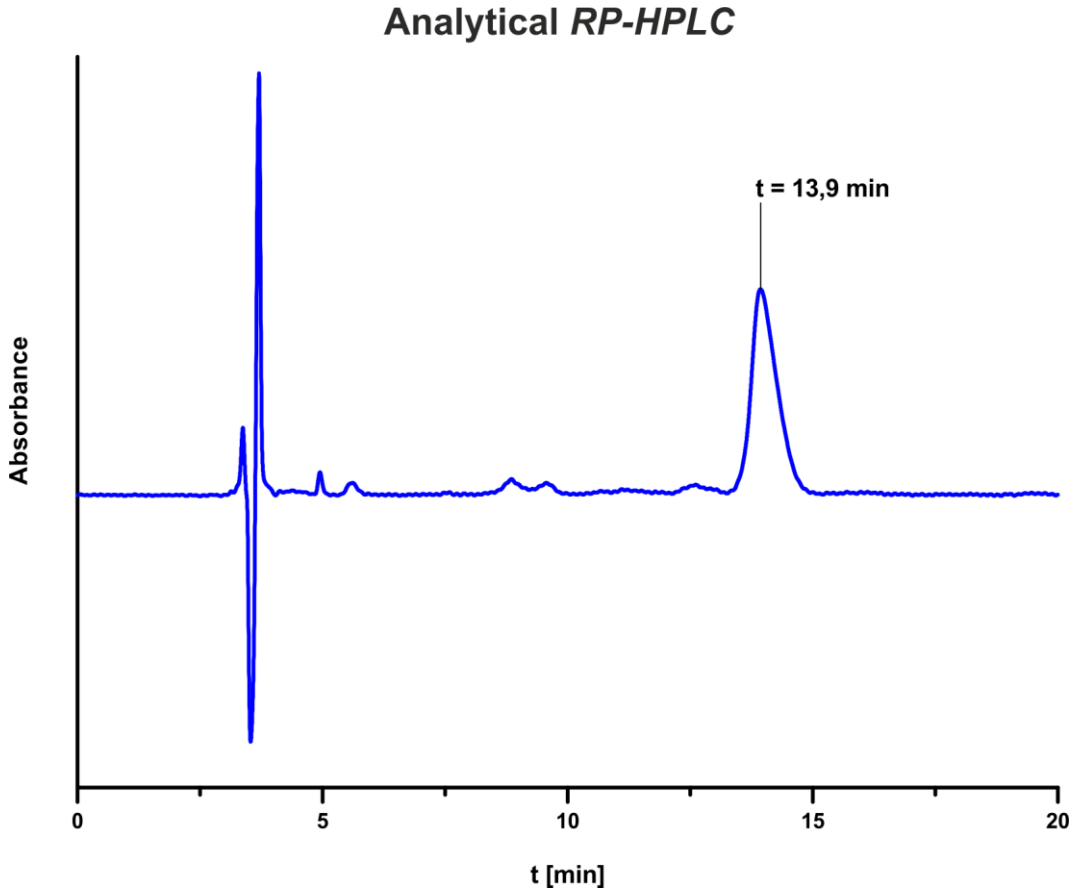
Analytical RP-HPLC
t = 13,9 min
Absorbance
t [min]

Glp-Asn-Ser-Thr-Thr-Asn-Tyr-His-Thr-Leu-Val-Arg-amide (7)

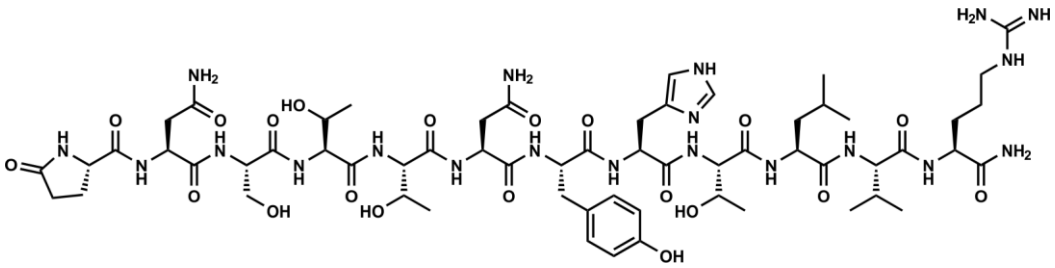

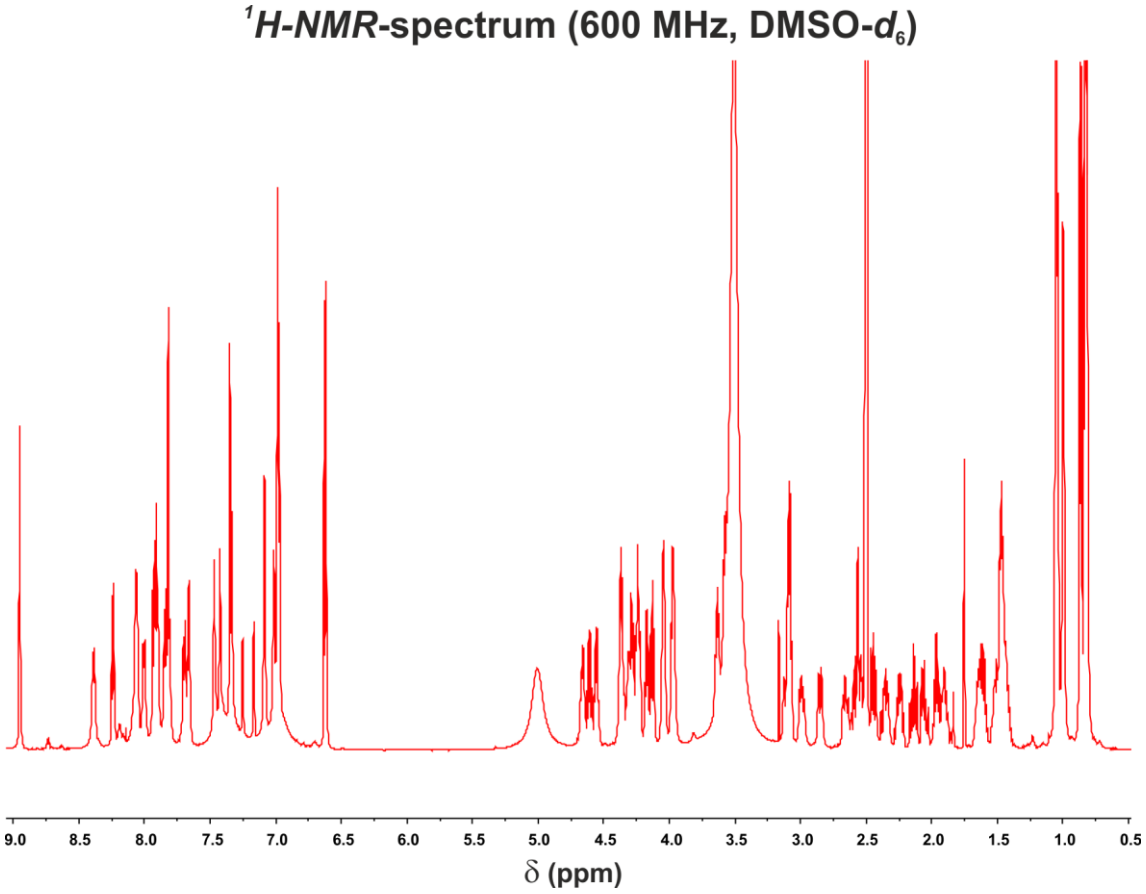

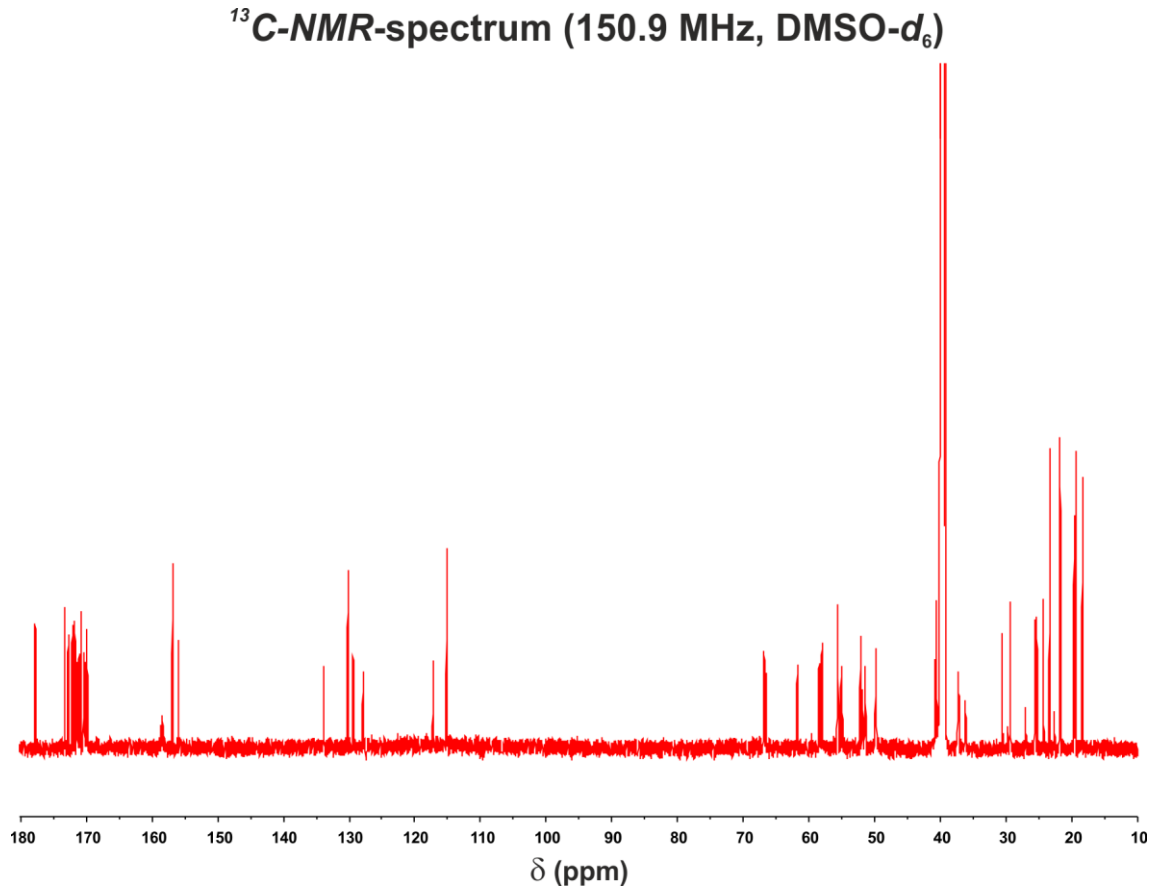
^{13}C-NMR-spectrum (150.9 MHz, DMSO-d_6)
180 170 160 150 140 130 120 110 100 90 80 70 60 50 40 30 20 10
δ (ppm)

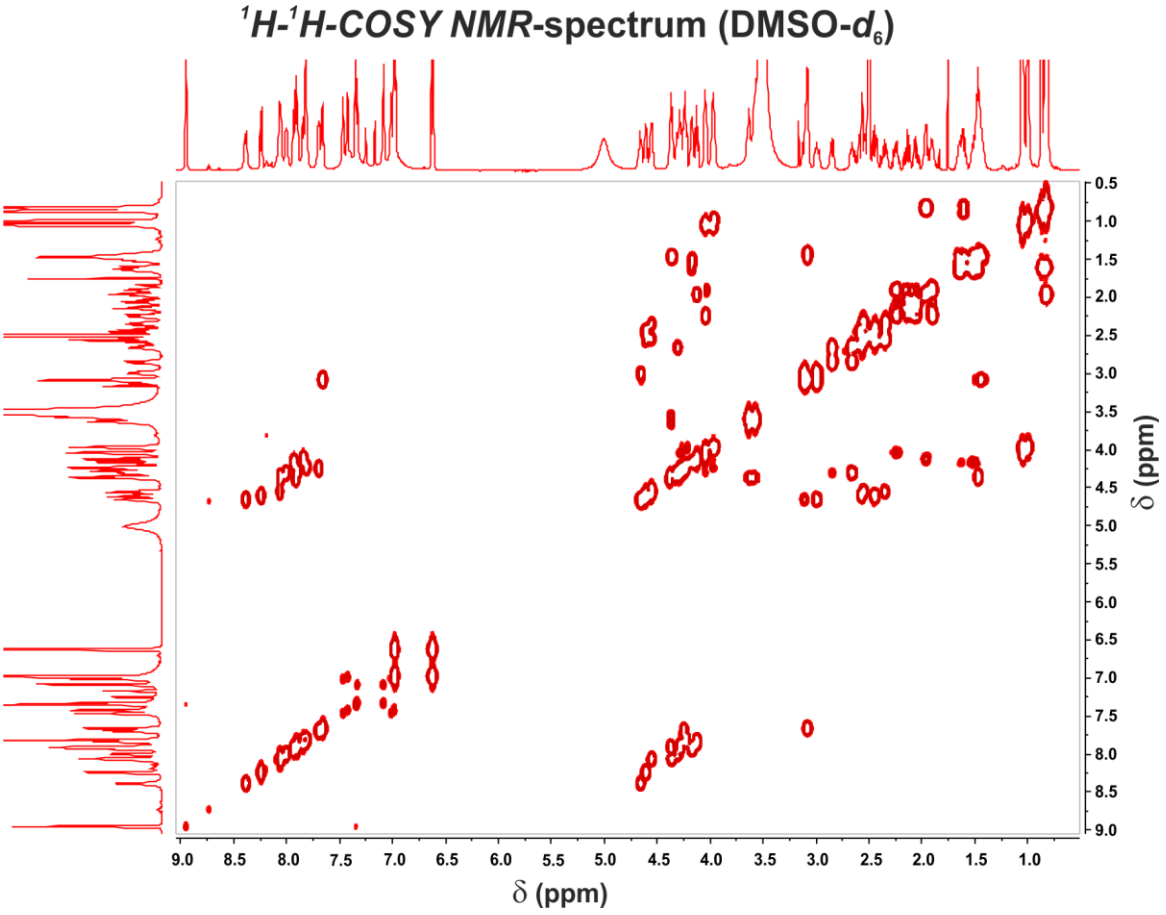
^{1}H-^{1}H-COSY NMR-spectrum (DMSO-d_6)
9.0 8.5 8.0 7.5 7.0 6.5 6.0 5.5 5.0 4.5 4.0 3.5 3.0 2.5 2.0 1.5 1.0
δ (ppm)
0.5 1.0 1.5 2.0 2.5 3.0 3.5 4.0 4.5 5.0 5.5 6.0 6.5 7.0 7.5 8.0 8.5 9.0
δ (ppm)

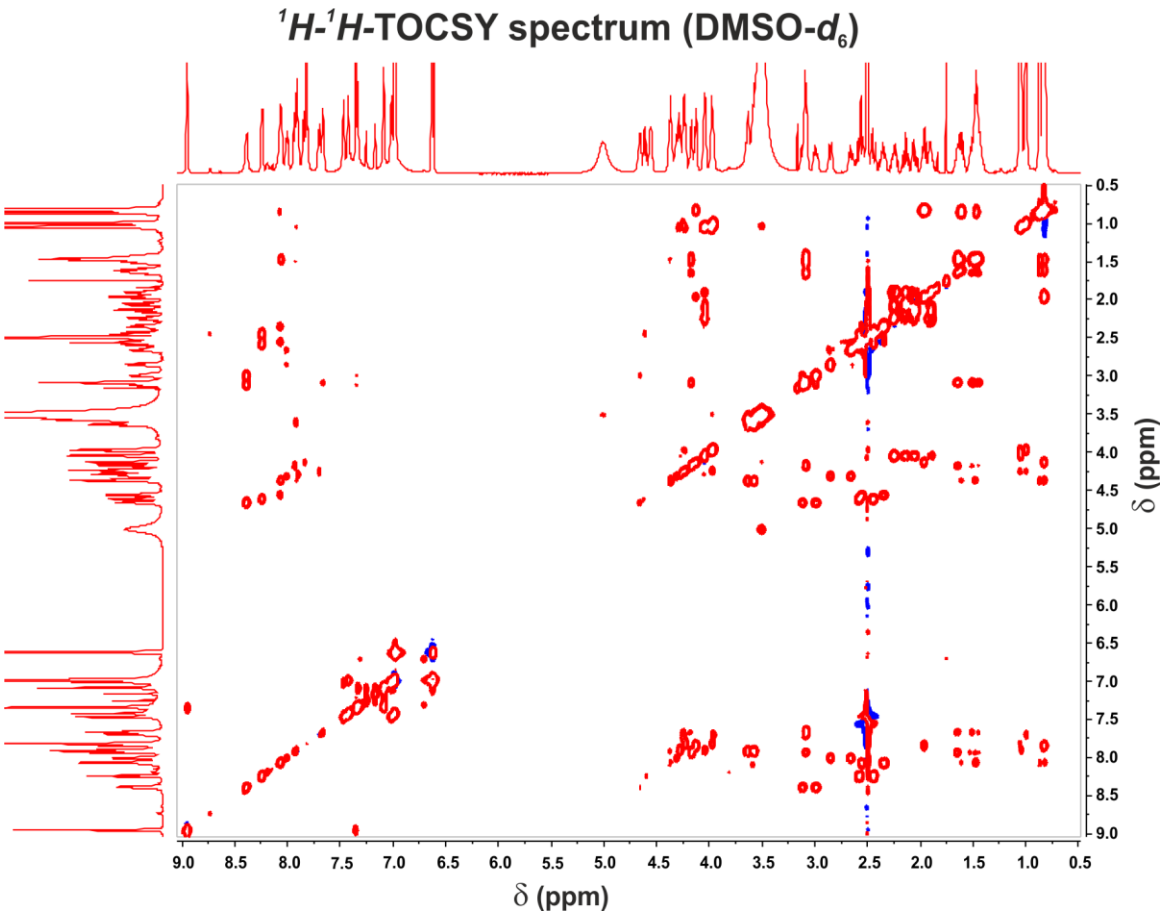
^{1}H-^{1}H-TOCSY spectrum (DMSO-d_6)
δ (ppm)
δ (ppm)

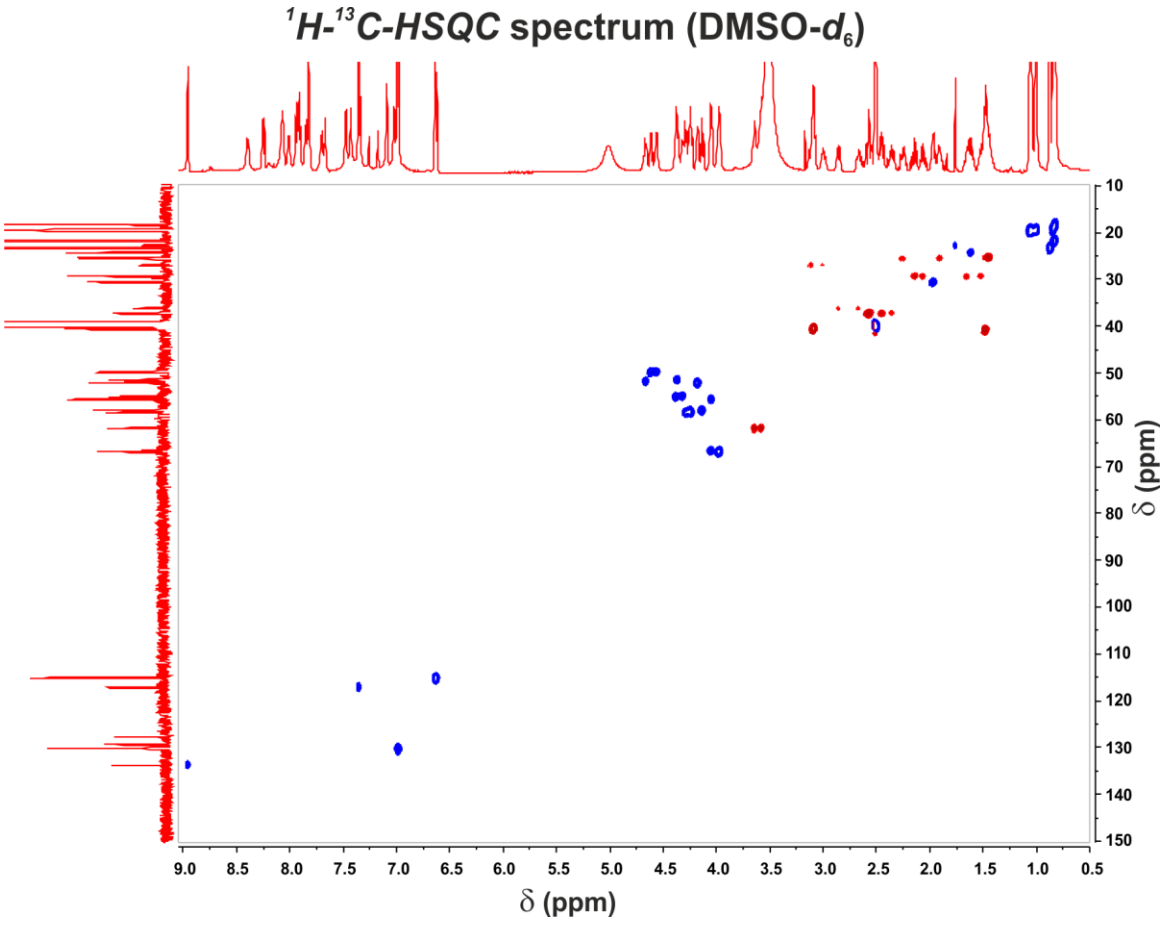
^{1}H-^{13}C-HSQC spectrum (DMSO-d_6)
δ (ppm)
δ (ppm)

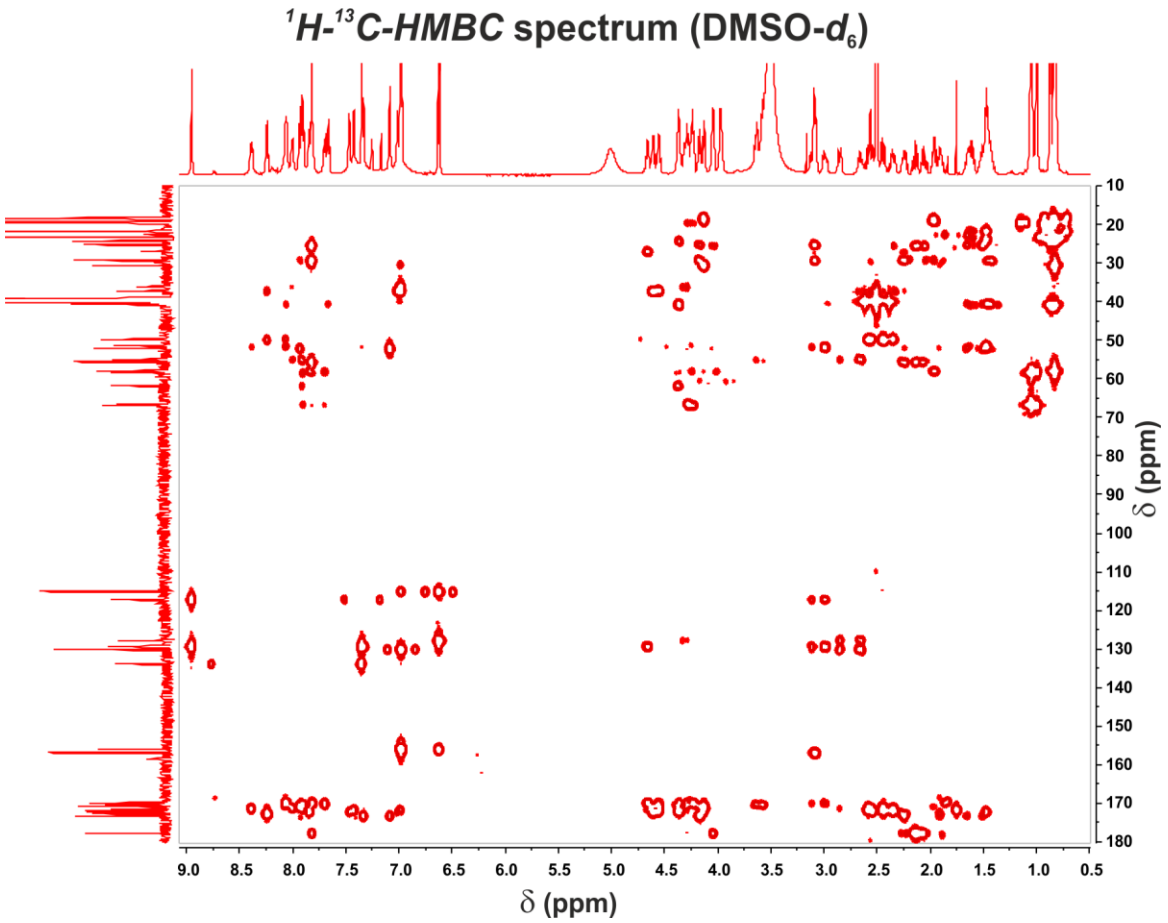
^{1}H-^{13}C-HMBC spectrum (DMSO-d_6)
δ (ppm)
δ (ppm)

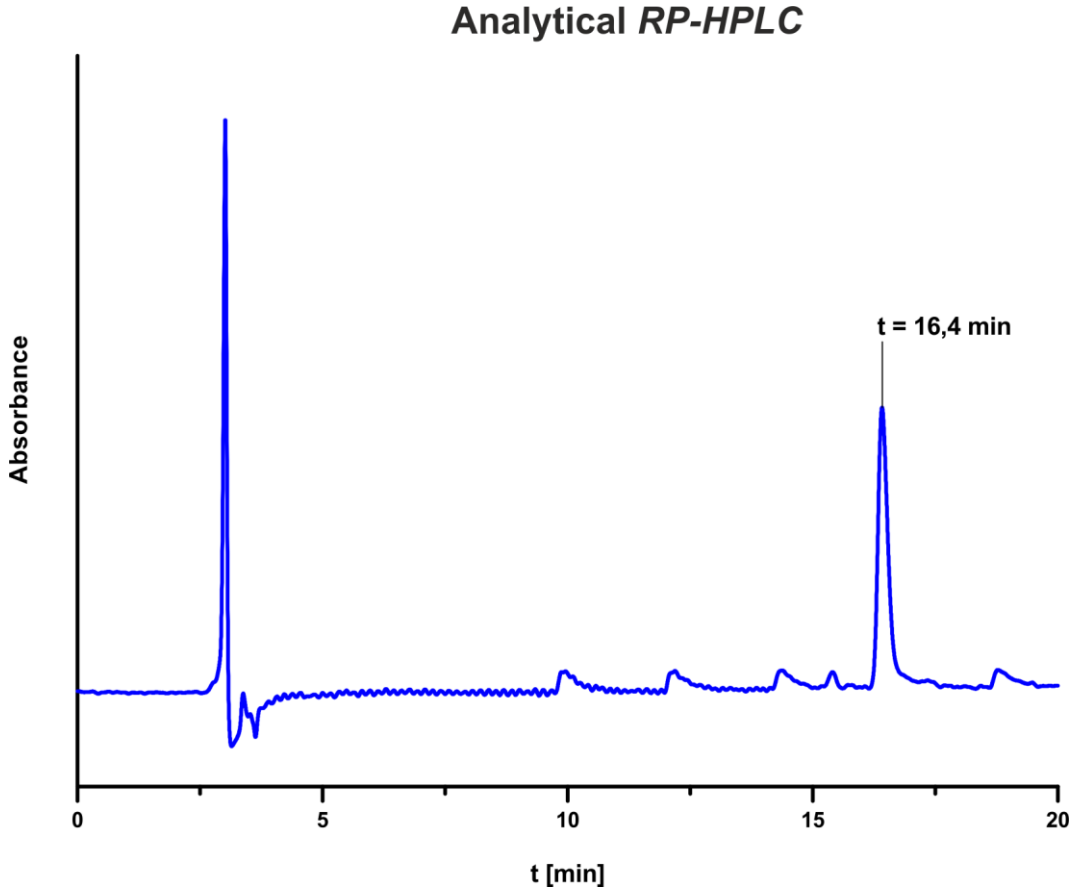
Analytical RP-HPLC
Absorbance
t = 16,4 min
t [min]

Gly-Gln-Asn-Ser-Thr-Thr-Asn-Tyr-His-Thr-Leu-Val-Arg-amide (8)

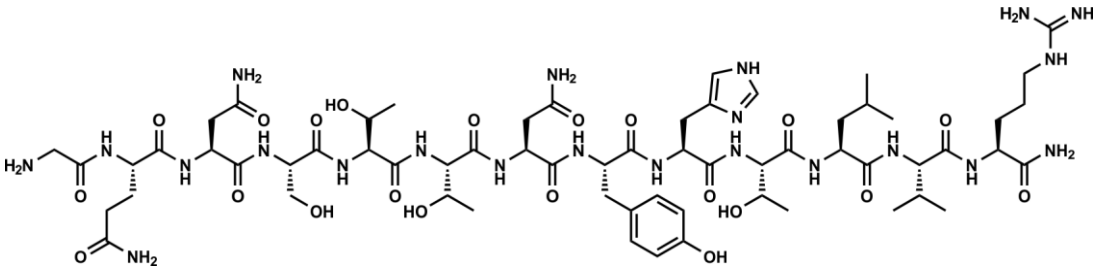

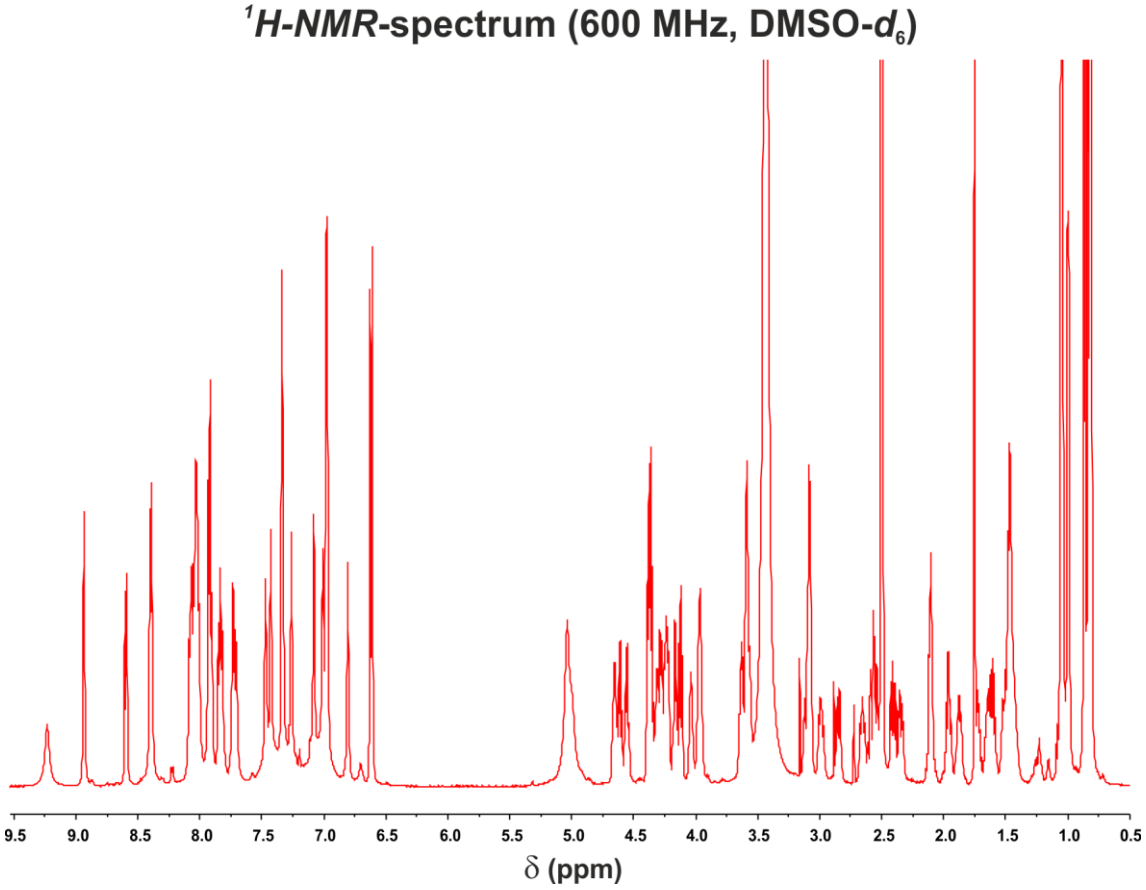

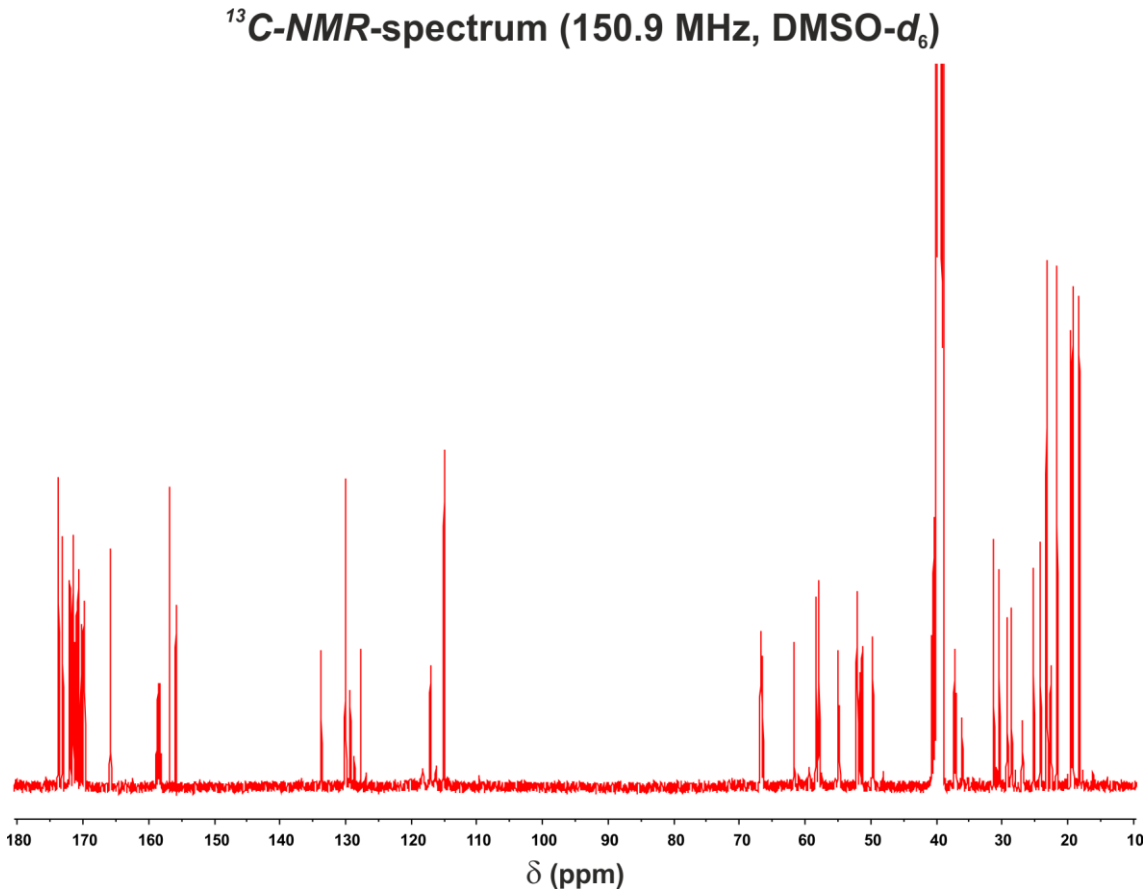
^{13}C-NMR-spectrum (150.9 MHz, DMSO-d_6)
180 170 160 150 140 130 120 110 100 90 80 70 60 50 40 30 20 10
δ (ppm)

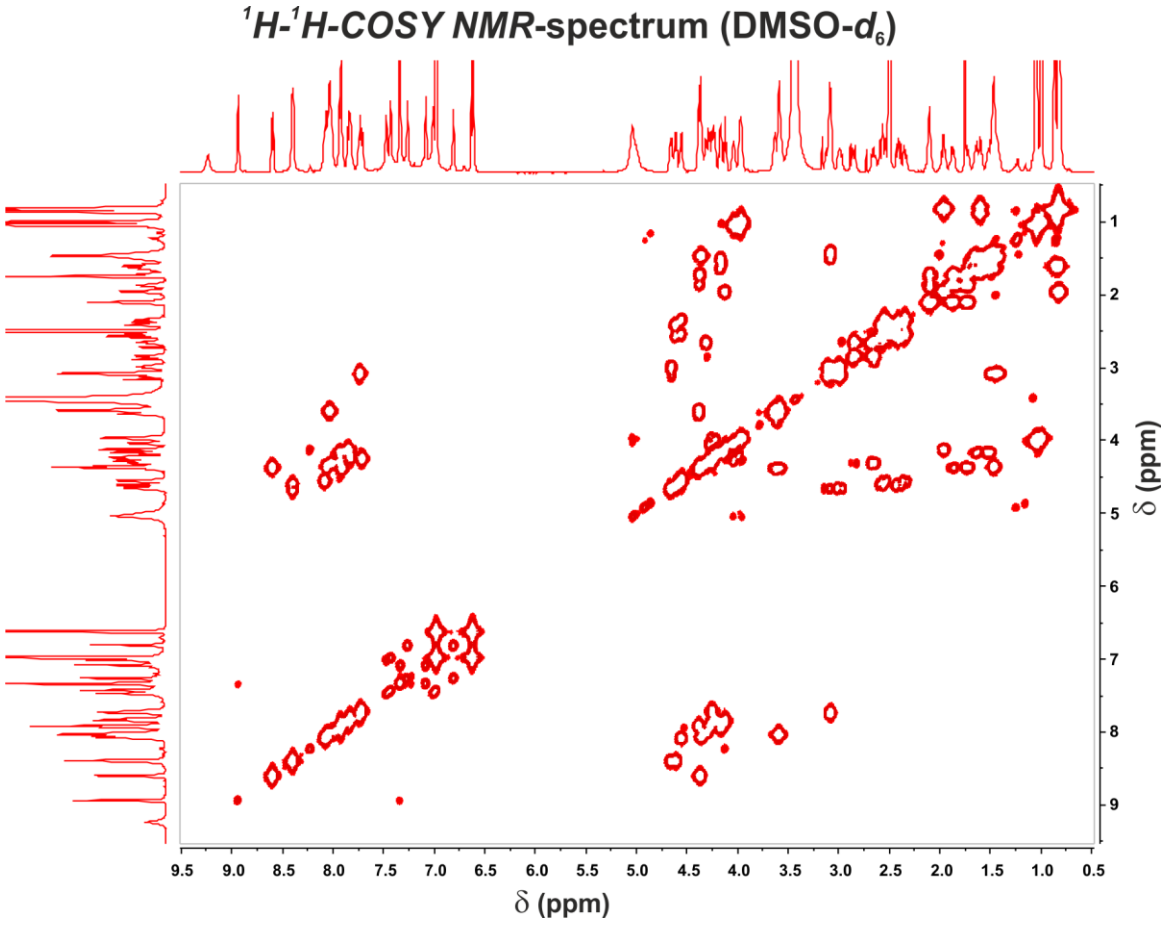
^{1}H-^{1}H-COSY NMR-spectrum (DMSO-d_6)
9.5 9.0 8.5 8.0 7.5 7.0 6.5 6.0 5.5 5.0 4.5 4.0 3.5 3.0 2.5 2.0 1.5 1.0 0.5
δ (ppm)
1 2 3 4 5 6 7 8 9
δ (ppm)

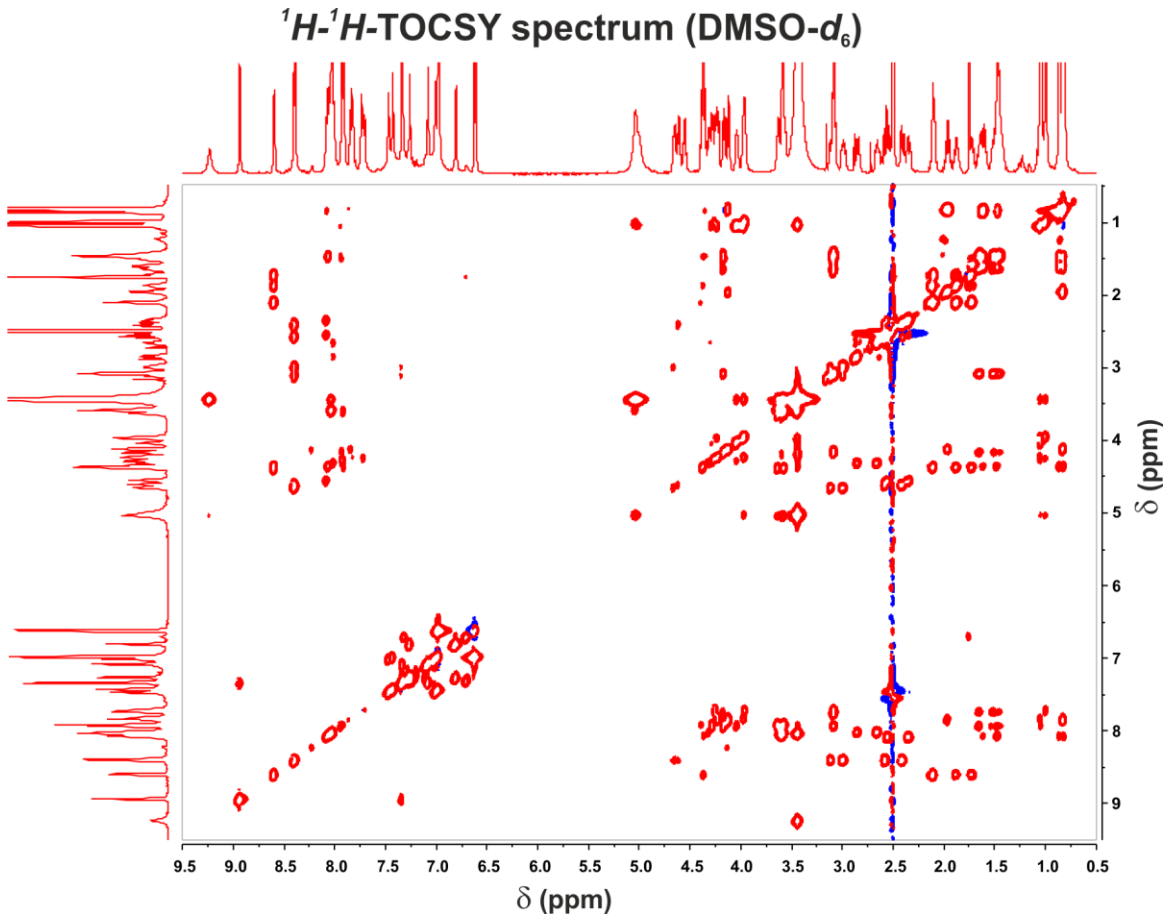
^{1}H-^{1}H-TOCSY spectrum (DMSO-d_6)
δ (ppm)
δ (ppm)

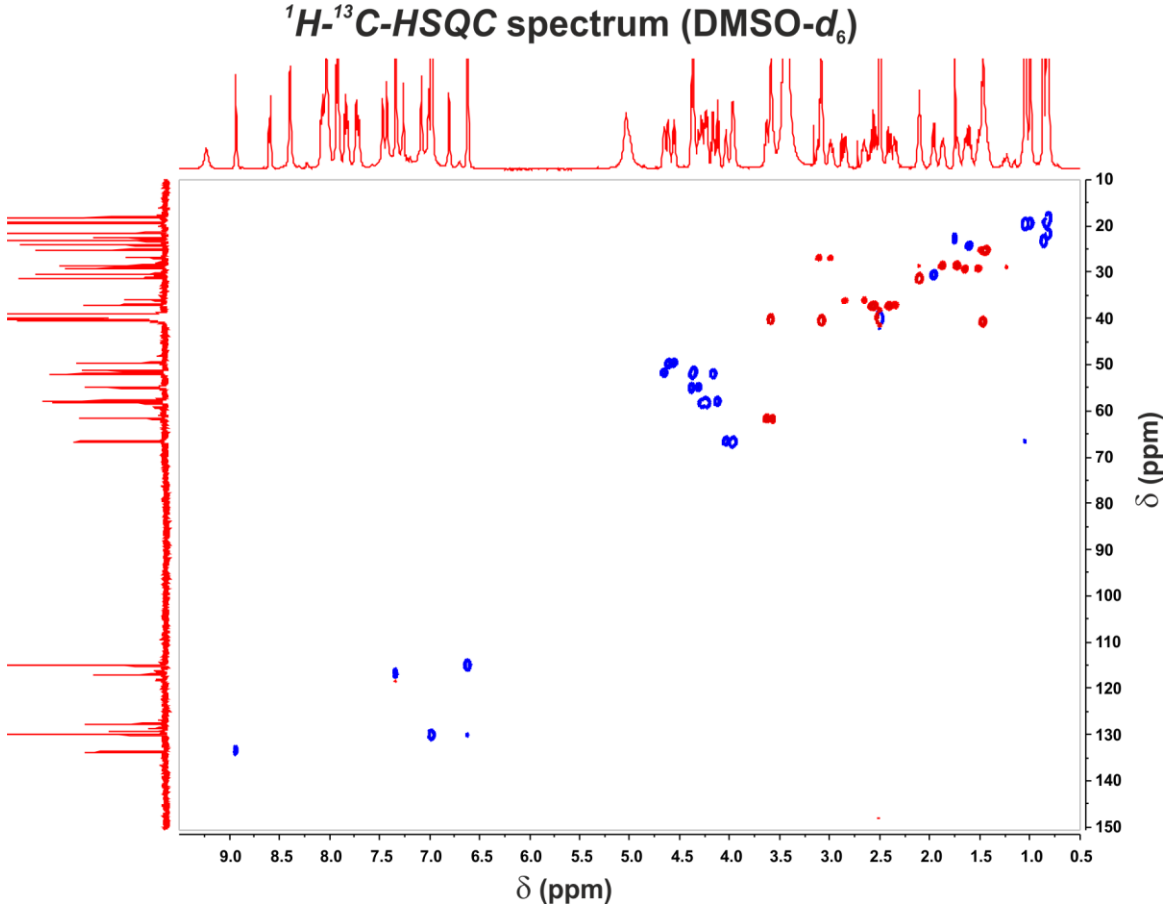
^{1}H-^{13}C-HSQC spectrum (DMSO-d_6)
δ (ppm)
δ (ppm)

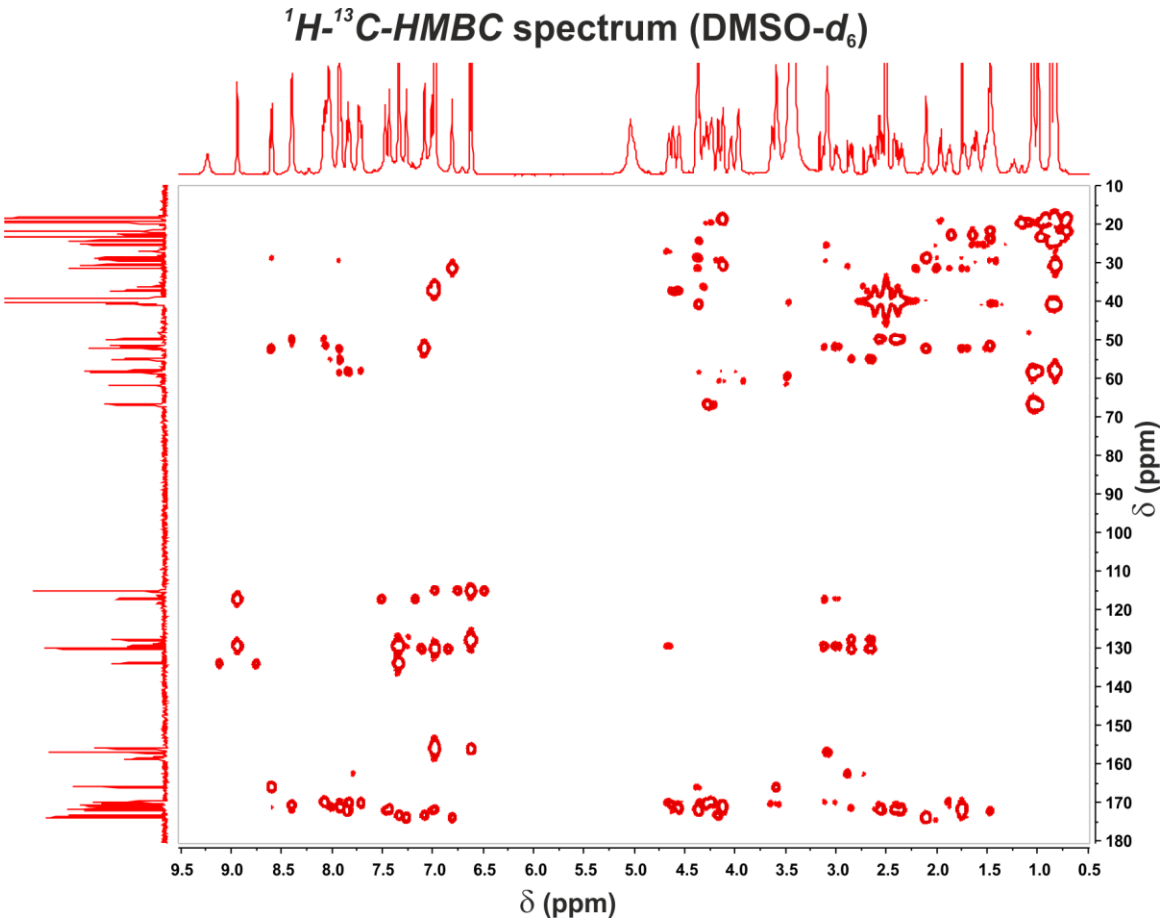
^{1}H-^{13}C-HMBC spectrum (DMSO-d_6)
δ (ppm)
δ (ppm)

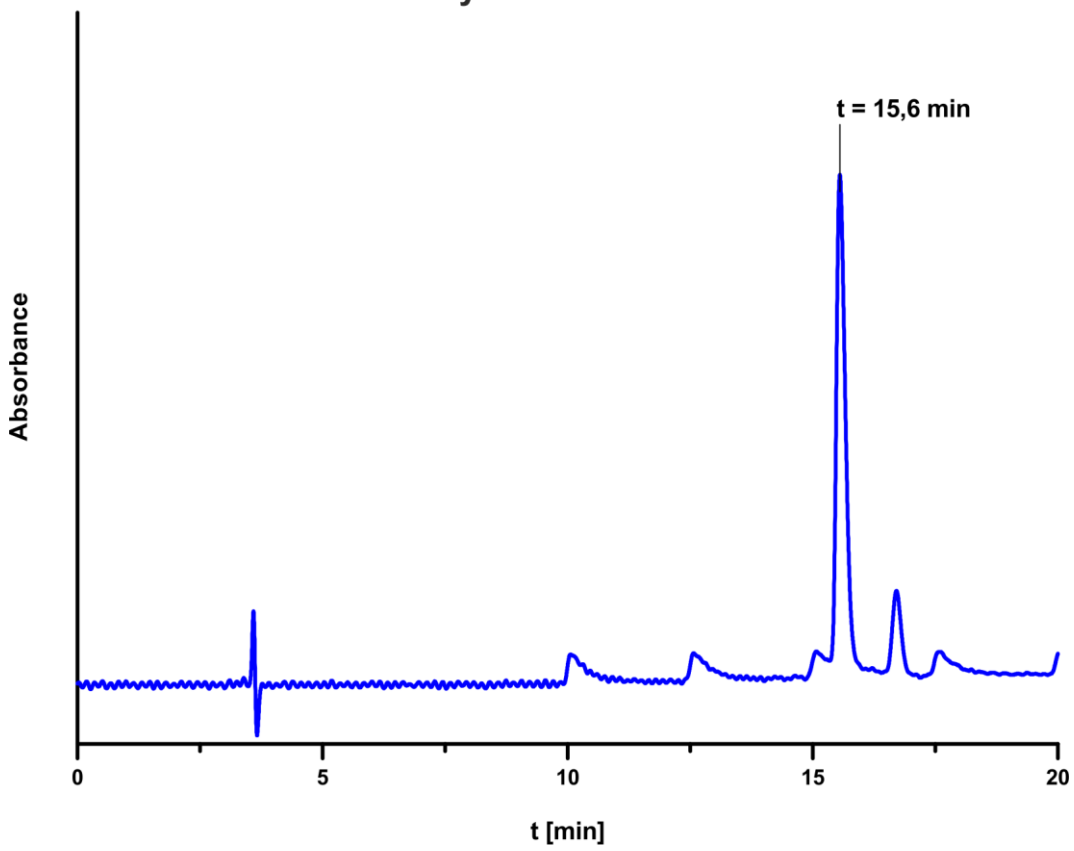
Analytical RP-HPLC
t = 15,6 min
Absorbance
t [min]

Ala-Val-Gly-Ser-Thr-Lys-His-Lys-Trp-Pro-Pro-Leu (9)

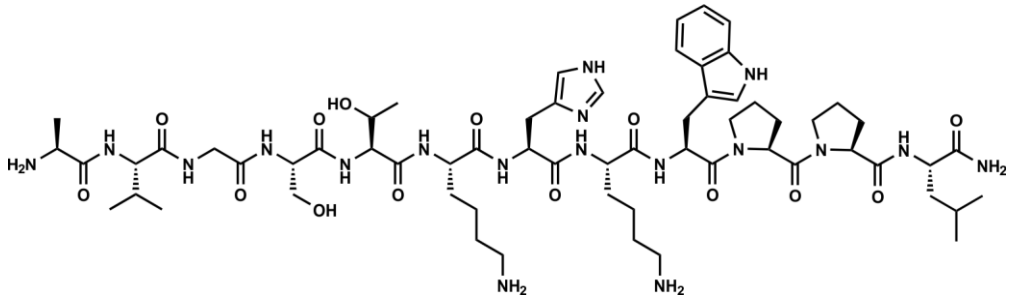

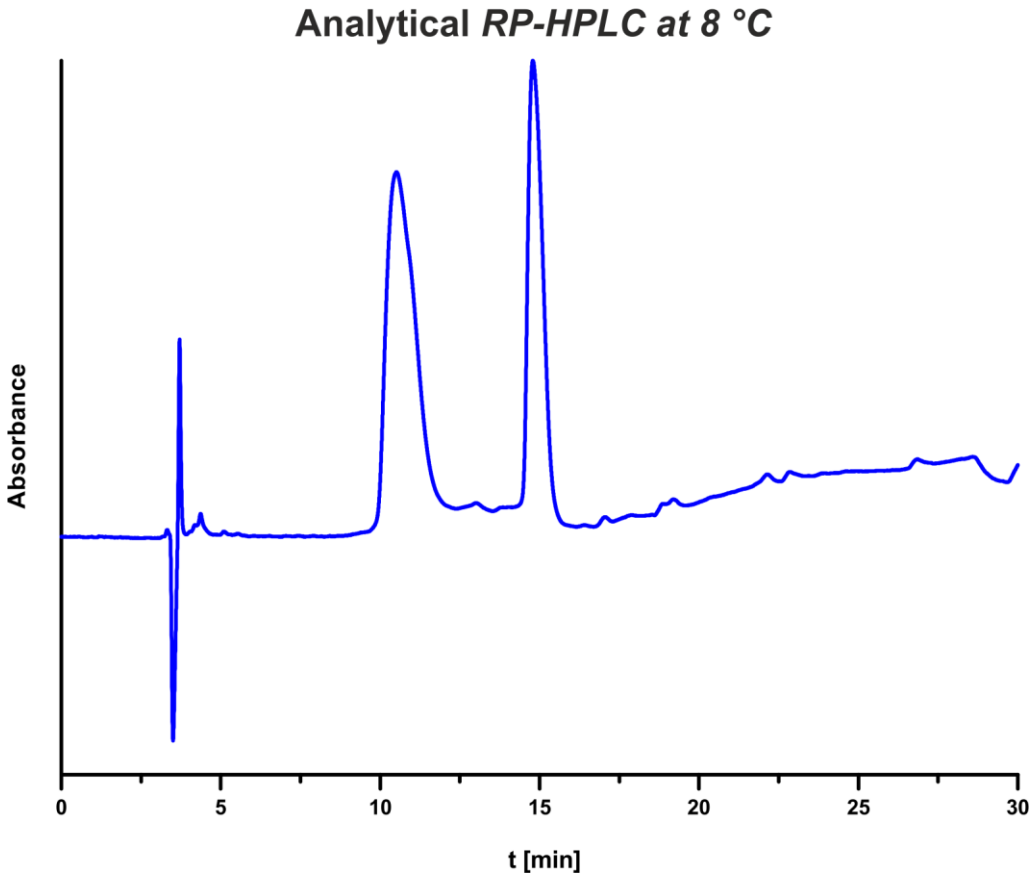

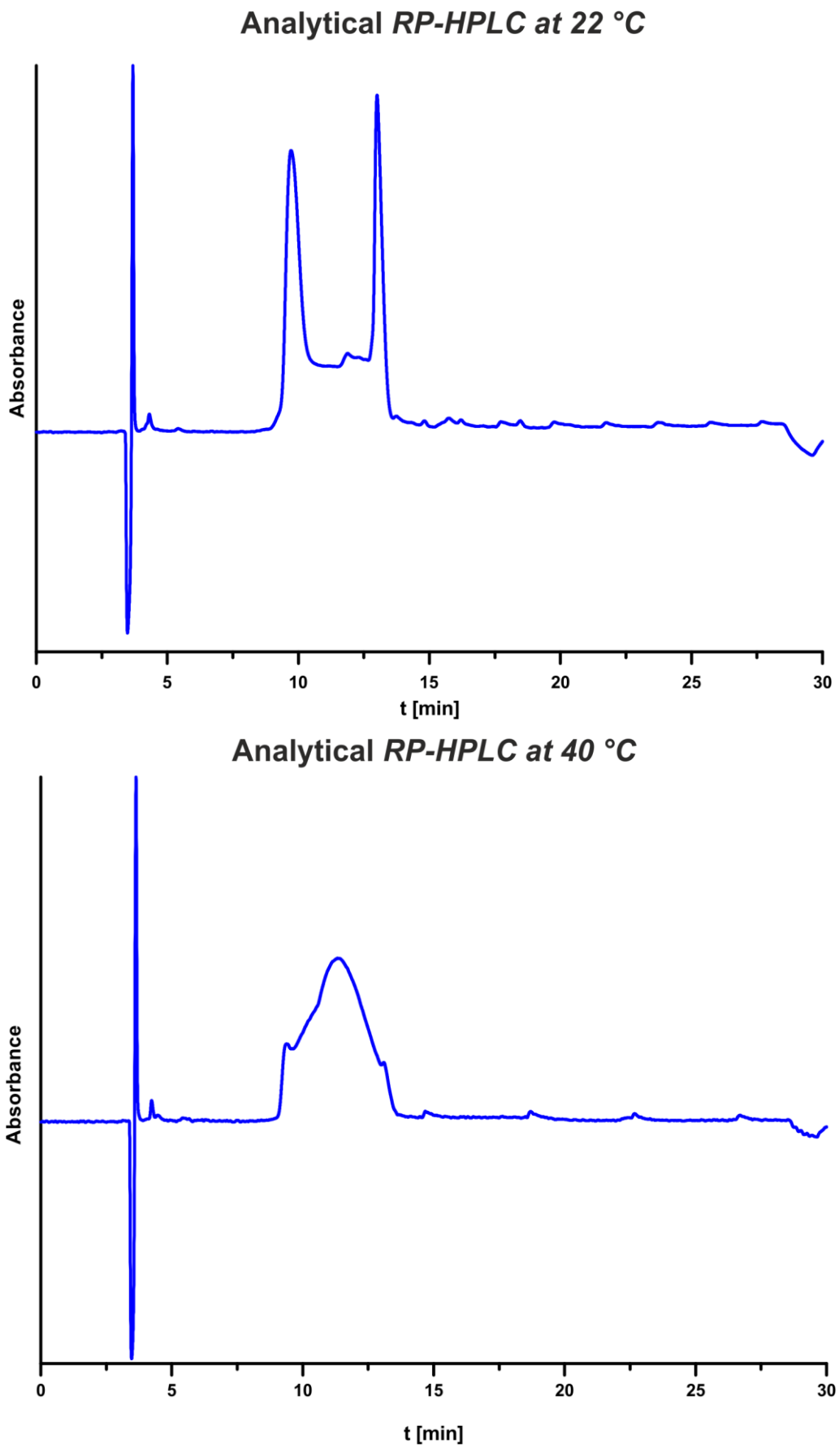
Analytical RP-HPLC at 22 °C
Absorbance
0
5
10
15
20
25
30
t [min]
Analytical RP-HPLC at 40 °C
Absorbance
0
5
10
15
20
25
30
t [min]

His-Thr-Gln-Asn-Met-Arg-Met-Tyr-Glu-Pro-Trp-Phe (10)

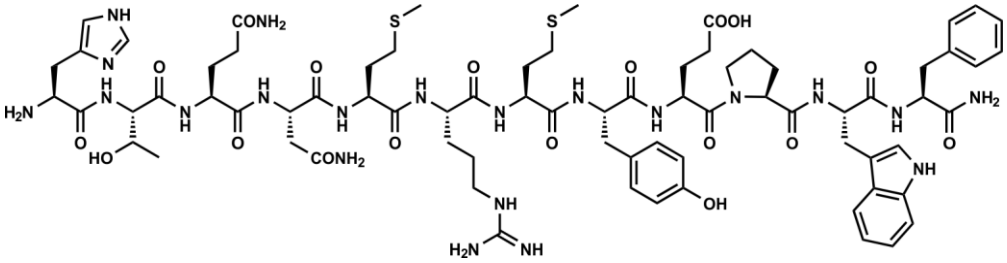

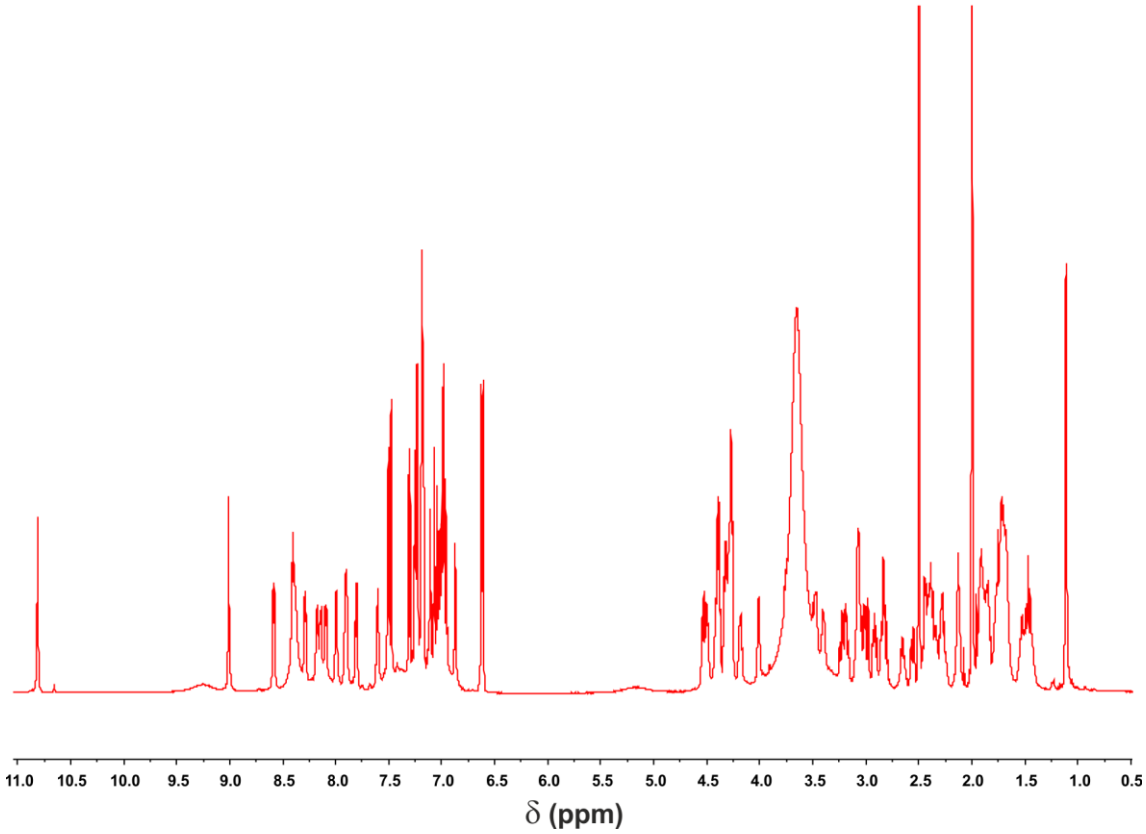

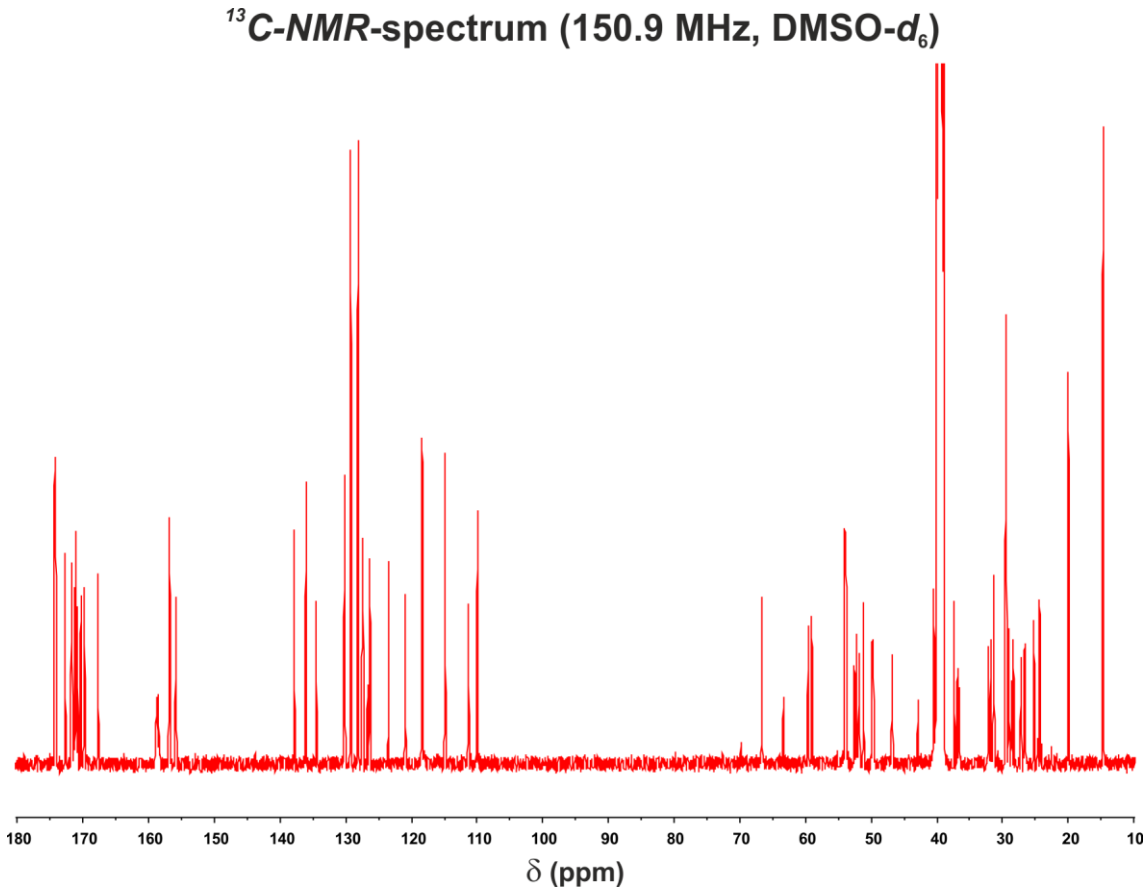
^{13}C-NMR-spectrum (150.9 MHz, DMSO-d_6)
180 170 160 150 140 130 120 110 100 90 80 70 60 50 40 30 20 10
δ (ppm)

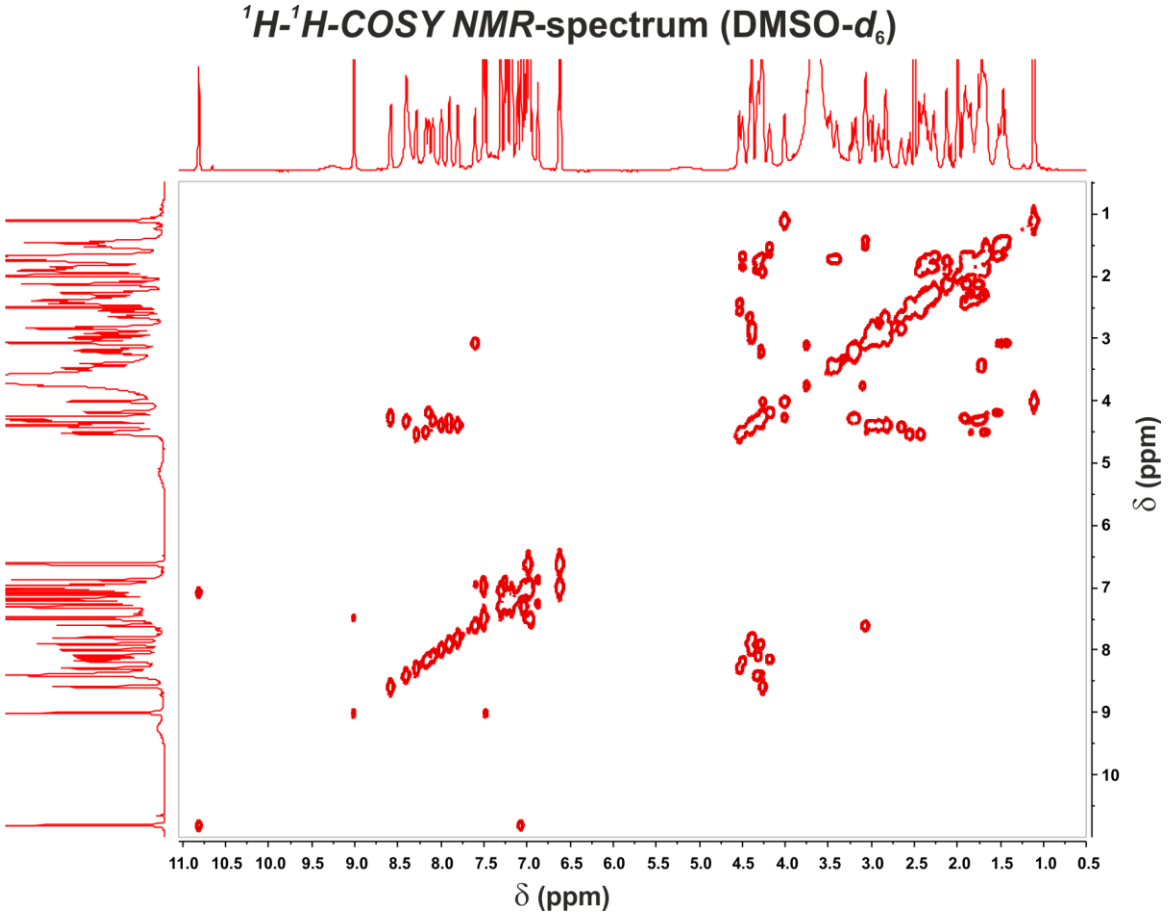
^{1}H-^{1}H-COSY NMR-spectrum (DMSO-d_6)
11.0 10.5 10.0 9.5 9.0 8.5 8.0 7.5 7.0 6.5 6.0 5.5 5.0 4.5 4.0 3.5 3.0 2.5 2.0 1.5 1.0 0.5
δ (ppm)
1 2 3 4 5 6 7 8 9 10
δ (ppm)

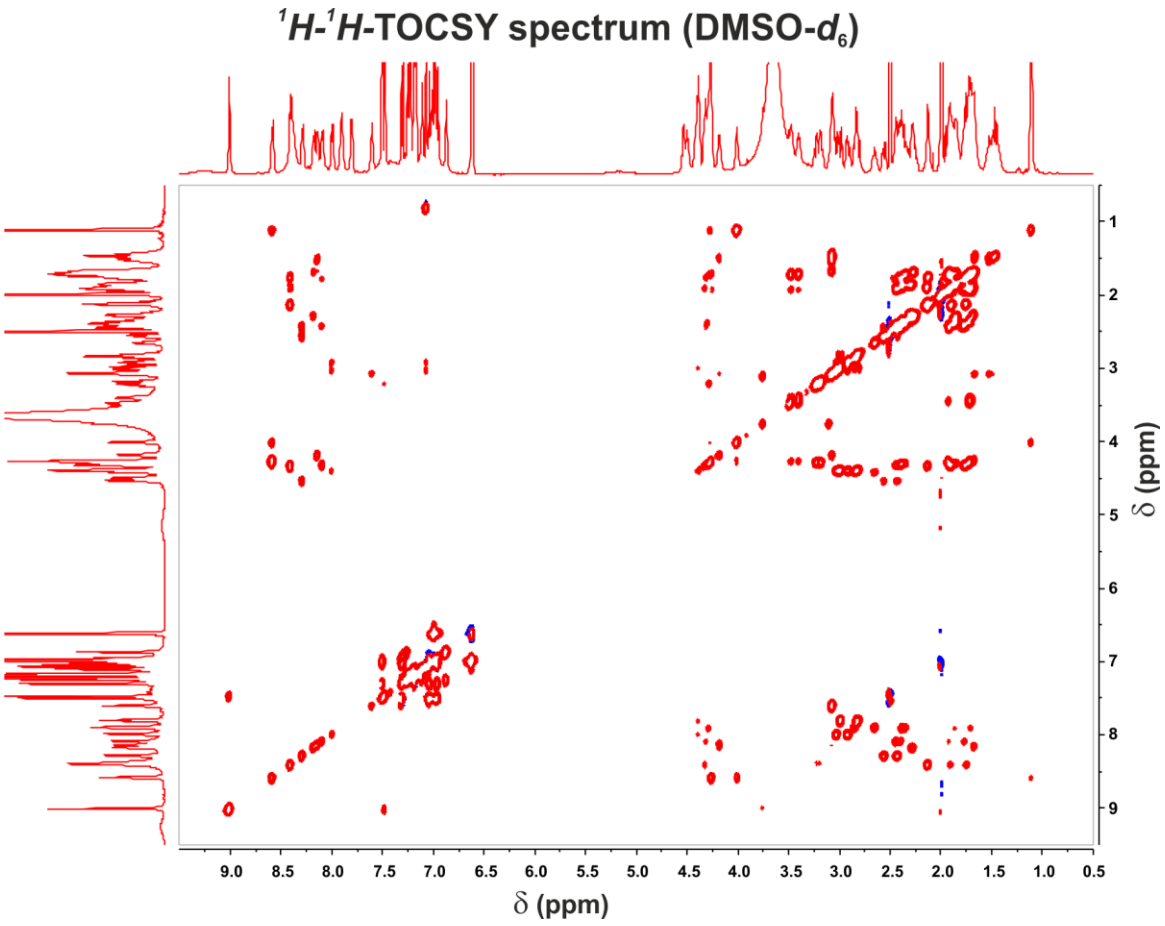
^{1}H-^{1}H-TOCSY spectrum (DMSO-d_6)
δ (ppm)
δ (ppm)

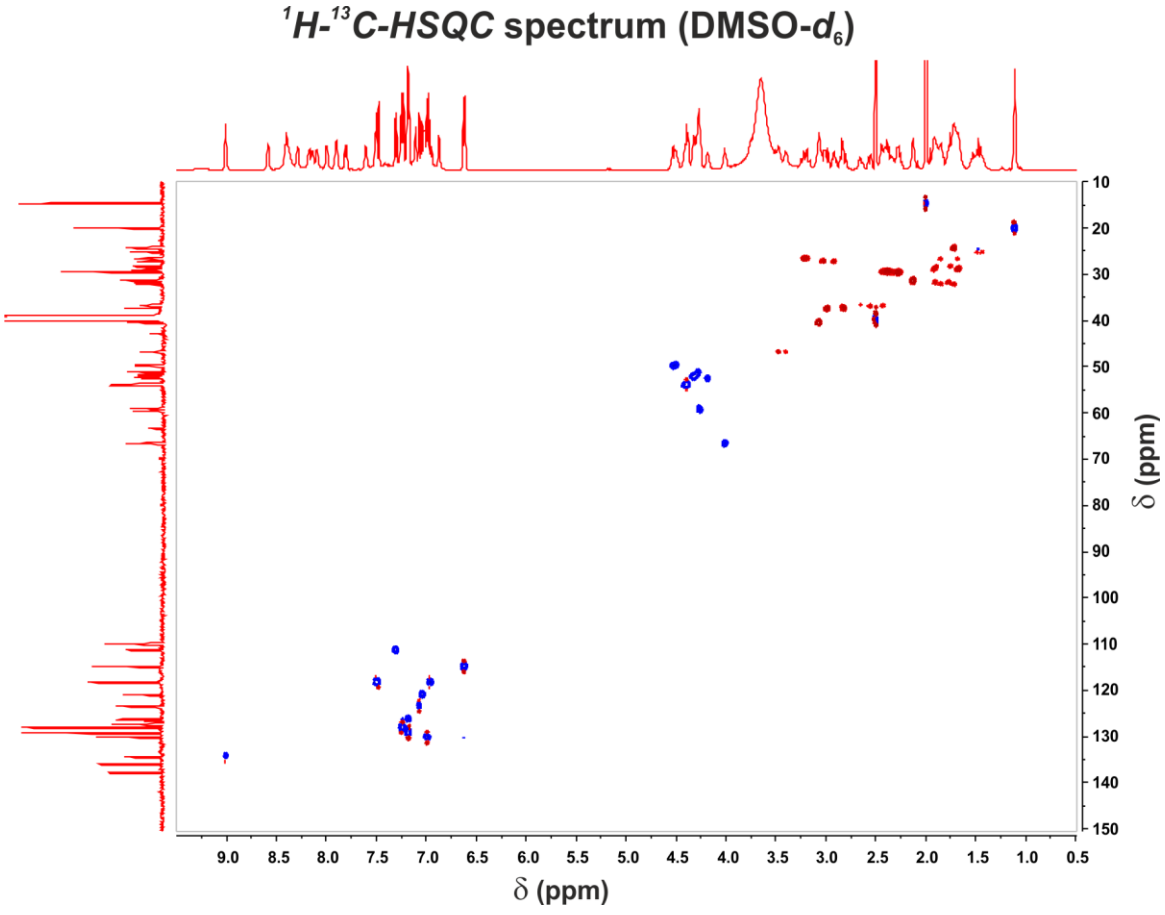
^{1}H-^{13}C-HSQC spectrum (DMSO-d_6)
δ (ppm)
δ (ppm)

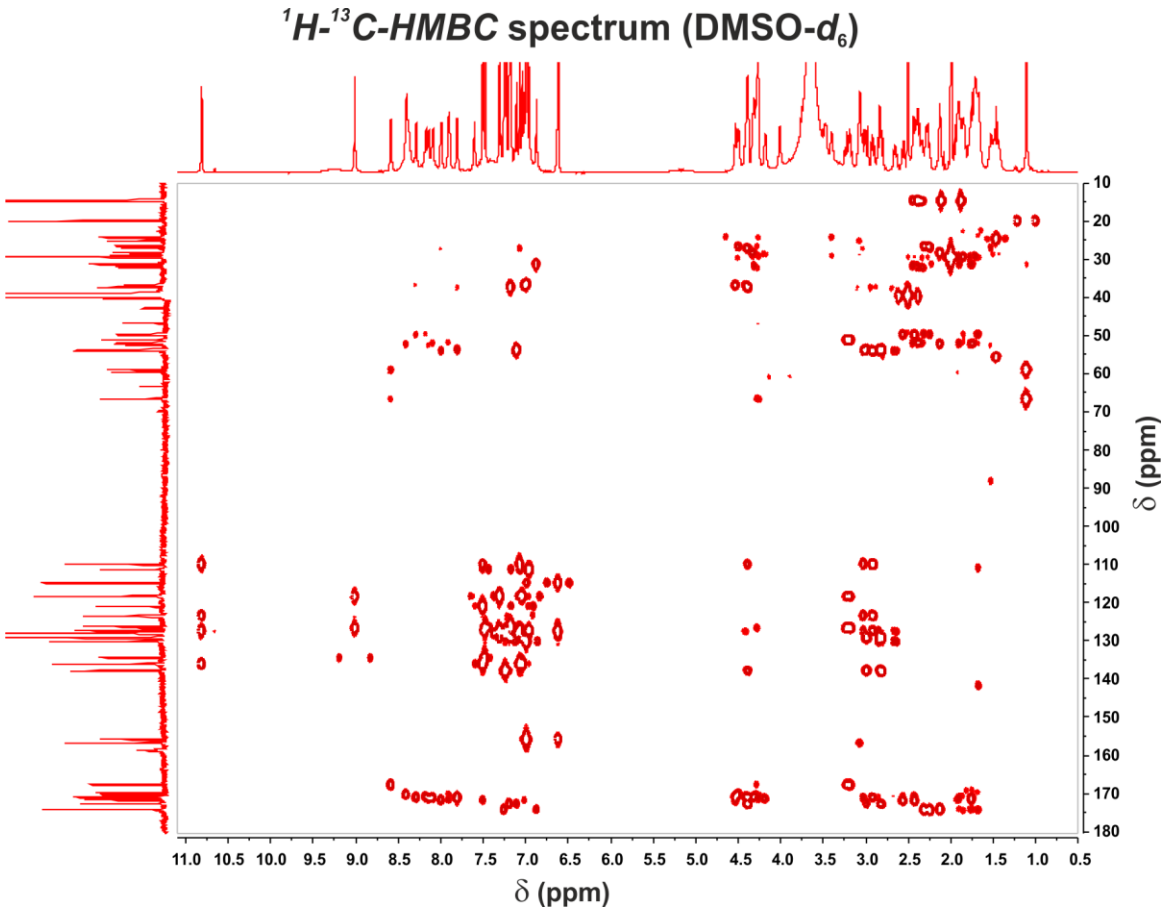
^{1}H-^{13}C-HMBC spectrum (DMSO-d_6)
δ (ppm)
δ (ppm)

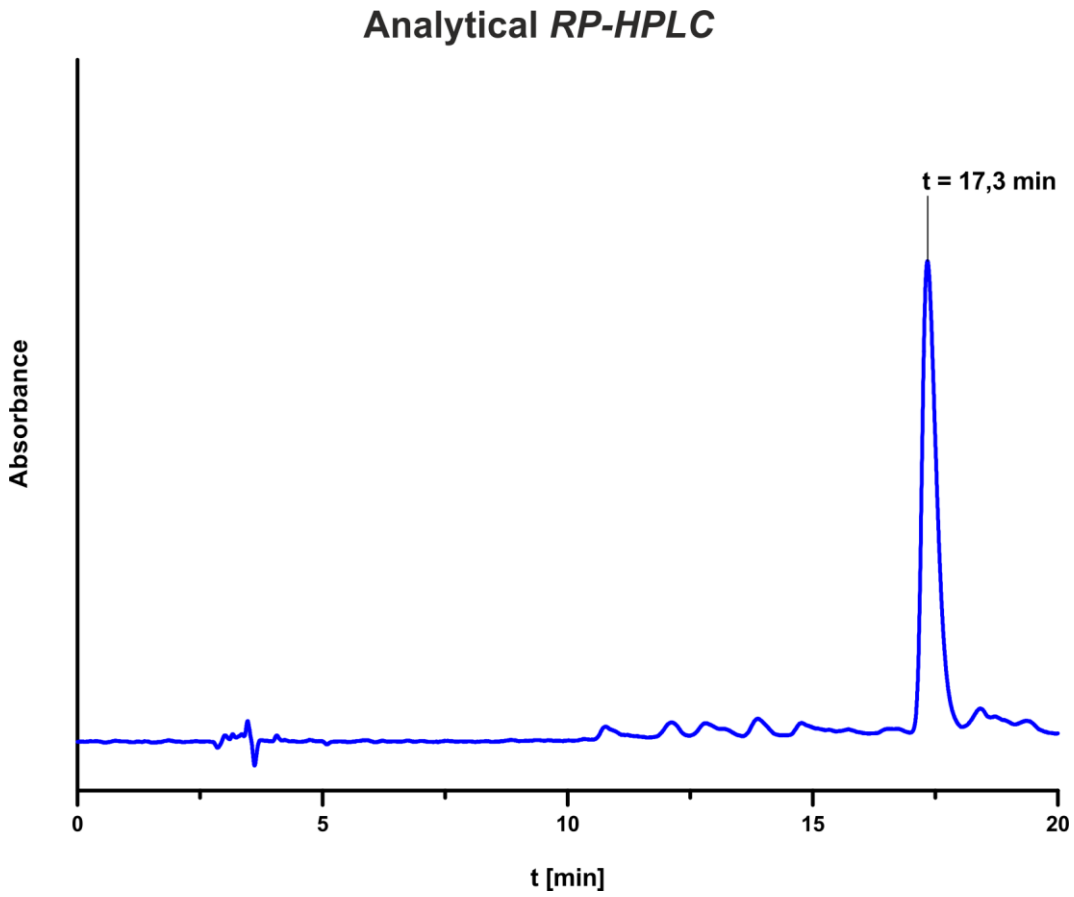
Analytical RP-HPLC
t = 17,3 min
Absorbance
t [min]

Ala-Ser-Thr-Gln-Pro-Leu-Arg-amide (11)

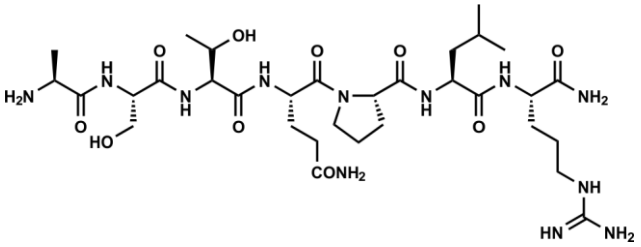

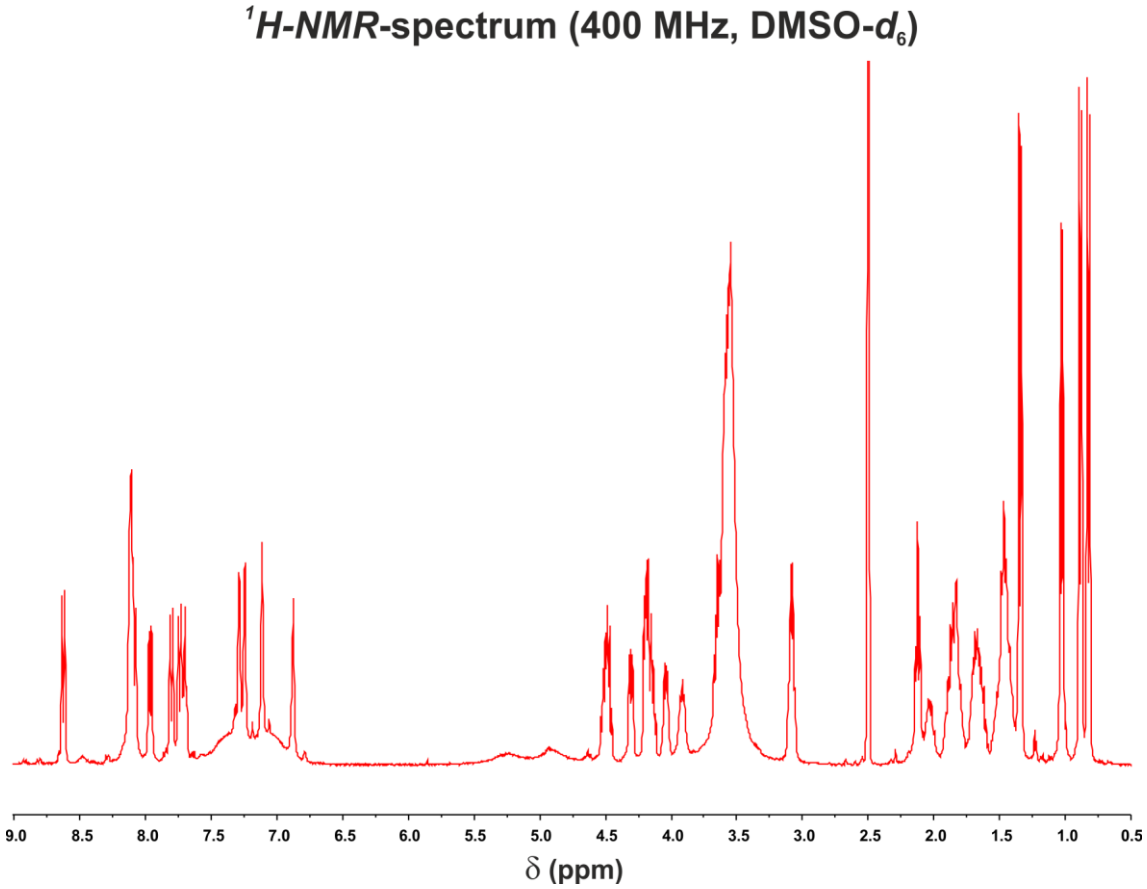

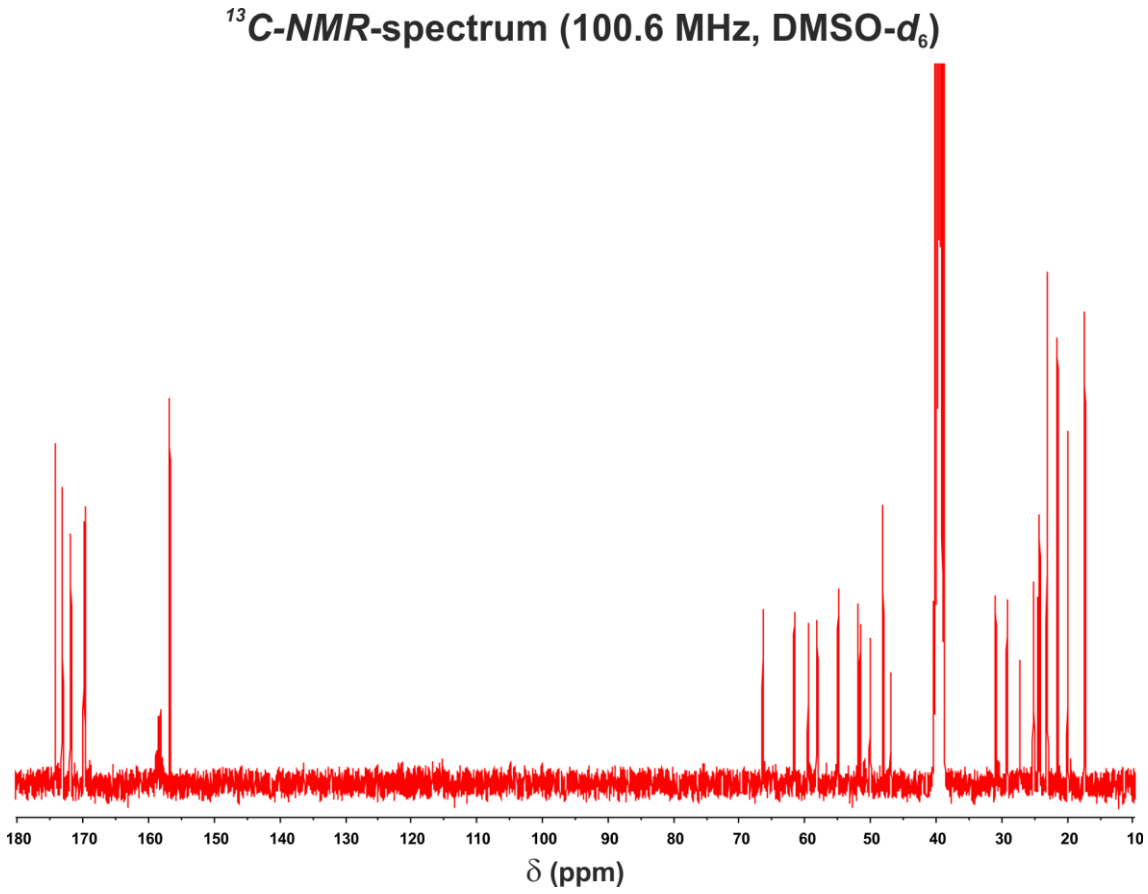
^{13}C-NMR-spectrum (100.6 MHz, DMSO-d_6)
180 170 160 150 140 130 120 110 100 90 80 70 60 50 40 30 20 10
δ (ppm)

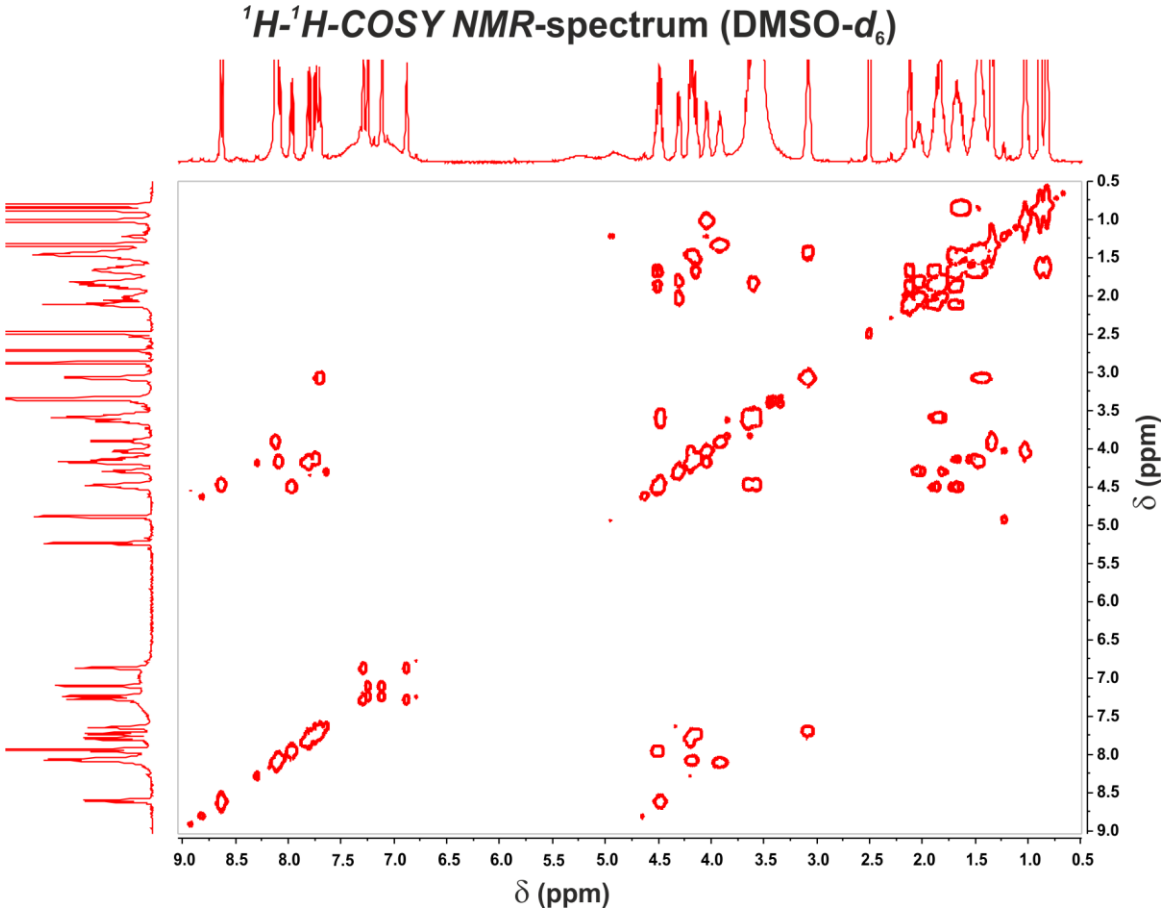
^{1}H-^{1}H-COSY NMR-spectrum (DMSO-d_6)
9.0 8.5 8.0 7.5 7.0 6.5 6.0 5.5 5.0 4.5 4.0 3.5 3.0 2.5 2.0 1.5 1.0 0.5
δ (ppm)
0.5 1.0 1.5 2.0 2.5 3.0 3.5 4.0 4.5 5.0 5.5 6.0 6.5 7.0 7.5 8.0 8.5 9.0
δ (ppm)

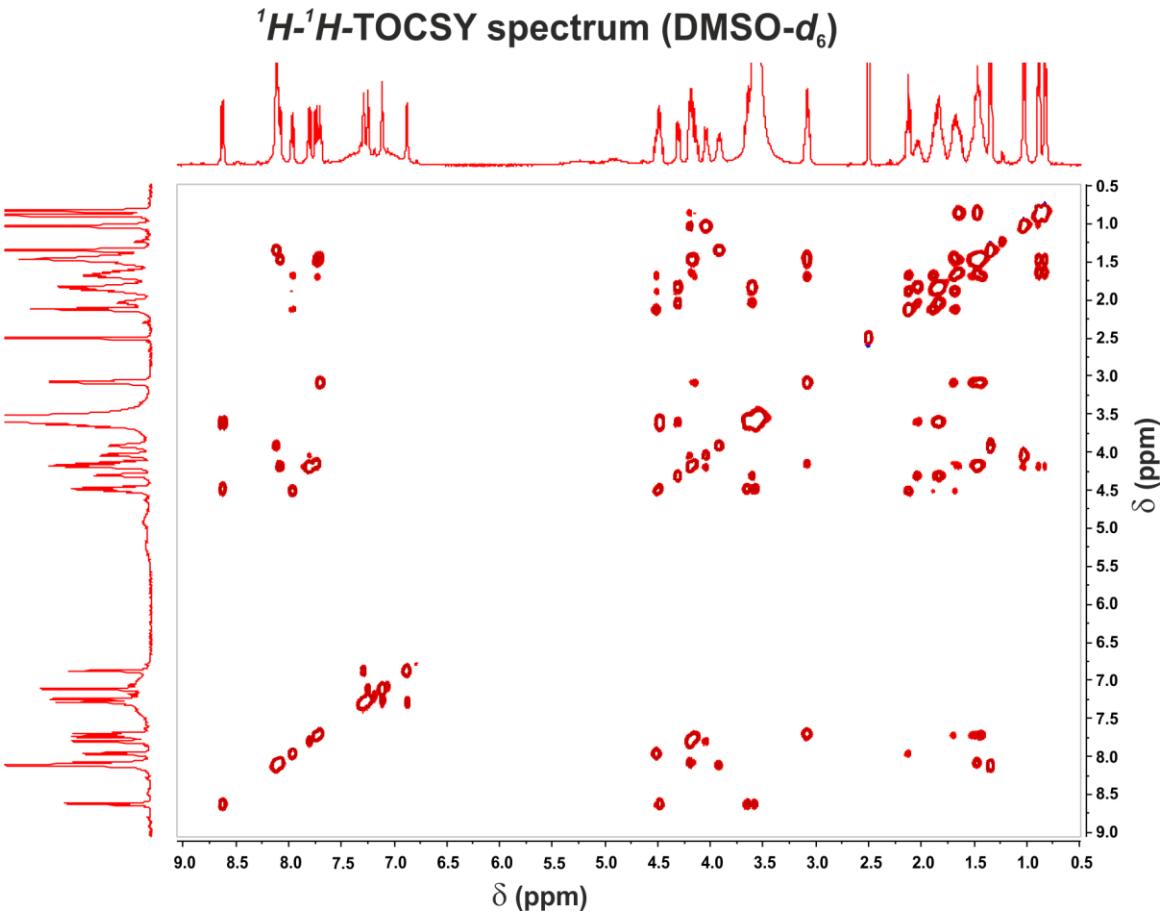
^{1}H-^{1}H-TOCSY spectrum (DMSO-d_6)
δ (ppm)
δ (ppm)

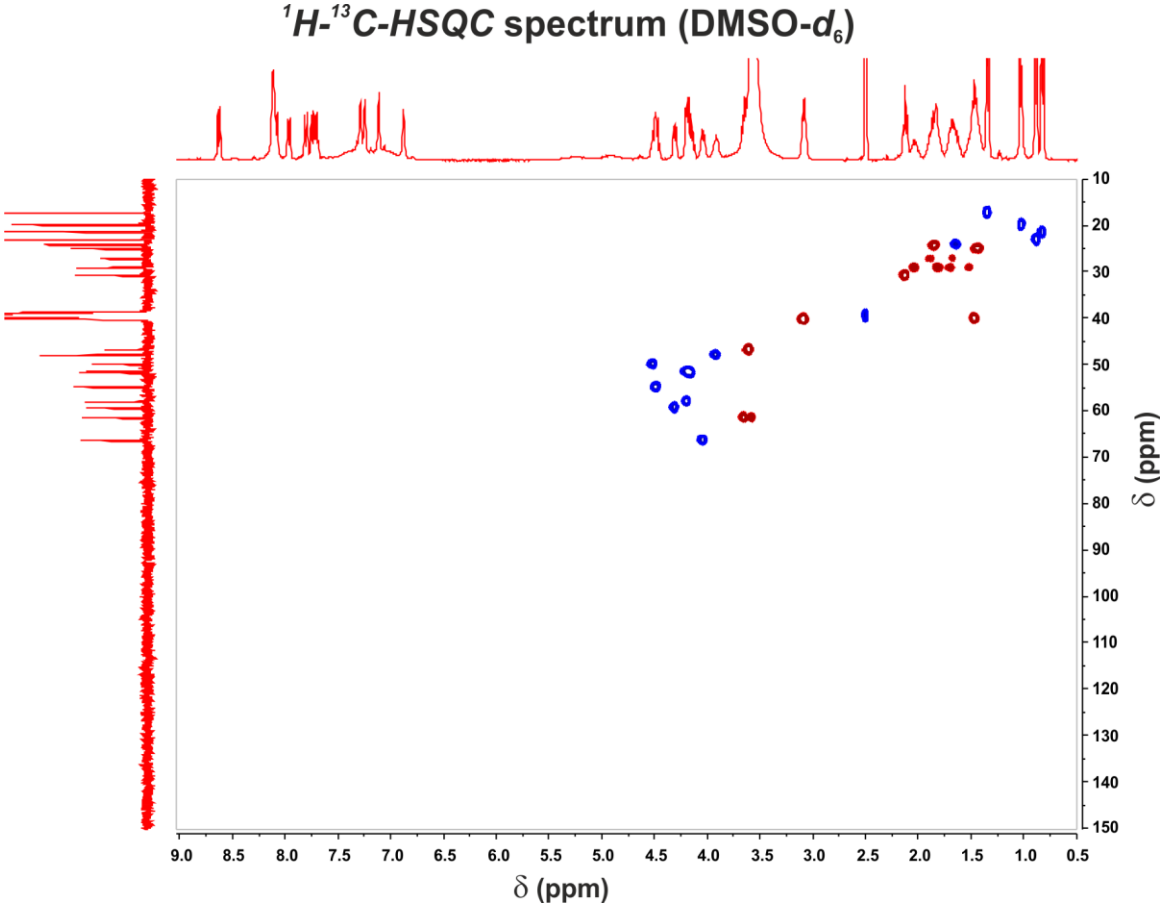
^{1}H-^{13}C-HSQC spectrum (DMSO-d_6)
δ (ppm)
δ (ppm)

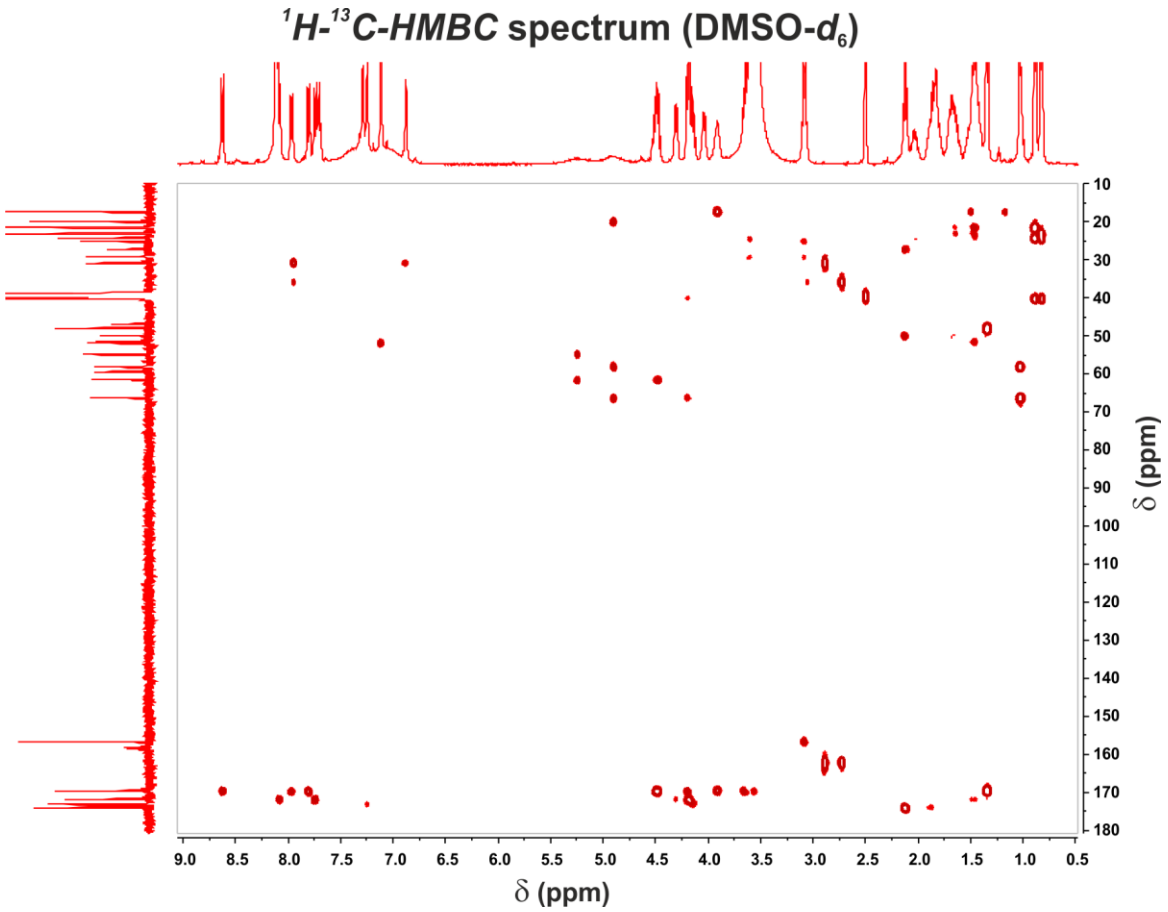
^{1}H-^{13}C-*HMBC* spectrum (DMSO-d_6)
δ (ppm)
δ (ppm)

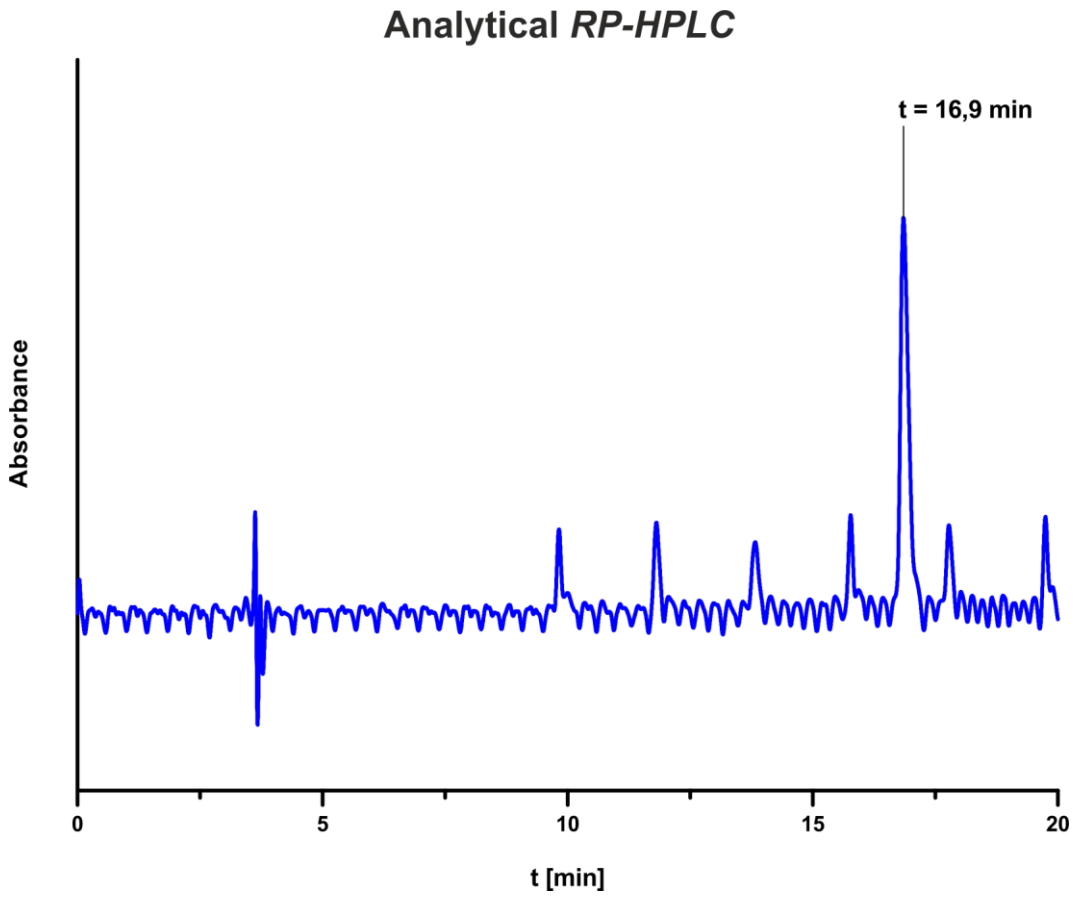
Analytical *RP-HPLC*
t = 16,9 min
Absorbance
t [min]

Val-Ala-Gln-Thr-Ala-Val-His-Gly-Val-Met-Gln-Lys-amide (12)

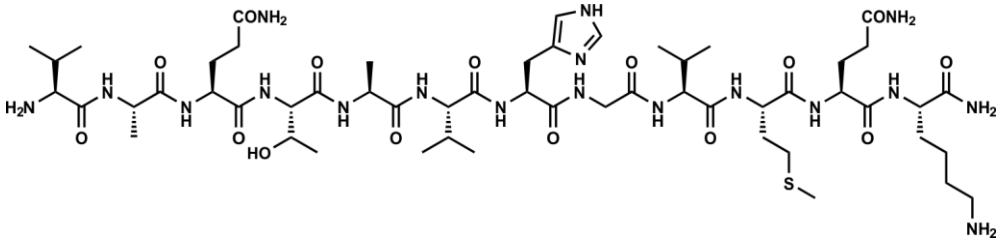

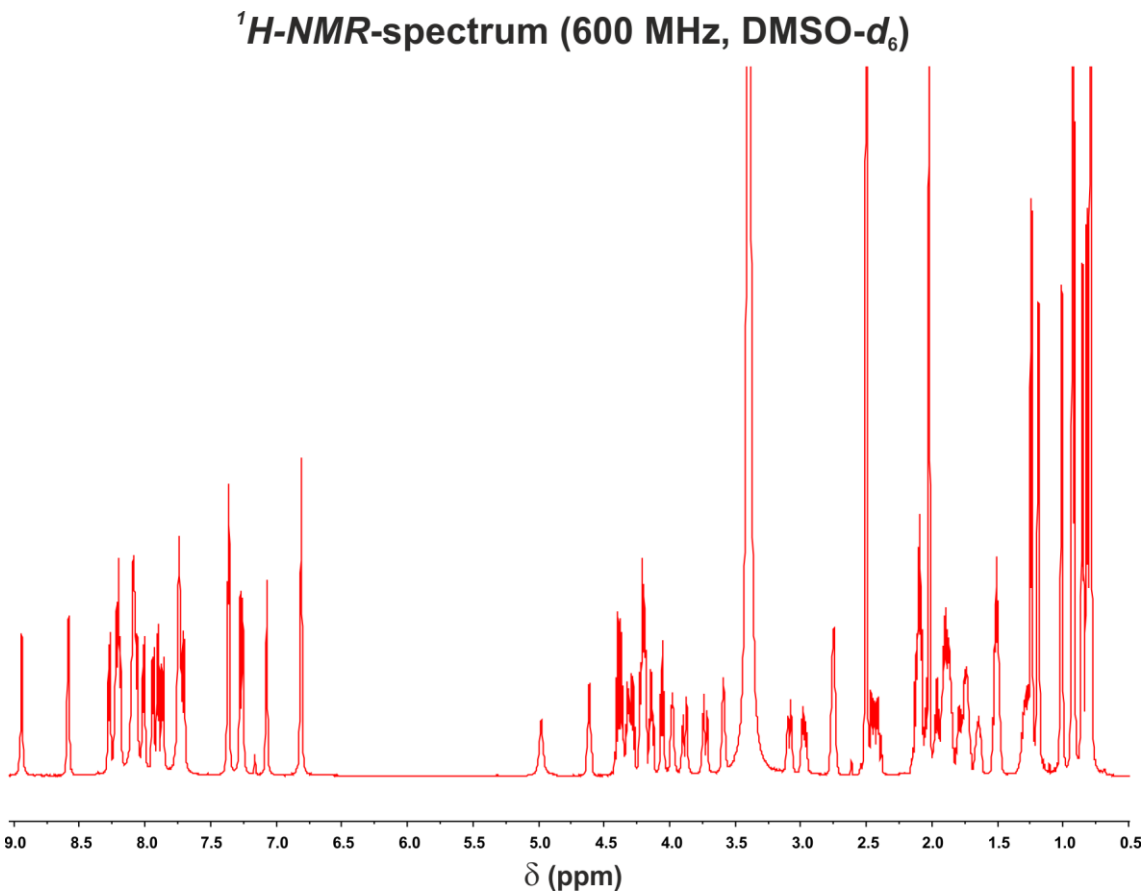

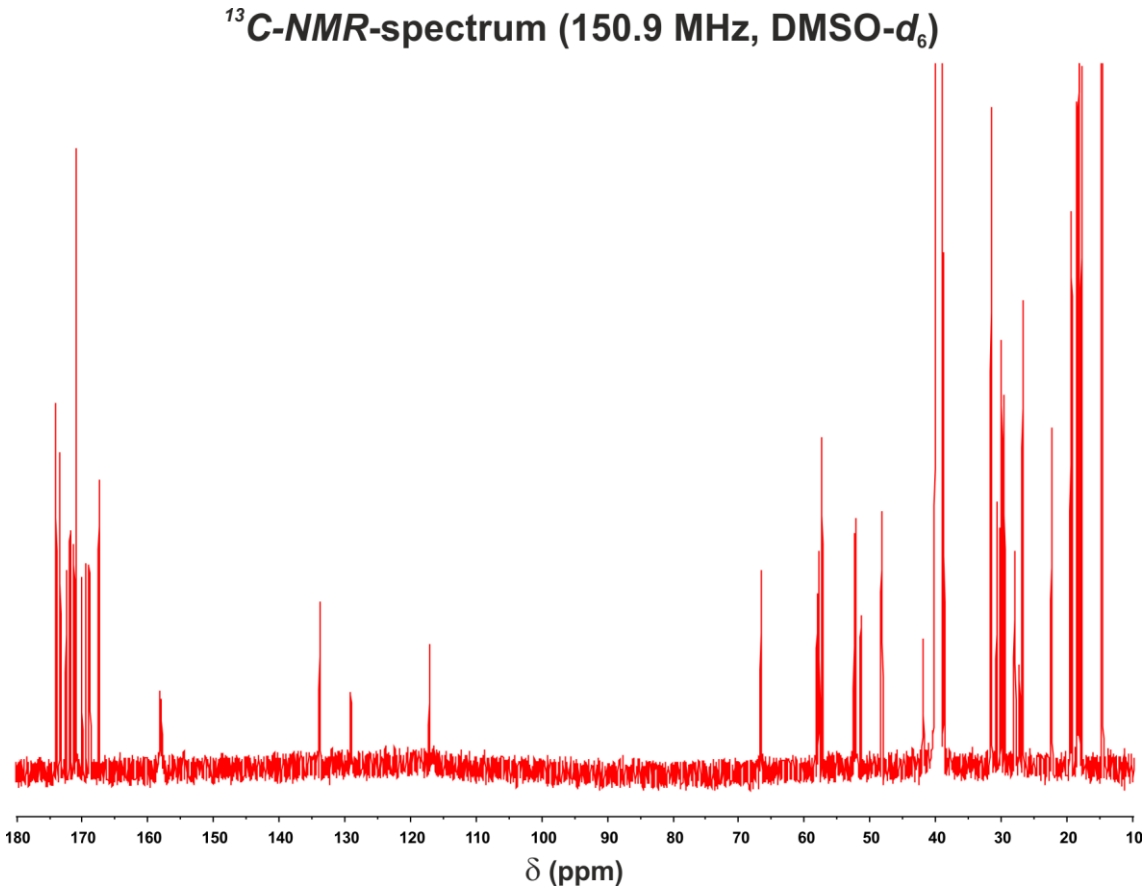
^{13}C-NMR-spectrum (150.9 MHz, DMSO-d_6)
180 170 160 150 140 130 120 110 100 90 80 70 60 50 40 30 20 10
δ (ppm)

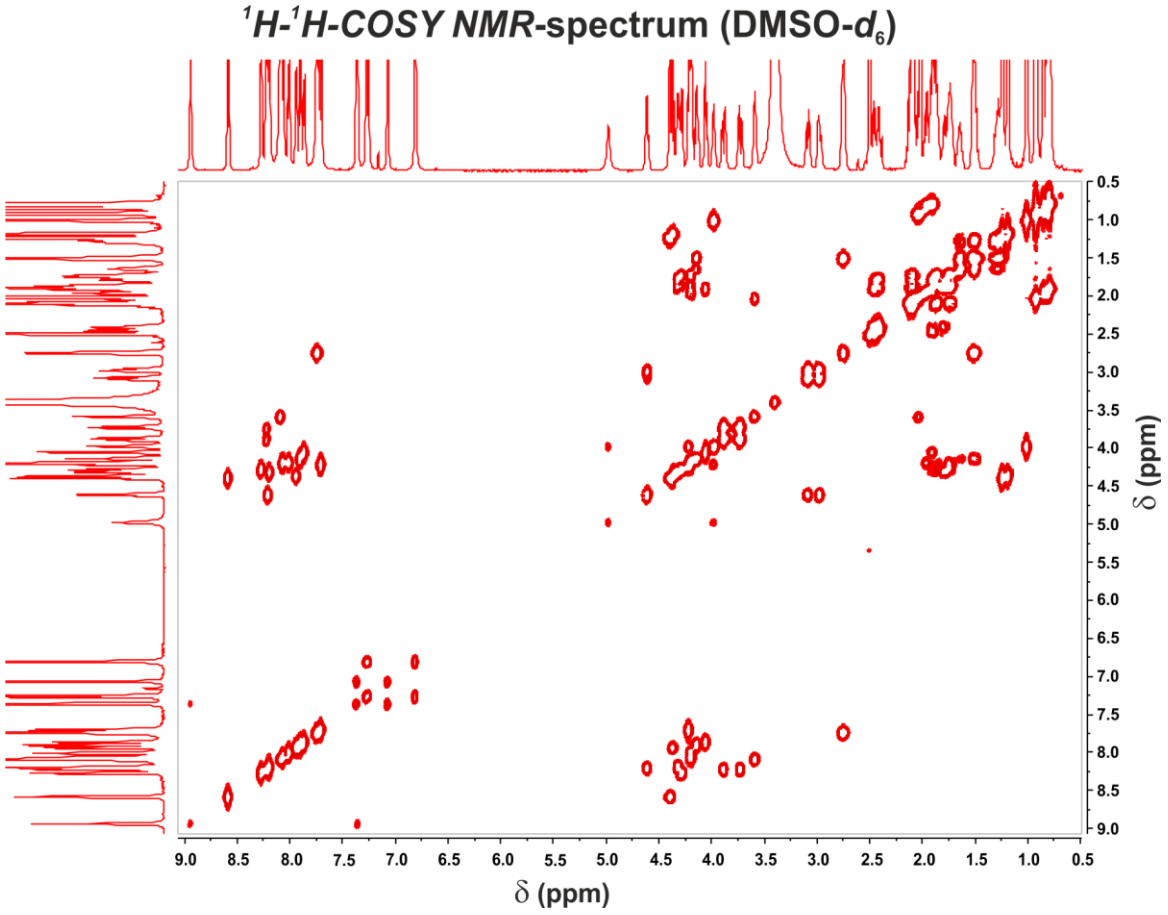
^{1}H-^{1}H-COSY NMR-spectrum (DMSO-d_6)
9.0 8.5 8.0 7.5 7.0 6.5 6.0 5.5 5.0 4.5 4.0 3.5 3.0 2.5 2.0 1.5 1.0 0.5
δ (ppm)
0.5 1.0 1.5 2.0 2.5 3.0 3.5 4.0 4.5 5.0 5.5 6.0 6.5 7.0 7.5 8.0 8.5 9.0
δ (ppm)

^{1}H-^{1}H-TOCSY spectrum (DMSO-d_6)

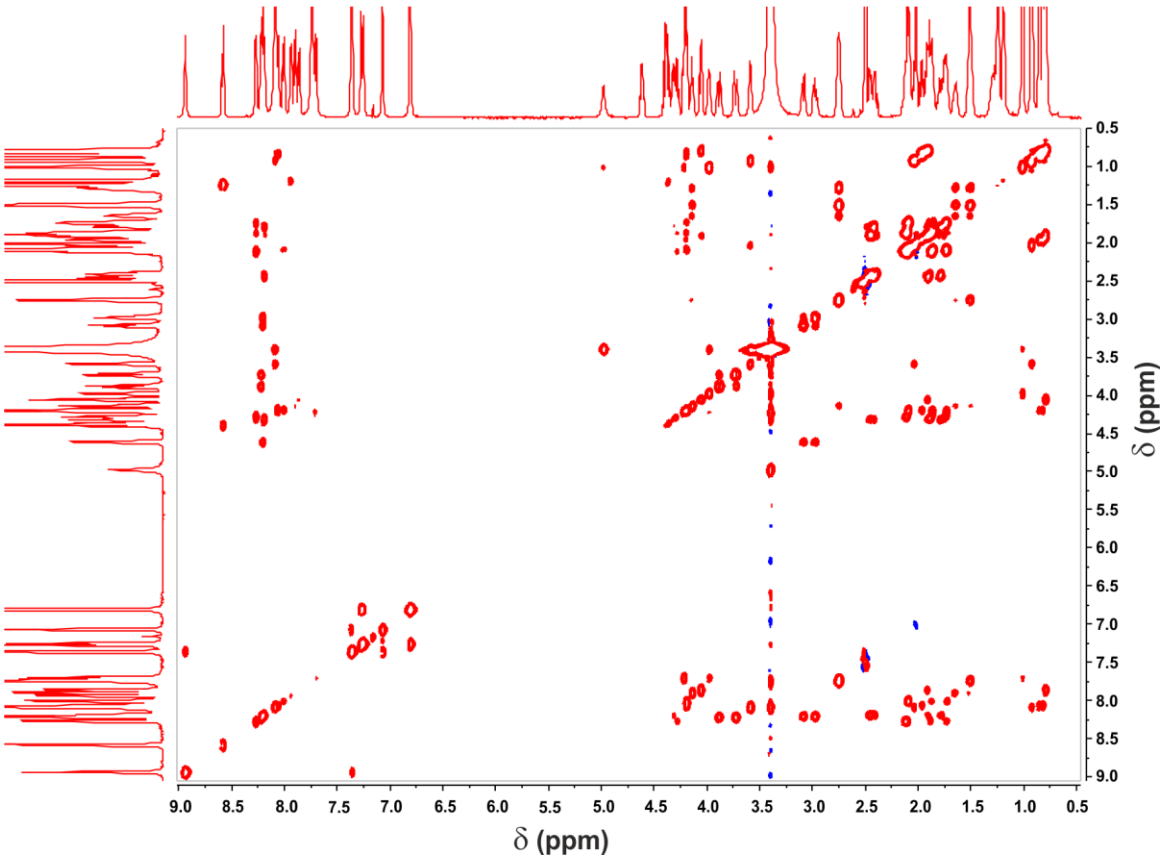

^{1}H-^{13}C-*HSQC* spectrum (DMSO-d_6)

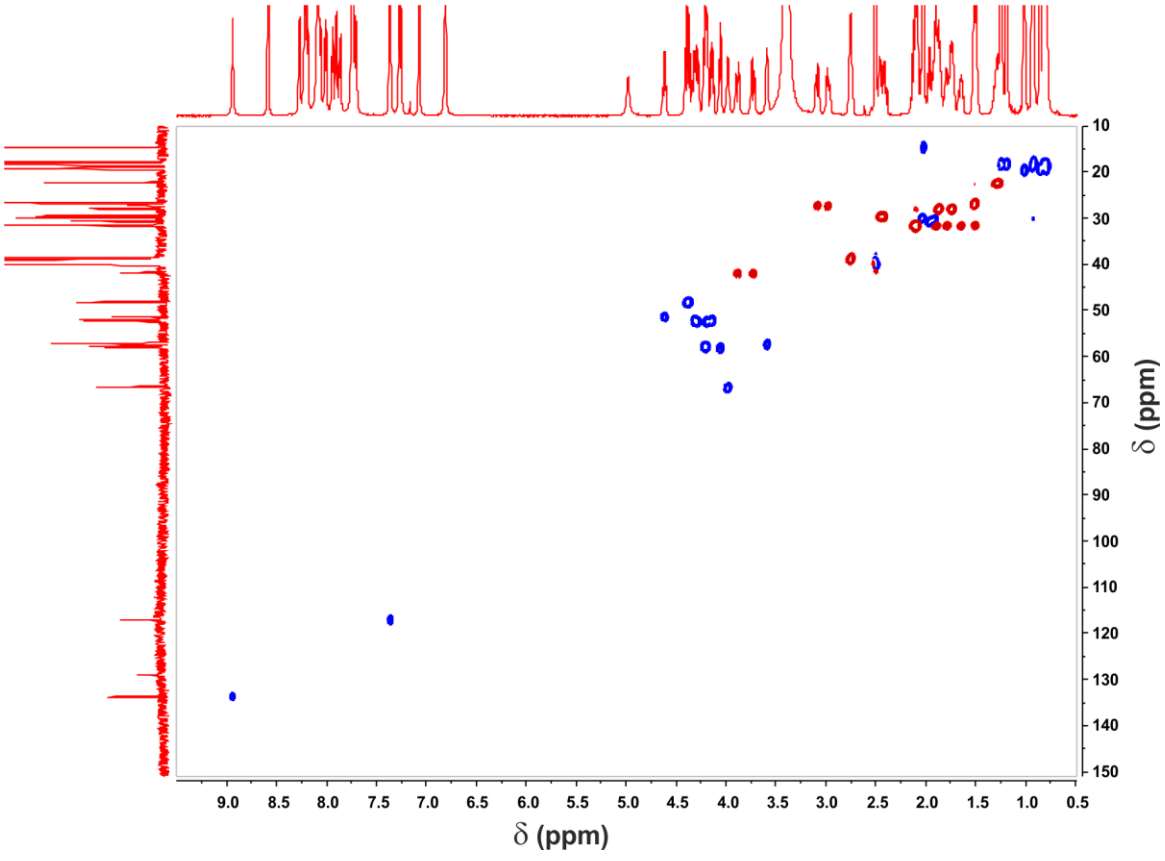

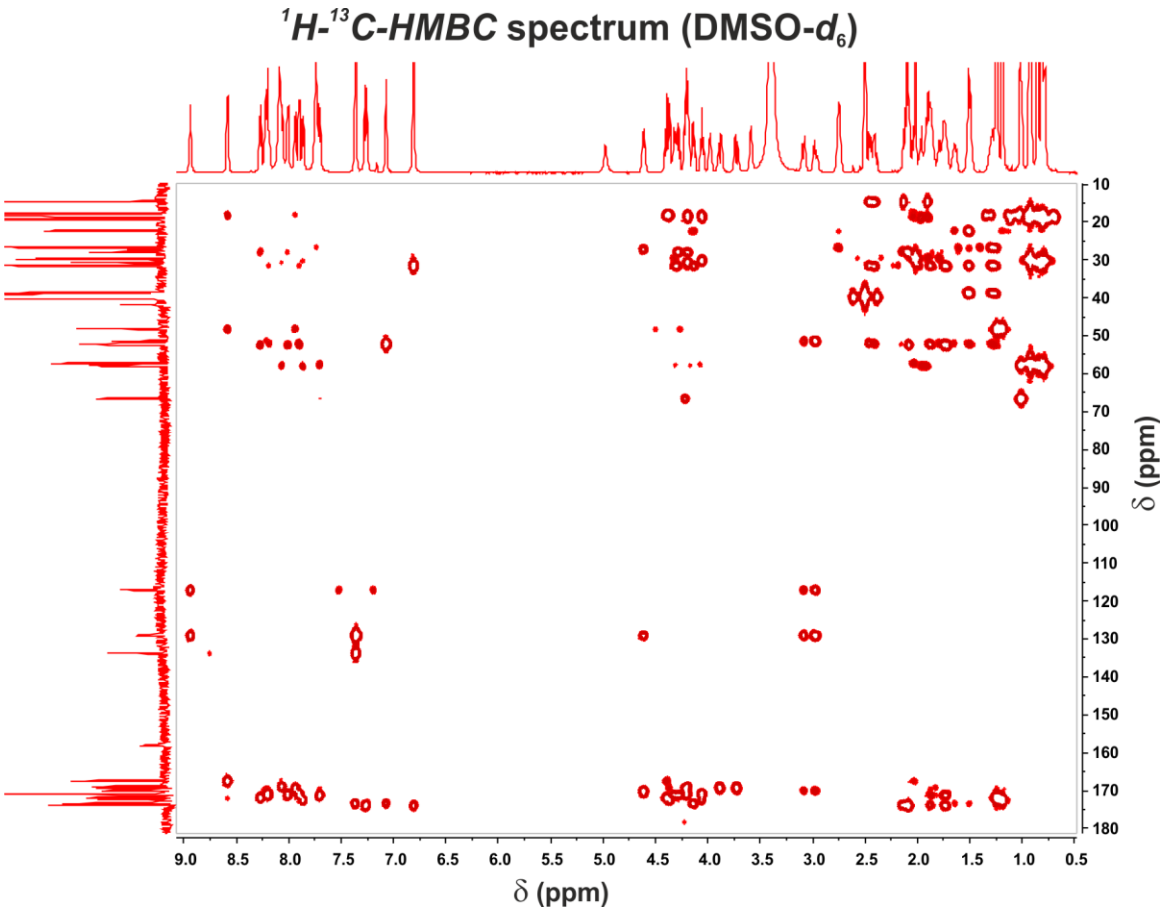
^{1}H-^{13}C-HMBC spectrum (DMSO-d_6)
δ (ppm)
δ (ppm)

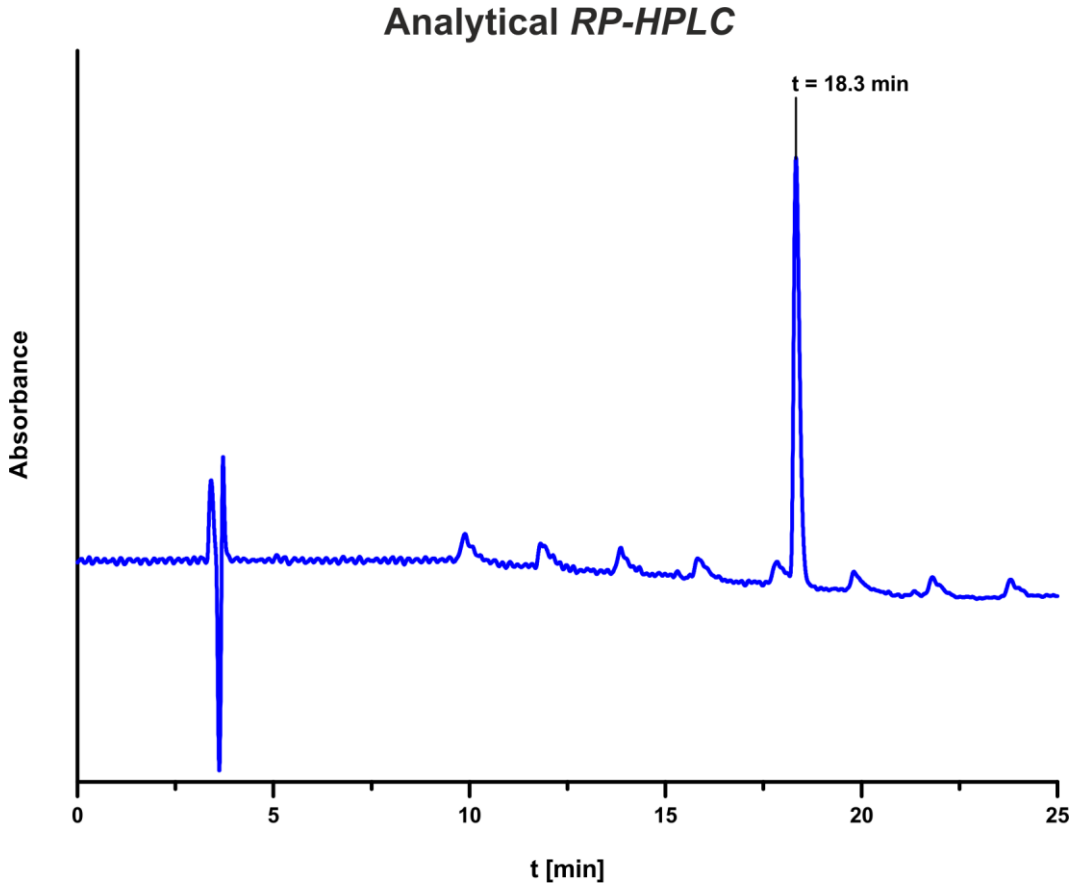
Analytical RP-HPLC
t = 18.3 min
Absorbance
t [min]

***N*-((9*H*-Fluoren-9-yl)-methoxycarbonyle)-Glycyl-(2-methyl-4-(o-tolyldiazen-yl)phenyl)-amide (18)**

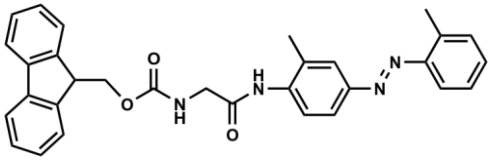

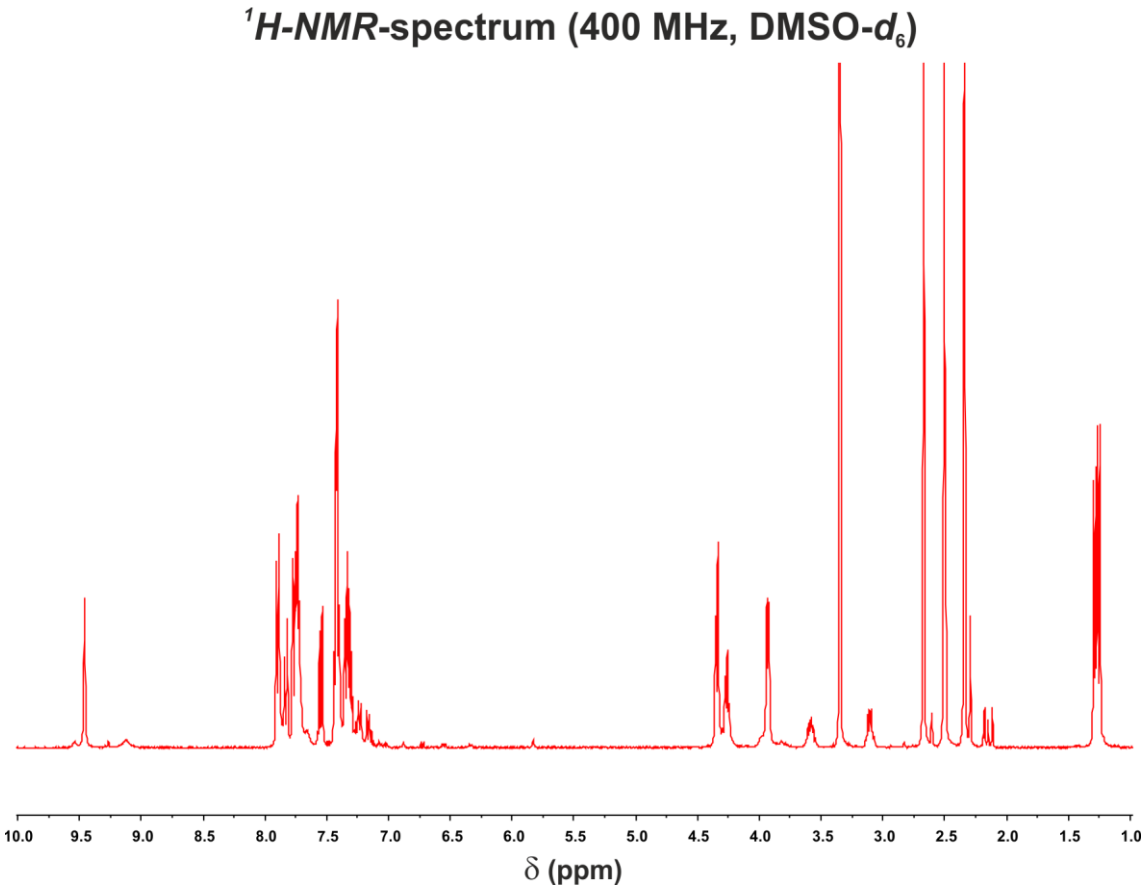

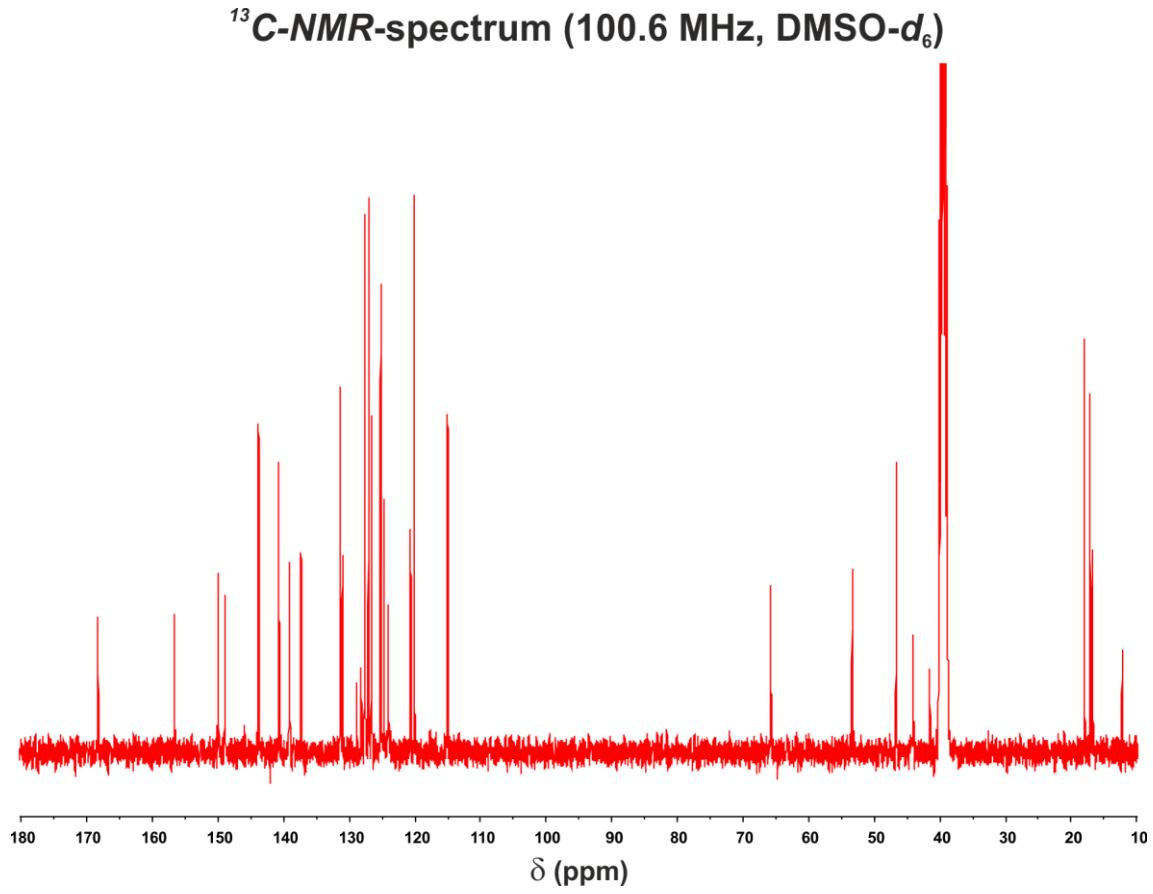
^{13}C-NMR-spectrum (100.6 MHz, DMSO-d_6)
180 170 160 150 140 130 120 110 100 90 80 70 60 50 40 30 20 10
δ (ppm)

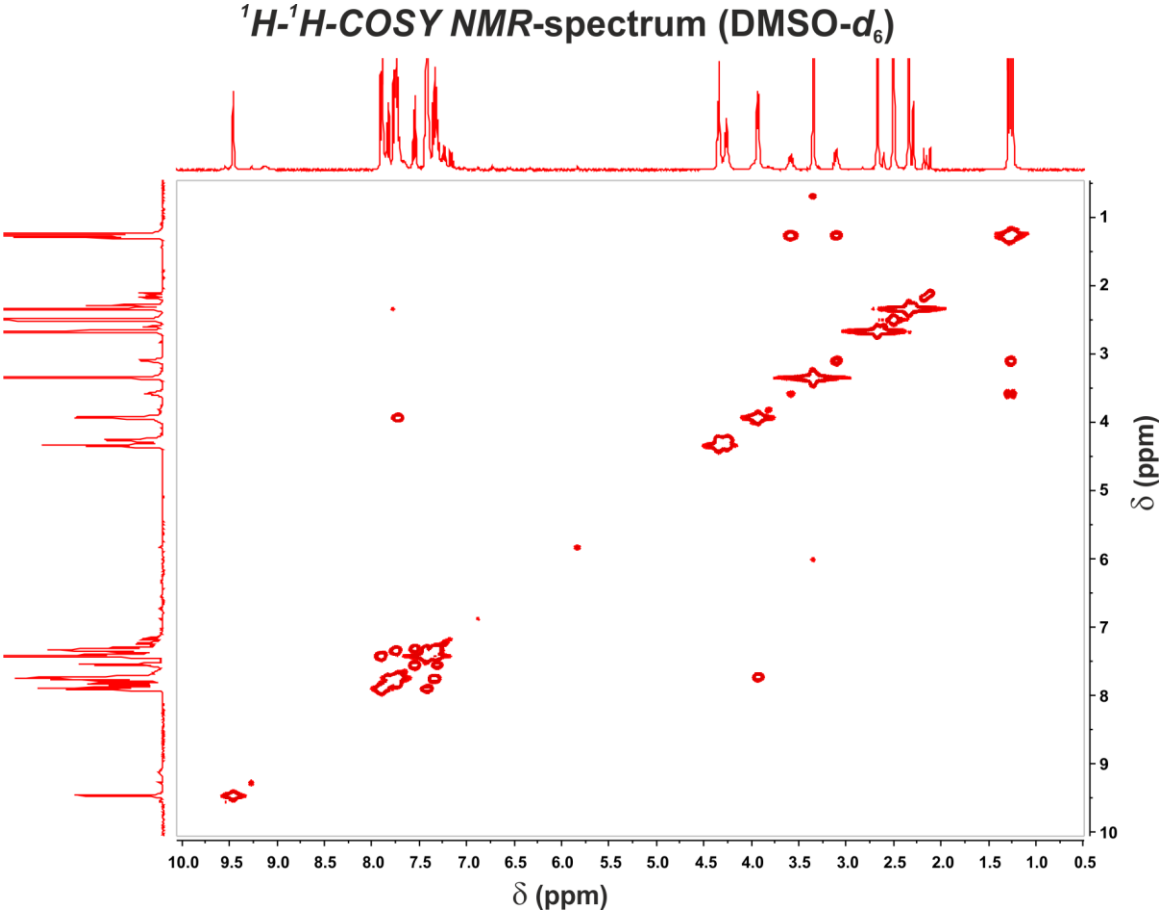
^{1}H-^{1}H-COSY NMR-spectrum (DMSO-d_6)
10.0 9.5 9.0 8.5 8.0 7.5 7.0 6.5 6.0 5.5 5.0 4.5 4.0 3.5 3.0 2.5 2.0 1.5 1.0 0.5
δ (ppm)
1 2 3 4 5 6 7 8 9 10
δ (ppm)

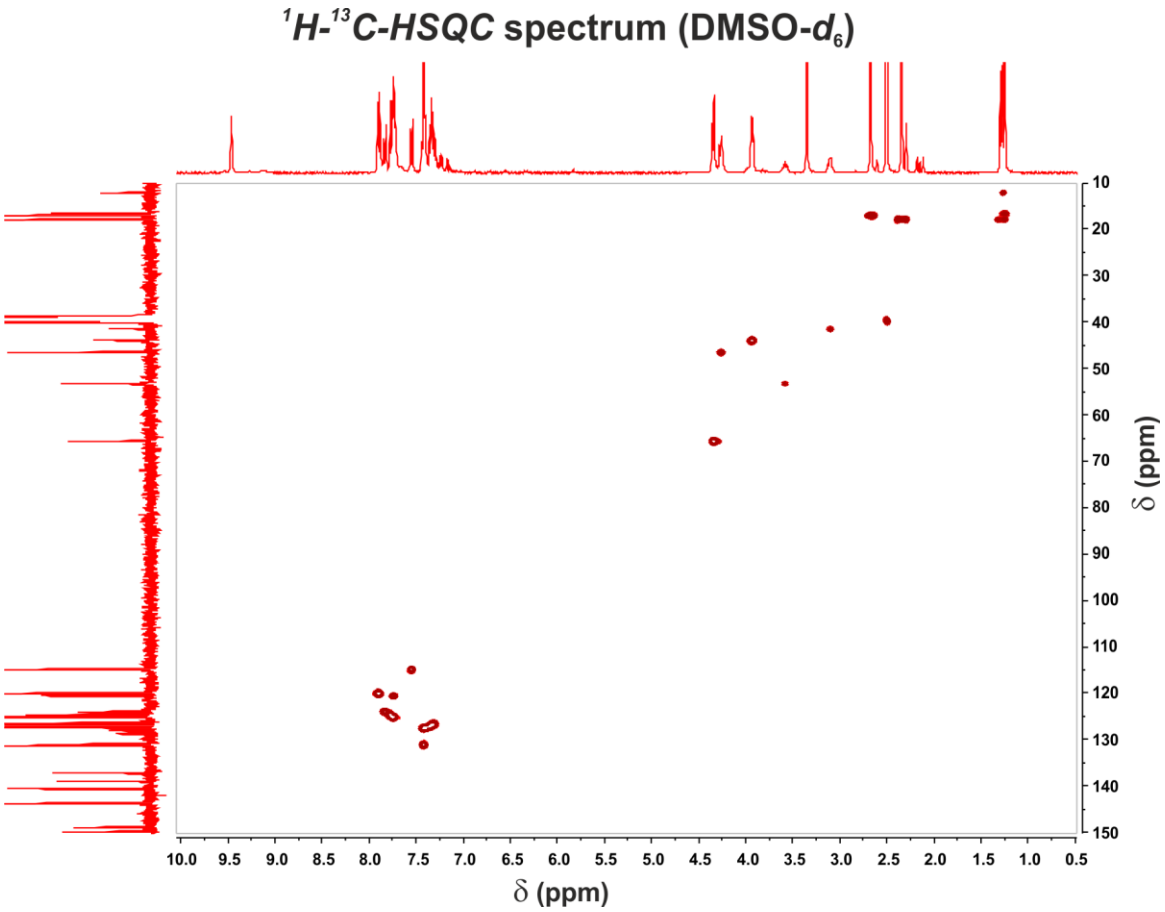
^{1}H-^{13}C-HSQC spectrum (DMSO-d_6)
10.0 9.5 9.0 8.5 8.0 7.5 7.0 6.5 6.0 5.5 5.0 4.5 4.0 3.5 3.0 2.5 2.0 1.5 1.0 0.5
δ (ppm)
10 20 30 40 50 60 70 80 90 100 110 120 130 140 150
δ (ppm)

***N*-((9*H*-Fluoren-9-yl)-methoxycarbonyle)-*L*-Glutamyl-(α-Glycyl-*N*-(2-methyl-4-(o-tolyldiazenyl)phenyl)-amid)-γ-*t*-butyl ester (19)**

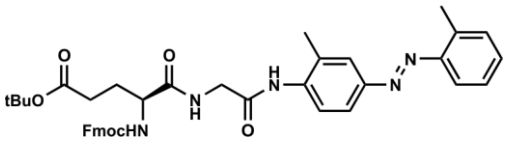

^{1}*H-NMR*-spectrum (400 MHz, DMSO-d_6)

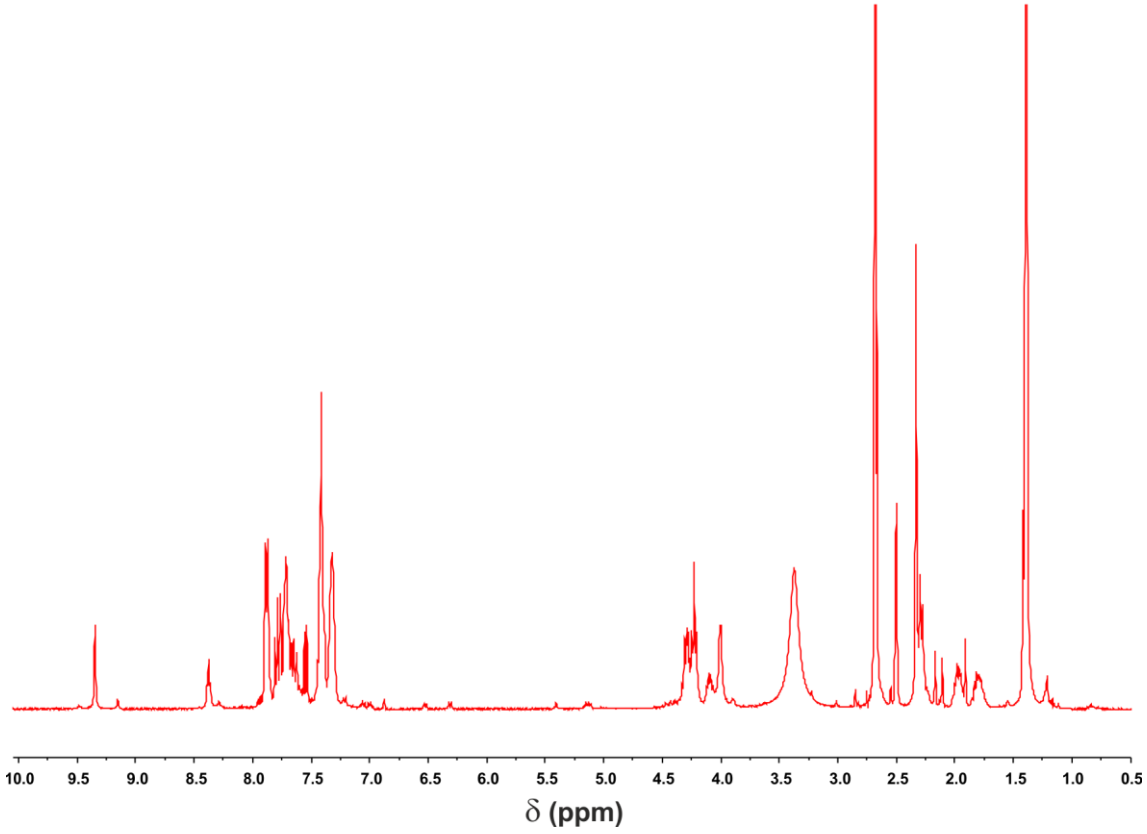

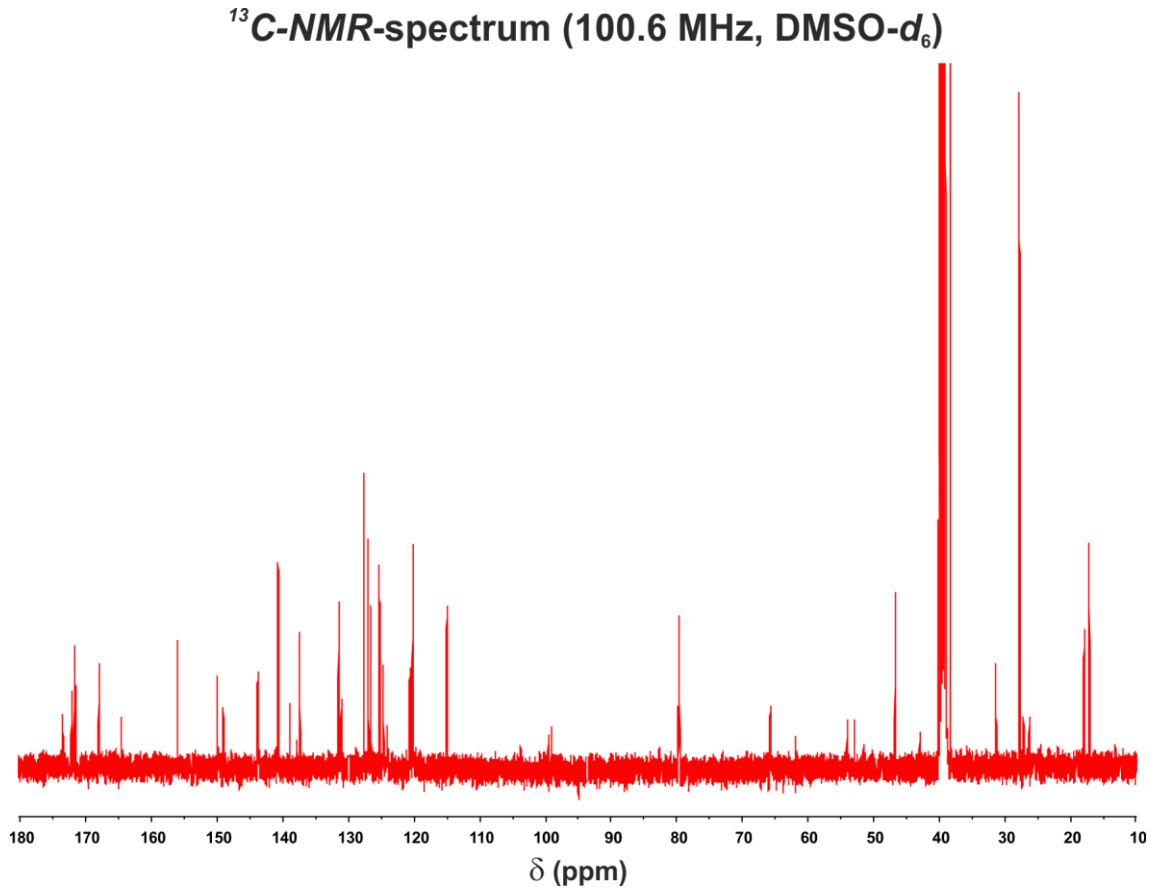
^{13}C-NMR-spectrum (100.6 MHz, DMSO-d_6)
180 170 160 150 140 130 120 110 100 90 80 70 60 50 40 30 20 10
δ (ppm)

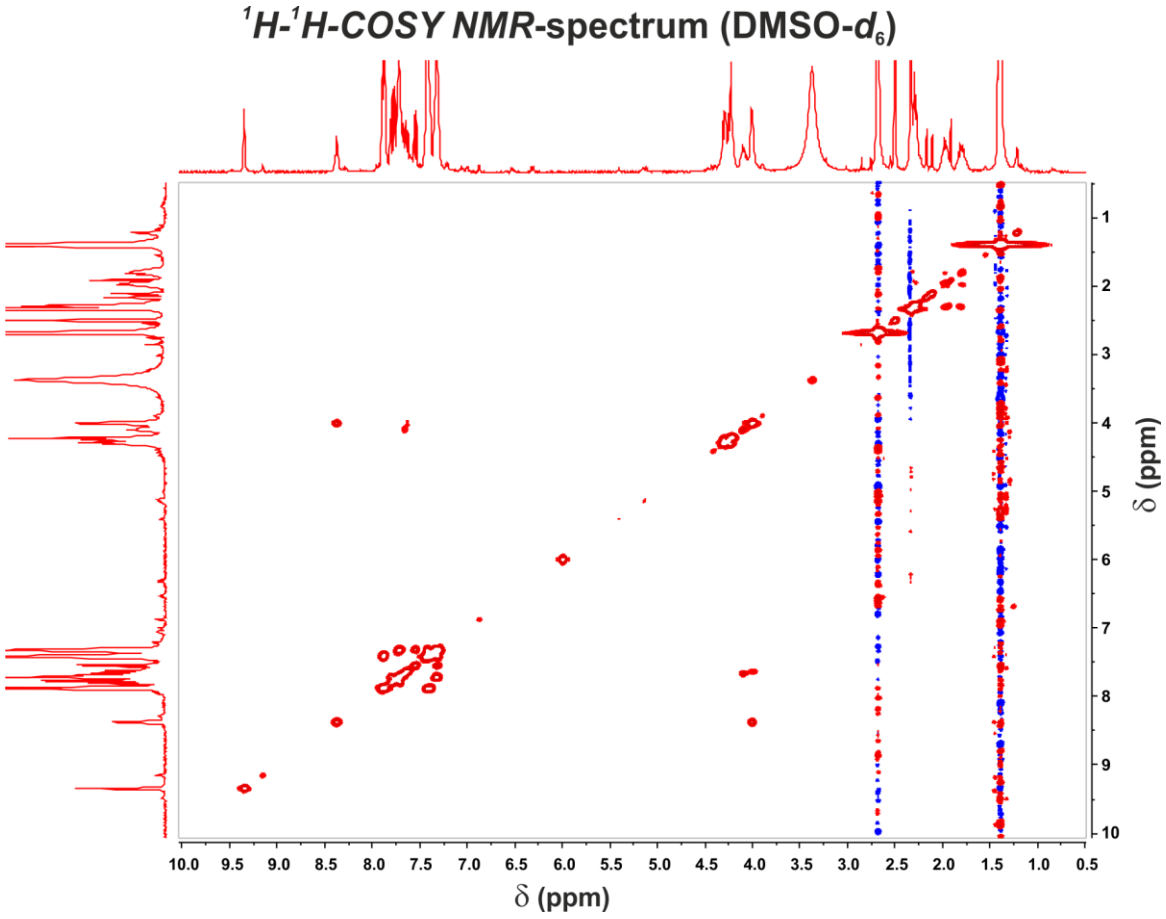
^{1}H-^{1}H-COSY NMR-spectrum (DMSO-d_6)
10.0 9.5 9.0 8.5 8.0 7.5 7.0 6.5 6.0 5.5 5.0 4.5 4.0 3.5 3.0 2.5 2.0 1.5 1.0 0.5
δ (ppm)
1 2 3 4 5 6 7 8 9 10
δ (ppm)

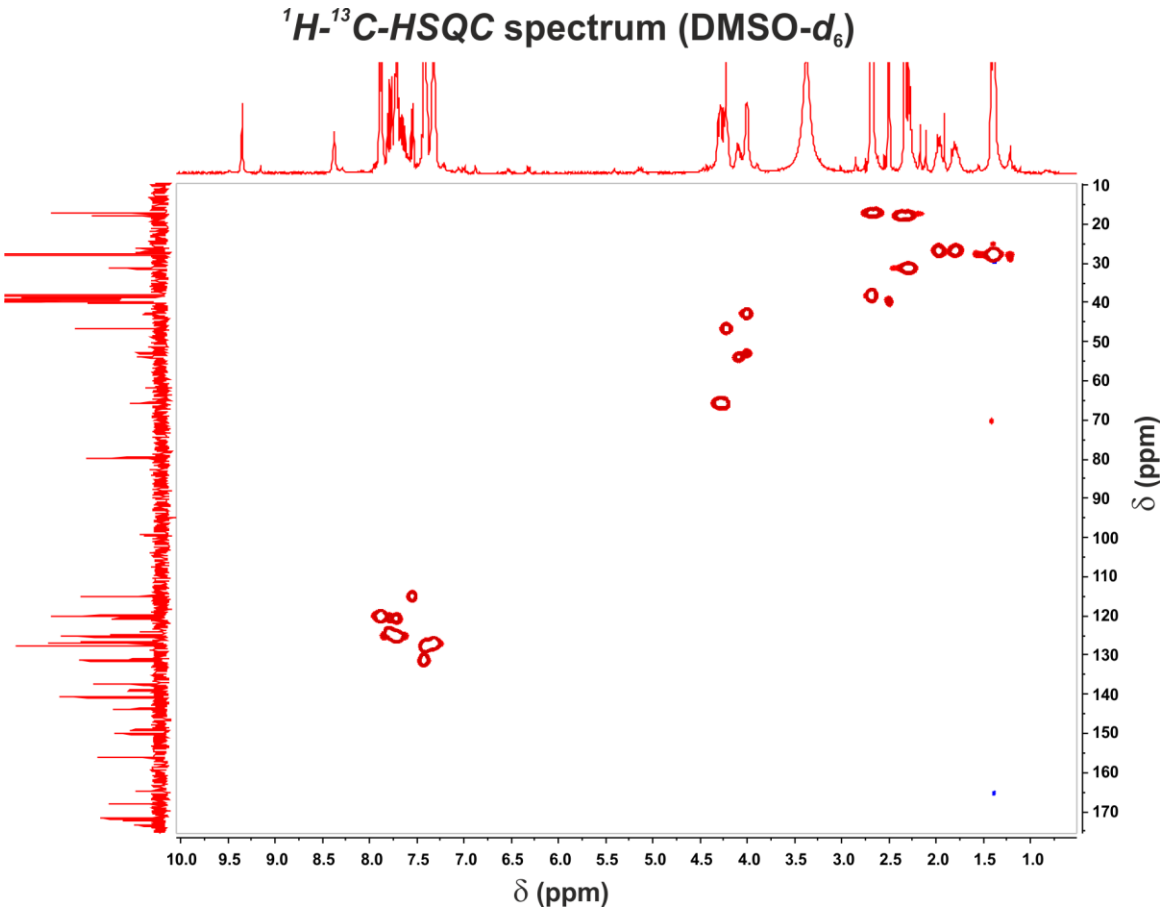
^{1}H-^{13}C-HSQC spectrum (DMSO-d_6)
10.0 9.5 9.0 8.5 8.0 7.5 7.0 6.5 6.0 5.5 5.0 4.5 4.0 3.5 3.0 2.5 2.0 1.5 1.0
δ (ppm)
10 20 30 40 50 60 70 80 90 100 110 120 130 140 150 160 170
δ (ppm)

***N*-((9*H*-fluoren-9-yl)-methoxycarbonyl)-*L*-Glutamyl-(α-Glycyl-*N*-(2-methyl-4-(o-tolyldiazenyl)phenyl)-amide) (16)**

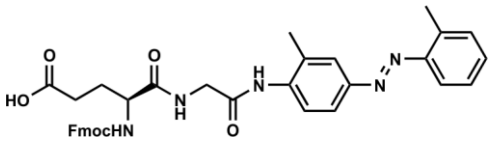

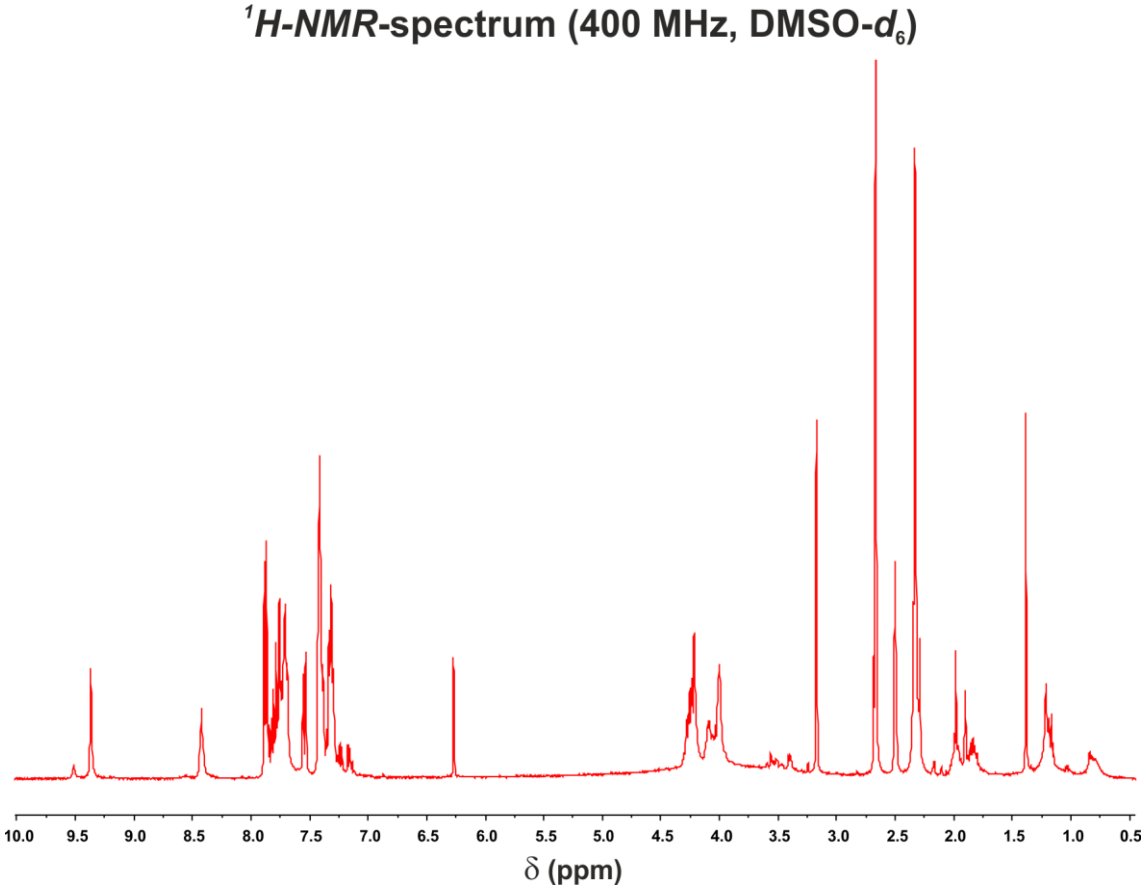

^{13}*C-NMR*-spectrum (100.6 MHz, DMSO-d_6)

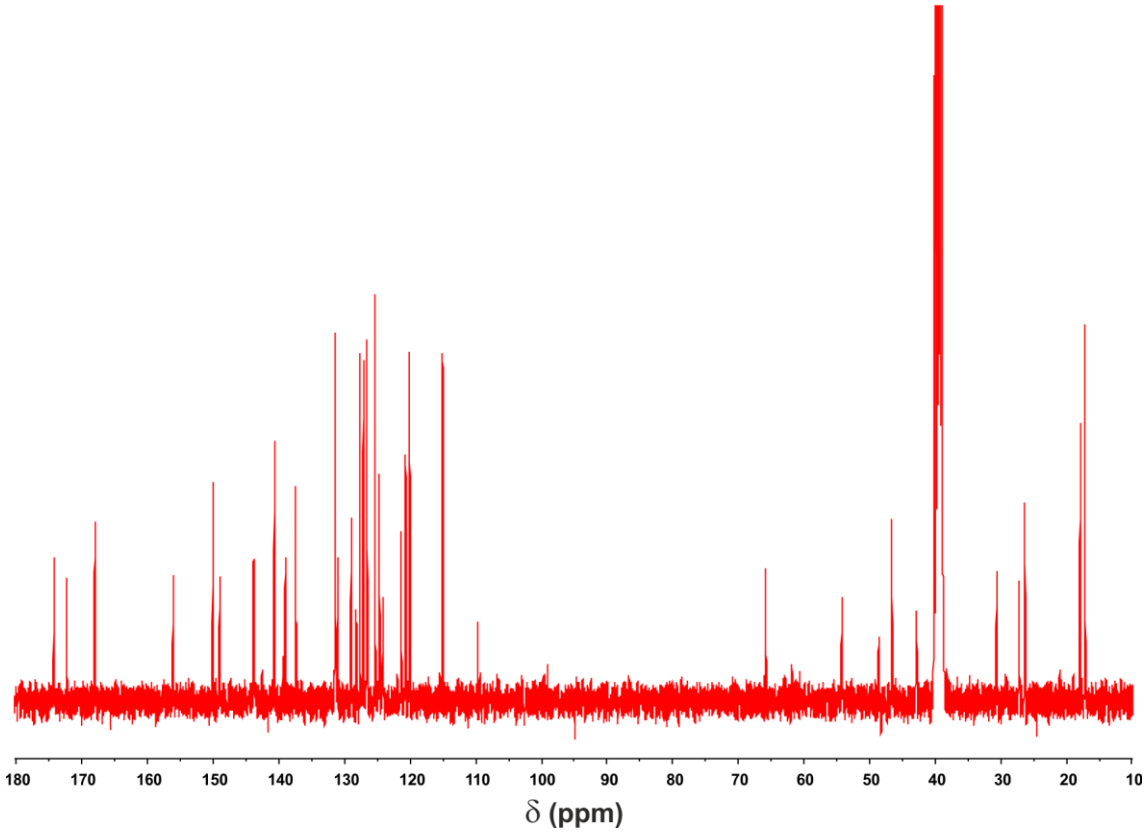

^{1}*H-*^{1}*H-COSY NMR*-spectrum (DMSO-d_6)

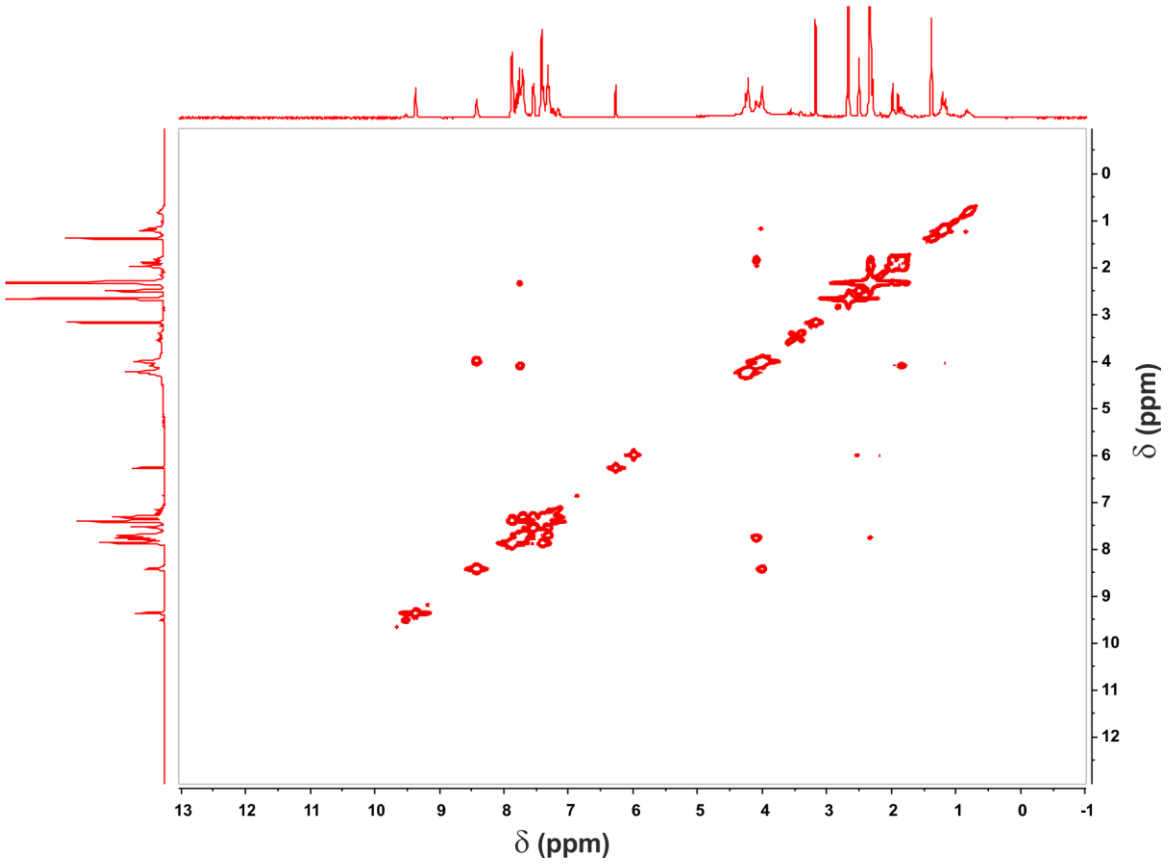

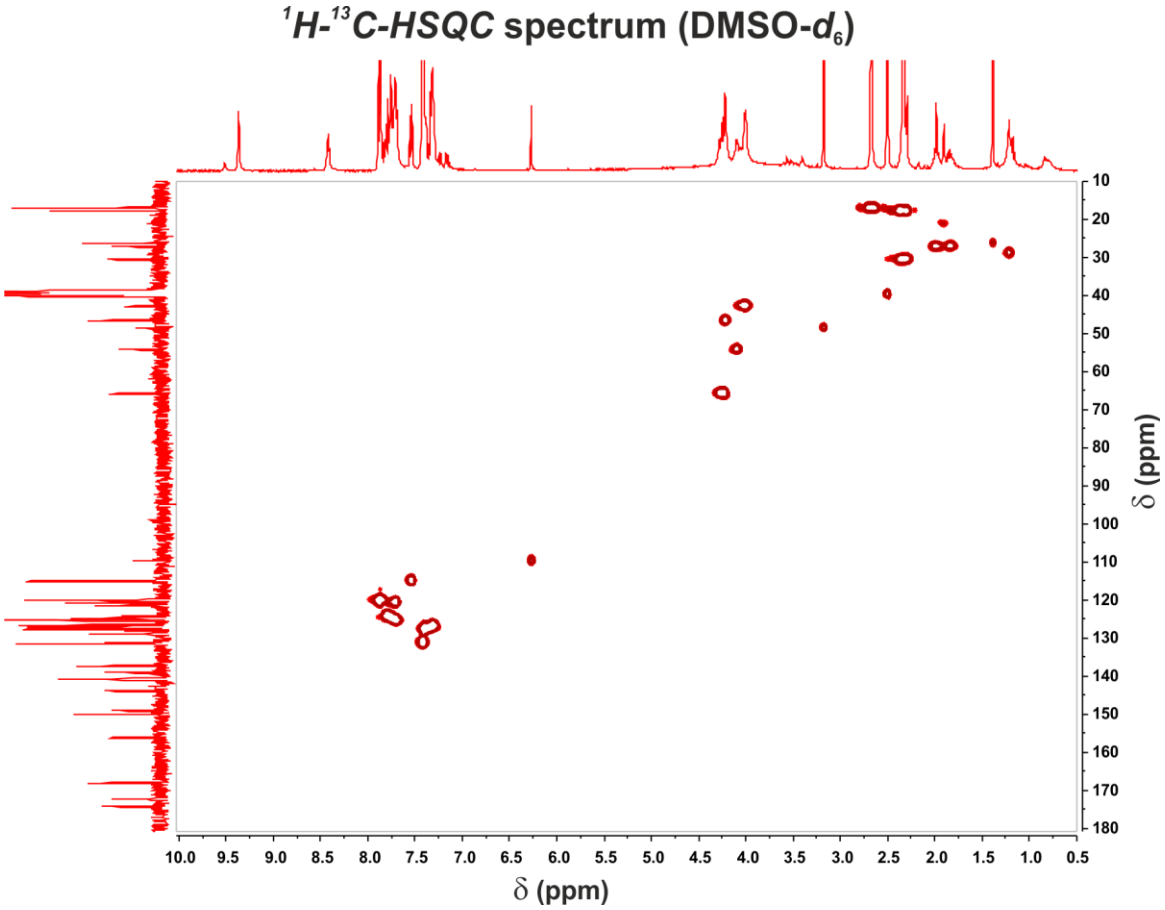
^{1}H-^{13}C-HSQC spectrum (DMSO-d_6)
δ (ppm)
δ (ppm)

Glycyl-*L*-glutaminyl-*L*-asparaginyl-*L*-seryl-*L*-threonyl-*L*-threonyl-*L*-asparaginyl-*L*-tyrosyl-*L*-histidyl-*L*-threonyl-*L*-leucyl-*L*-valyl-*L*-arginyl-amido-4,7,10-trioxa-dodecanylamido-*L*-Glutamyl-(α-Glycyl-*N*-(2-methyl-4-(o-tolyldiazenyl)phenyl)-amid)-γ-glycin-amide (20)

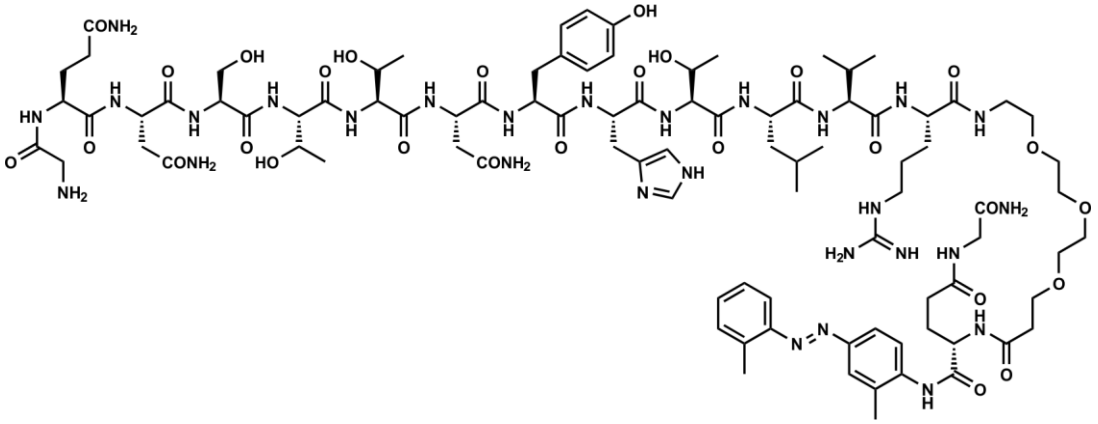

***^{1}H-NMR*-spectrum (600 MHz, DMSO-d_6)**

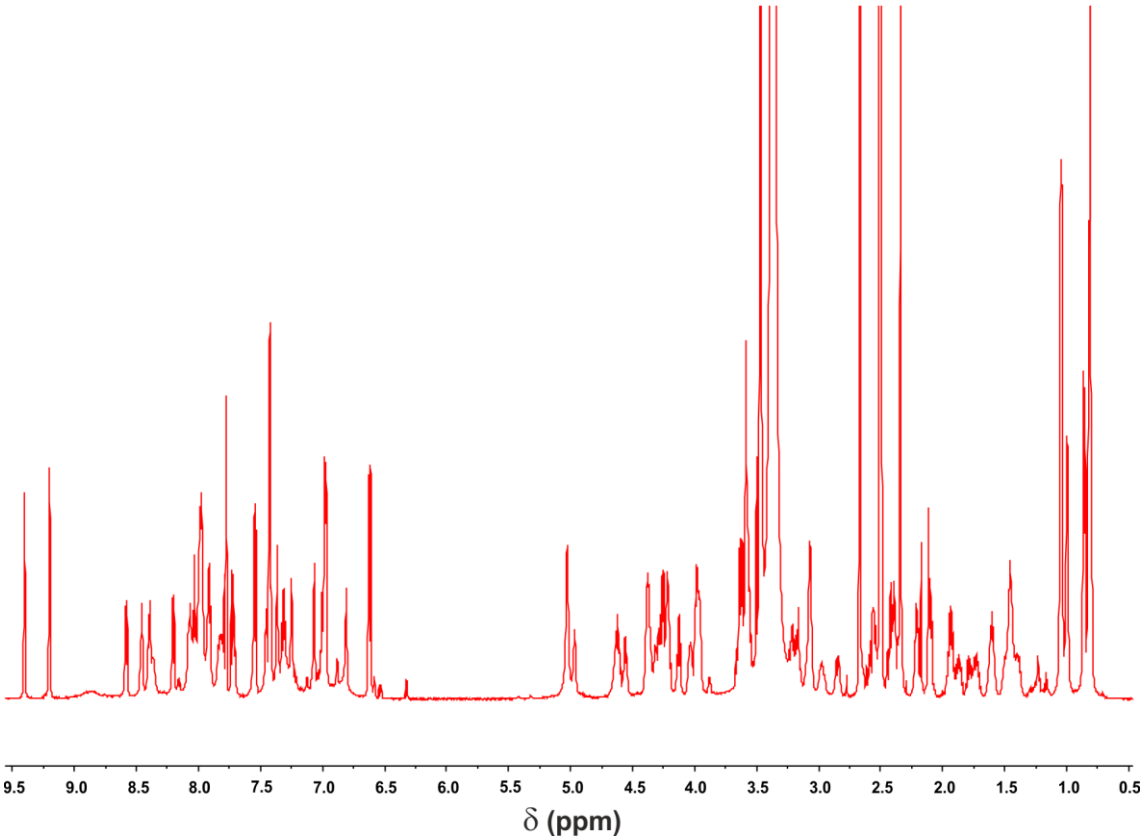

^{13}*C-NMR*-spectrum (150.9 MHz, DMSO-d_6)

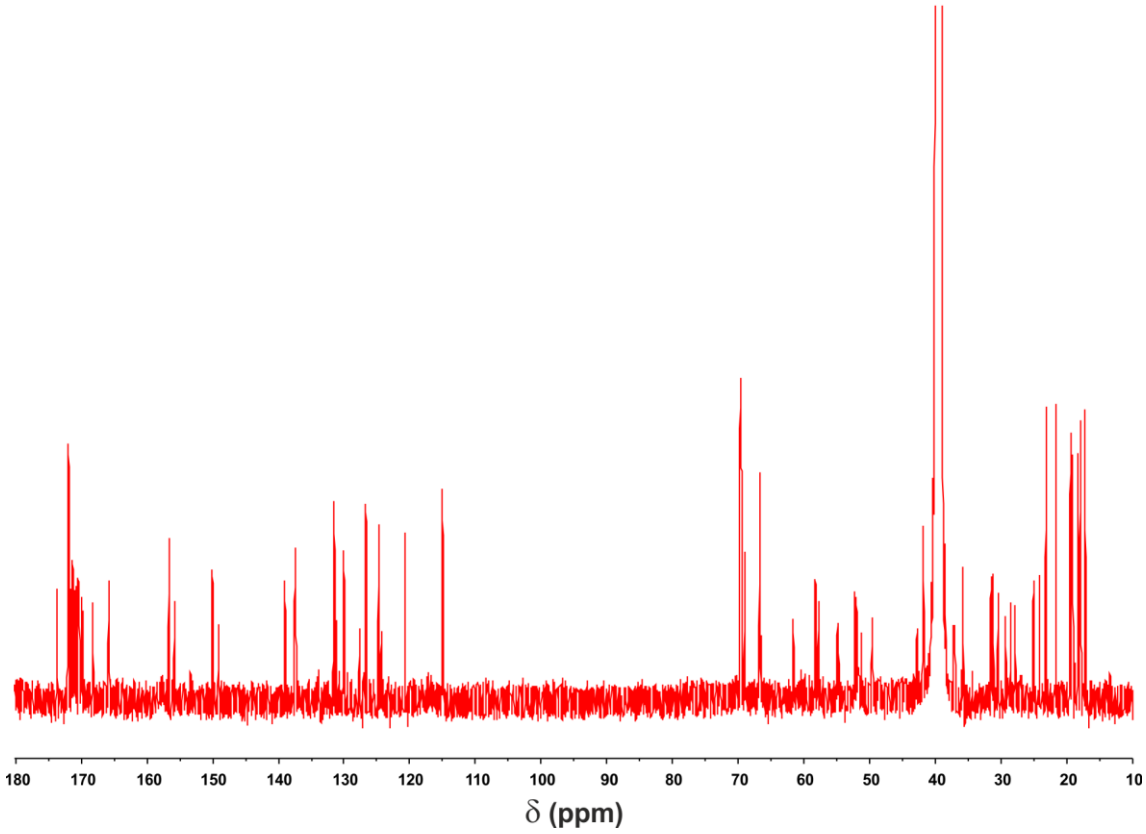

^{1}*H-*^{1}*H-COSY NMR*-spectrum (DMSO-d_6)

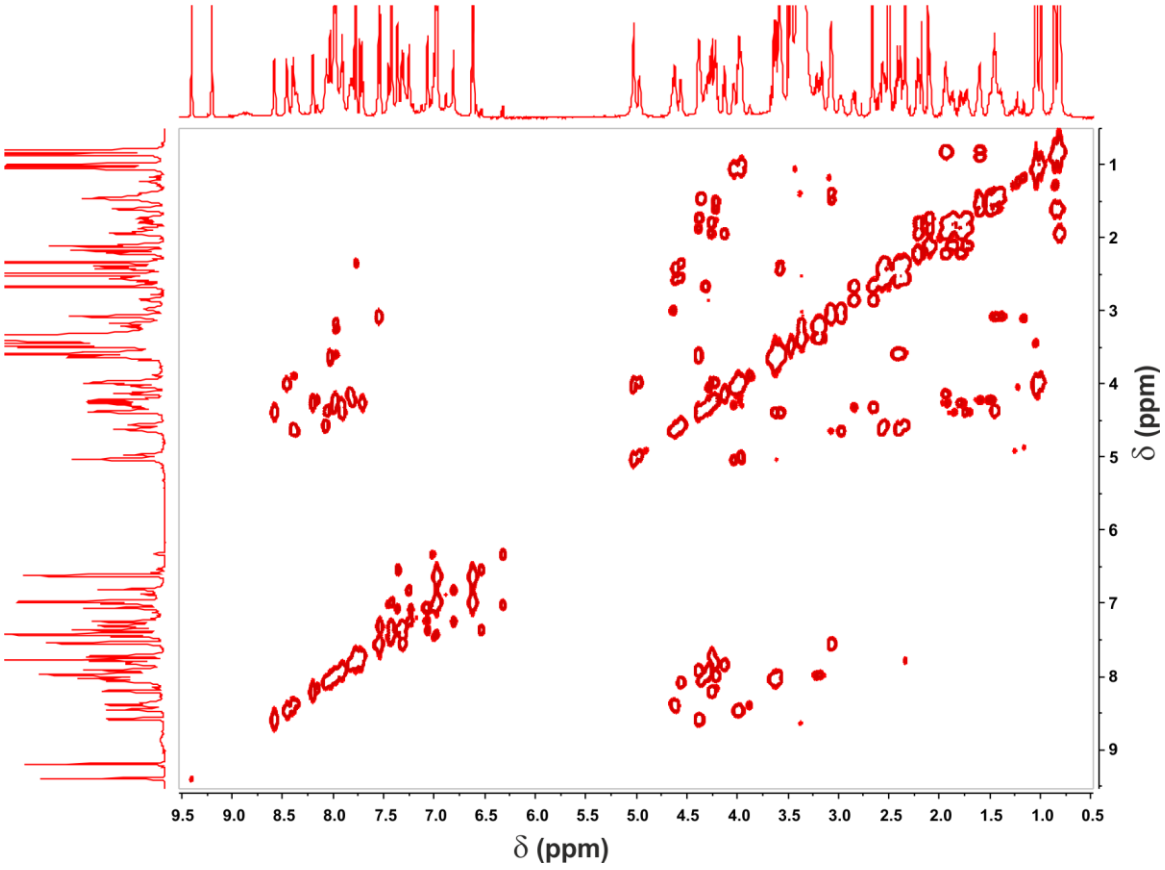

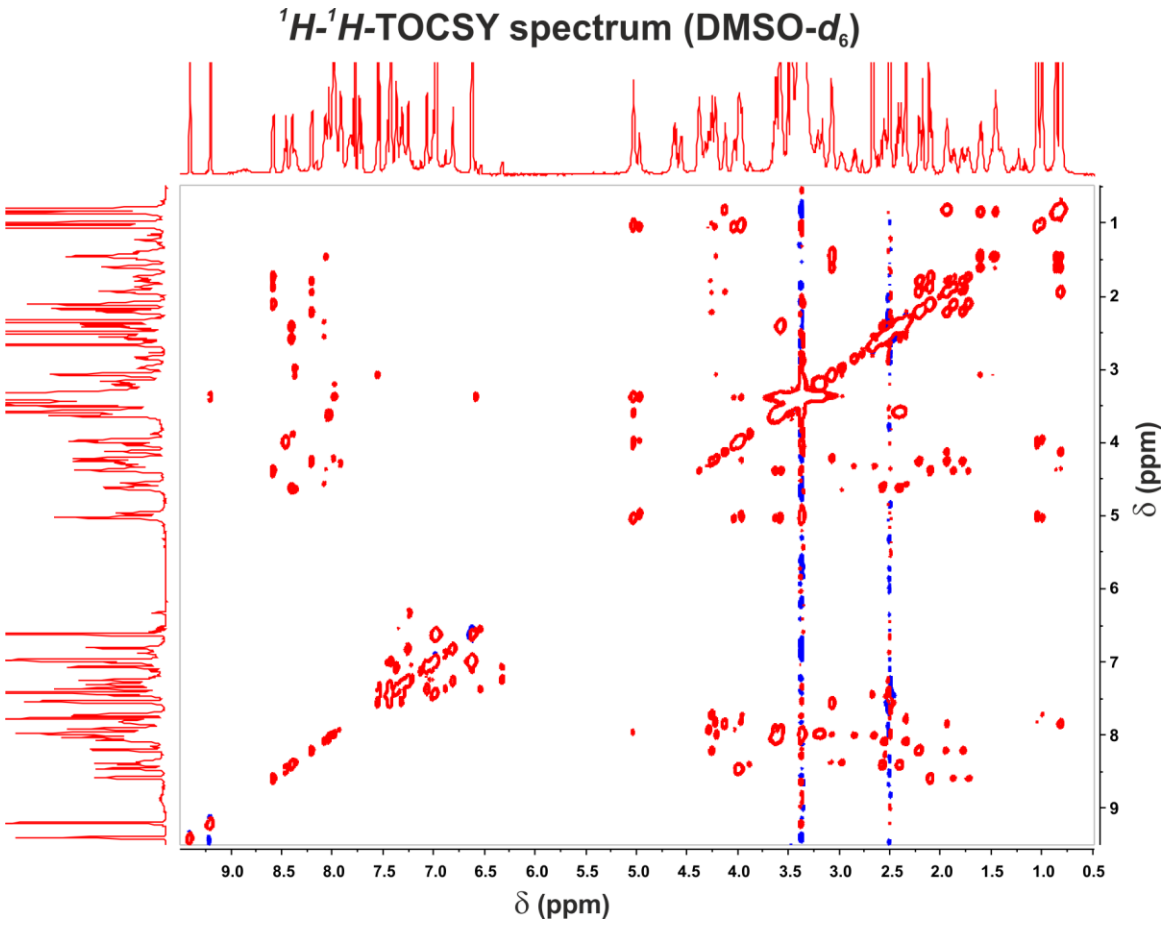
^{1}H-^{1}H-TOCSY spectrum (DMSO-d_6)
δ (ppm)
δ (ppm)

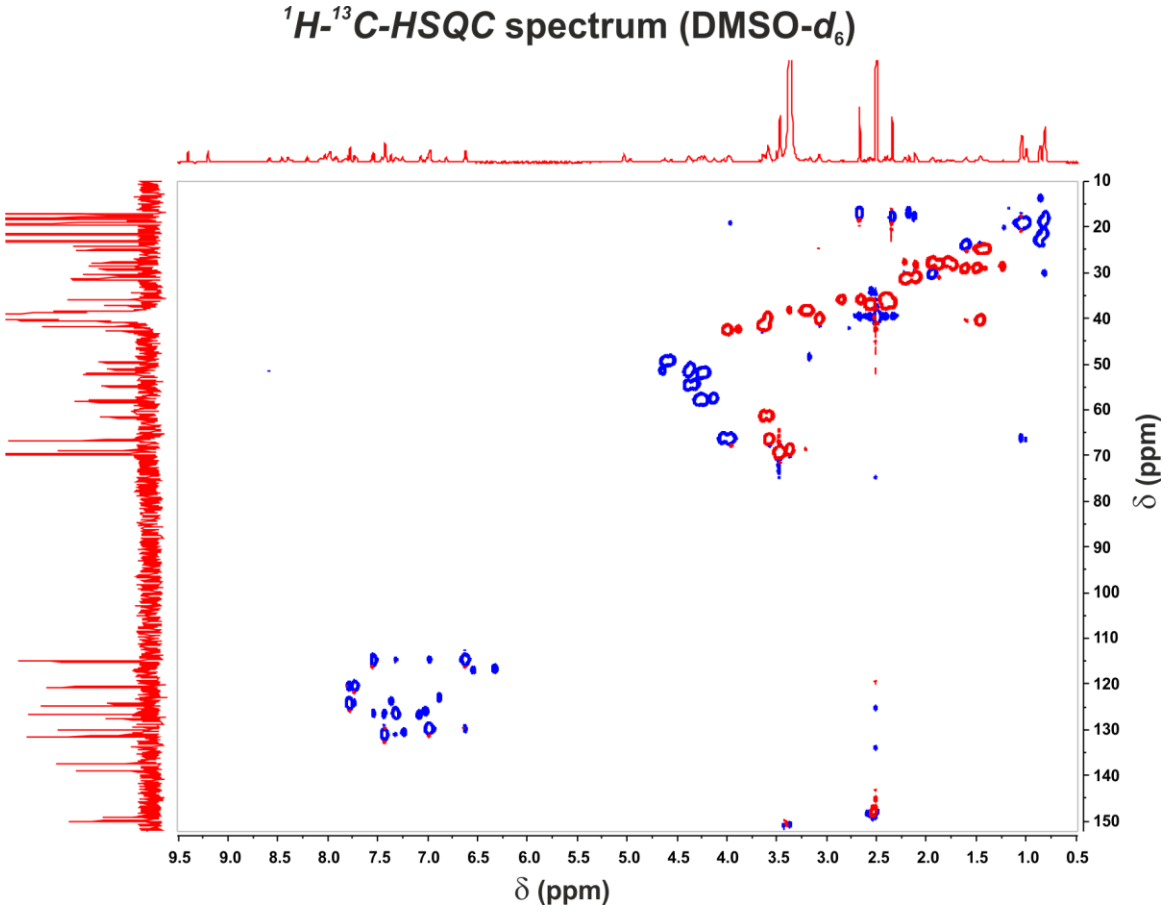
^{1}H-^{13}C-HSQC spectrum (DMSO-d_6)
δ (ppm)
δ (ppm)

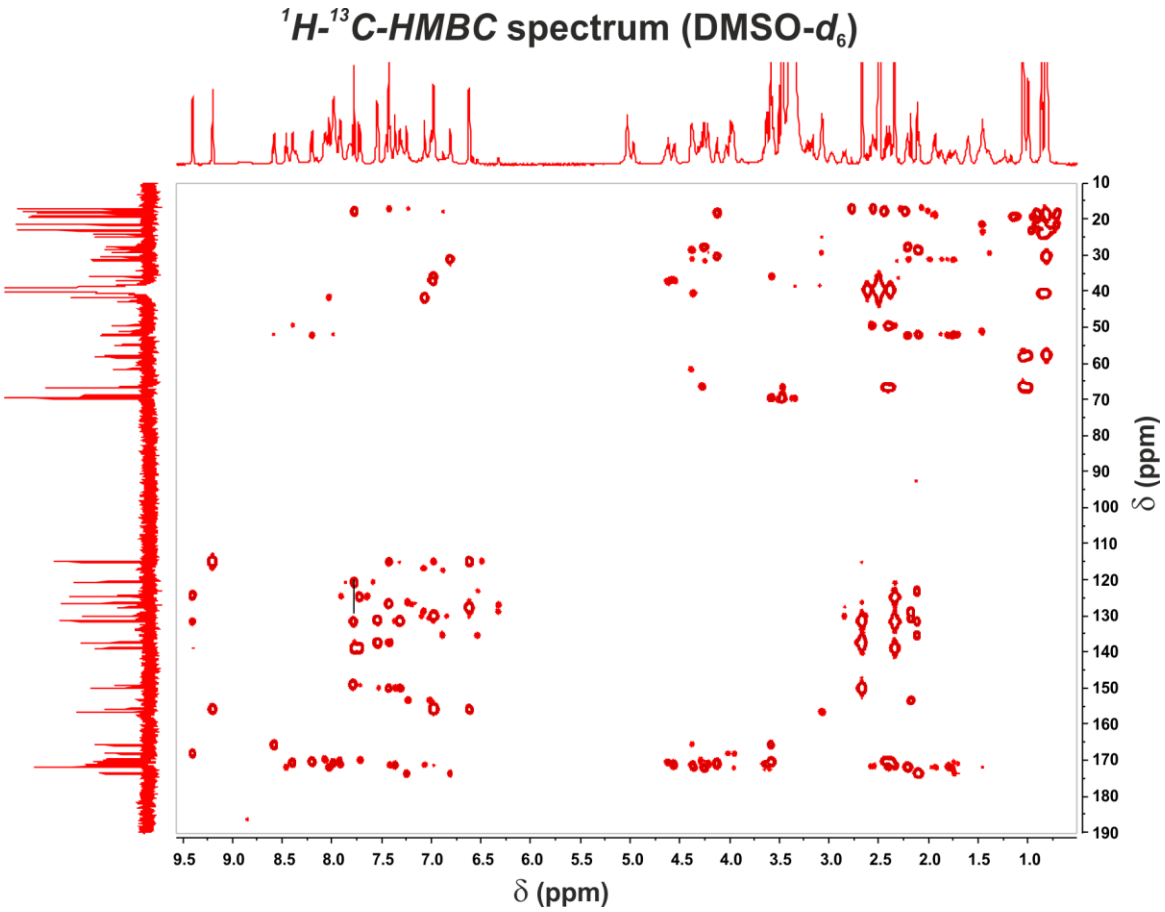
^{1}H-^{13}C-HMBC spectrum (DMSO-d_6)
δ (ppm)
δ (ppm)

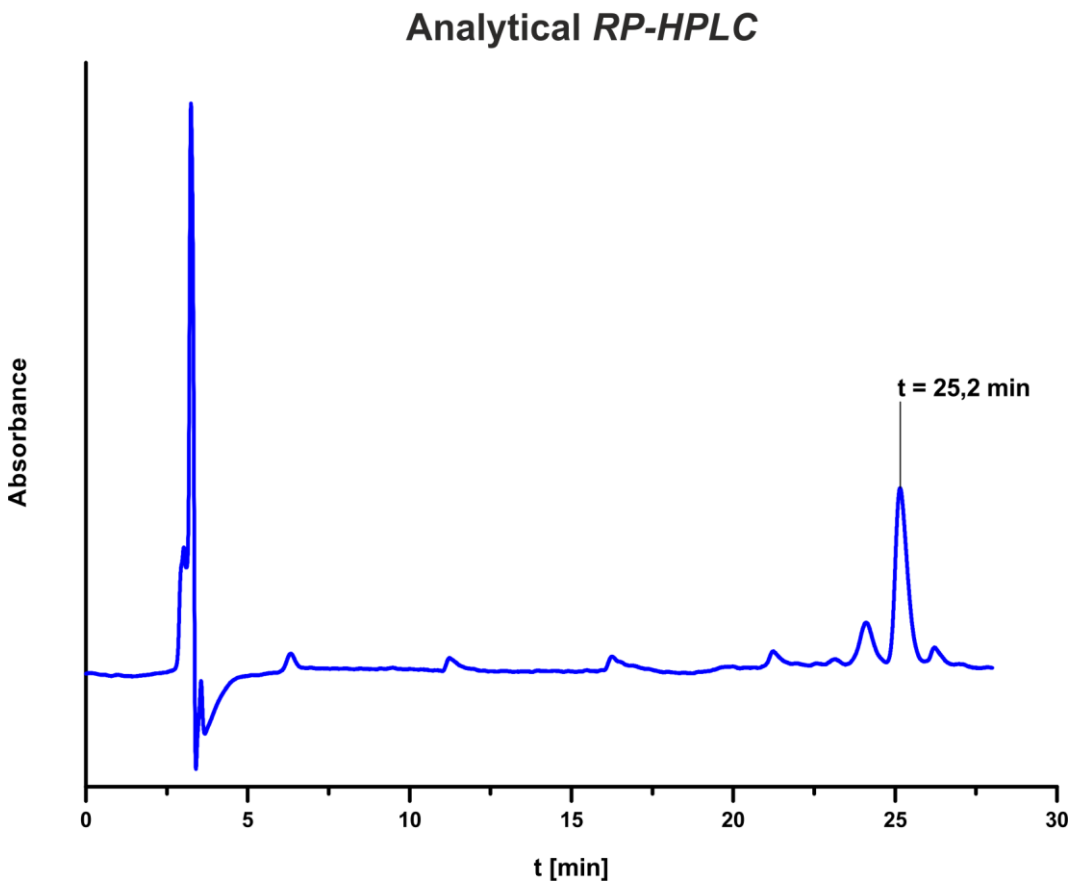
Analytical RP-HPLC
Absorbance
t = 25,2 min
t [min]

Appendix V:
Crystallisations: Data and Images

Appendix Va: Crystallisations of calcium carbonate in the presence of quartz glass slides

Crystallisations on quartz glass sildes after acidic wash steps

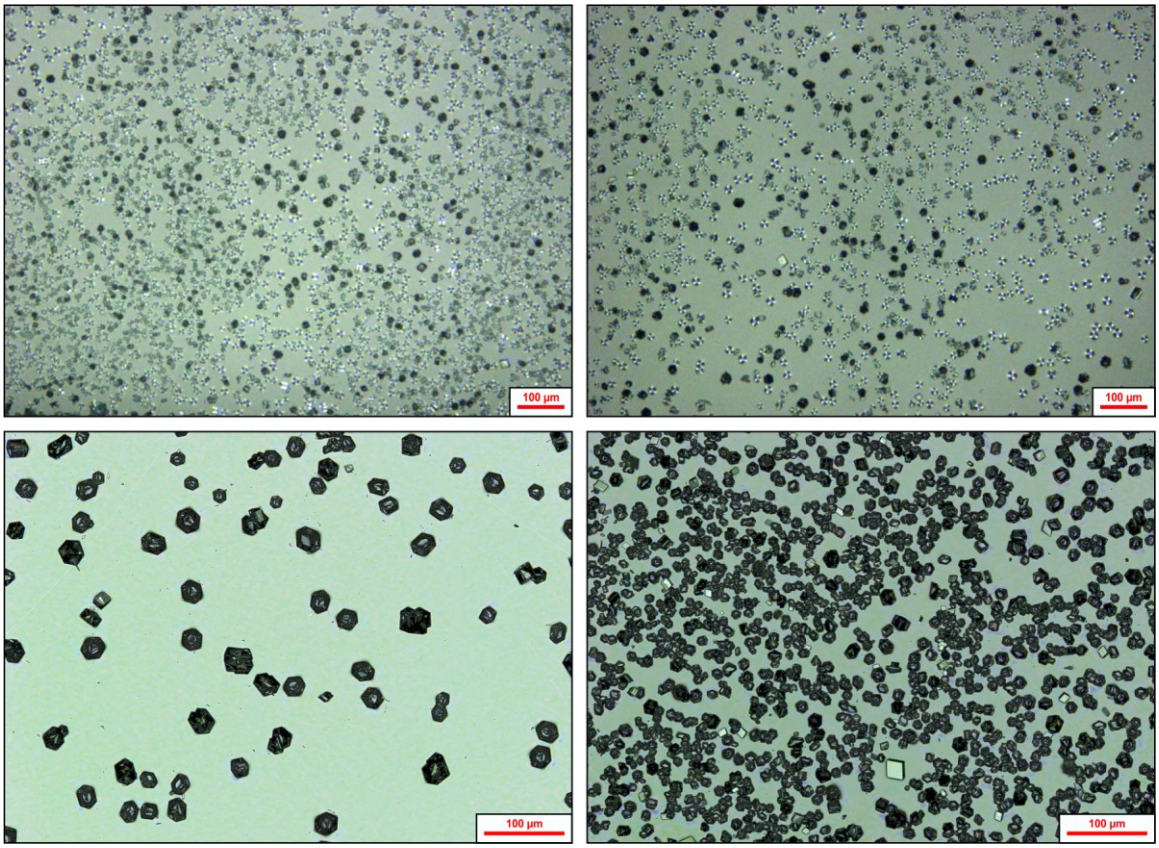

Figure 54) Upper row: Light microscopic images. **Lower row:** Overlayed Light-microscopic and *CLSM*-images.

Crystallisations on quartz glass sildes after basic wash steps

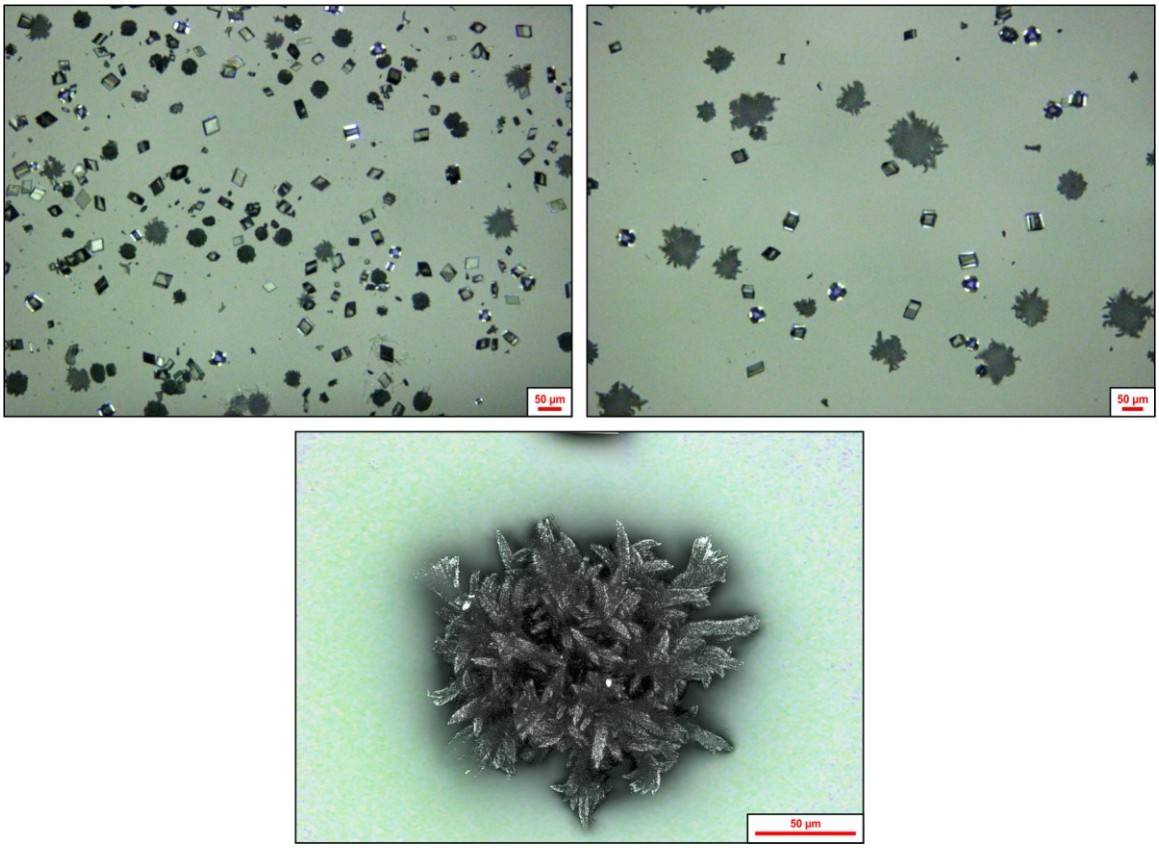

Figure 55) Upper row: Light-microscopic images. **Lower row:** Overlayed Light-microscopic- and ***CLSM*-images**.

Appendix Vb: Crystallisations of calcium carbonate in the presence of different concentrations of magnesium ions

Magnesium-free control sample

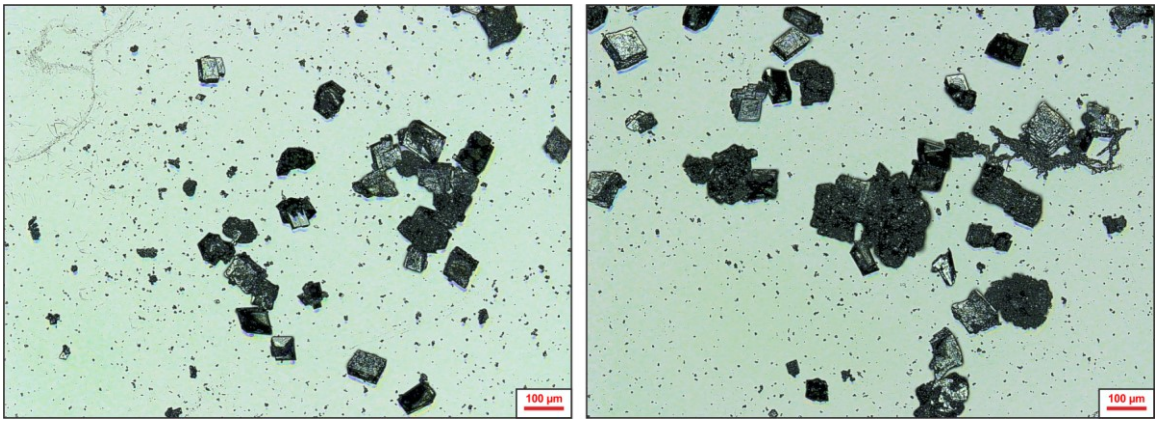

Figure 56) Both images: Overlayed Light-microscopic- and *CLSM*-images.

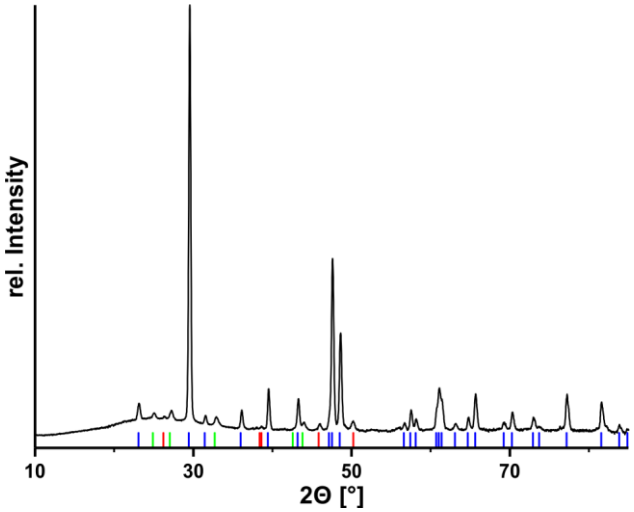

Figure 57) Powder X-ray diffractogram of the magnesium-free control sample. Referenced reflex position are indicated by the coloured lines. Colour code and references: **Blue** lines: calcite [140]; **Red** lines: aragonite [140]; **Green** lines: vaterite [284].

Sample containing a calcium/magnesium ratio of 1:1

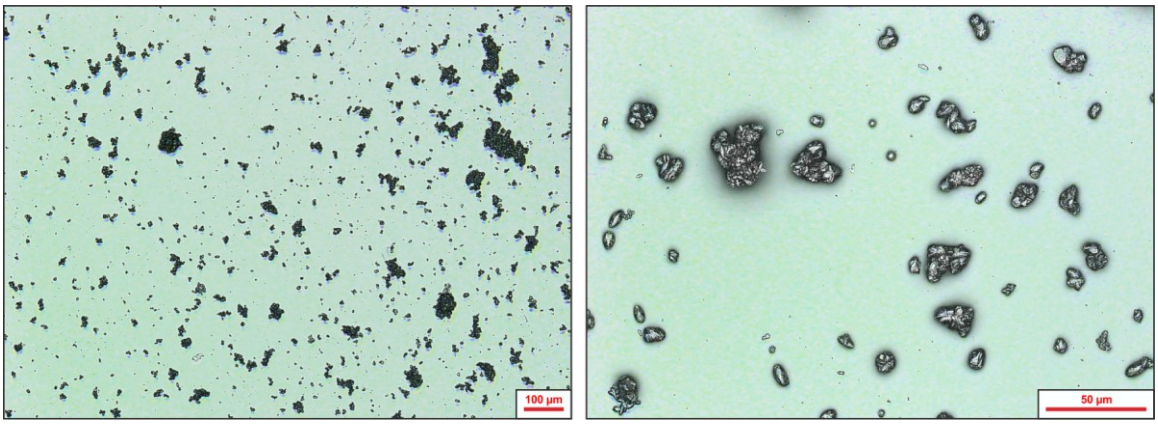

Figure 58) Both images: Overlayed of Light-microscopic- and *CLSM*-images.

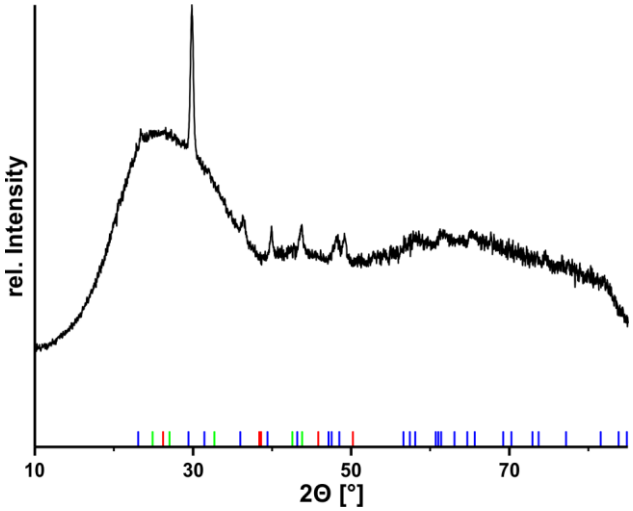

Figure 59) Powder X-ray diffractogram of the sample containing a calcium/magnesium ratio of 1:1. Referenced reflex position are indicated by the coloured lines. **Blue** lines: calcite [140]; **Red** lines: aragonite [140]; **Green** lines: vaterite [284].

Sample containing a calcium/magnesium ratio of 1:2

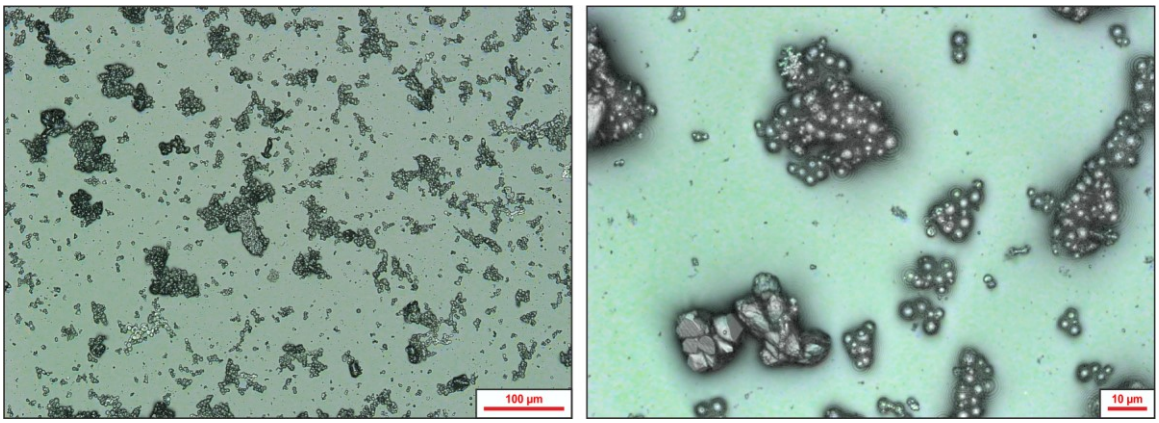

Figure 60) All images: Overlayed Light-microscopic- and *CLSM*-images.

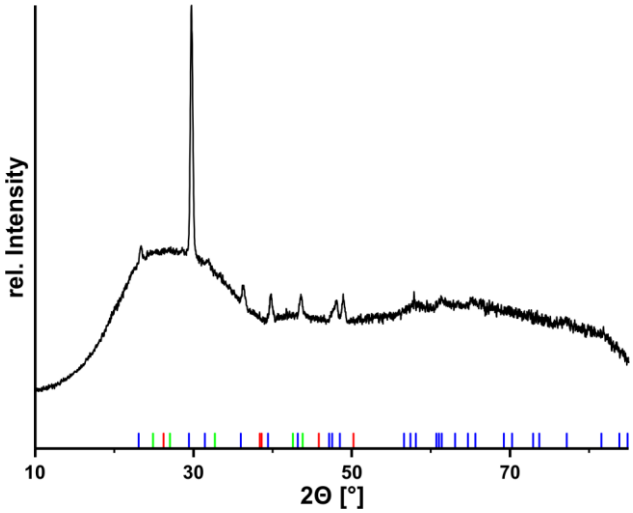

Figure 61) Powder X-ray diffractogram of the sample containing a calcium/magnesium ratio of 1:2. Referenced reflex position are indicated by the coloured lines. **Blue** lines: calcite [140]; **Red** lines: aragonite [140]; **Green** lines: vaterite [284].

Sample containing a calcium/magnesium ratio of 1:3

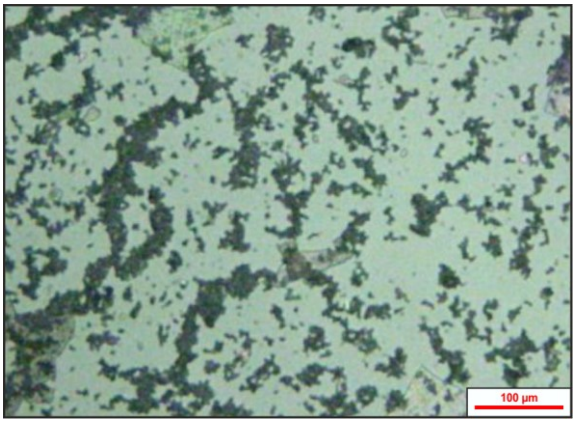

Figure 62) Overlayed light-microscopic and *CLSM*-images.

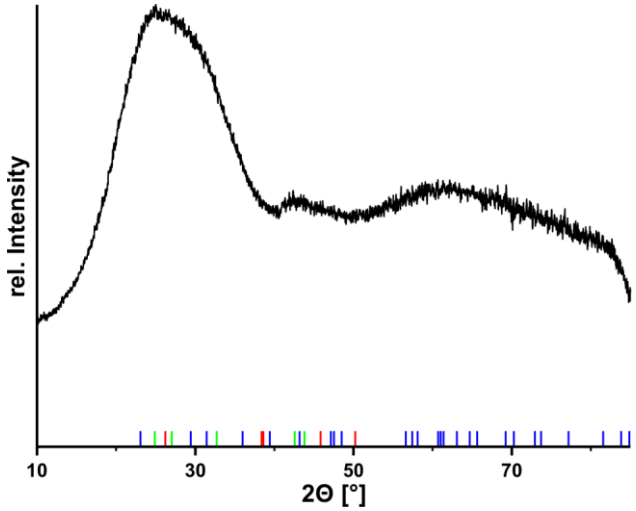

Figure 63) Powder X-ray diffractogram of the sample containing a calcium/magnesium ratio of 1:3. Referenced reflex position are indicated by the coloured lines. **Blue** lines: calcite [140]; **Red** lines: aragonite [140]; **Green** lines: vaterite [284].

Sample containing a calcium/magnesium ratio of 1:4

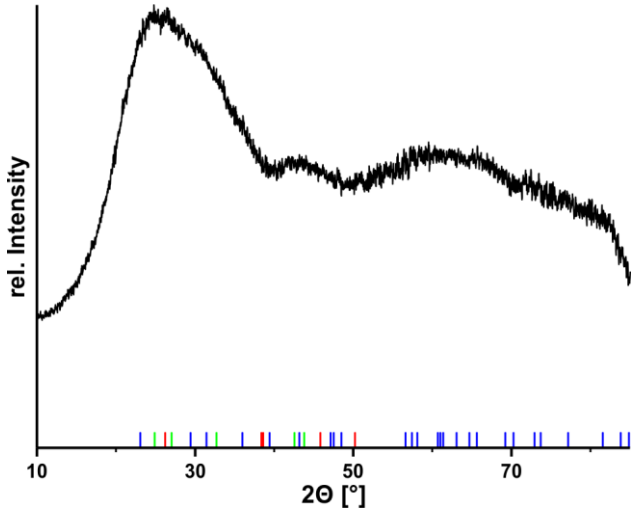

Figure 64) Powder X-ray diffractogram of the sample containing a calcium/magnesium ratio of 1:4. Referenced reflex position are indicated by the coloured lines. **Blue** lines: calcite [140]; **Red** lines: aragonite [140]; **Green** lines: vaterite [284].

Sample containing a calcium/magnesium ratio of 1:5

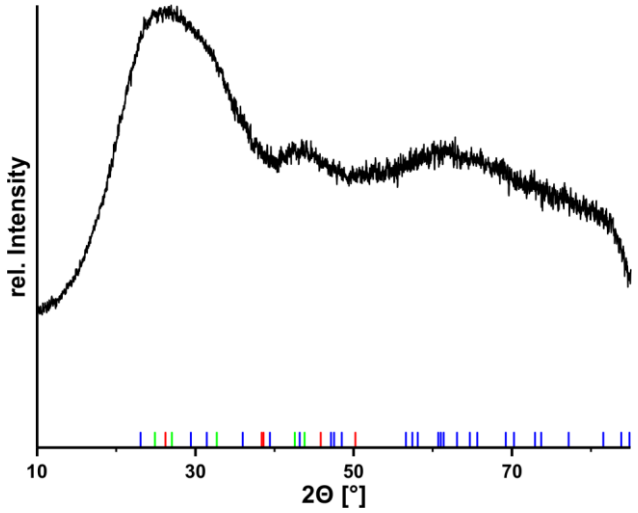

Figure 65) Powder X-ray diffractogram of the sample containing a calcium/magnesium ratio of 1:5. Referenced reflex position are indicated by the coloured lines. **Blue** lines: calcite [140]; **Red** lines: aragonite [140]; **Green** lines: vaterite [284].

Position of calcite`s {10.4}-reflex in the presence of different calcium-to-magnesium ratios

Ca^{2+}/Mg^{2+}-ratio	Position of the {10.4}-reflex (2Θ [°])
Control (1:0)	29.51
1:1	29.69
1:2	29.79
Referenced Position[141]	29.42

Appendix Vc: Phase composition at different temperatures

Crystallisation at 25 °C

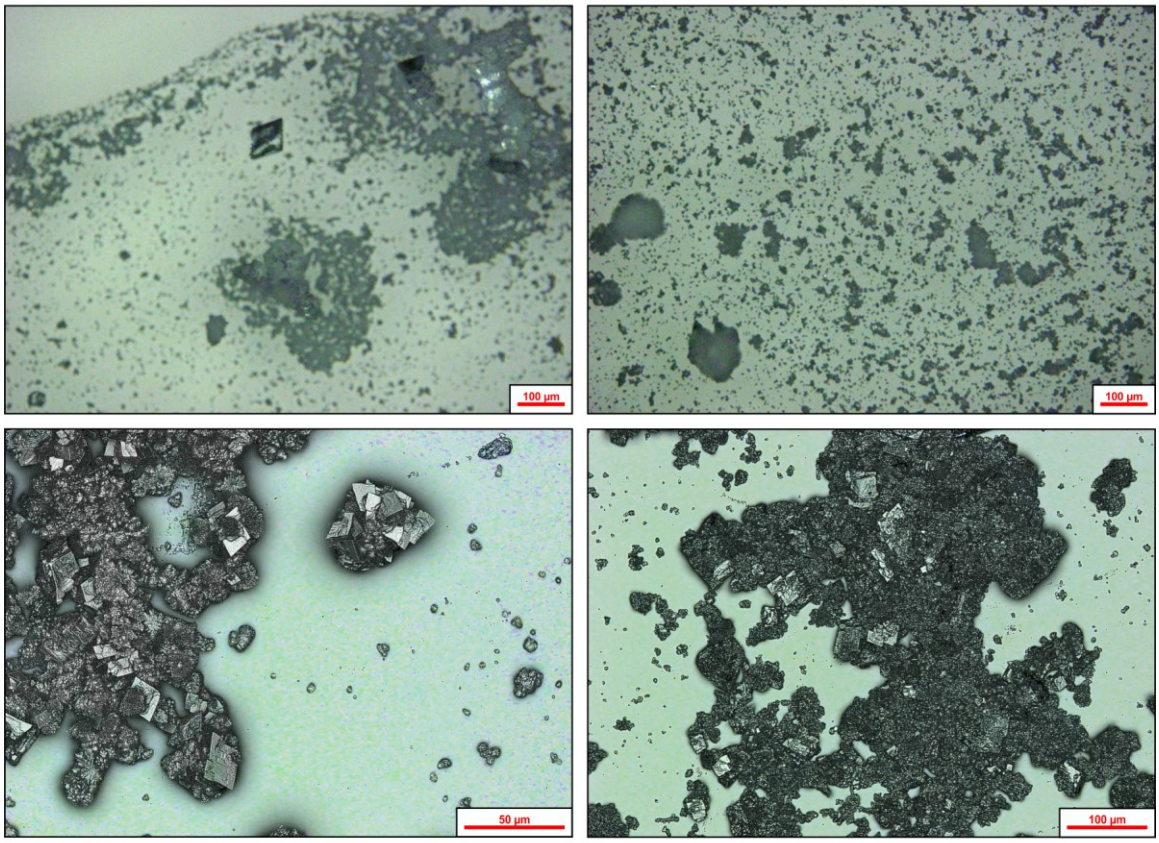

Crystallisation at 45 °C

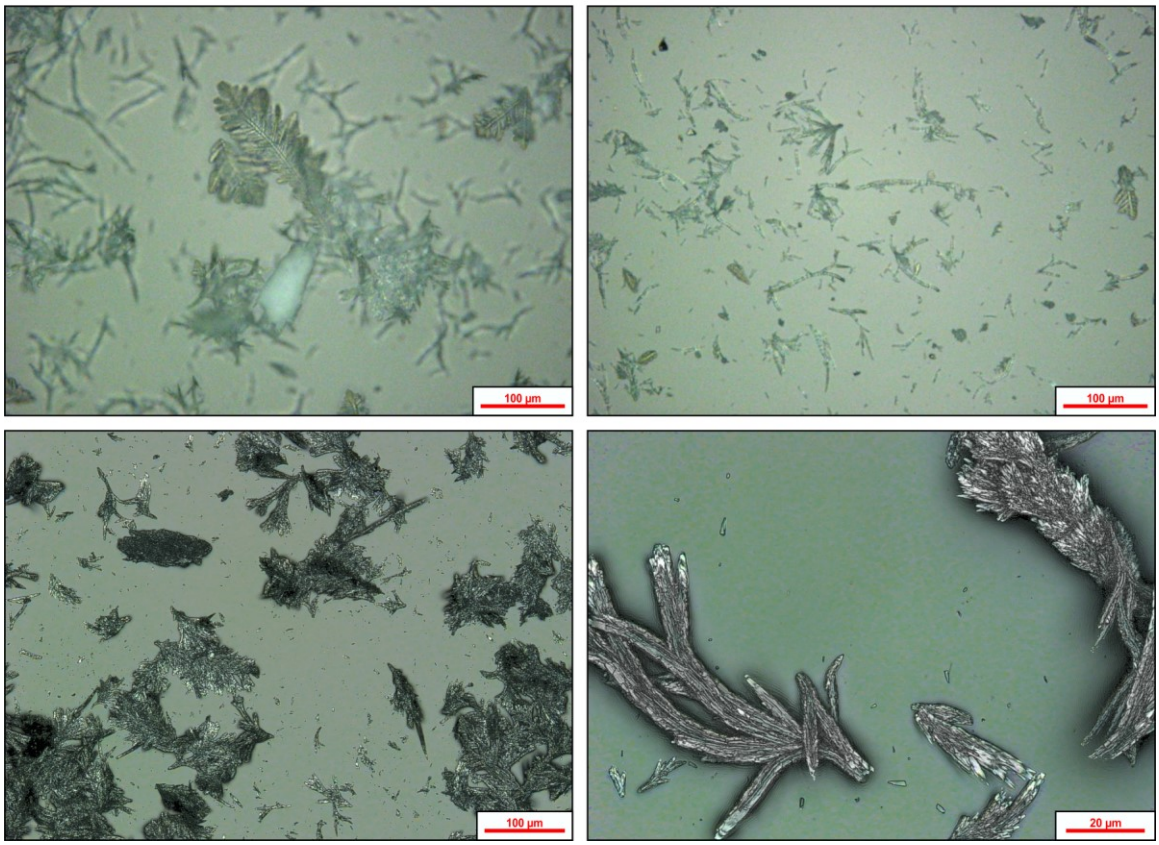

Figure 66) 1st and 3rd row: Light-microscopic images. **2nd and 4th row:** Overlayed light-microscopic and *CSLM*-images.

Crystallisation at 60 °C

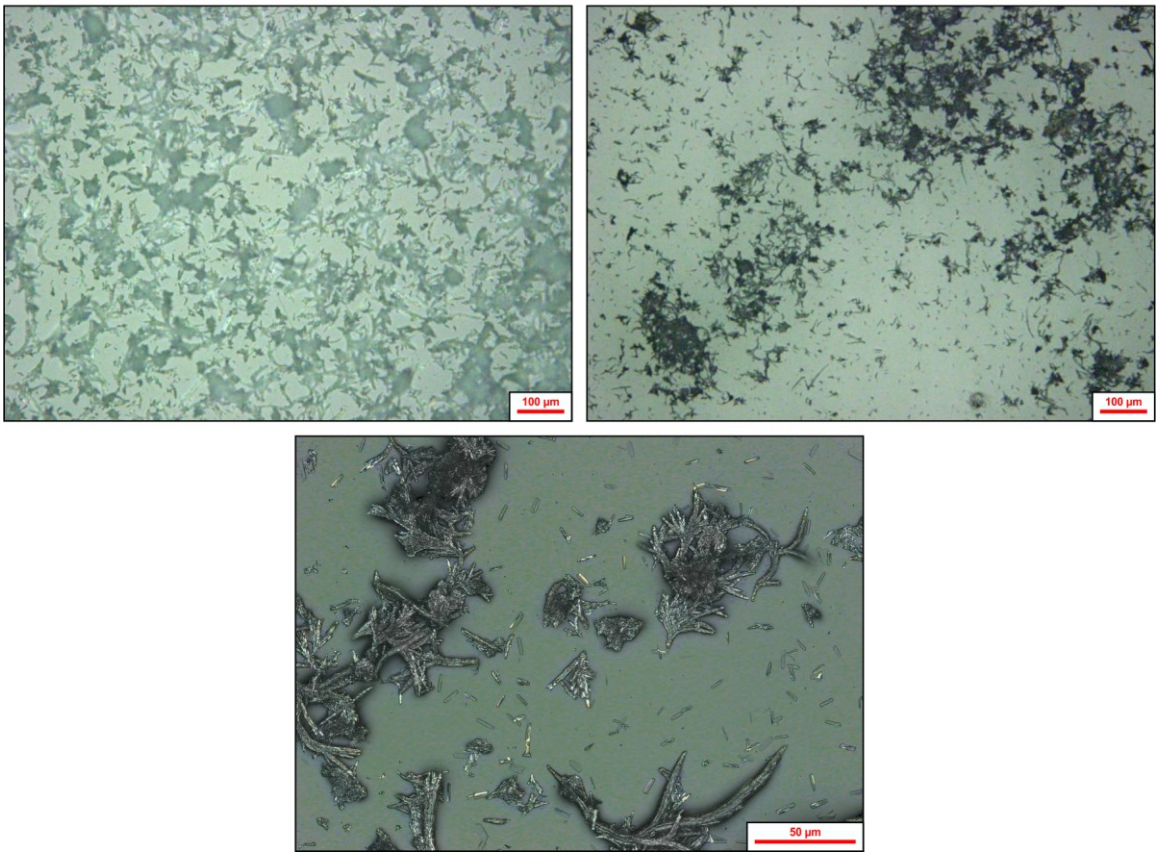

Figure 67) Upper row: Lightmicroscopic images. **Lower row:** Overlayed Light-microscopic and *CLSM*-images.

To assign the different morphologies to their respective polymorph Raman-microscopy was applied. Three references were used for the identification of the individual polymorphs. [307, 308, 309]

The rhombohedal crystallites were assigned to calcite.

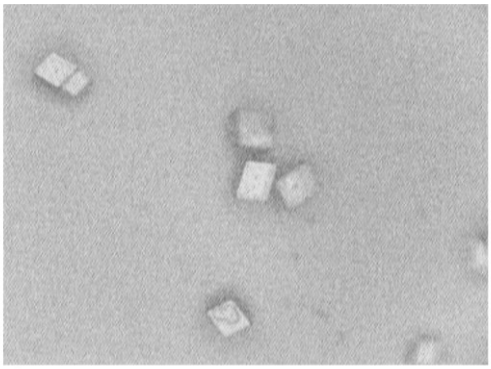

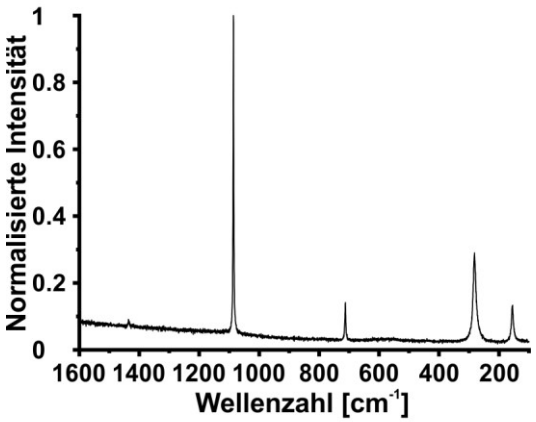

Peakliste	Referenz [1]
1437	1434
1086	1085
713	711
282	281
155	154

Figure 68) Raman-Microscopy of the rhombohedral crystallites. **a)** Image of the measured crystallite (in focus and center). **b)** Raman-spectrum of the same crystallites as well as the corresponding peaklist compared to a calcite reference [307].

The needle-like crystallites were assigned to aragonite.

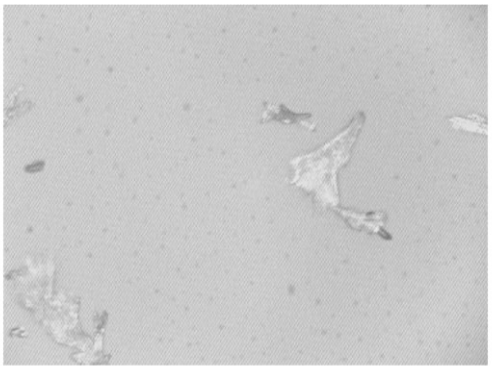

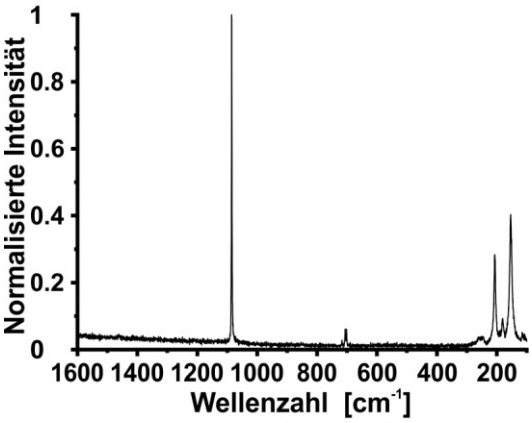

Peakliste	Referenz [2]
1085	1085
717	718
706	706
701	702
262	262
253	249
206	208
181	181
153	154

Figure 69) Raman-Microscopy of the needle-like crystallites. **a)** Image of the measured crystallite (in focus). **b)** Raman-spectrum of the same crystallites as well as the corresponding peaklist compared to a aragonite reference [308].

The feather-like crystallites were assigned to vaterite.

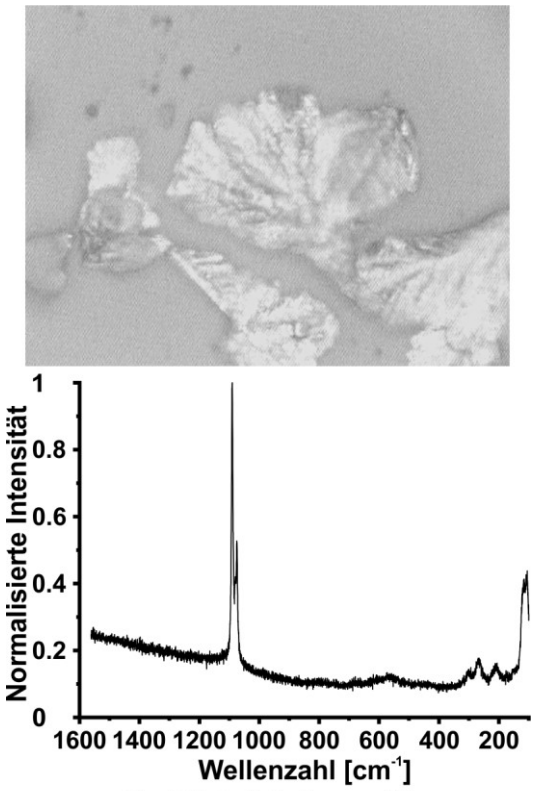

Peakliste	Referenz [2,3]
1090	1091
1078	1081
1075	1075
302	302
265	266
212	208
115	117

Figure 70) Raman-Microscopy of the feather-like crystallites. **a)** Image of the measured crystallite (in focus). **b)** Raman-spectrum of the same crystallites as well as the corresponding peaklist compared to a vaterite references [308, 309].

Appendix Vd: Crystallisation in presence of mixed, crude peptides (2/6)

Additive-free control

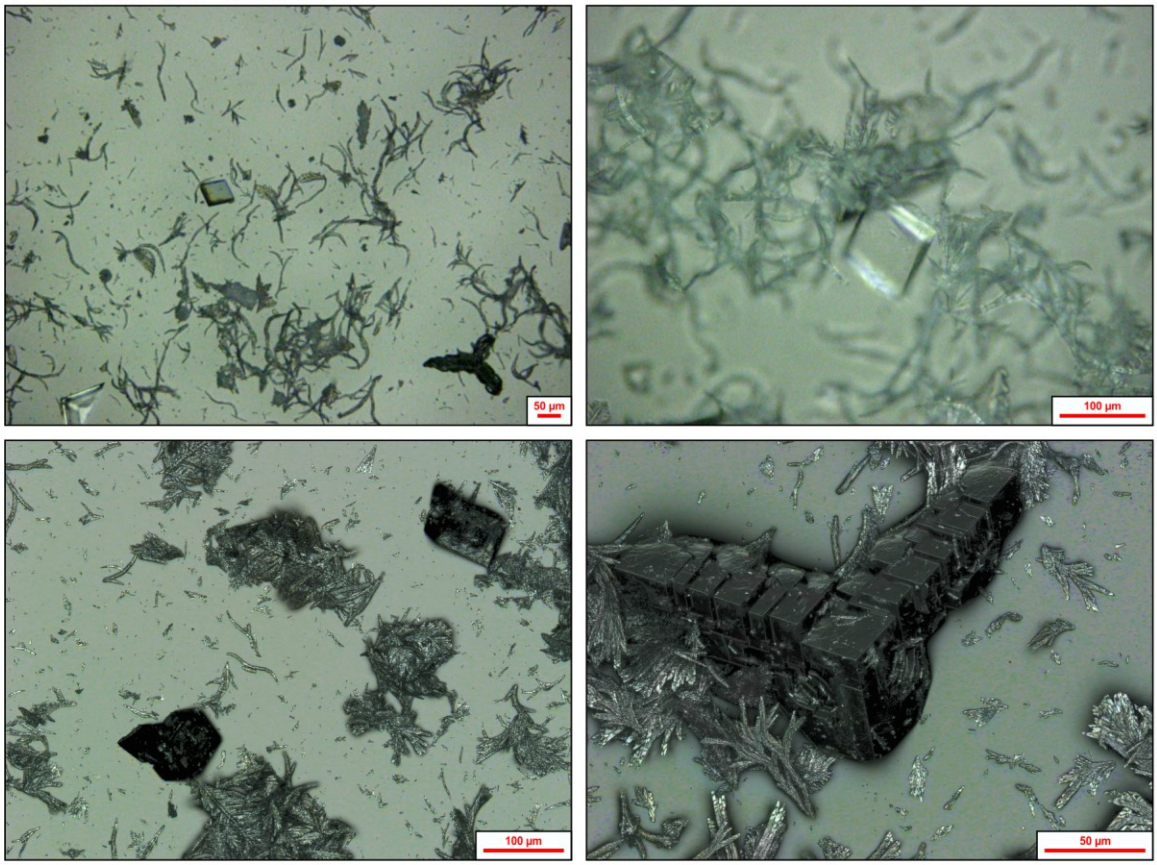

Crystallisation in presence of 0.337 mmol/L of the crude peptides (2) and (6)

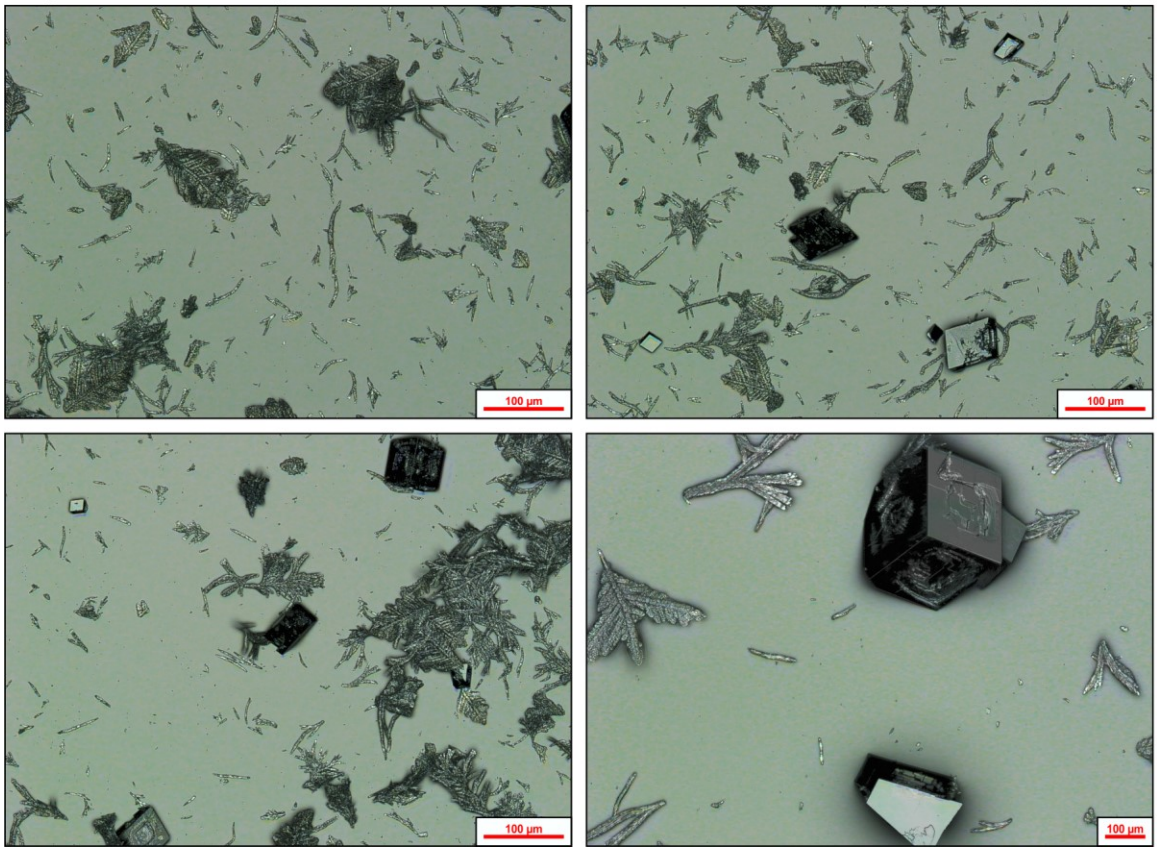

Figure 71) 1st and 3rd row: Light-microscopic images. **2nd and 4th row :** Overlayed Light-microscopic and *CLSM*-images.

Crystallisation in presence of 0.674 mmol/L of the crude peptides (2) and (6)

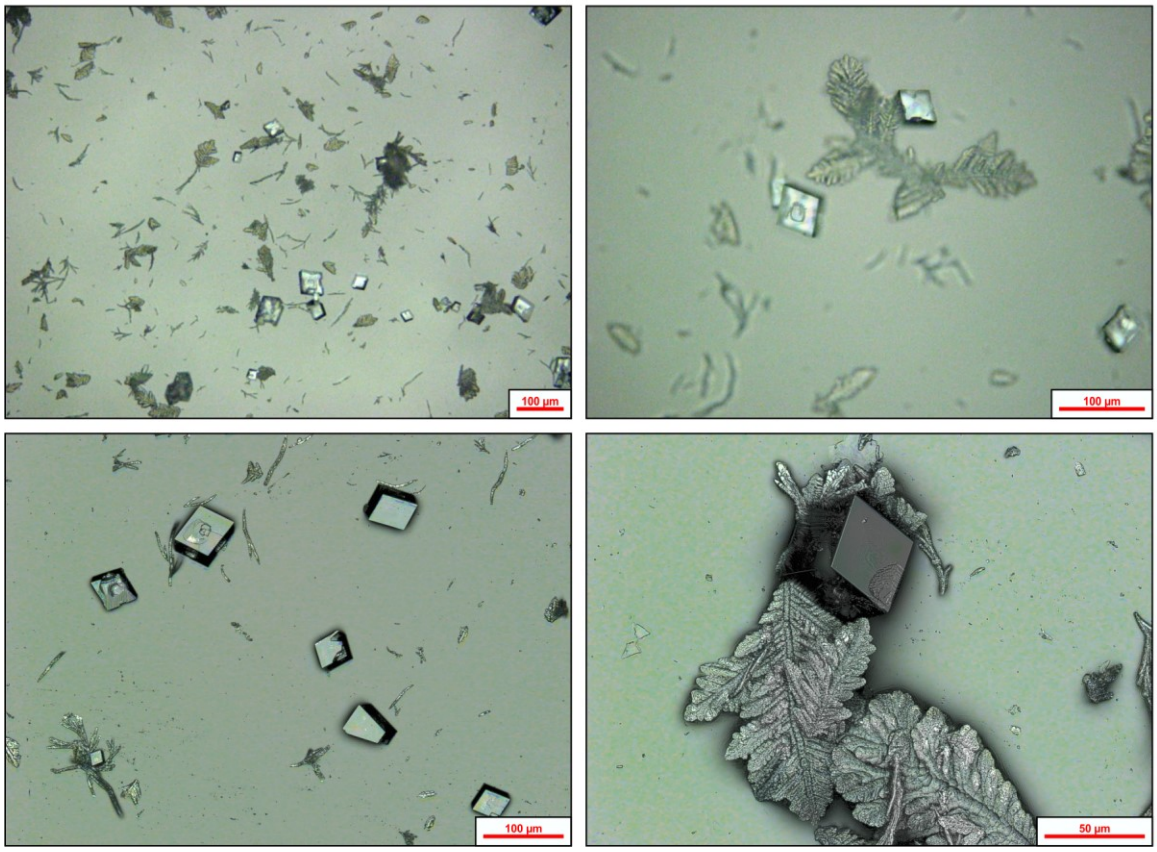

Figure 72) 1st row: Light-microscopic images. **2nd row:** Overlayed Light-microscopic and *CLSM*-images.

Appendix Ve: Precipitated calcium carbonate, crystallised in the presence of the mixed, crude peptides (2)/(6) and 0.5% Tween®20

Additive- and detergent-free control

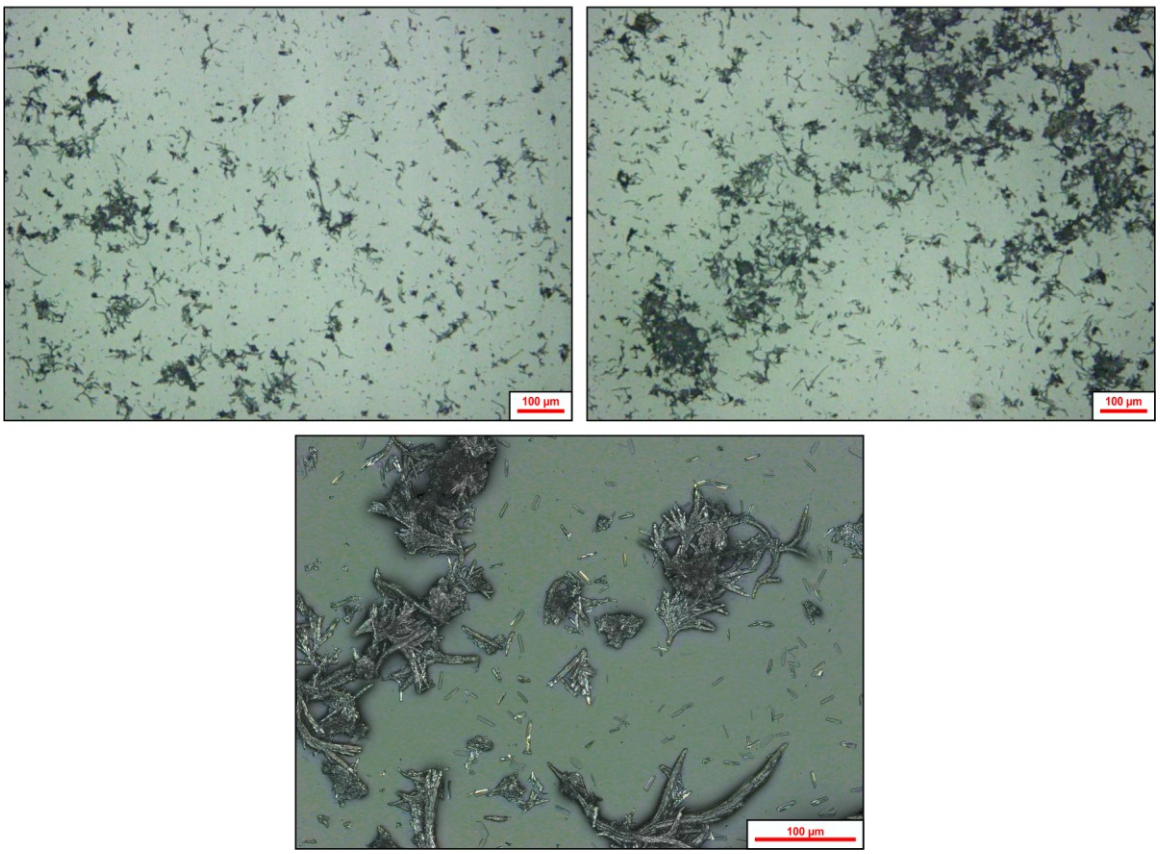

Figure 73) Upper row: Light-microscopic images. **Lower image:** Overlay of light-microscopic and *CLSM*-images.

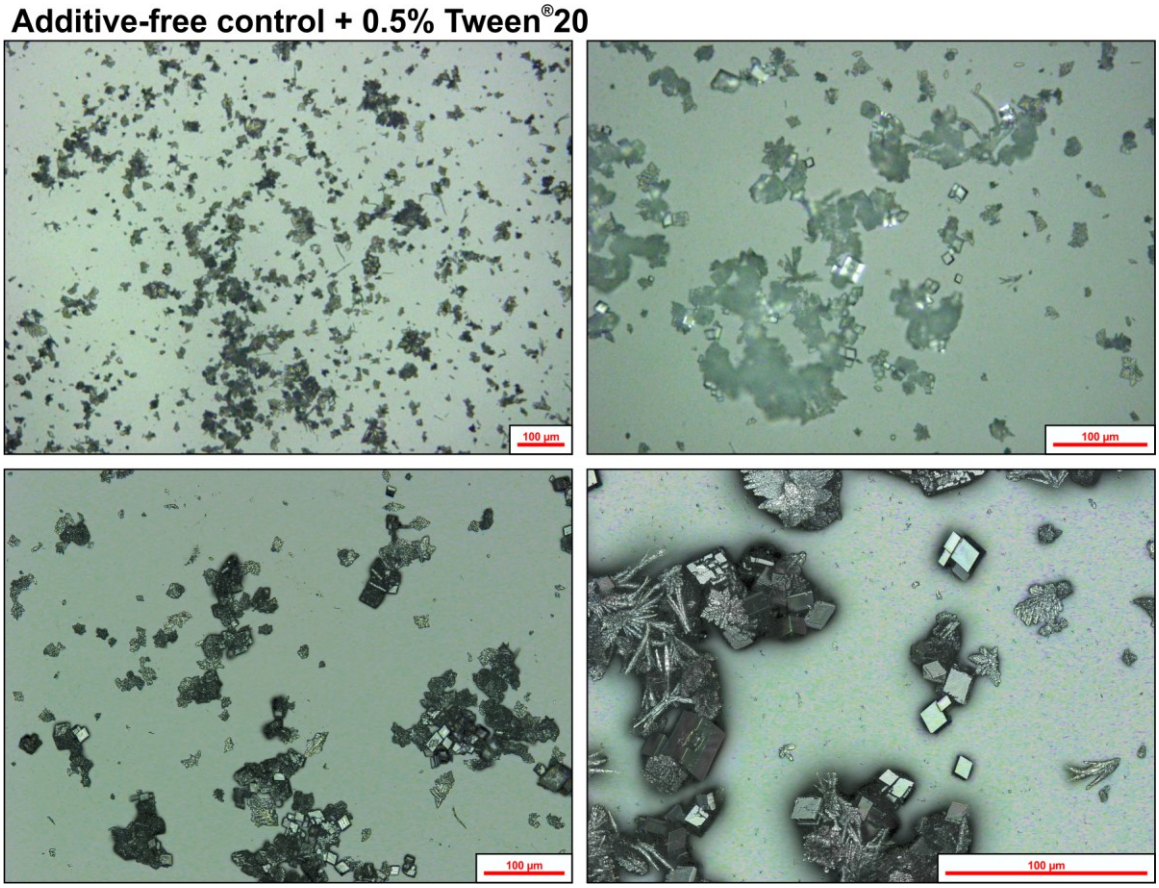

Figure 74) Upper row: Light-microscopic images. **Lower row:** Overlays of light-microscopic and *CLSM*-images.

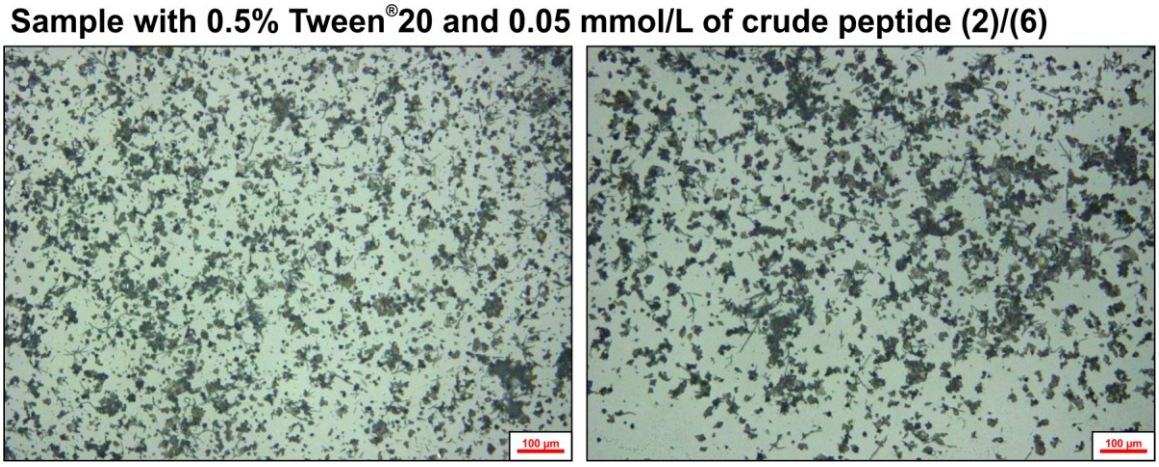

Figure 75) All images: Light-microscopic images.

Sample with 0.5% Tween®20 and 0.1 mmol/L of crude peptide (2)/(6)

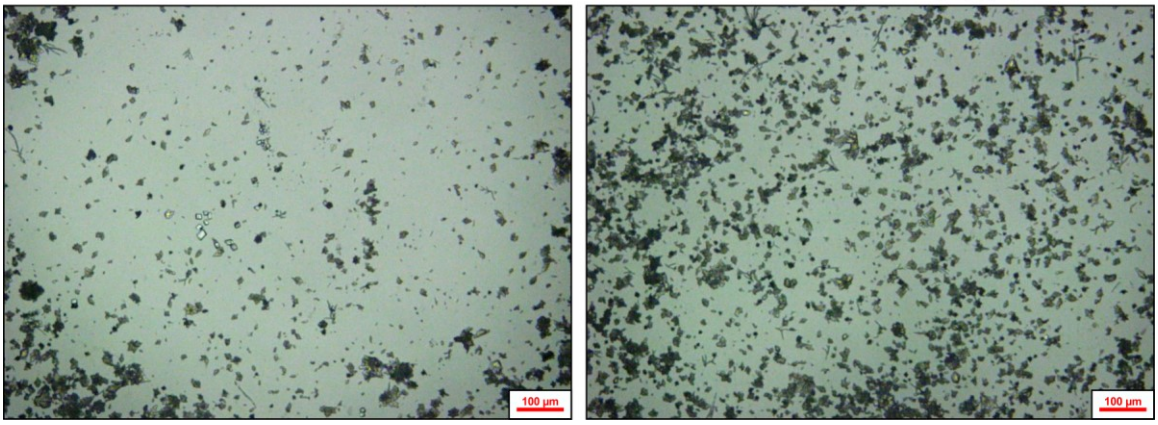

Figure 76) Light-microscopic images.

Sample with 0.5% Tween®20 and 0.2 mmol/L of crude peptide (2)/(6)

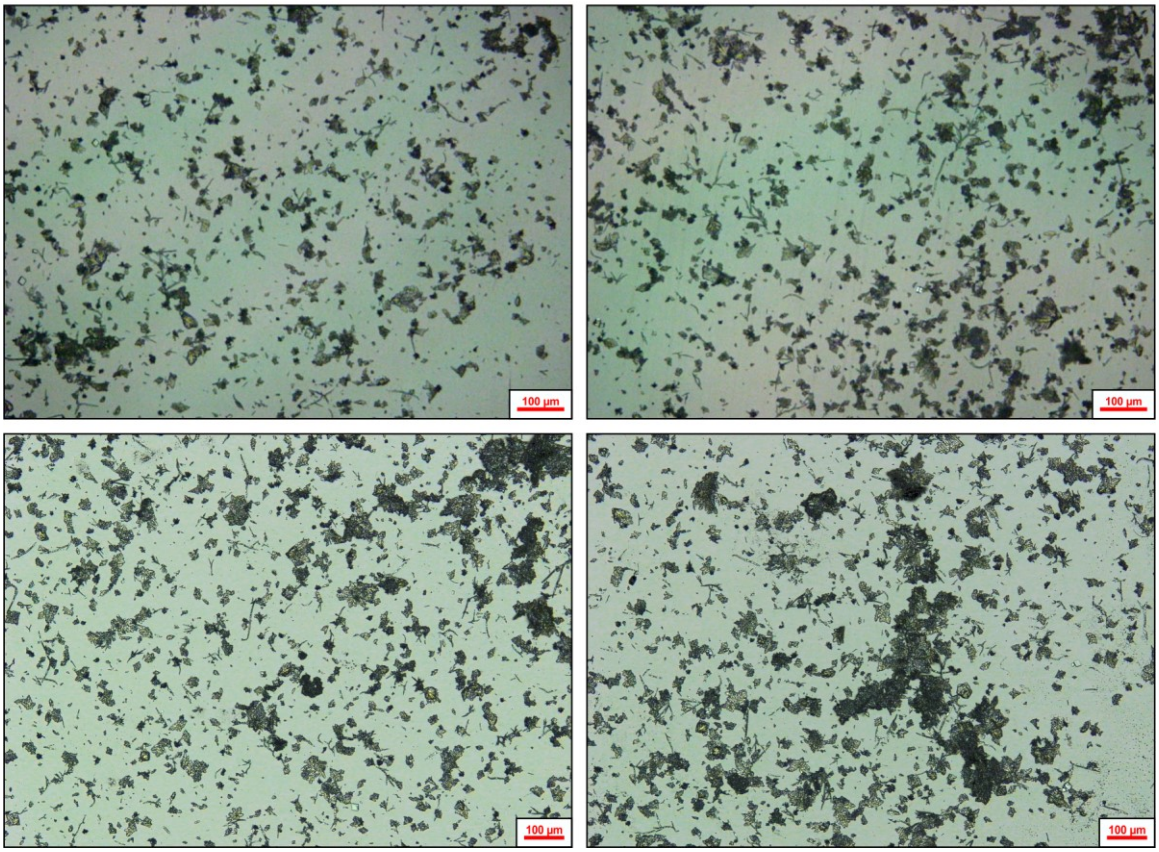

Figure 77) Upper row: Light-microscopic images. **Lower row:** Overlays of light-microscopic and *CLSM*-images.

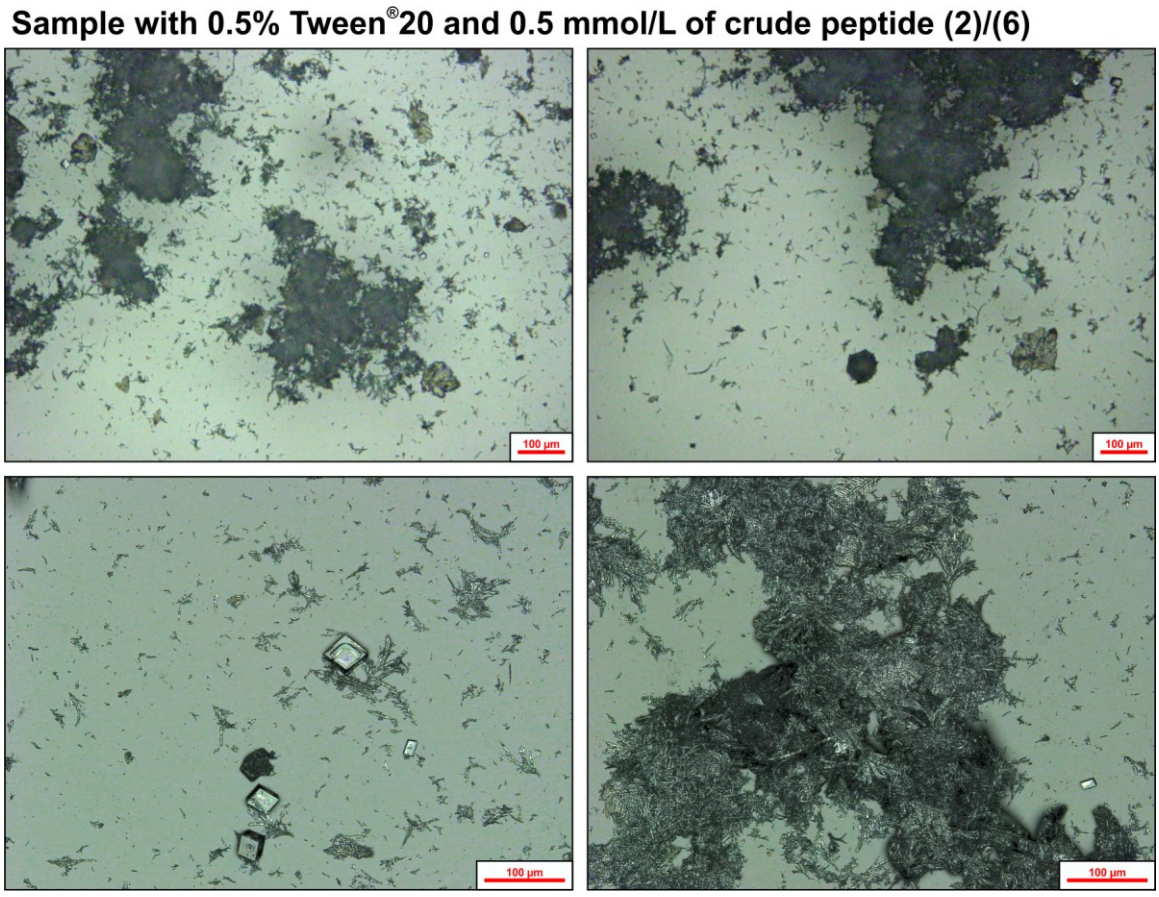

Figure 78) Upper row: Light-microscopic images. **Lower row:** Overlays of light-microscopic and *CLSM*-images.

Appendix Vf: Precipitated calcium carbonate, crystallised in the presence of the mixed, crude peptides (3)/(7)

Additive-free control sample

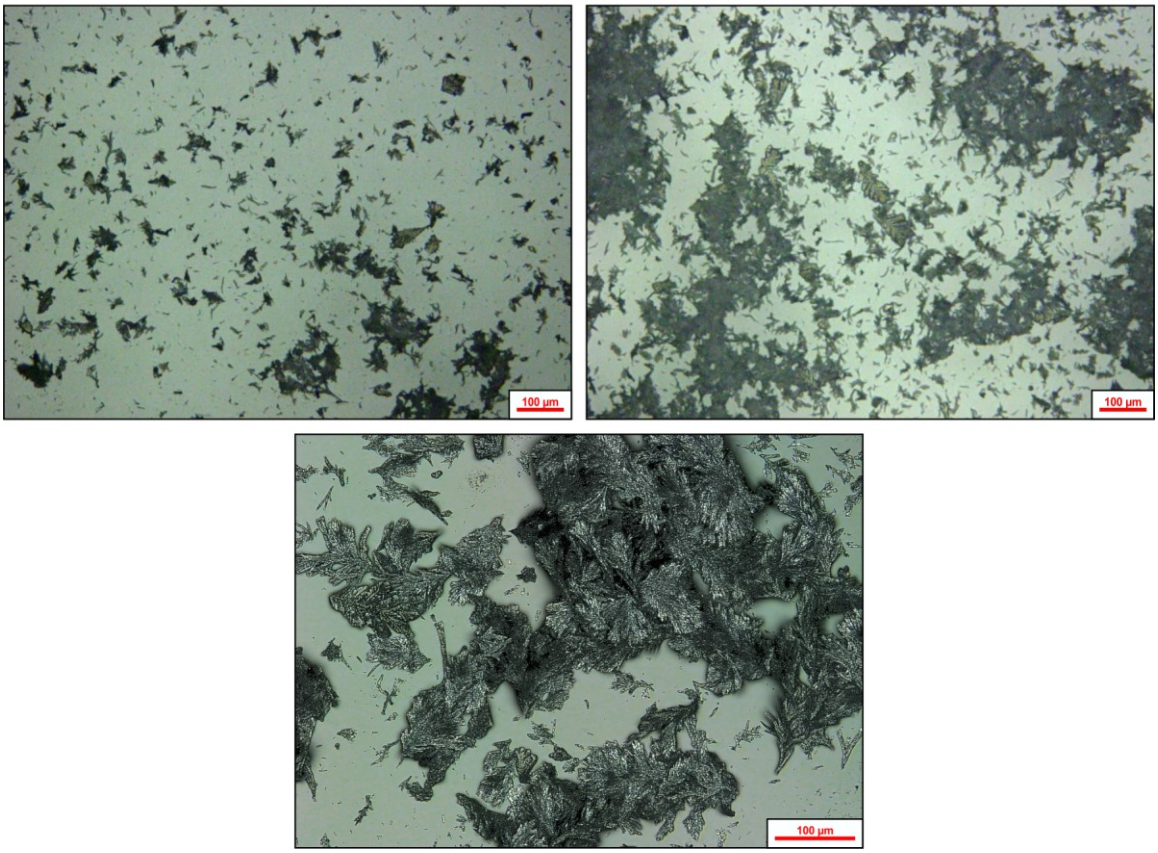

Figure 79) Upper row: Light-microscopic images. **Lower image:** Overlay of light-microscopic and *CLSM*-images.

Sample with 0.05 mmol/L of crude peptides (3)/(7)

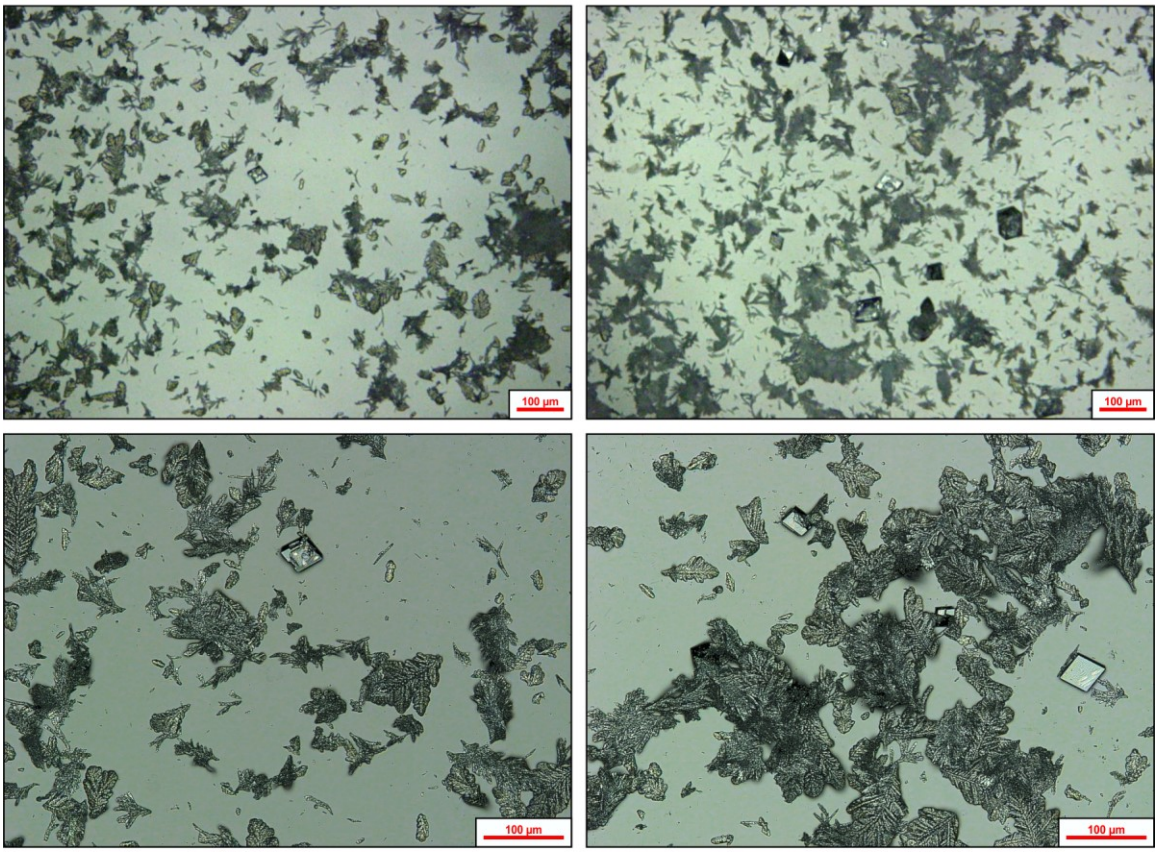

Sample with 0.1 mmol/L of crude peptides (3)/(7)

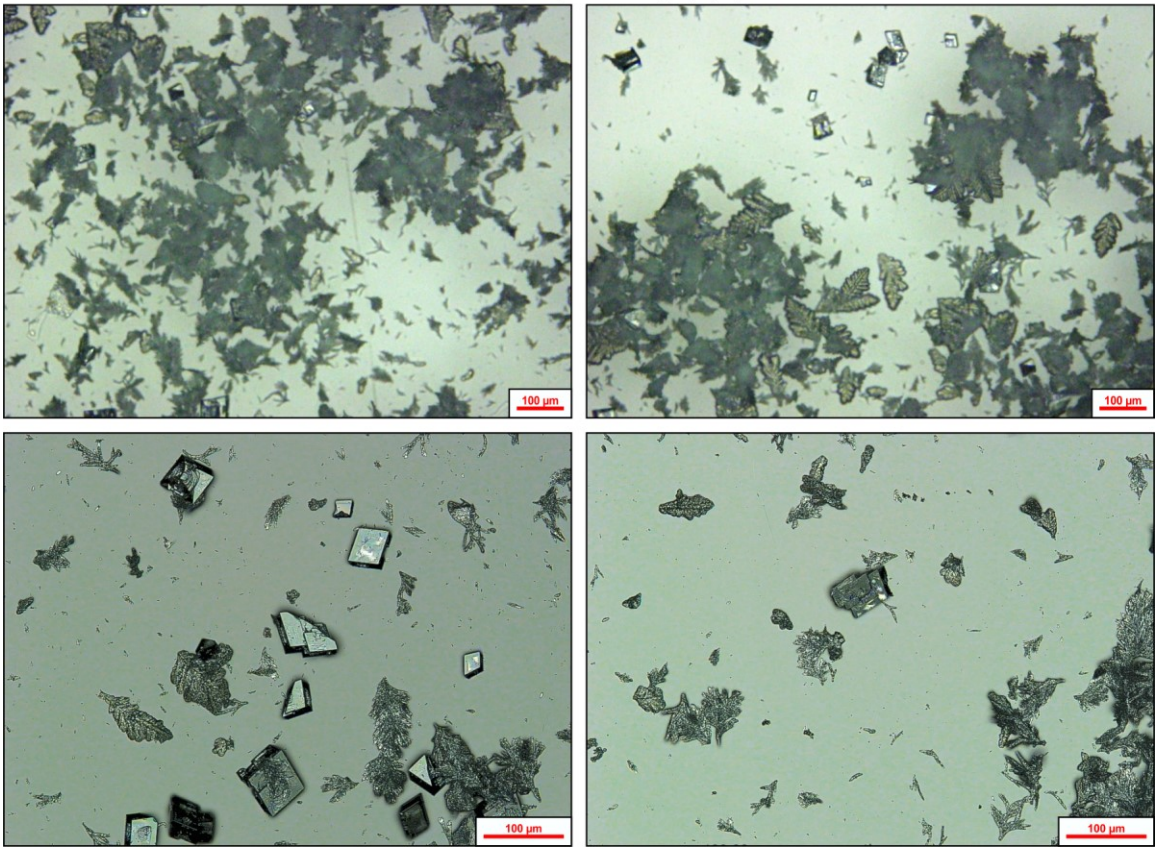

Figure 80) 1st row: Light-microscopic images. **2nd row:** Overlays of light-microscopic and *CLSM*-images. **3rd row:** Light-microscopic images. **4th row:** Overlay of light-microscopic and *CLSM*-images.

Sample with 0.2 mmol/L of crude peptides (3)/(7)

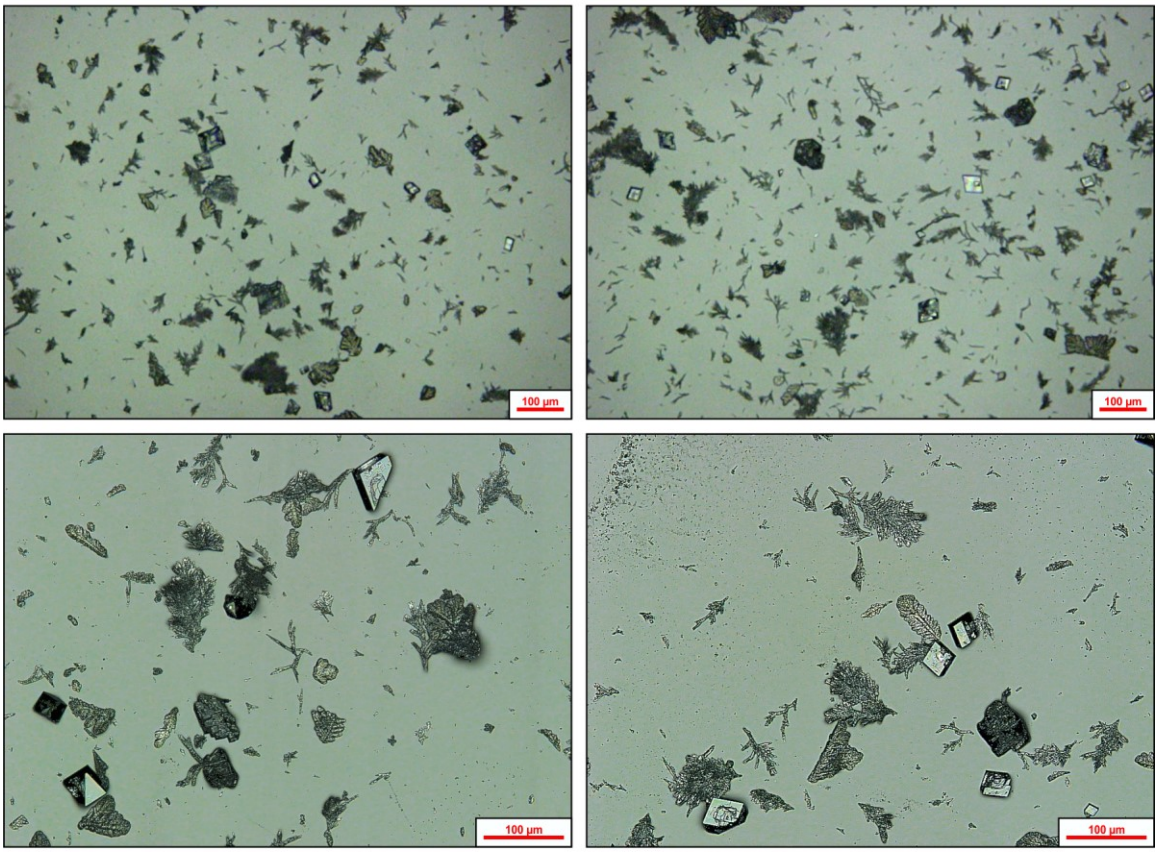

Sample with 0.5 mmol/L of crude peptides (3)/(7)

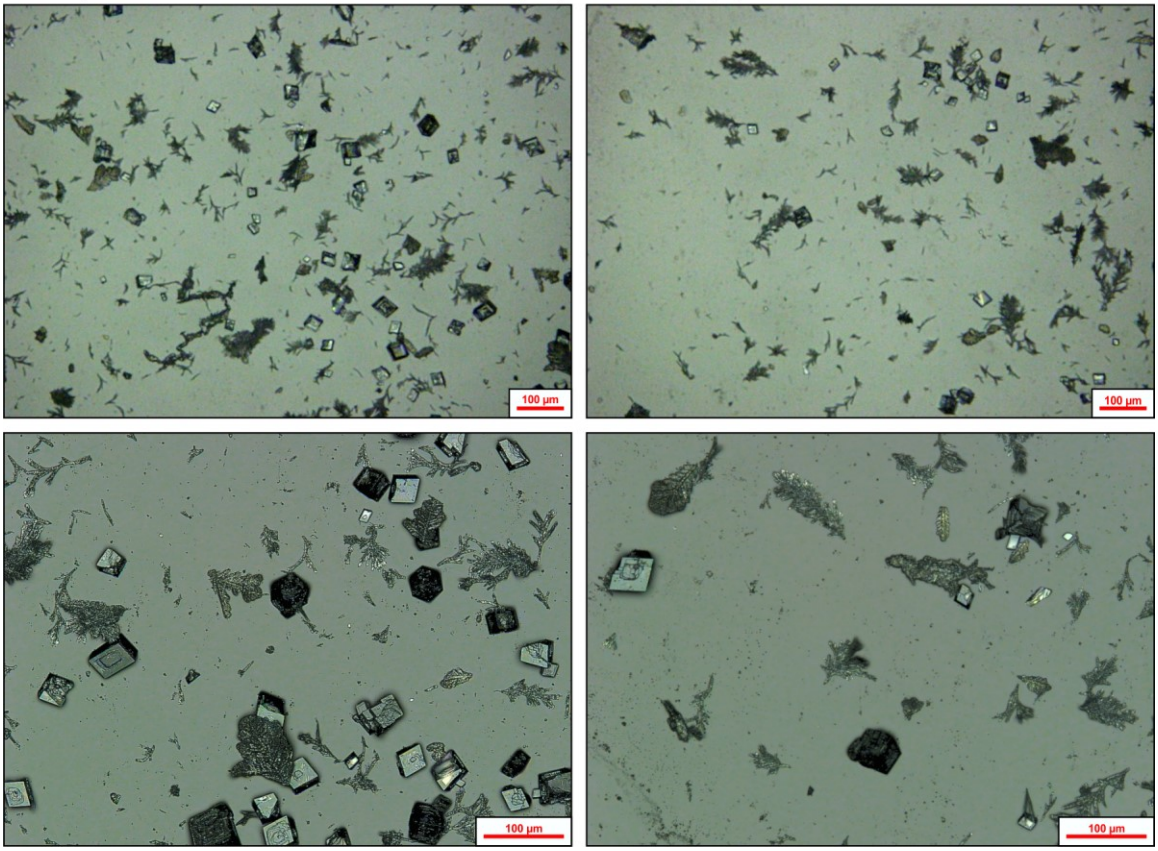

Figure 81) 1st row: Light-microscopic images. **2nd row:** Overlay of light-microscopic and *CLSM*-images. **3rd ow:** Light-microscopic images. **4th row:** Overlay of light-microscopic and *CLSM*-images.

Sample with 1 mmol/L of crude peptides (3)/(7)

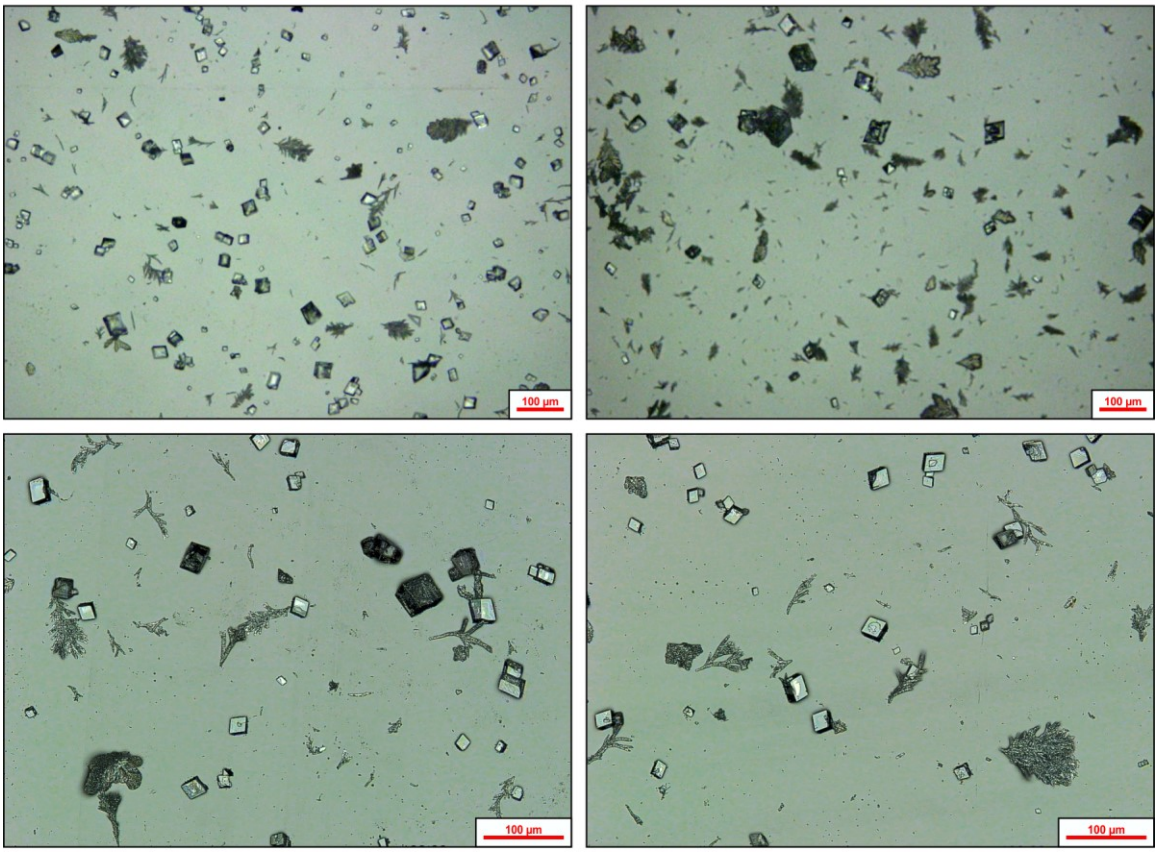

Sample with 2 mmol/L of crude peptides (3)/(7)

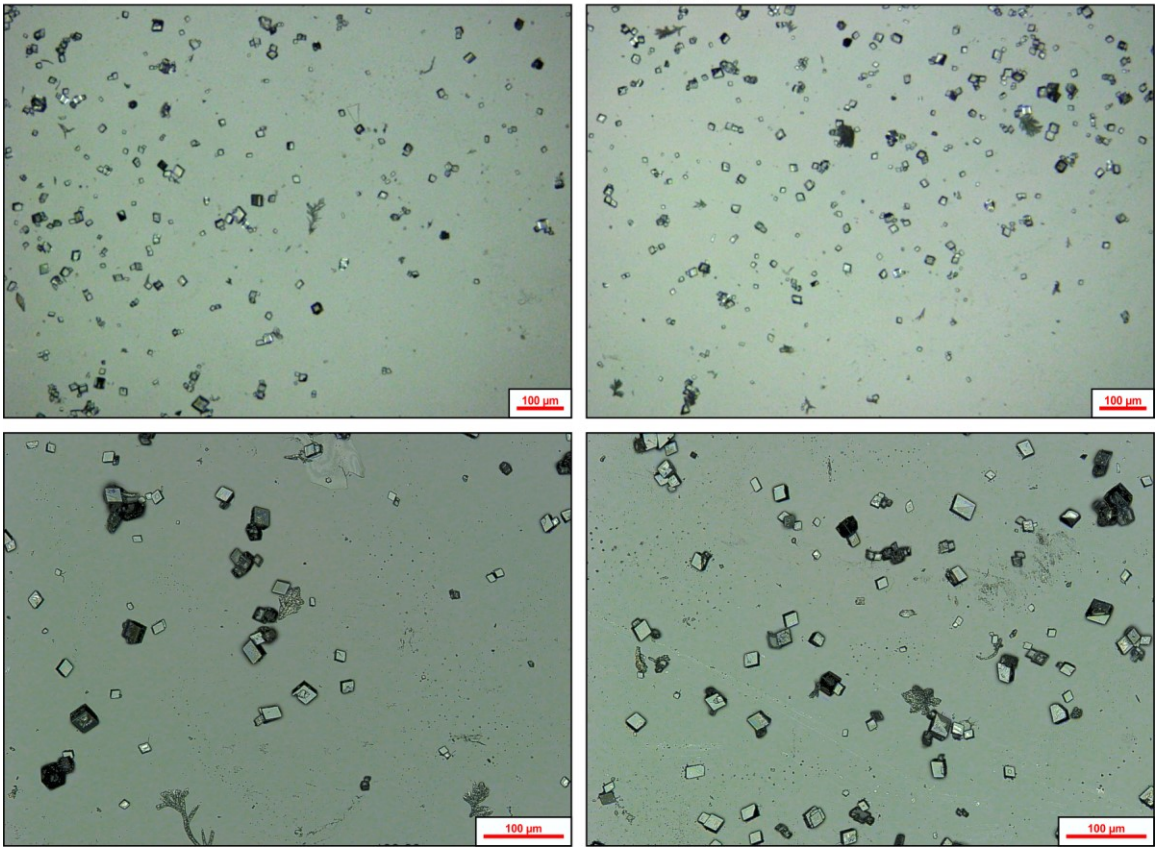

Figure 82) 1st row: Light-microscopic images. **2nd row:** Overlay of light-microscopic and *CLSM*-images. **3rd row:** Light-microscopic images. **4th row:** Overlay of light-microscopic and *CLSM*-images.

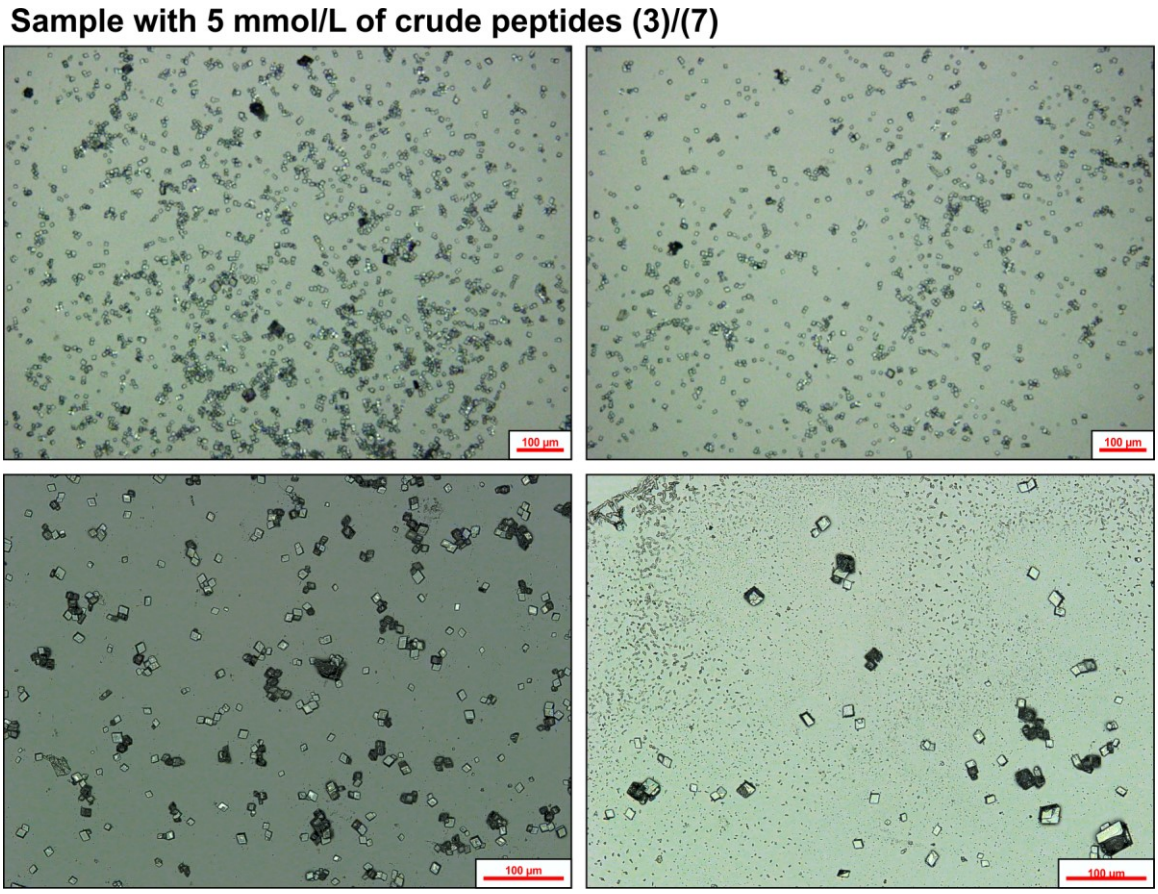

Figure 83) Upper row: Light-microscopic images. **Lower row:** Overlay of light-microscopic and *CLSM*-images.

Appendix Vg: Crystallisation in the presence of peptide (8)

Additive-free control sample

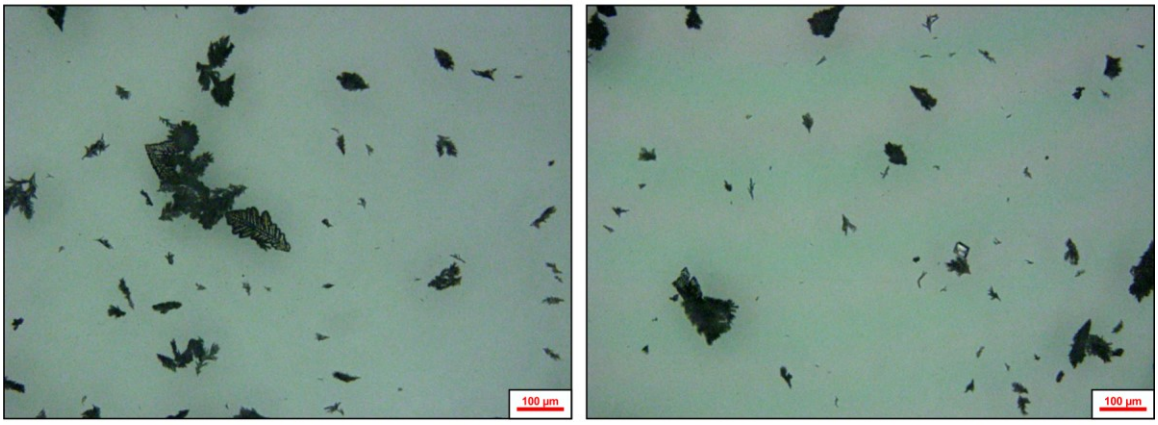

Sample with 0.05 mmol/L of the pure peptide (8)

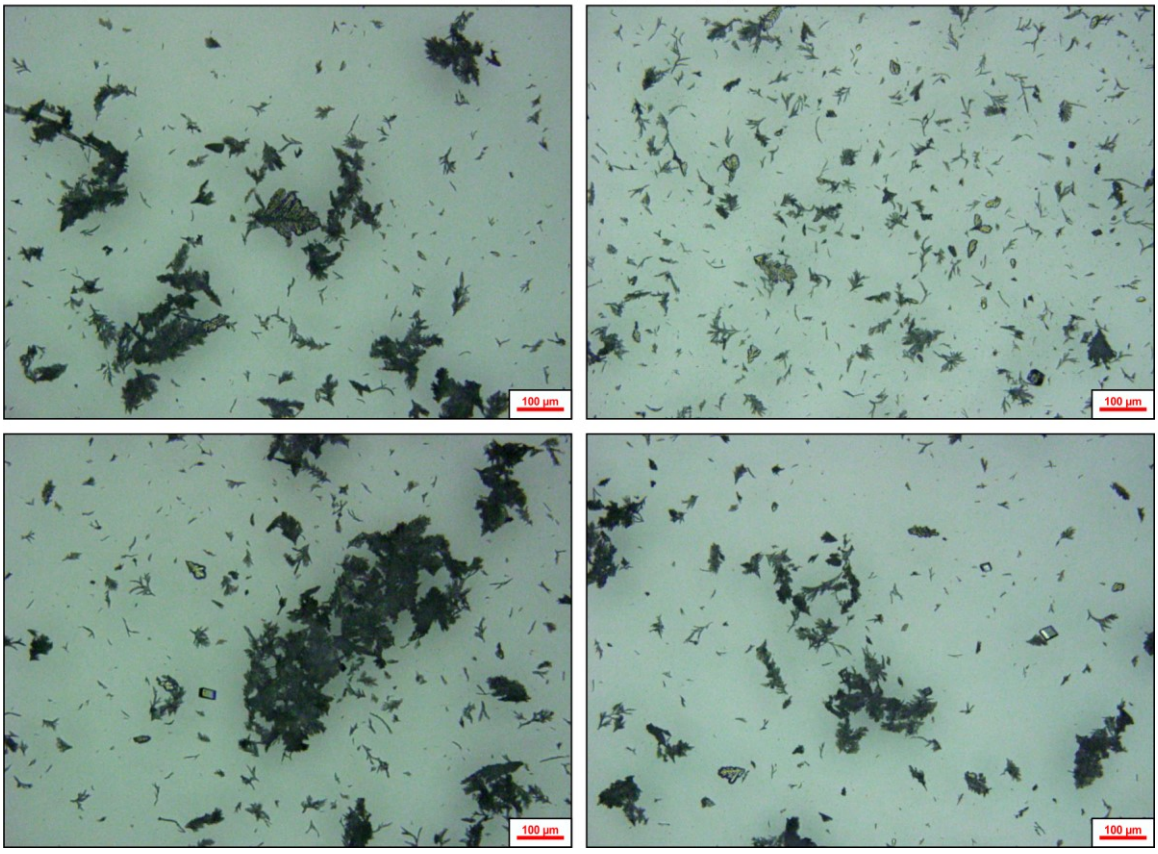

Figure 84) All images: Light-microscopic images.

Sample with 0.1 mmol/L of the pure peptide (8)

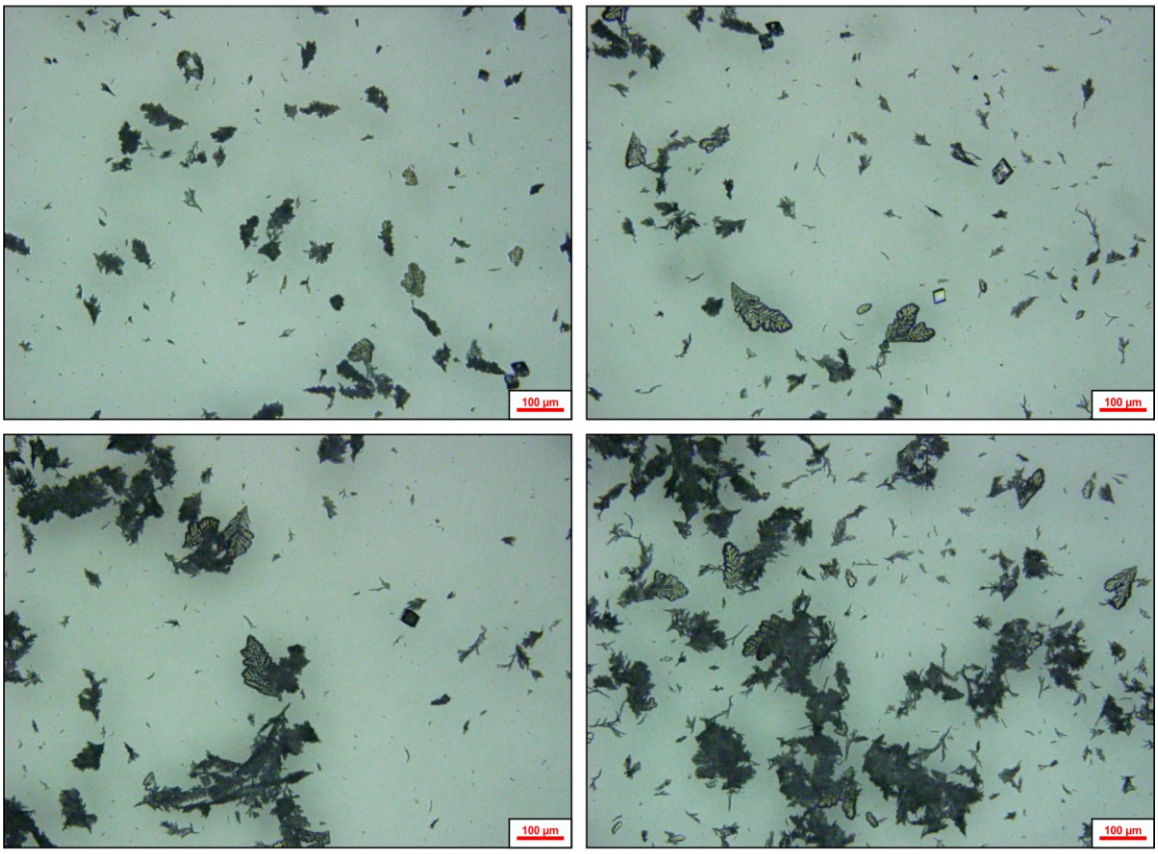

Sample with 0.2 mmol/L of the pure peptide (8)

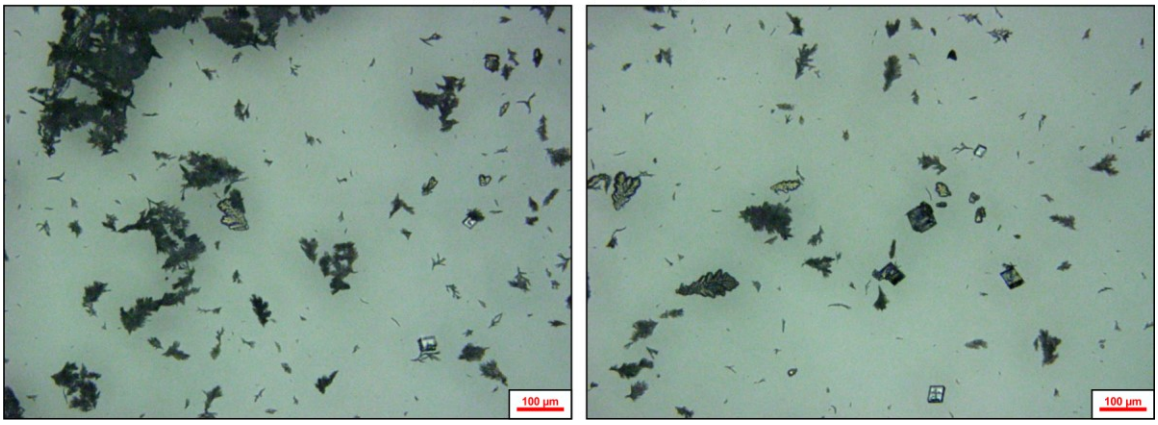

Figure 85) All images: Light-microscopic images.

Sample with 0.5 mmol/L of the pure peptide (8)

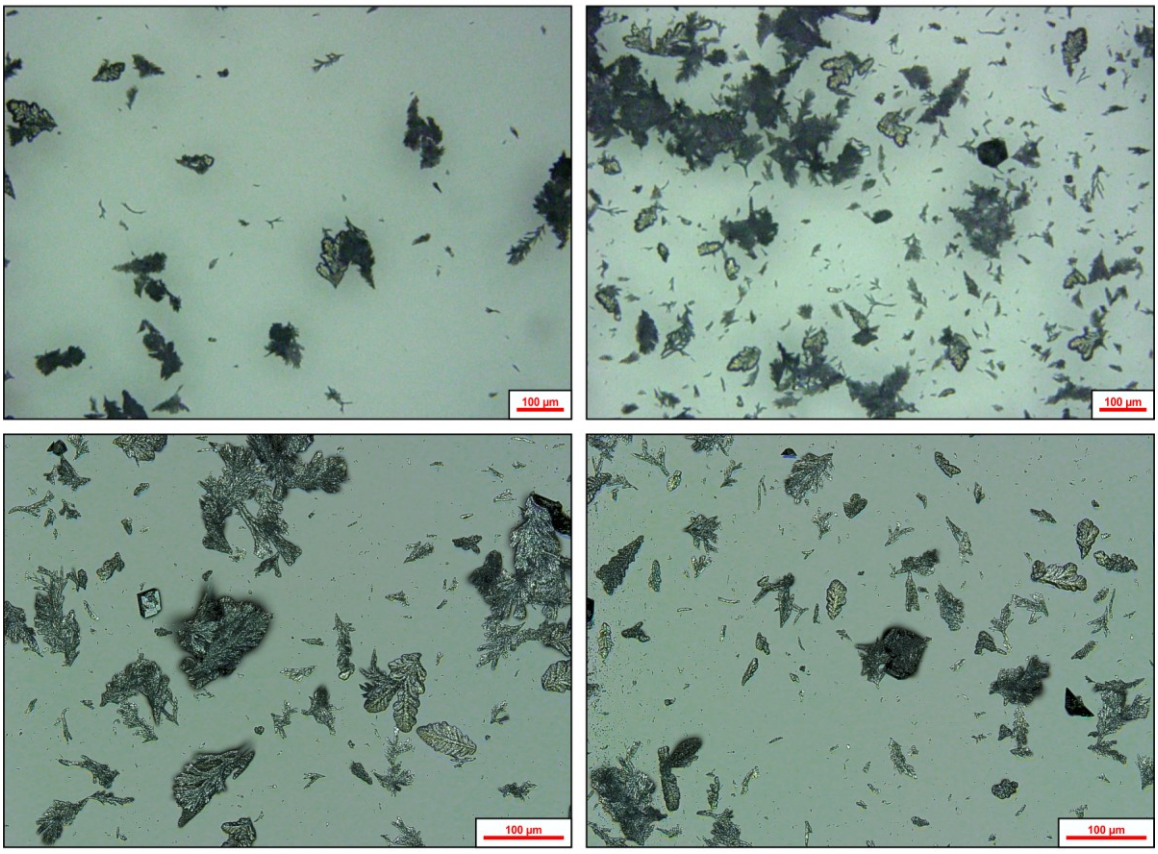

Sample with 1 mmol/L of the pure peptide (8)

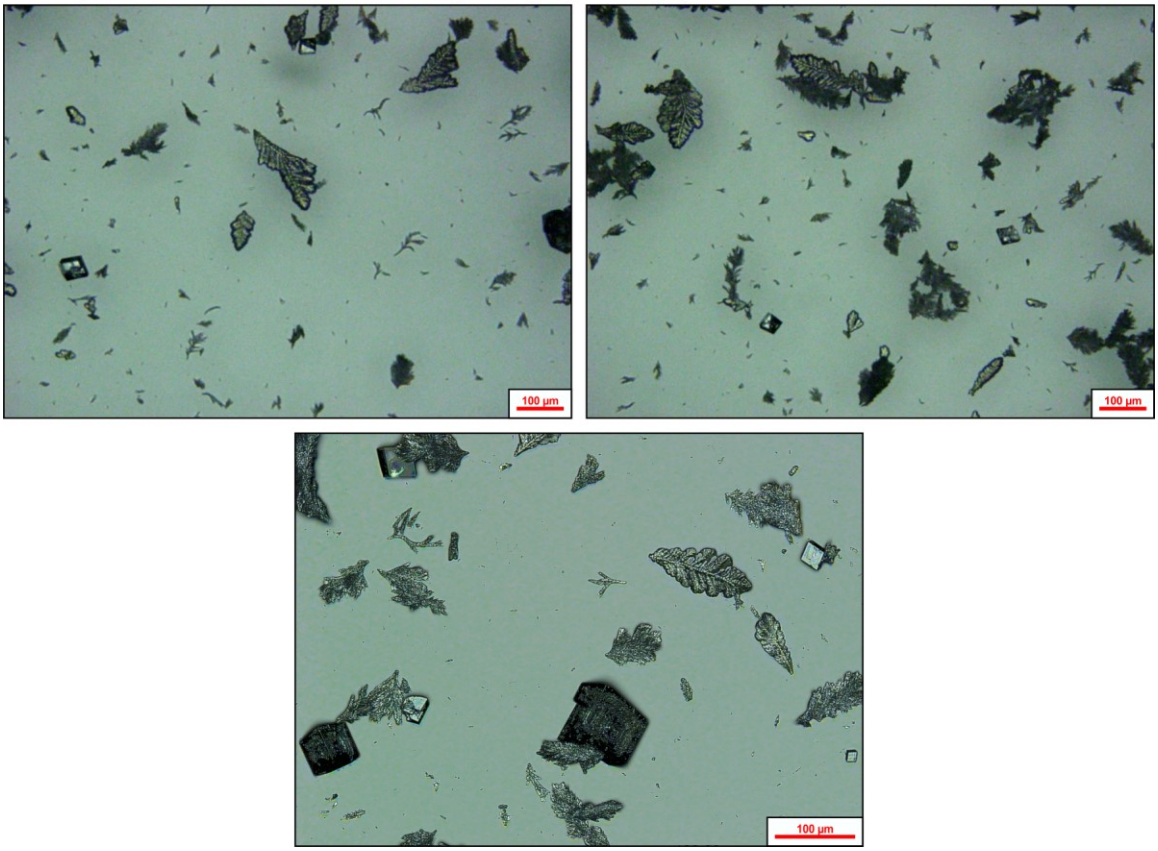

Figure 86) 1st row: Light-microscopic images. **2nd row:** Overlays of light microscopic and *CLSM*-images. **3rd row:** Light-microscopic images. **4th image:** Overlay of light microscopic and *CLSM*-image.

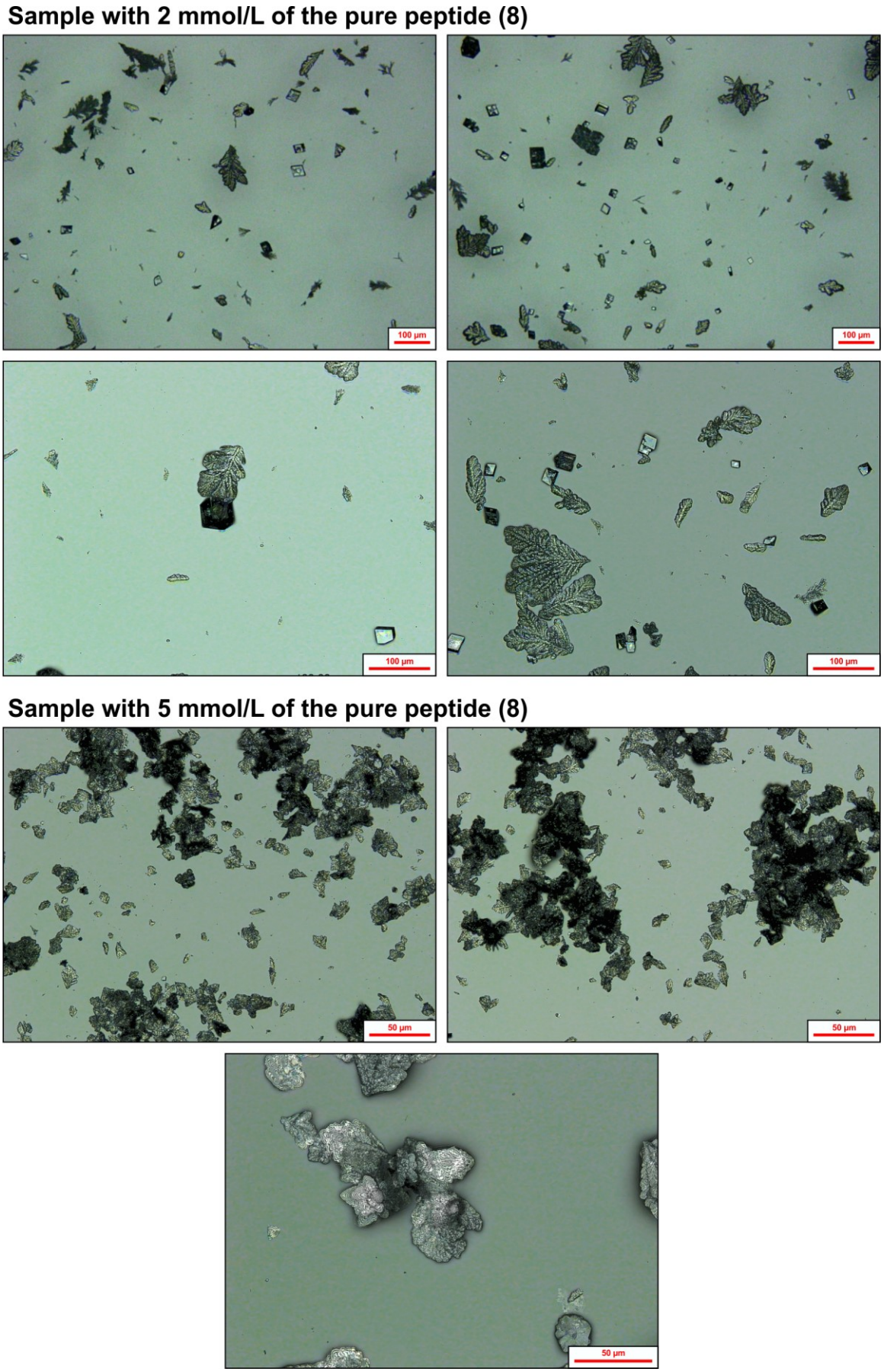

Figure 87) 1st row: Light-microscopic images. **2nd-4th row)** Overlays of light microscopic and *CLSM*-images.

Appendix Vh: Comparative crystallisations in the presence of peptide (7) and peptide (8) in different purities

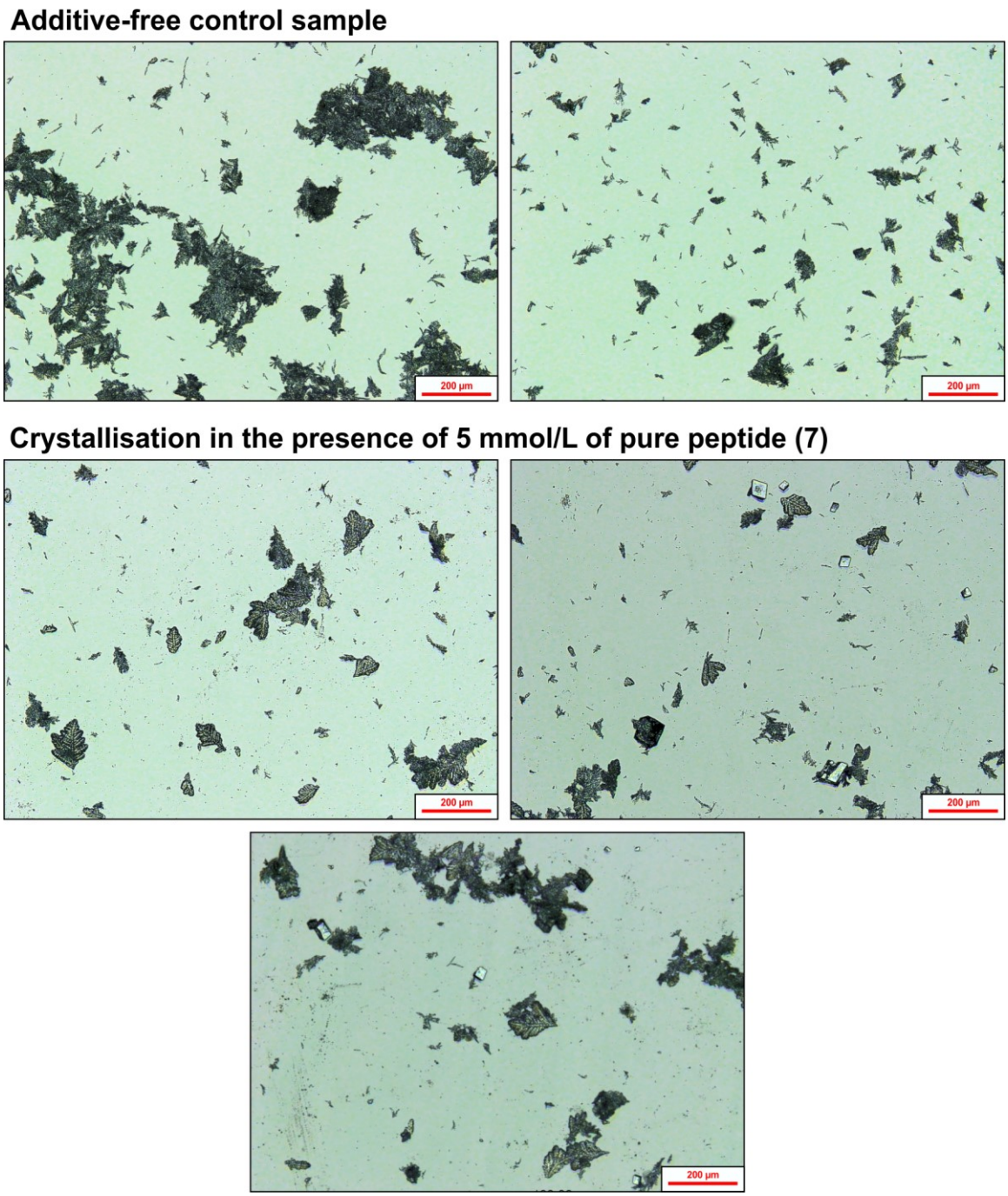

Figure 88) All images: Overlayed Light-microscopic and *CLSM*-images.

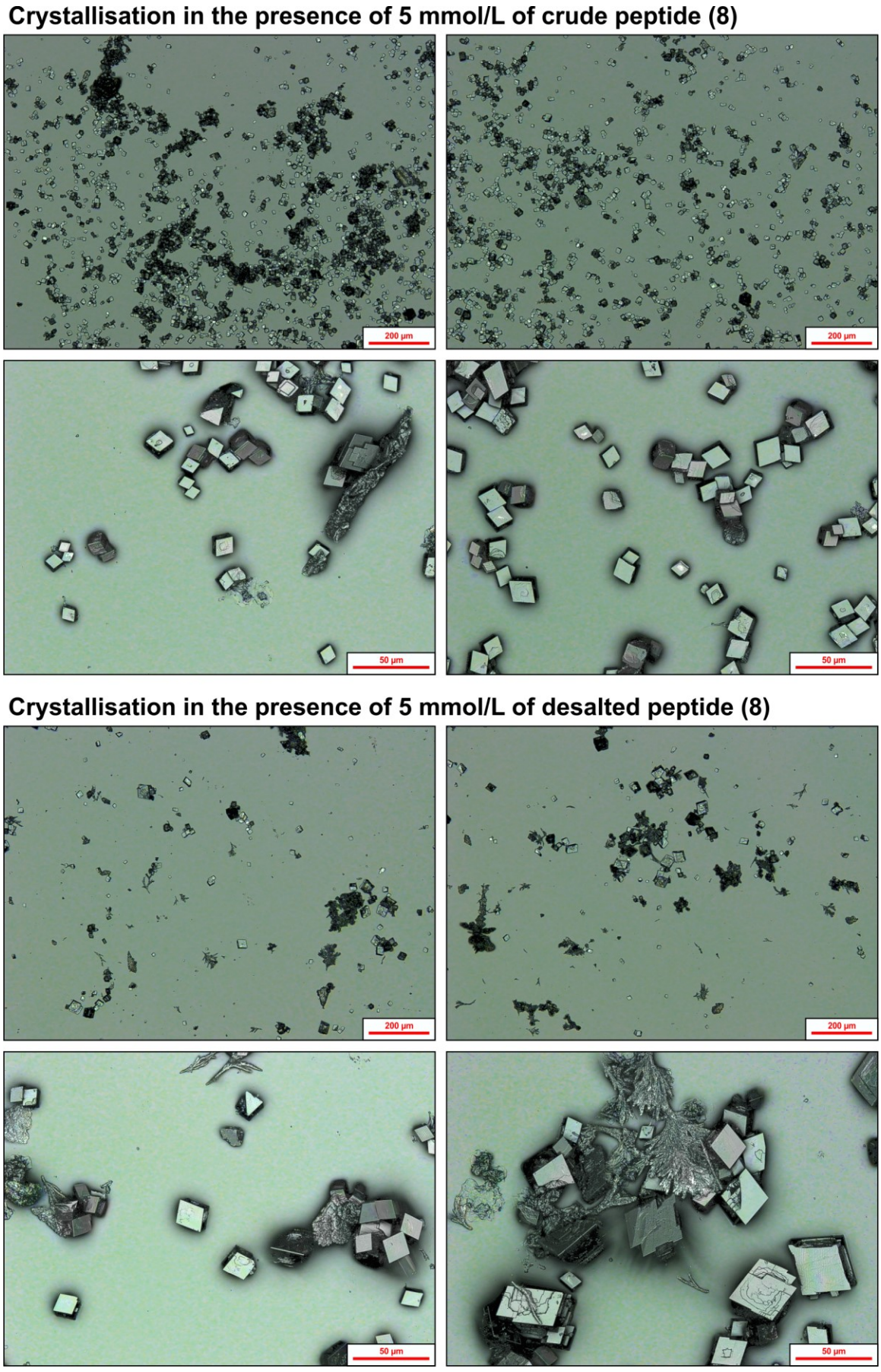

Figure 89) All images: Overlayed of Light-microscopic and *CLSM*-images.

Appendix Vi: Comparative crystallisations in the presence of the crude peptide (9) and the pure peptides (10), (11), (12) and (1)

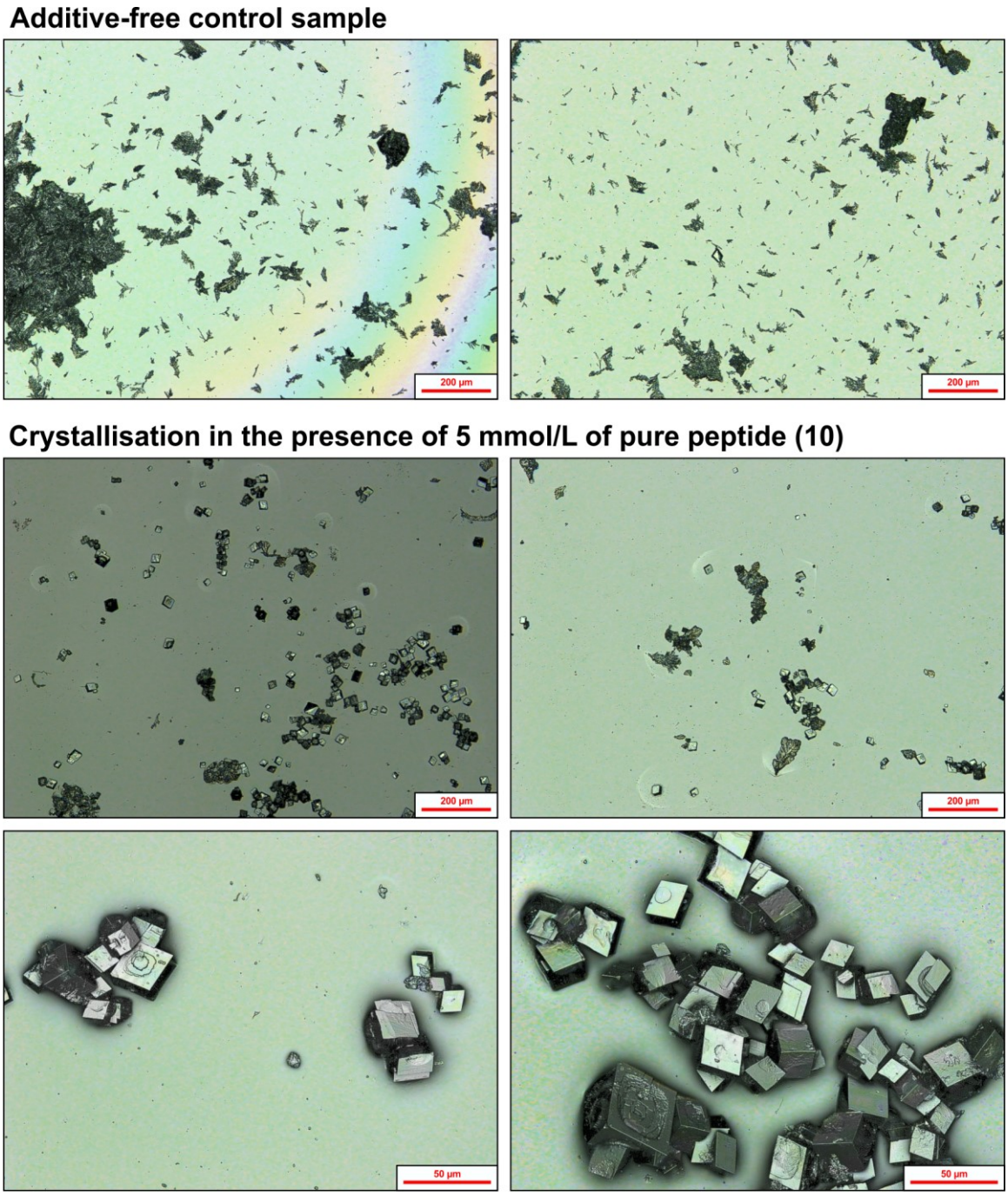

Figure 90) All images: Overlayed Light-microscopic and *CLSM*-images.

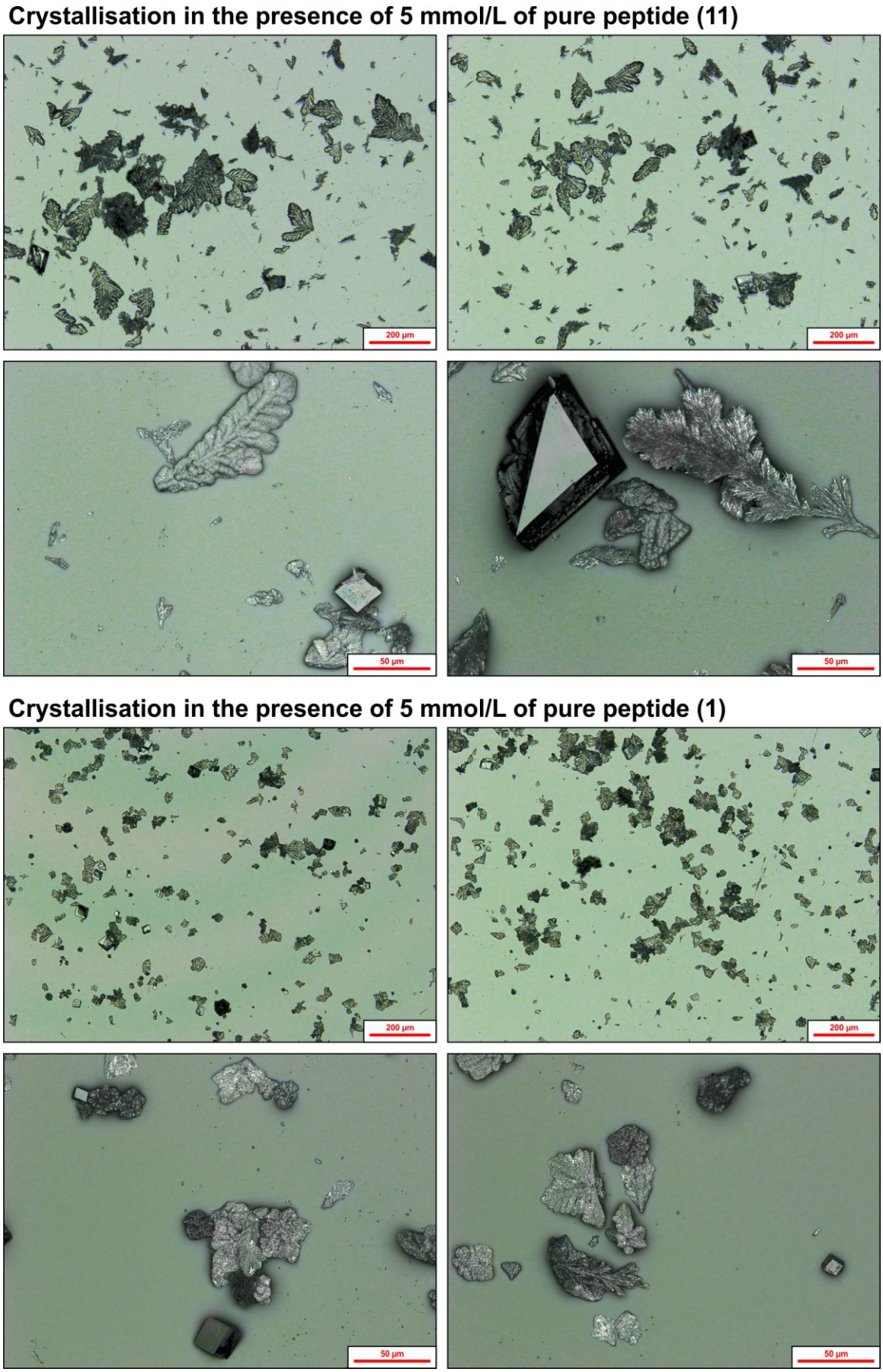

Figure 91) All images: Overlayed Light-microscopic and *CLSM*-images.

Crystallisation in the presence of 5 mmol/L of the crude peptide (9)

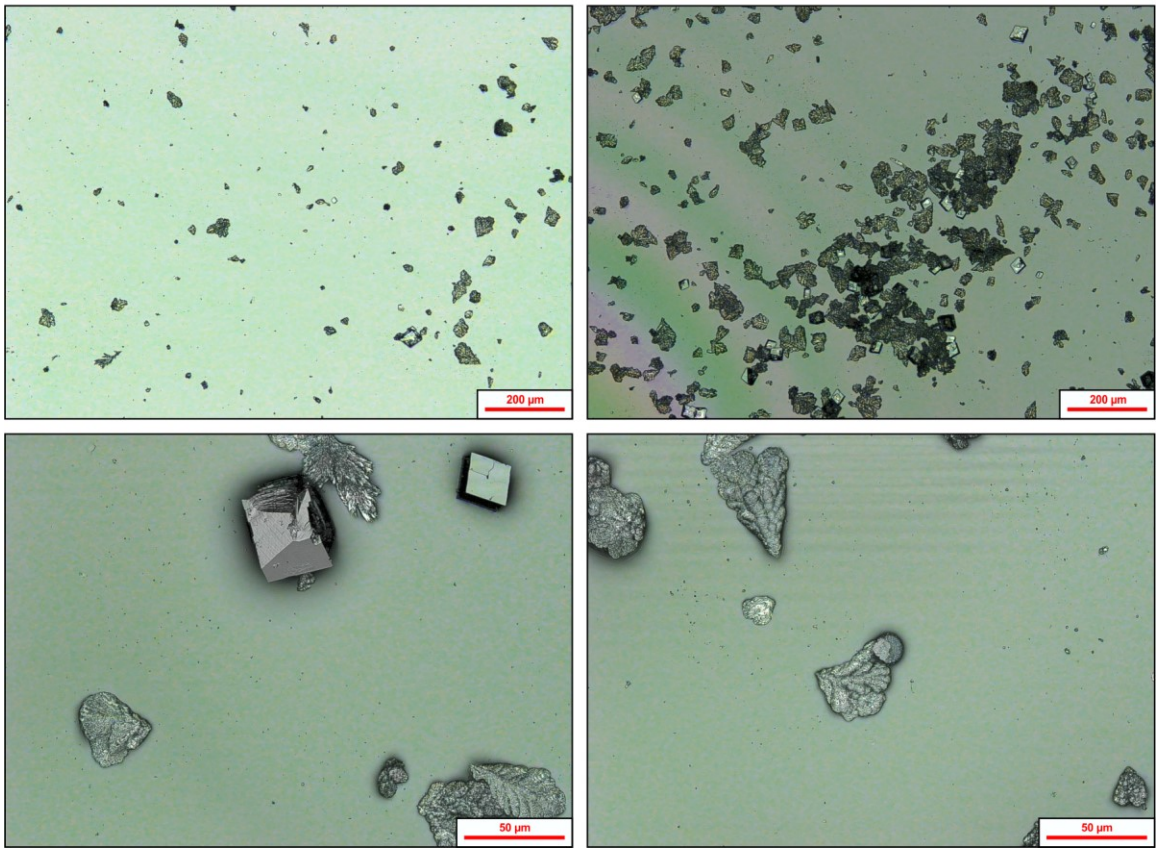

Figure 92) All images: Overlayeds Light-microscopic and *CLSM*-images.

Appendix VI:
Recrystallisations: Data and Images

Appendix VIa: Data of the utilised vaterite nanoparticles prior to a recrystallisation

X-ray powder diffractogram

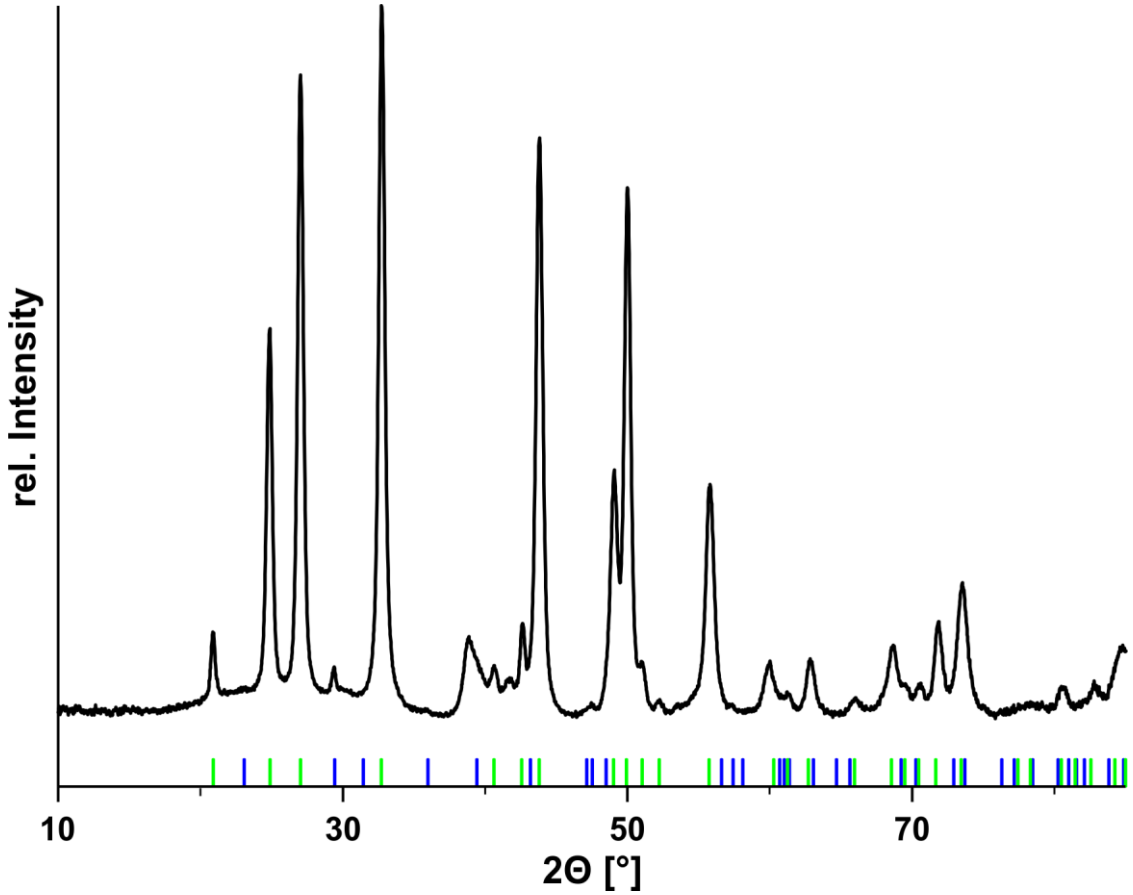

Figure 93) XRPD of the vaterite nanoparticles prior to a recrystallisation. Referenced reflex positions are indicated by the coloured lines. Colour code and references: **Blue** lines: calcite [140]; **Green** lines: vaterite [284]. Data were kindly provided by *Dr R. Schröder*.

SEM-images

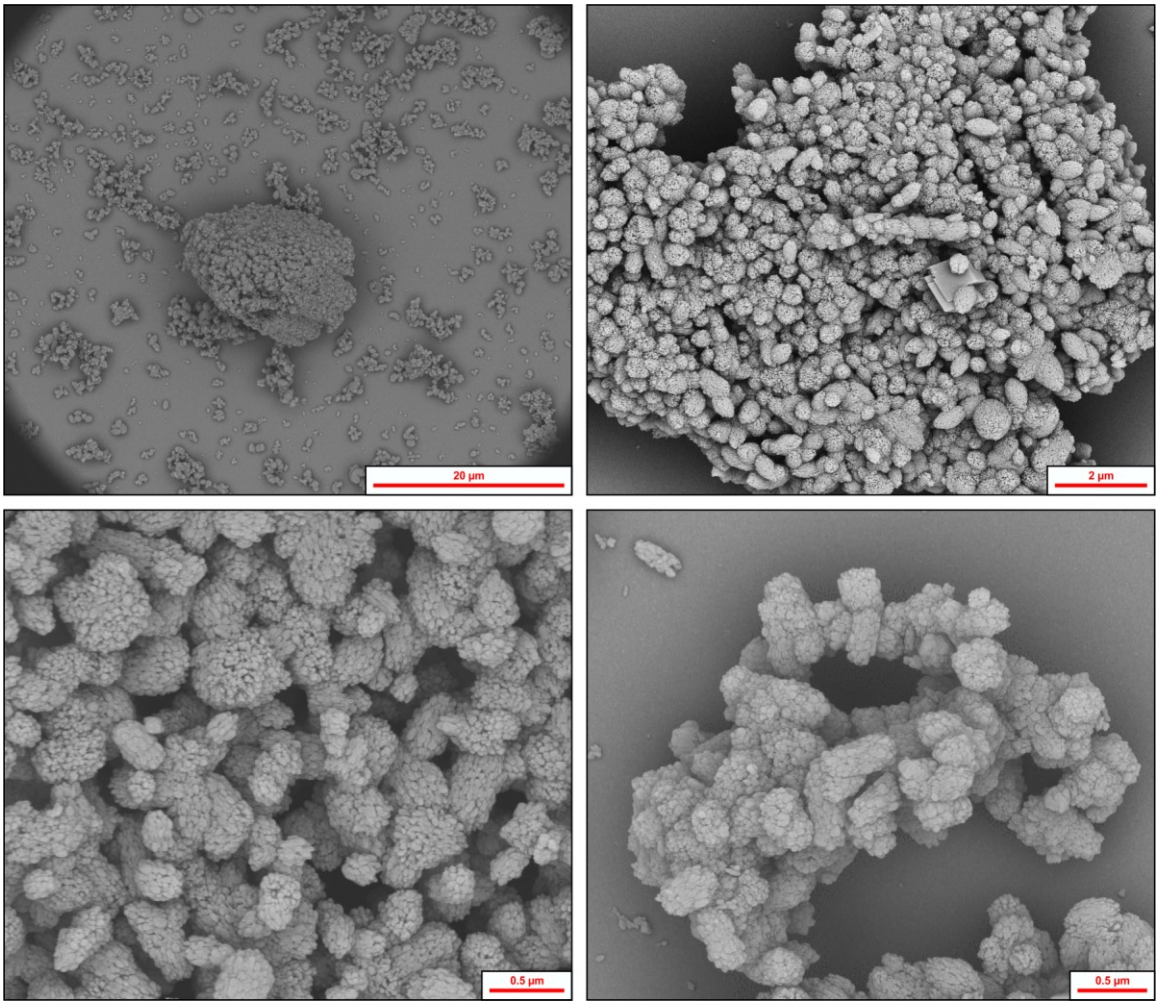

Figure 94) *SEM*-images of the vaterite nanoparticles prior to a recrystallisation The images were kindly provided by *Dr R. Schröder*.

Appendix VIb: Recrystallistions

Precipitate obtained from the additive-free control sample.

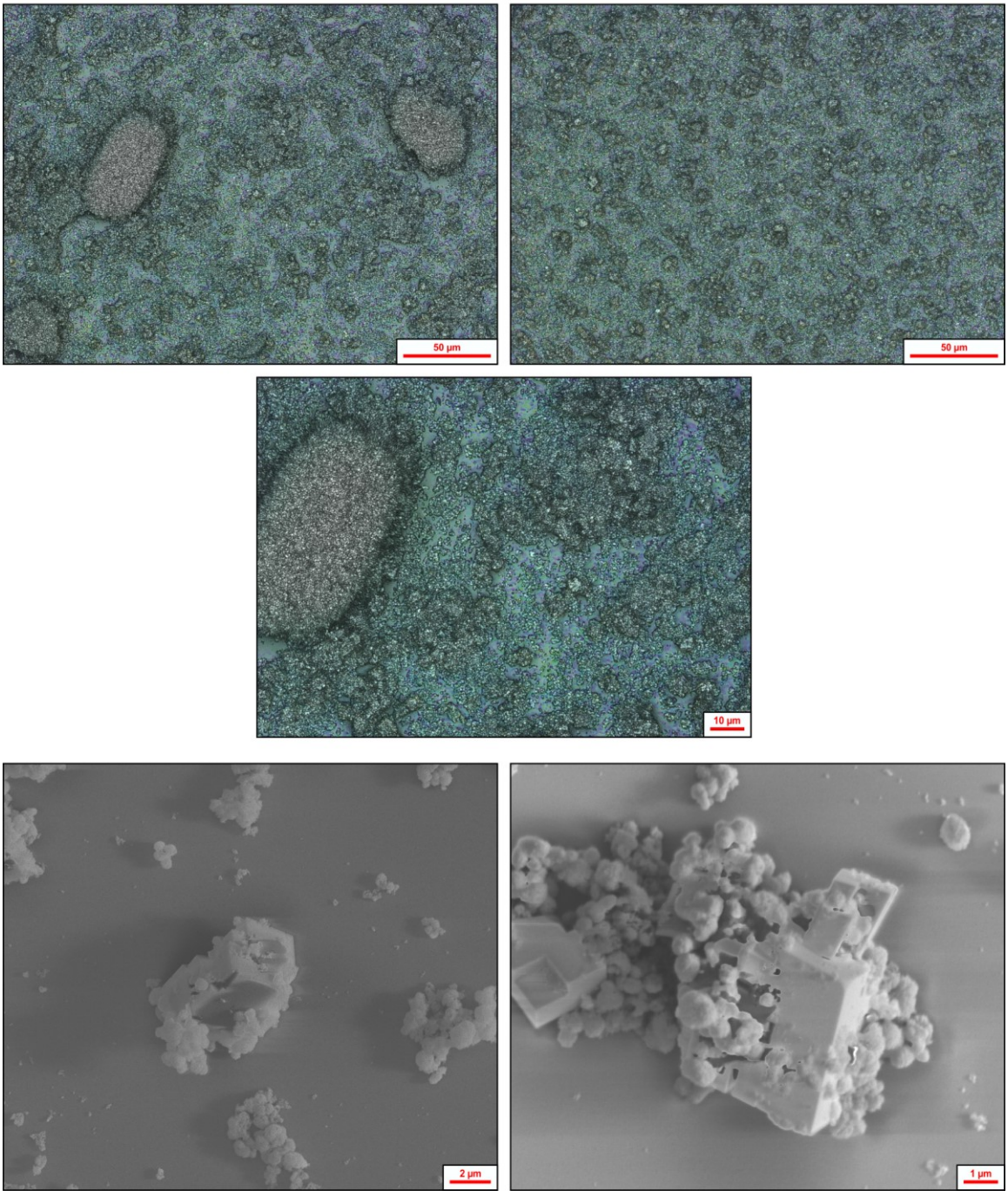

Figure 95) 1st and 2nd row: Overlayed Light-microscopic and *CLSM*-images. **3rd row:** *SEM*-images.

Precipitate obtained in the presence of 1 mmol/L of pure peptide (8)

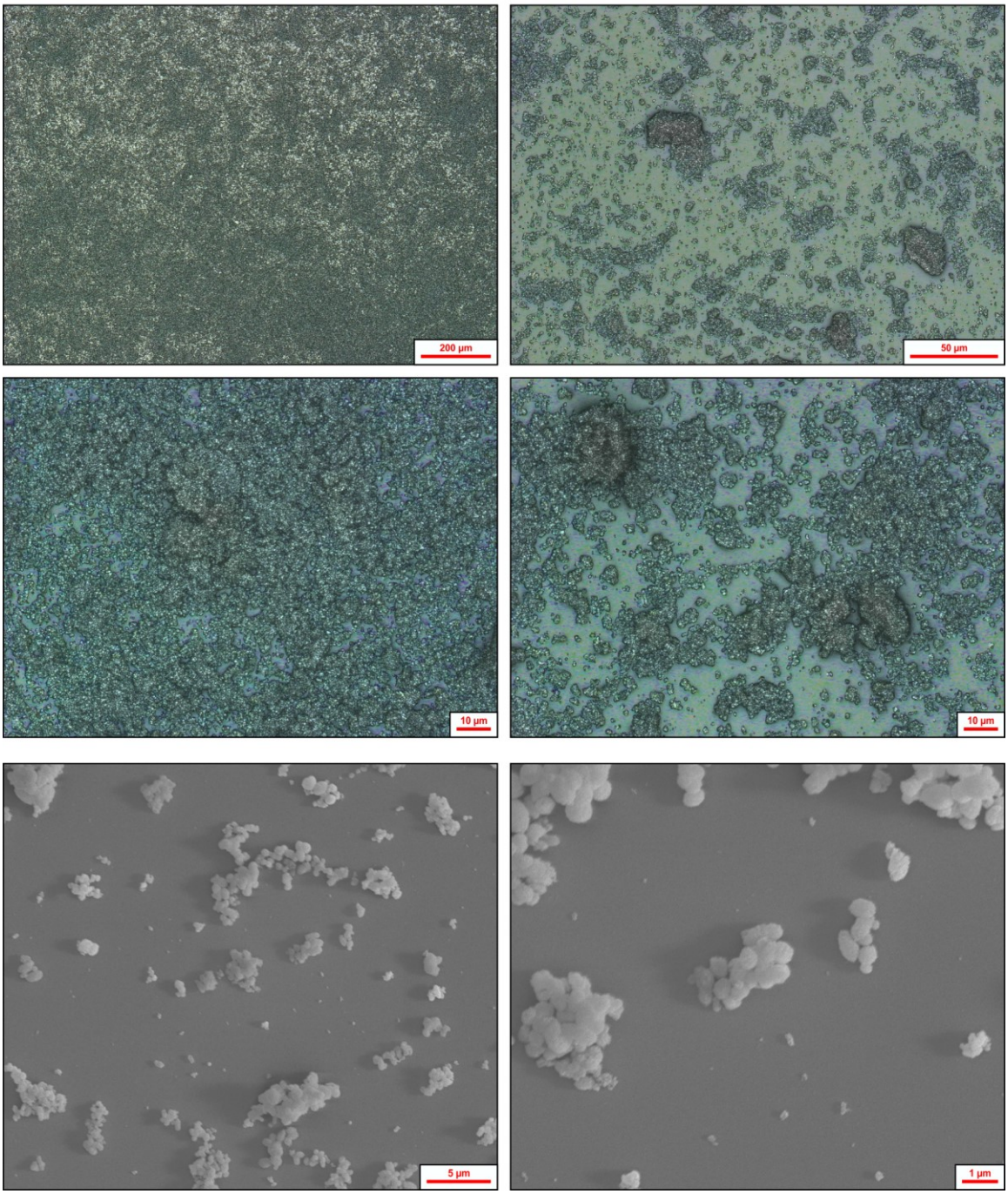

Figure 96) 1st and 2nd row: Overlayed Light-microscopic and *CLSM*-images. **3rd row:** *SEM*-images.

Precipitate obtained in the presence of 1 mmol/L of crude peptide (8)

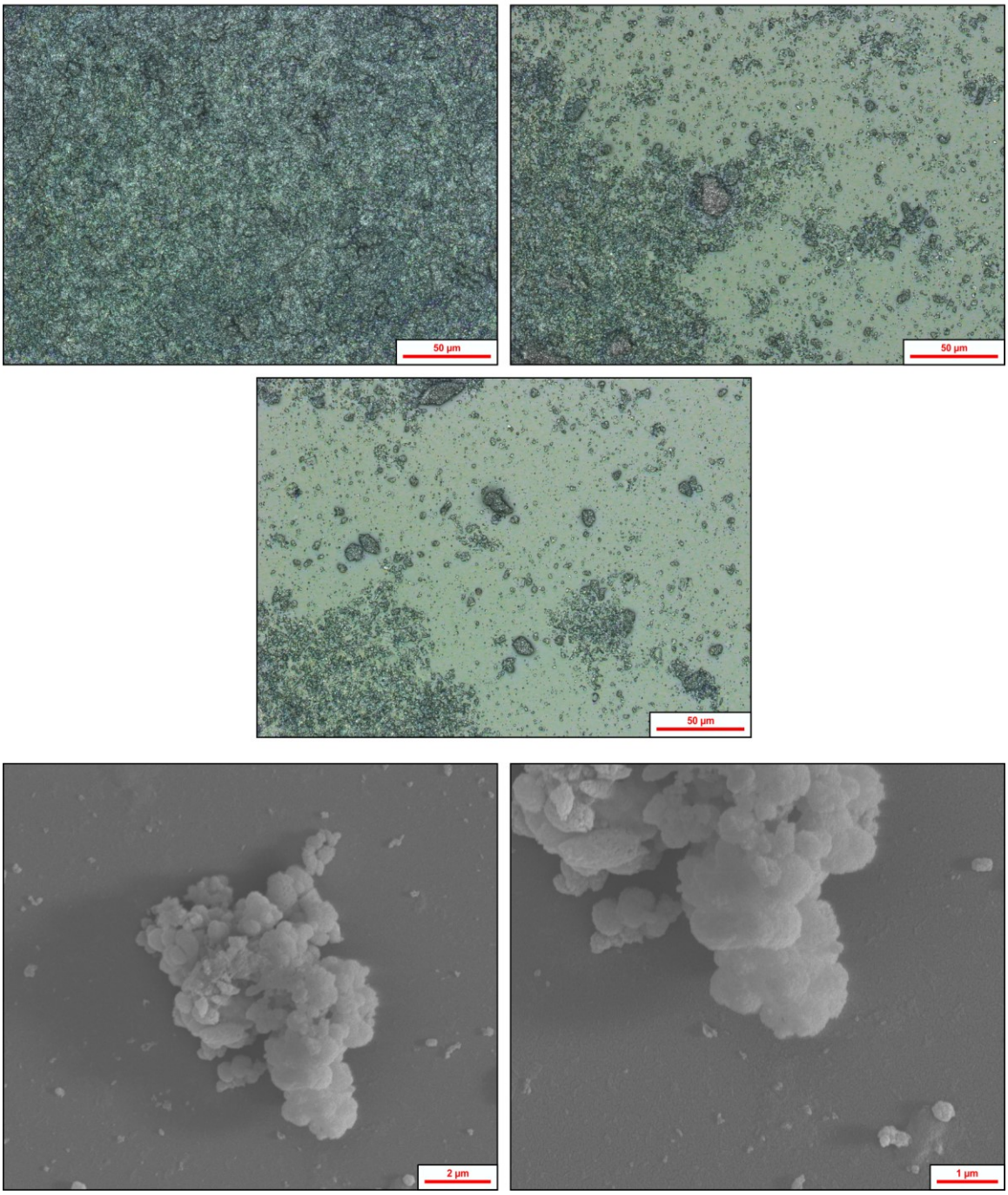

Figure 97) 1st and 2nd row: Overlayed Light-microscopic and *CLSM*-images. **3rd row:** *SEM*-images.

Precipitate obtained in the presence of 1 mmol/L of desalted peptide (8)

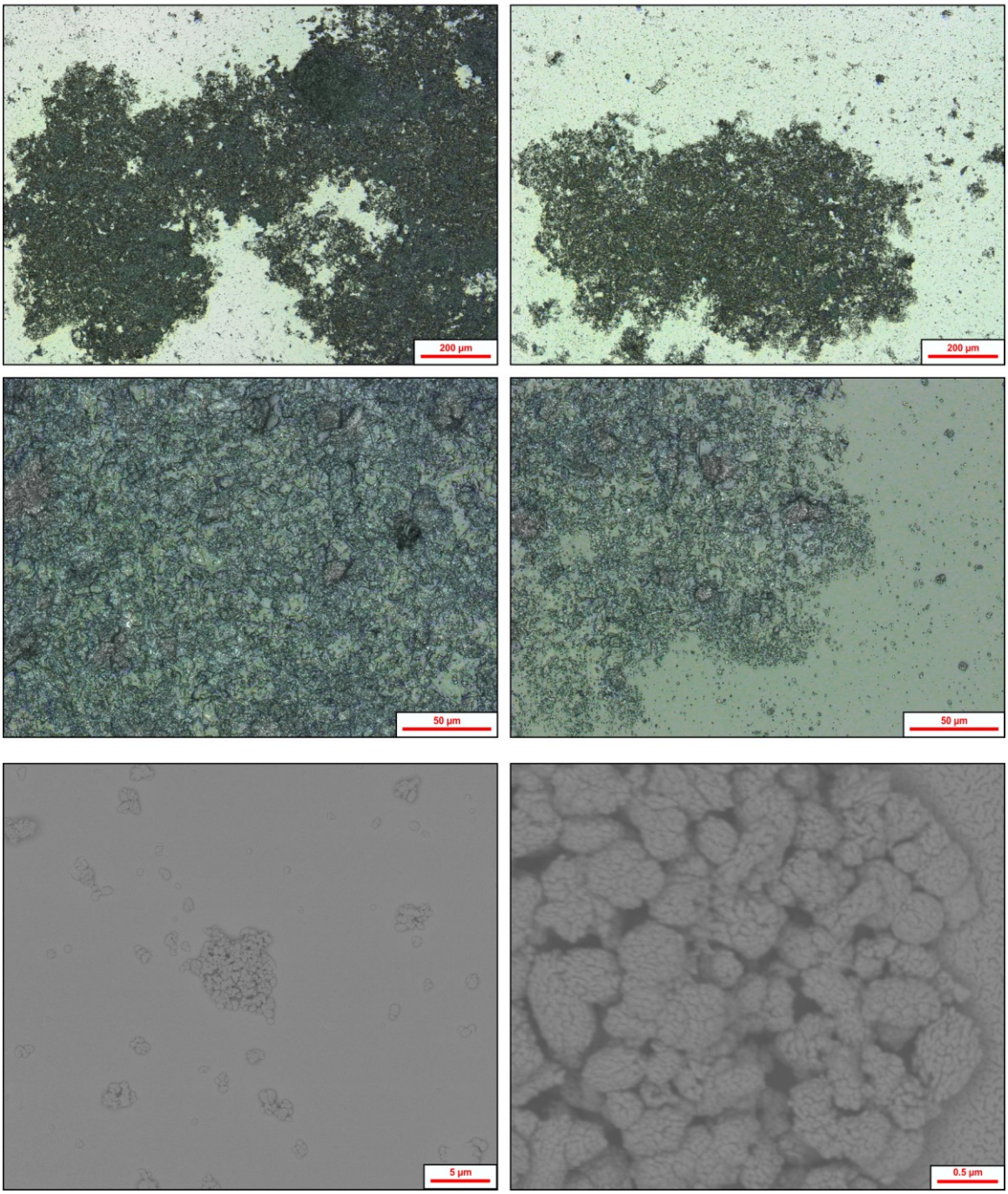

Figure 98) 1st and 2nd row: Overlayed Light-microscopic and *CLSM*-images. **3rd row:** *SEM*-images.

Precipitate obtained in the presence of 1 mmol/L of peptide (1)

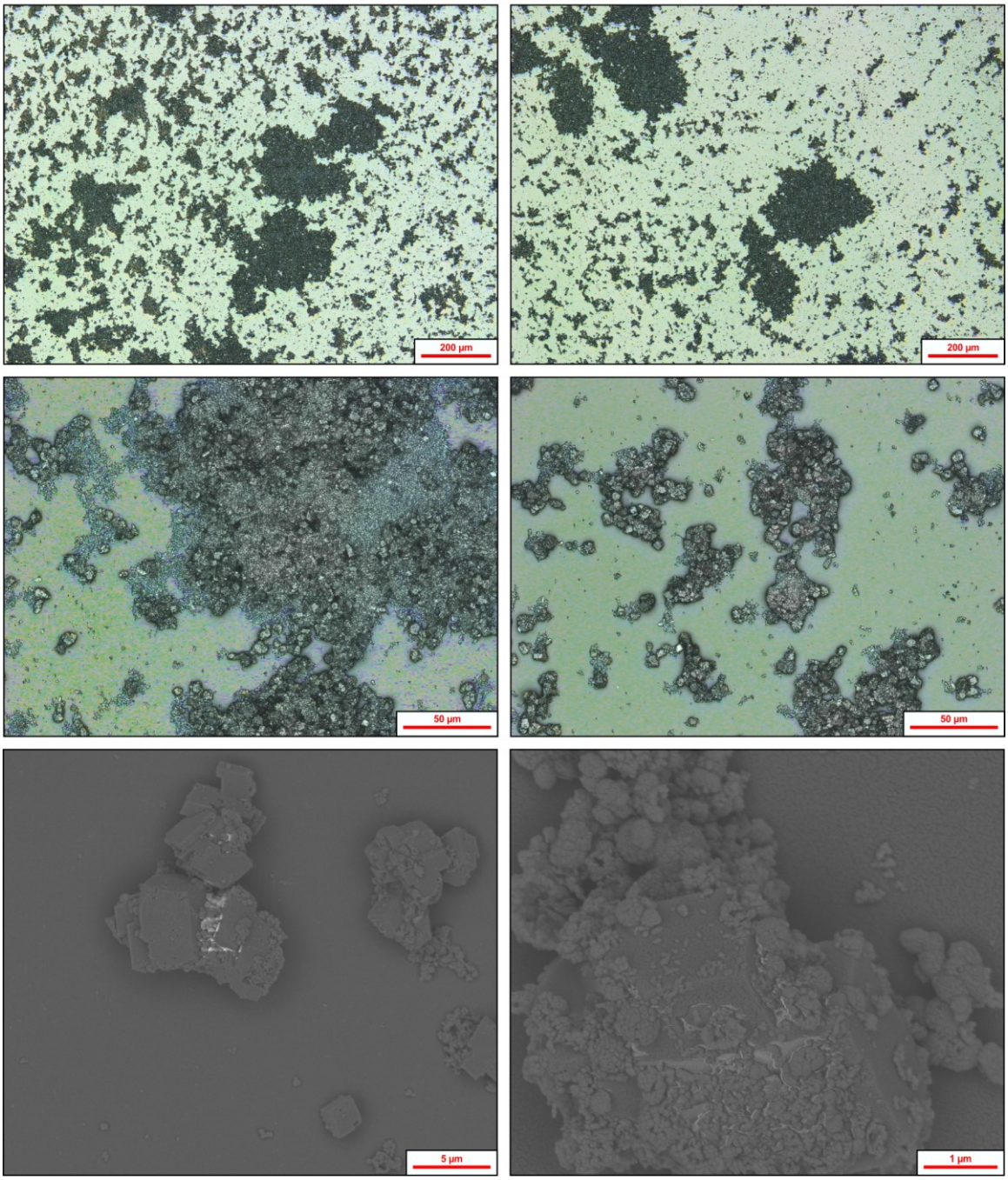

Figure 99) 1st and 2nd row: Overlayed Light-microscopic and *CLSM*-images. **3rd row:** *SEM*-images.

Precipitate obtained in the presence of 1 mmol/L of peptide (10)

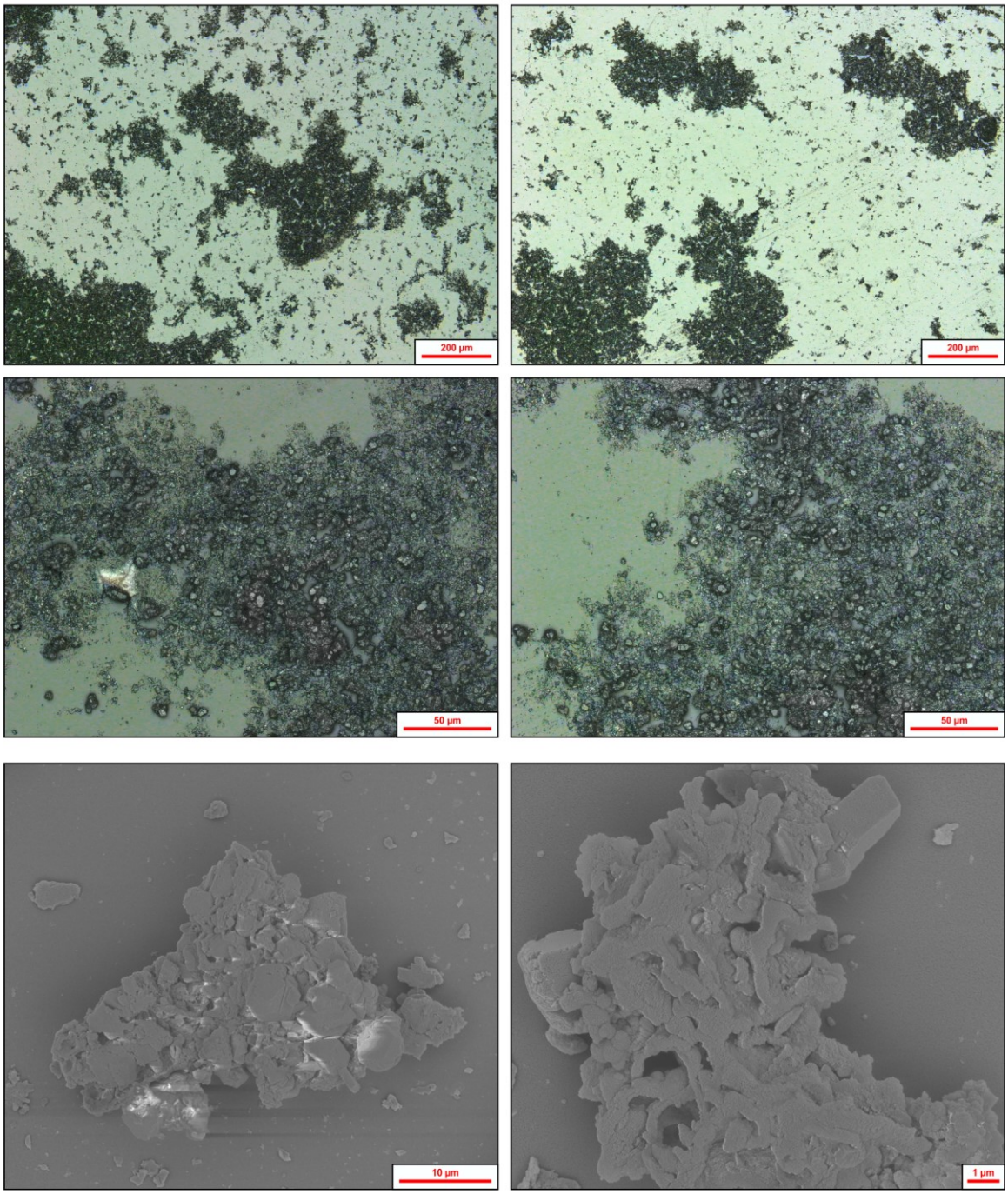

Figure 100) 1st and 2nd row: Overlayed Light-microscopic and *CLSM*-images. **3rd row:** *SEM*-images.

Precipitate obtained in the presence of 1 mmol/L of peptide (11)

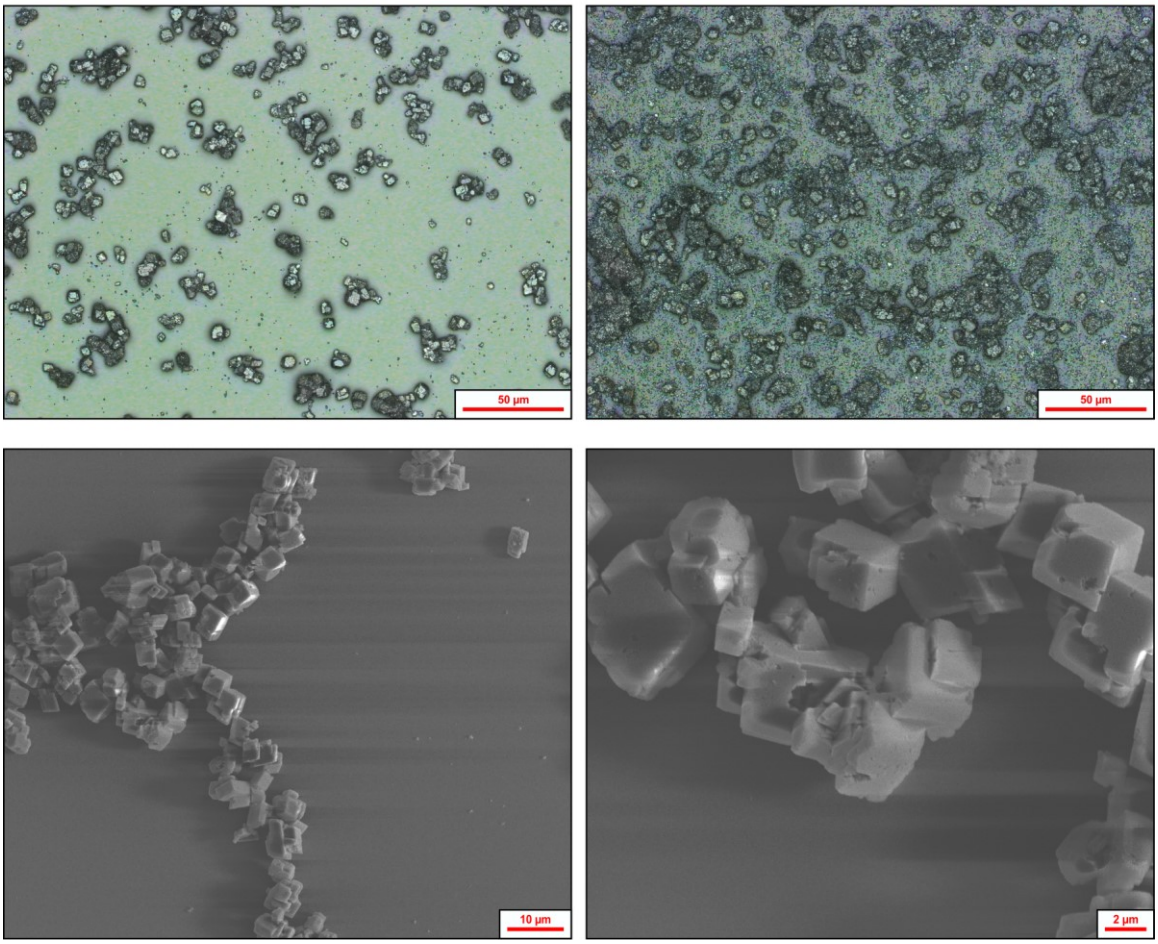

Figure 101) Upper row: Overlayed Light-microscopic and *CLSM*-image. **Lower row:** *SEM*-images.

Precipitate obtained in the presence of 1 mmol/L of crude peptide (9)

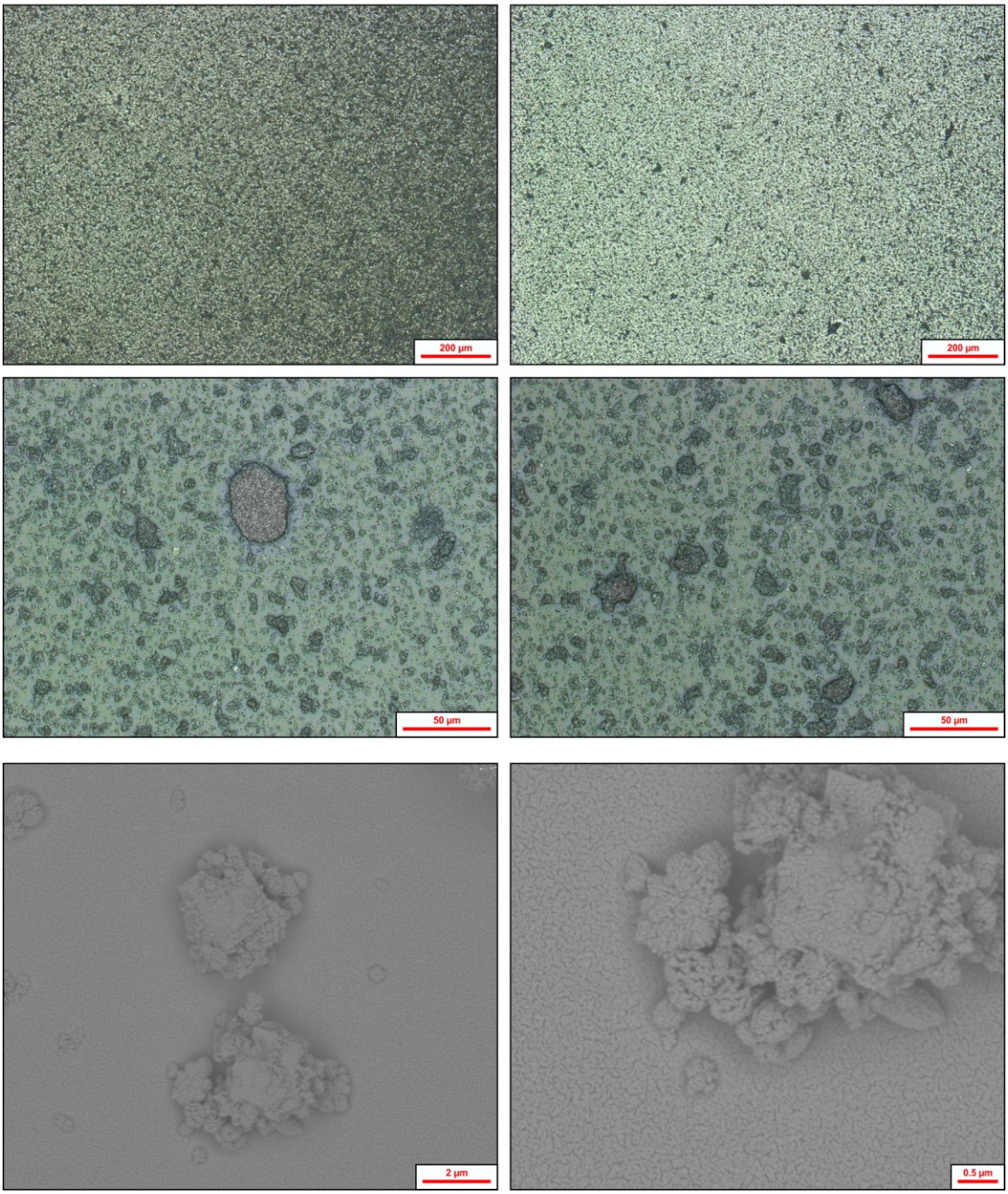

Figure 102) 1st and 2nd row: Overlayed Light-microscopic and *CLSM*-images. **3rd row:** *SEM*-images.

List of Figures

List of Tables